Integration of Hydrothermal Conversion and Anaerobic Fermentation for the Valorisation of High Ash Feedstocks

Aaron Ellis Brown

Submitted in accordance with the requirements for the degree of
Doctor of Philosophy as part of the Integrated PhD with MSc in Bioenergy

The University of Leeds
School of Chemical and Process Engineering

September 2021

The candidate confirms that the work submitted is his own, except where work which has formed part of jointly-authored publications has been included. The contribution of the candidate and the other authors to this work has been explicitly indicated below. The candidate confirms that appropriate credit has been given within the thesis where reference has been made to the work of others.

1. **Brown, A.E.**, Finnerty, G.L., Camargo-Valero, M.A. and Ross, A.B., 2020. Valorisation of macroalgae via the integration of hydrothermal carbonisation and anaerobic digestion. Bioresource Technology, 312, p.123539.

2. **Brown, A.E.**, Adams, J.M.M., Grasham, O.R., Camargo-Valero, M.A. and Ross, A.B., 2020. An Assessment of Different Integration Strategies of Hydrothermal Carbonisation and Anaerobic Digestion of Water Hyacinth. Energies, 13(22), p.5983.

Publications 1 and 2 have contributed towards some sections of Chapters 4, 5, 6, 7. The candidate designed the experiments, conducted the experimental work, conducted the data analysis and drafted the manuscripts for both Publication 1 and 2.

- Dr. Gillian Finnerty contributed, in part to Publication 1 by demonstrating the operation of the hydrothermal reactors and generating samples for downstream analysis by the candidate.
- Dr. Oliver Grasham provided advice on developing the methodology for developing the energy balance calculations used as part of Publication 2.
- Dr. Jessica Adams reviewed and provided feedback to Publication 2.
- Dr. Miller Alonso Camargo-Valero and Dr. Andrew Ross reviewed and provided feedback to both Publication 1 and 2.

Acknowledgements

First and foremost, I would like to express my sincere gratitude to my incredible supervisors, Dr. Andrew Ross and Dr. Miller Alonso Camargo-Valero, for their continued support, belief and advice. The guidance and encouragement you have provided has kept me on track through all the twists and turns of my PhD journey: I could not have done it without you.

I would also like to thank Dr. Jessica Adams (Aberystwyth University) and Dr. Sean Scully (University of Akureyri) for hosting me at their respective Universities during my placements – both were amazing experiences.

I would like to acknowledge the Engineering and Physical Sciences Research Council (EPSRC) for providing the funding to support this research degree. I must also thank the administrative and technical staff at the University of Leeds, in particular Emily Bryan-Kinns, James McKay, Simon Lloyd, Dr. Adrian Cunliffe, Karine Alves Thorne and Dr. David Elliott.

I would like to thank my friends and Leeds housemates: Andy Price-Allison, Matty Marshall and Alex Smith, who I lived with through the duration of the PhD. You really did make my time in Leeds an incredible experience, providing a constant source of fun and hilarity away from the office. I'd also like to give a special mention to: Tom Willmott, Vicky Holt, Danny Burkle, Sally Barton, Hannah Barton, Lizzie Palmer, India Lochhead, Becca Filewood and Nick Charman, who all kept me on track over the past 5 years.

Thank you to all my friends and colleagues that I have had the pleasure of meeting and working with throughout my time on the CDT. I'd like to thank Luke Higgins, Fernando Climent Barba, Iram Razaq, Jeanine Williams, Jessica Quintana-Najera, Jaime Borbolla-Gaxiola, James Hammerton, Toby Green, Aaron Carvell, Judith Ford, Kiran Parmar, Gillian Finnerty, Chris Holt, Doug Bray, Scott Wiseman, Ollie Grasham, Lee Roberts, Daisy Thomas, Christian Aragon-Briceño, Cynthia Okoro-Shekwaga and Aidan Smith.

Finally, a special thank you to my family, especially my mum Beverley, my dad Nicholas and my brother Ross. Your continued support has got me to the place I am today – I hope I can continue to make you proud.

Abstract

The generation of bioenergy is widely regarded as a key factor in reducing global GHG emissions. Alternative, high-ash feedstocks could provide an abundant source of sustainable biomass, which do not compete for valuable arable land with food or feed crops. However, thermal conversion of these biomass sources can prove problematic, due to a high moisture content, low bulk density and unfavourable ash chemistry. Biological conversion can also prove challenging, as recalcitrant biochemical structures limit the efficiency of biodegradation. The aim of this thesis was to investigate the potential for integrating hydrothermal and biological conversion technologies to improve the energy conversion efficiency (ECE) of alternative, high-ash biomass, compared to biological processing alone. This work focusses on the valorisation of two lignocellulosic feedstocks: water hyacinth (WH) and grass (GR), and three brown macroalgal species: *S. latissima* (SL), *F. serratus* (FS) and *L. digitata* (LD). A number of integration strategies exist between hydrothermal carbonisation (HTC) and anaerobic digestion (AD); including [i] AD of hydrochars, [ii] combustion of hydrochars and AD of process waters and [iii] AD of HTC slurry. The suitability of each integration strategy was assessed across a range of HTC reaction temperatures (150°C, 200°C and 250°C). The results show the separation of hydrochars for combustion and process waters for anaerobic digestion (AD) provides the greatest improvement in ECE. Higher HTC processing temperatures are associated with a lower energy output and lower ECE, due to decreased hydrochar yields and formation of inhibitory compounds in the process waters. However, hydrochar quality is compromised at lower processing temperatures, due to limited energy densification or removal of problematic ash species. This integration strategy proved particularly effective for SL, FS and GR. The ECE of SL (64%) was improved to between 71-90%, FS (31-35%) to between 57-91% and GR (50%) to between 63-82%. Although, HTC processing temperatures of between 200-250°C are recommended. The application of this HTC-AD integration strategy for LD appears to be seasonally variable. Winter-harvested LD shows an improvement in ECE from 59% to between 64-87%. However, the ECE of summer-harvested LD was not significantly improved using HTC-AD. WH-derived hydrochars showed no improvement in ash behaviour, potentially limiting the application as a combustion fuel. AD of WH-HTC slurry produced at 150°C improved the ECE of WH from 25% to 48% during one-stage digestion or 62% during two-stage digestion. Therefore, low-temperature hydrothermal pre-treatment could be a suitable valorisation strategy for WH. Overall, integrated hydrothermal and biological processing appears an effective strategy to improve the ECE of high ash feedstocks; overcoming the problems associated with thermochemical conversion. However, the optimised integration strategy and reaction conditions vary between different types of biomass.

Table of Contents

List of Tables

List of Figures

List of Acronyms and Abbreviations

AD	Anaerobic Digestion
ADF	Acid Detergent Fibre
ADL	Acid Detergent Lignin
AI	Alkali Index
AMPTS	Automatic Methane Potential Test System
ANOVA	Analysis of Variance
APHA	American Public Health Association
AR	As Received
BAI	Bed Agglomeration Index
BHP_{ex}	Experimental Biohydrogen Potential
BI	Biodegradability Index
BMP_{ex}	Experimental Biomethane Potential
BMP_{th}	Theoretical Biomethane Potential
COD	Chemical Oxygen Demand
DAF	Dry Ash Free
DB	Dry Basis
DF	Dark Fermentation
DIET	Direct Interspecies Electron Transfer
DIS	Distilled Water
DTG	Derivative Thermogravimetric
ECE	Energy Conversion Efficiency
ED	Energy Densification
EROI	Energy Return Upon Energy Invested
EY	Energy Yield
FC	Fixed Carbon
FI	Fouling Index
FID	Flame Ionisation Detection

FS	*Fucus serratus*
FTIR	Fourier Transform Infrared Spectroscopy
GC	Gas Chromatography
GCV	Gross Calorific Value
GHG	Greenhouse Gas
GR	Grass
HHV	Higher Heating Value
H_m	Maximum Biomethane/Biohydrogen Yield
HMF	5-Hydroxymethylfurfural
HPLC	High-Performance Liquid Chromatography
HTC	Hydrothermal Carbonisation
HTG	Hydrothermal Gasification
HTL	Hydrothermal Liquefaction
HY	Hydrochar Yield
IPCC	Intergovernmental Panel on Climate Change
ISR	Inoculum-to-Substrate Ratio
λ	Lag Phase
LD	*Laminaria digitata*
M	Moisture
MCF	Methylchloroformate
MS	Mass Spectrometry
ND	Not Detected
NDF	Neutral Detergent Fibre
NDIR	Non-Dispersive Infra-Red Detector
NH_4^+-N	Ammonium-Nitrogen
NO_x	Nitrogen Oxides
PID	Proportional Integral Derivative Controller
R b/a	Acid-Base Ratio
R_m	Peak Biomethane Production Rate

SE	Steam Explosion
SEA	Seawater
SF	Severity Factor
SI	Slagging Index
SL	*Saccharina latissima*
SLR	Solid Loading Ratio
SO_x	Sulphur Oxides
SVI	Slag Viscosity Index
T^{80}	Technical Digestion Time
TC	Total Carbon
TCD	Thermal Conductivity Analyser
TGA	Thermogravimetric Analysis
TIC	Total Inorganic Carbon
T_m	Peak Time of Fermentation
TN	Total Nitrogen
TOC	Total Organic Carbon
TP	Total Phenols
TS	Total Solids
VFA	Volatile Fatty Acid
VM	Volatile Matter
VS	Volatile Solids
WH	Water Hyacinth
WWTP	Waste Water Treatment Plant
XRF	X-Ray Fluorescence Spectrophotometry

Chapter 1
Introduction

The climate of our planet is drastically changing at an alarming rate, towards what has been termed a state of 'climate emergency' [1]. Greenhouse gas (GHG) emissions and global temperatures continue to rise, resulting in devastating environmental consequences, which include: rising sea levels, increased prevalence of extreme weather events and destruction of natural habitats. A rapid increase in atmospheric GHG emissions have been observed since the 1750s; driven by an increased uptake of fossil-fuel derived energy, initiated by the industrial revolution [2,3]. Since this time, GHG emissions have continued to rise, with a peak CO_2 concentration of 410ppm reported in 2019 [2]. Figure 1.1 shows this atmospheric CO_2 concentration is the highest of any point over the past 800,000 years. Higher GHG gas emissions are coupled with an increase in global surface temperatures; as heat becomes trapped by the Earth's atmosphere [1]. Global surface temperatures have shown a more rapid increase since 1970, compared to any 50-year period in the past 2000 years [2].

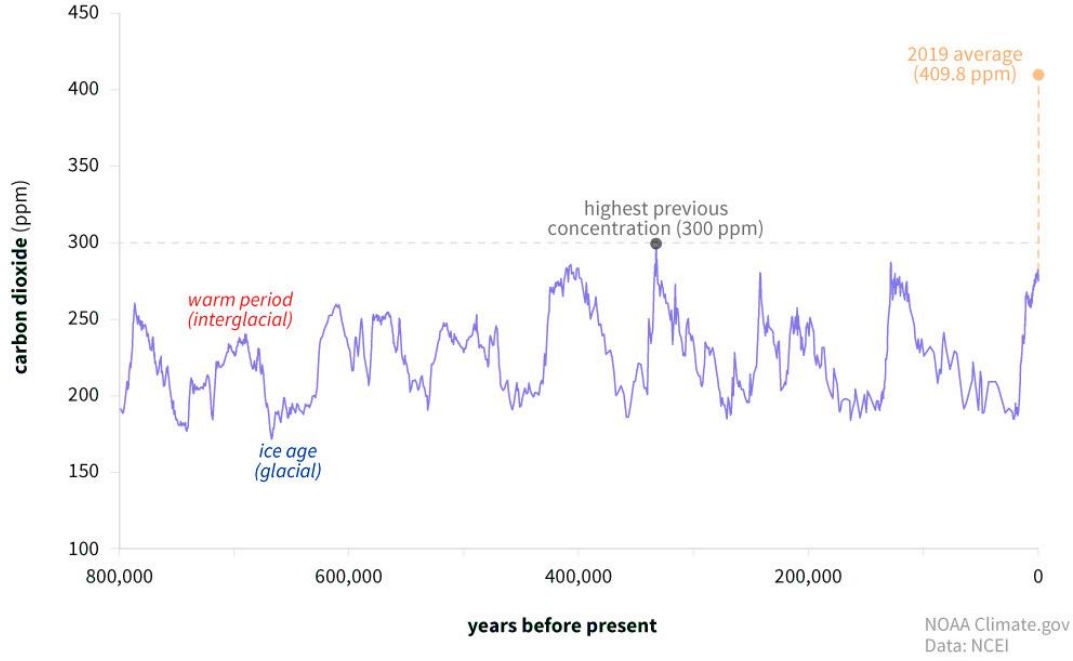

Figure 1.1. Global atmospheric carbon dioxide concentrations over the past 800,000 years. Sourced from [4]**.**

It is widely accepted that increasing GHG emissions are a result of anthropogenic-derived activity [1,2]. Since pre-industrial levels (c. 1750), human activity has resulted in a 1°C increase of the Earth's surface temperature [1,2], likely to increase to 1.5°C between 2030-2052, if current emission rates continue [1]. In 2015, the Paris Climate Agreement was

established [5]; with the aim of limiting global rising temperatures to below 2°C; ideally 1.5°C, compared to temperatures recorded in the pre-industrial era. The IPCC Climate Change report (2021) states that this limit will be exceeded during the 21st century, unless 'deep reductions' in GHG emissions occur over the coming decades [2]. In order to achieve the goal of limiting global warming to <1.5°C by the end of 2100, global GHG emissions must be maintained between 25-30 $GtCO_2e\ year^{-1}$ by 2030. However, current projections estimate global GHG emissions will reach between 52-58 $GtCO_2e\ year^{-1}$ by 2030. Therefore, a 40-50% reduction in anthropogenic-derived GHG gas emissions, compared to the 2010 levels, is required to achieve this goal [6].

Anthropogenically-derived GHG emissions are produced from many different aspects of living our day-to-day lives. Figure 1.2 shows the origins of GHG emissions across each economic sector. Electricity and heat production represents the greatest source of global GHG emissions (25%), due to the continued dependence on fossil-based energy sources. As a result, a shift away from fossil-based energy, towards renewable energy sources will play a significant role in achieving sufficient reductions in future GHG emissions.

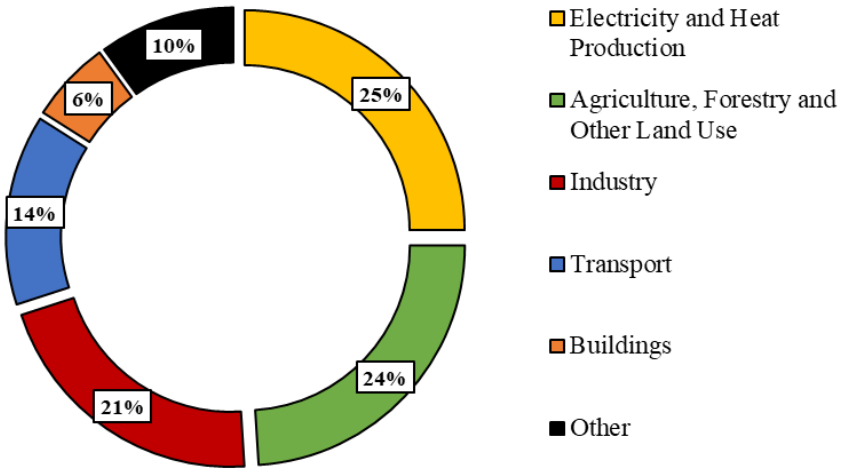

Figure 1.2. Global GHG emissions per economic sector. Data based on 2010 data, presented in the IPCC 2014 report [7].

1.1 Biomass & Bioenergy

The term 'biomass' refers to organic material of recent biogenic origin, which is either plant or animal derived. Plants-based biomass is produced by photosynthesis: a process where solar energy is converted into chemical energy in the form of plant structural components, such as

carbohydrates [8]. Photosynthesis is a natural method of CO_2 sequestration. Biomass can be processed and utilised as a source of bioenergy, chemicals or functional materials. Using biomass as an energy source allows for the exploitation of nature's energy cycle [9]. The CO_2 emissions generated during biomass conversion are reincorporated into other biomass sources, as they grow via photosynthesis; therefore, creating a closed carbon cycle [8].

The utilisation of biomass as an energy source has been exploited for thousands of years, with early civilisation burning wood to generate a heat source for cooking. Nowadays, bioenergy provides approximately 11.6% (c. 44 EJ) of the global total energy consumption, based on figures from 2019 [10]. More than half of this energy (c. 24.6 EJ) originates from the use of traditional biomass, such as wood, as a fuel for cooking and heating in developing nations [10].

The generation of bioenergy is attracting increased interest, as countries such as the UK, transition from fossil-derived energy to renewable energy. In 2008, the UK Government established the Climate Change Act; stipulating a legal requirement to reduce net UK GHG emissions to 80% lower than the 1900 baseline, by the year 2050 [11]. Bioenergy has been recognised as an important player in meeting this target by the UK Bioenergy Strategy [12]; which suggests bioenergy should contribute towards approximately 10% of the UK energy market to achieve this target. Bioenergy is one of the more versatile forms of sustainable energy: with the capability of producing a number of different energy vectors (solid, liquid or gaseous fuels) which can contribute towards each of the main areas of energy demand: heat, electricity and transportation fuels [12]. Biofuels pose a significant advantage over alternative renewable energy sources (wind, solar, hydropower), due to their potential for continuous production and capacity for storage and transportation.

1.1.1 Conversion Technologies

The combustion of biomass remains the most traditional method of converting chemical energy within biomass into heat energy. However, ever increasing interest in the utilisation of bioenergy into the global energy landscape has resulted in the development of multiple conversion approaches. These conversion technologies can be broadly categorised into: thermochemical and biological processing techniques; the characteristics of which are outlined in Table 1.1.

Thermochemical processing uses heat to convert organic material, such as biomass, into solids, liquids, gases or thermal energy [13]. Combustion involves the oxidation of biomass to release thermal energy. Pyrolysis describes the thermal decomposition of biomass, in the

absence of air. Varying the operational parameters of pyrolysis can generate different products. Generally, lower temperatures and retention times lead to the formation of a solid residue named biochar, whereas higher temperatures and shorter retention times lead to the formation of a liquid crude bio-oil [14]. Torrefaction is similar to slow pyrolysis, but occurs at lower processing temperatures. Finally, gasification involves the conversion of biomass under elevated temperatures and oxygen-starved conditions, to form a flammable syngas, containing mainly: CO, H_2, CH_4, N_2 and CO_2 [13]. Thermochemical processes are well established conversion methods for biomass. However, these often require dried feedstocks, which can be problematic when processing biomass.

Table 1.1. Overview of different biomass conversion techniques.

Conversion Technology	Process Conditions	Temperature (°C)	Pressure (bar)	Product	References
Thermochemical					
Combustion	Typically Dry & Oxidising	700-1400	1	Thermal energy	[14]
Torrefaction	Dry & Anoxic	200-300	1	Char	[14]
Slow Pyrolysis	Dry & Anoxic	400-600	1	Char	[14]
Fast Pyrolysis	Dry & Anoxic	650-1000	1	Bio-oil	[14]
Gasification	Dry & Limited O_2	500-1300	1	Syngas	[14]
HTC	Wet	180-250	20-100	Char	[15]
HTL	Wet	300-350	50-200	Bio-crude Oil	[15]
HTG	Wet	350-700	>220	Syngas	[15,16]
Biological					
AD	Wet & Anoxic	20-55	1	Biogas	[17]
Fermentation	Wet & Mostly Anoxic	25-37	1	Bioethanol	[18]

HTC=hydrothermal carbonisation. HTL=hydrothermal liquefaction. HTG=hydrothermal gasification. AD=anaerobic digestion.

Hydrothermal processing is an alternative thermochemical conversion route, which involves the conversion of biomass in hot compressed liquid water [19]; thereby negating the requirement to pre-dry biomass before processing. Different products can be produced from biomass during hydrothermal processing, depending on the severity of the reaction. Through varying the temperature of the process, biomass can be converted to a solid, liquid or gas, through hydrothermal carbonisation, hydrothermal liquefaction or hydrothermal gasification, respectively.

Biological conversion techniques utilise enzymes or microorganisms, such as bacteria or yeasts, to convert biomass into biofuels. During fermentation, simple sugars derived from the carbohydrate fraction of biomass are converted to bioethanol through the metabolic pathways of yeasts. Whereas, anaerobic digestion (AD) involves degradation of biomass into biogas through the sequential metabolic pathways of a mixed consortium of microorganisms, including bacteria and *Archaea*. Similarly to hydrothermal processing, biological conversion allows the processing of wet biomass. Biological conversion is often a much slower process compared to thermochemical conversion. However, the external energy requirements to carry out the biological conversion processes are often much lower than thermochemical conversion [14].

In addition to thermochemical and biological processes, biochemical conversion routes, such as transesterification can be used to generate biodiesel from lipid-rich biomass. Biodiesel is produced by mixing biomass-derived lipids, such as vegetable oils, with a NaOH catalyst and an alcohol, such as ethanol. The triglycerides within biomass-oils are converted to fatty acid methyl ester (biodiesel) and glycerol. Alternatively, diesel or gasoline fuels can be produced through Fischer-Tropsch synthesis of syngas [14].

1.1.2 Biomass Feedstocks

Worldwide, a large diversity of biomass exists, which can be converted into biofuels. Biofuels can be broadly categorised as first, second or third generation, dependent on the type of biomass used in their production. First generation biofuels are generated from biomass which is edible to humans, such as corn, sugarcane and rapeseed [20]. These biomass types tend to be rich in sugars, starches or lipids and are generally used to produce bioethanol or biodiesel [21]. However, the use of edible crops to generate energy results in the controversial ‘food vs fuel’ debate, where crops are deflected away from human consumption; causing additional strains to food supply [21] and potentially resulting in increased food prices [20].

Second generation biomass feedstocks utilise ‘non-food’ crops to generate biofuels, using more advanced conversion approaches [22]. Therefore, acting as a competitive solution for the generation of sustainable energy, whilst mitigating the use of food or feed crops. Lignocellulosic biomass is an example of a second generation feedstock and is one of the most abundantly available raw materials on the planet; with an estimated yield of 220 billion tonnes, per year, worldwide [23]. Therefore, representing an underutilised, alternative energy source for potential conversion into biofuels. Lignocellulosic biomass typically consists of woody biomass, agricultural residues or purpose-grown energy crops.

Lignocellulosic biomass is comprised of a complex interlinking network of polymers, including: cellulose (20-50%), hemicellulose (12-34%) and lignin (12-29%); which provide structural rigidity to the plant [24]. The typical structure of lignocellulosic biomass is displayed in Figure 1.3. Cellulose is a linear homopolysaccharide, comprised of β-(1-4) linked D-glucose monomers. Hemicellulose is a branched heteropolysaccharide comprised of hexose and pentose monosaccharides [24]. Whilst lignin is an amorphous polymer, consisting of three different types of phenylpropane alcohols: p-coumaryl, coniferyl and sinapyl. The presence of lignin is an evolutionary strategy; providing the plant with a defence mechanism against microbial attack or oxidative stress [25].

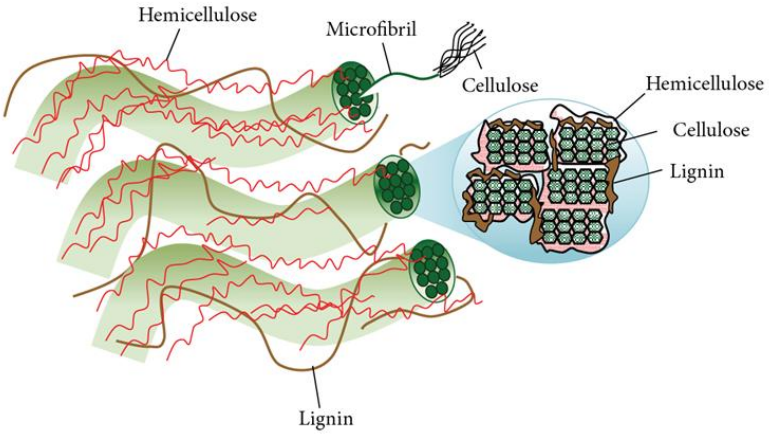

Figure 1.3. Structure of lignocellulosic biomass. Sourced from [26].

Third generation biofuels are generated from aquatic biomass, named algae. Broadly, two different types of algae exist: microalgal and macroalgal biomass. Microalgae are unicellular photosynthetic microorganisms, which are often used for the generation of biodiesel, due to their high lipid content [21]. Whereas, macroalgae are multicellular photosynthetic organisms, of which carbohydrates are typically the dominating biochemical fraction [21].

This work predominately focusses on two types of lignocellulosic biomass: water hyacinth and grass and three species of brown macroalgal biomass: *Saccharina latissima*, *Laminaria digitata* and *Fucus serratus*, which are described in more detail over the following sections.

1.1.2.1 Water Hyacinth

Water hyacinth (WH) (*Eichhornia crassipes* (Mart.) Solms) is a free-floating aquatic macrophyte, indigenous to South America [27]. Nowadays, WH is now widely regarded as one of the most prolific invasive macrophyte species in the world [27,28]; spreading to over 50 countries, across 5 continents, over the past 150 years [28]. WH was introduced to water bodies across the world as an ornamental plant, due to its attractive purple flowers [27]. However, WH now dominates fresh water bodies across Asia, Africa, Australia and North America. Lake Victoria is one of the worst affected areas of WH proliferation, following its introduction to the lake in the 1980s [29]. Early reports from 1998 estimated the total maximum WH coverage of Lake Victoria was at least 17,374 ha [30]. The successful proliferation of WH is attributed to its rapid growth rate, ability to outcompete native flora and the lack of natural control by native herbivores [31]. WH grows both sexually [32] and asexually [28] and can rapidly take up surrounding nutrients, facilitating rapid propagation of lakes and rivers.

WH forms cohesive floating mats atop water bodies, which can grow to high densities, of over 60kg/m^2 and contain up to two million plants per hectare; a total weight of between 270-400 tonnes [32]. Figure 1.4 displays an example of a WH mat in the Indryani River, Pune, India. The rapid growth of WH can result in devastating environmental effects on the natural ecosystem and socioeconomic implications on local communities; particularly those in developing countries. The environmental impacts include: deoxygenation of the water body, reducing the biodiversity of aquatic life and destroying ecosystems [33,34]. Whereas the social implications of WH invasion include irrigation issues, preventing operation of fishing boats; which impacts the economy of local communities and acting as a habitat for disease-carrying vector organisms; such as mosquitos [33,34].

Several efforts have been made to control the continued proliferation of WH, including biological, chemical and physical removal of biomass from the water. However, these methods are often time consuming, expensive or logistically complex [34,35]. An additional disadvantage to these methods is that no value is extracted from the WH. Therefore, recent interests have shifted towards the utilisation of WH as a source of fuels and chemicals [33]; taking advantage of the rapid growth rate of WH.

Figure 1.4. Water hyacinth mat located in the Indryani River, Pune, India. Photograph is courtesy of Douglas Bray.

WH is a lignocellulosic biomass, with the typical biochemical composition reported in Table 1.2. The moisture content of WH is typically high, due to the fact it is grown in an aquatic environment. Additionally, the ash content of WH represents a large fraction of the biochemical composition (16-25%). WH has excellent phytoremediative properties for both organic and inorganic pollutants [36], including heavy metals; which contribute towards the higher ash content [32]. The protein content of WH is also high (16-20%); suggesting it could also be used as a possible animal feed [34]. The carbohydrate and lignin contents of WH are highly varied across different samples. These variations could be linked to seasonal fluctuations in biochemical composition [37,38], plant maturity or spatial variation; resulting in differences between growth conditions.

Table 1.2. Typical biochemical composition of water hyacinth.

Parameter	Composition
Moisture[1]	91-94
Ash[2]	16-25
Carbon[2]	19-28
Cellulose[2]	18-31
Hemicellulose[2]	18-43
Lignin[2]	7-26
Protein[2]	16-20

Data obtained from Gunnarsson *et al*. [34]. [1]as received. [2]dry basis.

1.1.2.2 Grass

Grass (GR) is a widely abundant, terrestrial lignocellulosic biomass, which covers approximately 26% of total global land area [39]. Grasslands can be utilised for wide variety of purposes, such as: animal husbandry, carbon storage and preservation of ground or surface water quality [39]. The utilisation of GR as a feedstock to generate bioenergy is well established, with a particular interest for applications in biological conversion processes [40,41].

However, using GR as a feedstock for bioenergy generation often means displacing fertile land away from crop production or animal husbandry practices [42], creating negative competition between the production of food and the generation of biofuels [43]. Therefore, recently there is increased interest in using GR grown on marginal land as a feedstock source for bioenergy generation [43]. Such sources include: river banks [44], sports fields [45], roadside verges [46] and public spaces [47,48].

'Grass' is quite a broad term which encompasses a range of biomass types: from purpose-grown energy grasses, such as miscanthus [49], to mixed species of GR, such as those harvested from road-verges [46]. Grasses are typically defined as monocotyledonous plants which are part of the *Poaceae* family [50]. Table 1.3 displays the typical biochemical composition of GR; which generally contains a high moisture (58-76%) and high ash content (3-19%). Similarly to WH, large variances occur in the biochemical composition of GR. The biochemical composition of GR also varies according to species [39], harvesting season [51] and plant maturity [41].

Table 1.3. Typical biochemical composition of grass.

Parameter	Composition	References
Moisture[1]	58-76	[46,49]
Ash[2]	3-19	[46,47,49]
Carbon[2]	41-52	[46,49,52,53]
Cellulose[2]	25-40	[53]
Hemicellulose[2]	15-50	[53]
Lignin[2]	10-30	[53]
Protein[2]	5-16	[52,54]

[1]as received. [2]dry basis.

1.1.2.3 Macroalgae

Macroalgae, also referred to as seaweeds, are multicellular photosynthetic organisms belonging to the lower plants [55]. Globally, over 10,000 species of macroalgae exist [56], which can be broadly classified as green (*Chlorophyta*), red (*Rhodophyceae*) or brown (*Phaeophyceae*) algae; according to the pigmentation of different chlorophylls [55]. The number of species within each type of macroalgae varies, with the greatest diversity observed by red (c. 6000 species), then green (c. 4500 species) and finally brown macroalgae (c. 2000 species) [57]. The biochemical compositions of red, green and brown macroalgae vary both between and within the different algal groups. Numerous different applications exist for the utilisation of seaweed within the circular bioeconomy, including as food, nutraceuticals, pharmaceuticals, cosmetics, fertilisers and as a source for platform chemicals [56]. Recently, there has been increasing interest in the use of macroalgal biomass as a feedstock for bioenergy generation [58].

The utilisation of macroalgal biomass to produce third generation biofuels overcomes some of the disadvantages of using first, or even second generation biomass feedstocks. Seaweeds do not require arable land, freshwater, fertilisers or intensive human labour to grow [56]. Furthermore, macroalgae display faster growth rates compared to terrestrial biomass [9,56], which can be up to 2-20 times greater [59]; due to increased photosynthetic efficiency [57]. This increased rate in photosynthetic capability facilitates a reduction in atmospheric carbon; acting as a carbon sink, whilst simultaneously providing oxygen to the ocean, reducing acidification [56].

Of the different types of seaweeds, brown macroalgae tend to be the most widely studied in terms of biofuel production, due to their high carbohydrate content, coupled with successful mass cultivation [58]. The work conducted as part of this thesis has mainly focussed on the generation of bioenergy from two different types of brown macroalgae: kelps and wracks. Kelps refer to macroalgae within the *Phaeophyceae* class and *Laminariales* order [60], which have been referred to as the fastest growing plants in the world [9]. Whereas, wracks, also referred to as fucoids, belong to the *Fucaceae* family. The particular macroalgae used throughout this thesis are kelp species: *S. latissima* and *L. digitata* and wrack species: *F. serratus*; which are all common to UK waters.

The biochemical composition of brown macroalgae is significantly different to terrestrial biomass; in particular the carbohydrate fractions. The major structural carbohydrates found within macroalgal biomass are: alginate, laminarin, mannitol and fucoidan [61]. Although seaweeds contain cellulose [62], the levels of lignin are negligible [20]; therefore, the composition is largely different to lignocellulosic biomass. Alginates are comprised of uronic

acids: mannuroic and guluronic acids [55] and typically represent the major carbohydrate fraction of seaweeds. Alginates provide structural support to the algae, in a similar fashion to cellulose and lignin in terrestrial-based plants [9]. Whereas, laminarin and mannitol act as energy storage compounds [9]. Laminarin consists of a β-(1,3) glucan chain, with occasional a β-(1,6) linkages [60]. Whereas, mannitol is a type of sugar alcohol which is produced from the sugar mannose [60]. Finally, fucoidan is a polysaccharide, comprising of a sulphated fucose backbone, with small quantities of other sugars such as xylose, galactose and uronic acids [63].

The typical biochemical compositions of *S. latissima* and *L. digitata* and *F. serratus* are described in Table 1.4, Table 1.5 and Table 1.6, respectively. The moisture content of each macroalgal species is understandably high (67-89%), due to their growth in marine environments. In addition, the ash contents of macroalgal biomass are typically higher than WH (Table 1.2), GR (Table 1.3) and other conventionally used biomass feedstocks; such as oak wood or miscanthus [64]. The ash content of macroalgal biomass is predominately comprised of alkali metals (Na and K), Cl and Ca [65,66]. Large variations are observed between both the concentrations of ash and individual carbohydrate fractions of each seaweed. The biochemical composition of kelps has been widely reported to be to be seasonally variable, including: *S. latissima* [62] and *L. digitata* [60,62,67]. A simultaneous maximum carbohydrate content and minimum ash content was observed for *L. digitata* in July (summer), whilst the inverse trend was observed in March (winter) [60]. The composition of *F. serratus* has also been shown to vary seasonally [68,69]. The protein contents can be as high as 10%, 8% and 15% for *S. latissima* and *L. digitata* and *F. serratus*, respectively. Not only is this lower than WH (Table 1.2) or GR (Table 1.3), but it is also lower than red or green macroalgae (25-40%) [56]; suggesting these would be more suitable feedstocks for protein extraction.

Table 1.4. Typical biochemical composition of *S. latissima*.

Parameter	Composition	References
Moisture[1]	68-89	[62,70]
Ash[2]	11-41	[62,70,71]
Carbon[2]	21-37	[62,70–72]
Alginate[2]	16-31	[62]
Mannitol[2]	5-25	[62,70]
Laminarin[2]	1-15	[62]
Fucoidan[2]	2	[69]
Cellulose[2]	10-14	[62]
Protein[2]	1-10	[62,70]

Data from [62] was manually extrapolated. [1]as received. [2]dry basis.

Table 1.5. Typical biochemical composition of *L. digitata*.

Parameter	Composition	References
Moisture[1]	73-88	[62,70]
Ash[2]	19-43	[61,62,71]
Carbon[2]	26-38	[61,62,70,71]
Alginate[2]	23-31	[62]
Mannitol[2]	9-28	[62,70]
Laminarin[2]	2-18	[62]
Fucoidan[2]	2-4	[69]
Cellulose[2]	11-13	[62]
Protein[2]	2-8	[62,70]

Data from [62] was manually extrapolated. [1]as received. [2]dry basis.

Table 1.6. Typical biochemical composition of *F. serratus*.

Parameter	Composition	References
Moisture[1]	67-81	[68]
Ash[2]	20-31	[68,71]
Carbon[2]	37-44	[69,71]
Alginate[2]	9-23	[68,69]
Mannitol[2]	6-17	[68,69]
Laminarin[2]	2-45	[68]
Fucoidan[2]	4-8	[63]
Cellulose[2]	2-4	[73]
Protein[2]	6-15	[68]

[1]as received. [2]dry basis.

1.2 Identification of Research Problem

Alternative biomass sources such as WH, GR and macroalgal biomass provide enormous potential for the generation of sustainable bioenergy. These types of biomass represent abundant feedstocks which do not compete for valuable arable land with food or feed crops; an essential factor to the future development of generating sustainable biomass-derived energy. However, the inherent properties of these alternative feedstocks can be problematic during conventional conversion methods. The following section outlines the various issues involved in the conversion of these biomass-types. Therefore, contextualising the aims and objectives of this thesis.

1.2.1 Moisture Content

The moisture content of biomass does not contribute any energetic potential during conversion processes. WH, GR and macroalgal biomass generally contain high moisture contents (Table 1.2-1.6). A higher water content reduces the bulk density of biomass, increasing the transportation costs of a supply chain. In addition, hydrophilic biomass is subject to rapid biological deterioration, affecting the storage duration and time-frame for effective utilisation [74]. Thermochemical conversion methods such as: combustion, pyrolysis and gasification require dry feedstocks during operation. Therefore, the high moisture contents of WH, GR and macroalgal biomass means they are unsuitable feedstocks for these thermal conversion methods. Wet biomass can be dried prior to thermochemical processing, however, this is energy intensive; reducing the economic efficiency of a process [75].

1.2.2 Energy Density

In combination with a high moisture content, WH, GR and macroalgal biomass exhibit low energy densities. The typical higher heating values (HHVs) of dried WH, GR and macroalgal biomass are between 13.8-14.7 MJ/kg [76–78], 15.3-17.4 MJ/kg [64,74,79] and 10.8-16.1 MJ/kg [66,80], respectively. The HHVs of the selected biomass are lower than coal, which has a HHV between 28.3-36.3 MJ/kg, depending on coal quality [81]. The reduced energy density of biomass is due to the increased oxygen content [82].

1.2.3 Inorganic Content

Ash represents the inorganic species found within biomass [82]. The composition of biomass ash is largely different to coal ash, generally containing higher concentrations of alkali metals (Na and K), Cl, Mn, P, Ca and Mg, with lower concentrations of Al, Fe, S, Si and Ti [83]. A high concentration of biomass ash poses a number of problems, including: (i) reduced energy density (ii) increased costs of ash disposal (iii) unfavourable ash chemistry during thermal conversion.

The ash content itself does not contribute towards the energetic content of a fuel. As a result, an increase in the proportional ash fraction reduces the energy density of a biomass, due to a dilution effect of the carbon fraction. Furthermore, a higher ash content results in a greater

accumulation of bottom ash; increasing removal costs and the amount of industrial waste produced. High concentrations of alkali metals (Na and K) and Cl present within biomass can lead to problematic ash behaviour during large-scale combustion, including: slagging, fouling and corrosion issues.

Slagging occurs when ash deposits melt onto surfaces exposed to radiant heat [49]. Ashes which display a lower melting temperature fuse into a hard glassy slag, called a clinker [49]. Due to their fused nature, clinkers can be difficult to remove from the furnace surface and often require an operational shut-down to allow for cleaning; leading to unwanted economic costs [84]. Alkali metals generally reduce the melting temperature of ash, as these are easily volatilised [82] and act as a flux for alumina-silica ash [80]. Whereas, earth metals, such as Ca and Mg generally increase the ash melting temperature [64].

Fouling is a process where volatilised Na, K and Cl form alkali chlorides which deposit onto cool surfaces, such as heat exchangers [80]. Fouling can hinder heat exchange and potentially cause structural damage to the furnace, due to an uneven distribution of heat flow [82]. Again, these deposits are removed at an unwanted cost, but can also lead to corrosion issues which are catalysed by the presence of Cl [80]. Therefore, biomass with a high alkali metal and Cl content are not suitable for combustion, due to problematic ash behaviour.

WH, GR and macroalgal biomass all contain significant levels of alkali metals, as shown in Table 1.7. Macroalgae contain the highest concentrations of Na and K, but also a significant amount of Cl. Thermal conversion of macroalgal biomass is not recommended, due to problematic ash chemistry [65] leading to a high slagging and fouling potential [80]. Similar problems have been identified from the combustion of both WH [85] and GR [45].

Table 1.7. Typical alkali metal and chlorine contents of water hyacinth, grass and macroalgae.

Biomass	**Inorganic Element (wt% *db*)**			**References**
	Na	**K**	**Cl**	
Water Hyacinth	0.7-1.6	0.7-1.7	*	[38]
Grass	0.0-0.3	0.2-1.1	*	[64,74]
Macroalgae	2.1-5.9	0.7-4.4	2.1-5.3	[64–66]

*not reported. *db*=dry basis.

1.3 Research Gap

Alternative feedstocks such as WH, GR and macroalgal biomass could provide an abundant source of sustainable biomass for the generation of bioenergy. The inherent properties of these feedstocks means thermochemical processing is not an appropriate conversion method, due to: high moisture contents, low bulk densities and high ash contents. As a result, wet conversion processes are more suitable for these types of feedstocks. Anaerobic digestion (AD) is a biological conversion route which converts organic matter into a gaseous fuel named biogas. AD is a versatile technology, with the capability of processing feedstocks with a high moisture content [17]. However, the physical and biochemical properties of lignocellulosic and macroalgal biomass can limit the efficiency of biodegradation during biological conversion processes.

Hydrothermal carbonisation (HTC) is a wet thermochemical conversion process which utilises the solvent-like properties of hot, compressed subcritical water to convert biomass into an energy densified solid named hydrochar. HTC is an effective technology for the conversion of high moisture feedstocks, as reactions are conducted in an aqueous medium, negating the requirement for energy intensive pre-drying of biomass. During HTC, organic and inorganic species from the biomass are solubilised into the aqueous fraction; generating a by-product named process water. Hydrochar is typically utilised as a solid combustion fuel, with the process water traditionally considered a waste product.

Both AD and HTC provide suitable conversion routes for high moisture feedstocks which are otherwise problematic to process during typical thermochemical conversion routes: combustion, pyrolysis and gasification. However, recent interests have shifted towards the integration of HTC and AD [86] to maximise the energetic recovery of biomass by minimising waste streams, as part of a circular economy concept. A number of different HTC-AD integration strategies have been proposed, with little clarity of which strategy provides the greatest improvement in the energy conversion efficiency (ECE) of biomass. An additional complication is that the yields and composition of HTC products (hydrochars and process waters) vary according to both reaction severity (temperature and retention time) and feedstock composition. At present, no current studies exist which compare the effectiveness of different HTC-AD integration strategies for lignocellulosic or macroalgal biomass. Therefore, a research gap exists to determine the optimal processing conditions and HTC-AD integration strategies for improving the ECE of lignocellulosic or macroalgal biomass. Optimising the ECE of such feedstocks would allow for their successful integration into the future sustainable bioeconomy. These research gaps were considered in the development of the aims and objectives of this thesis and are described in Section 1.4.

1.4 Aims and Objectives

The overall aim of this thesis was to investigate the potential of integrating hydrothermal and biological conversion technologies to improve the energy conversion efficiency of alternative, high ash feedstocks, compared to biological processing alone. The effectiveness of different integration strategies were assessed over a range of hydrothermal treatment reaction severities, with differences between feedstocks highlighted. Determination of optimised treatment conditions and integration strategies allows for future recommendations of suitable valorisation routes, to incorporate high ash biomass feedstocks into the future sustainable bioeconomy. The feedstocks investigated as part of this study were: water hyacinth, grass and three macroalgal species: *S. latissima*, *F. serratus* and *L. digitata*.

The thesis aim was accomplished by achieving the following objectives:

(i) Assessment of the suitability of high ash feedstocks for conventional conversion routes.

- Feedstocks were characterised in terms of their proximate, ultimate and inorganic compositions.
- This allowed for an assessment of the behaviour of feedstocks during thermochemical conversion routes, such as: energy density and ash behaviour.
- The biomethane potential of each feedstock was determined to assess the biodegradability efficiencies and provide benchmark energy conversion efficiency values for comparison in later chapters.

(ii) Understand the effect of reaction severity on the yields and properties of HTC products.

- HTC reactions were conducted across a range of temperatures (150°C, 200°C and 250°C) at a fixed retention time of 60-min. The yields of HTC products were determined before separation and characterisation.
- The results of this section facilitates an understanding of how HTC reaction severity and feedstock differences affect the yields and composition of hydrochars and process waters.

(iii) Assess the potential applications of hydrochars and process waters as separate energy vectors.

- Following HTC reactions, the hydrochars and process waters were separated and their effectiveness as separate energy vectors assessed.
- Hydrochars were analysed for their potential as a combustion fuel, through determining their behaviour during combustion: energy density and ash behaviour.
- The behaviour of hydrochars as an AD feedstock was determined.
- The comparative generation of biomethane and biohydrogen from process waters was assessed to determine the optimal valorisation route.

(iv) Understand the effect of hydrothermal pre-treatment severity on the behaviour of high ash feedstocks during biological conversion.

- HTC reactions were conducted at 150°C, 200°C and 250°C and the biomethane potential of residual slurries (hydrochars and process waters) determined.
- Steam explosion (SE) reactions were conducted at 150°C and 200°C and the biomethane potential of residual slurries (hydrochars and process waters) determined.
- The comparative influence of HTC (150°C) and SE (150°C) pre-treatments on the energy conversion efficiency of water hyacinth during two-stage AD was assessed.

(v) Compare the effectiveness of different hydrothermal and biological integration strategies to improve the energy conversion efficiency of high ash feedstocks.

- The energy balance and energy conversion efficiencies of each hydrothermal and biological integration strategy were calculated to determine the optimal strategy and conditions recommended for each feedstock.

(vi) Assess the potential for using seawater as a HTC reactant medium for macroalgal biomass.

- The comparative influence of seawater and distilled water as a HTC reactant medium for macroalgal biomass was assessed.
- HTC products were characterised across a range of HTC temperatures (150°C, 200°C and 250°C).
- The resultant impact of using seawater on the integration of HTC-AD was also determined.

1.5 Organisation of Chapters

This thesis is comprised of 9 chapters, organised as follows:

Chapter 1 provided an introduction to the research problem, to contextualise and outline the significance of the work conducted as part of this thesis.

Chapter 2 provides an overview of the previous research conducted on the AD and HTC of WH, GR and macroalgal biomass. In addition, the current work conducted on the integration of HTC and AD was reviewed and discussed to highlight key challenges and knowledge gaps, which require further investigation.

Chapter 3 outlines the experimental protocols and methodologies used throughout the course of this thesis. This includes a description of biomass collection and characterisation, hydrothermal and biological conversion, product stream characterisation and calculation of the energy balance of the integrated processes.

Chapter 4 involves the characterisation of the selected high-ash feedstocks. This includes detailed analysis of the proximate, ultimate and inorganic compositions of each biomass. As part of this, the methodological limitations of working with high-ash feedstocks are discussed, alongside the implications of determining feedstock composition and conversion pathways. The biomethane potential was also determined, to obtain a benchmark energy conversion efficiency value, used to compare against integration strategies in later chapters.

Chapter 5 evaluates the product yields and characteristics obtained across a range of HTC processing temperatures. The characteristics of hydrochars are compared to the characteristics of the untreated biomass, described in **Chapter 4**. Process waters are characterised to assess their suitability for downstream biological conversion processes, such as AD.

Chapter 6 investigates the generation of different energy vectors from the separated hydrochars and process waters, with the aim of maximising the energy conversion efficiency of the selected feedstocks. The comparative energy output from the combustion or AD of hydrochars was determined. Improvements in the ash behaviour of hydrochars during combustion are also assessed. In parallel, the comparative energy output from the generation of biomethane or biohydrogen from the process waters was analysed. The overall energy balance of each integration option was determined, in order to find the most energetically-feasible integration strategy for the separated HTC products.

Chapter 7 evaluated the effectiveness of hydrothermal pre-treatment to enhance the energy conversion efficiency of high ash feedstocks, across a range of reaction severities. Initially, the biomethane potential of the HTC slurries were determined and the energy balances

directly compared those obtained in **Chapter 6**; allowing for recommendations of optimal integration strategy and conditions. Thereafter, the potential of steam explosion (SE) was assessed over a range of reaction severities. Finally, the comparative enhancement of HTC and SE to enhance the energy conversion efficiency of WH during two-stage digestion was assessed.

Chapter 8 investigated the comparative use of seawater and distilled water as a reactant medium for the HTC of macroalgal biomass, with an assessment of how this affects the product characteristics and energy balance obtained from optimal HTC-AD integration strategy identified in **Chapter 7**.

Chapter 9 outlines the key conclusions obtained throughout the work conducted in this thesis and provides suggestions for directions of future research.

Chapter 2
Literature Review

The aim of this chapter is to identify the key knowledge gaps which exist for the integration of hydrothermal and biological conversion processes, as a valorisation route for alternative, high-ash feedstocks. The identification of knowledge gaps contextualises the aims and objectives of this thesis; which aim to build on the current knowledge available in this ever-growing area of research. Initially, the concepts of biological and hydrothermal processing are introduced, with further discussion of the utilisation of these conversion methods for high-ash biomass feedstocks. Following this, the different hydrothermal-biological integration strategies are reviewed, whilst assessing their potential utilisation for the conversion of high-ash biomass.

2.1 Biological Conversion Processes

2.1.1 Anaerobic Digestion

Anaerobic digestion (AD) involves the biological conversion of organic matter into biogas through sequential microbial metabolic pathways, under oxygen-limited conditions. The process of AD is a naturally occurring phenomenon; existing across a range of anoxic environments, including: sediments, ruminant guts and waterlogged soils [17]. Traditionally, AD was applied as a method of processing sewage sludge to generate a more stable product and facilitate nutrient recovery [87]. However, advancements in the understanding of the AD process have seen the development of this technology into a viable method of generating renewable energy, through the production of gaseous fuels from biomass.

Biogas is mainly comprised of methane and carbon dioxide, with trace amounts of other gases, such as nitrogen, water vapour and hydrogen sulphide [88]. The typical composition of biogas is displayed in Table 2.1. The methane content of the biogas contributes towards its energetic value; whereas, CO_2 and other biogas components are not associated with any energetic value. Therefore, higher proportions of CO_2 lower the calorific value of the biogas.

Biogas is an adaptable fuel and can be used to generate renewable heat and electricity through direct combustion in a CHP engine. Alternatively, biogas can be upgraded to biomethane by removing the CO_2 fraction and other pollutants, or by CO_2 biomethanisation; improving the calorific value of the gas. Biomethane has the potential to be used as a transport fuel, or directly injected into the national gas grid; as observed across EU countries [89]. The residual

slurry generated after biogas production is a nutrient-rich effluent called digestate, which can be used as a natural fertiliser [89].

Table 2.1. Typical composition of biogas, adapted from [90]**.**

Gaseous Component	Chemical Formula	Content of Biogas
Methane	CH_4	45-75%
Carbon Dioxide	CO_2	15-60%
Hydrogen	H_2	Trace
Nitrogen	N_2	0-5%
Water Vapour	H_2O	1-5%
Hydrogen Sulphide	H_2S	0-5000ppm
Ammonia	NH_3	0-500ppm

2.1.1.1 Biochemistry

Biogas is generated from organic matter through a sequential four-stage metabolic pathway, which is carried out by a diverse consortium of bacteria and *Archaea* [91]. Each metabolic stage of AD is carried out by a different consortium of microorganisms, creating a syntrophic relationship between the different microbial populations [89]. The four stages of AD: hydrolysis, acidogenesis, acetogenesis and methanogenesis are outlined in Figure 2.1.

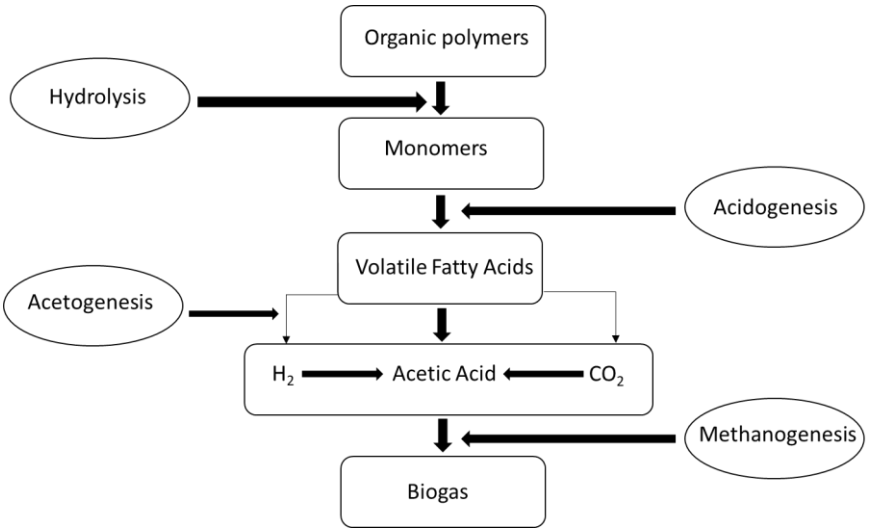

Figure 2.1. Outline of the four metabolic stages of anaerobic digestion, adapted from [90]**.**

Hydrolysis is the first metabolic stage of AD; which involves the anaerobic degradation of complex organic polymers: carbohydrates, lipids and proteins, into the corresponding monomeric or oligomeric constituents: sugars, fatty acids and amino acids, respectively. Hydrolysis involves the release of extracellular enzymes, such as: cellulases, lipases and proteases, by hydrolytic bacteria to catalyse the hydrolysis of polymers [90]. Equation 2.1 outlines the hydrolysis reaction, converting organic matter into solubilised monomers, in this case, glucose [92]. Hydrolysis is often described as the rate limiting stage of AD [92], this is particularly observed for feedstocks with a recalcitrant structure, such as lignocellulosic biomass [25].

Equation 2.1. Hydrolysis of organic matter.

$$n\mathrm{C_6H_{10}O_5} + n\mathrm{H_2O} \rightarrow n\mathrm{C_6H_{12}O_6}$$

The residual products from hydrolysis undergo further fermentation, named acidogenesis; a metabolic pathway of acidogenic bacteria. Acidogenesis produces acetate, hydrogen or intermediate products, such as: propionate and butyrate [93]. The metabolic formation of acetate, propionate and butyrate from glucose are outlined in Equation 2.2, Equation 2.3 and Equation 2.4, respectively [94]. Acetate formation from glucose is the favoured metabolic pathway for microorganisms, as this provides the greatest energy yield for subsequent growth. The formation of propionate and butyrate tends to occur as a metabolic response to hydrogen accumulation, such as that experienced during a high solid loading rate of an AD reactor [94].

Equation 2.2. Acetate formation from glucose during acidogenesis.

$$\mathrm{C_6H_{12}O_6} + 2\mathrm{H_2O} \rightarrow 2\mathrm{CH_3COOH} + 2\mathrm{CO_2} + 4\mathrm{H_2}$$

Equation 2.3. Propionate formation from glucose during acidogenesis.

$$\mathrm{C_6H_{12}O_6} + 2\mathrm{H_2} \rightarrow 2\mathrm{CH_3CH_2COOH} + 2\mathrm{H_2O}$$

Equation 2.4. Butyrate formation from glucose during acidogenesis.

$$\mathrm{C_6H_{12}O_6} \rightarrow \mathrm{CH_3CH_2CH_2COOH} + 2\mathrm{CO_2} + 2\mathrm{H_2}$$

Direct methanogenesis can occur through the utilisation of acetate or hydrogen and carbon dioxide. Products from acidogenesis which cannot be directly metabolised in methanogenesis are converted into methanogenic pre-cursors (acetate and hydrogen) during a process named acetogenesis [93]. This acetogenesis stage is conducted by acetogens. The metabolic pathways of propionate and butyrate conversion to acetate and hydrogen are outlined in Equation 2.5 and Equation 2.6, respectively [94].

Equation 2.5. Acetate formation from propionate during acetogenesis.

$$CH_3CH_2COOH + 2H_2O \rightarrow CH_3COOH + CO_2 + 3H_2$$

Equation 2.6. Acetate formation from butyrate during acetogenesis.

$$CH_3CH_2CH_2COOH + 2H_2O \rightarrow 2CH_3COOH + 2H_2$$

Methanogenesis is the final stage in the AD process, which is carried out by specialised *Archaea* named methanogens. Methanogenesis can occur through two different metabolic pathways: acetoclastic methanogenesis or hydrogenotrophic methanogenesis [91]. Acetoclastic methanogens directly metabolise acetate to produce methane, shown in Equation 2.7 [91]. Acetoclastic methanogenesis contributes approximately 70% of the total biomethane that is generated [90]. Alternatively, hydrogenotrophic methanogens exclusively utilise hydrogen and carbon dioxide to generate methane, as shown in Equation 2.8 [91].

Equation 2.7. Acetoclastic methanogenesis.

$$CH_3COOH \rightarrow CH_4 + CO_2$$

Equation 2.8. Hydrogenotrophic methanogenesis.

$$4H_2 + CO_2 \rightarrow CH_4 + 2H_2O$$

Anaerobic digesters can be broadly categorised as ‘wet’ (total solid content typically ≤16%) or ‘dry’ reactors (total solids content typically between 22-40%) [17]. Therefore, AD has the potential of digesting feedstocks with a high moisture content; this is particularly advantageous for the conversion of biomass. Digesters are normally maintained under mesophilic (35-42°C) or thermophilic (45-60°C) conditions [89], depending on the feedstock properties. AD can be conducted under psychrophilic temperatures (>20°C); however, this less common than mesophilic or thermophilic operation [17].

2.1.1.2 Anaerobic Digestion of Biomass

One of the main benefits of the AD process, is its capacity to utilise all of the macromolecular structures of the biomass: carbohydrates, lipids and proteins, during fermentation [58]. Therefore, resulting in a greater utilisation efficiency of biomass, compared to bioethanol production; which only utilises the carbohydrate fraction. Biogas can be generated from a diverse range of biomass feedstocks, including agricultural residues, sewage sludge, municipal solid wastes, industrial waste streams and algal biomass.

However, each biomass performs differently during AD, due to variations in biochemical composition. The theoretical biomethane yields obtained from typical carbohydrates, proteins and lipids are 415 mL CH_4/g VS, 496 mL CH_4/g VS and 1014 mL CH_4/g VS, respectively [95,96]. Although these maximum theoretical values are unlikely to be achieved, due to recalcitrant biochemical structures, or the presence of inhibitory compounds. The theoretical yields of biomethane (BMP_{th}) obtained from biomass can be calculated using predictive stoichiometric equations, such as the Buswell or Boyle's equations [97–99]. However, this does not differentiate between the biodegradable and non-biodegradable fractions of biomass and therefore, assumes complete stoichiometric conversion [100]. Experimentally-derived biomethane potential tests determine the maximum obtainable biomethane yields per mass of organic matter of a substrate (BMP_{ex}) [101], under idealised conditions. The subsequent biodegradability, or biodegradability index (BI), is calculated as BMP_{ex} as a fraction of the BMP_{th}; reflecting the methane conversion efficiency of a feedstock [40,100].

Table 2.2 shows the biomethane potential of a range of different biomass feedstocks. Variability in BMP_{th}, BMP_{ex} and BI exists both between and within the different biomass types; reflecting the large variations in biomass biochemical composition. Similar conclusions were obtained by Labatut *et al.* [102], who found the biodegradability for a variety of feedstocks ranged from 9-78%. The highest biomethane potential yields were obtained by substrates with a high lipid, or readily-digestible carbohydrate content. Whereas, substrates more recalcitrant structures, such as lignocellulosic biomass, resulted in a reduced BI.

Table 2.2. Analysis of biomethane potential across a range of feedstocks. Adapted from [103].

Biomass Type	BMP_{th} (mL CH_4/g VS)	BMP_{ex} (mL CH_4/g VS)	BI (%)	C:N
1st Generation Biomass Crops (*n*=16)	496 ± 118	370 ± 113	77 ± 25	44 ± 22
2st Generation Biomass Crops (*n*=15)	492 ± 49	356 ± 101	76 ± 16	30 ± 10
Agricultural Waste (*n*=11)	516 ± 82	199 ± 56	39 ± 11	18 ± 3
Food Processing Waste (*n*=15)	527 ± 127	387 ± 161	67 ± 18	16 ± 10
Municipal Wastes (*n*=13)	626 ± 158	434 ± 141	70 ± 18	18 ± 11
Macroalgae (*n*=12)	453 ± 86	231 ± 61	49 ± 17	17 ± 6

BMP_{th}=theoretical biomethane potential. BMP_{ex}=experimental biomethane potential. BI=biodegradability index. Data is presented as the average ± standard deviation.

Further to biochemical structure, maintaining an optimal carbon-to-nitrogen ratio (C:N) is important in sustaining a healthy microbial population and therefore, stable biogas production. The optimal C:N ratio is between 25-30:1 [17]. A lower C:N could result in a lack

of nutrients required for microbial growth, whereas, a higher C:N could result in the accumulation of ammonia, which is inhibitory to AD [104].

2.1.1.3 Pre-treatments

The biochemical structure of biomass can often limit biodegradability during AD. Lignocellulosic biomass can be particularly problematic during digestion, due to its recalcitrant structure. The interactions between holocellulose and lignin polymers limit hydrolysis; the rate limiting stage of AD, during lignocellulosic biomass digestion [25]. Pre-treatments are typically recommended for lignocellulosic biomass due to their inherent recalcitrant structural properties [41,105]. The overall aim of a pre-treatment is to disrupt the biochemical structure of biomass through the degradation of lignocellulose fibres, to facilitate enhanced hydrolysis during digestion [17]. A range of different pre-treatment methodologies exist which can be broadly categorised into mechanical, thermal, chemical and biological processing [41]. Physical pre-treatments involve milling, chopping or shredding biomass to reduce the particle size. Thermal pre-treatments use heat to break apart the lignocellulosic polymers; increasing the surface area for microbial interaction. Chemical pre-treatments use acidic or alkali solutions to solubilise the hemicellulose or lignin fractions. Whereas, biological pre-treatments use bacteria, fungi or enzymes to enhance the degradation of biomass [41]. The general advantages and disadvantages of each pre-treatment strategy are outlined in Table 2.3.

Table 2.3. Advantages and disadvantages of biomass pre-treatments, adapted from [41]**.**

Pre-treatment	Advantages	Disadvantages
Physical	Ease of biomass handling. Improved biomass rheology. Increased surface area.	High energy demand. High maintenance costs.
Thermal	High biomass solubilisation. Sanitation of biomass.	High energy demand. Inhibitory compound formation.
Chemical	Low energy input. Hemicellulose solubilisation.	Cost and recovery of chemicals. Inhibitory compound formation. Potential corrosion issues.
Biological	Low energy input. No inhibitory compound formation.	pH imbalances. Time consuming.

2.1.1.4 Generation of Biomethane from Water Hyacinth

The generation of biomethane from WH appears to be well explored throughout literature studies. However, the obtainable biomethane yields are highly varied, as displayed in Table 2.4. The biomethane yields generated from WH range from 57 mL CH_4/g VS to 252 mL CH_4/g VS. The reported biogas yields produced from WH also displayed a large range: from negligible production to 267 mL biogas/g VS. The majority of studies report either biogas or biomethane yields, resulting in incompatibilities between these value ranges.

Table 2.4. Biomethane potential of water hyacinth, reported across different studies.

Reactor Type	Operational Temperature (°C)	Biogas Potential (mL biogas/ g VS)	Biomethane Potential (mL CH_4/ g VS)	BI (%)	Reference
Batch	35	Negligible	-	-	[106]
ALBR-UASB	30	143	-	-	[107]
Batch	35	185	113[a]	-	[108]
Batch	38	267	140	61[b]	[109]
Batch	37	-	57[c]	12[d]	[110]
Batch	35	-	86	-	[111][e]
Batch	26-37	-	113	-	[112]
Batch	35	-	174	37	[113]
Batch	35-55	-	189-191	47	[114]
Batch	37	-	252	-	[115]

VS=volatile solid. BI=biodegradability index. ALBR=anaerobic leach bed reactor. UASB= Up-flow anaerobic sludge blanket. -=not reported. [a]based on 60.84% methane content of biogas. [b]calculated through VS removal. [c]calculated from methane yield obtained on a COD basis (L CH_4/kg COD). [d]determined by energy conversion efficiency (ECE). [e]study investigates WH stems only.

The variation in WH biomethane yields is likely to be related to a number of factors, including biomethane potential methodology, harvesting location, sample maturity and seasonal variation in biochemical composition [38]. Large variations are observed in the biochemical compositions of the WH samples presented in Table 2.4, including: cellulose (15-32%), hemicellulose (23-33%) and lignin (5-33%) [107,110–112,116]; likely to be related to both seasonal and spatial variation. The WH samples displayed in Table 2.4 were harvested across a range of countries: India [106–108,110], China [111], Egypt [112] and Australia [109] and

across a range of water bodies: ponds [108], lakes [106,107,109], rivers [111,112] or laboratory-grown conditions [114]. Each harvesting location would provide different growth conditions for the WH, resulting in variations in the biochemical composition of the biomass.

Differences in the morphological composition of WH could also lead to differences in the yields of biomethane produced. Shiralipour and Smith [117] report higher biomethane yields produced from WH shoots (0.26-0.43 m^3 CH_4/ kg VS), compared to WH roots (0.13-0.24 m^3 CH_4/ kg VS). Xia *et al*. [118] also identified variations in the digestion behaviour of different WH morphological components: WH roots generated a lower biomethane yield (21 L CH_4/ kg VS) compared to WH leaves (128 L CH_4/ kg VS) or WH stems (130 L CH_4/ kg VS). Therefore, the variability of biomethane generation from WH could be related to heterogeneous morphology of different WH plants. The digestion of WH plants with a higher proportion of root-mass could result in reduced biomethane production, compared to plants with a greater proportion of shoot-mass. However, the understanding of how WH morphological composition changes, both seasonally and spatially, is currently limited. Therefore, the significance of this hypothesis to explain the variation in WH biomethane yields observed in Table 2.4 is presently unknown.

The biodegradability of WH is not as commonly reported as the biomethane potential. However, Table 2.4 shows the reported BI of WH is between 12-61%. The limited conversion efficiency of WH during AD may be associated with the lignocellulosic structure of the plant. As a result, a number of pre-treatment technologies have been applied to improve the biodegradability of WH, including: alkali [106], drying [106,119], ionic liquid [111], microwave-heated alkali [120] and hydrothermal [112–115,121] pre-treatments. Improvements in biogas yields from WH have also been investigated through the utilisation of both co-digestion and thermophilic AD. The co-digestion of WH with sheep waste [108] and food waste [107] has been shown to produce higher biogas yields, compared to WH alone. Whereas, Ferrer *et al*. [114] found similar biomethane yields (189-191 mL CH_4/g VS) were obtained from both the thermophilic digestion (55°C) and mesophilic digestion (35°C) of WH.

2.1.1.5 Generation of Biomethane from Grass

GR is a well-established feedstock for AD, especially across European countries [39]. Similarly to WH, the biomethane potential of GR is largely varied across different studies, as displayed by Table 2.5. The biomethane yields generated from GR ranges from 122 mL CH_4/g to 403 mL CH_4/g VS. Again, this variation is likely due in part to differences in the biochemical composition of the different grass samples.

The biochemical composition of GR is known to vary across different species [39], which has a subsequent impact on obtainable biomethane yields [122]. The biochemical composition of grasses also varies according to the harvesting season [51] and GR maturity [41]. Figure 2.2 shows the proportion of recalcitrant lignocellulosic fibres increases as GR matures, whilst the presence of readily-digestible cell contents decreases. Generally, grasses can be harvested once or twice annually, with different harvesting periods associated with variations in biomethane yields. Chiumenti *et al.* [51] found the biomethane yields from spring-harvested GR (340 mL CH_4/g VS) was higher than summer harvested GR (308 mL CH_4/g VS); suggested to be due to a decreased lignin content. Early maturity GR contains more readily-digestible components, whereas, late maturity GR contains a higher proportion of recalcitrant cell wall constituents [41]. Although, the summer harvest was associated with a higher biomass yield production, per area of land. Therefore, the biomethane yield was higher for summer GR (1181 m^3/ha) than spring GR (263 m^3/ha) when normalised to a specific area of land.

Table 2.5. Biomethane potential of grass, reported across different studies.

Grass Sample	Reactor Type	Operational Temperature (°C)	Biomethane Potential (mL CH_4/ g VS)	BI (%)	Reference
Switchgrass	Batch	35	122	24	[102]
Roadside Grass	Batch	45	222	45	[46]
Meadow Grasses	Batch	35	51-406	32-73	[123]
Grass Silage	Batch	37	261	52	[124]
Sports Field Grass	Batch	37	292	-	[45]
Public Space Grass	Batch	37	327	44[c]	[47]
Ryegrass	Batch	37	400	90	[40]
Residential clippings	Batch	37	403	-	[125]
Riverbank Grass[a]	Batch	39	340	-	[51]
Riverbank Grass[b]	Batch	39	308	-	[51]
Ryegrass Silage	Batch	37-38	350-493	-	[52]
Ryegrass Silage	CSTR	37	363-451	-	[52]
Ryegrass Silage	SLBR-UASB	37	341	-	[52]

VS=volatile solid. BI=biodegradability index. SLBR=sequentially fed leach bed reactor. UASB=upflow anaerobic sludge blanket reactor. [a]spring harvest. [b]summer harvest. [c]calculated using the Boyle's equation. Spring harvest CSTR=continuously stirred tank reactor.

The variation in the biomethane potential of GR could be a result of both the variation in biochemical composition and differences between the experimental methodologies used to analyse the obtainable biomethane yields. The latter was highlighted by Nizami *et al*. [52], who showed the biomethane potential obtained from GR silage varied, whilst using three different sized reactors. The reactors were: 100 mL glass syringes (micro-BMP), serum bottles with 70 mL working volume (small-BMP) and larger bioreactors with a 1.5 L working volume (large-BMP). The biomethane yields obtained from micro-BMP, small-BMP and large-BMP were: 350 mL CH_4/g VS, 355-419 mL CH_4/g VS and 483-493 mL CH_4/g VS, respectively. In addition, the biomethane yields generated from GR silage were analysed using CSTR and SLBR-UASB reactors, again yielding different biomethane yields: 363-451 mL CH_4/g VS and 341 mL CH_4/g VS, respectively. Therefore, highlighting the variation in obtainable biomethane yields, according to the experimental set-up.

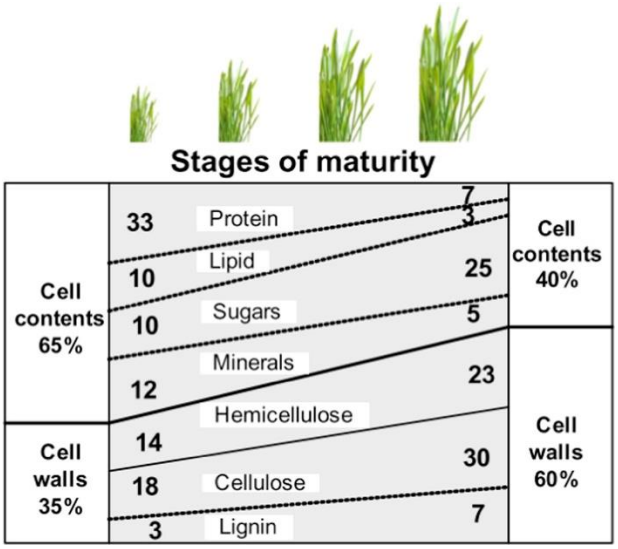

Figure 2.2. Changing biochemical composition of grass across different stages of maturity. Sourced from [41].

2.1.1.6 Generation of Biomethane from Brown Macroalgae

In recent years, macroalgal biomass have gained increasing popularity as a feedstock for AD, due to high carbohydrate and negligible lignin contents [126]. However, the biomethane yields generated from macroalgal biomass appears to display large interspecies and intraspecies variation.

Allen *et al*. [71] determined the biomethane potential of 10 different brown seaweeds, harvested from the Irish coastline. Large variations were observed in the BMP_{th} (249-540 mL CH_4/g VS), BMP_{ex} (101.7-341.7 mL CH_4/g VS) and BI (19-81%) across the seaweed species. This suggests the interspecies variation in biochemical composition affects the generation of

biomethane. *S. latissima* displayed the highest BMP_{ex} (341.7 mL CH_4/g VS) of all seaweed species, with a resulting BI of 81%. Whereas, *F. serratus* generated the lowest BMP_{ex} (101.7 mL CH_4/g VS) and BI (19%).

Similar conclusions were obtained by Vanegas and Bartlett [127], who found the biogas yields of *S. latissima* (244 mL biogas/g VS) and *L. digitata* (161 mL biogas/g VS) were higher than *F. serratus* (65 mL biogas/g VS). Despite this, Allen *et al*. [71] reported the BMP_{th} of fucoids: *F. serratus* and *F. spiralis* (532-540 mL CH_4/g VS) were higher than kelp species: *S. latissima* and *L. digitata* (422-479 mL CH_4/g VS): suggesting fucoids have a recalcitrant biochemical structure, which limits biodegradability during AD. *S. latissima* contains high levels of readily digestible sugars [71], resulting in higher biomethane yields. Whereas, *F. serratus* contains high concentrations of polyphenols [128], which have been shown to display an inhibitory effect during the digestion of fucoids [129]. Table 2.6 displays the typical biomethane potential values of *S. latissima*, *F. serratus* and *L. digitata* reported across literature studies. Again, kelp species: *S. latissima* and *L. digitata* generally produce higher biomethane yields and display a higher BI compared to the fucoid species *F. serratus*.

Table 2.6 also shows large intraspecies variations in the generated biomethane potential of brown macroalgae; likely due the seasonal variation in biochemical composition. Adams *et al*. [60] found the biomethane potential of *L. digitata*, harvested in the UK peaked in July (254 mL CH_4/g VS, BI=65%) and was lowest in March (196 mL CH_4/g VS, BI=55%). July-harvested *L. digitata* showed the highest carbohydrate content and lowest ash content, therefore, generated the highest biomethane yields. Whilst March-harvested *L. digitata* showed the inverse trend [60]. A similar study by Tabassum *et al*. [67] investigated the effect of seasonal variation on the biomethane yields obtained from *L. digitata* harvested in Ireland. A peak biomethane potential was observed in August (327 mL CH_4/g VS, BI=72%), whilst the lowest biomethane yield was observed in April (203 mL CH_4/g VS, BI=44%). Therefore, similar conclusions were obtained by Adams *et al*. [60] and Tabassum *et al*. [67]. *L. digitata* harvested in August had the lowest Ash:Volatiles ratio (0.2); suggesting the higher ash contents reduce the potential of biomethane generation [67].

The ash content of brown seaweeds (14-40% [71]) is typically higher than terrestrial biomass [65] due to the presence of alkali salts obtained from the surrounding marine environment. High concentrations of salts can become inhibitory to the AD process, due to increased osmotic stress on microorganisms [130]. Increased salinity and Ash:Volatiles ratio of seaweeds have been found to reduce gas production during AD [67]. Tabassum *et al*. [131] found washing *L. digitata* with hot water (40°C) can be an effective method of improving the obtainable biomethane yield, due to the removal of problematic salts. Washing *L. digitata* harvested in March reduced the ash content of the sample by 54%, resulting in a 31% increase

in biomethane yields, compared to unwashed samples. Although this effect was not as significant for September-harvested *L. digitata*, due to the initially lower ash content.

Table 2.6. Biomethane potential of brown macroalgae, reported across different studies.

Seaweed Species	Reactor Type	Operational Temperature (°C)	Biomethane Potential (mL CH_4/ g VS)	BI (%)	Reference
S. latissima	Batch	37	342	81	[71]
S. latissima	Batch	37	223	-	[132]
S. latissima	Batch	38	88-535	17-97	[133]
L. digitata	Batch	37	218	46	[71]
L. digitata	Batch	38	91-523	16-91	[133]
L. digitata[a]	Batch	39	187-195[b]	43	[134]
L. digitata	Batch	35	196-254	55-65	[60]
L. digitata	Continuous	37	221	-	[135]
L. digitata	Batch	37	245-280	52-62	[131]
F. serratus	Batch	37	102	19	[71]
F. serratus[a]	Batch	39	100**	17-22	[134]
F. serratus	Batch	38	63-416	13-78	[133]

VS=volatile solid. BI=biodegradability index. -=not reported [a]seaweed residues following biorefining. [b]data extrapolated manually from [134].

Similarly, to WH or GR, the BI of brown macroalgae varies across literature studies (Table 2.6). Of the 10 species of macroalgae analysed by Allen *et al.* [71], only 4 had a biodegradability >50%. Therefore, pre-treatment of macroalgal biomass is often recommended to improve biomethane yields [20], with hydrothermal pre-treatments identified as the most viable pre-treatment method for macroalgal biomass [126].

2.1.2 Dark Fermentation

Hydrogen has been described as a fuel of the future, due to its capability to decarbonise the energy sector; producing only water vapour as a combustion product [90]. Hydrogen also has the highest calorific value of any known fuel, on a mass basis; as shown in Table 2.7.

However, one of the major issues facing hydrogen generation is sustainable production. Currently, 96% of hydrogen is generated using fossil-fuel based conversion technologies [136] such as coal gasification or water electrolysis. Therefore, there is an ever-growing interest in the sustainable generation of hydrogen.

Table 2.7. Calorific values of various fuels, adapted from [136]**.**

Fuel	Calorific Value (J/kg)
Hydrogen	141.9
Methane	55.7
Natural Gas	50
Biodiesel	37
Ethanol	29.9

Dark fermentation (DF) involves the biological conversion of organic matter into biohydrogen, through the microbial fermentation of biomass. The metabolic pathways of biohydrogen production are similar to AD: hydrolysis, acidogenesis and acetogenesis. However, the methanogenesis stage is inhibited to facilitate biohydrogen accumulation [137]. Hydrogen is generated through the metabolic pathways of anaerobes from the *Clostridia* and *Enterobacter* genera [138]. Butyrate is produced through acidogenesis and acetate through acidogenesis and acetogenesis. Using one mole of glucose as a model compound, acetate generation produces 4 moles of hydrogen (Equation 2.2), whilst the generation of butyrate produces 2 moles of hydrogen (Equation 2.4). Alternatively, propionate generation creates a net yield deficiency of hydrogen of -2 moles (Equation 2.3). However, these are stoichiometric yields, which may not be achieved during experimental trials of dark fermentation. Yield inefficiencies can be associated with hydrogen consumption from propionate production, hydrogen consumption by homoacetogens [137] or glucose consumption for microbial growth [138].

2.1.3 Two-stage Digestion

Two-stage digestion involves the physical separation of AD across two different reactors. Hydrolysis, acidogenesis and acetogenesis occur in the first reactor, then the effluent is transferred to a secondary reactor, where the accumulated volatile fatty acids (VFAs) are converted to methane via methanogenesis. The separation of the AD stages allows optimisation of the different microbial conditions required for acidogenesis and methanogenesis to occur, leading to an overall increase in biogas yields [139]. For example,

the optimal pH range for biohydrogen generation is between 5.2-6.5 [140]. Whereas, the optimal pH range for methanogenesis is between 6.8-7.2 [17]; with inhibition of methanogens observed at pH 6.6 [22]. Therefore, the first reactor tank effectively acts as a buffer to prevent the inhibition of methanogens, as VFAs accumulate during acidogenesis and acetogenesis [141].

A two-stage digestion system allows for the co-production of biohydrogen and biomethane, during the first and second stages, respectively [140]. Numerous studies exist which show a higher energy recovery from two-stage digestion, compared to a one-stage system [142–145]. The higher energy recovery from two-stage digestions is generally associated with the formation of hydrogen and improved biomethane yields; due to the efficient conversion of accumulated VFAs during methanogenesis. Eluents from DF also contain dissolved hydrogen, which can stimulate the growth of hydrogenotrophic methanogens, further increasing methane yields [140]. However, a two-stage system adds an extra degree of complexity to scaling-up the technology. Therefore, the energy return must be significant to justify development of the technology.

The comparative effectiveness one-stage and two-stage digestion has been assessed for WH [110,120], GR [124,143] and *L. digitata* [135]. Varanasi *et al.* [110] reported a two-stage digestion of WH reflected a higher energy conversion efficiency (ECE) (19.04%), compared to one-stage DF (5.07%) or AD (11.94%), due to an increased COD removal. Conversely, Lin *et al.* [120] found a reduced ECE during two-stage digestion (40.0%) of sequentially microwave-heated alkali and enzymatically pre-treated WH, compared to one-stage digestion (49.5%). This was linked to higher biomethane yields obtained during one-stage digestion; highlighting how different behaviours can be observed across different WH samples and pre-treatments.

Massanet-Nicolau *et al.* [143] found two-stage digestion of grass pellets resulted in a 13.4% higher energy yield compared to one-stage digestion, using continuous digestion systems. The higher energy yield was associated with both the hydrogen formation and a 12.7% increase in biomethane yields after a 20-day retention time. Following a 12-day retention time, the energy yield from two-stage digestion was comparable to that obtained from one-stage digestion after 20-days. Therefore, process efficiency could be maintained, whilst reducing the hydraulic retention time. Similarly, Deng *et al.* [124] found an improvement in the ECE obtained from grass silage during two-stage digestion (83.5%), compared to one-stage digestion (54.7%); due to the metabolism of the accumulated VFAs. Interestingly, acid pre-treatment resulted in a reduction in the ECE of the grass silage, compared to not using pre-treatment.

2.2 Hydrothermal Carbonisation

2.2.1 Overview

Hydrothermal carbonisation (HTC) is a thermochemical conversion process, which involves the processing of biomass in hot compressed water [146]. HTC is thought to simulate the natural coalification process [147,148]; through the production of an energy-densified, 'coal-like' material from biomass. HTC is conducted under elevated temperatures (180°C-280°C) and autogenous pressures [146,149,150]; shifting the properties of the water into a subcritical condition [150]; maintaining water in a liquid state. Under these conditions, water adopts 'solvent-like' properties, forming reactive hydronium (H_3O^+) and hydroxide (OH^-) ions [151]; due to the weakening of hydrogen-bonds.

Subcritical water acts as a suitable medium to facilitate a number of complex reactions, which would normally require catalysis through acidic or alkali conditions [150]. Biomass conversion using subcritical water provides a non-toxic, cheaper alternative to chemical reagents [152]. HTC is also referred to as a wet torrefaction process [146]. One of the main advantages of HTC is it allows direct conversion of biomass with high moisture contents; negating the requirement for energy-intensive drying processes involved with alternative thermal conversion routes, such as pyrolysis or torrefaction [75,153]. Therefore, HTC appears to be a suitable technology for the conversion of biomass with undesirable fuel properties: low HHV, high ash content, high moisture content, and heterogeneity [148]. Furthermore, HTC also occurs at lower temperatures compared to pyrolysis; allowing for energy savings [154].

The major product of HTC is a carbon-rich solid product from biomass. Although, a process water fraction is also formed through the solubilisation of organic and inorganic matter from the biomass. A further increase in processing severity to temperatures between 300-350°C (approximately 50-200 bar pressure) results in the formation of a liquid product, named bio-oil [15]. This process is called hydrothermal liquefaction (HTL). An even further increase in the hydrothermal processing conditions leads to the formation of a gas, rich in H_2 or CH_4 [15]. This process is called hydrothermal gasification (HTG), which occurs at conditions beyond the critical point of water (374°C, 221 bar); shown in Figure 2.3. However, the focus of this thesis is to investigate the application of HTC for the conversion of biomass; associated with a lower energy demand, compared to HTL or HTG.

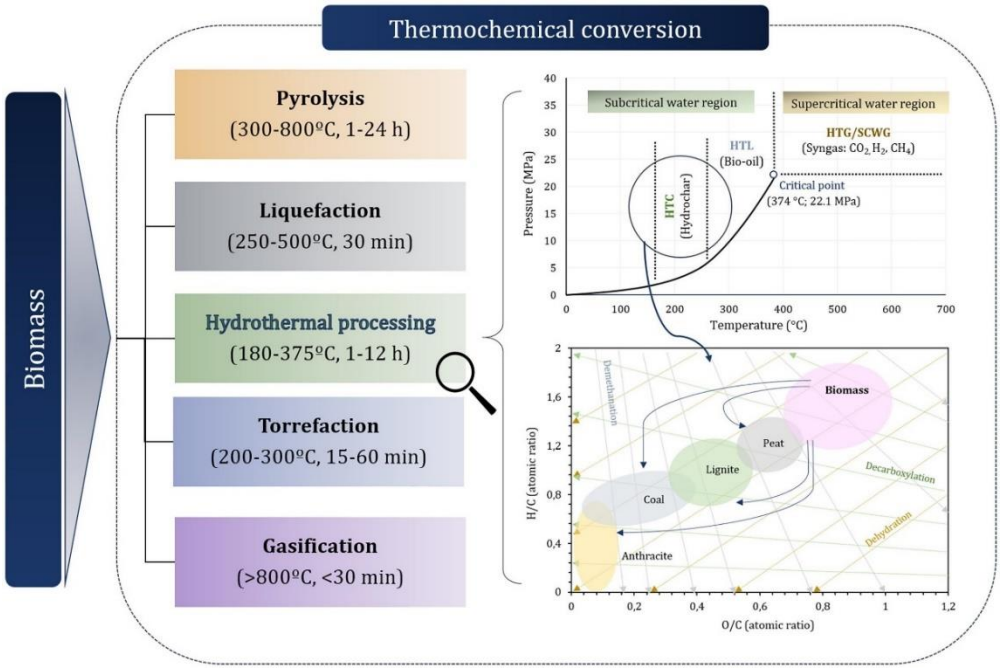

Figure 2.3. Thermochemical conversion routes of biomass, with an emphasis on hydrothermal carbonisation. Sourced from [155].

2.2.2 HTC Reaction Chemistry

The reaction chemistry associated with HTC is complex, with an outline of the reaction pathways shown in Figure 2.4. HTC reaction mechanisms have mainly been described for the carbohydrate fraction of lignocellulosic biomass; in particular cellulose [146,148,150,151]. A number of reaction mechanisms have been identified, including: hydrolysis, dehydration, decarboxylation, condensation, polymerisation and aromatisation [148]. These reaction mechanisms do not occur sequentially, as observed with AD, but simultaneously throughout HTC; adding to the complexity of the process [148,154].

Hydrolysis involves the cleavage of ester or ether bonds (mainly β-(1-4)) to generate a range of solubilised oligosaccharides from the carbohydrate fraction and phenols from the lignin fraction [146,148,150], which are solubilised into the aqueous phase. Hydrolysis of hemicellulose starts at around 180°C and cellulose around 230°C [146]. The lignin fraction of lignocellulosic biomass is more stable than cellulose or hemicellulose; degrading at approximately 250°C [149]. Therefore, the subsequent reaction mechanisms apply to the solubilised oligosaccharides.

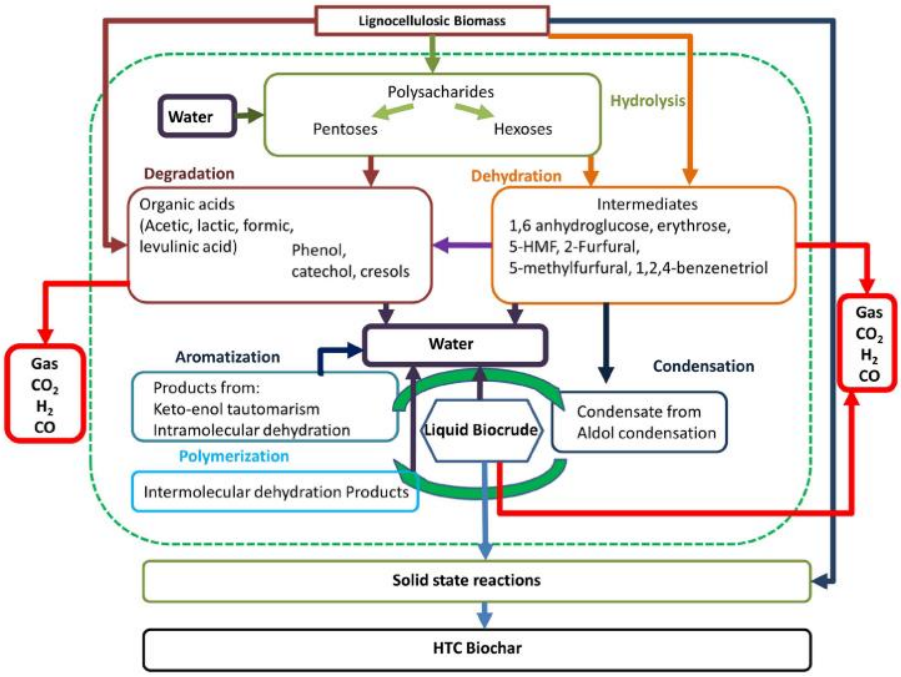

Figure 2.4. Overview of the reaction pathways of HTC. Sourced from [146]

Following hydrolysis, dehydration and decarboxylation reactions occur; with dehydration reactions removing hydroxyl groups (-OH) and decarboxylation reactions removing carboxyl (-COOH) and carbonyl groups (C=O) [64]; generating CO and CO_2 [149]. The combination of these reactions leads to a reduction in both the H:C and O:C ratios of the solid residue. Thereby creating an energy densification-effect through a simultaneous reduction in the O-content and a concentration of the C-fraction [64]. The dehydration of pentoses and hexoses leads to the formation of furfural and 5-hydroxymethylfurfural (5-HMF), respectively [149]. Further degradatory intermediates are also present within the process water phase, including: organic acids and aldehydes [146,156–158]. Elimination of carboxyl and hydroxyl groups leads to the formation of unsaturated compounds; which polymerise through simultaneous condensation, polymerisation and aromatisation reactions [146,148]. Hydrochar is formed by nucleation, either through solid-solid, liquid-solid, or liquid-liquid interactions [159].

HTC reactions result in the formation of a solid (hydrochar), aqueous phase (process water) and gaseous phase. Although, the gaseous phase only accounts for a small fraction of the overall mass balance. Currently, reaction mechanisms involved in the HTC of macroalgal biomass are not fully understood [80]; however, it is likely the reaction pathways are similar to the HTC of lignocellulosic-derived carbohydrates.

2.2.3 Hydrochar Properties and Applications

The primary product obtained from HTC is an energy-densified, carbon-rich solid residue, named 'hydrochar'. The generated hydrochars possess more 'coal-like' properties, compared to the original biomass, including: a higher energy content, improved grindability and increased hydrophobicity [15]. Therefore, hydrochars display enhanced properties for the application as solid combustion fuel [159], compared to the original biomass.

2.2.3.1 Energy Densification

HTC facilitates the energy densification of low bulk density biomass into a solid material, with enhanced properties as a combustion fuel. The HHV of hydrochars are generally higher than the original biomass. For example, Smith *et al*. [64] reported the HHVs of lignocellulosic biomass were between 15.4-16.4 MJ/kg, whereas, the resultant hydrochars displayed an increase in HHV, to between 19.3-25.0 MJ/kg and 27.8-32.1 MJ/kg, following HTC processing temperatures of 200°C and 250°C, respectively. This trend is also observed for macroalgal biomass; with Smith and Ross [80] reporting the HHV for a range of kelps was between 12.2-16.1 MJ/kg. Whereas, HTC treatment resulted in an increase in energy density to between 21.0-24.7 MJ/kg and 22.9-27.5 MJ/kg, at temperatures of 200°C and 250°C. The HHV of hydrochars are comparable to those of a low-ranking coal [80], especially when generated under the more severe reaction conditions. HTC has been shown to improve the HHV for a wide range of different biomass feedstocks, including lignocellulosic biomass [64,74,158], macroalgal biomass [66,80], microalgal biomass [160], cow manure [84] and spent coffee grounds [161].

The properties of hydrochars vary according to different HTC reaction conditions. The major variables during HTC reactions are: temperature, retention time and biomass composition. It is generally accepted that temperature is the most influential factor which governs the rate of HTC reactions [148,158,162–164]. Higher HTC temperatures typically generate hydrochars with increased HHV values. However, this is normally compromised by a reduced hydrochar yield [64,80]. The higher HHV displayed by higher-temperature hydrochars has been linked to increased dehydration and decarboxylation reactions, which reduce the oxygen content of the residual solid [64,80,160,163]. This concept is outlined by a Van Krevelen diagram, such as those shown in Figure 2.3 and Figure 2.5. Van Krevelen plots compare the atomic O:C to the atomic H:C, which highlights compositional changes of biomass during the HTC process. Figure 2.5 shows a Van Krevelen diagram obtained from the characteristics of miscanthus-

derived hydrochars generated at 200°C and 250°C, with a 1-hr retention time [49]. The hydrochars generated at 250°C had a much more 'coal-like' structure, compared to 200°C hydrochars, due to increased prevalence of dehydration and decarboxylation reactions.

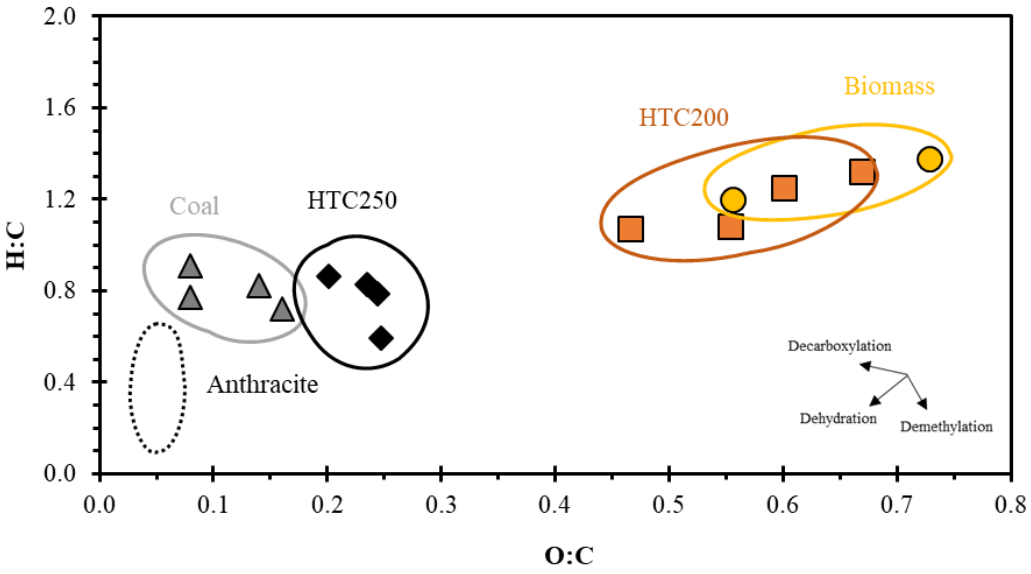

Figure 2.5. Van Krevelen diagram of miscanthus and miscanthus-derived hydrochars produced at 200°C and 250°C using data produced by [49]. Coal values adapted from [165], anthracite zone adapted from [160]. ●=Miscanthus Biomass. ■=HTC200. ♦=HTC250. ▲=Coal.

Additionally, in the case of lignocellulosic biomass, the degradation temperatures of hemicellulose (180°C), cellulose (220°C) and lignin (265°C) vary [76]. Therefore under progressively higher HTC temperatures, such as 250°C, hemicellulose and cellulose will be liberated, whilst lignin will not. The calorific value of lignin (23.3-26.6 MJ/kg) is higher than cellulose or hemicellulose (17-18 MJ/kg). Therefore, the selective removal of the less energy dense holocellulose polysaccharides at higher HTC temperatures will subsequently increase the energy density of the residual hydrochar. However, this also results in a reduction in hydrochar yield.

Increasing HTC reaction temperature is also associated with a simultaneous reduction in the volatile matter (VM) content and an increase in the fixed carbon (FC) content [64]. This is important in the application of hydrochar as a solid combustion fuel; as a higher FC:VM ratio creates a more stable flame during combustion, resulting in increased firing temperatures [160]. Despite the major influential effects of temperature on HTC reactions, the retention time can also influence hydrochar properties. HTC retention times range from several minutes to a few days [162]. A greater retention time is associated with an increase in reaction severity

[148]. Smith and Ross [164] reported increased retention time resulted in a greater number of dehydration reactions during the HTC of miscanthus, although temperature had a greater influence.

2.2.3.2 Hydrochar Demineralisation

Another significant advantage for the application of HTC to generate a solid combustion fuel from biomass, is the associated improvements in ash chemistry. As previously mentioned, the ash composition of biomass is typically problematic during large-scale combustion processes; resulting in issues such as: slagging, fouling and corrosion. HTC has the potential to overcome these issues by facilitating selective demineralisation of problematic elements [64,66,74,80]. Typically, HTC selectively removes alkali metals [64,80] and chlorine [66] from biomass, whilst other inorganic elements, such as Mg and Ca undergo more limited removal [64]. The removal efficiency of these problematic elements also appears to increase at higher HTC processing temperatures. Smith *et al*. [64] found the removal efficiencies of alkali metals in lignocellulosic biomass are higher under processing conditions of 250°C (Na=64-79%, K=84-88%), compared to 200°C (Na=46-74%, K=69-84%). Whereas, more limited removal of Mg and Ca were determined across a range of feedstocks [64]. Generally, Ca and Mg result in higher ash melting temperatures, whereas Na and K decrease the melting temperature of ash; meaning it is more likely to stick or melt onto furnace surfaces [64]. HTC also allows for significant removal of Cl [66,80], reducing potential corrosion issues. Smith and Ross [80] found a Cl removal efficiency between 93-99%, during the HTC of a range of macroalgal species. Inorganic species are removed from the solid phase and solubilised into the process water, during HTC.

Reza *et al*. [74] were the first to report that the changes in ash chemistry, associated with HTC, means hydrochars have the potential to display reduced slagging and fouling propensities compared to parent biomass [74]. This was determined by calculating a range of slagging and fouling indices, based on the biomass inorganic composition. These indices include: slagging index, fouling index, alkali index and slag viscosity index.

However, caution must be taken when applying predictive slagging and fouling indices to biomass, as these were originally developed for the analysis of coal ash samples [74], with alumina-silicate compositions [64]. Therefore, applications of the predictive indices assumes the biomass ash matrix undergoes similar behaviours to coal ash during combustion. As a result, a number of studies [49,64,80] have conducted ash fusion tests on hydrochars, alongside using predictive indices, to obtain a greater understanding of the slagging behaviour of hydrochar-derived ashes.

The ash fusion test identifies the temperatures at which ash undergoes transitional characteristic changes: shrinkage, deformation, hemisphere and flow. These transitions are associated with the different problematic stages of ash behaviour; for example during 'deformation' the ash becomes sticky and during 'flow' the ash melts [64]. The ash fusion test assesses the tendency of ashes to form fused deposits on heated surfaces; indicating its slagging potential. Samples which undergo the transitional changes at lower temperatures are associated with a higher slagging potential. Hydrochars derived from lignocellulosic [49,64] and macroalgal biomass [80] have been shown to have reduced slagging tendency, compared to the parent biomass, using ash fusion tests. Higher HTC processing temperatures generally produce hydrochars with reduced slagging potential; due to increased removal of problematic inorganics [64]. This displays the potential effectiveness of HTC for upgrading biomass with poor combustion properties into an energy densified solid fuel, with improved ash chemistry, during combustion.

2.2.3.3 Hydrochar Applications

Hydrochars are mainly utilised as a vector for energy generation through thermal conversion technologies, such as combustion [146]. Although, applications of hydrochars are not limited to energy generation. A recent review by Fang *et al*. [154] highlights a multitude of alternative applications for hydrochars, such as: soil amendment, energy storage, capacitors, carbon sequestration, or use as a low-cost sorbent for contaminant remediation. In addition, hydrochar has also been identified as a useful additive to facilitate AD [166–169]. Although these are all interesting areas of future development, the purpose of this study is to maximise the energy recovery from biomass. Therefore, the extent of this work focusses on the applications of hydrochar as an energy vector; mainly as a solid combustion fuel, although, the behaviour of hydrochars during AD is also investigated.

It is important to recognise that not all biomass feedstocks behave in a consistent manner during HTC. In fact, reports by Aragón-Briceño *et al*. [170] and Parmar and Ross [171] show limited energy densification for hydrochars generated from AD digestates. Aragón-Briceño *et al*. [170] found the HHVs of hydrochars generated from sewage sludge digestate range from 14.33-17.80 MJ/kg following HTC between 160-250°C; similar to the untreated digestate (16.61 MJ/kg). Similar conclusions were identified by Parmar and Ross [171]. The limited energy densification of these specific biomass-types could be linked to their collection, post-AD. During the AD process the C-content of a biomass is reduced during biogas generation. As a result, less carbohydrate-based matter is available to undergo HTC. Furthermore, Parmar and Ross [171] found HTC provided no significant improvement in the

ash behaviour of hydrochars; indicating digestate-derived hydrochars are a poor-quality fuel. Although, this was determined using predictive slagging and fouling indices; which are subject to error when applied to biomass feedstocks.

2.2.3.4 Generation of Hydrochar from Water Hyacinth

The behaviour of WH during HTC has been investigated by a number of studies [76–78,172–174]. The majority of published work has focussed on the utilisation of HTC to generate a solid combustion fuel from WH-hydrochars [76–78,172,173]; with the characteristics described in Table 2.8.

The early work of WH HTC appears to have been conducted by the same research group [78,172,173]. Initially, the group compared HTC (220°C, 4-hr) and HTL (300°C, 30-min) of WH [172], concluding HTC would be a more suitable technology for the conversion of WH, due to the higher costs and technological limitations involved with HTL [78]. Gao *et al*. [78] investigated the effect of HTC residence time (30-min to 24-hr) on hydrochar properties; whilst the temperature was fixed at 240°C. All hydrochars showed a higher HHV (16.83-20.63 MJ/kg), compared to the original WH (13.78 MJ/kg), due to decreased O:C and H:C ratios, indicating decarboxylation and dehydration reactions [64]. Although, retention time was found to have little effect on the hydrochar HHV after 4-hrs. The effect on hydrochar yield was not identified in this study.

Zhang *et al*. [76] investigated the effect of both HTC temperature (180-270°C) and HTC residence time (10-90 min) on the properties of WH-derived hydrochars. Interestingly, the retention times used in this study were lower than the optimal identified by Gao *et al*. [78]. An improvement in HHV was observed from 14.68 MJ/kg to 17.62-20.93 MJ/kg; with increased energy densification observed at higher temperatures and retention times. Concurrent with an increase in HHV, the generated hydrochars generally had a lower ash content, compared to the untreated WH. The authors speculated this could reduce the slagging and fouling potential of the hydrochars, although this was not experimentally determined. A novel conclusion of this study was that the hydrochars appeared to display lower NO_x and SO_x emissions during combustion, compared to untreated WH, following TG-FTIR analysis. This is an important consideration in the scale-up of these technologies, as NO_x and SO_x emissions are associated with severe environmental and human-health impacts [175]. Zhang *et al*. [76] also suggested that an alkali (NaOH) catalyst can further reduce NO_x and SO_x emissions, but this could compromise the hydrochar yield. NaOH was added to adjust the reactor contents to a pH of 9 and 11. However, the possible implications on the slagging and fouling potential of hydrochars was not discussed. The data presented from Zhang *et al*. [76]

in Table 2.8 is only the data from HTC reactions with a pH 7, to allow easier comparison to additional studies.

To provide a more in-depth understanding of the effect of HTC conditions on the properties of WH hydrochar, Román *et al*. [77] conducted a systematic study; varying temperature (160-250°C), retention time (30-120 min) and solid loading rate (10-50%). The effect of process conditions on hydrochar properties were analysed using a response surface methodology. Again, all hydrochars displayed an increase in HHV (16.8-21.8 MJ/kg), compared to the untreated WH (13.9 MJ/kg). Overall, temperature had the greatest effect on hydrochar yield, C-recovery and HHV. Retention time and solid loading ratio had an influence on the hydrochar properties, but to a lesser extent than temperature. With that said, an interaction between temperature and retention time was identified. This highlights the complexity of cross-comparing data between different studies. Variations in HTC processing conditions, reactor design and WH biochemical composition all have the potential to create differences in the results obtained across the different studies.

A further complication with comparing the cross-study data, presented in Table 2.8, is the use of different methodologies to calculate the HHV of hydrochars. Zhang *et al*. [76] and Román *et al*. [77] used bomb calorimetry to determine HHV, whilst the studies conducted by Gao *et al*. [78,172,173] used the predictive Dulong's equation. Bomb calorimetry is a measure of gross heating value, and is therefore considered an accurate determination of HHV. Dulong's equation calculates HHV according to the ultimate composition of biomass, by assuming the heat of combustion of a sample is equal to the heat of combustion of its elements. Smith and Ross [80] compared the HHV values for macroalgal biomass and macroalgal-derived hydrochars using bomb calorimetry and Dulong's equation. Although the HHV values correlated well, disparities occurred between specific samples; particularly for raw macroalgae. These disparities could be linked to errors in calculating the oxygen analysis by difference, which can prove challenging for high-ash feedstocks. The extent of this error and the resultant implications on future calculations, such as HHV and theoretical biomethane potential requires further investigation.

Overall, the studies shown in Table 2.8 suggest HTC is an effective conversion technology to produce a solid combustion fuel from WH. Generally, the HHV of untreated WH ranges from 13.78-14.68 MJ/kg [76–78], whereas the HHV values of WH hydrochars presented in Table 2.8 are generally higher; demonstrating the energy densification effect of HTC. This is further exemplified when comparing the HHV values of hydrochars in Table 2.8 to the HHV of pellets: 14.24-14.69 MJ/kg [85] or briquettes: 14.55-14.58 MJ/kg [35,176], generated from WH.

Table 2.8. Hydrochar properties obtained from the HTC of water hyacinth.

HTC Conditions			Hydrochar Properties		
Temperature (°C)	**Retention Time**	**Solid Loading (%)**	**Hydrochar Yield (%)**	**HHV (MJ/kg) *db***	**Reference**
220	240	5	48.7	9.2	[172]
220	240	4	16.5	20.8	[173]
240	30	6	ND	16.8	[78]
240	60	6	ND	18.4	
240	120	6	ND	17.7	
240	240	6	ND	19.2	
240	360	6	ND	18.6	
240	480	6	ND	20.6	
240	600	6	ND	19.0	
240	720	6	ND	19.8	
240	840	6	ND	18.6	
240	960	6	ND	20.2	
240	1080	6	ND	18.6	
240	1200	6	ND	18.6	
240	1440	6	ND	19.1	
180	60	10	47.9	18.2	[76]
210	60	10	48.0	19.4	
240	60	10	33.1	19.7	
270	60	10	28.8	20.3	
210	10	10	53.7	17.6	
210	30	10	51.6	18.8	
210	90	10	42.9	20.4	
178	36	18	69.3	17.2	[77]
178	36	42	68.7	16.9	
232	36	18	61.0	17.2	
178	99	18	50.4	18.5	
232	36	42	26.9	18.4	
178	99	42	66.3	16.8	
232	99	18	46.2	21.2	
232	99	42	47.1	21.8	
205	68	10	48.1	19.0	
160	68	30	76.9	17.1	
205	15	30	75.8	17.0	
205	68	49	60.7	16.8	
250	68	30	40.9	21.8	
205	120	30	49.2	18.9	
205	68	30	54.7	16.9	
205	68	30	53.1	18.7	
205	68	30	54.2	19.3	
205	68	29	50.6	19.3	

ND=not detected. HHV values have been corrected to a dry basis (*db*), where appropriate.

However, future research areas would focus on understanding the potential improvements in the slagging and fouling propensities of WH hydrochars, in order to further assess their suitability as a solid combustion fuel. Furthermore, no study in Table 2.8 reported on the characterisation and potential downstream applications of the process water phase from WH. In addition, an understanding of the energy balance for the HTC of WH would be particularly important in countries with limited energy infrastructure. Although, a recent study by Green *et al.* [177] identified the suitability of providing heating for HTC using concentrated solar-thermal energy for the conversion of different biomass types in Uganda; including WH.

2.2.3.5 Generation of Hydrochar from Grass

Similarly to WH, a number of studies have previously investigated the HTC of different GR feedstocks [49,64,74,79,164,178]. A summary of these studies, including HTC reaction conditions and hydrochar properties is shown in Table 2.9. The majority of work conducted on the HTC of grasses has focussed on miscanthus [49,64,74,164]. However, a few publications also investigate the behaviour of switch grass [74], lawn grass [79] and energy grass [178].

Reza *et al*. [74] investigated the HTC of a variety of lignocellulosic biomass, including: miscanthus and switch grass. The primary focus of this study was to understand the fate of inorganic matter during HTC and the resultant implications on the slagging and fouling potential of the hydrochars. HTC reactions were conducted across a range of temperatures (200-260°C) for a 5-min retention time; which appears a short time duration when compared with the HTC conditions presented across Table 2.8 or Table 2.9. Similarly to other studies, the HHV of the hydrochar increased at higher processing temperatures, with a simultaneous decrease in hydrochar yield. Predictive slagging and fouling indices suggested an improvement in the ash behaviour of lignocellulosic feedstocks during combustion. This was due to the removal of inorganics from the hydrochar; with up to 90% of Ca, S, P, Mg and K contents solubilised into the process water. However, as previously mentioned, predictive slagging and fouling indices should be interpreted with caution when discussing biomass.

Subsequent studies have further investigated the effect of HTC temperature [49,64,164] and retention time [164] on the inorganic and combustion chemistry of miscanthus-derived hydrochars. Each of these studies investigated the slagging and fouling potential using a combination of predictive indices and ash fusion testing; providing further evidence of the capability of HTC to improve the ash behaviour of biomass, during combustion. Smith *et al*. [64] reported the HHV of miscanthus-derived hydrochars to be 24.5 MJ/kg (200°C) and 32.1 MJ/kg (250°C); both greater than untreated miscanthus (16.1 MJ/kg); linked to

decarboxylation reactions decreasing the O:C ratio of the hydrochar. Miscanthus hydrochars showed a reduced ash content, compared to untreated miscanthus; as well as a significant reduction in the content of alkali metals. As a result, a reduced slagging and fouling propensity for the hydrochars was identified using predictive indices and ash fusion testing.

Smith *et al*. [49] investigated the application of HTC to upgrade early-harvested miscanthus, before it reaches senescence. Miscanthus harvested during this time is associated with higher crop yields, but this is compromised by unfavourable ash chemistry during combustion. This study showed HTC was able to successfully upgrade early-harvested miscanthus into a solid combustion fuel, with increased HHV and reduced slagging and fouling potential. Although, higher processing temperatures (250°C) produced a more 'coal-like' solid, compared to lower processing temperatures (200°C), with a higher HHV and reduced slagging potential, similar to results reported by [64]. Therefore, Smith *et al*. [49] recommends higher HTC processing temperatures to generate a better quality fuel. This is further supported by Smith and Ross [164] who investigated the HTC of miscanthus across a two processing temperatures (200°C and 250°C) and a wide range of retention times (0-24 hr). Temperature was found to have the greatest influence on bio-coal properties, although increased retention time resulted an increased prevalence of dehydration reactions.

The studies by Smith *et al*. [49,64,164] all recommend a higher HTC processing temperature for generation of bio-coal from miscanthus. However, what is not considered is the energy balance of the process; more specifically if the increased HHV the bio-coals warrants the increased energy input required to heat the HTC reactor to the required higher temperatures.

Table 2.9. Hydrochar properties obtained from the HTC of grasses.

Grass Sample	HTC Conditions			Hydrochar Properties		Reference
	Temperature (°C)	Retention Time (min)	Solid Loading (%)	Hydrochar Yield (%)	HHV (MJ/kg) *db*	
Miscanthus	200	5	20	79.0	19.8	[74]
	230	5	20	64.0	19.0	
	260	5	20	57.0	21.0	
Switch Grass	200	5	20	87.0	17.1	
	230	5	20	67.0	17.9	
	260	5	20	58.0	19.0	
Miscanthus	200	60	10	58.0	24.5	[64]
	250	60	10	45.0	32.1	
Miscanthus (Spring)	200	60	10	71.0	17.9	[49]
	250	60	10	47.0	24.8	
Miscanthus Autumn)	200	60	10	76.0	19.5	
	250	60	10	49.0	26.5	
Miscanthus** (Spring)	200	60	10	73.0	19.1	
	250	60	10	49.0	26.2	
Miscanthus** (Autumn)	200	60	10	76.0	16.2	
	250	60	10	48.0	28.4	
Miscanthus	200	0	10	67.0	18.5	[164]
	200	60	10	65.0	18.9	
	200	240	10	64.0	20.1	
	200	480	10	61.0	20.9	
	200	1440	10	56.0	22.6	
	250	0	10	52.0	21.1	
	250	60	10	46.0	24.2	
	250	240	10	44.0	27.5	
	250	480	10	43.0	28.2	
	250	1440	10	43.0	28.5	
Lawn Grass	200	30	3	50.0	*	[79]
	200	60	3	48.0	*	
	200	90	3	46.0	*	
	200	120	3	44.0	*	
	200	180	3	45.0	*	
	240	30	3	38.0	*	
	240	60	3	36.0	*	
	240	90	3	35.0	*	
	240	120	3	32.0	*	
	240	180	3	31.0	*	
Energy Grass	180	30	20	79.0	18.8	[178]
	210	30	20	69.3	21.0	
	240	30	20	61.1	22.8	
	180	0	20	95.4	18.0	
	180	20	20	72.9	19.7	

*Values not attainable from data available. **Biomass utilised as received. HHV values have been corrected to a dry basis (*db*), where appropriate.

2.2.3.6 Generation of Hydrochar from Brown Macroalgae

The HTC of macroalgal biomass has been much less widely studied than that of lignocellulosic biomass. However, there has been recent growing interest in the HTC of brown macroalgae [64,66,80,116,179,180]. Table 2.10 summarises the properties of hydrochars produced following HTC of brown macroalgae. The aim of each study presented in Table 2.10 was to optimise HTC conditions to generate a suitable solid combustion fuel from macroalgal biomass. A general observation from Table 2.10 is that higher HTC temperatures generally produce hydrochars with higher HHVs, but at the compromise of lower hydrochar yields. The hydrochar yields shown for macroalgal species (Table 2.10) are typically lower than for lignocellulosic biomass, such as WH (Table 2.8) and GR (Table 2.9). This suggests a greater yield distribution towards the aqueous phase; although the process water yields were not reported for any study reported in Table 2.10.

Xu *et al*. [180] investigated the application of HTC to convert *S. horneri*; a brown macroalgae, widely abundant across Chinese coastal areas, into a combustion fuel. This study has not been included in Table 2.10, due to the use of a citric acid catalyst. HTC was conducted across a range of temperatures (180-210°C) and retention times (2-16 hrs). The HHV of *S. horneri* was 17.4 MJ/kg, whereas the HHV of hydrochars ranged from 19.0-25.1 MJ/kg; reflecting an energy densification. Longer retention times generated hydrochars with higher HHVs, whilst it was reported increased temperature only influenced the HHV content of hydrochars beyond 200°C.

Smith and Ross [80] conducted an in-depth study on the applications of HTC to generate a solid combustion fuel from a range of kelps: *L. digitata*, *L. hyperborea*, and *A. esculenta*. The energy density of the seaweeds increased from around 10 MJ/kg, up to approximately 25 MJ/kg; with higher HHV values attained under higher HTC temperatures of 250°C, compared to 200°C. The effect of HTC retention time was not investigated in this study. The higher HHV values obtained are comparable to that of a low-ranking coal. HTC lead to a significant improvement in fuel quality through selective demineralisation of problematic alkali metals and chlorine; resulting in reduced slagging and fouling propensities of the hydrochars during combustion. The improvements in slagging and fouling potentials were determined through a combination of predictive indices and experimental ash fusion tests. Similar conclusions were reached by Smith *et al*. [64], also investigating the HTC of *L. hyperborea* under comparative conditions of 200°C and 250°C. Therefore, HTC could overcome the potential limitations associated with the ash chemistry of macroalgal biomass, during thermal conversion processes [65].

Table 2.10. Hydrochar properties obtained from the HTC of brown macroalgae.

Macroalgal Species	HTC Conditions			Hydrochar Properties		Reference
	Temperature (°C)	Retention Time (min)	Solid Loading (%)	Hydrochar Yield (%)	HHV (MJ/kg) *db*	
A. esculenta	200	60	10	30.0	22.9	[80]
	250	60	10	23.7	24.8	
L. digitata	200	60	10	21.8	21.0	[80]
	250	60	10	18.4	22.9	
L. hyperborea (Spring)	200	60	10	28.6	21.9	[80]
	250	60	10	24.7	23.0	
L. hyperborea (Summer)	200	60	10	31.2	24.4	[80]
	250	60	10	24.3	27.5	
L. hyperborea (Autumn)	200	60	10	33.0	24.7	[80]
	250	60	10	31.7	26.2	
L. hyperborea (Winter)	200	60	10	39.0	22.3	[80]
	250	60	10	23.6	26.3	
L. hyperborea	200	60	10	56.0	16.8	[64]
	250	60	10	36.0	24.6	
*Laminaria**	220	120	5	13.3	18.4	[179]
A. esculenta	200	30	25	29.0	17.7	[66]
	225	30	25	27.0	17.8	
	250	30	25	25.0	18.7	
Mixed Species**	200	30	25	40.0	18.1	[66]
	225	30	25	36.0	18.8	
	250	30	25	35.0	18.1	
F. serratus	200	30	25	40.0	23.2	[66]
	225	30	25	37.0	25.3	
	250	30	25	33.0	26.6	

*only the genus was specified; not the species. HHV values have been corrected to a dry basis (*db*), where appropriate.

The demineralisation potential of HTC during the processing of brown seaweeds was also analysed by Kantarli *et al*. [66]. The majority of literature studies have focussed on the HTC of kelps [64,80,179], whilst Kantarli *et al*. compared the HTC of a kelp (*A. esculenta*) and wrack (*F. serratus*), as well as a mixture of seaweeds (*Cystoseria* sp. and *Laurencia* sp.). In this study, three processing temperatures were analysed: 200°C, 225°C and 250°C, whilst

retention time was fixed (30-min). The hydrochars produced from *F. serratus* were shown to have a higher hydrochar yield and HHV, compared to those from *A. esculenta*; as seen in Table 2.10. Inorganic analysis of hydrochars generated at 225°C shows sufficient removal of Na and K from the seaweeds. The application of predictive indices suggested a reduction in the fouling potential of hydrochars; to a medium fouling potential. Whilst the slagging potential of hydrochars remained medium or high. The effectiveness of HTC to improve the ash behaviour of seaweed hydrochars was not as conclusive as the results presented by Smith and Ross [80]. However, this could be associated with the limitations of using the predictive slagging and fouling indices. Smith and Ross [80] used the predictive indices in combination with ash fusion tests, to obtain more rounded overview of the slagging behaviour of seaweed ash.

Taking a novel approach to macroalgae HTC, Wang *et al*. [179] studied the effect of recirculating of *Laminaria*-derived HTC process water back into the HTC reactor. Process water recirculation was conducted up to 12-times and the effect on hydrochar and process water properties investigated. HTC conditions remained fixed at 220°C, 12-hrs. The HHV of the resultant hydrochars (18.4-22.7 MJ/kg) were all higher than the HHV of *Laminaria*: 10.0 MJ/kg. After the 12^{th} reiteration of process water recycling, the hydrochar yield (17.1%) and HHV (20.5 MJ/kg) were both higher than the hydrochar generated with no process water recirculations (hydrochar yield=13.3% and HHV=18.4 MJ/kg). The authors concluded enhanced dehydration of *Laminaria* occurred during process water recirculation, suggested to be a result of the catalytic effect from organic acids solubilised in the process water phase. Wang *et al*. [179] propose recirculation of process water is an effective method to simultaneously enhance the energy recovery efficiency of macroalgal biomass and reduce the fresh water consumption of the HTC system. This opens up an interesting argument about the fresh water demand of the HTC process and perhaps, the utilisation of seawater as a HTC reactant medium could reduce this demand; especially whilst processing a marine-based biomass. Seawater has been used as a reactant medium during the HTC of marine plastic debris [181] and *Ulva* sp.; a green macroalgal biomass [182]. The hydrochar generated from *Ulva* sp. (at 180°C, 40-min) showed a HHV roughly double that of the untreated seaweed. Although, this study did not investigate the ash behaviour of the hydrochar during combustion; which is likely to become problematic, due to the high concentrations of mineral matter within seawater [183]. At the current time point, there is no published study available which investigates the use of seawater as a reactant medium during the HTC of brown macroalgae; with a subsequent understanding of the hydrochar and process water characteristics. Additionally, the studies reported in Table 2.10 all used dried macroalgae during HTC experiments; most likely to prolong storage of the sample. However, a further interesting research direction would be to compare the behaviour of dried and wet macroalgal

biomass during HTC, in a similar fashion to the study conducted by Smith *et al*. [49], comparing the HTC of dried and wet miscanthus.

Although not directly relevant to this study, it is also worth mentioning the increasing attention brought to the HTC of green [182,184–186] and red [187] macroalgal biomass. The majority focus of these studies is the generation of an energy densified hydrochar, typically for applications as a solid combustion fuel.

Overall, the studies presented in Table 2.10 suggest that HTC can be used as a suitable valorisation technology to convert macroalgal biomass into a solid combustion fuel. However, further knowledge is required to compare the fuel properties of hydrochars produced from different macroalgal species: such as wracks and kelps. This includes a particular emphasis on the understanding of the slagging and fouling propensity of macroalgal-derived hydrochars using a combination of predictive indices and ash fusion tests. In addition, the studies presented in Table 2.10 all used dried seaweeds during HTC reactions. Therefore, presenting another research gap: comparing the behaviour of 'wet' and 'dried' seaweeds during HTC.

2.2.4 Process Water Properties

Traditionally, the product of interest from the HTC process was directed towards production of hydrochar, with the process water previously regarded as a problematic residue, acting as a drawback for the full-scale development of HTC [86]. However, large quantities of process water are produced, which contain high concentrations of solubilised organics; associated with a potential energetic value [147,163]. Therefore, the process water can be considered a by-product, rather than a problematic waste product, if suitable downstream valorisation routes are present.

2.2.4.1 Process Water Composition

HTC process waters contain complex mixtures of organic matter; the composition of which varies across different feedstocks and reaction severities [86]. Becker *et al*. [157] found the total organic carbon (TOC) fraction of HTC process waters produced from lignocellulosic biomass and wheat straw digestate, at 270°C, represented 30-50% of the initial feedstock carbon. A recent review by Ipiales *et al*. [86] reported the characteristics of a range of HTC process waters, finding a TOC range between approximately 4-30 g/L: corresponding to between 16-61% of the carbon yield from the original feedstock.

Throughout literature studies, there appears to be disagreement as to the relationship between process water TOC concentration and HTC temperature. Various digestates show an increase in process water TOC concentration at higher HTC temperatures [171]. Whereas, orange pomace-process waters display the inverse relationship [163], which the authors suggested is due to the sequestering of carbon to the gaseous phase, at higher HTC temperatures. Alternative studies show an increase in TOC concentration between lower and intermediate HTC temperatures, but then a decrease at higher temperatures. Such biomass types include: woody biomass [157], cassava rhizome [188] coconut husk [158], rice husk [158]. Whilst some studies display no clear trend between TOC and HTC temperature, including: sewage digestate [170] microalgae [160] and olive mill waste [189]. The variation in the relationship between TOC and HTC temperature across literature studies suggests the differing biochemical composition of biomass feedstocks influences the solubilisation of organic degradation products into the process water, during HTC. Regardless, the high carbon content of process waters means effective downstream processing is required, in order to minimise serious environmental impacts [86].

HTC process waters contain a multitude of solubilised organic compounds, produced during the simultaneous reactions, which occur during HTC. Such compounds include: sugars, furfural, furfuryl alcohol, 5-HMF, formic acid, acetic acid and propionic acid [158]. HTC process waters generally display an acidic pH of 4.5 or below [147,152,157,158,188], due to the presence of organic acids [157]; mainly in the form of acetic acid [190]. Generally, the concentrations of VFAs solubilised in lignocellulosic-derived process waters are higher, following greater HTC reaction severities [152,158]. For example, the acetic acid concentration present in corn-stover HTC process waters, increased with HTC reaction temperature: 175°C (3760 mg/L), 200°C (4020mg/L), 225°C (4360 mg/L) and 250°C (5040 mg/L). The changing composition of brown macroalgal-derived HTC process waters over a temperature range has not yet been reported. Wang *et al*. [179] reported a VFA concentration of 3.4 g COD/L, during the HTC of *Laminaria*, at 220°C, 12-hrs. This concentration rapidly increased by 19.5 times to 85.2 g COD/L following recirculation of the process water 10-times.

The total sugar content of lignocellulosic-derived HTC process waters has been shown to rapidly decline between temperatures of 215°C (1.4 g/L) to 295°C (0.1 g/L) [191]. HMF and furfural are formed through dehydration of solubilised carbohydrate derivatives [150,192], typically around 200°C [152]. Although, during more severe reaction conditions, a decline in HMF and furfural concentrations are typically observed [152,157,158,163], due to further degradation to organic acids. Machado *et al*. [152] characterised HTC process waters produced from corn stover produced cross a range of temperatures: 175°C, 200°C, 225°C and 250°C. Both furfural (687-2832 mg/L) and HMF (444-494 mg/L) were detectable in high

concentrations between 175-200°C. However, beyond 200°C the concentrations began to decline; with treatments at 250°C resulting in no detectable HMF or furfural in the process water [152].

Higher severity HTC conditions have also been associated with an increased concentration of phenolic compounds solubilised within HTC process waters produced from: corn stover [152] digestates [171] and green macroalgal biomass [184]. Phenolic derivatives are generated during the degradation of aromatic structures, such as lignin [192,193], or polyphenols and phlorotannins; in the case of macroalgal biomass [128,194].

Generally, as HTC temperature increases, the concentration of total nitrogen solubilised in the process water also increases, due to the enhanced degradation of the protein fraction. This has been observed during the HTC of cow manure [84] and sewage digestate [170]. However, as HTC temperature increases, the proportion of organic-N to inorganic-N decreases [170]. Thereby, the concentration of ammonium generally increases at higher HTC processing temperatures [84,170].

2.3 Integration of HTC and AD Conversion Processes

The applications of both hydrothermal and biological conversion processes have been proven successful for the valorisation of second and third generation feedstocks. Although, recent interests have shifted towards the integration of HTC and AD, in order to maximise the full energetic potential of biomass. However, a major discrepancy which exists across literature studies is the differing HTC-AD integration strategies that exist, with little clarity as to the most effective strategy selection and processing conditions to optimise the ECE of biomass. This section outlines the different HTC-AD integration strategies and highlight studies where different integration strategies have been directly compared.

2.3.1 Digestion of Hydrochars

Despite the increased carbon-content of hydrochars, few studies have investigated the behaviour of hydrochars as a feedstock for mono-digestion, during AD [161,195,196]. Mumme *et al*. [196] studied the use of both hydrochars and biochars as a feedstock for AD. The hydrochar, produced from wheat straw digestate (230°C, 6-hrs), showed a low biomethane yield of 19mL CH_4/g VS; corresponding to a labile carbon fraction of 10.4%, which was degraded by AD. However, this was higher than the labile carbon fraction of pyrochar (0.6%). Zhao *et al*. [195] found hydrochar generated from food waste (260°C, 4-

hrs) generated a slightly higher biomethane yield of 144 mL CH_4/g hydrochar; approximately 137 mL CH_4/g VS. However, both [195,196] only investigated the behaviour of hydrochar generated from a single HTC processing condition during AD.

Luz *et al*. [161] determined the biomethane potential of spent coffee ground hydrochars, produced across a range of temperatures: 180°C, 220°C and 250°C. The biomethane yields obtained from hydrochars reduced with increasing HTC temperature: 491.4 mL CH_4/g VS (180°C), 465.5 CH_4/g VS (220°C) and 367.0 CH_4/g VS (250°C), as did their biodegradabilities: 78% (180°C), 61% (220°C) and 45% (250°C). This suggests increasing recalcitrance of higher-temperature hydrochars during AD. Although, Luz *et al*. [161] did not include a comparison of biomethane yields to untreated coffee grounds. Therefore, the effectiveness of the process to enhance biomethane yields cannot be assessed. The hydrochar biodegradabilities observed by Luz *et al*. [161] were higher than those observed by Mumme *et al*. [196]. However, it is difficult to interpret the significance of any difference between these studies; as different feedstocks, HTC conditions and biomethane potential methodologies were utilised.

An additional application for hydrochars during biological conversion processes is their addition as a supplement for AD [166–169]. The porous and functionalised structure of hydrochars can act as a support platform to facilitate direct interspecies electron transfer (DIET) across syntrophic microorganisms, involved in the AD process [195,197]. Hydrochar addition has been shown to improve biomethane yields from both fish processing waste [166] and pig carcass [167] in batch AD systems. Although, recent research by Quintana-Najera *et al*. [198] found that hydrochar supplementation can be inhibitory to the digestion of cellulose, compared to biochar supplementation. The inhibitory nature of hydrochars is thought to be related to their acidic properties and inhibitory compounds present on the hydrochar surface.

2.3.2 Digestion of HTC Process Waters

During the HTC process, organic and inorganic compounds are solubilised from the biomass and into the process water phase. These solubilised organics have an energetic value, which can be recovered through biological conversion processes, such as AD, to maximise the energy output obtained from the HTC process. The generation of biomethane from HTC process waters appears to be a growing topic of research interest [84,147,200–202,160,163,170,171,179,184,190,199]. Process waters contain readily digestible compounds which have the potential to bypass the hydrolysis stage of AD; often considered the rate-limiting step for recalcitrant biomass; such as lignocellulosic biomass [203].

The potential for biomethane generation from HTC process waters was initially investigated in the early 2010s by Oliveira *et al*. [200] and Wirth and Mumme [147]. Oliveira *et al*. [200] initially proved the generation of biomethane from HTC process waters was possible using batch systems. The process waters were produced from a combination of agricultural and forestry residues. Alternatively, Wirth and Mumme [147] compared the generation of biomethane from the HTC of corn silage across two reactors: a continuously stirred-tank reactor and a packed-bed anaerobic filter reactor. Both reactors showed high COD removal efficiency (up to 75%) and a maximum average methane yield of 0.236 L CH_4/g COD; suggesting HTC process waters are a suitable AD feedstock, with no evidence of inhibitory effects. However, the process waters digested by [147,200] were produced under a single HTC condition. As previously mentioned, the composition of HTC process waters is known to change across different HTC conditions; potentially affecting the digestion properties of the process waters.

Since these initial studies, the potential for biomethane production from HTC process waters has been assessed across a range of feedstocks and HTC conditions. The process water biomethane potential results obtained from these studies are displayed in Table 2.11; alongside the HTC processing conditions.

The results in Table 2.11 generally show that the biomethane yields obtained from HTC process waters varies between different feedstock types and HTC processing conditions; with higher processing temperatures typically resulting lower biomethane production. Similar conclusions were drawn in the review paper by Ipiales *et al*. [86], who indicate that the biomethane generation from process waters is optimised when HTC reactions are conducted below 200°C. HTC reactions above this temperature can result in the formation of recalcitrant compounds, which are inhibitory to AD. Furanic compounds such as 5-HMF and furfural are known inhibitors of AD [204] and DF [205,206] processes, due to the inhibition of both cell growth and enzymes associated with the glycolysis pathway [204]. Similarly, phenolic compounds are known inhibitors of AD processes, which alter the selective permeability cell membranes, causing cell disruption and termination of essential enzymatic pathways [204]. Although, there is evidence to suggest that a robust consortium of microorganisms can degrade phenolic compounds up to concentrations 2000 mg/L [207]. Further inhibitory compounds are also produced from the degradation products of proteins, including ammonia [208].

Table 2.11. Experimental biomethane potential yields for a range of HTC process waters.

Biomass	HTC Conditions		Biomethane Potential		Reference
	Temperature (°C)	Retention Time (min)	(mL CH_4/g COD)	(mL CH_4/g VS)	
Sewage Sludge	208	60	177	-	[201]
Sewage Sludge Digestate	160	30	260	-	[170]
	220	30	277	-	
	250	30	226	-	
Agricultural Residue Digestate[1]	150	60	100	-	[171]
	200	60	181	-	
	250	60	156	-	
MSW Residue Digestate[1]	150	60	85	-	[171]
	200	60	138	-	
	250	60	135	-	
Sewage Sludge Digestate[1]	150	60	100	-	[171]
	200	60	182	-	
	250	60	152	-	
Household Waste Digestate[1]	150	60	121	-	[171]
	200	60	159	-	
	250	60	125	-	
Cow Manure	170	60	-	294	[84]
	200	60	-	235	
	230	60	-	80	
Orange Pomace	190	120	214	-	[163]
	225	120	209	-	
	260	120	195	-	
Food Waste	260	240	58	-	[195]

Biomass	HTC Conditions		Biomethane Potential		Reference
	Temperature (°C)	Retention Time (min)	(mL CH_4/g COD)	(mL CH_4/g VS)	
OFMSW	180	60	205	-	[209]
	220	180	185[2]	-	
	250	360	166	-	
Pine Sawdust	220	60	253	-	[190]
Canola Oil Waste	220	60	108	-	[190]
Olive Oil Waste	220	60	91	-	[190]
Vineyard Waste	220	60	119	-	[190]
Microalgae	180	60	-	356	[160]
	210	60	-	226	
	240	60	-	188	
Macroalgae (*Laminaria*)	220	120	186	-	[179]

[1]based on 20% SLR. [2]approximate value OFMSW=organic fraction of municipal solid waste. MSW=municipal solid waste. COD=chemical oxygen demand. VS=volatile solid.

The potential for biomethane generation from different lignocellulosic-derived HTC process waters was studied by Pagés-Díaz *et al.* [190]: comparing four different biomass types (pine sawdust, canola oil waste, olive oil waste and vineyard waste), processed at 220°C, 60-mins. The generated biomethane yields appeared to drastically vary between the different feedstocks (Table 2.11); linked to the increased formation of inhibitory nitro-recalcitrant compounds for feedstocks with an initially high N-content. This re-iterates the complexity of the behaviour of HTC process waters during AD; which appears to be affected by both HTC reaction conditions (Table 2.11) and differences between biomass feedstocks. Currently, studies which have investigated the biomethane potential from lignocellulosic-derived HTC process waters have only assessed one reaction temperature: 220°C, 60-mins [190] or 220°C, 6-hrs [147]. Therefore, the effect of HTC reaction severity on biomethane production from lignocellulosic-derived process waters remains unexplored. Additionally, despite multiple studies on the HTC of WH (Table 2.8) and GR (Table 2.9), the potential for biomethane generation from these process waters has not been assessed.

Limited studies exist which have explored the behaviour of brown seaweed-derived HTC process waters during biological conversion. Smith and Ross [80] investigated the comparative potential of biohydrogen or biomethane generation from HTC process waters generated from a range of kelp species: *L. digitata*, *L. hyperborea*, and *A. esculenta*. It was concluded that biohydrogen generation obtained a higher energetic output from the process waters, compared to biomethane. However, the gas yields were theoretically determined, using stoichiometric equations. Therefore, the true biodegradability, or the effect of inhibitory compounds cannot be determined. Despite this, the generation of biohydrogen from HTC process waters appears to be a novel concept and, to the author's knowledge, this has not been experimentally investigated in current literature.

Wang *et al*. [179] experimentally determined the biomethane potential yield of *Laminaria*-derived HTC process water as 186 mL CH_4/ g COD. Interestingly, Wang *et al*. [179] found that repeated recirculation of the process water into the HTC reactor improved biomethane yields, due to the accumulation of VFAs and COD. However, these experiments were conducted using a single HTC process condition (220°C, 120-mins). Therefore, limited information is available on the effect of HTC processing temperature on the biomethane yields obtained from brown macroalgae-derived process waters. A more recent study by Shrestha *et al*. [184] found limited generation of biomethane from the co-digestion of green macroalgae (sea lettuce) HTC process waters and bananas. Therefore, highlighting differences in the behaviours of different types of macroalgal biomass, during integrated HTC and AD.

The potential for AD of HTC process waters has been investigated by many studies (Table 2.11), with the majority of work conducted in batch systems. It is therefore important to consider that methodological variations may affect the biomethane potential results obtained from process waters. De la Rubia *et al*. [199] recognised the selection of inocula can influence the biomethane potential of sewage sludge-derived HTC process waters. Whilst, Villamil *et al*. [201] found varying inoculum-to-substrate ratio can affect biomethane yields of sewage sludge-derived HTC process waters; with ratios ≥ 1 recommended to supress ammonia inhibition. Furthermore, it is also important to consider the behaviour of HTC process waters during continuous AD systems, to facilitate the transition to a scaled-up system. Wirth *et al*. [147], Wirth *et al*. [203] and Weide *et al*. [202] all report stable biomethane generation from the continuous AD of HTC process waters; with COD removal efficiencies of up to 75%. Therefore, suggesting that continuous AD is a suitable valorisation route for HTC process waters.

2.3.2.1 Combined Hydrochar Combustion and Process Water AD

The applications of hydrochar as a solid combustion fuel and biomethane generation from HTC process waters means that HTC can be utilised to generate separate energy vectors. The energetic output from each vector can be combined, to facilitate a more complete conversion of biomass. A number of studies exist which have explored the use of this HTC-AD integration strategy to improve the energetic recovery of biomass, compared to AD alone [84,160,170,209].

Aragón-Briceño *et al*. [170] determined that the energy output obtained from the AD of sewage sludge, containing 15% solids, was 7.08 MJ/kg; based on the energy content of biomethane produced. However, sequential AD, followed by HTC of the sewage sludge digestate improved the energetic output by 179%, 167% and 154% at HTC temperatures of 160°C, 220°C and 250°C, respectively. Therefore, the lower HTC processing temperature displayed the greatest improvement in obtainable energetic output.

Similar conclusions were obtained by Marin-Batista *et al*. [160], who found the integration of HTC-AD improved the net energy recovery of microalgae from 20%, to 91%, 72% and 62%, at HTC temperatures of 180°C, 210°C and 240°C, respectively. The authors suggested the reduction in net energy conversion at higher HTC temperatures was related to limited energy densification of the hydrochar and reduced biodegradability of the process waters; due to the presence of inhibitory compounds. An additional study by the same research group [84] also assessed this HTC-AD integration strategy for cow manure. The AD of cow manure represented an energy recovery yield of 26%; whereas integration of HTC-AD at HTC temperatures of 170°C and 200°C both obtained an increased energy recovery yield of 85% and 86%, respectively. However, a higher HTC processing temperature of 230°C resulted in a slightly reduced energy recovery yield of 74%; due to negligible biomethane yields generated from the process water; a result of nitrogenated inhibitory compounds, such as indoles.

Although, [84,160,170] all report an improvement in ECE using an integrated HTC-AD approach, it is worth considering that the HTC process is associated with an energetic input. Therefore, in order to be an energetically-feasible process, the energy output must out-weigh the energy input of the system. This was considered by Lucian *et al*. [209]; investigating the integration of HTC-AD from the organic fraction of municipal solid waste, with subsequent combustion of hydrochars and AD of process waters, across three different HTC conditions: 180°C: 1-hr, 220°C: 3-hr, 250°C: 6-hr. A similar process efficiency was obtained from the integration of AD-HTC at 180°C and 220°C (59-60%); although this decreased to 42%, under the more severe HTC conditions (250°C: 6-hr). However, it appears the energy input

outweighs the energy output of the system [209]. Aragón-Briceño *et al*. [210] determined the AD of sewage sludge, with sequential integrated HTC-AD of the digestate yields an energy positive process. Therefore, further investigation of the energy balance of integrated HTC-AD is required.

Overall, according to [84,160,170,209], the integration of HTC-AD through hydrochar combustion and process water AD is a suitable valorisation route to improve the ECE of biomass. Typically, lower processing temperatures are favoured, due to the improved energetics of the system. However, a factor that is not considered in these studies is the quality of the hydrochar which is generated; in terms of ash combustion chemistry. Generally, hydrochars produced at higher HTC processing temperatures display reduced slagging and fouling tendencies; linked to an increased removal efficiency of problematic alkali metals [64,80]. Although, limited information is available for the slagging and fouling tendencies of hydrochars generated at <200°C. The optimal HTC-AD temperatures identified to maximise the ECEs of sewage sludge digestate (160°C) [170], microalgae (180°C) [160], cow manure (170-200°C) [84] and organic fraction of municipal solid waste (180°C) [209] were all <200°C. However, the ash behaviour of these hydrochars during combustion is unknown; which could prove potentially problematic as the hydrochars were produced from high ash feedstocks, such as microalgae [160] and sewage sludge digestate [170]. This potential issue is highlighted by Parmar and Ross [171], in which HTC of various AD digestates at 150°C, 200°C and 250°C showed no significant reduction in slagging and fouling tendencies, according to predictive indices. Furthermore, the energy densification of the hydrochars was also limited; with Parmar and Ross [171] concluding that combustion of digestate-derived hydrochars was unsuitable and alternative applications should be sought; such as soil amendment. Overall, further work is required to determine the slagging and fouling propensity of hydrochars to confirm their viable application as a solid combustion fuel; especially when produced at lower HTC temperatures (<200°C).

A high slagging and fouling inclination can be a major issue for the large-scale combustion of a fuel [64]. This is an important factor to consider during the integration of HTC-AD; as the hydrochar combustion often represents a greater energy carrier, compared to AD of the process water [84,170,209]. Hydrochar combustion represented between 56-59%, 78-92% and 87-89% of the overall energy output from HTC-AD integration for sewage sludge digestate [170], cow manure [84] and the organic fraction of municipal solid waste [209], respectively. However, the distribution of energy obtained from the hydrochar and process water is likely to vary between feedstocks, according to the effectiveness of carbon distribution towards the process water. For instance, integration of HTC-AD for microalgae at 180°C resulted in a greater energy return from the AD of process water, compared to the combustion of the hydrochar [160].

2.3.3 Hydrothermal Pre-treatment

Hydrothermal pre-treatment involves the use of heated water as a reactant medium for the treatment of biomass. During this process, the structure of biomass is broken down, releasing readily-digestible material into the aqueous phase and disrupting the recalcitrant biochemical structure of biomass; such as lignocellulose polymers. Hydrothermal pre-treatment facilitates the hydrolysis of biomass; therefore, enhancing biodegradability during biological conversion. Therefore, a further integration strategy between HTC-AD is the application of HTC as a hydrothermal pre-treatment to enhance biological conversion, through the digestion of the residual slurry (hydrochar and process water), following HTC.

The severity of hydrothermal pre-treatment is dictated by the reaction temperature and retention time, which can lead to difficulties in cross-comparing data from multiple studies. In an attempt to overcome this, the reaction temperature and retention time of HTC or SE reactions can be combined into one single parameter, referred to as the 'severity factor' (SF) [164,211,212], described in Section 3.2.3. The application of the SF facilitates cross-study comparison of hydrothermal conversion processes, which is later explored in Chapters 5 and 7.

2.3.3.1 Digestion of HTC Slurries

AD of HTC-slurries has been investigated for a range of different feedstocks; including lignocellulosic biomass, such as rice straw [213–215] and WH [112,114,121], as well as macroalgal biomass [72,216]. Hydrothermal pre-treatment has been identified as a suitable pre-treatment for lignocellulosic biomass, due to the low operational costs and reduced use of environmentally-harmful chemicals [217].

Wang *et al*. [214] investigated the hydrothermal pre-treatment of rice straw across a range of temperatures (90°C, 150°C, 180°C and 210°C) for a retention time of 15-min. However, the authors reported that hydrothermal pre-treatments of 90-180°C did not significantly improve biomethane yields, compared to untreated rice straw. Pre-treatment at higher temperatures (210°C) resulted in a 30% reduction in biogas yields, due to the increased presence of fermentative inhibitors, such as furfural. Therefore, high-severity hydrothermal pre-treatment conditions were not recommended. Similar conclusions were obtained by He *et al*. [215], who reported rice straw pre-treatment at 210°C resulted in a decreased biomethane yield of between 51-100%, compared to the untreated biomass. However, optimal pre-treatment conditions of 150°C, 20-min resulted in a 31% improvement in biomethane yields [215]. Again, the authors suggest the more severe reaction conditions are associated with the

accumulation of fermentative inhibitors: furans and phenolics, which reduce the obtainable biomethane yields.

The effect of hydrothermal pre-treatment has also been investigated for WH, across a range of studies:[112,114,121]. Ferrer *et al*. [114] hydrothermally pre-treated WH using relatively mild conditions (80°C, 3-hrs). Despite an 8% increase in solubilised COD, no significant improvements in biomethane yields were observed, with the authors suggesting increased retention times or higher treatment temperatures should be explored. Subsequent studies have investigated higher temperature hydrothermal processing of WH [112,121]. Pre-treatment at 121°C, 30-min improved biomethane yields by 33% [112] and 170°C, 30-min by 51% [121]. Therefore, this suggests that increased pre-treatment severity results in a greater improvement in biomethane yields. However, it should be noted that all of these are separate studies, utilising WH samples collected from different sources. As a result, caution must be taken in comparing the results of these studies, due to the potential differences in the biochemical compositions of WH samples. Furthermore, limited information is available for the treatment of WH under more severe reaction conditions. Although, it is likely that more severe conditions (>200°C) will facilitate the generation of fermentative inhibitors, reducing biomethane yields, as was observed for rice straw [214,215].

In addition to lignocellulosic biomass, the effectiveness of hydrothermal pre-treatment to improve the digestion of macroalgal biomass has been investigated [72,216,218]. Lin *et al*. [72] determined the effectiveness of a range of hydrothermal pre-treatment temperatures (100-180°C) on the biohydrogen and biomethane yields generated from *S. latissima*, during two-stage digestion. During this study, the retention time was fixed to 30-min. An optimal pre-treatment temperature of 140°C was identified; which improved biomethane yields by 22.6%; linked to peak mannitol solubilisation. Increased temperatures (160-180°C) resulted in a reduced mannitol recovery, suggested to the linked to the increased degradation of solubilised carbohydrates into inhibitory compounds; such as furfural, or nitrogen-containing compounds, produced via Maillard reactions. As a result, the pre-treated *S. latissima* at 180°C displayed a slight (1%) reduction in biomethane yields, compared to the untreated seaweed. Following on from this study, the same research group took the identified optimal hydrothermal pre-treatment temperature (140°C, 20-min) and compared this hydrothermal pre-treatment condition to other pre-treatment methodologies, including: hydrothermal dilute acid pre-treatment, enzymolysis and a combination of pre-treatments [216]. The effectiveness of each pre-treatment to enhance biohydrogen and biomethane yields during two-stage digestion of *L. digitata* was compared. Hydrothermal pre-treatment was identified as the optimal pre-treatment; improving the ECE by 26.7%, compared to untreated *L. digitata*. Thompson *et al*. [218] investigated the use of hydrothermal pre-treatment to improve the biomethane yields obtained from the invasive brown macroalgae *Sargassum*. Interestingly,

the optimal pre-treatment conditions identified (140°C, 30-min) were identical to those found by Lin *et al*. [72]. The biomethane yields obtained from pre-treated *Sargassum* increased by 42%, compared to the untreated seaweed. However, under more severe reaction conditions (SF>2.77), a decrease in biomethane yields was observed, due to the formation of inhibitory compounds, such as ammonia, VFAs and phenolics [218]; echoing the conclusions obtained by Lin *et al*. [72].

2.3.3.2 Steam Explosion

Steam explosion (SE) is an alternative hydrothermal pre-treatment which uses high-pressure steam as a reactant medium, rather than subcritical water; which is utilised as part of HTC. During SE, steam is introduced to biomass, which generates a steam atmosphere associated with high temperatures (140-240°C) and pressures [219]. Following a certain retention time, the reactor contents undergoes rapid decompression to atmospheric conditions, causing mechanical disruption of the biomass. SE has been reported to improve the biomethane yields of a range of feedstocks [115,132,219–221], due to enhanced hydrolysis of the biomass.

SE pre-treatment has been used to improve the biomethane generation from lignocellulosic biomass, including: rice straw [219], bamboo [221] and WH [113,115]. Across each of these studies, intermediate SE conditions resulted in the highest biomethane yields. Indicating a balance between less severe conditions providing insufficient disruption of the lignocellulosic structure and too severe conditions resulting in the formation of inhibitory compounds, such as HMF and furfural [219].

Steinbach *et al*. [219] found optimal SE conditions with a SF of 4.1 (206°C, 30-min) improved biomethane yields from rice straw by 32%. However, SE conditions with a lower SF (3.05 and 3.54) showed similar biomethane yields to untreated rice straw, due to insufficient degradation of the lignocellulosic matrix. Harsher conditions of 229°C, 30-min (SF 4.32) caused inhibition of biomethane generation; with a 68% reduction, compared to untreated rice straw. The authors report an increase in HMF formation with increasing SF during the SE of rice straw; due to the higher prevalence of glucose dehydration. In addition, under more severe conditions, hemicellulose derivatives are suggested to re-polymerise with other hemicellulose or lignin derivatives to form pseudolignin; which are effectively inert during AD.

Similar conclusions were obtained by Alfageme *et al*. [115], investigating the application of SE to improve biomethane yields obtained from WH, across a range of SE conditions. SE conditions of 120°C, 60-min (SF=2.4) showed lower biomethane yields than untreated WH. Whereas, more severe conditions of 210°C, 10-min (SF=4.2) resulted in a 21% increase in

biomethane yields. However, similar to [219], Alfageme *et al*. [115] found intermediate SE conditions of 170°C, 60-min (SF=3.8) were the optimal pre-treatment conditions: improving biomethane yields by 38%. Kist *et al*. [113] determined investigated sequential thermal hydrolysis and SE for WH; finding optimal pre-treatment conditions of 170°C, 60-min (SF=3.5). Therefore, the combined work of [113,115] indicates a potential optimised SF range of between 3.5-3.8 for the hydrothermal pre-treatment of WH.

SE has also been investigated as a pre-treatment to enhance the biomethane yields from the macroalgal species *S. latissima* [132]. The obtainable biomethane yield was higher following SE conditions of 130°C, 10-min (268 mL CH_4/g VS) and 160°C, 10-min (260 mL CH_4/g VS), compared to untreated *S. latissima* (223 mL CH_4/g VS). Again, this study indicates more severe reaction conditions resulted in a slightly lower biomethane yields. Although, the variance between triplicate batch fermentations suggests these differences are not significant.

2.3.4 Comparison of HTC-AD Integration Strategies

Overall, there appears to be an increasing interest in the integration of HTC and AD to maximise the ECE of biomass feedstocks. Clearly, a number of HTC-AD integration strategies exist. However, only a limited number of studies include a direct comparison of these strategies [170,209], to determine which option appears the most energetically-feasible.

Aragón-Briceño *et al*. [170] compared the energetics of HTC-AD and thermal hydrolysis for the treatment of sewage sludge. The HTC-AD strategy selected involved AD of sewage sludge, with subsequent HTC of the digestate to generate a hydrochar for combustion and a process water for further AD. HTC was conducted at 160°C, 220°C and 250°C, with the lowest temperature reaction yielding the highest energy output of 19.77 MJ/kg; representing a 179% increase in obtainable energy output compared to the AD of sewage sludge. The energy output obtained from thermal hydrolysis pre-treatment was 10.13 MJ/kg; therefore, HTC-AD integration is a more energetically-feasible option.

Similar conclusions were obtained by Lucian *et al*. [209] who compared the energetics of two different HTC-AD integration options for the treatment of the organic fraction of municipal solid waste. The two options were (i) combustion of the hydrochars with AD of the process waters and (ii) AD of the mixed slurry. Again, the combustion of hydrochars and AD of process waters yielded a greater energy output compared to the AD of the slurry.

Therefore, both of these studies suggest the utilisation of HTC products as separate energy vectors provides the greatest energy output. However, the direct comparison of HTC-AD strategies has not yet been investigated for lignocellulosic or macroalgal feedstocks.

2.4 Research Gaps

In conclusion, current literature has highlighted that the integration of HTC-AD could provide a suitable strategy to enhance the ECE of biomass, compared to AD of the untreated biomass. This could provide a suitable conversion route for the valorisation of high-ash feedstocks, such as WH, GR and macroalgal biomass; which are unsuitable for conventional thermochemical conversion and display limited biodegradability during biological conversion processes. However, further work is required to determine the efficacy and suitability of integrated HTC-AD as a conversion strategy for high-ash biomass.

Therefore, this study aims to contribute towards this growing area of research, by addressing the current knowledge gaps:

The potential of HTC to generate a solid combustion fuel from WH has been well established. However, the ash behaviour of WH-derived hydrochars, during combustion, is not fully understood, with analysis of the slagging and fouling potential required to facilitate the scale-up of this technology.

Macroalgal-derived hydrochars appear more extensively characterised; demonstrating energy densification and selective demineralisation, compared to the original seaweed. However, the majority of work to date has been conducted on kelps, with limited knowledge of the behaviour of wracks during HTC. Furthermore, the majority of work conducted so far has used dried seaweed during HTC reactions. Therefore, a research gap exists in the comparative behaviour of 'wet' and 'dried' seaweed during HTC.

The characterisation of lignocellulosic-derived HTC process waters, produced across a range of reaction severities is currently limited, with no information available on the attainable biomethane yields from either WH or GR process waters. The theoretical biomethane and biohydrogen yields from macroalgal-derived process waters has been analysed [80]. However, the true biodegradability, or the effect of inhibitory compounds during digestion cannot be determined using predictive theoretical methods. Currently, no studies investigate the potential of biohydrogen generation from process waters using an experimental-based approach. The experimental biomethane potential of macroalgal-derived process waters have been assessed [179]. Nonetheless, this was conducted using a fixed HTC reaction severity. Therefore, the effect of HTC temperature on the properties and resultant biomethane yields from macroalgal-derived process waters remains unexplored.

A number of different HTC-AD integration strategies exist across literature studies, mainly (i) AD of hydrochars only (ii) combustion of hydrochars and AD of process waters and (iii) AD of HTC slurry. The optimal integration strategy used to improve the ECE of biomass is

likely to dependent upon biomass-type and HTC reaction conditions. Therefore, a systematic study to compare different HTC-AD integration strategies, across a range of HTC reaction severities and biomass types is required. Furthermore, the energy balance of each HTC-AD integration strategy needs to be considered, to ensure an energetically-feasible process. Currently, the potential integration of HTC-AD to improve the ECE of lignocellulosic biomass or macroalgal has not yet been assessed.

Hydrothermal pre-treatment appears to be a suitable technology to improve the biodegradability of biomass, in particular recalcitrant lignocellulosic biomass, such as WH. However, different methods of hydrothermal pre-treatment exist; including subcritical water (HTC) and steam explosion (SE). The comparative effectiveness of HTC and SE during the two-stage digestion of WH is currently unknown, especially across a range of reaction severities.

Chapter 3
Methodology

This chapter outlines the protocols and methodologies used whilst conducting the experimental work of this thesis. Initially, this includes a summary of methodologies involved in sample collection, hydrothermal conversion and characterisation of the solid and aqueous process streams. Following this, the methodologies used in the biological conversion of biomass and hydrothermal products are described. Finally, the calculations used to determine the energy balance of the different hydrothermal and biological conversion strategies are outlined.

3.1 Material Collection, Preparation and Storage

3.1.1 Biomass Feedstocks

Biomass feedstocks used as part of this thesis include: water hyacinth, grass and five brown macroalgal species; in order to compare the differences between species and between seasons. Table 3.1 describes the sampling dates and locations of each biomass, as well as the sample codes referred to hereafter.

Table 3.1. Sampling dates and locations for biomass.

Biomass	Collection				
	Sample Code	Location	GPS Co-ordinates	Month	Year
Water Hyacinth	WH	Lake Victoria, Uganda	0°17'21.6"N 32°39'16.6"E	December	2018
Grass	GR	UoL Campus, UK	53°48'25.9"N 1°33'18.8"W	August	2018
S. latissima	SL	Beadnell Bay, UK	-	June	2017
F. serratus	FS	Aberystwyth, UK	-	June	2015
L. digitata	LD	Clachan Sands, UK	-	January	2009
F. serratus	FS[19]	Aberystwyth, UK	52°25'11"N 4°05'16"W	July	2019
L. digitata	LD[19]	Aberystwyth, UK	52°25'11"N 4°05'16"W	July	2019

UoL=University of Leeds.

3.1.1.1 Preservation and Storage

The collected biomass samples were preserved through various drying methods. WH was air dried and oven dried to a moisture content of approximately 7% by the Centre for Research in Energy and Energy Conservation (CREEC, Makerere University Kampala, Uganda). GR, SL and LD were oven dried using at 60°C, for a minimum of 24-hrs, until constant weight was achieved. FS was air dried for 48-hrs, followed by subsequent oven drying at 50°C for approximately 24-hrs [69]. Oven dried biomass, corresponds to the 'as received' analysis of feedstocks herein. Subsequent analyses are presented on either an 'as received basis' (*ar*), 'dry basis' (*db*) or 'dry ash-free basis' (*daf*). The definitions and conversion calculations between bases are described in Appendix A.

FS[19] and LD[19] were prepared using two different methodologies. Approximately half the mass of each collected macroalgal sample was frozen (-20°C) and subsequently freeze dried. Whereas, the other half of each feedstock was submerged in seawater and stored at (4°C), to allow direct use of the wet, as received seaweeds during SE and HTC reactions; described in Chapters 7 and 8, respectively.

3.1.1.2 Particle Size Reduction

The particle size of each biomass was reduced to <1mm for HTC reactions and biomethane potential experiments. The particle size of WH was reduced to <4mm using a cutting mill (Retsch, Germany, SM300) and passed through a 1mm screen to obtain the correct particle size fraction. A NutriBullet was used to reduce the particle size of all other biomass to <1mm. The particle size of each biomass was further reduced to <100µm for proximate, ultimate and inorganic analysis. This reduction in particle size was achieved using a Cryomill (Retsch, Germany).

3.1.2 Inoculum

Inoculum was collected from the outlet of the anaerobic digester at Esholt wastewater treatment plant (WWTP) located in West Yorkshire, UK. The anaerobic digester operates under mesophilic temperatures (37°C) and processes wastewater biosolids from an urban population of approximately 750,000 people [222]. The inoculum was collected during steady-state operation of the anaerobic digester. Inoculum was passed through a 1mm sieve

to remove large particulates and stored at 4°C for approximately 1-month. Following this 1-month storage period, the inoculum was replaced with fresh samples collected from Esholt, to prevent the rate of microbial activity from slowing. It is assumed the microbial activity of the inoculum remains constant between the different time points of collection. However, the limitations of this are further discussed in Section 9.2.1.1. Prior to setting up an experimental biomethane potential or biohydrogen potential test, the inoculum was incubated at 37°C for approximately 48-hr to reduce residual methane emissions.

3.2 Hydrothermal Conversion

This section describes the different hydrothermal conversion processes investigated as part of this study, including hydrothermal carbonisation (HTC) and steam explosion (SE).

3.2.1 Hydrothermal Carbonisation

3.2.1.1 Reaction Conditions

Hydrothermal carbonisation experiments were conducted using bench-top Parr (USA) reactors. A combination of two non-stirred Parr reactors were used in this work, with volumes of; 600-mL and 2-L. The HTC reactions conducted on WH were carried out in duplicate using the 2-L reactor. Whereas, the 600-mL HTC reactor was used in the conversion of all other biomass types (SL, FS, LD, GR, FS[19] and LD[19]). Reactions for SL, FS, LD and GR were conducted in triplicate. Whereas, reactions for FS[19] and LD[19] were conducted in duplicate.

Whilst using the 600-mL reactor; 20g of oven dried biomass was added to 200-mL distilled water and whilst using the 2-L reactor; 96g biomass was added to 880-mL distilled water to achieve an approximate 10% solid loading ratio for each HTC reaction. Reactions were conducted within a custom-built quartz reactor liner to facilitate the transfer of material out of the reactor; allowing for more accurate mass balance calculations. HTC reactions were conducted at temperatures of 150°C, 200°C and 250°C; with a retention time of 60-min, once the desired temperature was reached. Temperatures of 150°C, 200°C and 250°C gave pressure gauge readings of approximately 0-bar, 14-bar and 43-bar, respectively. Reactors were heated using a surrounding heating jacket controlled by a proportional-integral-derivative (PID) controller. The heating rates of the 600-mL and 2-L reactors were approximately 8°C/min and 5°C/min, respectively. Following a 60-min retention time, the heating jacket was turned off and the reactor allowed to cool to ambient temperature.

Generally, HTC reactions were conducted on oven dried biomass. However, in the case of Chapter 8, the comparative HTC of wet seaweed in seawater and freeze dried seaweed in distilled water was conducted. 'Wet seaweed' refers to biomass which has not undergone preservation through drying, as described in Section 3.1.1.1. Seawater was collected alongside FS[19] and LD[19] biomass. The moisture content of FS[19] and LD[19] biomass was determined using a moisture analyser (Sartorius MA35) and the contents of the HTC reactor adjusted to contain 20-g of biomass solids and 200-mL of moisture. Therefore, the solid loading ratio was comparable to processing dried biomass. The particle size of the seaweeds was reduced to 5-10cm using scissors. This particle size was used for both the wet and freeze dried biomass. The moisture contents of the HTC reactor was adjusted to the correct solid loading ratio using seawater, whilst using wet seaweeds.

3.2.1.2 Mass Yields

Once cooled, HTC reactions were de-pressurised; by venting the gaseous fraction into a fume hood. The remaining solid (hydrochar) and aqueous (process water) fractions were separated through Büchner filtration through a Grade-4 Whatman® filter paper, for subsequent characterisation. The HTC products from the WH HTC reaction conducted at 150°C could not be separated through Büchner filtration, due to the absorbent, sponge-like properties of WH. Therefore, the products of this reaction were separated using a centrifuge (Sigma 4-5L) set at 4643x g, 10-min, with the process water collected through subsequent Büchner filtration. Hydrochars were dried overnight in a 60°C drying oven, with aqueous losses recorded gravimetrically. Process waters were frozen (-20°C) for preservation. Extracted HTC products were combined across reactions with the same reaction conditions to ensure enough material for characterisation and conversion.

HTC mass yields were all determined gravimetrically. Hydrochar yield (HY) was determined according to Equation 3.1. Where, *M*hc is the mass of oven dried hydrochar (g) and *M*b is the mass of oven dried biomass added to the HTC reactor (g). The gas yield was determined as the percentage difference between the total input and total output masses. Process water yield was calculated by difference.

Equation 3.1. Hydrochar Yield Calculation.

$$\text{Hydrochar Yield (\%HY)} = \frac{M\text{hc(g)}}{M\text{b (g)}} \times 100$$

3.2.1.3 Carbon Balance

The carbon distribution between the hydrochar and process water was determined by Equation 3.2 and Equation 3.3, respectively. To determine the hydrochar carbon-distribution (Equation 3.2): C%hc is the C-content of the hydrochar (% as received), *M*hc is the recovered mass of oven dried hydrochar (g), C%b is the C-content of the oven dried biomass (% as received) and *M*b is the mass of oven dried biomass added to the HTC reactions (g). The methodology used to determine C%hc and C%b is discussed in Section 3.3.1.2. To determine the process water carbon-distribution (Equation 3.3): TCpw is total carbon content of the process waters (g/L), *M*pw is the recovered mass of process water (kg), C%b is the as received C-content of the oven dried biomass and *M*b is the mass of oven dried biomass added to the HTC reactions. It is assumed 1mL of process water has mass of 1g. The methodology used to determine TCpw is discussed in Section 3.4.2.

Equation 3.2. Carbon distribution to the hydrochar.

$$\text{Carbon distribution to Hydrochar (\%)} = \frac{\left(\frac{\text{C\%hc}}{100} \times M\text{hc}\right)}{\left(\frac{\text{C\%b}}{100} \times M\text{b}\right)} \times 100$$

Equation 3.3. Carbon distribution to the process water.

$$\text{Carbon distribution to Process Water (\%)} = \frac{(\text{TCpw} \times M\text{pw})}{\left(\frac{\text{C\%b}}{100} \times M\text{b}\right)} \times 100$$

3.2.1.4 Ash Removal Efficiency

The ash removal efficiency from the biomass during HTC was calculated using Equation 3.4, where Ash%hc represents the ash content of the oven dried hydrochar (% as received), Ash%b represents the ash content of the oven dried biomass (% as received) and HY represents the hydrochar yield. The methodology used to determine Ash%hc and Ash%b is discussed in Section 3.3.1.1.

Equation 3.4. Ash removal efficiency from biomass during HTC.

$$\text{Ash Removal (\%)} = 100 - \left(\frac{\text{Ash\%hc}}{\text{Ash\%b}} \times \text{HY}\right)$$

3.2.1.5 Nitrogen Removal Efficiency

The nitrogen removal efficiency from the biomass during HTC was calculated using Equation 3.5, where N%hc represents the N-content of the oven dried hydrochar (% as received), N%b represents the N-content of the oven dried biomass (% as received) and HY represents the hydrochar yield. The methodology used to determine N%hc and N%b is discussed in Section 3.3.1.2.

Equation 3.5. Nitrogen removal efficiency from biomass during HTC.

$$\text{Nitrogen Removal (\%)} = 100 - (\frac{\text{N\%hc}}{\text{N\%b}} \times \text{HY})$$

3.2.2 Steam Explosion

Steam explosion (SE) reactions were conducted in duplicate using a 30-L thermal hydrolysis unit (Cambi, Asker, Norway) at the Institute of Biology, Environmental and Rural Sciences at Aberystwyth University (IBERS, Gogerddan, Aberystwyth University, UK). SE was conducted on WH, FS[19] and LD[19]. Oven dried WH was re-hydrated overnight, by adding approximately 8-kg of water per 1-kg of dried biomass. Whereas, wet macroalgal samples were used, as collected from the sea. A 1-kg of sample of wet biomass was added to the reactor and introduced to steam, to build the pressure of the reactor to 4.5-bar or 14.5-bar; giving approximate reaction temperatures of 150°C and 200°C, respectively. Following a 15-min retention time, the pressurised steam was rapidly released from the decompression chamber. The biomass effluent was collected and retained as a mixed slurry (solid and liquid). During SE an exogenous source of steam was introduced to the biomass. Steam can condense onto the biomass, causing water addition to the samples. Water addition during SE was calculated through the gravimetric difference of the total mass of the sample input to the SE reactor and the total mass of the effluent. A representative sub-sample of slurries were centrifuged at 4,265xg using a 4-5 L centrifuge (Sigma, Osterode am Harz, Germany), to separate the solid and aqueous fractions for characterisation. The aqueous fraction was decanted, and the residual solid pellet freeze dried using an ALPHA 1-2 LD plus freeze drier (CHRIST, Osterode am Harz, Germany) for further analysis. Solid yield was determined as the percentage mass of the remaining freeze dried solid compared to the total mass of SE slurry before centrifugation. Remaining slurries were stored in a freezer (-20°C), until required. The solid residues were combined across duplicate runs. Aqueous steams and slurries were analysed separately, in order to account for the addition of exogenous water.

3.2.3 Reaction Severity

In order to compare hydrothermal pre-treatments (HTC and SE) the severity of the pre-treatment was defined according to the severity factor (SF), shown in Equation 3.6 [211]. Here, *t* represents time (min) and *T* represents temperature (°C).

Equation 3.6. Calculation of hydrothermal reaction severity.

$$\mathrm{SF} = \log\left[\, t \times \exp\left(\frac{T - 100}{14.75}\right)\right]$$

3.3 Feedstock and Solid Residue Analysis

This section describes the characterisation methods applied to biomass feedstocks and the solid residues from HTC and SE pre-treatments.

3.3.1 Proximate, Ultimate and Biochemical Analysis

3.3.1.1 Proximate Analysis

Proximate analysis was conducted using a thermo-gravimetric analyser (TGA/DSC 1, Mettler Toledo). Approximately 10-mg of sample was accurately weighed into a pre-weighed ceramic crucible and heated according to the heating profile in Figure 3.1. Initially, the sample was heated, under nitrogen, from 25°C to 105°C at a rate of 25°C/min. The sample was held at 105°C for 10-min. Following this hold period, the sample was further heated, under nitrogen, from 105°C to 900°C at a rate of 25°C/min. Once a holding temperature of 900°C was reached, the sample was maintained at this temperature for 10-min, under nitrogen, then subsequently maintained under air, for 15-min. The sample mass was continually measured throughout the heating profile; allowing determination of the moisture, volatile matter, fixed carbon and ash fractionation of the sample.

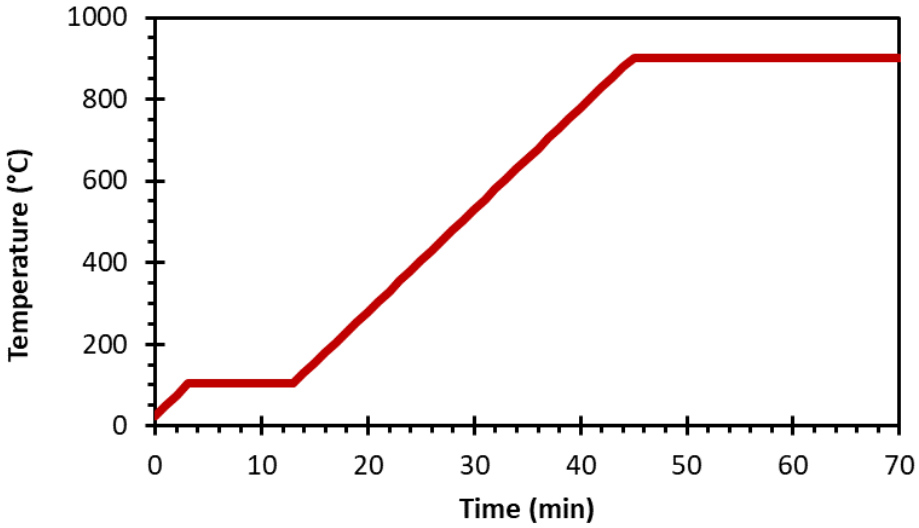

Figure 3.1. Heating profile of the thermo-gravimetric analyser for proximate analysis.

3.3.1.2 Ultimate Analysis

Ultimate analysis was conducted in duplicate, using a Flash 2000 CHNS analyser (Thermo Scientific) to determine the carbon (C), hydrogen (H), nitrogen (N) and sulphur (S) fractionation of the sample. The instrument was calibrated using certified reference materials (Elemental Microanalysis, Devon, UK). A 2-3mg sample was accurately weighed into a tin capsule before crimping to remove atmospheric air. Samples were introduced to the Flash 2000 via an autosampler, purged with Helium and combusted at 900°C, using a known quantity of oxygen. The combustion gases are converted to: carbon dioxide (CO_2), water (H_2O), nitrogen (N_2) and sulphur dioxide (SO_2). The gases then pass through a gas chromatography (GC) column to be separated and the gases detected by a thermal conductivity detector (TCD). Hydrogen-content was corrected for moisture content according to Equation 3.7. O-content can be calculated by difference, or measured directly. O-content calculated by difference was determined using Equation 3.8.

Equation 3.7. Hydrogen correction for moisture content.

$$\text{Corrected H}(\%) = \text{H}(\%) - (\text{Moisture}(\%) \times \left(\frac{2}{18}\right))$$

Equation 3.8. Calculation of oxygen-content, by difference, on an as received basis.

$$\text{O}(\%) = 100 - (\text{Moisture}\ (\%) + \text{Ash}\ (\%) + \text{C}(\%) + \text{H}(\%) + \text{N}(\%) + \text{S}(\%))$$

The Flash 2000 CHNS analyser was also fitted with an additional reactor which allowed O-content to be measured directly. Direct oxygen analysis was conducted in duplicate using the Flash 2000 elemental analyser, as a separate analysis to CHNS. Approximately 5mg of sample was accurately weighed into a silver capsule and crimped to remove atmospheric air. Samples were introduced to the Flash 2000 via an autosampler, purged with Helium and pyrolysed at 1060°C. Pyrolysis gases (CO, CO_2 and H_2O) were converted to carbon monoxide and quantified using GC with a TCD detector. O-content measured directly was corrected for moisture according to Equation 3.9. For selected samples, the O-content measured directly and by-difference was compared.

Equation 3.9. Oxygen correction for moisture content, if O-content is measured directly.

$$\text{Corrected O}(\%) = \text{O}(\%) - (\text{Moisture}(\%) \times \left(\frac{16}{18}\right))$$

3.3.1.3 Total Solids and Volatile Solids

Total solids (TS) and volatile solids (VS) of the untreated biomasses (SL, FS, LD, FS[19], LD[19], WH and GR) and hydrochars produced from both WH and GR were determined in duplicate according to APHA (2005), method 2540E [223]. Approximately 1g of sample was dried at 105°C (Memmert Drying Oven) with subsequent ashing at 550°C (Nabertherm B180 furnace). The TS of SE slurries were determined by drying at 60°C to reduce losses of volatile components. Approximately 20g of SE slurry was used for TS and VS analysis.

The VS-content of hydrochars produced from macroalgal biomass (SL and FS) were determined through the summation of fixed carbon and volatile matter, obtained by TGA proximate analysis (Figure 3.1), on an as received basis.

The VS-content of HTC slurries were calculated by determining the VS of the hydrochar and process water separately, before re-introducing the products as a mixed slurry, based on the yields obtained during HTC reactions.

The TS and VS-content of the inoculum was calculated by drying approximately 25mL of sample at 105°C (Memmert Drying Oven) with subsequent ashing at 550°C (Nabertherm B180 furnace).

3.3.1.4 Biochemical Composition

The neutral detergent fibre (NDF), acid detergent fibre (ADF) and acid detergent lignin (ADL) was determined for WH and GR biomass. Analysis was conducted externally by the University of Aberystwyth, using the Gerhardt Fibrecap system. Cellulose was determined as the difference between ADF and ADL. Hemicellulose was determined as the difference between NDF and ADF. Lignin was determined as equivalent to ADL

3.3.2 Inorganic Analysis

3.3.2.1 Inorganic Composition

The composition of the inorganic fraction of the biomass samples and solid residues were determined using X-ray fluorescence (XRF) spectroscopy (ZSX Primus II, Rigaku). Samples were prepared for XRF analysis by forming a pressed pellet.

The preparation of pressed pellets involved the weighing of 2.7g of sample and 0.3g of CEREOX® wax binder (FLUXANA®) into a sample container (MU-S Container, FLUXANA®). Three polyamine mixing balls (MU-MB-380-1, FLUXANA®) were added to the containers and the contents thoroughly mixed using a vortex mixer (MU-K-MIXER_50Hz, FLUXANA®) for approximately 5-min. The homogenised samples and binder were passed through a common kitchen sieve, to remove the mixing balls and transferred into a 35-mm steel pressing die. The die was compressed using 10-t of pressure, for approximately 5-min, using a Specac press. The pressed pellets were analysed using an ZSX Primus II, XRF analyser (Rigaku), using the EZ-Scan function. Sample and binder masses were included in the software calculation. The inorganic composition data was extracted in both elemental and oxide form.

3.3.2.2 Further Analysis of the Inorganic Content of Macroalgae

The characteristics of ashes produced from selected macroalgal species (SL, FS and LD) were further investigated. The changing carbon-content of seaweed derived-ashes was determined through sequential ashing and CHNS analysis. Initially, 1g of each seaweed was placed in a furnace at 550°C, 2-hrs (Nabertherm B180 furnace). Once cool, the ash content was determined through gravimetric difference and the C-content of the ash measured using a

Flash 2000 CHNS analyser. The ash was returned to the furnace for an additional 2-hrs and the analysis repeated to obtain the ash characteristics after 4-hrs and 6-hrs of ashing.

The reduction of macroalgal biomass ash content at increased residence times was also investigated through thermo-gravimetric analysis. Macroalgal samples (SL, FS and LD) were placed in a Nabertherm B180 furnace at 550°C, 2-hrs to obtain an ash. Approximately 400-mg of the generated ash was introduced to a TGA (Netzsch STA449) maintained at 550°C in air and the mass loss of the ash recorded over a 12-hr period.

3.3.3 Combustion Properties of Biomass and Hydrochars

3.3.3.1 Higher Heating Value and Energy Densification

The higher heating value (HHV) of feedstocks and solid residues was calculated according to Dulong's equation used by [64,80], shown in Equation 3.10. The Dulong's equation is based on the elemental composition of the sample and assumes the heat of combustion of a sample is equal to the combustion of its elements. HHV values were reported on a dry basis, unless otherwise specified. The methodology used in the conversion of analyses from an as received basis to a dry basis is outlined in Appendix A. The O-content applied to Dulong's equation was typically measured directly, unless otherwise specified. The HHV of GR and GR-derived hydrochars was calculated using Dulong's equation, using the O-content measured by difference. Appendices B and C display example calculations of determining HHV using Dulong's equation using O-content measured by difference and directly, respectively. The HHV obtained from the Dulong's equation were used in further energy balance calculations.

Equation 3.10. Dulong's equation for calculating HHV.

$$\mathrm{HHV(MJ/kg)} = \left(0.3383 \times \mathrm{C}(\%)\right) + \left(1.422 \times \left(\mathrm{H}(\%) - \left(\frac{\mathrm{O}(\%)}{8}\right)\right)\right)$$

The gross calorific value (GCV) of selected samples were determined by bomb calorimetry. GCV of samples were measured using a Parr (USA) 6200 bomb calorimeter, according to BS ISO 1928:2009. The GCV was corrected for the formation of nitric and sulphuric acid during the bomb calorimeter tests. The formation of these gases were corrected by applying a correction factor for the nitrogen and sulphur contents of the sample, determined by ultimate analysis, as outlined in BS ISO 1928:2009 [224].

The energy densification (ED) of the hydrochar, compared to the original feedstock was calculated according to Equation 3.11 [195]; using the HHV calculated from Equation 3.10 on a dry basis (*db*). The energy yield (EY) obtained from the hydrochars was determined using Equation 3.12 [195]; where ED represents the energy densification (Equation 3.11) and HY represents the hydrochar yield (Equation 3.1).

Equation 3.11. Calculation of the energy densification of hydrochars.

$$\mathrm{ED} = \frac{\mathrm{HHV\ of\ Hydrochar}}{\mathrm{HHV\ of\ Feedstock}}$$

Equation 3.12. Calculation of the energy yield obtained from hydrochars.

$$\mathrm{EY} = \mathrm{ED} \times \mathrm{HY}\ (\%)$$

3.3.3.2 Slagging and Fouling Indices

The slagging and fouling propensity of biomass and hydrochars were estimated using the predictive indices displayed in Table 3.2 [64]. Indices include: Alkali index (AI), bed agglomeration index (BAI), acid base ratio (Rb/a), slagging index (SI), fouling index (FI), and slag viscosity index (SVI). Originally derived from the combustion behaviour of coal, the indices are calculated using the inorganic composition of the biomass in the form of oxides. The composition of oxides of each biomass or hydrochar was determined by XRF, according to Section 3.3.2.1. The S-content required to calculate the SI was also determined by XRF. The interpretation of each index is displayed in Table 3.2.

Table 3.2. Predictive slagging and fouling indices.

Slagging/fouling Indices	Indices Initials	Equation	Analysis
Alkali index	AI	$\frac{kg\ (K_2O + Na_2O)}{GJ}$	AI < 0.17 safe combustion AI > 0.17 <0.34 probable slagging and fouling AI > 0.34 almost certain slagging and fouling
Bed agglomeration index	BAI	$\frac{\%(Fe_2O_3)}{\%(K_2O + Na_2O)}$	BAI < 0.15 bed agglomeration likely
Acid base ratio	$R\frac{b}{a}$	$\frac{\%(Fe_2O_3 + CaO + MgO + K_2O + Na_2O)}{\%(SiO_2 + TiO_2 + Al_2O_3)}$	$R\frac{b}{a}$ < 0.5 low slagging risk
Slagging index	SI	$\left(\frac{\%(Fe_2O_3+CaO+MgO+K_2O+Na_2O)}{\%(SiO_2+TiO_2+Al_2O_3)}\right)$ * %S (dry)	SI < 0.6 low slagging indication SI > 0.6 < 2.0 medium slagging indication SI > 2.0 high slagging indication
Fouling index	FI	$\left(\frac{\%(Fe_2O_3+CaO+MgO+K_2O+Na_2O)}{\%(SiO_2+TiO_2+Al_2O_3)}\right) * \%(K_2O + Na_2O)$	FI < 0.6 low fouling FI > 0.6 < 40.0 medium fouling FI > 40.0 high fouling
Slag viscosity index	SVI	$\frac{(\%SiO_2 * 100)}{\%(SiO_2 + MgO + CaO + Fe_2O_3)}$	SVI > 72 low slagging indication SVI > 65 < 72 medium slagging indication SVI < 65 high slagging indication

3.3.3.3 Ash Fusion Test

Ash fusion tests were conducted in duplicate, in accordance with DD CEN/TS 15370-1:2006 using an ash fusibility test furnace (CAF, Carbolite). The ash fusion test provides further information of the slagging behaviour of a fuel. Ash was generated from samples by heating at 550°C for 2-hrs using a Nabertherm B180 furnace. The residual ashes were mixed with 10% dextrin solution to create a paste, which was formed into cylindrical test pieces using a sample mould. Test pieces were allowed to dry overnight before analysis.

Test pieces were introduced to the Carbolite furnace, where samples were heated in an oxidising environment, from 550°C to the furnace limit of 1550°C at a rate of 7°C minute^{-1}. A digital camera was mounted to the front of the furnace to take photographs of the test pieces during every 5°C increase in furnace temperature. The key stages of ash transformation were identified according to DD CEN/TS 15370-1:2006: shrinkage, deformation, hemisphere and

flow. A depiction of these stages is shown in Figure 3.2. The transition temperature between each ash transformation stage was reported to the nearest 10°C, in accordance with DD CEN/TS 15370-1:2006. Due to the complex nature of the samples, the 'shrinkage' phase could not be identified for all samples.

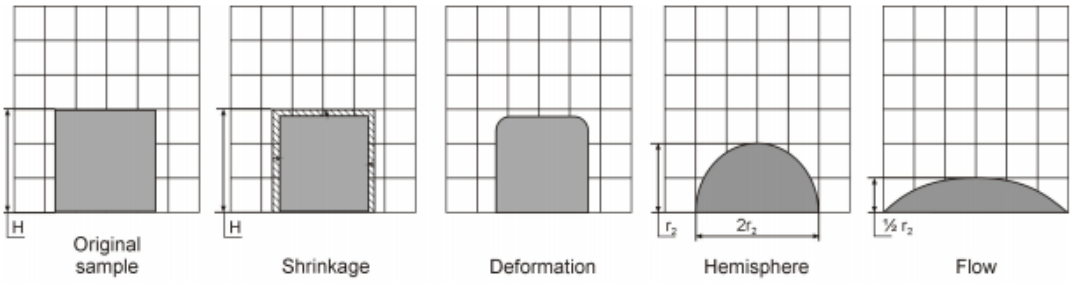

Figure 3.2. The different stages of ash transformation during ash fusion testing. Sourced from DD CEN/TS 15370-1:2006 [225].

3.4 Aqueous Residue Analysis

The following section outlines the methodologies used to characterise the aqueous fractions obtained from HTC and SE.

3.4.1 Chemical Oxygen Demand, Total Phenols, Total Nitrogen and Ammonium-Nitrogen

Chemical oxygen demand (COD), total phenols (TP), total nitrogen (TN) and ammonium-nitrogen (NH_4^+-N) were determined using HACH-Lange cuvettes: LCK014, LCK346, LCK338 and LCK303, respectively. A combination of the HACH HT200S and Dr Lange LT 100 Thermostat heating blocks were used to heat the LCK014 and LCK338 cuvettes to their recommended conditions. A combination of DR3900 and Dr Lange Lasa 100 UV-Vis spectrophotometers were used to measure the absorbance of the individual HACH cuvettes.

3.4.2 Total Organic Carbon

Total organic carbon (TOC) concentration of aqueous residues were determined differentially using a HACH IL 500 TOC-TN analyser. The differential method determines the total carbon (TC) and total inorganic carbon (TIC) concentration of the sample; with TOC calculated as the difference between TC and TIC. TC content is determined through combustion (950°C)

of the sample, where any carbon is converted to carbon dioxide. Gaseous products are subsequently passed to a non-dispersive infra-red (NDIR) detector to be quantified. Carbon dioxide concentrations are proportional to the carbon content of the sample. TIC concentration is determined through introducing the sample to acid, which reacts with the inorganic carbon to form carbon dioxide; which is quantified by the NDIR detector. TOC analysis was based upon multiple injections until a maximum standard deviation of ±2% was achieved.

3.4.3 pH

The pH of the aqueous samples were measured using a digital pH meter (HQ11D, HACH).

3.4.4 Total Solids and Volatile Solids

The TS and VS concentrations of the aqueous residues were determined following an adapted method from APHA [223]. Approximately 5-mL of aqueous samples were accurately weighed and dried at 60°C (Memmert Drying Oven) to determine the Total Solids (TS). A drying temperature of 60°C was selected over 105°C; as per the standard, to reduce the losses of volatile compounds. After drying, samples were subsequently heated at 550°C for 2-hour (Nabertherm B180 furnace) and recorded gravimetric losses used to determine the VS-content.

3.4.5 Volatile Fatty Acids

The volatile fatty acid (VFA) composition of the process waters was determined through gas chromatography (GC, Agilent 7890 A) with flame ionisation detection (FID), according to [226]. Initially, samples were acidified to pH 2.0 ± 0.1 using phosphoric acid, centrifuged (16,000x *g*, 5-min) and passed through a 0.2µm syringe filter into a GC vial. A 10µl sample was automatically injected onto a DB-FFAP column (30m, 0.32mm ID, 0.5µm film), using a 5:1 split ratio and an inlet temperature of 150°C. Helium was used as a carrier gas, at a flow rate of 10mL/min. The oven heating profile was hold at 60°C for 4-min, ramp at 10°C/min to 140°C, ramp at 40°C/min to 200°C and hold for 5-min. The FID detector was maintained at 200°C with Nitrogen make-up gas. The GC was calibrated with SUPELCO Volatile Acid Standard Mix. Total VFA was calculated through the summation of the concentrations of;

acetic, propionic, isobutyric, butryric, isovaleric, valeric, isocaproic, caproic and heptanoic acids, on a mass basis (mg/L).

3.4.6 Sugars

The sugar composition of the aqueous phases was determined using a high-performance liquid chromatography (HPLC) system (UltiMate 3000, Thermoscientific) equipped with a refractive index detector (Shodex RI-101, Japan). Samples were previously passed through a 0.45µm syringe filter. A 10µl aliquot of sample was injected onto a Supelcogel C-610H column (30cm x 7.8mm), maintained at 30°C using a column oven (Shimadzu CTO-10AC, Japan). A 0.1% H_3PO_4 mobile phase was used, set at a flow rate of 0.5 mL/min. Total sugar concentration was calculated through the summation of the concentrations of: glucose, maltose, lactose, fructose and arabinose.

3.4.7 Aldehydes

The concentrations of the aldehydes; 5-hydroxymethylfurfural (HMF) and furfural were determined though gas chromatography-mass spectrometry (GC-MS) using a Shimadzu 2010QE GC-MS (Shimadzu, Kyoto, Japan). A 1µl aliquot of sample was injected onto a Restex wax capillary column (Rtx®-Wax; 30-m, 0.25-mm ID and 0.25-µm film) using a split ratio of 10:1 and a GC inlet temperature of 250°C. The heating programme started at 40°C and was ramped to 220°C at a rate of 20°C/min and a final hold time of 5-min. Helium as used as the carrier gas. The mass spectrometer transfer line and ion source were held at 200°C, with a solvent delay of 2.6min. Electron impact ionization was employed at 70eV and the data was acquired in scan mode (35–500 m/z).

3.4.8 Process Water Derivatization (GC-MS)

Additional compounds were identified in the process waters using a derivatization method with methyl chloroformate (MCF); optimised by Madsen *et al.* [227], and subsequent GC-MS analysis. A 200µl aliquot of process water was mixed with 40µl sodium hydroxide (5% w/w), 200µl methanol and 50µl pyridine. MCF was added in two parts (2 x 25µl). The samples were vortexed (30s) after each addition of MCF using a Mini Vortex Mixer (Fisher Scientific). 400µl of chloroform containing 4-bromotoulene (20.8 µg/mL) was added and vortexed (10s).

Finally, 400µl of sodium bicarbonate solution (50 mM) was added and vortexed (10s). The top-floating aqueous layer was removed and discarded. The remaining chloroform layer was transferred into a GC vial containing an insert for GC-MS analysis.

GC-MS analysis was conducted using a Shimadzu 2010QE GC-MS (Shimadzu, Kyoto, Japan). A 1µl aliquot of sample was injected onto a Restex capillary column (Rtx®-5; 60-m, 0.25-mm ID and 0.25-µm film) using a split ratio of 50:1 and a GC inlet temperature of 260°C. The heating programme started at 60°C and was ramped to 300°C at a rate of 5°C/min and a final hold time of 3-min. Helium as used as the carrier gas.

3.4.9 Proximate and Ultimate Analysis

Determination of the proximate and ultimate composition of HTC process waters was conducted by drying a known volume (c. 10mL) of process water at 60°C for approximately 48-hrs. The dried residue was analysed by TGA (Section 3.3.1.1) and by Flash 2000 Elemental analysis (Section 3.3.1.2) to determine the proximate and ultimate composition. Oxygen-content was calculated by difference.

In order to account for evaporative organic losses during the drying process, a separate aliquot (c. 10mL) of each process water was dried at 60°C for approximately 48-hrs. Evaporative losses of water and potential organics were determined by gravimetric difference. The dried residues were then rehydrated using the exact mass of water lost during the drying process. TOC of the rehydrated process waters were then measured (Section 3.4.2) and compared to the original TOC value before drying. Losses in TOC concentration were assumed to be proportional to the loss of organic matter during drying. The resulting ultimate (CHNS) values of the process waters were corrected for these evaporative losses. The influence of these evaporative losses are further explored in Chapter 5.

3.5 Biological Conversion

A number of biological conversion methods were applied for biomass samples and products following hydrothermal treatment. This includes (i) biomethane production through anaerobic digestion; AD (ii) biohydrogen production through dark fermentation; DF and (iii) combined biohydrogen and biomethane production through two-stage digestion; sequential DF and AD. All biological conversion routes were measured using an Automatic Methane Potential Test

System II (AMPTS II, Bioprocess Control, Lund, Sweden), as shown in Figure 3.3. The AMPTS II is comprised of three units: a water bath containing the batch reactors, a CO_2 removal system and a gas collection and measurement unit. The AMPTS II has the capacity to analyse 15 different samples simultaneously. The batch bioreactors were incubated by a water bath, under mesophilic conditions (37°C) and agitated for 60-s every 10-min, using an automated stirrer. Biogas generated from each reactor passes along Tygon® tubing to the CO_2 removal system. This system contains a 3M NaOH solution which removes CO_2 and other acidic gases from the biogas, by diffusion. The remaining biomethane continues to the gas measurement unit, where the volume of methane is measured by liquid displacement and normalised to standard conditions (1atm, 0°C, zero moisture content). A modified methodology was applied for the determination of biohydrogen yields from feedstocks; outlined in Section 3.5.2 and Chapter 6.

Figure 3.3. Automatic Methane Potential Test System II.

3.5.1 Biomethane Potential

3.5.1.1 Theoretical Biomethane Potential

The theoretical biomethane potential (BMP_{th}) of samples were determined stoichiometrically from the elemental composition of the sample, using the Boyle's equation; Equation 3.13 [100,170] and the Buswell Equation; Equation 3.14 [170]. Where; *c*, *h*, *o* and *n* represent the molar fraction of C, H, O and N, respectively. Both the Boyle's and the Buswell equations have the units; mL CH_4/g VS and assume 1-mol of gas (0°C, 1-atm) has a volume of 22,400mL, under normalised conditions. Boyle's equation was developed in 1977 [228], following a modification of the Buswell Equation. The Buswell equation is a stoichiometric

equation developed in 1952 by Buswell and Mueller [99] which calculates the complete microbial metabolism of organic matter to CO_2 and CH_4. Boyle's equation has been suggested to be a more accurate representation of theoretical biomethane generation [170], as the Boyle's equation accounts for the nitrogen-containing fractions of biomass, such as protein [100]. Therefore, the Boyle's equation is mainly used throughout this thesis.

Equation 3.13. Boyle's Equation for theoretical biomethane potential (BMP_{th}) determination.

$$\mathrm{BMP_{th}\ Boyle's\ (mL\ CH_4/\ gVS)} = \frac{22\,400\left(\frac{c}{2}+\frac{h}{8}-\frac{o}{4}-\frac{3n}{8}\right)}{12c+h+16o+14n}$$

Equation 3.14. Buswell Equation for theoretical biomethane potential (BMP_{th}) determination.

$$\mathrm{BMP_{th}\ Buswell\ (mL\ CH_4/\ gVS)} = \frac{22\,400\left(\frac{c}{2}+\frac{h}{8}-\frac{o}{4}\right)}{12c+h+16o}$$

The Boyle's equation assumes complete stoichiometric conversion of a substrate [97] with no differentiation between biodegradable and non-biodegradable matter [100]. Therefore, BMP_{th} was assumed to be the maximum achieveable biomethane potential.

The comparative BMP_{th} of HTC process waters was determined using the Boyle's equation (Equation 3.13), as well as the theory that 1g COD theoretically yields 350mL CH_4, under standard conditions [97]. The utilisation of both methodologies is further discussed in Chapter 6.

3.5.1.2 Experimental Biomethane Potential

The experimental biomethane potential (BMP_{ex}) was determined for all samples using an AMPTS II (Figure 3.3) maintained at 37°C for a 30-day retention time, unless otherwise specified. For solids samples and slurries, a 2:1 inoculum-to-substrate ratio (ISR), on a VS basis was used by diluting samples to 10 g VS/L and inoculum to 20 g VS/L, using distilled water, unless otherwise specified. A 200mL aliquot of both sample and inoculum was added to each reactor to create a 400mL working volume; and a 100mL headspace. Blank reactors were run in parallel with each BMP_{ex} experiment to account for the residual biomethane emissions from the inoculum. Blank reactors contained only inoculum (200mL at 20g VS/L)

and distilled water (200mL). The volume of biomethane generated from solid and slurry samples were normalised to be expressed on a VS basis, using Equation 3.15. Where, $V\mathrm{CH_4}$Sample is the volume of biomethane originating from the sample (mL), $V\mathrm{CH_4}$Blank is the volume of biomethane originating from the blank (mL), *C*VS represents the concentration of volatile solids added (10 g VS/L) and *V*sample is the volume of sample added to the reactor (0.2 L).

Equation 3.15. Calculation of experimental biomethane potential ($\mathrm{BMP_{ex}}$) determination of solid samples and residues.

$$\mathrm{BMP_{ex}\ Solids} = \frac{(V\mathrm{CH_4Sample} - V\mathrm{CH_4Blank})}{C\mathrm{VS}\ \times V\mathrm{Sample}}$$

For aqueous samples, a 2:1 ISR, on a COD basis was used by diluting samples to 10 g COD/L and inoculum to 20 g COD/L, using distilled water. A 200mL aliquot of both sample and inoculum were added to each reactor. Again, blank reactors were run in parallel, containing only inoculum (200mL at 20g COD/L) and distilled water (200mL). The volume of biomethane generated from aqueous samples were normalised to be expressed on a COD basis, using Equation 3.16. Where, $V\mathrm{CH_4}$Sample is the volume of biomethane originating from the sample (mL), $V\mathrm{CH_4}$Blank is the volume of biomethane originating from the blank (mL), *C*COD represents the concentration of volatile solids added (10 g COD/L) and *V*sample is the volume of sample added to the reactor (0.2 L).

Equation 3.16. Calculation of experimental biomethane potential ($\mathrm{BMP_{ex}}$) determination of aqueous residues.

$$\mathrm{BMP_{ex}\ Aqueous\ Residues} = \frac{(V\mathrm{CH_4Sample} - V\mathrm{CH_4Blank})}{c\mathrm{COD}\ \times V\mathrm{Sample}}$$

The headspace of each reactor was flushed with nitrogen gas to ensure anaerobic conditions. The pH of the reactors remained unadjusted. All measured gas volumes were automatically normalised to standard conditions (1 atm, 0°C and zero moisture content). Reactions were conducted in duplicate, with the average values reported alongside the maximum and minimum values.

3.5.1.3 Biodegradability Index

The biodegradability index (BI); derived from [40] defines the methane conversion efficiency of a sample. The BI was calculated using Equation 3.17 and expressed as a percentage (%).

Equation 3.17. Calculation of Biodegradability Index.

$$\mathrm{BI} = \frac{\mathrm{BMP_{ex}}}{\mathrm{BMP_{th}}} \times 100$$

3.5.2 Biohydrogen Potential

The experimental biohydrogen potential (BHP_{ex}) of samples was determined using an AMPTS II using a similar methodology used to determine BMP_{ex}: described in Section 3.5.1.2. Although, the methodology is slightly modified to facilitate biohydrogen generation, rather than biomethane generation. Prior to starting a BHP_{ex} experiment, the inoculum was heat-treated using an autoclave (CertoClav, A-4050) maintained at 115°C, 30-min to inhibit methanogens and select for hydrogen-producing micro-organisms. Reactors were set-up in a similar manner to in Section 3.5.1.2, however the reactor contents were adjusted to pH 6.0 ± 0.1 using phosphoric acid. Reactions were typically run in triplicate, for 5-day duration. Biohydrogen production was confirmed using a sodium acetate standard. The confirmation of biohydrogen generation is further discussed in Chapter 6.

The volume of biohydrogen generated from solid samples were normalised to be expressed on a VS basis, using Equation 3.18. Where, $V\mathrm{H_2Sample}$ is the volume of biohydrogen originating from the sample (mL), $V\mathrm{H_2Blank}$ is the volume of biohydrogen originating from the blank (mL), CVS represents the concentration of volatile solids added (10 g VS/L) and Vsample is the volume of sample added to the reactor (0.2 L).

Equation 3.18. Calculation of experimental biohydrogen potential (BHP_{ex}) determination of solid samples.

$$\mathrm{BHP_{ex}\ Solids} = \frac{(V\mathrm{H_2Sample} - V\mathrm{H_2Blank})}{C\mathrm{VS} \times V\mathrm{Sample}}$$

The volume of biohydrogen generated from aqueous samples were normalised to be expressed on a COD basis, using Equation 3.19. Where, $V\mathrm{H_2Sample}$ is the volume of biohydrogen originating from the sample (mL), $V\mathrm{H_2Blank}$ is the volume of biohydrogen originating from

the blank (mL), *C*COD represents the concentration of volatile solids added (10 g COD/L) and *V*sample is the volume of sample added to the reactor (0.2 L).

Equation 3.19. Calculation of experimental biohydrogen potential (BHP_{ex}) of aqueous residues.

$$\mathrm{BHP_{ex}\ Aqueous\ Residues} = \frac{(V\mathrm{H_2Sample} - V\mathrm{H_2Blank})}{C\mathrm{COD}\ \times V\mathrm{Sample}}$$

3.5.3 Two-stage Digestion

Two-stage digestion involves the sequential production of biohydrogen during DF and biomethane during conventional AD. Batch two-stage digestions of selected solid residues were conducted in triplicate using an AMPTS II. The first stage; DF was conducted according to the specifications described in Section 3.5.2. However, only half of the working volume of the reactor was used (200mL), with slightly different solid loading masses. The sample and inoculum was diluted to 15g VS/L and 30g VS/L, respectively and a 100mL aliquot added to the batch reactors. Therefore, maintaining a 2:1 ISR. The DF stages were conducted at 37°C for 5-days. The yields of biohydrogen were calculated according to Equation 3.18. However, in this case, *C*VS was 15 g VS/L and *V*sample was 0.1 L. Following incubation, the reaction was stopped and a 5mL aliquot of digestion medium collected for VFA analysis. Subsequently, un-conditioned, methanogen-containing inoculum was diluted to 15 g VS/L using distilled water and 200mL added to each reactor to create an approximate 2:1 ISR. The same volume and concentration of un-conditioned inoculum was added to the blank reactors to account for residual biomethane production. For the second stage, biomethane potential yields were determined performed using an AMPTS II, maintained at 37°C. Due to time restrictions, the second AD stage was conducted for only 14-days. Biomethane yields were calculated according to Equation 3.15. However, in this case, *C*VS was 15 g VS/L and *V*sample was 0.1 L.

3.5.4 Modelling of Digestion Kinetics

3.5.4.1 Modified Gompertz Model

The modified Gompertz model; as described by Equation 3.20, was used to fit the cumulative BMP_{ex} curves to describe the process kinetics [229]. Where, H_m is the maximum biomethane

yield (mL CH_4/g VS), R_m is the peak biomethane production rate (mL CH_4/g VS/d), λ is the lag phase (d), t is the time (d) and e=2.71828 [179,230]. The parameters: H_m, R_m and λ were estimated by the least squares method using the Solver Function in Microsoft Excel [44]. The accuracy of the modified Gompertz model fit was determined through a squared correlation coefficient (R^2) between the experimental and model data.

Equation 3.20. Modified Gompertz equation.

$$H = H_m \exp[-\exp(\frac{R_m e}{H_m}(\lambda - t) + 1)]$$

The modified Gompertz model was also used to fit the cumulative BHP_{ex} curves, again using the least squares method in Microsoft Excel. Here, H_m represents the maximum biohydrogen yield (mL H_2/g VS), R_m is the peak biohydrogen production rate (mL H_2/g VS/hr), λ is the lag phase (hr), t is the time (hr) and e=2.71828 [179,230].

3.5.4.2 Peak Time of Digestion

The peak time of fermentation (T_m) can be identified by Equation 3.21 [229]. Prediction of T_m uses parameters defined by the modified Gompertz equation. Here, H_m is the maximum biomethane yield (mL CH_4/g VS), R_m is the peak biomethane production rate (mL CH_4/g VS/d), λ is the lag phase (d) and e=2.71828 [179,230]. A lower T_m is preferable, linked to an increased digestion rate; indicative of reduced retention times in larger-scale systems.

Equation 3.21. Calculation of the peak time of fermentation.

$$T_m = \frac{H_m}{R_m e} + \lambda$$

Equation 3.21 can also be used to predict the peak time of fermentation for BHP_{ex} curves. Where, H_m is the maximum biohydrogen yield (mL H_2/g VS), R_m is the peak biohydrogen production rate (mL H_2/g VS/hr), λ is the lag phase (hr) and e=2.71828 [179,230].

3.5.4.3 Technical Digestion Time

The technical digestion time (T^{80}) is reported as the time duration taken for the digestion to generate 80% of the total cumulative yield [226]. This was reported for both BMP_{ex} and BHP_{ex} curves.

3.6 Energy Balance

The energy balance was calculated for both HTC and SE hydrothermal processes. This included an assessment of energy input: the energy required to heat the contents of the hydrothermal reactors and energy output recovered from the conversion of the hydrothermal products.

3.6.1 Energy Input

3.6.1.1 HTC Energy Input

The energy input of the HTC reactor is based on the energy required to heat the contents of the biomass and water within the reactor, based on 1-kg of oven dried biomass as a starting material. The term 'oven dried' biomass refers to the biomass once it has been preserved, as described in Section 3.1.1.1. Therefore, the moisture contents of the biomass ranged from approximately 5-9%. The energy input associated with AD has not been considered as part of this study. HTC energy input was calculated according to Equation 3.22, adapted from [72]. Here, *V*w is the volume of water added to the HTC reactor (L), *C*w and *C*b represent the specific heating capacities (MJ/kg/K) of water and biomass, respectively, *M*b is the mass of oven dried biomass added to the HTC reactor (kg), *T*reac is the final temperature of the reaction (°C) and *T*amb is the ambient temperature; assumed to be 25°C. Water had an assumed specific heating capacity of 4200 J/kg/K [72] and biomass was 1455 J/kg/L [177]. In addition, 1 mL of water had an assumed mass of 1g.

Equation 3.22. Calculation of HTC energy input.

$$\text{Energy Input HTC (MJ/kg)} = \frac{(VwCw + MbCb) \times (T\text{reac} - T\text{amb})}{Mb}$$

3.6.1.2 Steam Explosion Energy Input

The energy input for SE was determined by the combined energy required to generate enough steam to pressurise the reactor and the energy required to heat the biomass added to the SE reactor to the desired temperature. The energy input was calculated according to the operational parameters and loading rates according to Section 3.2.2, but then divided by the mass of the dry fraction of biomass, to obtain comparable units to the energy input of HTC (MJ/kg). Wet biomass was added to the SE reactor, with moisture contents of 76% (FS[19]), 87% (LD[19]) and assumed at 90% (WH). SE energy input was calculated using Equation 3.23. It is assumed that pressurised steam will occupy 29-L of the 30-L SE reactor volume and the 1-kg of wet biomass sample; will occupy a 1-L volume within the reactor. It is also assumed there will be 20% vapour losses during the heating of the reactor [231].

For Equation 3.23, *Vs* is for the volume of the steam in the SE reactor (0.029-m^3), ρ is the density of steam at the desired pressure (kg/m^3) and *h* is the specific enthalpy of steam (MJ/kg) at the desired pressures. Values for steam characteristics; ρ and *h* were extracted from [232], no information was available for steam pressures at 14.5-bar, therefore ρ and *h* values for steam at 14-bar were used. Additionally; *Vw* is the volume of water in the rehydrated biomass added to the SE reactor (L), *Cw* is the specific heat capacity of water (MJ/kg/K), *Mb* is the dry fraction mass of the biomass added to the SE reactor (kg), *Cb* is the specific heat capacity of biomass (MJ/kg/K), *T*reac is the final temperature of the reaction (°C) and *Tamb* is the ambient temperature (assumed 25°C).

Equation 3.23. Calculation of SE energy input.

$$\text{Energy Input SE (MJ)} = \frac{\left((Vs \times 1.2) \times \rho\right) \times h) + ((Vw Cw + Mb Cb)) \times (T\text{reac} - T\text{amb}))}{Mb}$$

3.6.2 Energy Output

The energy output from the AD of untreated biomass and each integration strategy is detailed as part of this section. Throughout this Section it is assumed the HHV of methane is 39.8 MJ/m^3 and hydrogen is 12.7 MJ/m^3 [233].

The energy output from the AD of un-treated feedstocks is based upon the calorific value of the biomethane produced from a starting material of 1-kg of oven dried feedstock. This was calculated using Equation 3.24. Here, *M*b is the starting mass of oven dried biomass (1-kg), VS is the volatile solid content (%*ar*), BMP_{ex} is the experimental biomethane potential (L CH_4/kg VS) and 39.8 denotes the assumed HHV of methane (MJ/m^3).

Equation 3.24. Calculation of energy output obtained from the AD of untreated biomass.

$$\text{Energy Output AD Biomass (MJ/kg)} = \frac{(M\text{b} \times \frac{\text{VS}}{100} \times \text{BMP}_{\text{ex}})}{1000} \times 39.8$$

The energy output from the DF of un-treated feedstocks is based upon the calorific value of the biohydrogen produced from a starting material of 1-kg of oven dried feedstock. This was calculated using Equation 3.25. Here, *M*b is the starting mass of oven dried biomass (1-kg), VS is the volatile solid content (%*ar*), BHP_{ex} is the experimental biohydrogen potential (L H_2/kg VS) and 12.7 denotes the assumed HHV of hydrogen (MJ/m^3).

Equation 3.25. Calculation of energy output obtained from the DF of untreated biomass.

$$\text{Energy Output DF Biomass (MJ/kg)} = \frac{\left(M\text{b} \times \frac{\text{VS}}{100} \times \text{BHP}_{\text{ex}}\right)}{1000} \times 12.7$$

The calculation of energy output obtained from the two-stage digestion of untreated biomass was obtained through the addition of Equation 3.24 and Equation 3.25.

3.6.2.1 HTC Energy Output

The energy output from HTC was based upon a starting point of 1-kg of oven dried feedstock, processed using an approximate 10% solid-loading-ratio. Multiple integration strategies exist; alongside the potential for multiple energy vectors. The energy output of these energy vectors were determined using the same unit (MJ/kg) to allow direct cross-comparisons of integration options. The residual masses of hydrochars and process waters were calculated based on a starting material of 1-kg oven dried biomass, using yield data extrapolated from the HTC reactions described in Section 3.2.1.2.

The energy output obtained from the combustion of the residual hydrochar after HTC, was calculated according to Equation 3.26. Here, *M*hc represents the residual mass of oven dried hydrochar (kg) recovered after HTC of 1-kg of oven dried biomass and HHV is the higher heating value of the hydrochar, on an as received basis (MJ/kg), calculated using Dulong's equation.

Equation 3.26. Calculation of energy output obtained from the combustion of hydrochars.

$$\text{Energy Output Hydrochar Combustion (MJ/kg)} = M\text{hc} \times \text{HHV}$$

The energy output obtained from the AD of the residual hydrochar after HTC, was calculated according to Equation 3.27. Here, *M*hc represents the residual mass of oven dried hydrochar (kg) recovered after HTC of 1-kg of oven dried biomass, *VS* is the volatile solid content of the hydrochar (%*ar*), BMP_{ex} is the experimental biomethane potential of the hydrochar (mL CH_4/g VS) and 39.8 denotes the assumed HHV of methane (MJ/m^3).

Equation 3.27. Calculation of energy output obtained from the AD of hydrochars.

$$\text{Energy Output Hydrochar AD (MJ/kg)} = \frac{\left(M\text{hc} \times \frac{\text{VS}}{100}\right) \times \text{BMP}_{ex}}{1000} \times 39.8$$

The energy output from the AD of process waters was determined using Equation 3.28. Where, *M*pw is the residual mass of process water (kg) following the HTC of 1-kg of oven dried biomass, COD is the chemical oxygen demand of the process water (g/L), BMP_{ex} is the experimental biomethane potential of the process water (mL CH_4/g COD) and 39.8 denotes the assumed HHV of methane (MJ/m^3). It is assumed 1 mL of process water is equal to 1g.

Equation 3.28. Calculation of energy output obtained from the AD of process waters.

$$\text{Energy Output Process Water AD (MJ/kg)} = \frac{M\text{pw} \times \text{COD} \times \text{BMP}_{\text{ex}}}{1{,}000{,}000} \times 39.8$$

The energy output from the DF of process waters was determined using Equation 3.29. Where, *M*pw is the residual mass of process water (kg) following the HTC of 1-kg of oven dried biomass, COD is the chemical oxygen demand of the process water (g/L), BHP_{ex} is the experimental biohydrogen potential of the process water (mL H_2/g COD) and 12.7 denotes the assumed HHV of hydrogen (MJ/m^3). It is assumed 1 mL of process water is equal to 1g.

Equation 3.29. Calculation of energy output obtained from the DF of process waters.

$$\text{Energy Output Process Water DF (MJ/kg)} = \frac{M\text{pw} \times \text{COD} \times \text{BHP}_{\text{ex}}}{1{,}000{,}000} \times 12.7$$

The energy output obtained from the AD of the residual HTC slurries, was calculated according to Equation 3.30. Here, *M*s represents the residual mass of slurry (kg) after HTC of 1-kg of oven dried biomass, VS is the volatile solid content of the slurry (%*ar*), BMP_{ex} is the experimental biomethane potential of the slurry (mL CH_4/g VS) and 39.8 denotes the assumed HHV of methane (MJ/m^3). The VS content of HTC slurries was determined according to Section 3.3.1.3.

Equation 3.30. Calculation of energy output obtained from the AD of HTC slurries.

$$\text{Energy Output Slurry AD (MJ/kg)} = \frac{\left(Ms \times \frac{\text{VS}}{100}\right) \times \text{BMP}_{ex}}{1000} \times 39.8$$

The energy output obtained from the DF of the residual HTC slurries, was calculated according to Equation 3.31. Here, *M*s represents the residual mass of slurry (kg) after HTC of 1-kg of oven dried biomass, *VS* is the volatile solid content of the slurry (%*ar*), BHP_{ex} is the experimental biohydrogen potential of the slurry (mL H_2/g VS) and 12.7 denotes the assumed HHV of hydrogen (MJ/m^3).

Equation 3.31. Calculation of energy output obtained from the DF of HTC slurries.

$$\text{Energy Output Slurry DF (MJ/kg)} = \frac{\left(Ms \times \frac{\text{VS}}{100}\right) \times \text{BHP}_{ex}}{1000} \times 12.7$$

The calculation of energy output obtained from the two-stage digestion of HTC slurries was obtained through the addition of Equation 3.30 and Equation 3.31.

3.6.2.2 Steam Explosion Energy Output

The energy output from SE was calculated based on the energy obtained from the residual slurry produced after SE, described in Section 3.2.2. This energy output value was then divided by the dry mass fraction of biomass, which was added to the SE reactor. This allows the SE energy output to be normalised to the unit MJ/kg: allowing direct comparison with the energy output values obtained from HTC products.

The energy output obtained from the AD of the residual SE slurries, was calculated according to Equation 3.32. Here, *M*s represents the residual mass of slurry (kg) after SE, *VS* is the volatile solid content of the slurry (%*ar*), BMP_{ex} is the experimental biomethane potential of the slurry (mL CH_4/g VS), *M*b is dry fraction mass of the biomass added to the SE reactor (kg) and 39.8 denotes the assumed HHV of methane (MJ/m^3).

Equation 3.32. Calculation of energy output obtained from the AD of SE slurries.

$$\text{Energy Output SE AD (MJ/kg)} \frac{= \left(\frac{\left(Ms \times \frac{\text{VS}}{100}\right) \times \text{BMP}_{ex}}{1000} \times 39.8\right)}{Mb}$$

The energy output obtained from the DF of the residual HTC slurries, was calculated according to Equation 3.33. Here, *M*s represents the residual mass of slurry (kg) after SE, *VS* is the volatile solid content of the slurry (%*ar*), BHP_{ex} is the experimental biohydrogen potential of the slurry (mL H_2/g VS), *M*b is dry fraction mass of the biomass added to the SE reactor (kg) and 12.7 denotes the assumed HHV of hydrogen (MJ/m^3).

Equation 3.33. Calculation of energy output obtained from the DF of SE slurries.

$$\text{Energy Output SE DF (MJ/kg)} = \left(\frac{\frac{\left(Ms \times \frac{\text{VS}}{100}\right) \times \text{BHP}_{ex}}{1000} \times 12.7}{Mb}\right)$$

The calculation of energy output obtained from the two-stage digestion of SE slurries was obtained through the addition of Equation 3.32 and Equation 3.33.

3.6.3 Energy Balance

Energy return upon energy invested (EROI) was calculated according to Equation 3.34. Previous studies have assumed 85% energy recovery efficiency from HTC processes [234]. However, in this work, a more conservative estimate of 55% heat recovery efficiency was assumed for both HTC and SE, calculated using Equation 3.35.

Equation 3.34. Calculation of energy return upon energy invested.

$$\text{EROI} = \frac{\text{Energy Output}}{\text{Energy Input}}$$

Equation 3.35. Calculation of energy return upon energy invested, with 55% energy recovery.

$$\text{EROI} = \frac{\text{Energy Output}}{(\text{Energy Input} \times 0.45)}$$

Energy conversion efficiency (ECE) is based on the percentage of energy recovered from the HHV of the starting biomass material. ECE was calculated according to Equation 3.36 [72]. HHV of the biomass was determined on an as received basis, using Dulong's equation, following preservation (Section 3.1.1.1).

Equation 3.36. Calculation of energy conversion efficiency.

$$\text{ECE}\ (\%) = \frac{\text{Energy Output}\ \left(\frac{\text{MJ}}{\text{kg}}\right)}{\text{HHV of Biomass}\ \left(\frac{\text{MJ}}{\text{kg}}\right)} \times 100$$

3.7 Statistical Analysis

Where applicable, Analysis of Variance (ANOVA), with Tukey *post hoc* tests, Spearman's rank correlation coefficient and Pearson's Correlation analysis were conducted using the SPSS Statistics software (Version 23) to identify significant differences to a confidence level of $p<0.05$.

Chapter 4
Feedstock Characterisation

The aim of this chapter is to understand the differences in the biochemical compositions of the feedstocks used throughout this thesis. The composition of biomass provides useful information to determine the suitability of different conversion technologies for generating bioenergy.

Initially, proximate, ultimate and inorganic compositions were compared across each feedstock. Subsequently, the energy output from the AD of feedstocks was assessed. The energy output from AD provides a benchmark figure to compare against other conversion methods in the later chapters of this thesis.

The feedstocks used throughout this thesis can be broadly grouped into macroalgal and lignocellulosic biomass. Macroalgal feedstocks include the species: *S. latissima* (SL), *F. serratus* (FS and FS[19]) and *L. digitata* (LD and LD[19]). The lignocellulosic feedstocks used in this work were water hyacinth: (WH) and grass (GR).

4.1 Objectives

The objectives of this chapter are to:

- Compare the biochemical compositions of selected feedstocks.
- Understand the effect of the biochemical composition on the thermal conversion of the selected feedstocks.
- Highlight and discuss the methodological limitations of working with high-ash feedstocks.
- Assess the ECE from the AD of the selected feedstocks.

4.2 Proximate, Ultimate and Biochemical Analysis

4.2.1 Proximate Analysis

Proximate analysis was performed to understand the proportion of volatile matter (VM), fixed carbon (FC) and ash within the feedstocks; values of which are presented in Figure 4.1. The values were determined by thermogravimetric analysis and presented on a dry basis; therefore the proportional fraction of moisture is not included.

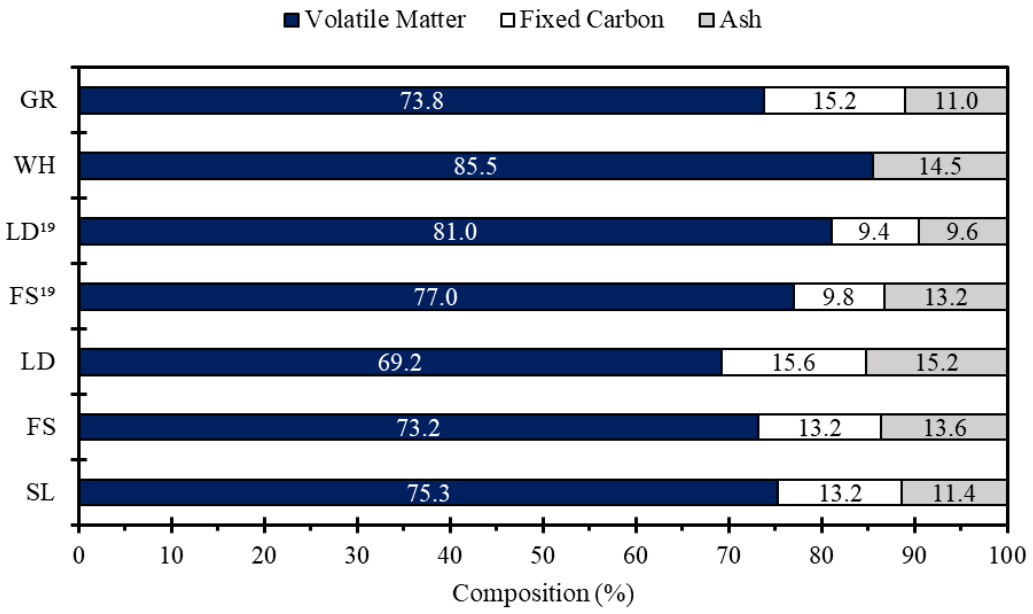

Figure 4.1. Proximate composition of biomass feedstocks, determined by TGA. Data presented on a dry basis (*db*).

VM represents the greatest proximate fraction across all feedstocks, ranging from 69.2% (LD) to 85.5% (WH). There appears to be no real trend for FC content. Previous studies found macroalgal biomass contained a higher FC content (12-33%) than terrestrial, lignocellulosic biomass (14-19%) [65]. The FC content of GR (15.2%) is similar to the lignocellulosic FC contents found by Ross *et al.* [65]. However, the seaweed species shown in Figure 4.1 all have a lower FC content than GR, except LD (15.6%). FC was not detected in WH. The organic fraction of biomass; VM and FC, contains carbon, which contributes towards the energetic potential of a feedstock during conversion processes. Therefore, the ash and moisture contents can be considered inert, in terms of energy potential.

The ash contents presented in Figure 4.1, are generally higher than conventionally used bioenergy feedstocks; such as oak wood (7.4%), miscanthus (4.9%) and willow (4.1%) [64]. The highest ash content; 15.2% (LD) and the lowest ash content; 9.6% (LD[19]) both originate

the same macroalgal species: *L. digitata*, albeit different samples. Ash composition is seasonally variable for *L. digitata* [61] and is at a minima in July (summer months) and a maxima in March (winter months). LD^{19} was harvested in July and LD in January, therefore agreeing with the conclusions of Adams *et al*. [61].

The ash contents of the macroalgal species, shown in Figure 4.1, are typically lower than values reported in previous studies. SL had an ash content of 11.4%, whereas a *S. latissima* sample harvested in a similar season had an ash content of 34.9% [71]. FS and FS^{19} had similar ash contents; 13.6% and 13.2% respectively, whereas literature values for the ash content of *F. serratus* are: 21.2% [66] and 29.4% [71]. LD was harvested in January and displayed an ash content of 15.2%, whereas a similar *L. digitata* sample, described by [61], also harvested in January had an ash content of 27.7%. LD^{19} was harvested in July and displayed an ash content of 9.6%, whereas, a similar *L. digitata* sample, described by [61], also harvested in July, had an ash content of 13.8%. Additional literature values for the ash content of *L. digitata* include: 27.2% [71] and 12.4% [80]. Therefore, large variability is seen between literature values.

4.2.2 Total Solids and Volatile Solids Analysis

Total solids (TS) and volatile solids (VS) analysis is an alternative approach of reporting the proximate composition of a biomass. Table 4.1 displays the TS and VS-contents for each biomass.

Table 4.1. Total solid and volatile solid determination using APHA method [223].

Feedstock	TS (% *ar*)	VS (% *ar*)	VS (% TS)	Ash (% TS)*
SL	92.2 ± 0.1	65.7 ± 0.0	71.3 ± 0.1	28.7 ± 0.1
FS	90.5 ± 0.0	65.8 ± 0.1	72.7 ± 0.1	27.3 ± 0.1
LD	88.8 ± 0.0	57.0 ± 0.1	64.2 ± 0.1	35.8 ± 0.1
FS^{19}	85.5 ± 0.0	63.5 ± 0.0	74.2 ± 0.0	25.8 ± 0.0
LD^{19}	89.4 ± 0.0	71.4 ± 0.5	79.9 ± 0.5	20.1 ± 0.5
WH	93.1 ± 0.1	76.7 ± 0.0	82.3 ± 0.1	17.7 ± 0.1
GR	95.4 ± 0.9	84.3 ± 0.7	88.3 ± 1.1	11.7 ± 1.1

*calculated by difference 100-[VS(% TS)]. Average values are presented ± standard deviation (*n*=2). TS=total solids. VS=volatile solids. *ar*= as received.

The VS-contents of the seaweeds are consistently lower than WH or GR, due to a higher ash content. Despite reporting on the same biomass feedstocks, the ash contents shown in Table 4.1 are all consistently higher than those presented in Figure 4.1, particularly for the seaweeds. A difference between these two methodologies is the temperature used to determine ash concentration. Ash content using the TGA (Figure 4.1) is determined as the residual matter following combustion at 900°C. Whilst the ash contents presented in Table 4.1 were determined at 550°C. Therefore, the results of Table 4.1 and Figure 4.1 suggest the temperature of which ash is determined influences the concentration of ash measured. This concept is further explored as part of Section 4.3.2.

4.2.3 Ultimate Analysis

The carbon (C), hydrogen (H), nitrogen (N), sulphur (S) and oxygen (O) contents of each biomass are reported on a dry basis in Table 4.2, alongside the atomic ratios presented on a dry ash free basis. Whereas, Figure 4.2 displays the CNHSO contents of each biomass on a dry ash free basis. The C-content represents the highest elemental fraction across all biomass feedstocks, if O-content is measured directly. Lignocellulosic biomass contains a higher carbon fraction; WH (38.7%) and GR (44.2%) compared to the macroalgal feedstocks (26.5-35.7%); this is typically found across literature studies [64,65,103]. Oxygen is the second most abundant element across all feedstocks (Table 4.2) if measured directly, ranging from 23.2% (LD) to 30.0% (LD[19]).

Table 4.2. Ultimate analysis of biomass feedstocks.

Feedstock	Ultimate analysis (%wt *db*)						Element Ratios (*daf*)			
	C	H	N	S	O[a]	O[b]	H:C[c]	O:C[a,c]	O:C[b,c]	C:N[d]
SL	33.0 ± 0.7	2.9 ± 0.1	1.9 ± 0.1	ND	23.7 ± 2.6	50.8 ± 1.0	1.07	0.54	1.16	17.5
FS	35.7 ± 0.1	3.9 ± 0.6	2.0 ± 0.1	ND	27.8 ± 0.2	44.8 ± 0.4	1.32	0.58	0.94	17.5
LD	26.5 ± 0.3	3.4 ± 1.0	2.1 ± 0.1	ND	23.2 ± 0.0	52.7 ± 1.3	1.55	0.66	1.49	12.4
FS[19]	33.7 ± 0.2	4.2 ± 0.2	2.1 ± 0.0	1.6 ± 0.4	26.8 ± 0.0	45.3 ± 0.2	1.51	0.60	1.01	16.2
LD[19]	33.5 ± 0.1	4.4 ± 0.1	1.5 ± 0.1	0.8 ± 0.2	30.0 ± 0.0	50.2 ± 0.1	1.56	0.67	1.12	21.8
WH	38.7 ± 0.0	3.4 ± 0.0	2.7 ± 0.1	0.1 ± 0.1	27.4 ± 0.5	40.7 ± 0.2	1.04	0.53	0.79	14.5
GR	44.2 ± 1.0	6.9 ± 0.8	3.9 ± 0.1	ND	26.0 ± 0.5	34.0 ± 1.7	1.88	0.44	0.58	11.3

[a]oxygen measured directly.[b]oxygen measured by difference, using the ash content determined in Figure 4.1. [c]atomic ratio. [d]mass ratio. *db*=dry basis. *daf*=dry ash free basis. ND=not detected.

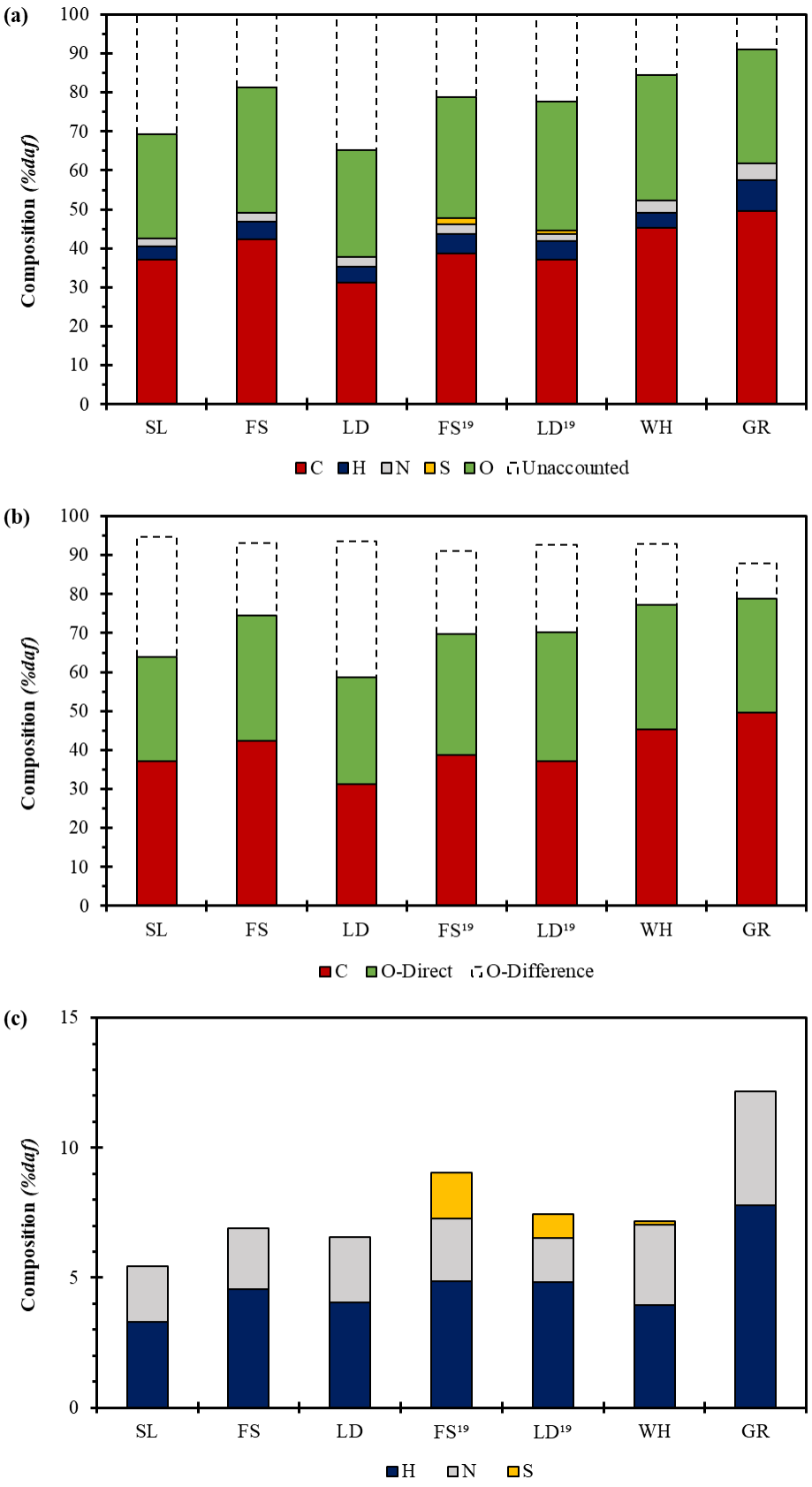

Figure 4.2. Ultimate composition of biomass feedstocks **(a)** C, H, N, S & O **(b)** C & O and **(c)** H, N & S. Values are presented on a dry ash free basis (*daf*).

O-content can be measured either by difference (100-[C%+H%+N%+S%+Ash%]), or directly measured using a CHNS-O analyser (Flash 2000 CHNS-O analyser). Table 4.2 and Figure 4.2b also shows the O-content, if measured through difference. If oxygen was to be measured by difference, the oxygen content would represent a greater fraction of the organic matter compared to carbon for seaweeds (Figure 4.2b). The oxygen content measured directly and by difference is more similar for WH and GR than macroalgal feedstocks. This concept is further explored in Section 4.3.2.1.

The H, N and S contents represent a smaller fraction of the biomass feedstocks than C and O. Figure 4.2c shows similar H and N values across macroalgal feedstocks; however, GR contains a higher proportion of both H and N. A sulphur content of 1.6% and 0.8% was detected in FS[19] and LD[19] (Table 4.2). However, sulphur was not detected in the other seaweed feedstocks: SL, FS or LD. Seaweeds typically contain approximately 1% sulphur [61,66,80], but this can increase to around 2-4% [64,65].

4.2.4 Biochemical Analysis

The biochemical compositions of the lignocellulosic biomasses: WH and GR are presented in Table 4.3 and are shown to be broadly similar. Although, the lignin content is slightly higher for WH, whilst the non-structural carbohydrate content is higher for GR, compared to WH.

Table 4.3. Biochemical composition of lignocellulosic feedstocks.

Composition (wt% *ar*)	**Water Hyacinth**	**Grass**
Moisture	6.7	5.9
Cellulose	25.1	23.2
Hemicellulose	23.1	22.6
Lignin	6.8	3.5
Ash*	13.5	10.3
Crude Protein**	15.6	23.0
Non-structural Carbohydrates**	9.2	11.5

*Determined by TGA. **Crude Protein = %N(*ar*)×6.25 [235]. ***calculated by difference. Data presented on an as received basis (*ar*) of the oven dried biomass.

4.3 Inorganic Analysis

4.3.1 Inorganic Composition

The composition of the inorganic fraction of biomass can be highly problematic during conversion processes; particularly through thermal processing routes [65]. High concentrations of alkali metals and chlorine can lead to slagging, fouling and corrosion issues [64,65,74]; reducing plant efficiencies and inferring un-desired maintenance costs. The ash composition of each biomass is shown in Figure 4.3. Additionally, the concentrations of the major inorganic elements in the biomass feedstocks are shown in Table 4.4.

Figure 4.3 shows the major ash components of the macroalgal feedstocks are Cl (23-41%), K (20-33%) and Na (14-23%). Lignocellulosic feedstocks; WH and GR, showed reduced proportions of Cl (13-24%) and Na (1-3%), compared to macroalgal feedstocks, but the proportion of K remained high; 31-32%. In addition, the proportions of Si, Ca and P were higher for lignocellulosic feedstocks, than macroalgal feedstocks.

The concentration of ash varies between feedstocks (Figure 4.1). Therefore, the concentrations of inorganic components, within each biomass, will vary in proportion to the overall ash concentration. Table 4.4 displays the concentrations of the major inorganic components across each biomass feedstock. The values shown in Table 4.4 were directly determined by XRF analysis, but have been corrected to a dry basis.

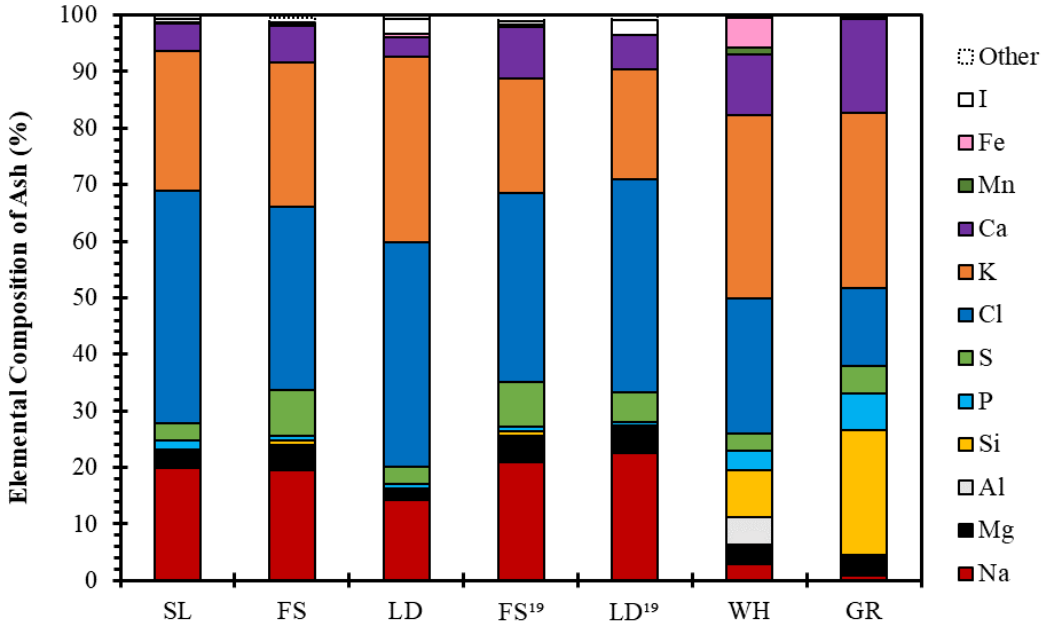

Figure 4.3. Composition of ash in each biomass feedstock, determined by XRF analysis.

Table 4.4. Inorganic composition of biomass feedstocks, determined by XRF analysis.

Feedstock	Inorganic element concentration (wt% feedstock *db*)											
	Na	**Mg**	**Al**	**Si**	**P**	**S**	**Cl**	**K**	**Ca**	**Mn**	**Fe**	**I**
SL	5.0	0.7	0.0	0.1	0.4	0.8	10.3	6.2	1.2	0.0	0.0	0.2
FS	3.8	0.8	0.1	0.2	0.2	1.6	6.3	4.9	1.2	0.0	0.0	0.1
LD	4.8	0.6	0.0	0.1	0.3	1.0	13.5	11.2	1.2	0.0	0.2	0.9
FS[19]	4.1	0.8	0.1	0.2	0.2	1.5	6.6	3.9	1.8	0.0	0.1	0.1
LD[19]	3.6	0.7	0.0	0.1	0.1	0.8	6.1	3.1	1.0	0.0	0.0	0.4
WH	0.5	0.6	0.8	1.4	0.5	0.5	3.9	5.2	1.7	0.2	0.8	0.0
GR	0.1	0.3	0.0	1.9	0.6	0.4	1.2	2.7	1.5	0.0	0.0	0.0

db=dry basis.

Table 4.4 shows Na concentrations are considerably higher for macroalgal biomass (3.6-5.0%), compared to WH (0.5%) and GR (0.1%). The concentrations of K are lowest for GR (2.7%), however, WH contains a higher concentration of K than FS, FS[19] and LD[19]. The concentrations of alkali metals for the feedstocks in Table 4.4 are higher than conventionally-used biomass feedstocks [64]; willow (Na=0.01%, K=0.28%), miscanthus (Na=0.02%, K=0.17%) and oak wood (Na=0.01%, K=0.16%). Therefore, indicating potential problematic slagging and fouling tendencies. The concentrations of alkali metals are known to be seasonally variable for *L. digitata*; with the lowest concentrations found in July [61]. LD shows higher Na (4.8%) and K (11.2%) concentrations than LD[19] (Na=3.6%, K=3.1%). LD[19] was harvested during July 2019, whereas, LD was collected in January 2009. Therefore, the higher alkali content of LD enforced the findings of [61]. However, there is also likely to be variation according to geographical location [61,65].

High Cl concentrations results in unfavourable ash chemistry behaviour during thermal conversion [80]. The Cl concentrations described in Table 4.4 were higher for macroalgal species (6.1-13.5%), compared to WH (3.9%) and GR (1.2%). In addition, macroalgal species contain higher levels of iodine, in particular LD (0.9%) and LD[19] (0.4%). Total halogens have been previously reported to be higher for macroalgal biomass (up to 11%) than terrestrial biomass (1-1.5%) [65], agreeing with the values presented in Table 4.4. Cl values reported in Table 4.4 are significantly higher than wood (0.02-0.03%) and coal (0.06%) [236]. Therefore, all feedstocks are expected to have problematic ash behaviour during thermal conversion. WH contains a higher Cl content then GR, likely because WH is an aquatic biomass. Previously,

Hudakorn and Sritrakul [85] generated pellets for combustion from WH, assessing the quality according to the US Peller Fuel Institute Standard Specification. The pellets pass most of the standard criteria, except for the ash and chloride contents; suggesting the chlorine content is problematic to the thermal conversion of WH.

Ultimate analysis (Table 4.2) only detected significant sulphur values for FS^{19} (1.6%) and LD^{19} (0.8%). These values closely match the sulphur concentrations of determined by XRF (Table 4.4) for the same samples: FS^{19} (1.5%) and LD^{19} (0.8%). However, XRF also detects sulphur for SL (0.8%), FS (1.6%), LD (1.0%), WH (0.5%) and GR (0.4%). Whereas, ultimate analysis (Table 4.2) detected low or negligible concentrations of sulphur for these samples; highlighting potential differences in analytical techniques.

4.3.2 Limitations of Determining the Ash Content of High Ash Biomass

The ash content of a biomass can be determined using several different methods. As part of this thesis, the ash content of the biomasses was measured using three different methodologies: (i) ashing at 550°C in a furnace (Table 4.1), (ii) ashing at 900°C in a TGA (Figure 4.1), or (iii) calculating the total sum of all inorganic elements detected by XRF (Table 4.4). The results of each ash determination method are presented in Figure 4.4. Generally, Figure 4.4 shows the determination of ash content for macroalgal biomass is highly variable, whereas, the observed differences are not as severe for lignocellulosic biomass: WH and GR. The ash contents of seaweeds were between 50-60% lower when determined at 900°C, compared to 550°C. However, the difference is not as significant for WH (18% lower) and GR (7% lower).

Ross *et al*. [65] previously highlighted discrepancies in calculating the ash content of macroalgal biomass, following ashing at two temperatures: 550°C; using a furnace and 950°C; using TGA. Therefore, applying similar methodologies to those shown in Figure 4.4 to determine ash contents. Ross *et al*. [65] showed the ash concentrations determined by TGA at 950°C were lower than the ash contents determined using a furnace at 550°C for a range of macroalgal species, including; *L. digitata* (550°C=25.8%, 950°C=10.0%), *L. hyperborea* (550°C=18.0%, 950°C=11.2%), *F. serratus* (550°C=23.4%, 950°C=18.6%) and *F. vesticulosus* (550°C=22.8%, 950°C=11.8%). Therefore, reflecting similar conclusions to Figure 4.4.

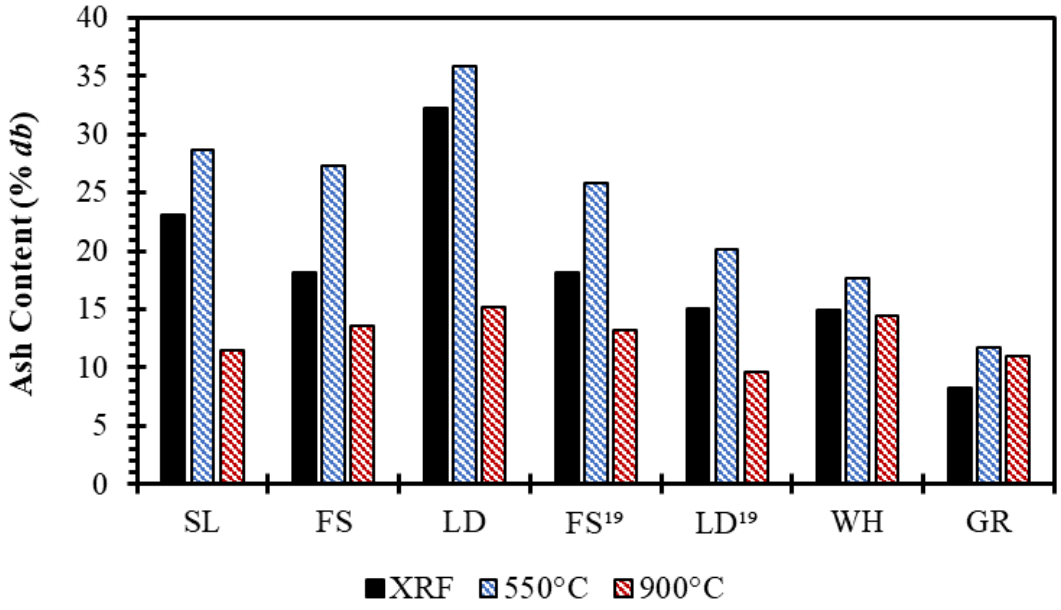

Figure 4.4. Ash composition of biomass using different methods of determination.

Additional studies have also shown that increasing the biomass ashing temperature results in a reduction in the calculated ash content [83,237,238], although the effect is feedstock dependent [83]. The ash content of marine macroalgal biomass has been shown to reduce by 17%, 27%, 39% and 59% at ashing temperatures of 700°C, 900°C, 1100°C and 1300°C, compared to ash determined at 500°C [83]. Whereas, lignocellulosic feedstocks, such as rice husks and switchgrass show more a limited reduction in ash; 19% and 7%, respectively, even at higher temperatures. These conclusions are reflected by the differences shown in Figure 4.4. The increased ash losses at higher temperatures for macroalgal biomass is likely due to volatilisation of alkali metals and decomposition of carbonate species [65,83]. Whereas, losses are minimalised high-silica containing biomass [83], such as WH and GR.

Figure 4.5 shows that a strong positive correlation (R^2=0.88) was identified between the loss of ash content between 550°C and 900°C and the concentration of alkali metals (Na and K) present within each biomass. Therefore, this reflects the conclusions obtained by [65,83,238], that higher ashing temperatures are associated with increased losses of volatile alkali metals. Table 4.4 shows the concentrations of alkali metals were greater for macroalgal biomass (8.0-16.0%), compared to lignocellulosic feedstocks (2.7-5.7%). Therefore, macroalgal biomass experienced a greater volatilisation of ash at 900°C, compared to lignocellulosic biomass. As a result, the measured ash contents of lignocellulosic biomass are more similar between the ashing temperatures of 550°C and 900°C, compared to macroalgal biomass (Figure 4.4).

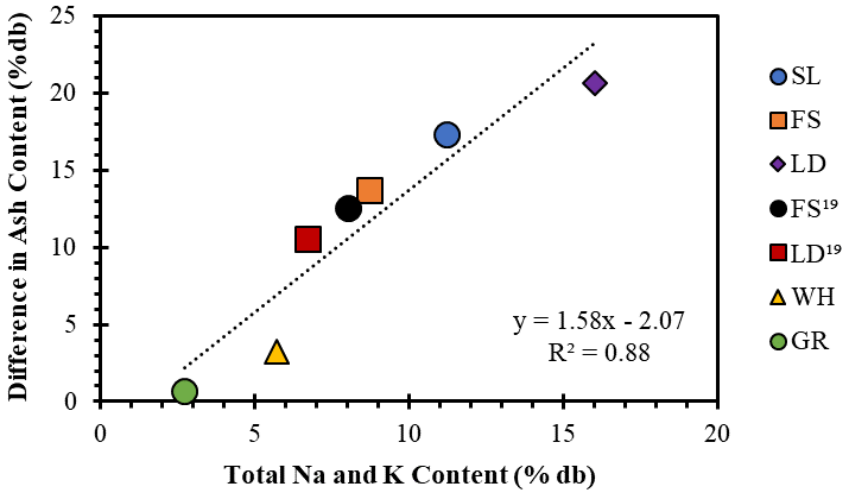

Figure 4.5. Effect of alkali metal concentration of biomass on the loss of ash between temperatures of 550°C and 900°C.

Furthermore, Figure 4.6 shows a stronger positive correlation (R^2=0.91) between the loss of ash content between ashing temperatures of 500°C and 900°C and the total concentration of Na, K and Cl. Therefore, this suggests the increased ashing temperature is associated with the volatilisation of mineral salts; such as NaCl and KCl. Table 4.4 showed the Cl contents of macroalgal species (6.1-13.5%) were higher than lignocellulosic biomass (1.2-3.9%). Therefore, greater losses of ash were observed for macroalgal species at the higher ashing temperatures. According to Figure 4.6, the volatilisation of mineral salts are expected to represent the greatest contribution to the ash losses displayed by macroalgal biomass. However, further losses are also expected from the decomposition of carbonate species; forming CO_2 [238].

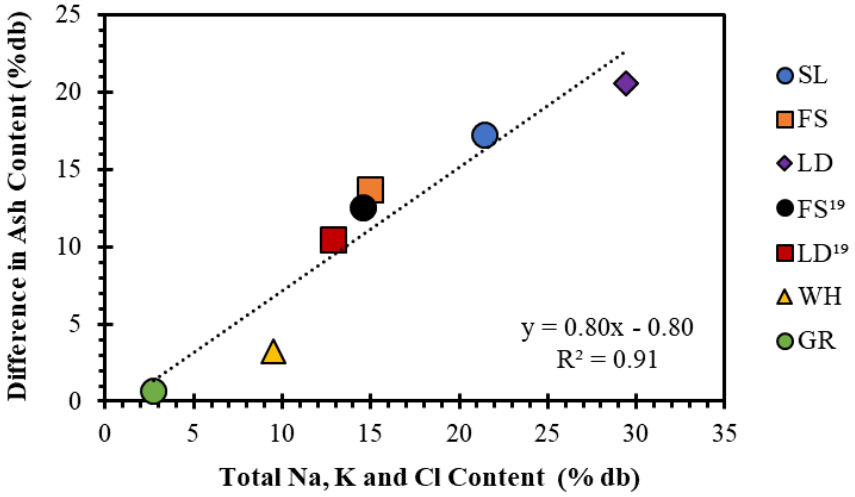

Figure 4.6. Effect of combined alkali metal and chlorine concentration of biomass on the loss of ash between temperatures of 550°C and 900°C.

Figure 4.4 shows the ash determined by XRF was lower than the ash determined through ashing at 550°C, across all seaweed samples; ranging from 4% lower (LD) to 9% lower (FS). This suggests the presence of potentially unburnt carbon in the seaweed ash at 550°C, leading to an overestimation of the ash content. Previous work conducted by Anastasakis [238] found the presence of unburnt carbon within seaweed-derived ash, produced at 550°C. Initially, this was noticed due to the visible dark grey colour of the ash following a 5-hour ashing period at 550°C. Anastasakis [238] further analysed the C-content of the ashes from *L. digitata*, and observed that ash generated at 550°C, 5-hours contained approximately 3% carbon. An increased ashing retention time of 12-hours caused a decrease in the C-content of the ash to approximately 1.5%.

In order to understand this behaviour for the seaweeds species used in this thesis, a similar experiment to Anastasakis [238] was conducted. Figure 4.7 shows the effect of ashing residence time on both the ash content and the carbon content of the ashes produced from SL, FS and LD. Ashing temperature was maintained at 550°C. Increased residence time is associated with a reduction in the C-content of the ashes, along with an overall reduction in ash content. However, the extent of these reductions appears to vary between different macroalgal species.

Fucoid species: FS shows a greater reduction in the ash and carbon content compared to kelp species: SL and LD. The C-content of SL ashes reduced from 1.5% to 0.8% between 2-hours and 6-hours ashing retention time. Similarly, the C-content of LD reduced from 1.8% (2-hours) to 0.9% (6-hours). Whilst the ash contents of the kelps typically reduced by 1-2% between 2-hours and 6-hour retention time; reflecting similar conclusions observed by [238]. Alternatively, FS displays a greater reduction in ash and carbon content at increased retention times. FS ash contents decreased from 24.3% (2-hours) to 20.8% (6-hours); a reduction of 3.5%. Whilst the C-content of the FS ash decreased by 9% between 2-hours (11.3%) and 6-hours (2.3%). The values obtained for FS-ashes in Figure 4.7 are much higher than those described by [238].

To further investigate the influence of retention time on the reduction of the ash contents of seaweeds, a subsample of ash produced at 550°C, 2-hours was placed in a TGA, maintained in an air atmosphere at 550°C and the mass losses recorded across a further 12-hour period. The analysis was again determined for SL, FS and LD ashes, with the results presented in Figure 4.8. Again, the mass loss of kelp ashes is minimal; with both SL and LD ashes showing a mass loss of <1% between 0-mins and 720-mins. Whereas, the ash loss observed for FS-ash was much greater; decreasing by 5.4% between 0-mins and 720-mins, with 3% losses observed within the first 180-mins, indicating the presence of unburnt carbon in the ash.

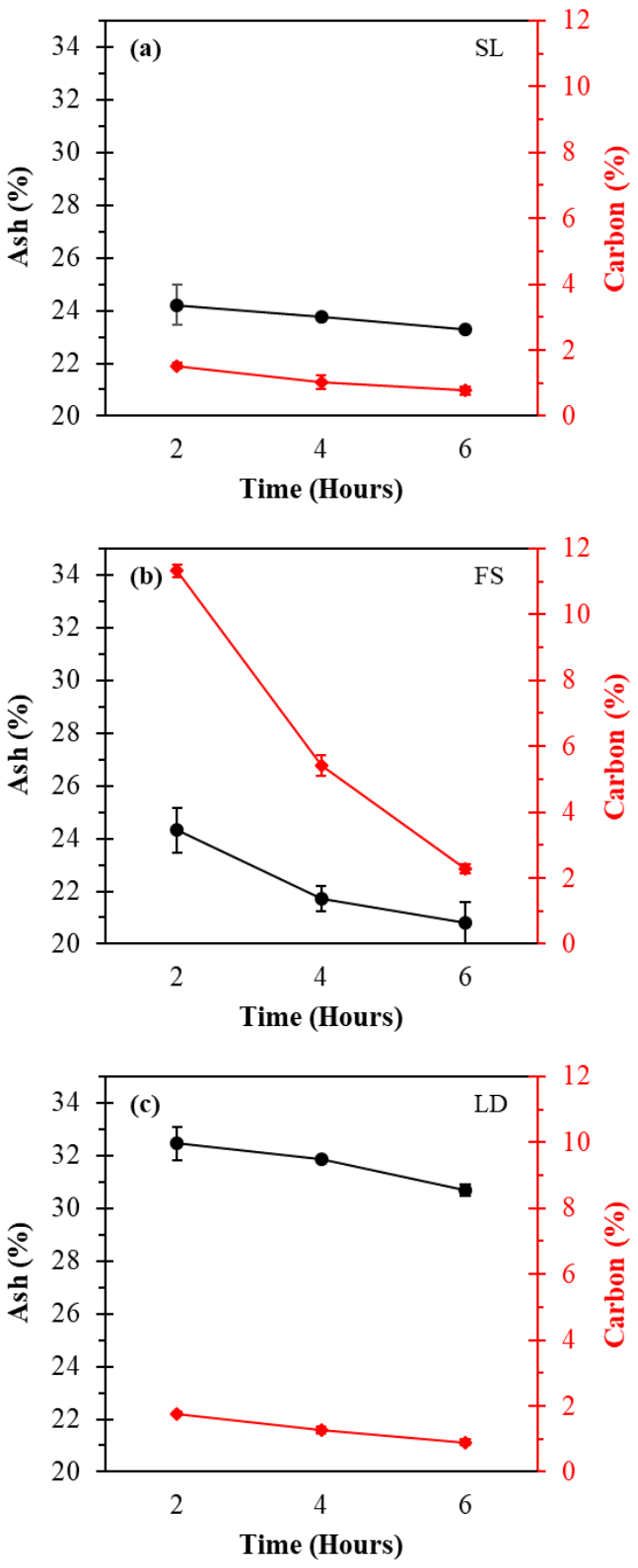

Figure 4.7. Influence on residence time on the ash content and carbon content of the ashes produced from (a) SL, (b) FS and (c) LD. Ashing was conducted at 550°C. Data is presented as average values, on an as received basis (*ar*). Error bars represent the standard deviation (*n*=4).

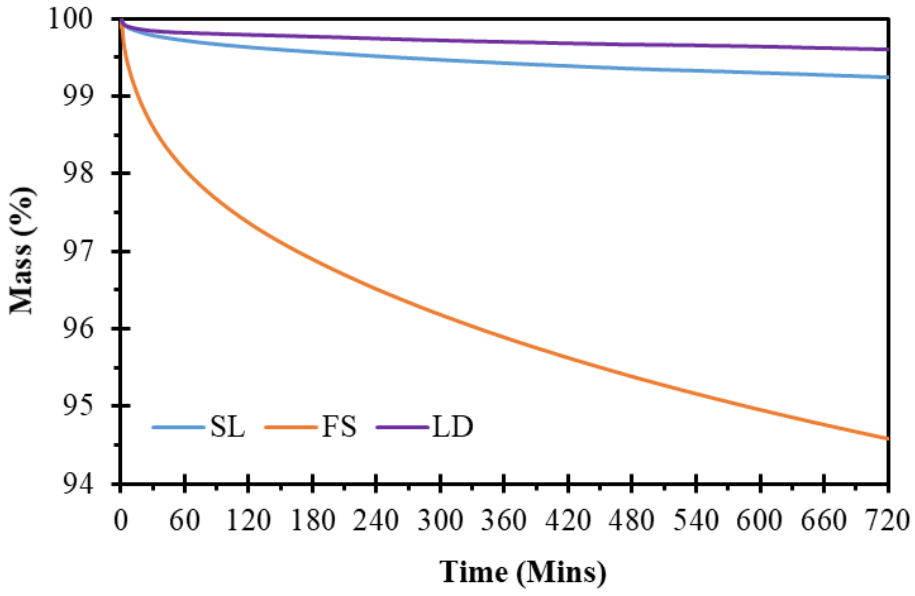

Figure 4.8. Influence of residence time on the mass loss of seaweed-derived ashes during ashing at 550°C.

4.3.2.1 Influence of Ash Determination Method on Measuring Oxygen by Difference

Previously, Table 4.2 showed inconsistent O-content measurement of the biomasses, when determined either directly, or by difference. Measuring oxygen by difference resulted in an increased O-content, compared to direct measurement; especially for macroalgal species. The methodology of calculating O-content by difference is reliant upon the accurate determination of proximate and ultimate composition. However, if ash losses are experienced at higher ashing temperatures, this will, in turn lead to an overestimation of O-content, if measured by difference.

This hypothesis is exemplified by Figure 4.9 which shows a strong positive correlation (R^2=0.89) between the loss of ash observed between temperatures of 550°C and 900°C and the difference in O-content when determined by difference and directly. Therefore, confirming the higher ashing temperature causes a volatilisation of ash, resulting in an overestimation of O-content, when calculated by difference. Again, this is related to both the alkali metal and Cl concentrations biomass; with Figure 4.10 showing this has a strong positive correlation (R^2=0.93) to the difference observed between O-content determined directly, or by difference. This effect is more exaggerated for macroalgal biomass, than lignocellulosic biomass; due to the higher concentrations of alkali metals and Cl.

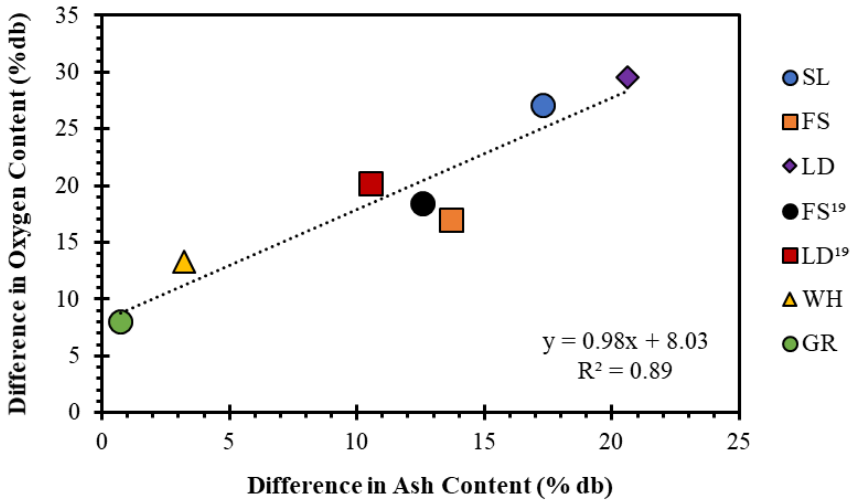

Figure 4.9. Correlation of the loss of ash between temperatures of 550°C and 900°C and the difference between O-content measured directly and by difference.

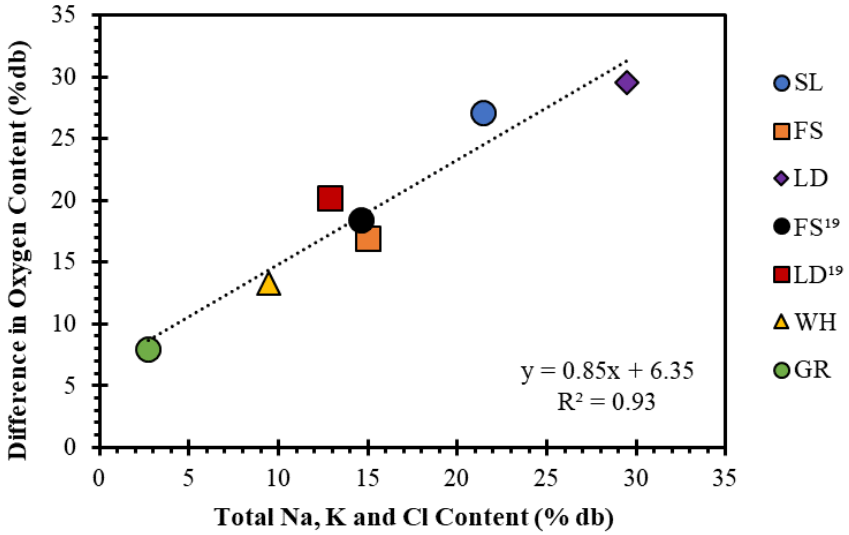

Figure 4.10. Effect of combined alkali metal and chlorine concentration of biomass on the difference between O-content measured directly and by difference.

4.3.2.2 Influence of Ash Determination Method on Volatile Solid Measurement

The standard method for VS determination involves calculating the weight loss on ignition (550°C) of a previously dried sample (105°C) [223]. However, Figure 4.7 shows the presence of unburnt carbon in seaweed-derived ashes, in particular *F. serratus*, resulting in a potential under-estimation of VS-content. Therefore, an alternative approach could be to determine the VS-content of biomass through the summation of FC and VM, on an as received basis, from

the TGA proximate analysis. The ashing step of TGA was determined at 900°C; allowing for complete combustion of carbon within the ash.

The comparative VS-contents of each biomass, whether determined at an ashing temperature of 550°C or 900°C are displayed in Table 4.5. The VS-content of each biomass was generally lower when determined at 550°C, compared to 900°C. The difference in VS-content, between the two determination methods is greater for seaweeds, compared to lignocellulosic biomass; due to higher Na, K and Cl concentrations. According to Figure 4.6, a higher ashing temperature of 900°C leads to the volatilisation of alkali metals and Cl. Increased losses of Na, K and Cl at 900°C would result in an underestimation of ash content and a subsequent overestimation of VS-content. This is evidenced by Table 4.5, which shows a consistently lower ash content through determination at 900°C, compared to 550°C.

Overall, it appears that determining the VS-content of biomass appears to be balance between ensuring total carbon burnout, whilst minimising losses of ash through volatilisation. This becomes particularly important whilst determining the VS-content of biomass which contain high concentrations of alkali metals and chlorine, such as seaweeds. The effect of different VS-determination methodologies on subsequent biochemical methane potential and biodegradability calculations are further explored in Section 4.5.1.1.

Table 4.5. Comparative total solid and volatile solid determination of biomass using two methods: (i) APHA method [223], ashing at 550°C (ii) TGA method ashing at 900°C.

Feedstock	APHA Method (550°C)			TGA Method (900°C)		
	TS (% *ar*)	VS (% *ar*)	Ash (% TS)*	TS (% *ar*)**	VS (% *ar*)***	Ash (% TS)*
SL	92.2 ± 0.1	65.7 ± 0.0	28.7 ± 0.1	92.4	81.8	11.4
FS	90.5 ± 0.0	65.8 ± 0.1	27.3 ± 0.1	93.8	81.1	13.6
LD	88.8 ± 0.0	57.0 ± 0.1	35.8 ± 0.1	94.9	80.4	15.2
FS[19]	85.5 ± 0.0	63.5 ± 0.0	25.8 ± 0.0	92.8	80.6	13.2
LD[19]	89.4 ± 0.0	71.4 ± 0.5	20.1 ± 0.5	93.6	84.6	9.6
WH	93.1 ± 0.1	76.7 ± 0.0	17.7 ± 0.1	93.3	79.8	14.5
GR	95.4 ± 0.9	84.3 ± 0.7	11.7 ± 1.1	94.1	83.8	11.0

*calculated by difference [100-(VS %ar/TS %ar)×100]. **Calculated by summation [VM+FC+Ash]. ***Calculated by summation [VM+FC]. Average values are presented ± standard deviation, where appropriate (*n*=2). TS=total solids. VS=volatile solids. *ar*= as received.

4.4 Higher Heating Value

The HHVs of the biomass feedstocks are presented in Table 4.6; calculated using three different methods: bomb calorimetry, Dulong's equation using the O-content measured by difference and Dulong's equation using the O-content measured directly. All values in Table 4.6 are presented on a dry basis, to allow direct comparison. Bomb calorimetry provides the GCV of a sample and can therefore be considered an accurate measurement of HHV. Dulong's equation is a calculation of HHV, based on the ultimate analysis of a sample. Therefore, there is the assumption that the heat of combustion of a sample is equal to the heat of combustion of its elements. The calculation of HHV using Dulong's equation with oxygen measured directly more closely matches the values from bomb calorimetry than using the Dulong's equation where oxygen is measured by difference, for the majority of feedstocks shown in Table 4.6.

This is particularly prevalent for seaweeds, where applying the Dulong's equation using oxygen values calculated by difference underestimates HHV by 49%, 30% and 57% for SL, FS and LD, respectively, compared to bomb calorimetry. Calculating HHV using Dulong's equation with oxygen values measured directly also underestimates HHV compared to bomb calorimetry for seaweeds, but the underestimation is reduced: 10% (SL), 8% (FS) and 7% (LD). Unfortunately, the HHVs of FS[19] and LD[19] were unable to be determined by bomb calorimetry.

Table 4.6. Higher heating value of biomass feedstocks.

Feedstock	**HHV (MJ/kg) (*db*)**		
	Bomb calorimetry	**Dulong's Equation (Oxygen calculated by difference)**	**Dulong's Equation (Oxygen measured directly)**
SL	12.4	6.3	11.1
FS	13.8	9.7	12.7
LD	10.4	4.5	9.7
FS[19]	-	9.4	12.6
LD[19]	-	8.6	12.2
WH	15.7	10.6	13.0
GR	18.2	18.8	20.2

HHV=higher heating value. *db*=dry basis.

WH showed a similar trend in HHV to macroalgal biomass (Table 4.6), using the Dulong's equation with oxygen values determined by difference and directly, both provided an underestimation of HHV, by 32% and 18%, respectively, compared to bomb calorimetry.

GR is an exception compared to the macroalgal biomass and WH feedstocks. Calculating HHV for GR using Dulong's equation provided an overestimation compared to bomb calorimetry, regardless of whether O-content was measured by difference or directly. Conversely to the other feedstocks, measuring oxygen by difference provided a HHV value closer to the HHV determined by bomb calorimetry. Using Dulong's equation with O-content calculated by difference gave a 3% overestimation in HHV determined by bomb calorimetry. Whereas, measuring oxygen directly overestimated HHV by 11% (Table 4.6).

Overall, the decision was made that the HHV of solid samples would be determined using Dulong's equation, measuring O-content directly, for SL, FS, LD, FS^{19}, LD^{19} and WH biomasses and their resulting solid products, discussed in later chapters. These values most closely match the HHV values determined by bomb calorimetry. Furthermore, the HHV of GR and GR-related solid residues were calculated by applying the O-content calculated by difference, herein.

Table 4.6 shows the HHVs of seaweeds ranged from 9.7 MJ/kg to 12.7 MJ/kg, whereas WH had a slightly higher HHV of 13.0 MJ/kg. GR displayed a much greater HHV of 18.8 MJ/kg. The HHV of a fuel is related to the carbon, hydrogen and oxygen content of the sample [64,239]. Increased carbon content and reduced oxygen content typically leads to an increase in HHV [64]. Table 4.2 shows the C-content of the lignocellulosic biomass: WH (38.7%) and GR (44.2%) was higher than the seaweeds (26.5-35.7%); a trend observed in previous studies [64,65,103]. The higher C-content of the lignocellulosic biomass explains the higher HHVs, compared to macroalgal samples (Table 4.6); despite variable oxygen content between the samples (Table 4.2). *F. serratus* samples (FS and FS^{19}) have a higher HHV (12.6-12.7 MJ/kg), compared to kelps (SL, LD and LD^{19}), due to the increased C-content of *F. serratus* samples (Table 4.2). Higher C-content of *F. serratus* compared to kelp species has also been previously observed [71].

With the exception of GR, the HHV of all biomasses presented in Table 4.6 are all lower than the HHV of conventional biomass feedstocks, including: oak wood (15.4 MJ/kg) [64], miscanthus (16.1 MJ/kg) [64], willow (16.4 MJ/kg) [64] and domestic firewood (18.8-19.5 MJ/kg) [236]. In addition, all feedstocks have a lower HHV than coal (36.3 MJ/kg) [236], due to a higher concentration of oxygen.

4.5 Biomethane Potential

4.5.1 Experimental Biomethane Potential

4.5.1.1 Influence of Biomass Characterisation Method on Experimental Biomethane Potential

During a biomethane potential experiment (BMP_{ex}), the obtainable biomethane yields are typically expressed as mL CH_4/ g VS [240]. Previously, Table 4.5 showed the VS-content of the biomass can vary according to the method of determination. The different methods of VS calculation are likely to affect the interpretation of measured BMP_{ex} yields. As a result, Table 4.7 shows the implications of VS method determination on the calculated BMP_{ex} yields of each biomass.

Table 4.7. Volatile solid content and resultant biomethane potential of biomass, following VS determination, following ashing at 550°C or 900°C.

Biomass	VS Ashing Temperature (°C)	BMP_{ex} (mL CH_4/g VS)
SL	550	249.5
	900	200.4
FS	550	157.4
	900	127.9
LD	550	241.0
	900	170.7
FS[19]	550	143.8
	900	117.5
LD[19]	550	307.6
	900	259.6
WH	550	103.1
	900	95.5
GR	550	261.2
	900	262.5

VS=volatile solids. BMP_{ex}=experimental biomethane potential.

Generally, Table 4.7 shows higher BMP_{ex} yields when the VS-content is determined at 550°C, compared to 900°C, especially for macroalgal biomass. The BMP_{ex} yields of SL, with VS determined at 550°C (249.5 mL CH_4/ g VS) were more similar to literature values: 281.4 mL CH_4/ g VS [72] and 341.7 mL CH_4/ g VS [71], compared to determination of VS at 900°C. This is due to [71,72] using a similar temperature (550°C) to calculate the VS-content of seaweeds. Ashing temperatures of 900°C causes a volatilisation of alkali metals (Figure 4.5), resulting in an overestimation of VS-content (Table 4.5) and subsequent underestimation of BMP_{ex} (Table 4.7). However, a lower ashing temperature of 550°C could underestimate VS-content, due to the presence of unburnt carbon, resulting in an overestimation of BMP_{ex}. Therefore, determination of VS-content appears a balance of ensuring complete carbon burn-out, whilst minimising losses of volatile inorganics.

A potential method of achieving this balance is to determine the ash content at a low ashing temperature (550°C) for a longer residence time (12-hours) [238]. Although, perhaps the most accurate method of determining the VS-content of seaweeds is to ash the biomass at 550°C, 2-hours, then subsequently measure the C-content of the ash and adjust the VS-content accordingly. For example, the VS-content of FS determined after ashing at 550°C, 2-hours was 65.8% (Table 4.5), whilst the C-content of the ash was 11.3% (Figure 4.7); representing an additional VS-content of 3.1% within the ash; present as unburnt carbon. Therefore, the summation of original VS-content (65.8%) and the VS present in the ash (3.1%), results in an adjusted VS-content of 68.9% for FS. The BMP_{ex} curves for the different methods of VS determination are shown in Figure 4.11, including: ashing at 550°C, ashing at 900°C and adjustment of ashing at 550°C according to the carbon content of the ash. FS was selected for this comparison as this was the seaweed with the highest C-fraction in the ash (Figure 4.7). Overall, Figure 4.11 shows that the presence of the C-fraction in the ash contributes a negligible contribution towards biomethane production. Whereas, ashing at 900°C causes an underestimation in BMP_{ex} yields. Therefore, the BMP_{ex} of each untreated biomass was calculated using VS-content determined at an ashing temperature of 550°C, henceforth.

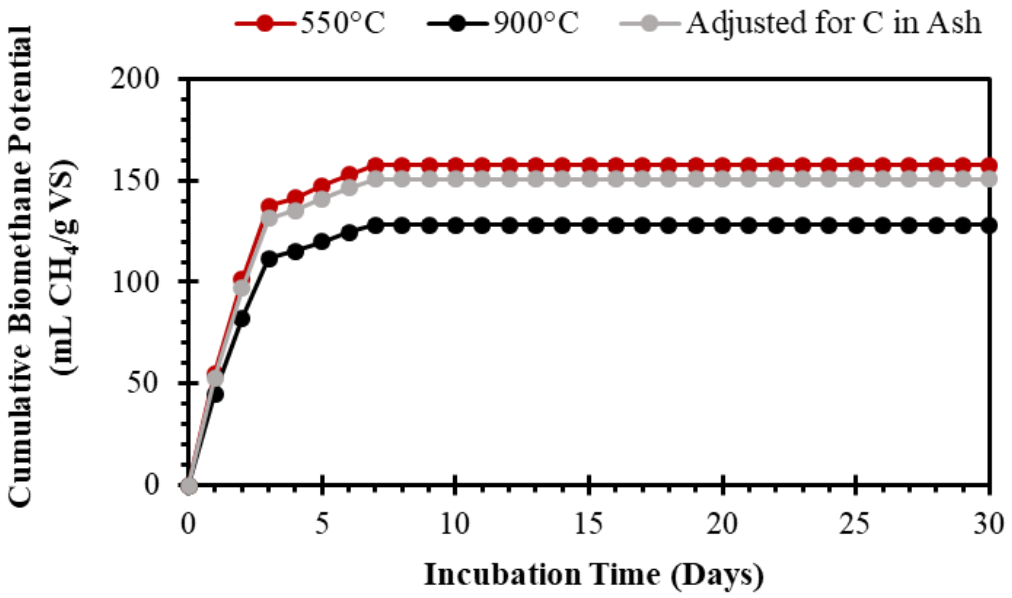

Figure 4.11. Biomethane potential of FS according to different methods of VS determination: ashing at 550°C, ashing at 900°C and adjustment of ashing at 550°C according to the carbon content of the ash.

4.5.1.2 Measured Experimental Biomethane Potential

The experimental biomethane potential (BMP_{ex}) of each oven dried biomass is displayed in Figure 4.12, calculated using the VS-content determined at 550°C (Table 4.1). BMP_{ex} yields are reported numerically in Table 4.7. The BMP_{ex} yields were highly variable across feedstocks, ranging from 103.1 mL CH_4/g VS (WH) to 307.6 mL CH_4/g VS (LD^{19}). This suggests the differing biochemical composition of each biomass affected the generation of biomethane during AD.

Fucus serratus; FS and FS^{19}, generated the lowest biomethane yields compared to the other species of macroalgal biomass; SL, LD and LD^{19}, a similar finding to previous studies [71,127,134]. The lower biomethane yield generated by *F. serratus* is thought to be related to the presence of inhibitory, or recalcitrant compounds within its biochemical structure [127]. *F. serratus* is known to contain higher concentrations of polyphenols, compared to other seaweed species, including *L. digitata* [128]. Tabassum *et al.* [129] found polyphenol concentration had a significant negative impact on the biomethane yields of *A. nodosum*; another fucoid seaweed. Therefore, this could be linked to the lower biomethane yields from *F. serratus*, shown in Figure 4.12.

Despite lower biomethane yields, the BMP_{ex} of both samples of *F. serratus* was similar; 157.4 mL CH_4/g VS (FS) and 143.8 mL CH_4/g VS (FS^{19}). Both *F. serratus* samples were harvested

from a similar location; Aberystwyth, during summer months; FS (June 2015) and FS[19] (July 2019). Therefore, the biochemical composition of the two *F. serratus* samples is expected to be similar. Previously reported BMP_{ex} values for *F. serratus* have been; 101.7 mL CH_4/g VS [71] and approximately 100 mL CH_4/g VS [134]; slightly lower than the values shown in Figure 4.12. However, slight discrepancies between interlaboratory studies are to be expected, due to differences in sample harvesting location and time, as well as variation in biomethane potential methodologies.

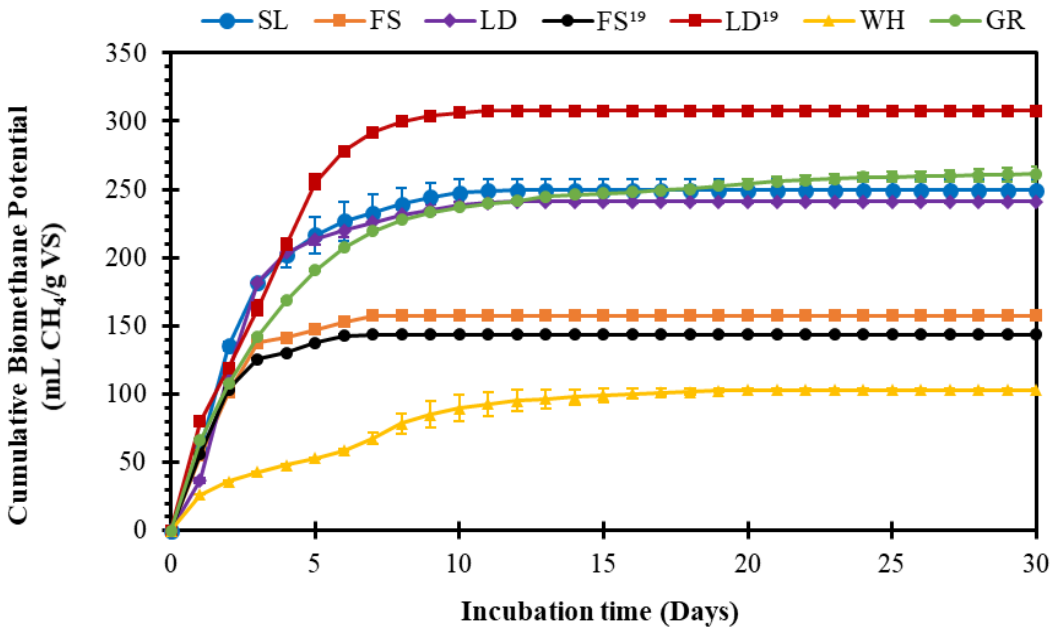

Figure 4.12. Experimental biomethane potential (BMP_{ex}) of the oven dried feedstocks used in this study. Data is presented as average values. Error bars represent the maximum and minimum values (n=2). VS-content of each biomass was determined at 550°C [223].

Kelp seaweed species *S. latissima* and *L. digitata* showed a higher BMP_{ex} than *F. serratus*. Again, this is in agreement with literature studies that find that kelp species *S. latissima* and *L. digitata* generate higher levels of biomethane [71] or biogas [127,134] than *F. serratus*. SL BMP_{ex} yield was 249.5 mL CH_4/g VS; typically low, compared to literature values [71,72,241]. However, BMP_{ex} yields of *S. latissima* are known to be highly variable with harvesting location and season [241].

L. digitata samples generated different biomethane yields; 241.0 mL CH_4/g VS (LD) and 307.6 mL CH_4/g VS (LD[19]), despite both samples being of the same species. LD was harvested during winter (January 2009), whereas LD[19] was harvested during summer (July 2019). Additionally, LD and LD[19] were harvested from different locations; Clachan Sands

and Aberystwyth, respectively. Spatial variation in the biochemical composition [70] and biomethane potential [241] of kelp species has been reported across different harvesting sites. Furthermore, the biochemical composition of *L. digitata* has been shown to vary seasonally within the UK [60,61], which has a subsequent impact on the generation of biomethane [60]. July was identified as the optimum harvesting month for conversion of *L. digitata* into biofuels; where the carbohydrate content is highest and ash content is lowest [61]. Whereas, *L. digitata* samples from winter months had lower carbohydrate concentrations and a higher ash content; reducing the biomethane yields, compared to the sample harvested in July [60]. Figure 4.1 shows the ash content of LD (15.2%) was higher than LD^{19} (9.6%), supporting the conclusions of Adams *et al*. [61]. Additionally, it is expected that the carbohydrate content of LD^{19} is higher than LD [60]; therefore higher biomethane yields would be expected.

LD^{19} generated higher levels of biomethane than SL (Figure 4.12). Whereas, previous studies report *S. latissima* generated higher biomethane yields than *L. digitata* [71,127]. Both LD^{19} and SL were collected during the summer. However, LD was collected during the winter and showed a lower BMP_{ex} (241.0 mL CH_4/g VS), compared to SL.

WH displayed a BMP_{ex} of 103.1 mL CH_4/g VS; the lowest of any feedstock in Figure 4.12. The biomethane potential of GR was higher: 261.2 mL CH_4/g VS, highlighting the variation in biomethane yields obtained from different lignocellulosic biomass samples. WH is, therefore, likely to contain more recalcitrant or inhibitory biochemical components than GR. Table 4.3 shows WH contains a higher lignin and ash fraction, compared to GR; which would negatively impact biomethane yields. Additionally, the non-structural carbohydrate fraction was slightly higher in GR (11.5%) than WH (9.2%); which would positively impact biomethane yields.

The biomethane yields obtained from WH are largely varied across literature studies; ranging from negligible amounts [106] to 252 mL CH_4/g VS [115]. This variation is likely due variability associated in the biochemical composition of WH biomass used and differences in the BMP_{ex} methodologies. The BMP_{ex} value of WH in Figure 4.12 is most similar to the value reported by Ali and Sun [112]: 113 mL CH_4/ g VS.

GR generated lower biomethane yields compared to LD^{19}, contrary to previous findings that grass generates higher biomethane yields than *L. digitata* [103]. Although, Vanegas and Bartlett [127] found similar biogas yields for grass (168 mL biogas/g VS) and *L. digitata* (161 mL biogas/g VS) during small-scale, batch digestions. The BMP_{ex} yield of GR (261.2 mL CH_4/g VS) is slightly lower than most literature values; 222 mL CH_4/g VS [46] 288 mL CH_4/g VS [123], 327 mL CH_4/g VS [47], 341 mL CH_4/g VS [52] and 400 mL CH_4/g VS [40]. Again, this is likely due to the variability in grass samples across different studies.

4.5.2 Theoretical Biomethane Potential and Biodegradability

4.5.2.1 Influence of Biomass Characterisation Method on Calculating Theoretical Biomethane Potential and Biodegradability

Theoretical biomethane potential (BMP_{th}) is a measure of the maximum theoretical yields of biomethane from a given feedstock [96,97]. BMP_{th} is calculated stoichiometrically by applying the elemental composition from the ultimate analysis, presented to either the Boyle's or Buswell equations [97,100]. As a result, the methodology used to determine elemental composition will affect the subsequent calculation of BMP_{th}. This is exemplified by Table 4.8, which shows large variations in BMP_{th}, whilst applying the O-content measured by difference and directly (Table 4.2) to either the Boyle's or Buswell equations. Measuring O-content by difference consistently resulted in a reduced BMP_{th} yield compared to measuring O-content directly; a result of an overestimation of O-content, when measured by difference, due to the increased volatilisation of inorganics. Applying the Boyle's equation resulted in comparatively lower BMP_{th} yields compared to the Buswell equation, due to the consideration of the N-fraction.

Table 4.8. Comparative theoretical biomethane potentials (BMP_{th}) of feedstocks, through measuring O-content both by difference and directly to both the Boyle's and Buswell Equations.

Sample	BMP_{th} (mL CH_4/g VS) Boyle's Equation		BMP_{th} (mL CH_4/g VS) Buswell Equation	
	O-Content measured by difference	**O-Content measured directly**	**O-Content measured by difference**	**O-Content measured directly**
SL	226.3	481.0	244.3	515.1
FS	317.6	480.8	339.8	513.5
LD	172.1	451.5	192.0	493.7
FS[19]	307.1	488.7	329.8	523.7
LD[19]	279.4	462.3	294.8	486.4
WH	347.3	475.9	377.8	517.3
GR	521.5	607.7	573.0	668.9

Table 4.9 shows the calculation of biodegradability (BI) for each biomass; comparing how the interpretation of different BMP_{ex} yields obtained across different VS-determination temperatures (Table 4.7) can affect the calculation of BI. Furthermore, the effect of calculating BMP_{th} values by applying the O-content measured directly or by difference (Table 4.8) and their application to Boyle's or Buswell equations is also assessed.

Table 4.9. Comparison of the biodegradabilities of feedstocks when determining the O-content directly and by difference. O-content by difference calculated after determining ash content at 900°C.

Biomass	VS Ashing Temperature (°C)	BI (%)			
		Boyle's Equation		Buswell Equation	
		O-content measured directly	O-content measured by difference	O-content measured directly	O-content measured by difference
SL	550	52	110	48	102
	900	42	89	39	82
FS	550	33	50	31	46
	900	27	40	25	38
LD	550	53	140	49	126
	900	38	99	35	89
FS[19]	550	29	47	27	44
	900	24	38	22	36
LD[19]	550	67	110	63	104
	900	56	93	53	88
WH	550	22	30	20	27
	900	20	27	18	25
GR	550	43	50	39	46
	900	43	50	39	46

VS=volatile solid. BI=biodegradability index.

Generally, Table 4.9 shows that the calculation of BI is largely variable for macroalgal species, dependent on: the application of either the Boyle's or Buswell equation, the measurement of O-content, either directly, or by difference and the ashing temperature during VS determination. Greater variation is observed in the BI values of macroalgal biomass, compared to lignocellulosic biomass. For example, LD shows the greatest difference in calculated BI: 35-140%, whilst GR shows smallest range in BIs: 39-50%. Again, this is because of a greater difference in the O-content, measured directly and by difference for macroalgal biomass (Table 4.2); linked to volatilisation of ash (Figure 4.9). SL, LD and LD[19]

all display a BI >100%, when O-content was calculated by difference; indicating overestimation of O-content, resulting in the underestimation of BMP_{th} and subsequent overestimation of BI. Furthermore, the BI values calculated whilst determining VS-contents at 900°C were generally lower than where the VS was determined at 550°C; due to the lower BMP_{ex} values.

The BI values calculated using the Buswell equation were all higher, compared to the corresponding sample calculated using the Boyle's equation. The Boyle's equation accounts for the nitrogen-containing fraction of biomass [100] and is therefore suggested to be a more accurate prediction of BMP_{th} [170]. However, discrepancies still exist between the BIs calculated through measuring O-content directly and by difference; highlighting how different methodologies can yield different results.

Overall, the results of this section suggests that 900°C is an unsuitable temperature for determining the VS-content of biomass, especially macroalgal biomass. Although this higher ashing temperature eliminates the presence of unburnt carbon in the ash, it also volatilises a significant fraction of alkali metals and Cl; overestimating VS-content and, therefore, underestimating BMP_{ex} yields. Figure 4.11 demonstrates the contribution of unburnt carbon to BMP_{ex} yields is minimal and the underestimation of BMP_{ex} yields through volatilisation of inorganics at higher ashing temperatures (900°C) introduces a greater degree of error.

As previously mentioned, BMP_{ex} of each untreated biomass was calculated using VS-content determined at an ashing temperature of 550°C. The data presented in Table 4.8 and Table 4.9 allows a number of decisions to be made for the calculation of the BMP_{th} and BI of each biomass. Henceforth, BMP_{th} of seaweeds and WH were calculated using the O-content measured directly, applied to Boyle's equation. This is to prevent the overestimation of O-content, if measured by difference, due to inorganic volatilisation.

Alternatively, the BMP_{th} of GR was calculated by applying the O-content measured by difference, to the Boyle's equation. Table 4.8 shows the BMP_{th} values of GR using the Boyle's equation were 521.5 mL CH_4/g VS and 607.7 mL CH_4/g VS, whilst applying O-content measured by difference and directly, respectively. A BMP_{th} of 607.7 mL CH_4/g VS appears unrealistically high for GR, given the composition is mainly carbohydrates (c. 57% *ar*) and protein (23% *ar*) (Table 4.3), with respective theoretical methane yields of: 415 mL CH_4/g VS, 496 mL CH_4/g VS [95]. Generally, BMP_{th} yields of lignocellulosic biomasses range between 426-599 mL CH_4/g VS [103], again suggesting 607.7 mL CH_4/g VS is too high. Previously, Table 4.6 suggested the stoichiometric prediction of HHV for GR more closely matched the HHV measured by bomb calorimetry when O-content was measured by difference, rather than directly. The results of Table 4.6 and Table 4.8 suggest a potential under-estimation of the direct measurement of O-content from GR. Although, the variation in

calculated BMP_{th} for GR is expected to have little impact on the overall conclusions of this thesis, due to the Table 4.9 showing GR showed the least variation in BI (43-50%) using different methods to interpret the biodegradability; linked to the lowest alkali metal and Cl concentration of the biomasses (Table 4.4).

4.5.2.2 Measured Theoretical Biomethane Potential and Biodegradability

The BMP_{th} of GR (521.5 mL CH_4/g VS) was higher than the BMP_{th} of all other feedstocks in Table 4.10, which all appear to have a similar BMP_{th} (451.5-488.7 mL CH_4/g VS). The higher BMP_{th} of GR is related to its higher C-content (Table 4.2). Generally, lignocellulosic biomass have been shown to have a higher BMP_{th} compared to macroalgal biomass [103]. Allen *et al.* [71] report the BMP_{th} values of *S. latissima*, *F. serratus* and *L. digitata* to be 422 mL CH_4/g VS, 532 mL CH_4/g VS and 479 mL CH_4/g VS, respectively. Similar values were obtained for the seaweeds presented in Table 4.10. BMP_{th} of WH is scarcely reported, however Kist *et al.* (2018) [113] report at BMP_{th} of 466.5 mL CH_4/g VS, similar to that of WH in Table 4.10: 475.9 mL CH_4/g VS.

Table 4.10. Experimental and theoretical biomethane potential of feedstocks, alongside biodegradabilities.

Sample	BMP_{ex} (mL CH_4/g VS)	BMP_{th} (mL CH_4/g VS)	BI (%)
SL	249.5	481.0 [a]	52
FS	157.4	480.8 [a]	33
LD	241.0	451.5 [a]	53
FS[19]	143.8	488.7 [a]	29
LD[19]	307.6	462.3 [a]	67
WH	103.1	475.9 [a]	22
GR	261.2	521.5 [b]	50

[a]O-content measured directly. [b]O-content measured by difference. BMP_{th}=theoretical biomethane potential calculated using the Boyle's Equation. BMP_{ex}=experimental biomethane potential. BI=biodegradability index.

Table 4.10 shows the biodegradability index (BI) varies across the different biomass samples. WH gave the lowest BI (22%); linked to low BMP_{ex} yields. The BI of WH is scarcely reported, however, Kist *et al*. (2018) [113] report a BI of 37%; a higher value than reported in Table 4.10.

The BI of FS (33%) and FS^{19} (29%) were lower than SL (52%), LD (53%) and LD^{19} (67%). Allen *et al*. [71] found the BI of *F. serratus*, *S. latissima* and *L. digitata* to be 19%, 81% and 46%, respectively, suggesting *F. serratus* had a lower BI than kelps. However, the BI value found for *S. latissima* [71] is significantly higher than the value reported for SL in Table 4.10. This is because of lower BMP_{ex} yields for SL (249.5 mL CH_4/g VS) compared to Allen *et al*. [71]; 341.7 mL CH_4/g VS; likely due to variations in *S. latissima* samples.

Despite the highest BMP_{th}, GR had a BI of 50%; lower than SL, LD and LD^{19}. The biodegradability of grass samples varies across the literature: 24% [102] 43% [46], 90% [40], again, likely to vary with sampling season, location and the species of grass analysed, as well as differences between experimental methodologies.

Generally, the feedstocks exhibited quite low biodegradabilities; with only one feedstock (LD^{19}) displaying a BI >55% (Table 4.10). Therefore, the full energetic potential of the feedstocks is not being achieved, suggesting alternative or integrated conversion technologies may be able to enhance the energy output of the biomass feedstocks.

4.5.3 Energy Output and Energy Conversion Efficiency

Figure 4.13 shows the HHV associated with the total volume of biomethane generated from the AD of 1-kg of each oven dried feedstock. The ECE of AD was then calculated as a proportion of the HHV of the original dried feedstock, described in Section 3.6.3. This acts as a benchmark value for the comparison of energy output obtained from integrated conversion strategies, later explored in this thesis. The drying methods, described in Section 3.1.1.1 reduced the moisture content to between 5-8%.

The ECE is particularly low for the *F. serratus* samples, FS (35%) and FS^{19} (31%) and WH (25%), due to the lower BMP_{ex} yields shown in Figure 4.12. The kelp seaweed species demonstrate the highest ECEs; SL (64%), LD (59%) and LD^{19} (76%). The ECE of GR was 50%, despite the energy output calculated from the generated biomethane being similar to LD^{19}; 8.76 MJ/kg dry feedstock and 8.74 MJ/kg dry feedstock. GR represents the feedstock with the greatest HHV (Table 4.6), therefore has the potential to return the greatest energy output.

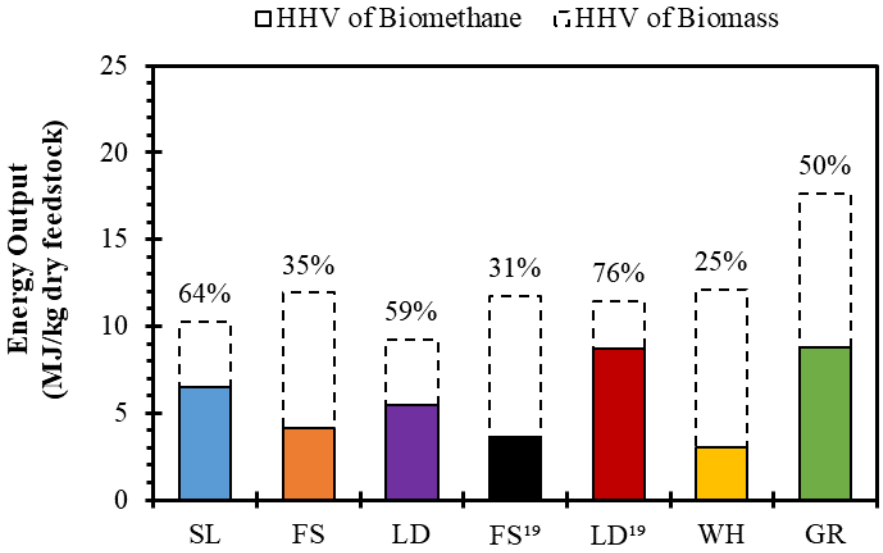

Figure 4.13. Energy output of dry biomass and biomethane generated from 1-kg of oven dried feedstock. The values above the bars represents the energy conversion efficiency from the original biomass. HHV of biomass calculated on an as received basis (*ar*).

The HHV of the dried biomass was calculated using the Dulong's equation; based on the elemental composition of the feedstock. Therefore, the ECE is a measurement of energy output, as a proportion of the theoretical maximum. Similarly, BMP_{th}, shown in Table 4.10, is the maximum theoretical biomethane yield, calculated by the stoichiometric conversion of the elemental composition of a feedstock [100]. Correspondingly, the BI of a feedstock (Table 4.10) is a measurement of the conversion of a feedstock, as a proportion of the theoretical maximum. Based upon these assumptions it can be postulated that the BI in Table 4.10 and the ECE in Figure 4.13 should be equal. However, discrepancies are observed between these values; with the BI reported as lower than the ECE across all feedstocks. The degree of difference between BI and ECE is different for each feedstock type. The difference is minimal for *F. serratus* and lignocellulosic feedstocks: FS (BI=33%, ECE=35%), FS^{19} (BI=29%, ECE=31%). WH (BI=22%, ECE=25%) and GR (BI=50%, ECE=50%), each showing a difference of 0-3% between BI and ECE. However, it is the kelp seaweed species where the greatest difference between BI and ECE was observed, with a difference of 12% for SL (BI=52%, ECE=64%), 6% for LD (BI=53%, ECE=59%) and 9% for LD^{19} (BI=67%, ECE=76%).

Despite AD being a versatile and well established conversion technology, Figure 4.13 suggests the ECEs of the feedstocks can be further improved to maximise the energetic potential of each biomass. Therefore, the overall aim of this project is to maximise the energy recovery from these feedstocks, by investigating integration strategies between hydrothermal treatment and anaerobic conversion.

4.6 Conclusions

The aim of this chapter was to characterise the biomass feedstocks used throughout this thesis, to assess their suitability for different conversion routes. The feedstocks include macroalgal biomass: *S. latissima* (SL), *F. serratus* (FS and FS[19]) and *L. digitata* (LD and LD[19]) and lignocellulosic feedstocks: water hyacinth (WH) and grass (GR).

Each biomass contains a high proportion of ash; of which the ash composition is unsuitable for thermal conversion routes to generate bioenergy. This is because of the high concentrations of alkali metals (Na and K) and chlorine within the ash; which can lead to slagging, fouling and corrosion problems during thermal conversion. Macroalgal feedstocks contain higher concentrations of these problematic inorganic, although they are still present in high concentrations in WH and GR.

The methodology used to determine the ash content of biomass can lead to large variations in the results obtained. Higher ashing temperatures (900°C) result in a lower ash content compared to lower temperatures (550°C); related to losses of alkali metals (Na and K), as well as Cl. Macroalgal biomass experienced larger discrepancies between the measured ash contents at 550°C and 900°C, compared to lignocellulosic biomass; due to increased Na, K and Cl concentrations. Volatilisation of low-molecular weight ash components can subsequently result in an overestimation of O-content, if determined by difference. This, in turn, can lead to an underestimation in calculated HHV content, especially for macroalgal biomass, if calculated using predictive equations, such as the Dulong's equation. However, lower ashing temperatures can result in the presence of unburnt carbon within the residual seaweed ash. The concentration of unburnt carbon remaining in the ash appears to vary according to the species of macroalgae used. The ash produced from kelp species (SL and LD) contained between 1.5-1.8% carbon following ashing at 550°C, 2-hrs. Whereas, fucoid species (FS) ash contained an even higher carbon content (11.3%), under similar ashing conditions. Increasing the retention time of ashing leads to a simultaneous reduction in ash content and C-concentration, although the observed effect was more exaggerated for FS than SL or LD.

This creates complications in determining the VS-content of macroalgal biomass: as a compromise is made between minimising the volatilisation of inorganic components, whilst simultaneously eliminating the presence of unburnt carbon within the ash. The determination of experimental biomethane potential (BMP_{ex}) appears to widely vary for macroalgal biomass, depending on the method of VS determination. This has a successive impact on the determination of the biodegradability (BI) of macroalgal biomass, where largely varied BI results are obtained. Although, this effect is reduced for lignocellulosic feedstocks. Overall,

it appears higher temperature ashing (900°C) is unsuitable for the determination of VS of macroalgal biomass. Lower ashing temperatures (550°C) show reduced losses of volatile inorganics and longer ashing retention times (12-hrs) can facilitate the elimination of unburnt carbon in the residual ash.

The HHV of GR (18.8 MJ/kg) was higher than WH (13.0 MJ/kg) and macroalgal samples (9.7-12.7 MJ/kg); due to the higher carbon content of GR. Although, as expected, the HHV of biomass remains significantly lower than coal.

The energy conversion efficiency (ECE) from the AD of these selected feedstocks was particularly low for *F. serratus* (FS= 35% and FS^{19}=31%), water hyacinth (25%) and GR (50%). Therefore, suggesting the ECE can be further improved to maximise the energy output obtained from the feedstocks. Such improvements to the ECE are explored across subsequent thesis chapters.

Chapter 5
Hydrothermal Carbonisation (HTC) of High Ash Feedstocks: Product Yields and Characterisation

HTC is a thermal conversion technology with the capability of processing biomass with a high moisture content. During HTC, biomass is converted to several hydrothermal products: hydrochar, process water and a gaseous phase, through a number of complex reaction pathways. This chapter investigates the effect of HTC temperature on the mass yield distribution and resultant characteristics of the hydrothermal products. Evaluating the properties of hydrochars and process waters, across a range of HTC temperatures allows an assessment of their suitability for subsequent downstream conversion processes.

This chapter determines the properties and characteristics of hydrochars and process waters following the HTC of macroalgal species (*S. latissima*-SL; *F. serratus*-FS; *L. digitata*-LD), water hyacinth (WH) and grass (GR) biomass feedstocks, across a range of temperatures (150°C, 200°C and 250°C). Therefore, allowing for a direct comparison between the behaviour of macroalgal and lignocellulosic biomass during HTC. Initially, the effect of HTC temperature on both the mass yield and carbon distribution was assessed. Following this, hydrochars were separated and their proximate, ultimate and inorganic compositions characterised, in order to understand the influence of HTC temperature on the energy densification and ash composition of the residual solid fraction. Finally, the composition of process waters were determined, in order to understand the effect of feedstock and HTC temperature on the properties of the process waters.

5.1 Objectives

The objectives of this chapter are to:

- Assess the influence of HTC temperature on the mass yield and carbon distributions across the HTC products.
- Understand the effect of HTC temperature on the compositions of hydrochars and process waters.
- Compare the characteristics of hydrochars and process waters generated from macroalgal and lignocellulosic feedstocks.

5.2 HTC Yields

5.2.1 Mass Yields

During HTC, the structure of biomass is broken down through a number of complex and simultaneous reactions [159], with different biomass-derived species distributed across three possible phases. These phases include the solid phase (hydrochar), aqueous phase (process water) and gaseous phase (gas). The mass distribution of the original biomass across each of the three phases, after HTC, are referred to as 'mass yields'. The mass yields of macroalgal species (SL, FS and LD), water hyacinth (WH) and grass (GR) following HTC reactions are displayed in Table 5.1.

Table 5.1 Yields of products following HTC reactions.

Sample	Yield (wt%)		
	Hydrochar	Process Water	Gas
SL150	37.5 ± 1.0	61.8 ± 0.7	0.7 ± 0.3
SL200	28.4 ± 0.8	70.9 ± 0.5	0.7 ± 0.3
SL250	22.0 ± 0.8	76.7 ± 0.6	1.3 ± 0.3
FS150	44.7 ± 3.7	54.6 ± 3.6	0.7 ± 0.1
FS200	32.7 ± 0.7	66.4 ± 0.8	0.9 ± 0.1
FS250	27.6 ± 1.7	71.0 ± 1.7	1.4 ± 0.2
LD150	40.4 ± 1.8	58.7 ± 1.7	1.0 ± 0.2
LD200	30.3 ± 0.3	68.6 ± 0.3	1.1 ± 0.2
LD250	22.1 ± 1.0	76.8 ± 0.9	1.2 ± 0.1
WH150	79.9 ± 1.8	20.1 ± 0.9	0.6 ± 0.0
WH200	57.8 ± 0.9	41.4 ± 0.9	0.9 ± 0.0
WH250	37.9 ± 0.4	60.5 ± 0.4	1.7 ± 0.0
GR150	73.4 ± 2.7	26.0 ± 2.8	0.6 ± 0.1
GR200	57.0 ± 2.6	42.2 ± 2.7	0.8 ± 0.1
GR250	37.4 ± 4.2	61.1 ± 4.0	1.4 ± 0.5

Data is presented as average ± standard deviation.

The hydrochar yields decreased with increasing HTC temperature across all biomass feedstocks presented in Table 5.1. This trend is well defined in previous studies across a range of biomass types, including: lignocellulosic biomass [49,64,74], microalgal biomass [160], macroalgal biomass [66,80,184,185] and digestates [170,171].

The hydrochar yields observed in Table 5.1 are lower for macroalgal feedstocks than lignocellulosic biomass, across comparative HTC processing temperatures. The average hydrochar yield for macroalgal species (SL, FS and LD) was: 40.9% (150°C), 30.5% (200°C)

and 23.9% (250°C). Whereas, the average hydrochar yield for the lignocellulosic biomass (WH and GR) was; 76.7% (150°C), 57.4% (200°C) and 37.7% (250°C). The lower hydrochar yields of macroalgal hydrochars is thought to be due to differences between the biochemical compositions [64,80]. The carbohydrate fractions of macroalgal biomass include: alginates, laminarin, mannitol, fucoidan and other polysaccharides [65,80]. Whereas, lignocellulosic biomass is comprised of cellulose and hemicellulose polysaccharides, with interlinking lignin polymers [24]. Hydrolysis of hemicellulose starts around 180°C [159] and cellulose around 230°C [159,242]. However, seaweed polymers begin to hydrolyse at lower temperatures than hemicellulose and cellulose: including, alginates; 150-160°C [69,243], laminarin; 140°C [69] and fucoidan; 140°C [69]. The HTC reactions conducted as part of this thesis were carried out at 150°C, 200°C and 250°C. Therefore, seaweed polysaccharides are more readily degraded at the lowest HTC processing temperature used in this study. Whereas, hemicellulose and cellulose polymers would degrade during the reactions conducted at 200°C and 250°C, respectively. Therefore, a higher hydrochar yield would be expected for lignocellulosic feedstocks, compared to macroalgal biomass, at the selected HTC processing temperatures used in this study.

FS displayed higher hydrochar yields than SL and LD, across comparative HTC processing temperatures. Hydrochar yields were 44.7%, 37.5% and 40.4% (150°C), 32.7%, 28.4% and 30.3% (200°C) and 27.6%, 22.0% and 22.1% (250°C), for FS, SL and LD, respectively. This suggests potential differences in the behaviour of wracks (FS) and kelps (SL and LD) during HTC, due to variances between biochemical compositions. Kantarli *et al.* [66] have also shown that wracks (*F. serratus*) generated higher hydrochar yields compared to kelps (*A. esculenta*), across comparable HTC conditions. GR and WH display similar hydrochar yields (Table 5.1), particularly at HTC temperatures of 200°C and 250°C. GR and WH have been shown to have a similar carbohydrate composition (Chapter 4). Therefore, it would be expected that the carbohydrate fractions would degrade in a similar manner; producing similar hydrochar yields. Although, slight variations would be expected as different sized HTC reactors were used for WH (2-L) and GR (600-mL).

Hydrochar yields outlined in Table 5.1 reduced by: 9% (SL), 12% (FS), 10% (LD), 22% (WH) and 16% (GR), between temperatures of 150°C to 200°C. Moreover, hydrochar yields reduced by 6% (SL), 5% (FS), 8% (LD), 20% (WH and GR), between temperatures of 200°C to 250°C. The reduction in hydrochar yield across the temperature range used in this study is greater for lignocellulosic biomass than macroalgal biomass; also highlighted by previous studies [66]. Again, this is likely related to the differences in the degradation temperatures of different macroalgal and lignocellulosic polysaccharides. Processing at 150°C allows for the degradation of macroalgal polysaccharides, whilst hemicellulose and cellulose fractions remain relatively intact. Increasing the HTC processing temperature to 200°C and 250°C will

degrade the hemicellulose and cellulose fractions within WH and GR, explaining the increased reduction in hydrochar yield, compared to SL, FS and LD. Despite this, an ANOVA analysis with a Tukey *post hoc* test showed hydrochar yield significantly (p<0.05) decreased with increasing HTC temperature for SL and LD. However, the hydrochar yield of FS200 (32.7%) and FS250 (27.6%) did not significantly differ (p>0.05). Kantarli *et al*. [66] observed a similar finding; suggesting HTC temperature did not largely effect hydrochar yield between 200-250°C. Hydrochar yield decreases with temperature in a sigmoidal fashion [152]. This suggests the degradation of carbohydrate fractions reaches a maximum at a certain temperature, which is likely to vary between feedstocks with different biochemical compositions. However, as HTC reactions in this thesis were only conducted across three temperatures, this sigmoidal relationship cannot be observed.

Table 5.1 shows the process water yield increased at higher HTC processing temperatures, across all feedstocks. All seaweed species (SL, FS and LD) have a higher process water yield, compared to hydrochar yield across all HTC temperatures. Again, this is likely due to the degradation of seaweed carbohydrates across all temperatures tested. The average process water yield for the seaweeds was: 58.4% (150°C), 68.6% (200°C) and 74.8% (250°C). Whereas, the average process water yield for lignocellulosic biomass (WH and GR) was: 23.1% (150°C), 41.8% (200°C) and 60.8% (250°C). Therefore, for lignocellulosic feedstocks, the process water yield was lower than the hydrochar yield at HTC temperatures of 150°C and 200°C. However, a processing temperature of 250°C gave a higher process water yield, compared to the hydrochar yield, due to cellulose degradation. Furthermore, the yield of gas also increased with increasing HTC temperature across all feedstocks in Table 5.1. However, in all cases, the gas yield did not exceed 2%; suggesting the yield of gas is negligible compared to the hydrochar and process water yield.

Cross-comparing data from published studies can prove challenging, due to variations of multiple factors between HTC reactions. For example, Kantarli *et al*. [66] found hydrochar yields of approximately 40% and 33% from *F. serratus* at temperatures of 200°C and 250°C, respectively. These values are slightly higher than the hydrochar yields of FS200 and FS250, shown in Table 5.1. However, Kantarli *et al*. [66] used a shorter retention time (30-min), compared to this study (60-min). A shorter retention time reduces the HTC reaction severity and is therefore likely to lead to higher hydrochar yields. To facilitate easier comparison between studies, the HTC reaction temperature and retention time can be combined into one single parameter defined as the severity factor (SF) [164,211,212], as described in Section 3.2.3. The SFs of the HTC reactions used in this study were: 3.3, 4.7 and 6.2, for processing temperatures of 150°C, 200°C and 250°C, respectively.

Figure 5.1 displays a correlation of HTC SF and hydrochar yield from brown macroalgae, using a combination of values from literature studies [64,66,80,179] and data presented in Table 5.1. Xu *et al.* [180] and Rasam *et al.* [116] were excluded from the correlation due to the use of a citric acid catalyst during the HTC of *Sargassum horneri*. In addition, studies of green [184,185] and red [187] macroalgal species were also excluded. A Spearman's rank correlation coefficient found a significant negative correlation between HTC severity factor and hydrochar yield produced from brown macroalgae; in Figure 5.1 (ρ= -0.620, N=33, p<0.05).

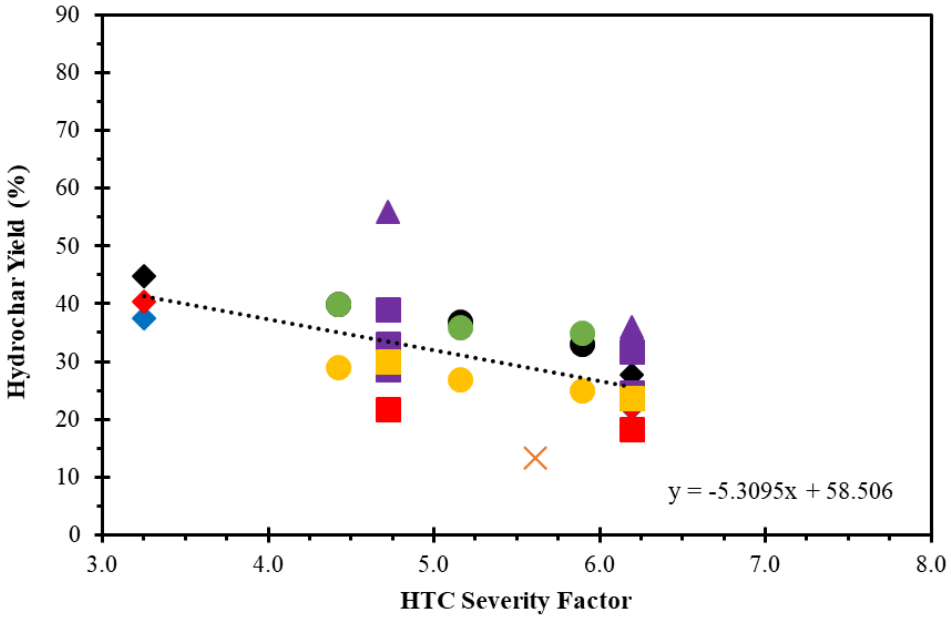

Figure 5.1. Correlation of severity factor and hydrochar yield for brown macroalgae. Data points are a combination of literature values and values found in this work. The different colours represent different macroalgal species; blue=*S. latissima*, red=*L. digitata*, black=*F.serratus*, *purple=L. hyperborea*, yellow=*A. esculenta*, green=mixed species and orange=*Laminaria*. The different shapes represent different studies; ♦ =this work, ▲ =[64], ■ =[80], ● =[66], × =[179].

In addition, Figure 5.2 displays a correlation of HTC SF and hydrochar yield for WH using a combination of literature studies [76,77,172,173] and data from Table 5.1. Zhang *et al.* [76] examined the effect of pH on WH HTC; only tests conducted at pH 7 were included in Figure 5.2. There was a significant negative correlation between HTC SF and hydrochar yield produced from WH (ρ= -0.756, N=30, p=0.000), according to a Spearman's rank correlation co-efficient analysis.

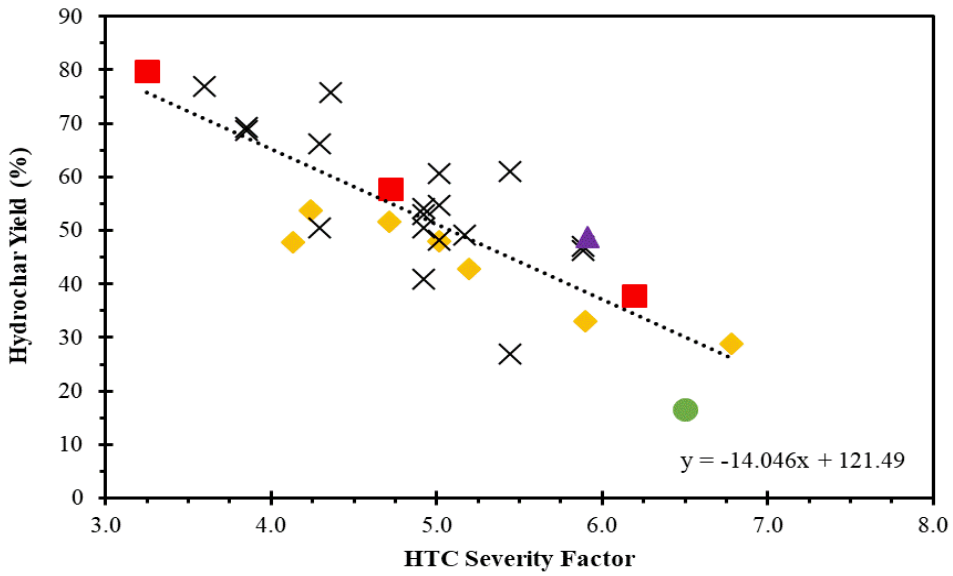

Figure 5.2. Correlation of severity factor and hydrochar yield for water hyacinth. Data points are a combination of literature values and values found in this work. The different shapes represent different studies; ■= this work, ♦ =[76], × =[77] , ▲=[172] and ● =[173].

Furthermore, Figure 5.3 displays a correlation of HTC SF and hydrochar yield from GR species, using a combination of literature studies [49,64,74,79,164,178] and data from Table 5.1. Data points where the retention time was 0-min [164,178] have been eliminated from Figure 5.3; as this gives a SF of 0. There was a significant negative correlation between HTC SF and hydrochar yield produced from GR (Spearman ρ= -0.791, N=41, p=0.000), again, according to a Spearman's' rank correlation co-efficient analysis.

Figure 5.1, Figure 5.2 and Figure 5.3 all show a significant (p<0.05) negative correlation between HTC SF and hydrochar yield for the different feedstock types: brown macroalgal species, WH and GR. Although, these correlations must be interpreted with caution. Figure 5.1 groups different species of brown seaweeds together, which may display different behaviours during HTC; as shown in Table 5.1 and [66]. However, the extent of inter-species differences is difficult to analyse, as there are limited amount of studies which focus on the HTC of brown macroalgae. Again, this is an issue for Figure 5.3, where different species of GR are compared together. An additional factor to be considered is the effect of seasonal variation of biomass composition on subsequent hydrochar yields and characteristics. Harvesting season appears to have an effect on the hydrochar yields obtained from the seaweed species *L. hyperborea* [80], as well as miscanthus [49], due to changes in the biochemical composition. However, there is no current information available which identifies the impact of seasonal variation on the behaviour of WH during HTC.

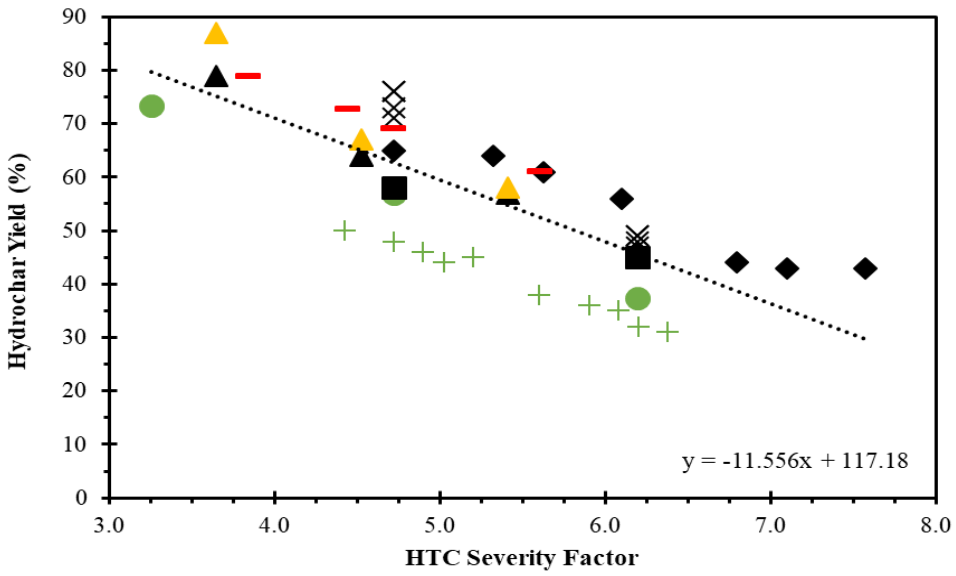

Figure 5.3. Correlation of severity factor and hydrochar yield for grass. Data points are a combination of literature values and values found in this work. The different colours represent different grasses; green=lawn/campus grass, black=miscanthus, yellow=switch grass and red=energy grass. The different shapes represent different studies; ● =this work, ♦ =[164], ■ =[64], × =[49], ▲ =[74], + =[79], – =[178].

5.2.1 Carbon Balance

Increasing HTC processing temperatures causes a reduction in hydrochar yield and an increase in process water yield. All seaweed species showed a greater process water yield than hydrochar yield across all three HTC temperatures (Table 5.1). WH and GR also displayed this trend, when processed at the highest HTC temperature; 250°C. This suggests increased solubilisation of organic and inorganic species into the process water. Table 5.2 displays the percentage distribution of carbon, from the original feedstock, across the hydrochar and the process water fractions.

Overall, the carbon yield recovered in the hydrochar fraction decreased with increasing HTC temperature, across all feedstocks; likely because of reduced hydrochar yields, shown in Table 5.1. This trend is observed in other feedstocks, such as: cow manure [244], digestates [170,245], olive oil waste streams [189]. The distribution of carbon in the hydrochars (Table 5.2) is constantly higher than the corresponding hydrochar yield (Table 5.1) across all feedstocks, suggesting the carbon becomes concentrated in the hydrochar.

However, the behaviour of carbon yield recovery from process waters across different temperatures varied between feedstocks. The process water carbon yield decreased with increasing HTC temperature for FS. Kelp species (SL and LD) showed an increased in process water carbon yield between 150°C and 200°C. However, a decline was observed between

200°C and 250°C. Conversely, WH process water carbon yields showed the reverse trend; increasing with HTC reaction severity: 18% (WH150), 29% (WH200) and 32% (WH250). GR process water carbon yields remained relatively similar (31-33%) across the different HTC reaction temperatures. However, GR150 process water had a slightly higher carbon yield compared to GR200 and GR250.

Becker *et al*. [245] found carbon yield recovered in hydrochar produced from a range of lignocellulosic biomass decreased with increased HTC temperature: 68-70% (190°C), 58-69% (230°C), 59-66% (250°C) and 54-63% (270°C). The same research group later confirmed the carbon within the process water accounted for 30-50% of the original biomass carbon at a HTC temperature of 270°C [157]. These values are in line with WH and GR values presented in Table 5.2. At present, there is no macroalgal-derived HTC carbon balance data available in literature.

Table 5.2. Average carbon distribution between hydrochars and process waters.

Sample	Carbon Yield (%)		
	Hydrochar	Process Water	Total
SL150	48	54	102
SL200	40	59	99
SL250	34	53	87
FS150	60	53	112
FS200	49	46	94
FS250	44	43	87
LD150	54	60	115
LD200	45	61	106
LD250	37	55	91
WH150	83	18	101
WH200	71	29	100
WH250	55	32	87
GR150	74	33	108
GR200	64	31	95
GR250	50	31	81

Table 5.2 displays the total carbon yield for each HTC reaction; calculated through a summation of the carbon recovered from both the hydrochar and process water. The total yield was greater than 100% for all feedstocks processed at 150°C, as well as LD200. Therefore, the methodology of predicting carbon balance may overestimate carbon availability at lower HTC processing temperatures. Conversely, higher HTC processing temperatures gave a total carbon yield lower than 100%. Processing at 250°C means between 9-19% of the carbon is unaccounted for across the feedstocks in Table 5.2. As a result of this, the total carbon yield decreased with increased HTC temperature across all feedstocks. The unaccounted fraction of total carbon can be attributed to losses into the gaseous fraction [244], as gas yield increases with increased HTC temperature (Table 5.1). The composition of gas is typically expected to be >95% CO_2, with trace quantities of CO, CH_4 and lightweight hydrocarbons [189]. The gas fraction obtained from HTC has not been analysed as part of this study.

Accordingly, Figure 5.4 shows the normalised distribution of carbon between the hydrochar and the process water fractions. Once normalised, the carbon distribution of the hydrochar decreased with increasing HTC temperature, whilst the carbon distribution in the process water increased, across all feedstocks. The HTC process waters from kelp species (SL and LD) had a normalised carbon distribution of 53% (150°C), 57-60% (200°C) and 60-61% (250°C). Additionally, the process water carbon distribution of FS150, FS200 and FS250 was 47%, 48% and 49%, respectively.

The carbon distribution of the kelp macroalgal species was greater in the process water than hydrochar. Furthermore, wrack species; FS showed almost equal carbon distribution between the hydrochar and process waters, across all HTC processing temperatures. Conversely, Figure 5.4d-e show the normalised carbon distribution of lignocellulosic feedstocks was shifted towards the hydrochar, compared to the process water. The normalised carbon yields of WH150, WH200 and WH250 hydrochars were 82%, 71% and 63%, respectively. Whereas, the normalised carbon yield of GR150, GR200 and GR250 hydrochars were 69%, 68% and 62%, respectively. The carbon recovery of hydrochars remains high across all feedstocks, despite the overall low mass of hydrochars recovered.

Overall, a significant proportion of carbon was distributed towards the HTC process waters; particularly for macroalgal species. Therefore, in order to maximise the energetic output from HTC reactions, the process waters must also be considered as a significant energy carrier and the value of this product extracted alongside the hydrochar.

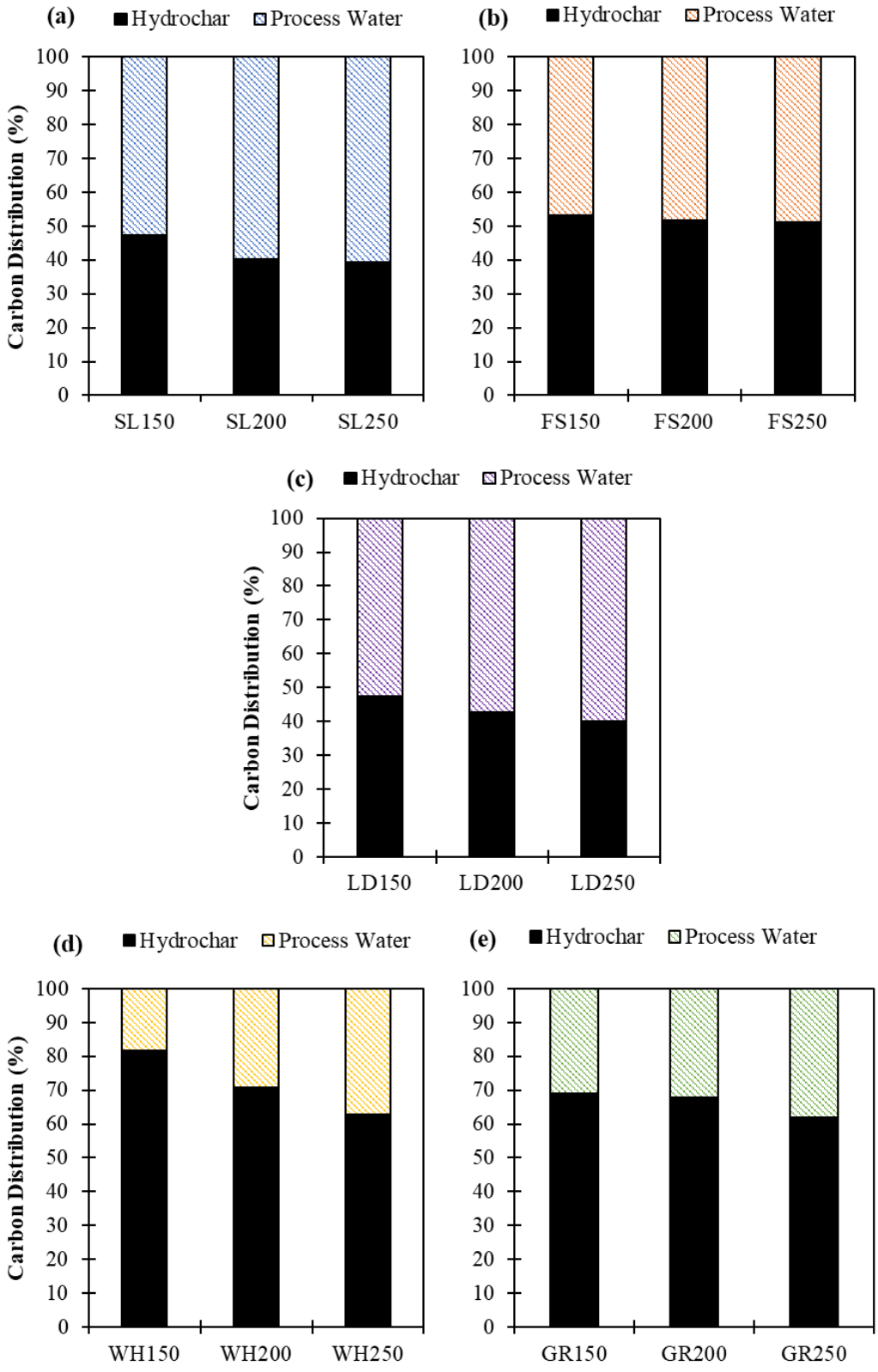

Figure 5.4. Normalised carbon distribution between hydrochars and process waters following the HTC of (a) SL (b) FS (c) LD (d) WH (e) GR. Gaseous phase is excluded from the carbon distribution.

5.3 Hydrochar Characteristics

5.3.1 Proximate and Ultimate Composition

The proximate and ultimate compositions of the hydrochars are shown in Table 5.3, alongside the compositions of the original biomass. The carbon content of hydrochars increased with increasing HTC temperature, whilst the oxygen content of the hydrochars generally displayed the inverse trend; decreasing as HTC temperatures increased. The O-contents of SL, FS, LD and WH and associated hydrochars were determined directly, whilst the O-contents of GR and GR-derived hydrochars were calculated by difference; due to the conclusions obtained from Section 4.4. The largest increase in carbon content is observed between FS (35.7%) and FS250 (54.6%). The increasing C-content between untreated seaweeds and 150°C hydrochars is greater than the increase in C-content between untreated WH or GR and WH150 or GR150. This suggests limited energy densification occurs for lignocellulosic biomass at 150°C; whereas energy densification occurs at this temperature for macroalgal species.

The de-oxygenation of hydrochars is further highlighted by a Van Krevelen diagram (Figure 5.5). The Van Krevelen diagram compares the atomic H:C and O:C ratios of biomass, hydrochars and coals and highlights the effect of temperature on the compositional changes to the biomass, during the HTC process. Generally, a reduction in H:C and O:C was observed with increasing HTC temperature, across each biomass feedstock. Decreased H:C and O:C ratios are associated with dehydration and decarboxylation reactions, respectively. Decarboxylation reactions are associated with the removal of carboxyl (-COOH) and carbonyl groups (C=O). Whereas, dehydration reactions are associated with the removal of hydroxyl groups (-OH) [64]. Both reactions reduce the oxygen content, whilst concentrating the carbon content of the solid; reflected by the ultimate analysis shown in Table 5.3. Figure 5.5 also shows that hydrochars produced at higher temperatures display the more ‘coal-like’ properties [49], in this case, HTC250.

Despite the general decrease in H:C with increasing HTC temperature, SL, LD, WH and GR hydrochars produced at 150°C showed a slight increase in H:C, compared to the untreated biomass. Smith and Ross [80] report differences in the H:C ratios between different feedstocks; with H:C in macroalgal-dervied hydrochars remaining similar at each HTC temperature. Whereas, H:C decreased with increasing HTC temperature in lignocellulosic feedstocks.

Table 5.3. Proximate and ultimate composition of biomass feedstocks and hydrochars.

Sample	Ultimate Analysis (wt% *db*)					Proximate Analysis (wt%)			
						(*ar*)	(*db*)		
	C	H	N	S	O	M	VM	FC	Ash
SL	33.0 ± 0.7	2.9 ± 0.1	1.9 ± 0.1	ND	23.7 ± 2.6*	7.6	75.3	13.2	11.4
SL150	41.1 ± 1.0	4.4 ± 0.0	2.8 ± 0.0	ND	26.1 ± 0.2*	4.4	73.3	16.1	10.6
SL200	43.2 ± 0.6	3.7 ± 0.2	2.2 ± 0.0	ND	20.3 ± 0.6*	2.3	69.4	17.4	13.2
SL250	48.3 ± 0.3	4.2 ± 0.3	2.2 ± 0.0	ND	15.2 ± 0.4*	2.0	63.0	18.9	18.1
FS	35.7 ± 0.1	3.9 ± 0.6	2.0 ± 0.1	ND	27.8 ± 0.2*	6.2	73.2	13.2	13.6
FS150	46.8 ± 0.4	3.8 ± 0.1	3.0 ± 0.0	ND	25.0 ± 0.0*	4.4	72.3	18.4	9.3
FS200	51.1 ± 0.0	4.3 ± 0.1	2.8 ± 0.0	ND	20.3 ± 0.8*	2.6	67.1	20.5	12.5
FS250	54.6 ± 0.1	4.1 ± 0.1	2.4 ± 0.0	ND	15.0 ± 0.1*	1.8	61.9	20.7	17.4
LD	26.5 ± 0.3	3.4 ± 1.0	2.1 ± 0.1	ND	23.2 ± 0.0*	5.1	69.2	15.6	15.2
LD150	35.0 ± 0.1	4.8 ± 0.8	2.8 ± 0.0	ND	23.7 ± 0.5*	3.4	72.8	15.3	11.8
LD200	38.3 ± 0.0	4.9 ± 0.3	2.6 ± 0.0	ND	20.5 ± 0.1*	1.9	68.6	17.4	14.0
LD250	42.2 ± 0.5	5.1 ± 0.2	2.4 ± 0.0	ND	16.9 ± 0.5*	1.7	63.4	16.6	20.1
WH	38.7 ± 0.0	3.4 ± 0.0	2.7 ± 0.1	0.1 ± 0.1	27.4 ± 0.5*	6.7	85.5	ND	14.5
WH150	39.3 ± 0.2	3.5 ± 0.0	2.5 ± 0.0	ND	27.3 ± 0.3*	4.9	77.2	7.9	15.0
WH200	45.5 ± 0.1	3.7 ± 0.0	2.6 ± 0.0	ND	25.0 ± 0.2*	3.0	70.8	14.8	14.4
WH250	53.0 ± 0.7	4.0 ± 0.5	3.4 ± 0.0	ND	14.9 ± 0.3*	1.7	55.3	22.9	21.8
GR	44.2 ± 1.0	6.9 ± 0.8	3.9 ± 0.1	ND	34.0 ± 1.7**	5.9	73.8	15.2	11.0
GR150	45.2 ± 0.4	6.1 ± 0.2	3.0 ± 0.1	0.4 ± 0.0	39.7 ± 0.3**	6.8	77.7	16.6	5.6
GR200	49.0 ± 0.6	6.3 ± 0.4	3.0 ± 0.0	0.4 ± 0.0	31.8 ± 0.2**	3.9	69.7	20.7	9.6
GR250	57.2 ± 0.2	6.1 ± 0.2	3.4 ± 0.0	0.4 ± 0.0	18.9 ± 0.1**	2.3	58.6	27.4	14.0

*Oxygen measured directly. **Oxygen measured by-difference. ND=not detected. *ar*=as received. *db*=dry basis. M=moisture. VM=volatile matter. FC=fixed carbon. Proximate analysis determined by TGA analysis.

The nitrogen and sulphur concentrations are crucial to the application of hydrochars as a solid combustion fuel, due to the formation of NO_x and SO_x emissions. The release of NO_x and SO_x emissions can result in severe environmental and human health impacts [175]. NO_x is formed through the oxidation of the N-containing species within a fuel [236]. Figure 5.6 shows the nitrogen removal efficiency from the biomass increased as HTC temperature increased. The nitrogen is removed from the original biomass and solubilised into the process water [244,246]. Nitrogen removal from the hydrochars was highest at 250°C, with the seaweed samples and GR showing the highest nitrogen removal at this temperature: SL (72%), FS (66%), LD (64%) and GR (66%). Hydrochars produced from WH had the lowest nitrogen removal efficiency across all HTC temperatures: 24% (WH150), 43% (WH200) and 49% (WH250).

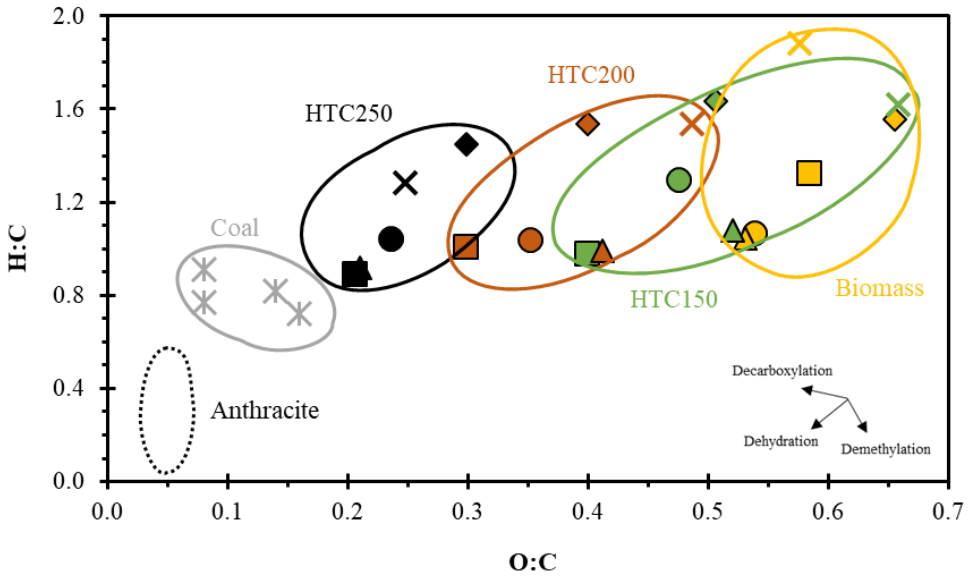

Figure 5.5. Van Krevelen diagram for biomass and resultant hydrochars. Coal values adapted from [165], anthracite zone adapted from [160]. H:C and O:C atomic ratios are presented on a dry ash free basis (*daf*). ●=SL. ■=FS. ♦=LD. ▲=WH. ×=GR.

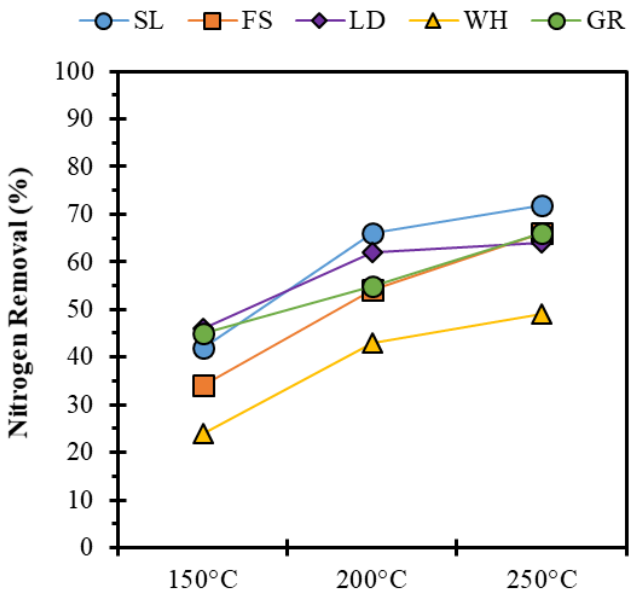

Figure 5.6. Nitrogen removal efficiencies from the biomass into the process water.

Despite Figure 5.6 showing nitrogen removal efficiency increased at higher HTC temperatures, Table 5.3 shows the N-content of the hydrochars remains high (2.2-3.4%). Nitrogen removal efficiency increases due to a reduction in overall hydrochar yield (Table 5.1), meaning there is a reduced mass of the solid fraction following HTC. Compared on a like-for-like basis, all seaweed hydrochars contained a higher N-content compared to the parent biomass. This has been previously observed by [80]. Although, N-content reduced with

increasing HTC temperature across all seaweed hydrochars. WH150, WH200, GR150 and GR200 had a lower N-content, compared to the original parent biomass. However, the N-content remained high (2.5-3%). WH250 had an N-content of 3.4%; higher than WH. GR250 also displayed an N-content of 3.4%; although this was slightly lower than the N-content of GR.

Linear relationships have been shown between fuel-N content and NO_x emissions for solid fuels with a N-content of up to 2% [236] and between 1-10% [247]. Conversely, N-content was found not to be causally related to the NO_x emission during thermochemical conversion of microalgae [248]. Furthermore, the conversion rate of fuel-N to NO_x has been shown to decrease at higher fuel-N concentrations [247]. Therefore, it remains unclear whether the hydrochars in Table 5.3 would generate high levels of NO_x emissions during combustion. However, it remains true that the N-content of the hydrochars remains high, which could create potential problems downstream. Zhang *et al*. [76] found lower NO_x emissions for WH-derived hydrochars, compared to untreated WH. Although, NO_x emissions from hydrochars are likely to be feedstock dependent, with the study of the mechanisms of NO_x emissions requiring further study.

Sulphur was not detected across SL, FS, LD and WH hydrochars (Table 5.3), suggesting SO_x emissions would not be problematics during combustion of these hydrochars. However, all GR hydrochars contain 0.4% sulphur; which could cause the release of SO_x emissions. The S-content of hydrochars is typically lower than the parent biomass [64]. Again, Zhang *et al*. [76] showed a reduction in SO_2 emissions in WH-derived hydrochars, compared to the parent biomass.

In addition to the ultimate composition, Table 5.3 also displays the proximate composition of the hydrochars and original biomass. The moisture contents of hydrochars displayed in Table 5.3 are derived from TGA analysis, following drying the hydrochars at 60°C. The moisture contents range from 5.1-7.6% (untreated biomass), 3.4-6.8% (150°C hydrochars), 1.9-3.9% (200°C hydrochars) and 1.7-2.3% (250°C hydrochars). Therefore, the moisture content of hydrochars decreased with increased HTC temperature. Hydrochars display hydrophobic properties [75,212,249], allowing greater stability during transportation and storage. Higher HTC processing temperatures are associated with generating hydrochars with enhanced hydrophobic properties. Increased hydrophobicity is associated with the removal of hydroxyl and carboxyl groups during HTC [64,250].

Generally, as HTC processing temperature increased, the VM content of the hydrochars decreased, whilst the FC content increased (Table 5.3). The increase in FC corresponds to a simultaneous increase in C-content. However, the VM still represents the greatest fraction across each biomass and hydrochar shown in Table 5.3. The VM contents were: 72.3-77.7%,

67.1-70.8% and 55.3-63.4% for hydrochars produced at 150°C, 200°C and 250°C, respectively.

The fuel ratio describes the ratio of FC to VM (FC/VM) and is used to rank hydrochars as alternative, coal-like fuels [251]. A high VM content reduces the quality of a solid combustion fuel by causing flame instability and subsequent losses in heat. Whereas, a high FC content can increase combustion temperatures by producing a more stable flame [160]. Figure 5.7 shows a general increase in the fuel ratio with increasing HTC temperature for all feedstocks. The lignocellulosic feedstocks (WH and GR) showed a greater increase in FC/VM, compared to the macroalgal feedstocks. WH, WH150, WH200 and WH250 had a FC/VM of 0.00, 0.10, 0.21 and 0.41, respectively. GR, GR150, GR200 and GR250 had a FC/VM of 0.21, 0.21, 0.30 and 0.47, respectively. GR250 had the greatest FC/VM of any sample in Figure 5.7. The macroalgal feedstocks generally showed a slight increase in FC/VM with increasing HTC temperature; increasing from 0.18-0.23 for untreated seaweed to 0.26-0.33 for hydrochars produced at 250°C. Therefore, hydrochars produced at higher HTC temperatures; 250°C, displayed more favourable FC/VM. However, the fuel ratio remained significantly lower than coal: 1.5 [236].

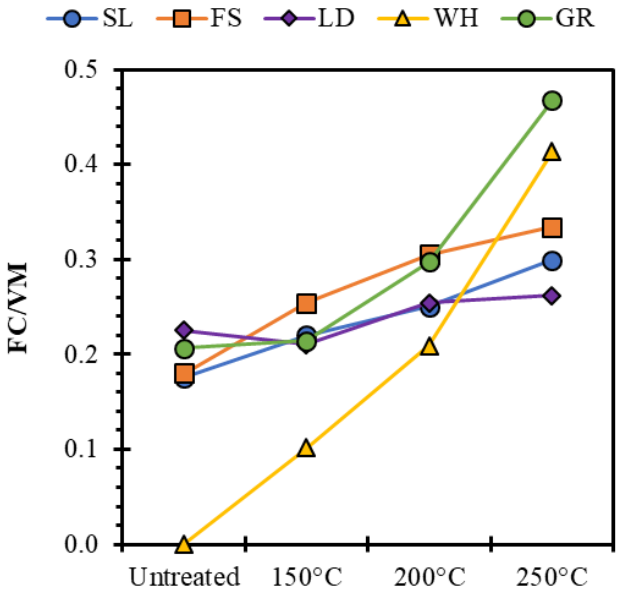

Figure 5.7. Fuel ratio (FC/VM) of biomass and hydrochars

The ash content of a biomass or hydrochar is crucial for its application as a solid combustion fuel. The energy potential is associated with the carbon-fraction, with the ash effectively inert, in relation to energy generation. Therefore, combustion of high ash feedstocks in industrial biomass boilers can be problematic, as large amount of ash residue can accumulate, with

induced additional removal costs. Additionally the composition of ash may create slagging, fouling and corrosion issues [64].

The ash removal efficiencies from the different biomass are displayed in Figure 5.8. The ash removal efficiency remains relatively stable for all macroalgal biomass (63-71%), across all HTC temperatures. Although, a slight decrease in ash removal efficiency is seen between 200°C and 250°C, for example FS200: 69% and FS250: 63%; suggesting re-incorporation of inorganics into the hydrochar at higher temperatures. The efficacy of ash removal in WH150 is low (16%), however the ash removal observed for WH200 and WH250 remains stable at a higher level (40%). The removal of ash between GR200 and GR250 also remains stable (49-50%). However, GR150 showed a higher ash removal, of 63%. Macroalgal-derived hydrochars display a greater removal of ash than lignocellulosic hydrochars at higher processing temperatures (200°C and 250°C). This suggests variations in inorganic composition between the biomass types and the removal efficiencies of different inorganic species from the solid phase.

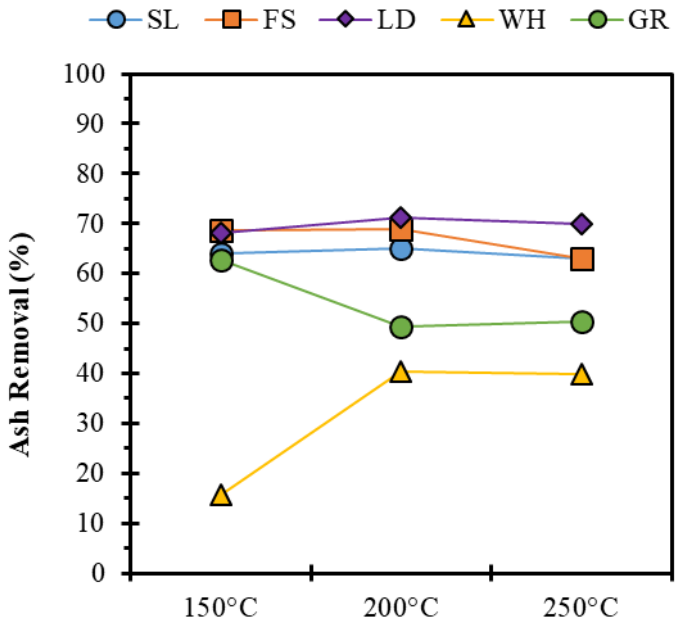

Figure 5.8. Ash removal efficiencies from the biomass into the process waters.

The ash contents, derived from TGA analysis of the original biomass and resultant hydrochars are displayed in Table 5.3. The ash content decreased between the untreated biomass and hydrochars generated at 150°C; with the exception of WH150. Following this, the ash content increased between HTC temperatures of 150°C and 200°C to concentrations which were generally similar to the parent feedstock. A further increase in ash content is observed between 200°C and 250°C to levels above that of the parent feedstock. This trend occurs across all biomass types presented in Table 5.3. Therefore, despite Figure 5.8 showing high removal of

ash from the original biomass, during HTC, Table 5.3 shows the ash content of the hydrochars can be higher than the parent feedstock, especially at higher processing temperatures (250°C). Ideally, the ash content of a solid combustion fuel would be minimised, due the inert contribution of ash to the calorific value of the fuel, or the potential problematic ash behaviour in the form of slagging, fouling and corrosion.

5.3.2 Inorganic Composition

The inorganic composition of a fuel is crucial to its application in large-scale combustion. Unfavourable ash composition of a solid combustion fuel can result in issues with the operation of a commercial furnace, including; reduced thermal efficiency, corrosion and manual removal of the ash from the furnace [64].

Previously, Table 5.3 showed the proximate compositions of hydrochars were altered compared to the original biomass, with further changes observed across increasing HTC temperatures. However, the composition of the residual ash also changes with increased HTC severity [64,74]. Selective demineralisation of the biomass during HTC has been shown to improve the ash chemistry of the resultant hydrochar; therefore, reducing the slagging and fouling propensities during combustion [64,74]. Table 5.4 displays the concentrations of the major ash components of the different biomass types and hydrochars. Whereas, Table 5.5 shows the removal efficiencies of each inorganic species from the hydrochars, compared to the original biomass; accounting for the reduction in solid mass observed during HTC (Table 5.1).

High concentrations of alkali metals; Na and K are particularly problematic in the slagging and fouling tendencies of a solid combustion fuel [64]. All hydrochars contained lower concentrations of alkali metals, compared to the parent biomass. The concentration of Na decreased with increasing HTC temperature, across all biomass types (Table 5.4). However, Na concentrations remained higher in macroalgal-derived hydrochars, compared to lignocellulosic-derived hydrochars, due to a higher concentration in the initial biomass [65]. Table 5.4 also shows the concentrations of K decreased with increasing HTC temperature for all feedstocks.

Table 5.4. Inorganic composition of biomass feedstocks and hydrochars, determined by XRF analysis.

Sample	Inorganic Content (% Feedstock *db*)							
	Na	Mg	Si	P	Cl	K	Ca	Fe
SL	5.0	0.7	0.1	0.4	10.3	6.2	1.2	0.0
SL150	2.8	0.6	0.1	0.4	6.1	4.1	1.8	0.0
SL200	2.4	0.8	0.1	1.1	5.9	3.9	2.6	0.1
SL250	1.6	2.1	1.2	1.6	3.9	2.6	3.4	0.1
FS	3.8	0.8	0.2	0.2	6.3	4.9	1.2	0.0
FS150	2.1	0.5	0.2	0.1	3.2	2.9	1.3	0.1
FS200	1.6	0.5	0.2	0.3	2.4	2.2	1.7	0.1
FS250	1.0	1.7	1.0	0.5	1.6	1.4	2.8	0.1
LD	4.8	0.6	0.1	0.3	13.5	11.2	1.2	0.2
LD150	3.1	0.6	0.1	0.4	8.4	7.6	1.6	0.2
LD200	3.1	0.7	0.1	0.9	8.1	7.4	2.2	0.3
LD250	1.9	1.8	0.7	1.4	5.6	5.1	3.2	0.5
WH	0.5	0.6	1.4	0.6	3.9	5.2	1.7	0.8
WH150	0.4	0.4	1.4	0.5	2.9	4.0	1.9	0.9
WH200	0.3	0.4	1.7	0.5	2.1	3.0	2.4	1.0
WH250	0.2	0.7	1.7	1.2	0.9	1.3	2.8	1.8
GR	0.1	0.3	1.9	0.6	1.2	2.7	1.5	0.0
GR150	0.0	0.2	2.4	0.6	0.8	1.8	1.6	0.0
GR200	0.0	0.2	2.6	0.7	0.7	1.6	1.7	0.1
GR250	0.0	0.4	3.9	1.5	0.2	0.6	2.9	0.1

db=dry basis.

Table 5.5 shows high removal efficiencies of Na and K, particularly at higher temperatures. The removal of Na and K for macroalgal-derived hydrochars ranged from 74-79%, 80-86% and 90-93%, for hydrochars generated at 150°C, 200°C and 250°C, respectively. Previous studies have reported significant removal of Na and K from brown macroalgae during HTC [66,80]. Smith and Ross [80] reported Na and K removal efficiencies of 95-99% from macroalgal biomass treated at 200°C and 250°C. The removal efficiencies of Na and K of macroalgal-derived hydrochars processed at 200°C are slightly reduced compared to [80]. However, this still represents significant levels of alkali metal removal. Na and K removal was also significant for the lignocellulosic-derived hydrochars; 35-52%, 66-68% and 87-92%, for hydrochars generated at 150°C, 200°C and 250°C, respectively. Smith *et al.* [64] found Na removal from lignocellulosic feedstocks; willow, miscanthus and oak wood was between 46-74% and 64-79% during HTC at 200°C and 250°C. Whereas, K removal was between 69-84% and 84-88% at 200°C and 250°C [64]. The problematic alkali metals are selectively removed from the solid phase, during HTC, especially at higher temperatures, as shown by

[64,74,80] and Table 5.5. Most (>90%) of the Na and K present in biomass are in the form of ionic salts, which are easily removed during HTC [64].

Table 5.5. Removal efficiencies of individual inorganic species from hydrochars, compared to the original biomass.

Sample	% Removal							
	Na	Mg	Si	P	Cl	K	Ca	Fe
SL	-	-	-	-	-	-	-	-
SL150	79	70	48	63	78	75	45	38
SL200	86	70	61	15	84	82	40	36
SL250	93	37	-307	8	92	91	39	35
FS	-	-	-	-	-	-	-	-
FS150	75	70	54	69	77	73	51	36
FS200	86	79	64	38	87	86	53	43
FS250	93	39	-65	2	93	92	37	45
LD	-	-	-	-	-	-	-	-
LD150	74	58	58	54	75	73	46	62
LD200	80	64	59	11	82	80	43	53
LD250	91	34	-210	1	91	90	40	41
WH	-	-	-	-	-	-	-	-
WH150	35	37	17	26	39	38	11	16
WH200	66	61	28	43	69	67	19	32
WH250	87	55	53	15	91	90	38	20
GR	-	-	-	-	-	-	-	-
GR150	52	45	7	21	55	53	22	13
GR200	68	59	22	33	68	67	33	15
GR250	87	56	24	1	93	92	25	14

A high Cl content is also an unfavourable characteristic of a solid combustion fuel, due to associated corrosion issues [64]. Table 5.4 shows that Cl represents the dominant inorganic species for the macroalgal-derived hydrochars. WH hydrochars contained higher Cl levels, compared to GR (Table 5.4). This suggests the aquatic biomass absorbs chlorine-containing ionic salts are from the surrounding water bodies. Removal of Cl followed a similar trend to alkali metals; showing increased removal as HTC temperature increased (Table 5.5). Hydrochars produced at 250°C showed over 90% Cl removal. Again, Cl exists mainly in the form of water-soluble ionic salts [64]. Therefore, Table 5.5 suggests a high removal of salts, such as NaCl and KCl.

Table 5.5 shows that Mg, Ca and P undergo more limited removal during HTC. Table 5.4 shows the Mg concentration of hydrochars generated at 150°C and 200°C are similar to the parent biomass. However, hydrochars generated at 250°C showed an increased Mg concentration, especially for macroalgal-derived hydrochars. This is reflected in Table 5.5,

where SL250, FS250 and LD250 all show a dramatic decrease in Mg removal efficiency, compared to SL200, FS200 and LD200. Ca and P shows a similar trend to Mg; with the highest concentrations present in the hydrochars generated at 250°C (Table 5.4). Smith *et al*. [64] also previously reported limited removal of Mg, Ca and P during HTC. In addition, the percentage removal of Mg, Ca and P decreased between hydrochars generated at 200°C and 250°C; suggesting re-incorporation of these inorganics into the hydrochars. Hydrochars generated at higher temperatures are thought to show an increased surface functionality; therefore have the potential to re-absorb selected inorganics from the process water [64]. The removal of Si is also limited, compared to alkali metals and Cl. Although, SL250, FS250 and LD250 all showed negative Si removal efficiencies. This is because of an initially low concentration of Si in the initial macroalgal feedstocks (0.1-0.2%); therefore, the removal efficiency appears exaggerated.

Overall, HTC appears to selectively remove the inorganic species which are associated with problematic slagging, fouling and corrosion issues during thermal conversion processes. This includes enhanced removal of alkali metals: Na and K, as well as Cl, particularly at higher HTC processing temperatures. Therefore, HTC appears to suitably upgrade biomass to generate a solid fuel with enhanced combustion properties.

5.3.3 HHV and Energy Densification

HTC is thought to simulate the natural coalification process; [147,159]; generating an energy densified, coal-like solid; hydrochar [150]. Figure 5.9 shows the changing appearance of WH hydrochar under the different HTC conditions. A darker, more coal-like appearance was observed at higher processing temperatures. The darker appearance is likely due to increased carbon content; reflected in Table 5.3.

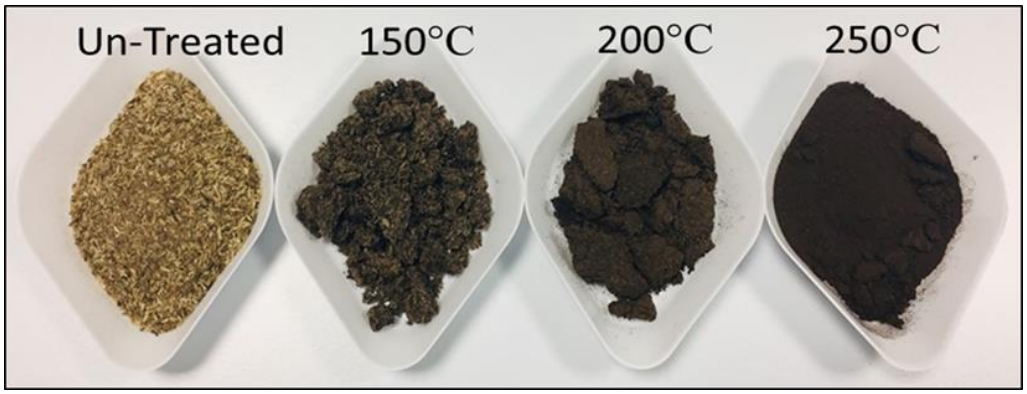

Figure 5.9. Images of untreated water hyacinth (WH) and hydrochars produced from WH during hydrothermal carbonisation at 150°C, 200°C, and 250°C.

Table 5.6 displays the HHVs of the hydrochars, calculated by Dulong's equation using the O-content measured both directly and by difference and through bomb calorimetry. The data is presented alongside each untreated biomass, to ease comparison.

Table 5.6. Effect of determining oxygen content directly or by difference on the HHV of hydrochars.

Sample	O-Content (%*db*)			HHV (MJ/kg *db*)		
	Determined by Difference	Determined Directly	Difference in O-contents	Dulong's (Oxygen Determined by difference)	Dulong's (Oxygen Determined Directly)	Bomb Calorimetry (MJ/kg)
SL	50.8 ± 1.0	23.7 ± 2.6	27.1	6.3	11.1	12.4
SL150	41.1 ± 1.1	26.1 ± 0.2	15.0	12.9	15.6	15.7
SL200	37.7 ± 0.4	20.3 ± 0.6	17.4	13.2	16.3	17.0
SL250	27.2 ± 0.1	15.2 ± 0.4	12.0	17.5	19.6	22.0
FS	44.8 ± 0.4	27.8 ± 0.2	17.0	9.7	12.7	13.8
FS150	37.1 ± 0.5	25.0 ± 0.0	12.1	14.7	16.8	18.0
FS200	29.4 ± 0.1	20.3 ± 0.8	9.1	18.1	19.8	21.4
FS250	21.5 ± 0.0	15.0 ± 0.1	6.5	20.4	21.6	23.6
LD	52.7 ± 1.3	23.2 ± 0.0	29.5	4.5	9.7	10.4
LD150	45.7 ± 0.9	23.7 ± 0.5	22.0	10.5	14.4	13.8
LD200	40.2 ± 0.3	20.5 ± 0.1	19.7	12.8	16.3	15.2
LD250	30.2 ± 0.4	16.7 ± 0.5	13.5	16.1	18.5	18.2
WH	40.7 ± 0.2	27.4 ± 0.5	13.3	10.6	13.0	15.7
WH150	39.7 ± 0.2	27.3 ± 0.3	12.4	11.2	13.5	16.0
WH200	33.9 ± 0.1	25.0 ± 0.2	8.9	14.7	16.3	18.8
WH250	17.7 ± 0.3	14.9 ± 0.3	2.8	20.5	21.0	22.0
GR	34.0 ± 1.7	26.0 ± 0.5	8.0	18.8	20.2	18.2
GR150	39.7 ± 0.3	24.8 ± 0.0	14.9	16.9	19.5	19.9
GR200	31.8 ± 0.2	22.3 ± 0.8	9.5	19.8	21.5	22.0
GR250	18.9 ± 0.1	13.3 ± 0.2	5.6	24.7	25.7	25.8

HHV=higher heating value. *db*=dry basis.

The O-content determined by difference is consistently higher than when O-content is determined directly, across all biomass and hydrochars. Generally, the difference in the O-contents between the different determination methods is greater for macroalgal-derived hydrochars, compared to lignocellulosic-derived hydrochars produced at equivalent temperatures. This is due to the greater Na, K and Cl concentrations found within macroalgal-derived hydrochars (Table 5.4). Another trend observed in Table 5.6 is the difference in the O-contents determined by the different methods generally decreases with increased hydrochar production temperature, with the exception of GR-hydrochars. For example, the difference in O-contents between the different methods for LD, LD150, LD200 and LD250 was 29.5%, 22.0%, 19.7% and 13.5%, respectively. Table 5.5 shows an increasing removal efficiency of

Na, K and Cl from hydrochars at higher HTC temperatures. Therefore, higher-temperature hydrochars would experience reduced volatilisation of ash at 900°C, due to reduced concentrations of Na, K and Cl. The reduced volatilisation of ash means the overestimation of O-content, when determined by difference, is reduced. This concept is illustrated by Figure 5.10, which shows a strong positive correlation (R^2=0.87) between the difference in O-content, determined by the different methods and the Na, K and Cl contents of the hydrochars and biomass. Furthermore, Table 5.6 also shows that using the Dulong's equation with O-content determined directly consistently generates a HHV more closely matching the value obtained by bomb calorimetry, compared to O-content measured by difference; with the exception of GR. However, with increasing HTC temperature, the HHV using the O-content by difference more closely matches the HHV obtained by bomb calorimetry; indicating reduced volatilisation of ash.

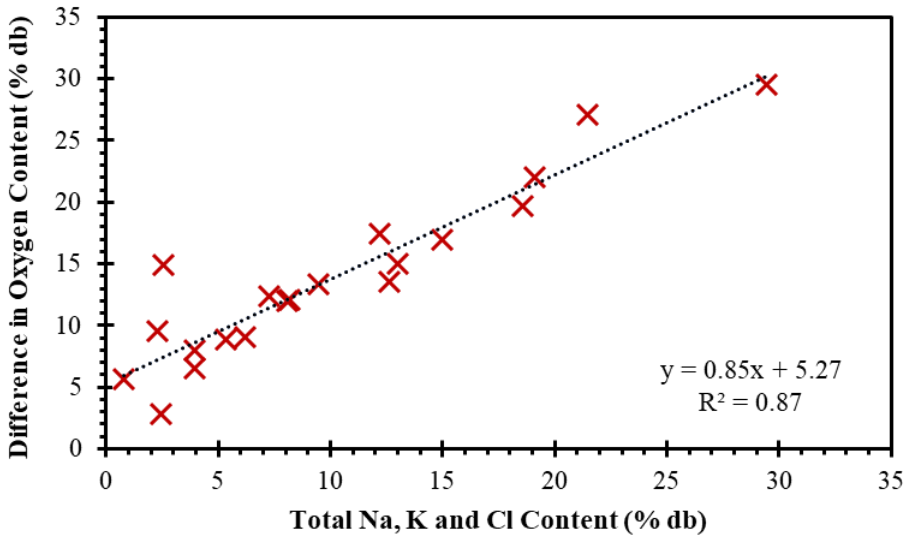

Figure 5.10. Effect of combined alkali metal and chlorine concentration of biomass and hydrochars on the difference between O-content measured directly and by difference.

Generally, HHV values calculated using the O-determined directly more closely matched the values obtained through bomb calorimetry, with the exception of GR. Applying the O-values calculated by difference typically caused an underestimation in HHV, especially for macroalgal-biomass, due to ash volatilisation resulting in an overestimation of O-content. The resulting higher predicted O-content would relate to a decrease in HHV of the biomass [64]. Therefore, the HHVs of macroalgal and WH-derived hydrochars were calculated using Dulong's equation, with the O-content measured directly. Whereas, the HHVs of GR-derived hydrochars were calculated using Dulong's equation with the O-content measured by difference, to maintain consistency with GR.

The HHVs of the untreated biomass and resultant hydrochars are presented in Figure 5.11. Generally, an increase in HHV with increasing HTC temperature was observed. Higher HHVs are related to both an increase in carbon content and a reduction in oxygen content, observed in Table 5.3 and Figure 5.5. GR250 had the highest HHV; 24.7 MJ/kg, with coincides with the highest carbon and fixed carbon contents (Table 5.3).

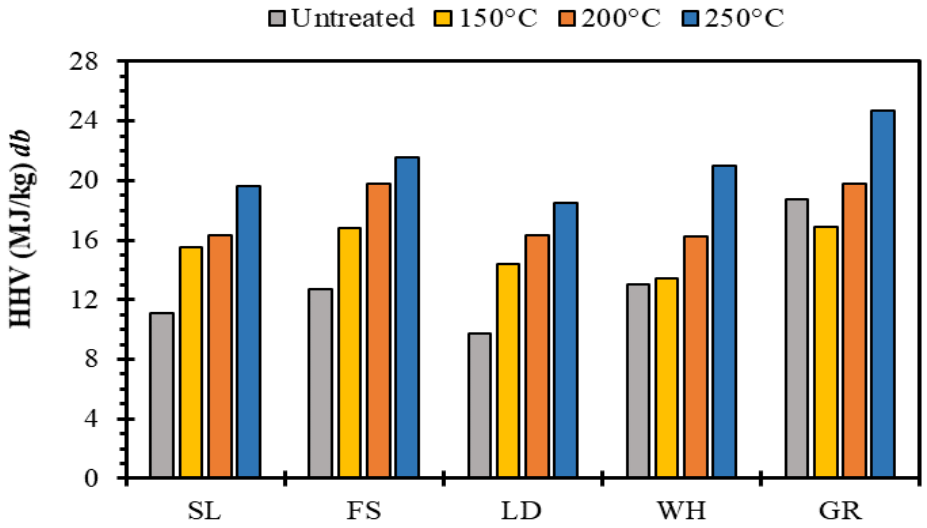

Figure 5.11. HHVs of biomass feedstocks and hydrochars, calculated using Dulong's equation, using the ultimate analysis presented in Table 5.3.

FS hydrochars had greater HHVs than hydrochars generated from kelp species (SL and LD), across comparable processing temperatures. Figure 5.11 shows the HHVs of FS150, FS200 and FS250 were 16.8 MJ/kg, 19.8 MJ/kg and 21.6 MJ/kg, respectively. Whereas, the HHV of SL and LD hydrochars ranged from 14.4-15.6 MJ/kg, 16.3 MJ/kg and 18.5-19.6 MJ/kg, at processing temperatures of 150°C, 200°C and 250°C, respectively. Again, this is due to the lower O:C content of the FS hydrochars (Figure 5.5). In addition, FS hydrochars have a lower ash content compared to SL and FS hydrochars, produced at the same temperature; potentially linked to higher HHVs. Similar trends are reported by Kantarli *et al* [66], comparing fucoid species; *F. serratus* and kelp species *A. esculenta*.

The HHV of WH150 (13.5 MJ/kg) was only slightly higher than the HHV of untreated WH (13.0 MJ/kg). Whereas, WH200 and WH250 had higher HHVs of 16.3 MJ/kg and 21.0 MJ/kg, respectively. A similar trend was observed for GR hydrochars, where the HHV of GR150 (16.9 MJ/kg) slightly decreased compared to GR (18.8 MJ/kg). Whilst GR200 and GR250 showed higher HHVs of 19.8 MJ/kg and 24.7 MJ/kg, respectively. As previously mentioned, HTC reaction temperatures of 150°C would result in limited hemicellulose and cellulose degradation. Therefore, limited energy densification would be expected at these temperatures. Despite this, GR hydrochars had the highest HHV across all feedstocks in Figure 5.11, at

comparable HTC processing temperatures. This is likely because of the initially high HHV of GR (18.8 MJ/kg), compared to other feedstocks (9.7-13.0 MJ/kg).

The energy densification (ED) of the hydrochars are displayed in Figure 5.12. ED was calculated using the HHV values shown in Figure 5.11. ED increased with increasing HTC temperature across all feedstocks, due an increasing HHV. Macroalgal-derived hydrochars showed a greater ED compared to lignocellulosic-derived hydrochars, across all HTC processing temperatures. The average EDs for macroalgal-derived hydrochars were 1.40, 1.57 and 1.79, generated at 150°C, 200°C and 250°C, respectively. WH150 showed limited ED (1.03), whilst GR150 had an ED of 0.90, due to a slight reduction in HHV compared to GR (Figure 5.11). The ED of WH200 (1.25), GR200 (1.06), WH250 (1.62) and GR250 (1.31) were lower than the hydrochars generated from SL, FS and LD, across the same HTC temperature. LD250 had the greatest ED (1.91), potentially due to LD having the lowest HHV of all the untreated feedstocks (Figure 5.11).

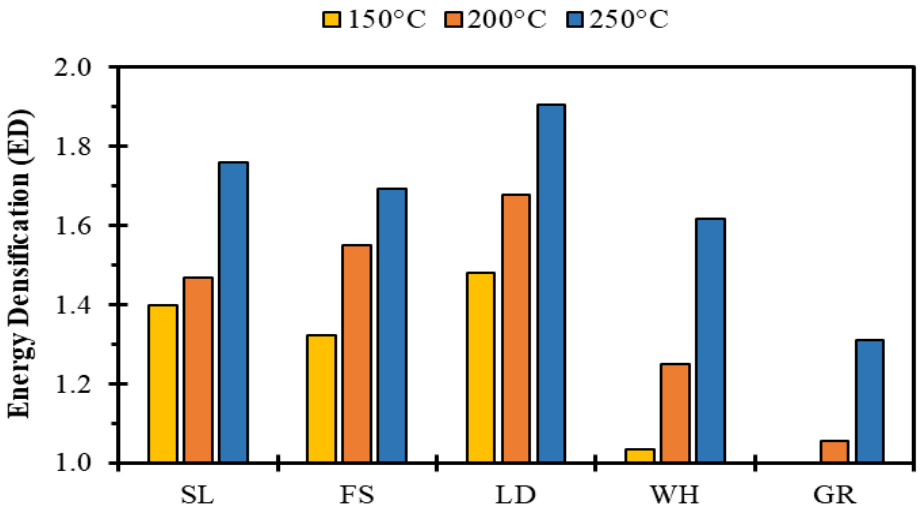

Figure 5.12. Energy densification (ED) of hydrochars.

The energy yield (EY) recovered by each hydrochar is shown in Figure 5.13. EY showed the inverse relationship to HHV and ED; decreasing with increasing HTC temperature, across all feedstocks. The reduction in EY is linked to reduced hydrochar yields at higher HTC temperatures (Table 5.1). Therefore, despite the greater ED of hydrochars produced at higher HTC temperatures, the reduced hydrochar yield causes a reduction in the overall EY.

Figure 5.13 shows the EY was lower for hydrochars generated from macroalgal biomass, compared to lignocellulosic-derived hydrochars. The EY ranges from 53-60%, 42-51% and 39-47% for SL, FS and LD hydrochars generated at 150°C, 200°C and 250°C, respectively. Whereas, the EY ranges from 66-82%, 60-72% and 49-61% for WH and GR hydrochars

generated at 150°C, 200°C and 250°C, respectively. The HHVs of GR hydrochars were higher than macroalgal-derived hydrochars. Whereas, the HHVs of WH hydrochars were more similar to the macroalgal-derived hydrochars. However, the hydrochar yield was higher for lignocellulosic biomass, compared to macroalgal biomass (Table 5.1); explaining the higher EY. The EYs reported in Figure 5.13 are calculated just from the hydrochars. The lower EYs, especially at higher HTC processing temperatures, suggest valorsation of the process waters, can maximise the energy recovery efficiency of a feedstock.

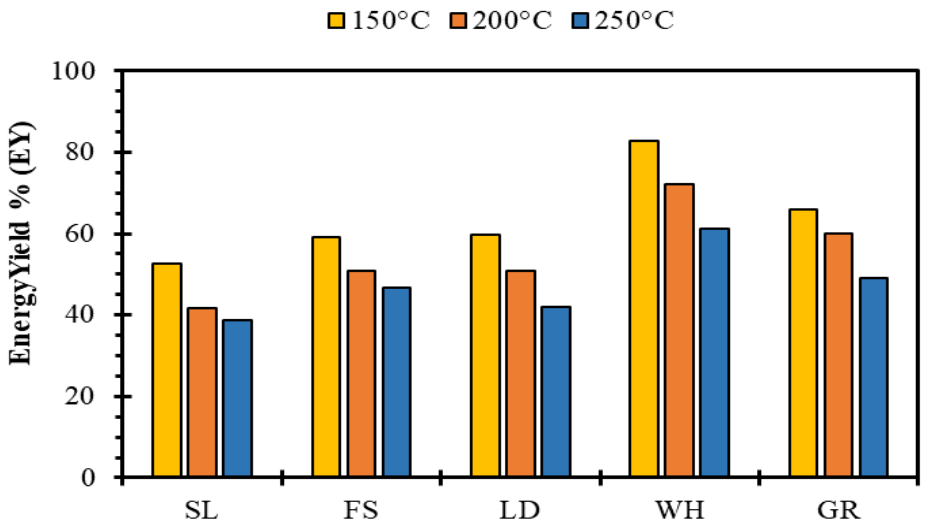

Figure 5.13. Energy yield (EY) of hydrochars.

These trends of increasing HHV and ED, whilst EY decreases, with increasing HTC severity are observed across literature studies of brown seaweeds, water hyacinth and grasses. These trends are observed in Figure 5.14, Figure 5.15 and Figure 5.16. respectively; which combines literature data and data from this thesis. Again, SF is used to compare studies, rather than just HTC temperature to facilitate easier comparison.

HHV significantly increases with increased HTC SF for brown macroalgae (Spearman ρ= 0.554, N=33, p<0.05), WH (Spearman ρ= 0.462, N=43, p<0.05) and GR (Spearman ρ= 0.858, N=31, p<0.05), according to Figure 5.14a, Figure 5.15a and Figure 5.16a, respectively. ED significantly increases with increased HTC SF for brown macroalgae (Spearman ρ= 0.693, N=33, p<0.05), WH (Spearman ρ= 0.556, N=43, p<0.05) and GR (Spearman ρ= 0.685, N=31, p<0.05), according to Figure 5.14b, Figure 5.15b and Figure 5.16b, respectively. EY significantly decreases with increased HTC SF for brown macroalgae (Spearman ρ= -0.424, N=33, p<0.05), WH (Spearman ρ= -0.633, N=30, p<0.05) and GR (Spearman ρ= -0.459, N=31, p<0.05), according Figure 5.14c, Figure 5.15c and Figure 5.16c respectively. Therefore, the HHV, ED and EY values generated in this study agree with the findings of previous literature studies.

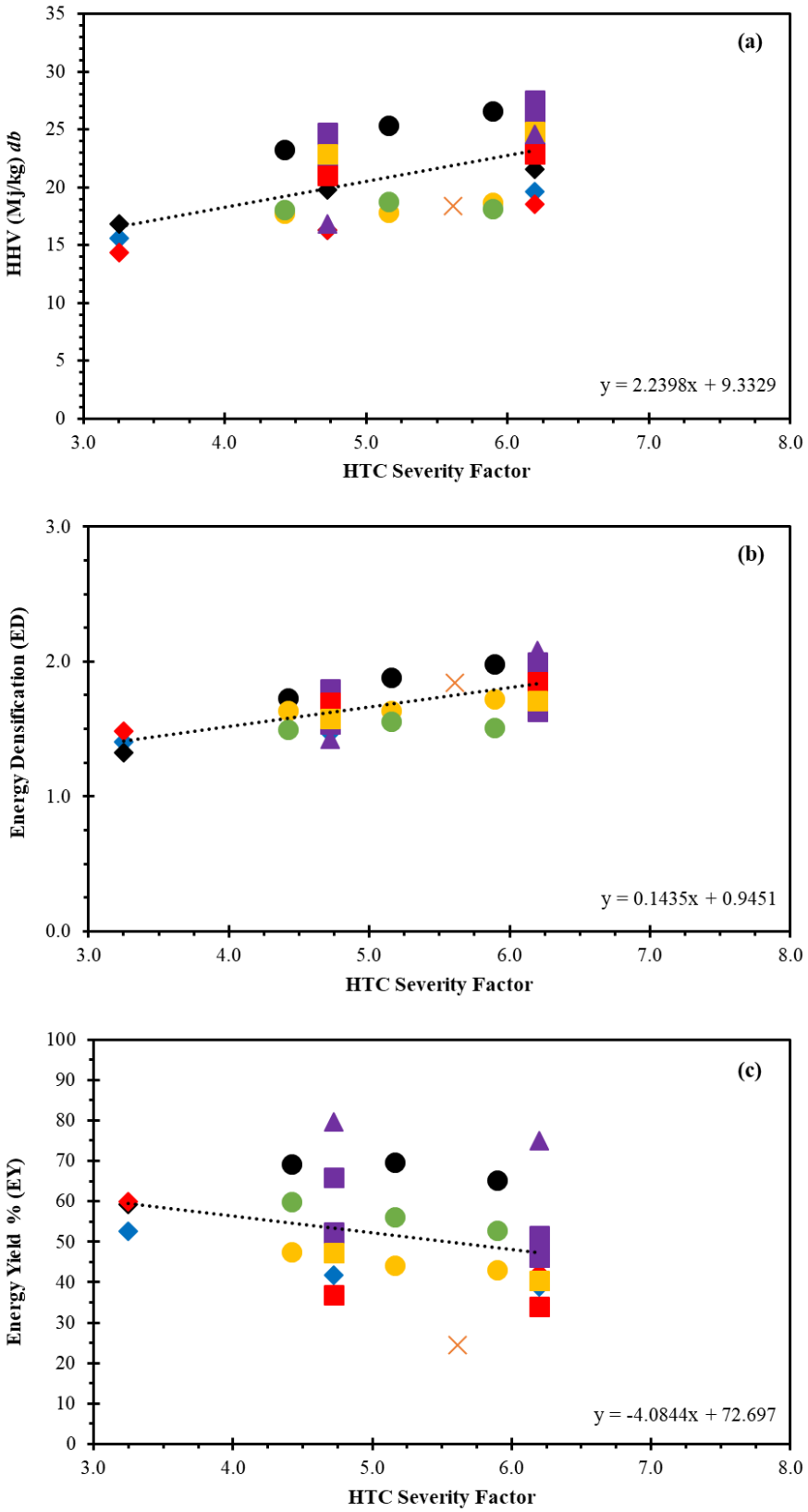

Figure 5.14. Correlation of severity factor and (a) HHV, (b) energy densification and (c) energy yield for brown macroalgae. Data points are a combination of literature values and values found in this work. The different colours represent different macroalgal species; blue=*S. latissima*, red=*L. digitata*, black=*F.serratus*, *purple=L. hyperborea*, yellow=*A. esculenta*, green=mixed species and orange=*Laminaria*. The different shapes represent different studies; ♦ =this work, ▲ =[64], ■ =[80], ● =[66], × =[179].

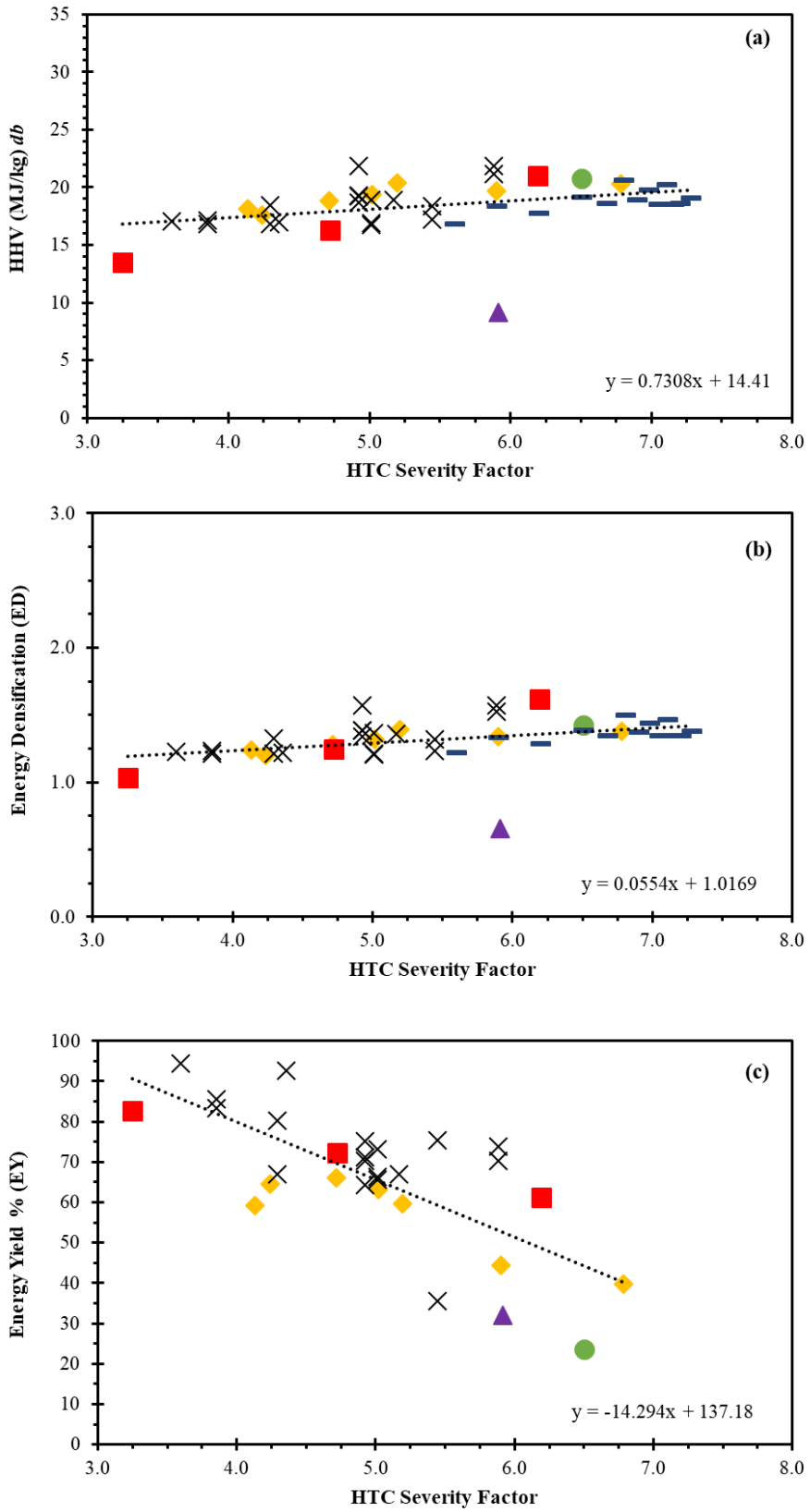

Figure 5.15. Correlation of (a) HHV, (b) energy densification and (c) energy yield for water hyacinth. Data points are a combination of literature values and values found in this work. The different shapes represent different studies; ■= this work, ♦ =[76], × =[77] , ▲=[172] and ● =[173] - = [78].

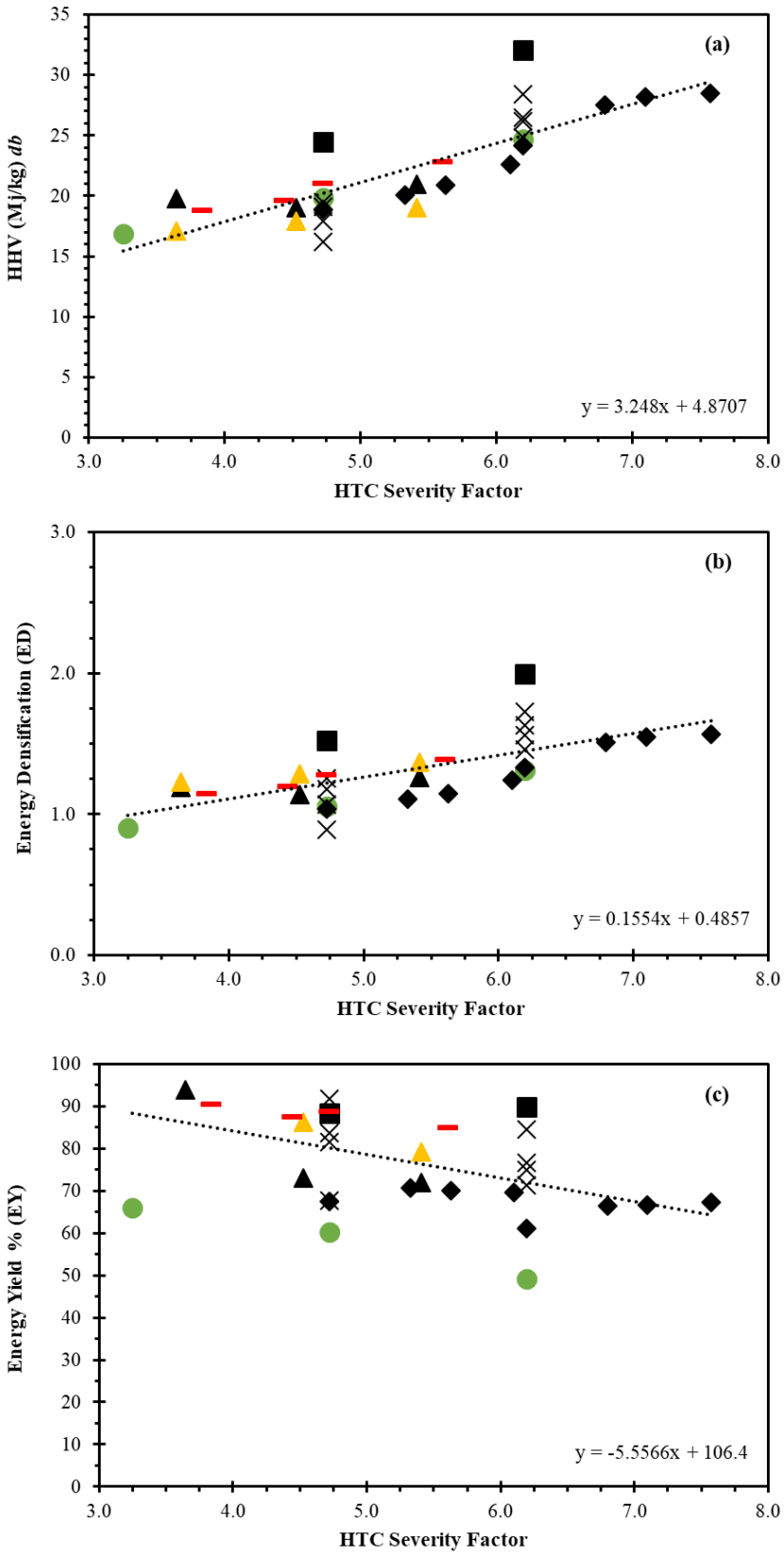

Figure 5.16. Correlation of severity factor and (a) HHV, (b) energy densification and (c) energy yield for grass. Data points are a combination of literature values and values found in this work. The different colours represent different grasses; green=lawn/campus grass, black=miscanthus, yellow=switch grass and red=energy grass. The different shapes represent different studies; ● =this work, ♦ =[164], ■ =[64], × =[49], ▲ =[74], + =[79], – =[178].

5.4 Process Water Composition

5.4.1 Chemical Oxygen Demand and Total Organic Carbon

The chemical oxygen demand (COD) and total organic carbon (TOC) concentrations of each of the HTC process waters are presented in Table 5.7. There appears to be no real trend between COD concentration and HTC temperature for macroalgal-derived process waters. The COD concentration of process waters generated from FS slightly decreased as HTC temperature increased: 41.4 g/L (FS150), 37.1 g/L (FS200) and 35.2 g/L (FS250). Whereas, COD values remain similar for SL (39.0-40.7 g/L) and LD (34.6-36.6 g/L). COD concentrations can be difficult to compare across literature studies, as higher solid-loading-ratios can result in a higher COD content in the process water [171], although this effect is not always additive. Few studies report the process water composition produced from the HTC of macroalgal biomass. Wang *et al*. [179] report a concentration of 23 g COD/L for the process water generated from *Laminaria* (220°C, 120-min); lower than LD200 or LD250 (Table 5.7). Although, a more dilute SLR of 1:20 was used.

Table 5.7. Chemical oxygen demand (COD) and total organic carbon (TOC) concentrations of HTC process waters.

Sample	COD (g/L)	TOC (g/L)
SL150	39.0 ± 0.7	15.6 ± 0.0
SL200	42.9 ± 0.0	16.8 ± 0.0
SL250	40.7 ± 0.0	15.1 ± 0.0
FS150	41.4 ± 0.8	16.8 ± 0.0
FS200	37.1 ± 0.3	14.5 ± 0.0
FS250	35.2 ± 0.4	13.4 ± 0.0
LD150	35.7 ± 0.3	14.6 ± 0.0
LD200	36.6 ± 0.3	14.6 ± 0.0
LD250	34.6 ± 0.1	13.0 ± 0.0
WH150	19.0 ± 0.2	7.1 ± 0.0
WH200	27.5 ± 0.2	11.1 ± 0.0
WH250	31.4 ± 0.1	12.1 ± 0.1
GR150	34.6 ± 1.3	13.5 ± 0.0
GR200	33.0 ± 0.6	12.3 ± 0.0
GR250	34.2 ± 0.4	12.4 ± 0.1

GR-derived process waters also had similar COD concentrations (33.0-34.5 g/L) across all HTC temperatures. WH is the only biomass which displays an obvious trend. WH150, WH200 and WH250 showed COD concentrations of 19.0 g/L, 27.5 g/L and 31.4 g/L, respectively. Increasing COD concentrations suggests greater solubilisation of organic matter under more severe reaction conditions. There is no current information available on the composition of WH-derived HTC process waters. However, Hudakorn and Sritrakul [85] found the liquid squeezed from untreated WH had a concentration of 6 g COD/L. Therefore, the higher COD values of WH process waters, displayed in Table 5.7 reflects the effectiveness of HTC to further solubilise organic matter, even at the lowest HTC temperature; WH150. Typical COD concentrations of lignocellulosic HTC process waters are between 14-26 g/L (220 °C, 1 h, SLR 1:12) [252]; similar to WH150 and WH200. Although, this was not assessed over a range of HTC temperatures.

The TOC values presented in Table 5.7 show an almost identical trend to the COD values. This is because TOC represents a similar proportion (36-41%) of the COD concentrations, across all process water samples. Erdogan *et al*. [163] also report a linear relationship between COD and TOC concentrations in orange pomace HTC process waters. The authors suggest the presence of inorganic compounds in the process waters is the reason COD values exceed TOC values [163]. Although, this is unlikely, as COD concentration should represent an indirect measurement of organic matter [97]. The presence of chlorides can cause interference and provide an overestimation of COD concentration (BS 6068-2.34:1988) [253]. However, the pre-dilution of process waters and the presence of mercury (II) sulphate in the LCK014 HACH cuvettes used in this study, mask this interference. The difference between COD and TOC in Table 5.7 is due to COD measuring the total oxygen consumed during the complete oxidation of the total organic constituents. Whereas, TOC is a measure of just the organic carbon fraction. TOC concentrations remains relatively constant for SL (15.1-16.8 g/L), FS (13.4-16.8 g/L), LD (13.0-14.6 g/L) and GR (12.3-13.5 g/L) process waters (Table 5.7). However, WH150 had a lower TOC value (7.1 g/L) compared to WH200 (11.1 g/L) or WH250 (12.1 g/L).

5.4.2 Total Nitrogen and Ammonia

The total nitrogen (TN) and ammonium-nitrogen (NH_4^+-N) concentrations of each HTC process water are shown in Table 5.8. Process waters generated at higher temperatures; 200°C and 250°C have a greater TN concentration than process waters generated at 150°C. Previous studies have found an increased N-content of HTC process waters generated under more severe conditions [84,170]; likely due to degradation of proteins. This result is also consistent

with Figure 5.6; showing a greater removal of nitrogen from the solid phase at higher HTC processing temperatures. GR process waters showed the greatest TN concentration across each HTC temperature, due to GR containing the highest initial N-concentration (Table 5.3). Conversely, SL process waters contained the lowest TN concentrations across each HTC temperature; linked to SL having the lowest N-content of the initial feedstocks. WH250 had a lower TN concentration than FS250 and LD250, despite the initial N-content of WH being higher than FS and LD. Although, this finding is again consistent with Figure 5.6; showing WH had the lowest nitrogen removal efficiency from the solid fraction, across each HTC temperature.

Table 5.8. Total nitrogen (TN) and ammonium-nitrogen (NH_4^+-N) concentrations of HTC process waters.

Sample	TN (mg/L)	NH_4^+-N (mg/L)	NH_4^+-N (%TN)
SL150	462 ± 25	28 ± 1	6
SL200	771 ± 7	133 ± 1	17
SL250	849 ± 41	225 ± 2	27
FS150	649 ± 16	89 ± 0	14
FS200	844 ± 37	196 ± 6	23
FS250	948 ± 23	340 ± 1	36
LD150	919 ± 7	69 ± 1	7
LD200	1208 ± 99	197 ± 1	16
LD250	1154 ± 20	354 ± 2	31
WH150	725 ± 13	166 ± 2	23
WH200	836 ± 31	195 ± 1	23
WH250	868 ± 11	280 ± 1	32
GR150	1236 ± 25	224 ± 1	18
GR200	1520 ± 17	218 ± 6	14
GR250	1482 ± 20	260 ± 2	18

Table 5.8 shows a linear increase in the concentration of NH_4^+-N with increasing HTC temperature, across the seaweed feedstocks. Whilst the higher-temperature, lignocellulosic-derived process waters (WH250 and GR250) showed a higher NH_4^+-N concentration, compared to lower-temperature lignocellulosic process waters. In addition, the contribution of NH_4^+-N to the overall TN concentration generally increased under more severe HTC conditions. Therefore, at lower processing temperatures more of the solubilised nitrogen is in the organic form. Whereas, increased concentrations of inorganic-nitrogen are observed at higher processing temperatures. Similar conclusions are observed by previous studies [16,170]. Ammonia is a well described inhibitor of the AD process [104,254]. Therefore,

Table 5.8 suggests higher-temperature HTC process waters may be more inhibitory than lower-temperature HTC process waters.

5.4.3 Proximate and Ultimate Composition

The proximate and ultimate composition of the HTC process waters were determined by drying a known volume at 60°C for a minimum of 48-h, with subsequent analysis of the residue by TGA and CHNS analysis. The proximate and ultimate analysis of the process water residues are presented in Table 5.9. In this instance, the O-content was calculated by difference, rather than measured directly. Generally, Table 5.9 suggests that oxygen represents the most significant fraction of macroalgal-derived HTC process water residues. Only GR200 and GR250 gave a greater C-content, compared to O-content, across all process water residues. This is reflected in the calculated HHV for the residues, which shows SL and LD process water residues have negligible, or even negative HHVs. The negative HHV values indicate a potential limitation with determining the proximate and ultimate composition through this method.

Table 5.9. Proximate and ultimate analysis of the dried residue of HTC process waters.

Sample	Ultimate analysis (wt%) *db*					Proximate analysis (wt%) *db*			HHV (MJ/kg)
	C	H	N	S	O*	VM	FC	Ash	
SL150	22.2 ± 0.2	2.1 ± 0.0	0.9 ± 0.0	0.6 ± 0.5	60.6 ± 0.7	57.2	28.4	14.4	0.0
SL200	22.4 ± 3.3	1.7 ± 0.4	0.9 ± 0.2	0.4 ± 0.1	72.6 ± 3.7	64.2	27.9	7.9	-3.4
SL250	23.4 ± 0.5	2.6 ± 0.1	0.9 ± 0.0	0.1 ± 0.0	71.4 ± 0.6	69.1	23.2	7.7	-5.3
FS150	27.5 ± 0.2	2.9 ± 0.0	1.5 ± 0.0	ND	51.9 ± 0.3	67.9	15.9	16.2	4.2
FS200	27.2 ± 0.7	3.1 ± 0.1	2.0 ± 0.0	1.0 ± 0.7	52.0 ± 0.1	79.5	5.6	14.8	4.3
FS250	24.8 ± 1.0	2.7 ± 0.2	1.7 ± 0.1	2.0 ± 1.4	53.2 ± 2.6	79.8	4.5	15.7	2.8
LD150	21.9 ± 0.3	2.0 ± 0.1	1.8 ± 0.0	1.1 ± 0.8	53.8 ± 0.5	56.1	24.5	19.4	0.7
LD200	16.7 ± 0.4	1.6 ± 0.0	1.8 ± 0.0	1.2 ± 1.0	66.2 ± 1.5	68.2	19.3	12.5	-3.9
LD250	21.9 ± 0.1	2.3 ± 0.0	2.0 ± 0.0	1.0 ± 0.8	63.1 ± 0.9	73.3	17.0	9.7	-0.5
WH150	24.5 ± 0.1	2.4 ± 0.0	3.3 ± 0.0	ND	53.0 ± 0.1	59.2	23.9	16.9	2.2
WH200	32.9 ± 0.0	3.6 ± 0.7	4.9 ± 0.0	ND	43.0 ± 0.7	66.6	17.8	15.6	8.6
WH250	25.7 ± 0.5	3.7 ± 0.8	1.0 ± 0.0	ND	62.9 ± 1.4	76.8	16.4	6.8	2.7
GR150	37.6 ± 0.1	3.5 ± 0.0	4.1 ± 0.0	ND	43.8 ± 0.1	67.4	21.6	11.0	10.0
GR200	40.4 ± 0.0	3.4 ± 0.1	5.8 ± 0.0	ND	34.3 ± 0.1	66.0	17.9	16.1	12.4
GR250	42.1 ± 0.0	4.2 ± 0.0	5.5 ± 0.0	ND	36.6 ± 0.1	76.9	11.5	11.6	13.7

*Oxygen measured by difference. *db*=dry basis. VM=volatile matter. FC=fixed carbon. HHV=higher heating value.

The negligible HHV values reported in Table 5.9 could be linked to an underestimation of ash content, leading to a consequential overestimation of O-content; as a result of calculating O-content through difference. Table 5.10 shows the TS and VS concentrations of the process waters, determined using the standard APHA method [223]. Here, the ash concentration is determined by difference, following incineration at 550°C. The concentrations of ash in Table 5.9 appear to represent a much lower proportion of the overall dry residue, compared to Table 5.10. For instance, Table 5.9 shows the ash content of SL150, SL200 and SL250 represents 14.4%, 7.9% and 7.7% of the respective dried process water residue. Whereas, using the values in Table 5.10, the ash content represents a greater proportion of the TS fraction: 42.5% (SL150), 42.7% (SL200) and 45.5% (SL250). The ash concentrations presented in Table 5.10 were determined at 550°C. Whereas, the ash contents shown in Table 5.9 were determined at 900°C. Previously, Table 5.5 demonstrated that alkali metals underwent the greatest removal and subsequent solubilisation into the process water, during HTC. Therefore, determining the ash content of process water residues at 900°C is likely cause volatilisation of these alkali metals and consequentially, an underestimation of ash concentration.

Table 5.10. Total solids (TS), volatile solids (VS) and ash composition of HTC process waters.

Sample	TS (g/L)	VS (g/L)	Ash* (g/L)	Ash (%TS)
SL150	64.6 ± 2.8	37.1 ± 0.6	27.5 ± 2.9	42.5
SL200	59.6 ± 0.3	34.1 ± 0.2	25.5 ± 0.4	42.7
SL250	54.4 ± 0.3	29.6 ± 0.1	24.8 ± 0.3	45.5
FS150	61.8 ± 1.3	42.1 ± 0.2	19.7 ± 1.3	31.9
FS200	56.2 ± 0.9	34.9 ± 1.2	21.3 ± 1.5	37.8
FS250	59.8 ± 9.0	41.9 ± 8.5	17.9 ± 12.4	30.0
LD150	59.1 ± 0.3	31.3 ± 0.3	27.8 ± 0.4	47.1
LD200	55.8 ± 0.2	27.7 ± 0.0	28.1 ± 0.2	50.4
LD250	49.3 ± 0.3	23.1 ± 0.3	26.2 ± 0.4	53.1
WH150	22.0 ± 0.5	11.9 ± 0.2	10.1 ± 0.5	45.8
WH200	31.1 ± 0.4	19.2 ± 0.1	11.9 ± 0.4	38.4
WH250	19.0 ± 0.0	13.6 ± 0.0	5.4 ± 0.0	28.7
GR150	33.0 ± 0.1	27.2 ± 0.1	5.8 ± 0.1	17.6
GR200	27.1 ± 0.1	20.9 ± 0.0	6.2 ± 0.1	22.7
GR250	23.4 ± 0.0	18.2 ± 0.1	5.2 ± 0.1	22.2

*Calculated by difference.

Additionally, HTC process waters are likely to contain volatile organic compounds, such as VFAs, which are potentially driven-off during the drying process (60°C) [80]. This is exemplified in Table 5.10, where a reduction in TS is observed between WH200 (31.1%) and WH250 (19.0%), despite an increasing COD concentration (Table 5.7). In order to obtain an understanding of the significance of these volatile organic losses, a subsample of each dried process water was rehydrated, by adding the exact mass of water lost during drying. The TOC was subsequently measured and compared to the original TOC concentrations. The reduction in TOC after drying provides an indication of the proportion of organic compounds volatilised during the drying process.

The differences between the process water TOC values, before and after drying are displayed in Table 5.11. With the exception of SL150, TOC concentrations are lower for all the rehydrated HTC process waters, compared to process waters before drying. Therefore, indicating the loss of organic matter through volatilisation. Higher temperature process waters: 200°C and 250°C display greater TOC losses compared to process waters generated at 150°C, across all feedstocks. Although, the degree of TOC losses appears to vary between different feedstock types. Process waters derived from lignocellulosic biomass exhibit greater TOC losses during the drying process, than those generated from macroalgal biomass. WH200 and WH250 showed the greatest loss in TOC, reducing by 49.0% and 46.1%, respectively.

Table 5.11. Total organic carbon (TOC) losses from the HTC process waters during the drying process.

Sample	TOC before drying (g/L)	TOC after drying (g/L)	Change in TOC (%)
SL150	15.6	16.0	+3.1
SL200	16.8	15.2	-9.7
SL250	15.1	14.1	-6.9
FS150	16.8	16.6	-1.3
FS200	14.5	13.7	-5.3
FS250	13.4	12.5	-6.6
LD150	14.6	14.2	-2.1
LD200	14.6	12.8	-12.0
LD250	13.0	11.7	-9.6
WH150	7.1	5.1	-28.3
WH200	11.1	5.7	-49.0
WH250	12.1	6.5	-46.1
GR150	13.5	13.0	-4.2
GR200	12.3	9.8	-20.5
GR250	12.3	8.9	-28.2

The combined losses in organic compounds (Table 5.11) and potential underestimation of the ash fraction, could result in incorrect determination of the ultimate composition of dried process water residues. In particular, an overestimation of the O-content; leading to a prediction of low HHV, which was observed in Table 5.9.

Therefore, the re-calculated ultimate analysis results of the dried process water residues are presented in Table 5.12. The CHNS-fractions have been adjusted according to the percentage TOC losses reported in Table 5.11. However, unlike Table 5.9, the ash content of the residue was calculated based on the values in Table 5.10, where ash was determined at 550°C; reducing the potential for alkali metal volatilisation, compared to 900°C. Therefore, reducing the risk of overestimating the O-content; which was still determined by difference.

Table 5.12. Corrected proximate and ultimate analysis of the dried residue of HTC process waters. Values corrected for organic and inorganic losses from the drying and ashing processes.

Sample	Ultimate Analysis (wt%) *db*					Proximate Analysis (%TS)		HHV (MJ/kg)
	C	H	N	S	O*	VS	Ash	
SL150	19.9	2.1	1.0	0.6	40.0	57.5	42.5	3.6
SL200	24.5	1.7	1.2	0.4	29.5	57.3	42.7	5.5
SL250	19.8	2.1	1.4	0.1	31.1	54.5	45.5	4.1
FS150	27.9	2.9	2.1	ND	35.2	68.1	31.9	7.3
FS200	28.7	3.2	2.7	1.0	26.6	62.2	37.8	9.5
FS250	26.6	2.7	2.3	2.0	36.4	70.0	30.0	6.4
LD150	22.4	2.1	2.3	1.1	25.0	52.9	47.1	6.0
LD200	19.0	1.6	2.2	1.2	25.7	49.6	50.4	4.1
LD250	24.8	2.4	2.6	1.0	16.7	46.9	53.1	8.6
WH150	34.1	2.5	4.4	ND	13.3	54.2	45.8	12.7
WH200	64.6	9.8	7.3	ND	-14.0	61.6	38.4	29.7
WH250	47.7	3.7	1.3	ND	18.7	71.3	28.7	18.1
GR150	39.3	3.7	6.6	ND	32.8	82.4	17.6	12.7
GR200	50.8	3.6	9.7	ND	13.2	77.3	22.7	20.0
GR250	58.7	4.4	9.5	ND	5.2	77.8	22.2	25.2

*Oxygen measured by difference. *db*=dry basis. TS=total solids. VS=volatile solids. HHV=higher heating value.

The macroalgal-derived process water residues presented in Table 5.12 have a much lower O-content than Table 5.9. The HHV of the dried process waters are also higher, for both macroalgal and lignocellulosic process waters, with no negative values present. However, WH200 has a negative O-content (-14.0%) and GR250 has a very low O-content (5.2%). This

results in a high HHV content for WH200 (29.7 MJ/kg) and GR250 (25.2 MJ/kg); suggesting this method of re-calculating the ultimate composition of dried HTC process water residues is still subject to some flaws. Perhaps different feedstock types require different methods of re-calculation, based on the properties of the process water. For instance, the ultimate composition of macroalgal-derived process waters could be re-calculated using the method presented in Table 5.12. Whereas, lignocellulosic process waters could be calculated using the method in Table 5.9. However, further work is required to refine this method of process water ultimate composition recalculation.

5.4.4 Volatile Fatty Acids

VFAs are intermediates from the HTC process, which are solubilised into the process water. Figure 5.17 shows the concentrations of VFAs present in the HTC process waters, determined by GC-FID. Higher temperature process waters (200°C and 250°C) contain a higher concentration of VFAs, compared to process waters generated at 150°C. FS, WH and GR process waters showed an increased VFA concentration as HTC temperature increased. However, VFA concentrations remained similar between SL200 and SL250, as well as LD200 and LD250.

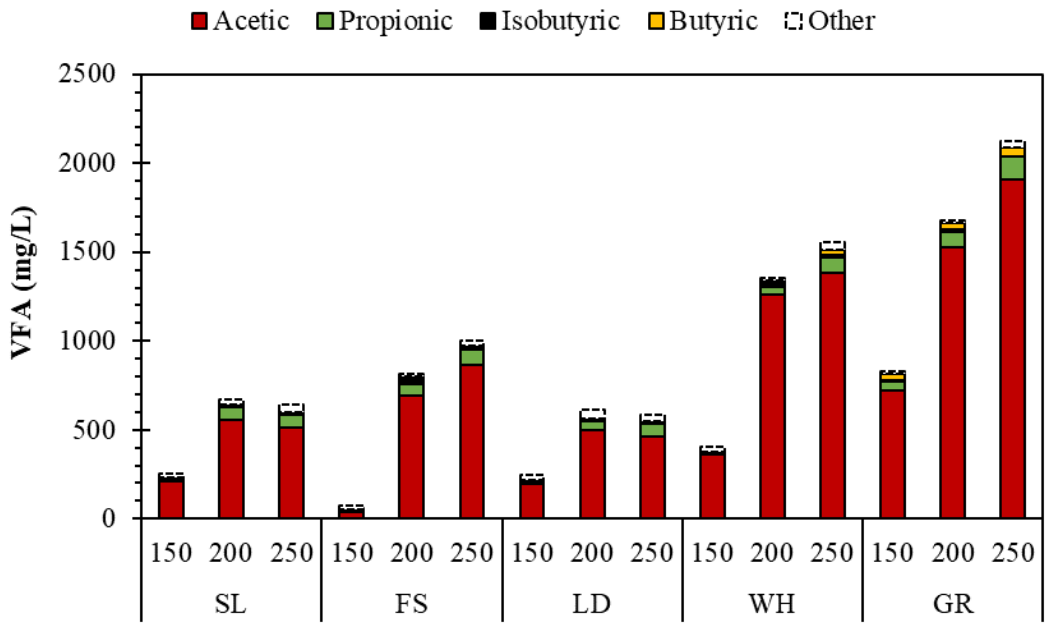

Figure 5.17. Volatile fatty acid concentrations of HTC process waters, determined by GC-FID.

Higher temperature (200°C and 250°C) HTC process waters, derived from lignocellulosic biomass (WH and GR) have a greater concentration of VFAs compared to process waters generated from macroalgal biomass, across comparable temperatures. This could explain why high levels of TOC losses are observed for WH200, WH250, GR200 and GR250, whilst drying the process waters (Table 5.11). Acetic acid represents the majority fraction (79-91%) of the solubilised VFAs, across all process waters, except FS150; where the concentration of total VFA is low (75 mg/L). Previous studies have also reported how acetic acid is the dominant VFA in HTC process waters [157,158]. VFAs are pre-cursors for biomethane generation, during AD. Acetic acid can be directly converted to biomethane by acetoclastic methanogens [255]. Higher VFAs, such as propionic and butyric acids, are further converted to acetic acid, during acetogenesis [93] which can then be converted to biomethane.

5.4.5 Total Sugars and Aldehydes

During hydrolysis, sugars are liberated from biomass and solubilised into the process waters. Sugars are readily digestible and can be fermented by anaerobic systems to generate biofuels, such as: biomethane and biohydrogen. Table 5.13 shows the concentrations of individual and total sugars of each of the process waters. The concentration of total sugars was determined through the summation of maltose, lactose, glucose, fructose, ribose and arabinose concentrations. Unfortunately, due to time restraints, the sugar and aldehyde composition of GR-derived process waters could not be determined.

Table 5.13. Sugar and aldehyde (HMF and furfural) concentrations of HTC process waters.

Sample	Sugar (g/L)							Aldehyde (mg/L)	
	Maltose	Lactose	Glucose	Fructose	Ribose	Arabinose	Total	HMF	Furfural
SL150	ND	ND	3.53	ND	0.64	ND	4.17	360.9	490.4
SL200	ND	2.88	ND	13.23	1.33	ND	17.44	ND	ND
SL250	ND	2.65	ND	12.61	ND	ND	15.25	ND	ND
FS150	ND	4.84	ND	9.11	ND	ND	13.95	ND	ND
FS200	ND	ND	ND	9.70	ND	ND	9.70	ND	ND
FS250	ND	ND	ND	9.50	ND	ND	9.50	ND	ND
LD150	ND	ND	3.63	ND	ND	6.62	10.25	ND	ND
LD200	ND	ND	ND	6.41	ND	ND	6.41	ND	ND
LD250	ND	ND	ND	6.56	ND	ND	6.56	ND	ND
WH150	0.33	ND	0.31	0.80	ND	1.05	2.49	ND	ND
WH200	ND	ND	0.24	0.36	0.63	ND	1.23	587.3	382.0
WH250	ND	ND	0.07	0.20	0.57	ND	0.83	264.6	ND

ND=not detected.

During more severe reaction conditions; typically around 200°C, solubilised sugars begin to further degrade into furanic compounds [152,163]. Such furanic compounds include: HMF (5-hydroxymethylfurfural) and furfural; formed by the dehydration of solubilised sugar derivatives [150,192]. This relationship between the sugar and furanic concentrations is exemplified by the WH-derived process waters shown in Table 5.13. A gradual reduction in total sugar concentration is observed between WH150, WH200 and WH250; indicating further degradation to furanic compounds. No detectable levels of HMF or furfural are observed in WH150. However, WH200 contains the highest concentrations of HMF (587.3 mg/L) and furfural (382.0 mg/L), of all WH-derived process waters. However, a reduction in HMF and furfural concentrations was observed between WH200 and WH250. This suggests the higher HTC temperatures of 250°C degrades furanic compounds; similar findings were reported by [152,163,256].

HMF and furfural was not detected in macroalgal-derived process waters, with the exception of SL150. Lin *et al*. [72] found the monosaccharic mannitol yield of *S. latissima* started to decrease at temperatures >140°C; suggesting the degradation of mannitol into inhibitory furanic compounds, beyond this temperature. SL150 showed the presence of HMF and furfural; whereas, neither is detected in SL200 and SL250. This is contradictory to the argument of Lin *et al*. [72] and the results of WH-derived process waters in Table 5.13. In addition, SL200 and SL250 showed a higher total sugar concentration than SL150, which would be unexpected; as degradation of sugars would be expected under more severe reaction conditions. FS and LD-derived process waters show an expected trend in total sugar composition; with the process waters generated at 150°C displaying a higher sugar concentration than the waters produced at 200°C or 250°C.

Overall the total sugar concentration of macroalgal-derived process waters was much higher than process waters generated from WH. SL200 had the highest total sugar concentration (17.44 g/L); significantly higher than WH150; the highest sugar yielding WH-process water. According to Table 5.13, fructose represents the highest sugar concentration for macroalgal-derived process waters. However, the biochemical composition of seaweeds is comprised of polysaccharides which differ to those within lignocellulose; such as: laminarin, fucoidan and mannitol. Therefore, the expected monomeric sugars liberated from the hydrolysis of seaweed polysaccharides would be mainly glucose, fucose and mannose [60,63]. Table 5.13 shows high concentrations of fructose for seaweed-derived process waters, which would not be expected. In addition, the HPLC used to determine the sugar composition was not able to detect fucose or mannose. Overall, this highlights potential flaws with determining the sugar contents of macroalgal-derived HTC process waters using this HPLC methodology; with complex matrix effects leading to overestimations of the total sugar content.

5.4.6 Total Phenols

The total phenol (TP) concentration of each process water is displayed in Figure 5.18. Generally, the phenol concentration was higher during more severe reaction temperatures (200°C and 250°C). Similar trends have been observed for process waters generated from corn stover [152] and digestates [171] and green macroalgal biomass [184]. Phenols are known inhibitors to anaerobic microbial systems [192,206]. Therefore, Figure 5.18 suggests higher-temperature process waters are likely to be more inhibitory to AD or DF.

The higher-temperature (200°C and 250°C) lignocellulosic-derived HTC process waters contained higher phenol concentrations than macroalgal-derived process waters. The phenol concentrations of WH200 and GR200 ranged from 342-346 mg/L and WH250 and GR250 ranged from 423-590 mg/L. Whereas, the process waters produced from macroalgal species ranged from 196-297 mg/L (200°C) and 236-255 mg/L (250°C). The phenols generated from lignocellulosic biomass are derived from the lignin fraction [192,193]. Seaweeds generally contain a negligible lignin content [257]; therefore, a lower concentration of phenols in the process waters would be expected. Alternative sources of phenols within seaweeds exist, in the form of polyphenols and phlorotannins [128,194]. Although, little is known about the behaviour of these sources of seaweed-based phenols during HTC; the evidence from Figure 5.18 and [184] indicates increased phenol solubilisation into the process water, at higher HTC temperatures.

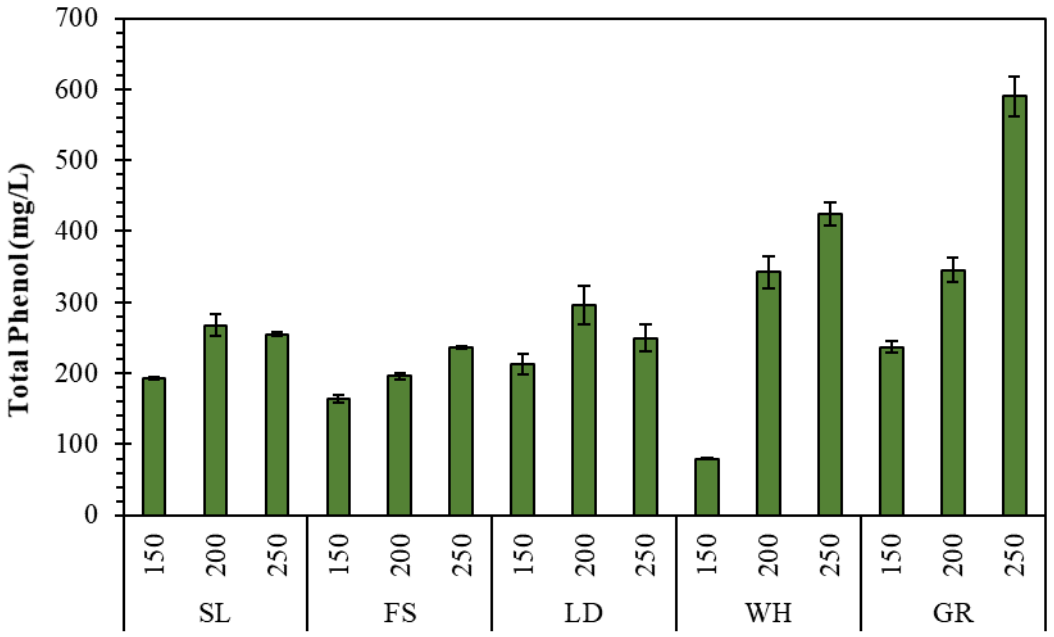

Figure 5.18. Total phenol concentrations of HTC process waters, determined by LCK345 HACH cuvettes.

5.4.7 pH

The pH of each HTC process water is shown in Figure 5.19. Macroalgal-derived process waters produced at 150°C and 200°C all displayed an acidic pH. In addition, the pH remained fairly constant as the temperature increased from 150°C to 200°C. The pH of SL150, FS150 and LD150 ranged between 4.42-4.80 and SL200, FS200 and LD200 ranged between 4.62-4.76. However, during HTC at 250°C, the pH of macroalgal-derived process waters increased to between 6.57-6.82. Generally, the pH of process waters reduces, or remains constant, when produced at higher HTC temperatures [152,158,188], due to the solubilisation of organic acids. Therefore, the increased pH observed for SL250, FS250 and LD250 is an unusual trend. However, Table 5.8 indicates the ammonia concentration of macroalgal-derived HTC process waters increased sharply between HTC temperatures of 200°C and 250°C. This could provide a possible explanation for the increased pH of macroalgal-derived process waters produced at 250°C [16].

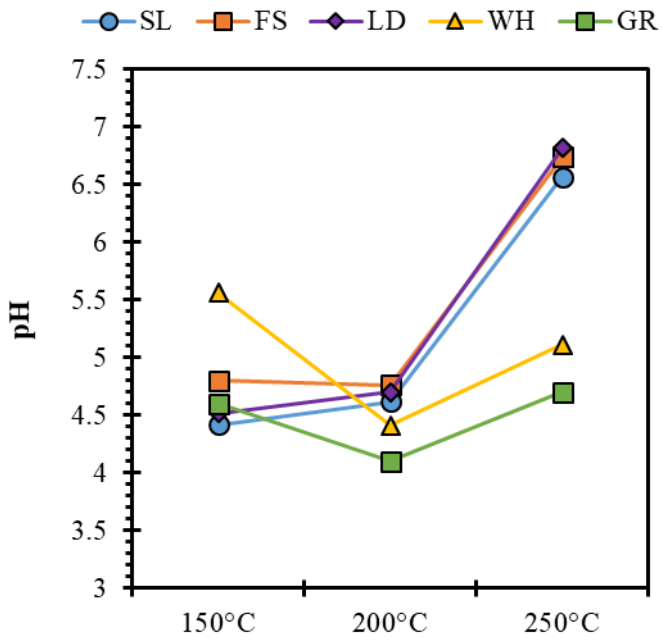

Figure 5.19. pH of HTC process waters.

Lignocellulosic-derived process waters all displayed an acidic pH; comparable to literature values [147,152,158,258]. The pH values of WH150, WH200 and WH250 were 5.56, 4.41 and 5.11, respectively. Whereas, the pH values of GR150, GR200 and GR250 were 4.65, 4.13 and 4.65, respectively. Therefore, both WH and GR process waters follow a similar pH trend. An initial decrease in pH is observed between 150°C and 200°C, due to an accumulation of VFAs (Figure 5.17). However, despite a further increase in VFA content between process

waters generated at 200°C and 250°C, a slight increase in pH is observed. Again, this could be linked to a higher concentration of solubilised ammonia; although the effect is not as dramatic as was observed for macroalgal-derived process waters.

5.4.8 Compound Identification (GC-MS)

HTC process waters are complex mixtures of a variety of different compounds; in which the composition varies according to biomass feedstock and HTC severity [157]. GC-MS can be used to identify key groups of compounds within HTC process waters, produced at different reaction severities [84,160]. Table 5.14 displays the concentrations of different groups of compounds solubilised within the process waters, which have been identified by GC-MS. The grouping structures of the compounds are listed in Appendix D. It was not possible to analyse WH150 and GR150 process waters using this method, due to the formation of a thick gel during the derivatization stage. This thick gel-like material was unable to be injected onto the GC-column.

Carboxylic acids and pyridines are the dominating compounds identified across each of the HTC process waters shown in Table 5.14. The concentrations of carboxylic acids identified by GC-MS generally follows the same trends for the VFA concentrations displayed in Figure 5.17. Overall, the carboxylic acid concentrations increased at higher temperature process waters (200°C and 250°C), compared to lower temperatures (150°C). In addition, lignocellulosic-derived process waters showed a higher carboxylic acid concentration compared to macroalgal-derived process waters, generated at comparable HTC temperatures. However, the concentrations of carboxylic acids are significantly higher when identified by GC-MS (Table 5.14), compared to GC-FID (Figure 5.17). This is due to the capacity of GC-MS to identify succinic and levulinic acids; which is not possible using the GC-FID methodology.

Pyridines represent the additional dominating compounds found within HTC process waters, according to Table 5.14. However, the only pyridine compound identified by the GC-MS was 3-hydroxypyridine; a N-containing heterocyclic organic compound. Generally, the concentrations of pyridines increased with increasing HTC temperature. Additionally, higher N-containing biomass: WH and GR showed higher concentrations of pyridines at 250°C. Severe reaction conditions can cause the formation of N-containing compounds through Maillard reactions between the carbohydrate and protein fractions of biomass [72,259]. Previous studies have reported an increase in nitrogenated aromatic compounds under more severe HTC reaction conditions [84,160]; due to the degradation of protein and subsequent Maillard reactions. This is reflected in the increased pyrazine and pyridine concentrations, at

higher HTC temperatures, shown in Table 5.14. Although, these compounds are generally removed by the AD process [84].

Table 5.14. Concentrations of groups of compounds in HTC process waters, determined by GC-MS.

Sample	Analyte (mg/L)					
	Carboxylic Acids	Aromatic Carboxylic Acids	Aromatic Ketones	Phenolics	Pyrazines	Pyridines
SL150	1911	55	47	ND	16	2300
SL200	3202	4	64	24	11	4001
SL250	2078	57	62	41	24	3253
FS150	734	ND	7	38	2	ND
FS200	2385	ND	49	ND	9	3293
FS250	2889	56	80	ND	50	3767
LD150	1386	ND	16	14	22	3176
LD200	2771	56	21	ND	23	4604
LD250	4060	5	151	26	65	4976
WH150	*	*	*	*	*	*
WH200	4572	ND	23	ND	17	3578
WH250	6583	59	109	28	179	5336
GR150	*	*	*	*	*	*
GR200	3915	ND	14	ND	124	6653
GR250	9266	72	113	110	269	10040

*unable to be analysed, due to method limitations. ND=not detected.

The phenolic concentrations determined by GC-MS (Table 5.14) are significantly lower than those determined by LCK345 HACH-cuvettes (Figure 5.18). For example, for WH250, Table 5.14 shows a phenolic concentration of 28 mg/L; whereas, Figure 5.18 displays a yield of 425 mg/L. This is due to the GC-MS identifying specific phenolic species: phenol and P-cresol, while the HACH-cuvettes measure total phenol content; without identifying specific species. However, Table 5.14 generally shows the concentration of phenolics was highest, under the most severe reaction conditions; similar to the conclusions obtained from Figure 5.18.

5.5 Conclusions

The aim of this chapter was to understand the use of HTC for processing alternative macroalgal and lignocellulosic feedstocks. This includes the effect of HTC processing temperature (150°C, 200°C and 250°C) on the product yield distribution, as well as the properties of the residual hydrochar and process water.

Hydrochar yield decreased with increasing HTC temperature, across all feedstocks used in this study. However, hydrochar yields were lower for macroalgal feedstocks, compared to lignocellulosic feedstocks, across comparable treatment temperatures. A significant proportion of carbon is solubilised into the process water fraction during HTC. However this is greater for macroalgal biomass (43-61%), than lignocellulosic feedstocks (18-33%). Regardless, this presents an opportunity to valorise the carbon in the process water and maximise the ECE of the feedstocks.

The HHV of hydrochars increased with increasing HTC temperature; due to an increased carbon content and reduced oxygen content. Higher-temperature hydrochars display more coal-like properties, in relation to the H:C, O:C and FC:VM. Limited energy densification was observed for WH and GR at 150°C, due to limited disruption of the biochemical composition at these temperatures. Alternatively, macroalgal-derived polysaccharides degrade at lower temperatures and therefore, undergo energy densification at lower temperatures. Energy densification of hydrochars is typically higher for macroalgal species, compared to lignocellulosic; due to the initial lower HHVs of the biomass. However, the energy yield of lignocellulosic-derived hydrochars is higher; due to increased hydrochar yields.

HTC can selectively remove problematic inorganics from the biomass, which may cause slagging, fouling and corrosion issues during thermal conversion processes. These inorganic species include: Na, K and Cl. The removal efficiency of alkali metals and Cl increases with increasing HTC temperature. However, macroalgal-derived hydrochars contain higher concentrations of these problematic inorganics, compared to lignocellulosic-derived hydrochars, due to initial higher concentrations in the parent biomass.

Overall, hydrochars generated at higher temperatures (250°C) display the highest HHV and removal of problematic inorganics. Although, this is compromised with a reduced hydrochar yield. In addition, the ash content and N-content of the hydrochars remains high; creating undesirable residual ash after combustion and unwanted NO_x emissions, which should be investigated in future research.

The TOC and COD concentrations of the process waters remain fairly constant across each processing temperature, with the exception of WH. This suggests a high concentration of

organic matter is solubilised within the process waters. Although, the composition of the process waters changes across the HTC temperature range. More severe HTC conditions are generally associated with higher VFA concentrations; beneficial to further conversion by AD. Although, an increase in inhibitory compound formation is also observed at higher HTC temperatures; such as ammonia and phenols.

Chapter 6
Integration of HTC and Biological Processing: Utilisation of HTC Products as Separate Energy Vectors

The separation of HTC products: hydrochars and process waters, allows for the co-generation of multiple energy vectors to maximise the obtainable energy recovery from a biomass. Hydrochars are energy-densified solids, with multiple potential applications as either an energy vector, or as a functional material. Process waters are often considered a waste product to the HTC process. However, biological processing can recover value from the solubilised organic matter within the process waters. The co-generation of energy from the hydrochars and process waters can help maximise the obtainable energy recovered from the initial biomass feedstock.

This chapter compares the generation of different energy vectors from both hydrochars and process waters; with a view of maximising the ECE of the feedstocks: SL, FS, LD, WH and GR. The comparative behaviour of hydrochars during combustion and AD were assessed. Whilst the comparative generation of biomethane and biohydrogen from process waters was assessed. The overall energetics of each integration option was determined, in order to find the most energetically-feasible integration strategy between HTC and biological processing.

6.1 Objectives

The objectives of this chapter are to:

- Assess the properties of hydrochars for use as a solid combustion fuel, including: ash behaviour and energy output.
- Evaluate the behaviour of hydrochars during AD.
- Evaluate the comparative yields of biohydrogen and biomethane generated from HTC process waters.
- Compare the energetics of the different integration strategies between HTC and biological processing.

6.2 Combustion Behaviour of Hydrochars

Chapter 5 previously demonstrated hydrochars displayed an increased HHV and removal of problematic alkali metals, compared to the parent biomass; indicating enhanced properties for applications as a solid combustion fuel. Therefore, this section focuses on assessing the slagging and fouling potential of the hydrochars.

6.2.1 Slagging and Fouling Indices

Slagging and fouling indices predict the likelihood of a fuel-derived ash to display problematic slagging and fouling tendencies during combustion [64,74,171]. These indices are calculated based on the inorganic oxide content of the sample; in this case, determined by XRF. Indices include: the alkali index (AI), bed agglomeration index (BAI), acid base ratio (Rb/a), slagging index (SI), fouling index (FI), and slag viscosity index (SVI). Table 6.1 displays how each of the different indices are interpreted. Whereas, Table 6.2 displays the calculated indices for the hydrochars generated during this study.

Table 6.1. Interpretation of slagging and fouling indices [64].

Colour Key	Interpretation	Slagging and Fouling Indices					
		AI	**BAI**	**Rb/a**	**SI**	**FI**	**SVI**
	Low/safe	<0.17	>0.15	<0.5	<0.6	<0.6	>72
	Medium/likely	>0.17<0.34	<0.15	-	>0.6<2.0	>0.6<40.0	>65<72
	High/certain	>0.34	-	>0.5	>2.0	>40.0	<65

All indices presented in Table 6.2 suggest macroalgal species (SL, FS and LD) possess certain or likely slagging and fouling tendencies. This agrees with similar findings in literature for *L. digitata*, *A. esculenta*, *L. hyperborea* and *F. serratus* macroalgal species, through applying the same indices [61,66,80]. According to the predictive indices presented in Table 6.2, the seaweed-derived hydrochars showed no real improvement in ash behaviour during combustion, compared to the parent biomass. The calculated indices for AI (>0.34), Rb/a (>0.5), SI (>2.0), FI (>40.0) and SVI (<65) generally indicated high, or certain slagging and fouling behaviour from macroalgal-derived hydrochars. However, there are the exceptions of SL250 and FS250, which both displayed a slight improvement in the FI (>0.6 < 40.0); indicating a medium fouling tendency.

Table 6.2. Slagging and fouling indices for untreated biomass and hydrochars.

Sample	Slagging and Fouling Index					
	AI	BAI	R_a^b	SI	FI	SVI
SL	12.77	0.00	92.0	72.5	1305.7	4.4
SL150	5.63	0.01	43.7	29.1	383.1	5.1
SL200	4.90	0.01	47.1	35.5	376.8	3.6
SL250	2.64	0.02	5.2	5.4	26.7	23.2
FS	8.67	0.00	28.7	44.9	316.8	10.9
FS150	3.77	0.01	17.6	19.7	111.5	12.1
FS200	2.42	0.02	13.0	15.8	62.1	11.0
FS250	1.38	0.04	4.1	5.8	12.1	24.6
LD	20.52	0.01	167.9	169.9	3347.6	3.4
LD150	9.30	0.02	113.0	107.6	1511.8	2.9
LD200	8.04	0.03	89.4	87.3	1171.1	2.9
LD250	4.72	0.08	11.1	14.6	96.7	15.0
WH	5.26	0.17	2.6	1.2	17.6	39.1
WH150	3.95	0.24	2.1	0.8	11.3	39.4
WH200	2.43	0.36	1.6	0.6	6.3	40.0
WH250	0.87	1.39	1.5	0.6	2.8	32.0
GR	1.66	0.02	1.4	0.6	4.8	61.3
GR150	1.11	0.03	0.9	0.3	2.0	66.5
GR200	0.91	0.04	0.8	0.3	1.6	66.5
GR250	0.27	0.17	0.7	0.3	0.5	63.4

Previous studies have applied the slagging and fouling indices to macroalgal-derived hydrochars and found an improvement in the ash behaviour, compared to the parent feedstock [66,80]. In particular, hydrochars generated from seaweeds at higher HTC temperatures show improvements in the slagging propensity and are deemed safe for combustion [80]; linked to the reduced alkali metal content [66]. Alternatively, only minor improvements in the fouling indices were found for seaweed-derived hydrochars [66,80], with Smith and Ross [80] reporting high fouling propensity for seaweed hydrochars. Despite the high removal of Na and K from SL, FS and LD during HTC (Chapter 5), the indicative slagging and fouling capacities remain high.

Similarly to macroalgal-derived hydrochars, Table 6.2 suggests WH hydrochars showed little improvement in the slagging and fouling tendencies and, therefore, ash behaviour during combustion. The only improvement was displayed by WH250; where the SI indicated a low slagging propensity, compared to WH, WH150 and WH200, which displayed a medium slagging inclination. Alternatively, the AI and SVI predict a high slagging risk for WH and

all WH-derived hydrochars. A medium fouling propensity for WH and WH hydrochars was predicted by the FI (>0.6 < 40.0). The BAI predicted unlikely bed agglomeration for WH and WH-hydrochars. Although, this could be because of the increased Fe concentration, compared to the other feedstocks.

GR hydrochars show the greatest improvement in ash behaviour according to the slagging and fouling indices, compared to any other biomass feedstock presented in Table 6.2. The AI suggests GR, GR150 and GR200 had an almost certain slagging and fouling potential. Whereas, GR250 (AI=0.27) had a probable risk of slagging and fouling. GR250 also displays an improvement in the BAI and FI; suggesting bed agglomeration is unlikely and a low fouling propensity. The SI and SVI indicates a reduction in the slagging propensity for GR-derived hydrochars, compared to GR, with the SI predicting the hydrochars have a low slagging inclination and SVI predicting a medium slagging propensity.

Overall, according to Table 6.2, the majority of hydrochars displayed no reduction in slagging and fouling tendencies, compared to the parent feedstocks. However, a trend which can be observed from Table 6.2, is that as HTC temperature increased, the predictive indices values became closer to the lower/safer limits. Although, this was not always enough to reach the value to qualify for the specification. For example, values >0.34 indicate almost certain slagging and fouling, according to the AI. The AI values of SL, SL150, SL200 and SL250 were 12.77, 5.63, 4.90 and 2.64, respectively. Therefore, this suggests a reduced slagging and fouling propensity with increased HTC temperature. Although, the values are not low enough to qualify for probable slagging and fouling (>0.17 <0.34). This reflects the removal of alkali metals, described in Chapter 5, but suggests the removal is not sufficient to prevent slagging and fouling occurring.

6.2.2 Ash Fusion Testing

The results of the slagging and fouling indices must be interpreted with caution, as these indices were originally used to analyse coal samples, rather than biomass [74]. Therefore, creating an assumption that biomass ash will show similar slagging and fouling behaviours to coal ash; with alumina-silicate compositions [64]. This assumption is potentially incorrect due to the unknown matrix-effect from biomass ash, which is likely to vary between different biomass feedstocks. Therefore, in order further understand the ash behaviour of the biomass and hydrochar ashes, ash fusion tests were conducted.

Ash fusion tests provide a greater understanding of the slagging behaviour of an ash, through identifying the temperatures at which different transitional phases of ash behaviour are

observed. For example, the deformation temperature is the point ash becomes ‘sticky’, and therefore, problematic. Whereas, the flow temperature is the ash melting point [64]. Transitional stages recorded at higher temperatures are indicative of a reduced slagging potential [64]. The temperatures of the different ash transitional stages are reported for the different biomass-types and hydrochars; as shown in Figure 6.1. The dotted line present on each figure indicates the maximum temperature of the furnace (1550°C). Any transitional change beyond the furnace limit cannot be determined. Additionally, it is worth noting that the shrinkage transitional stage is the most difficult to observe and therefore, could not be recorded for each sample.

Figure 6.1a-c displays the ash behaviour of the macroalgal biomass and the macroalgal-derived hydrochars. FS and LD showed similar improvements in ash behaviour, compared to the respective parent feedstocks. The untreated FS and LD ashes were shown to deform between 560°C-580°C and flow between 700°C-720°C. Hydrochars generated from FS and LD underwent the different ash transitional changes at consistently higher temperatures compared to their respective parent biomass; suggesting improvements in the slagging propensities. Although, the hydrochars generated at the higher HTC temperatures appear to demonstrate the greatest improvement in ash behaviour. Ash deformation occurred at 640°C for FS150, but this increased to 1170°C and 1180°C for FS200 and FS250, respectively (Figure 6.1b). A similar behaviour was observed in Figure 6.1c, where the ash deformation temperature increased from 640°C (LD150) to 1140°C (LD250). Furthermore, Figure 6.1b showed that ash from FS-derived hydrochars, produced at higher HTC temperatures underwent flow at higher temperatures. The flow transitional stage was recorded at 1470°C for FS150 and above the furnace limit for FS200 and FS250. Figure 6.1c showed the flow temperature of all LD-derived hydrochars were above the furnace limit.

Figure 6.1a also suggests hydrochars generated from SL may show an improvement in ash behaviour, compared to the untreated seaweed. This is because of an increased deformation temperature of SL150 (1460°C) and SL200 (1290°C), compared to untreated SL (850°C); consistent with the findings of Figure 6.1b. However, untreated SL exhibited a flow temperature higher than the furnace limit, indicating this seaweed may have a low slagging propensity. This observation is inconsistent with the results of FS and LD. Smith and Ross [80] previously described a high flow temperature for certain species of seaweed, including: *A. esculenta* and *L. hyperborea*. Work presented in Chapter 4 and literature studies [61,65,80] show high concentrations of alkali metals are associated with macroalgal biomass. Therefore, untreated seaweeds, such as SL are unlikely to display low slagging propensities and the high temperature recorded for the flow (Figure 6.1a) could be related to complex ash matrices affecting the behaviour of seaweed ash. The complex interpretation of seaweed ash behaviour is further exemplified by the shrinkage temperature of untreated SL (1060°C) being higher

than the deformation temperature (850°C). This suggests seaweed ash may not always behave as conventionally expected during these ash fusion tests.

Despite this anomalous result for untreated SL, both SL150 and SL200 also record flow temperatures above the furnace limit; suggesting a low slagging propensity. However, the flow temperature of SL250 (1400°C) was slightly reduced; suggesting a slightly higher slagging tendency than untreated SL, SL150 and SL200. This result is conflicting to the behaviour found in Figure 6.1b-c; where FS and LD hydrochars produced at a higher HTC temperatures display reduced slagging tendencies. However, this again could be linked to the unusual behaviour of seaweed-derived ash.

This highlights the discrepancies between determining the slagging potential according to the predictive indices (Table 6.2) and ash fusion testing (Figure 6.1). For example, the AI, Rb/a, SI and SVI all indicated high/certain slagging tendencies for LD150, LD200 and LD250 (Table 6.2). Whereas, Figure 6.1c shows all flow temperatures are above the furnace limit for LD-derived hydrochars. Similar discrepancies are highlighted by Smith *et al*. [64] for macroalgal-derived hydrochars. These inconsistencies are linked to the differences in ash chemistry between macroalgal biomass and coals, with seaweeds containing high levels of alkali metals and coal containing high levels of silicon dioxide, iron oxide and aluminium oxide [80]. The predictive indices are based on calculations from coal ash and therefore, assumes similar compositions. The Si content of macroalgal biomass is low [80], therefore, overestimation of slagging and fouling indices are predicted.

Figure 6.1d shows that the untreated WH ash underwent the transitional changes at consistently higher temperatures, compared to WH-derived hydrochar ashes. Therefore, WH-derived hydrochars display no significant improvement in ash behaviour, compared to untreated WH. This behaviour is not typically expected, as previous studies have highlighted the potential of HTC to reduce the slagging potential of a range of biomass types, including: algae and lignocellulosic material [64,80,164]. Furthermore, Chapter 5 shows sufficient removal of problematic alkali metals from WH-derived hydrochars. Therefore, the results in Figure 6.1d could be due to further complex matrix effects of the WH.

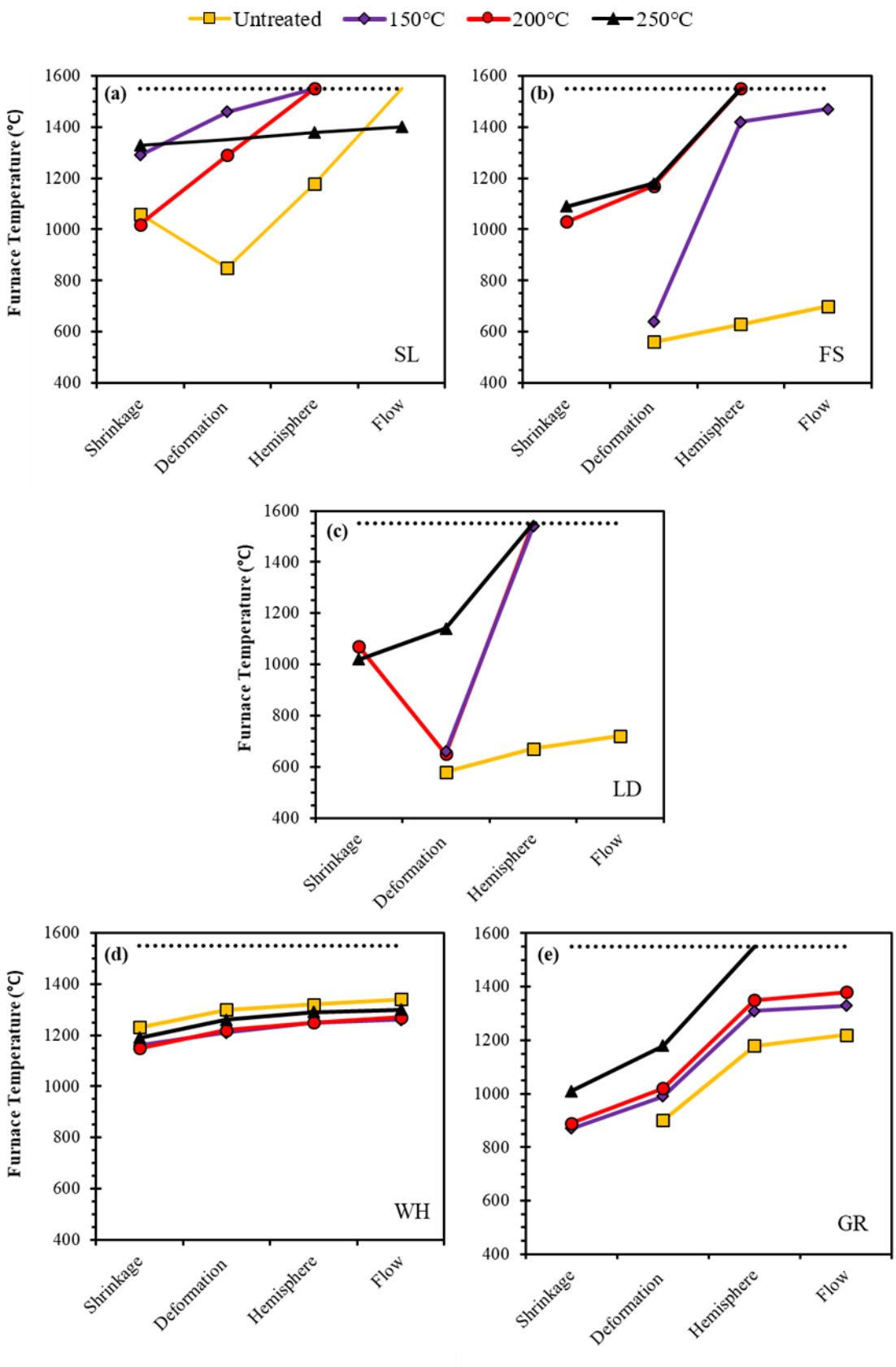

Figure 6.1. Ash fusion transition temperatures of untreated biomass and hydrochars for (a) SL, (b) FS, (c) LD, (d) WH and (e) GR. The dotted line depicts the furnace temperature limit (1550°C).

The application of WH-derived hydrochars in large-scale combustion could be problematic due to slagging and fouling issues. Therefore, the utilisation of WH-hydrochars for small-scale combustion, such as a cooking fuel, could serve as a potential alternative application; as slagging and fouling issues are not a significant problem at smaller-scales. Parmar and Ross [171] previously found hydrochars derived from AD digestate were unsuitable for large-scale combustion due to limited energy densification or improvements in ash behaviour. Therefore, using the hydrochars as a soil-amendment material was suggested as an alternative application. WH-derived hydrochars could also be better suited towards alternative applications, such as: energy storage, soil amendments and low-cost sorbents for phytoremediation applications and carbon sequestration [146,154], should large-scale combustion prove problematic.

GR-derived hydrochars showed improvements in ash behaviour, compared to untreated GR (Figure 6.1e). The deformation temperatures of GR, GR150, GR200 and GR250 were: 900°C, 990°C, 1020°C and 1180°C, respectively. Whereas, the flow temperatures of GR, GR150, GR200 and GR250 were: 1220°C, 1330°C, 1380°C and beyond the furnace limit, respectively. Therefore, the ash behaviour of GR-derived hydrochars improved with increased HTC temperature; following similar conclusions to [64,164]. This is linked to a higher removal efficiency of problematic alkali metals from hydrochars produced at a higher temperature (Chapter 5).

Overall, Figure 6.1 shows that hydrochars generally showed an improvement in ash behaviour compared to the parent feedstock; with the exception of WH. Higher HTC processing temperatures were generally associated with a reduced slagging propensity. According to Figure 6.1 and previous work [80], macroalgal-derived hydrochars show improvements in ash behaviour when processed at across all HTC temperatures. Whereas, GR-derived hydrochars showed only limited improvements in ash behaviour when processed at 150°C or 200°C. Therefore, in order to minimise the slagging potential of GR the HTC reaction should be conducted at higher temperatures (250°C).

6.3 Biomethane Production from Hydrochars

6.3.1 Theoretical Biomethane Potential

Previously, Chapter 5 demonstrated that hydrochars contain a higher carbon content compared to the original parent biomass; with a higher carbon fraction observed at higher HTC temperatures. The carbon content of a biomass feedstock is of particular significance during AD; where accessible carbon is converted to biogas through microbial metabolic pathways. Therefore, hydrochars have the potential to generate higher levels of biomethane,

compared to the parent biomass, on a like-for like mass basis, due to the increased carbon fraction.

Table 6.3 displays the TS and VS content of each biomass feedstock and resultant hydrochars. LD and LD-derived hydrochars have not been analysed as part of this section. Due to insufficient sample, the VS content of hydrochars produced from SL and FS could not be analysed using the furnace method; ashing at 550°C. Therefore, TGA analysis was used to analyse these samples, through the summation of FC and VM, on an as received basis with an ashing temperature at 900°C. Previously, Section 4.3.2.2 demonstrated an increased ashing temperature can result in volatilisation of inorganics, resulting in an overestimation of VS-content. However, Table 5.6 showed macroalgal-derived hydrochars display reduced losses of inorganics during high-temperature ashing, compared to the parent biomass, due to increased solubilisation of alkali metals and chlorine into the process water at higher HTC temperatures. Furthermore, the temperature recommended for determining the ash content of coals (>800°C, BS ISO 1171:2010 [260]) is greater than for biomass (550°C, BS EN 14775:2009 [261]). Chapter 5 showed hydrochars possess more coal-like properties, compared to biomass. Therefore, the error associated with determining the VS-content at higher ashing temperatures is not expected to be as significant for hydrochars, than would be expected for biomass.

According to Table 6.3, the theoretical biomethane potential (BMP_{th}) of all hydrochars were consistently higher than the parent feedstocks and the BMP_{th} increased with increasing HTC temperature. Hydrochars produced at 250°C displayed the highest BMP_{th} of 717.2 mL CH_4/g VS (SL), 730.6 mL CH_4/g VS (FS), 710.0 mL CH_4/g VS (WH) and 721.7 mL CH_4/g VS (GR). Representing an increase of 49%, 52%, 49% and 38%, compared to the untreated biomass, for SL, FS, WH and GR, respectively. Higher BMP_{th} yields are linked to an increased carbon concentration, which causes a stoichiometric shift towards increased theoretical methane generation.

Similar results were discovered for the BMP_{th} of spent coffee ground hydrochars; increasing from 633.4 mL CH_4/g VS (180°C), 758.2 mL CH_4/g VS (220°C) and 823.5 mL CH_4/g VS (250°C) [161]. Although, these values are slightly higher than the values presented in Table 6.3. This is due to a higher carbon content of the coffee grounds-derived hydrochars. For example, FS250 displayed the greatest BMP_{th} in Table 6.3; 730.6 mL CH_4/g VS, with a respective carbon content of 54.6% (Chapter 5). Whereas, the coffee ground-derived hydrochar, produced at 250°C recorded a BMP_{th} of 823.5 mL CH_4/g VS, with a respective carbon content of 71.7% [161].

The improvement in BMP_{th} is related to the degree of energy densification (ED) of a hydrochar. For instance, WH only showed a 3% increase in BMP_{th} from the original biomass

to the respective hydrochars generated at 150°C. Whereas, GR150 displayed an 11% reduction in BMP_{th}, compared to GR. Alternatively, SL150 and FS150 exhibited an increase of 12% and 16%. Again, this is linked to differences in the increased carbon content, with lignocellulosic-derived hydrochars displaying limited ED at 150°C, compared to macroalgal-derived hydrochars.

Due to the increased carbon fraction, higher-temperature hydrochars are typically associated with an increased C:N ratio. The optimal C:N range for AD is between 25-30:1 [17]. Figure 6.2 shows hydrochars produced at 200°C and 250°C have an improved C:N for AD. However, all biomass feedstocks and hydrochars fall short of the optimum C:N range; associated with high concentrations of nitrogen.

Table 6.3. Total solids, volatile solids and theoretical biomethane potential for untreated biomass and hydrochars.

Sample	**TS (%)** *ar*	**VS (%)** *ar*	**BMP_{th} (mL CH_4/g VS)**
SL	92.2	65.7 [a]	481.0
SL150	95.6	85.5 [b]	537.2
SL200	97.7	84.7 [b]	610.9
SL250	98.0	80.3 [b]	717.2
FS	90.5	65.8 [a]	480.8
FS150	95.6	86.7 [b]	558.4
FS200	97.4	85.3 [b]	648.6
FS250	98.2	81.1 [b]	730.6
WH	93.1	73.7 [a]	476.0
WH150	92.9	75.6 [a]	488.8
WH200	95.6	78.4 [a]	555.1
WH250	97.2	74.9 [a]	710.0
GR	95.4	84.3 [a]	521.5
GR150	93.8	83.0 [a]	463.3
GR200	95.6	84.0 [a]	558.4
GR250	97.5	81.5 [a]	721.7

[a]Determined by APHA method [223]; ashing at 550°C, [b]Determined by TGA; ashing at 900°C. TS=total solids. VS=volatile solids. BMP_{th}=theoretical biomethane potential. *ar*=as received. BMP_{th} calculated using elemental composition data presented in Table 5.3, applied to the Boyle's equation.

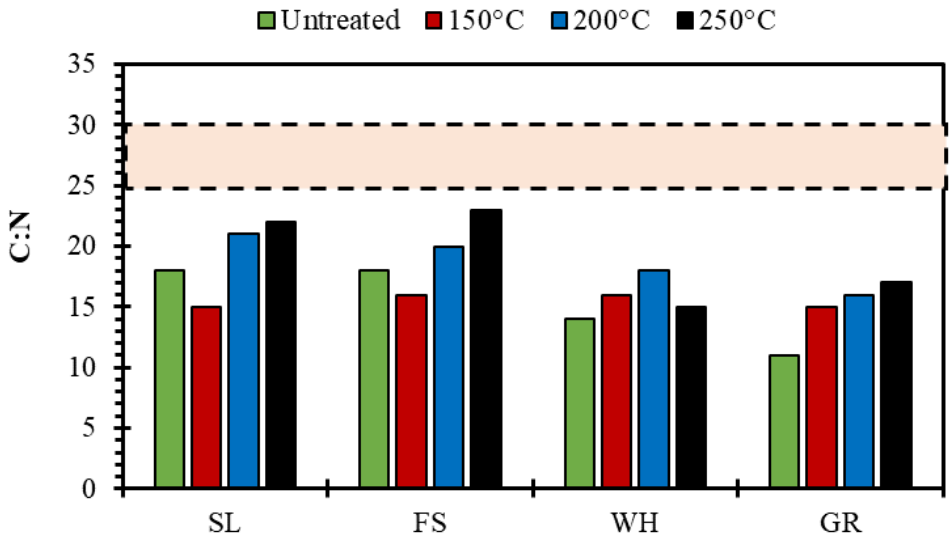

Figure 6.2. Carbon-to nitrogen ratio of untreated biomass and hydrochars.

6.3.2 Experimental Biomethane Potential

Overall, from a theoretical perspective, hydrochars have the potential to generate improved biomethane yields, compared to the respective parent feedstocks. Hydrochars demonstrate higher BMP_{th} (Table 6.3) and enhanced C:N (Figure 6.2) particularly when produced at higher HTC temperatures; due to an increased carbon content. However, BMP_{th} does not represent true BMP, as complete stoichiometric conversion is assumed [97], with no understanding of the degree of biodegradability of a feedstock during AD. Therefore, batch experimental biomethane potential experiments were conducted on SL, FS, WH and GR hydrochars and original biomass, to determine the true biomethane potential (BMP_{ex}).

Figure 6.3 displays the cumulative biomethane potential yields of the hydrochars and parent biomass material, with final BMP_{ex} yields reported in Table 6.4. In addition, Table 6.4 describes the process kinetics of the BMP_{ex} curves shown in Figure 6.3, according to the modified Gompertz Model [229], peak fermentation time (T_m) [44] and technical digestion time (T^{80}) [226].

Figure 6.3a shows all SL-derived hydrochars had a lower BMP_{ex} yield than untreated SL (249.5 mL CH_4/g VS). SL150 and SL200 showed BMP_{ex} yields of 184.5 mL CH_4/g VS and 161.6 mL CH_4/g VS, corresponding to a 26% and 35% reduction in BMP_{ex}, compared to untreated SL, respectively. The biomethane yield from SL250; 28.1 mL CH_4/g VS was much lower than any other sample in Figure 6.3a, representing an 89% reduction in BMP_{ex}, compared to the untreated SL. Furthermore, Table 6.4 shows untreated SL displayed the most

favourable digestion kinetics compared to SL150, SL200 and SL250. Untreated SL had the highest peak biomethane production rate (R_m), as well as the lowest peak fermentation time (T_m) and technical digestion time (T^{80}); suggesting more rapid digestion, compared to SL-derived hydrochars.

Figure 6.3b shows the BMP_{ex} of FS150 (151.1 mL CH_4/g VS) and FS200 (126.3 mL CH_4/g VS) were both lower than the BMP_{ex} yield obtained from untreated FS (157.4 mL CH_4/g VS). FS250 generated the lowest BMP_{ex}; 86.8 mL CH_4/g VS in Figure 6.3b; following a similar trend to SL250. Overall, SL-derived hydrochars generated higher BMP_{ex} yields than FS-derived hydrochars produced across comparable HTC temperatures.

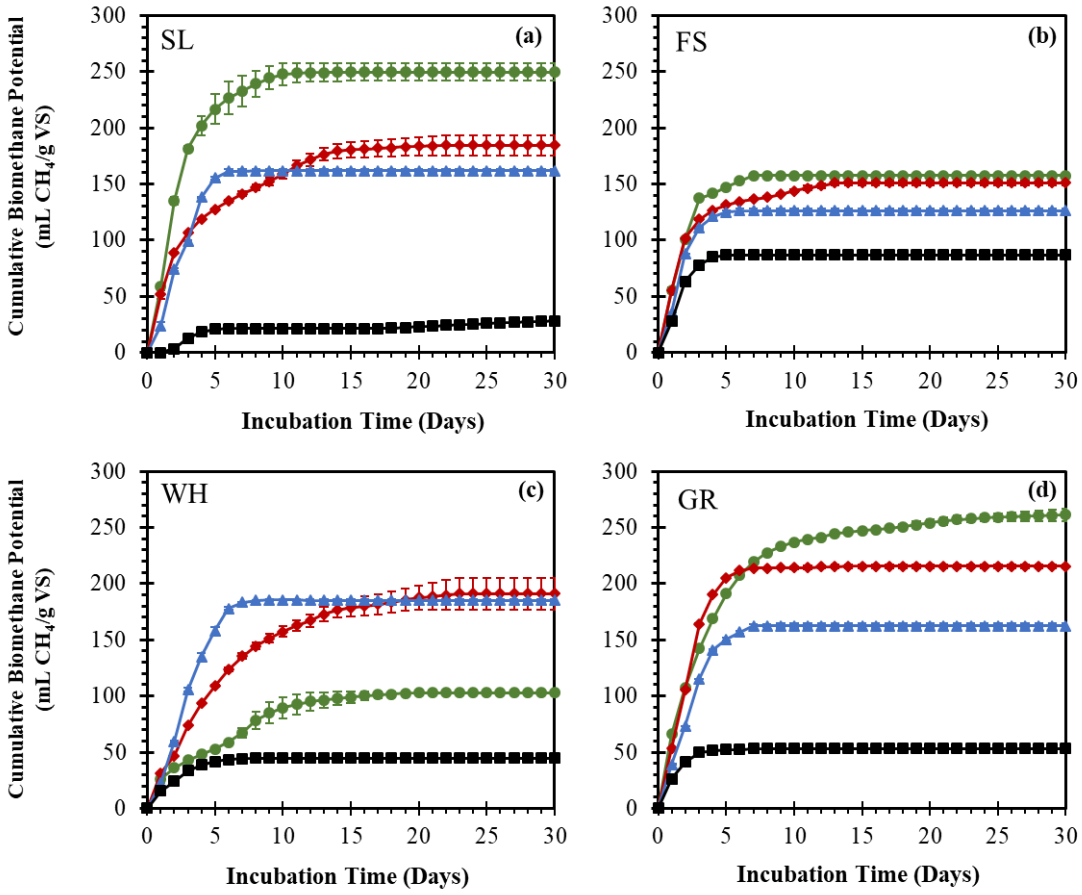

Figure 6.3. Experimental biomethane potential (BMP_{ex}) of untreated biomass and hydrochars for (a) SL, (b) FS, (c) WH and (d) GR. Data is presented as average values. Error bars represent the maximum and minimum values (n=2).

Table 6.4. Digestion kinetics from the anaerobic digestion of untreated biomass and hydrochars.

Sample	BMP_{ex} mL CH_4/g VS	Modified Gompertz Model				T_m (d)	T^{80} (d)
		H_m mL CH_4/g VS	R_m mL CH_4/g VS/d	λ (d)	R^2		
SL	249.5	248.0	62.1	0.0	0.99	1.5	4
SL150	184.5	179.6	28.9	0.0	0.95	2.3	9
SL200	161.6	162.1	47.4	0.6	0.99	1.8	4
SL250	28.1	23.5	8.2	1.5	0.92	2.6	20
FS	157.4	157.0	53.4	0.0	0.99	1.1	3
FS150	151.1	147.9	48.1	0.0	0.97	1.1	4
FS200	126.3	126.3	55.4	0.3	0.99	1.2	3
FS250	86.8	86.8	40.0	0.3	0.99	1.1	3
WH	103.1	103.1	11.2	0.0	0.99	3.4	9
WH150	191.1	187.6	21.0	0.0	0.99	3.3	10
WH200	185.0	185.6	46.1	0.7	0.99	2.2	5
WH250	44.9	44.9	12.6	0.0	0.99	1.3	4
GR	261.2	252.4	44.3	0.0	0.99	2.1	7
GR150	215.4	215.5	64.1	0.2	0.99	1.5	4
GR200	162.6	162.9	44.2	0.2	0.99	1.6	4
GR250	53.2	53.1	24.7	0.0	0.99	0.8	3

BMP_{ex}=experimental biomethane potential. H_m=maximum biomethane yield. R_m=peak biomethane production rate. λ=lag phase. T_m=peak time of fermentation. T^{80}=technical digestion time.

WH-derived hydrochars (Figure 6.3c) underwent slightly different digestion behaviours, compared to SL and FS hydrochars. WH150 and WH200 both generated similar yields of biomethane; 191.1 mL CH_4/g VS and 185.0 mL CH_4/g VS; 85% and 79% higher than untreated WH (103.1 mL CH_4/g VS), respectively. However, Table 6.4 shows WH200 had more favourable digestion kinetics than WH150; with a higher peak methane production rate (R_m) as well as a lower peak time of fermentation (T_m). The technical digestion time (T^{80}) of WH200 suggests this hydrochar could generate 80% of the overall total methane in half the time of WH150; 5 and 10 days, respectively. Although, WH200 has more favourable

digestion kinetics than WH150, WH200 is likely to be less energetically feasible to produce, due to the higher energy input required for the HTC reaction. Similarly to SL and FS, the WH-hydrochar produced at the highest HTC temperature (250°C) generated the lowest biomethane yields in Figure 6.3c. WH250 generated 44.9 mL CH_4/g VS; which corresponded to a 56% reduction in BMP_{ex}, compared to untreated WH.

The BMP_{ex} yields of all GR-derived hydrochars presented in Figure 6.3d were lower than untreated GR. GR150. GR200 and GR250 displayed BMP_{ex} yields of 215.4 mL CH_4/ g VS, 162.6 mL CH_4/ g VS and 53.2 mL CH_4/ g VS, respectively; corresponding to 18%, 38% and 80% reductions in BMP_{ex}, compared to untreated GR. Digestion of GR-hydrochars were conducted at an ISR of 1.9:1, due to the initial VS of the inoculum batch being slightly lower. Table 6.4 displays evidence that GR150 underwent more favourable digestion kinetics than untreated GR; with an increased R_m as well as decreased T_m and T^{80}. However, the slightly improved digestion kinetics may not warrant the reduced BMP_{ex} yield.

Overall, Figure 6.3 highlights clear differences between different feedstock types and the behaviour of hydrochars during AD. All hydrochars generated from SL, FS and GR generated lower biomethane yields, compared to the untreated parent biomass. Whereas, WH150 and WH200 showed an improvement in biomethane generation compared to the untreated parent biomass; albeit each displaying different degrees of improvement. A common trend observed across all feedstocks in Figure 6.3 is that hydrochars generated at lower temperatures (150°C) appear to generate higher BMP_{ex}, compared to hydrochars generated at higher temperatures (250°C).

6.3.3 Biodegradability Index (BI)

The biodegradability index (BI) of each biomass feedstock and hydrochar is presented in Figure 6.4; calculated using the BMP_{th} (Table 6.3) and BMP_{ex} (Figure 6.3). Previously, Table 6.3 showed that hydrochars generated at higher HTC temperatures had a greater BMP_{th}, because of an increased carbon content. However, this trend is not reflected in the BIs shown in Figure 6.3.

Figure 6.4a shows a decreasing BI with increased HTC temperature; with SL, SL150, SL200 and SL250 recording respective BIs of 52%, 34%, 26% and 4%. Figure 6.4b shows the BIs of FS-derived hydrochars are also lower than untreated FS (33%): FS150 (27%), FS200 (19%) and FS250 (12%). GR-derived hydrochars followed a similar trend (Figure 6.4d), with the BIs of GR, GR150, GR200 and GR250 being 50%, 46%. 29% and 7%, respectively. Whereas,

the BI of WH150 (39%) and WH200 (33%) are higher than untreated WH (22%) (Figure 6.4c), due to higher BMP_{ex} yields. Although, the BI of WH250 reduced to 6%.

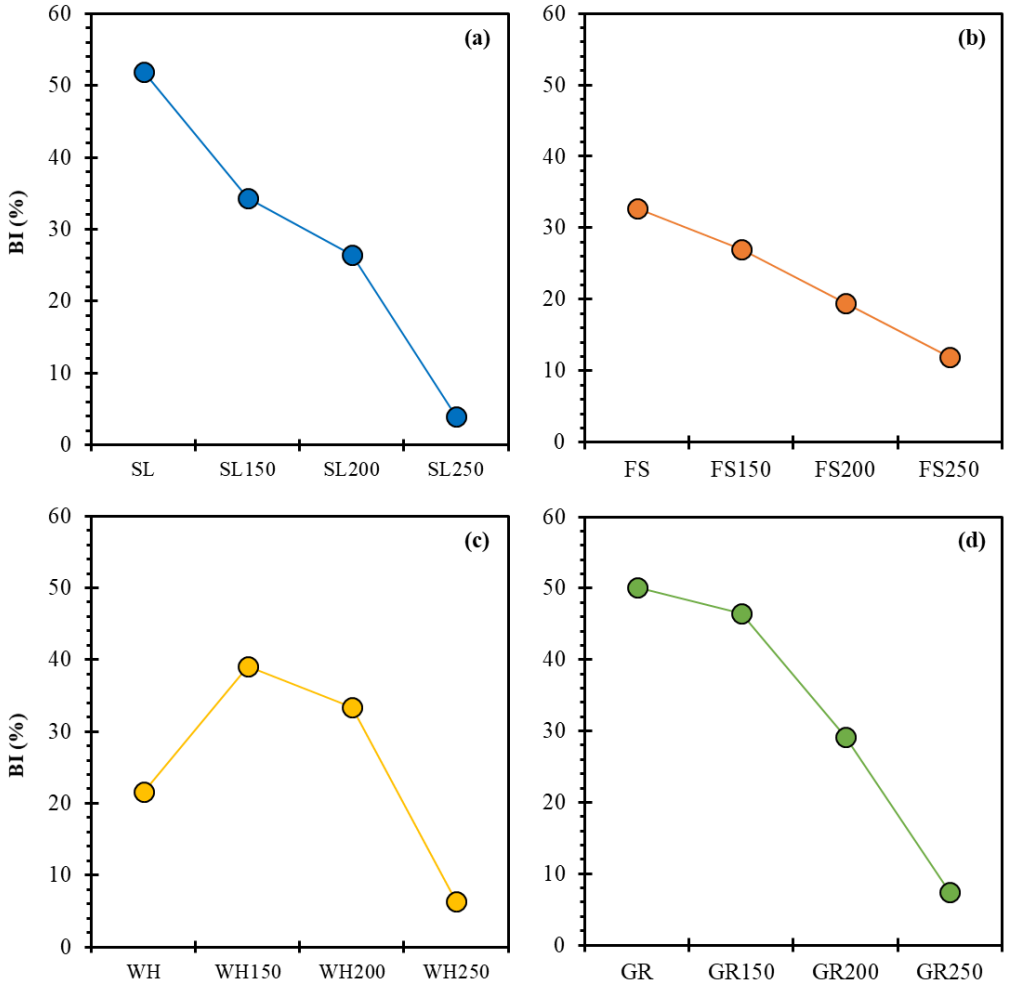

Figure 6.4. Biodegradabilities of untreated biomass and hydrochars for (a) SL, (b) FS, (c) WH and (d) GR.

Figure 6.4 highlights that hydrochars produced at 250°C exhibited the lowest BIs across all biomass types. Despite an increase in the carbon content of hydrochars, the carbon availability for biomethane generation appears to be limited. The BI of SL250, FS250, WH250 and GR250 hydrochars are lower than conventional AD feedstocks [102], suggesting the structure is recalcitrant to anaerobic microbial degradation. Mumme *et al*. [196] found only 10.4% of the carbon within hydrochar produced from wheat digestate (230°C, 6-hr), was labile for anaerobic degradation during AD. This value is similar to the BI values obtained for SL250, FS250, WH250 and GR250 hydrochars. The reduced BI of hydrochars generated at higher HTC temperatures is believed to be linked to the increase in aromatic structure [161]. Hydrochar structures have been shown to have an increased degree of aromatisation under

more severe HTC conditions [148,161,262,263]. These aromatic structures have been described as 'lignin-like' [196] and therefore, inert to microbial degradation [196].

Overall, Figure 6.4 suggests AD of hydrochars produced at higher temperatures is not a suitable conversion route. This is supported by work conducted by Quintana-Najera *et al*. [198] who found the addition of hydrochars produced from FS and WH at 250°C caused an inhibitory effect during cellulose AD. Selected lower temperature hydrochars (WH150 and WH200) showed an improvement in BMP_{ex} and BI; however, this trend appears to vary across different biomass types.

6.4 Anaerobic Biological Conversion of Process Waters

Traditionally, the main product of interest from the HTC process was the solid hydrochar. The multiple applications of hydrochars typically results in its separation from the process water fraction. Chapter 5 demonstrated that the process water fraction contains high concentrations of organic and inorganic matter from the original biomass; the composition of which changes with increased HTC severity. Potential applications for HTC process waters have been suggested, including: re-circulation into HTC [179,264] or as a nutrient-rich fertiliser [262].

However, this work focusses on the valorisation of the solubilised organic fraction of the process waters through the generation of energy by biological processing. This includes a direct comparison of the available energy recovered from the generation of biomethane and biohydrogen from the process waters, through AD and DF, respectively. The solubilised organic matter within process waters can bypass the rate limiting step of biological conversion; hydrolysis [265]. Although, the increased concentration of inhibitory compounds present within higher-temperature process waters could limit biological conversion.

6.4.1 Biomethane Generation

This section investigates the potential for biomethane generation from the separated HTC process waters from SL, FS, LD, WH and GR. Initially, batch BMP_{ex} experiments were conducted to determine the cumulative biomethane potential of the process waters. Following this, the influence of the process water biochemical composition on the generated biomethane yields was investigated. Finally, methodologies for determining the BI of the process waters were assessed.

6.4.1.1 Experimental Biomethane Potential

The BMP_{ex} of the HTC process waters are displayed in Figure 6.5. Final BMP_{ex} yields are presented in Table 6.5, alongside the digestion kinetics according to the modified Gompertz Model [229], peak fermentation time (T_m) [44] and technical digestion time (T^{80}) [226]. BMP_{ex} experiments were conducted using an AMPTS II; using a similar methodology which was used to determine the BMP_{ex} of hydrochars. The key difference between the BMP_{ex} experimental set-up of the hydrochars and process waters is the unit of expression; with the biomethane yields of hydrochars expressed as: mL CH_4/g VS and the process waters expressed as: mL CH_4/g COD. Determining the BMP_{ex} of process waters on a COD (mL CH_4/g COD) basis is common practice [147,163,170,171,179,190,195]. Although, some studies report process water biomethane yields on a VS basis (mL CH_4/g VS) [84,160]. This method is advantageous as it would allow for direct comparison of the BMP_{ex} yields with hydrochars. However, Chapter 5 demonstrated the evaporative loss of volatile organic compounds whilst determining the TS/VS concentration of process waters, suggesting this methodology may be subject to errors. Alternatively, determining the COD of solid heterogeneous samples is considered to be difficult and generate erroneous results [97,266]. Therefore, the BMP_{ex} of solid samples; hydrochars were determined on a VS basis.

The BMP_{ex} of SL150 was 221.9 mL CH_4/g COD; higher than both SL200 (185.7 mL CH_4/g COD) and SL250 (179.2 mL CH_4/g COD), which generated similar yields (Figure 6.5a). Although, Table 6.5 suggests SL200 and SL150 had more favourable digestion kinetics than SL150; showing higher R_m, as well as lower T_m and T^{80} values, indicating a more rapid digestion. However, this is compromised by the lower BMP_{ex} yield. Figure 6.5b shows the cumulative BMP_{ex} values for FS-derived process waters are more similar across the three HTC treatment temperatures, compared to SL: 214.5 mL CH_4/g COD (FS150), 201.2 mL CH_4/g COD (FS200) and 190.4 mL CH_4/g COD (FS250). Although, the BMP_{ex} yield of FS-derived process waters decreased as HTC production temperature increased; similar to SL. The digestion kinetics of FS-derived process waters were more similar across the different HTC temperatures, compared to SL-derived process waters.

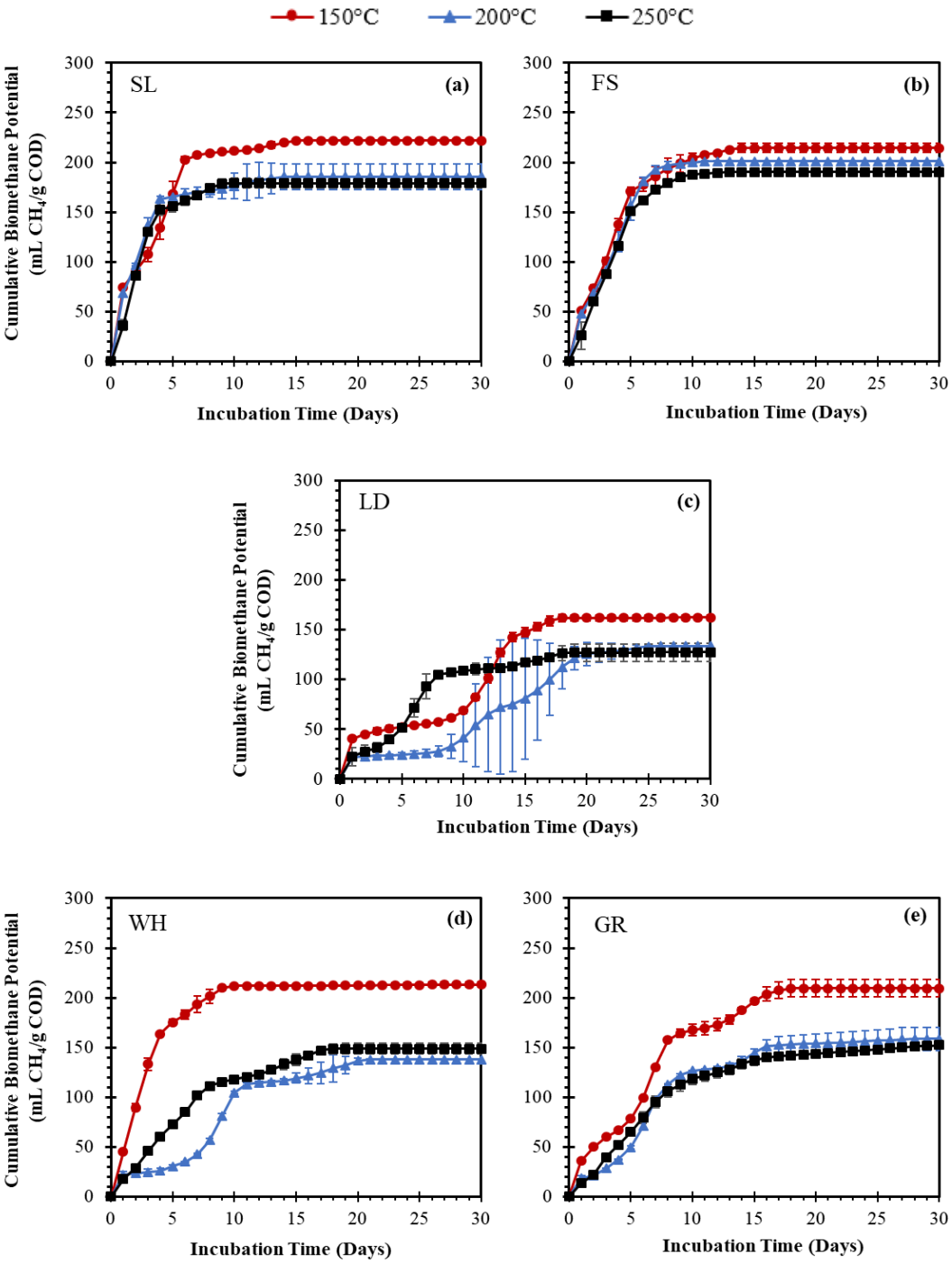

Figure 6.5. Experimental biomethane potential (BMP_{ex}) of HTC process waters from (a) SL, (b) FS, (c) LD, (d) WH and (e) GR. Data is presented as average values. Error bars represent the maximum and minimum values (n=2).

Table 6.5. Digestion kinetics from the anaerobic digestion of HTC process waters.

Sample	BMP_{ex} mL CH_4/g COD	Modified Gompertz Model				T_m (d)	T^{80} (d)
		H_m mL CH_4/g COD	R_m mL CH_4/g COD /d	λ (d)	R^2		
SL150	221.9	221.2	39.2	0.0	0.98	2.1	6
SL200	185.7	182.9	50.6	0.0	0.98	1.3	4
SL250	179.2	178.4	46.1	0.1	0.99	1.6	4
FS150	214.5	213.8	35.7	0.0	0.99	2.2	6
FS200	201.2	202.6	35.3	0.1	0.99	2.2	6
FS250	190.4	190.7	35.0	0.4	0.99	2.4	6
LD150	162.4	179.1	9.5	0.0	0.94	6.9	14
LD200	133.9	157.1	7.2	2.9	0.97	10.9	18
LD250	127.4	126.9	13.3	0.4	0.98	3.9	8
WH150	213.4	212.1	43.6	0.0	0.99	1.8	5
WH200	137.9	140.7	11.6	2.0	0.98	6.4	11
WH250	148.8	184.7	14.2	0.0	0.99	3.9	11
GR150	209.3	212.0	18.5	0.0	0.99	4.2	10
GR200	158.7	157.0	15.6	1.2	0.99	4.9	11
GR250	152.4	148.1	13.8	0.2	0.99	4.2	12

BMP_{ex}=experimental biomethane potential. H_m=maximum biomethane yield. R_m=peak biomethane production rate. λ=lag phase. T_m=peak time of fermentation. T^{80}=technical digestion time.

LD-derived process waters (Figure 6.5c) appear to undergo different digestion behaviours compared to SL and FS-derived process waters, during AD. LD150 generated a higher final BMP_{ex} (162.4 mL CH_4/g COD), compared to LD200 (133.9 mL CH_4/g COD) and LD250 (127.4 mL CH_4/g COD); following a similar trend to SL and FS process waters. However, Table 6.5 shows the behaviour of the digestion kinetics are different; showing a much slower generation of biomethane and large variations between duplicate runs, especially for LD200. In addition, the final BMP_{ex} yields of LD-derived process waters are lower than the equivalent produced from SL and FS process waters. Table 6.5 shows the peak biomethane production

rate (R_m) was lower for LD process waters (7.2-13.3 mL CH_4/g VS/d) compared to SL (39.2-50.6 mL CH_4/g VS/d) and FS (35.0-35.7 mL CH_4/g VS/d) process waters. Moreover, the T_m and T^{80} values were also greater for LD-derived process waters, than SL and FS; signifying a slower digestion. This suggests the formation of inhibitory compounds during the HTC of LD, which are not present, or present in a reduced concentration within SL and FS process waters. Although, the complex HTC reaction pathways are not yet fully understood in relation to macroalgal polysaccharides [80]. Therefore, further work is required to identify the potential inhibitory compound generated from the HTC of LD.

Overall, Figure 6.5a-c shows seaweed-derived HTC process waters produced at lower temperatures (150°C) produced higher biomethane yields, compared to those produced at higher temperatures (200°C and 250°C). This trend is typically observed across previous studies, including the digestion of HTC process waters from microalgae [160], cow manure [84] orange pomace [163] and the organic fraction from municipal solid waste [209]. The reduced biomethane yields of higher-temperature HTC process waters is thought to be related increased formation of inhibitory compounds, coupled with a reduction in readily-digestible sugars. Lin *et al*. [72] determined a maxima mannitol extraction from *S. latissima* at 140°C during hydrothermal pre-treatment. Further increasing the hydrothermal treatment temperatures to 160°C and 180°C decreased the mannitol recovery yield; indicating further degradation into inhibitory compounds, such as furfural and levulinic acid [72]. In addition, inhibition has been linked to the formation of nitrogen-containing compounds, derived from Maillard reactions [72]. Chapter 5 indicated an increase in NH_4^+-N and total phenol concentrations of higher-temperature seaweed process waters; known inhibitors of the AD process [104,192]. However, no HMF or furfural were detected in the macroalgal-derived process waters produced at 200°C or 250°C.

Few studies previously report the BMP_{ex} of macroalgal-derived process waters. Furthermore, no current studies are available which compare the biomethane yields from brown macroalgal-derived HTC process waters produced across a range of HTC temperatures. Despite this, Wang *et al*. [179] reported a BMP_{ex} of 186 mL CH_4/g COD for a *Laminaria* species generated at 220°C (2-hrs). This value agrees with the higher temperature process waters generated from SL, another kelp species, at 200°C (SL200) and 250°C (SL250). Interestingly, the value reported by Wang *et al*. [179] was not as comparable to LD200 (133.9 mL CH_4/g COD) and LD250 (127.4 mL CH_4/g COD); despite both seaweeds sharing the same genus origin. The disparity between the results of Wang *et al*. [179] and Figure 6.5c could potentially be linked to differences in the seaweed harvesting period. As previously mentioned, the biochemical composition of *Laminaria digitata* is seasonally variable, including the variation in the polysaccharide composition [60,61]. The effect of seasonality on biomethane yields from *A. esculenta*-derived HTC process waters was theoretically

determined by Smith and Ross [80]. It was suggested summer-harvested seaweed would generate higher theoretical biomethane yields, due to an increased carbohydrate content; with winter-harvested seaweed displaying the inverse relationship [80]. LD used in Figure 6.5c was collected during a winter period (January 2009), therefore, lower biomethane yields would be expected, according to [80]. Wang *et al*. [179] do not report information regarding the *Laminaria* collection time; however, it can be speculated the seaweed was collected during a season which favours a higher carbohydrate content, explaining the higher BMP_{ex} yields of the process waters. Although, further work is required to confirm this theory, as currently, the seasonal variation of biomethane generation from macroalgal-derived HTC process waters has only been theoretically calculated. Future work would aim to investigate this seasonal variation using experimentally-derived biomethane yields across a range of HTC temperatures and different macroalgal species. A more recent study [184] investigated the biogas generation from the co-digestion of food waste with HTC process waters produced from sea lettuce, a green macroalgal species, across a range of HTC temperatures (180°C, 200°C and 220°C). However, the process waters showed minimal biogas production and were not deemed suitable for AD. This highlights differences potential differences between the suitability of green and brown macroalgal-derived HTC process waters to generate biogas or biomethane; with Figure 6.5a-c indicating the process waters from brown macroalgae generate significant yields of biomethane.

Figure 6.5d displays the BMP_{ex} of the WH-derived process waters. WH150 generated the highest BMP_{ex} shown by Figure 6.5d (213.4 mL CH_4/g COD). WH200 and WH250 produced biomethane yields of 137.9 mL CH_4/g COD and 148.8 mL CH_4/g COD, respectively. The process water compositional analysis from Chapter 5 showed WH150 had a greater concentration of total sugar, compared to WH200 and WH250, as well as the lowest concentration of phenols and no detectable HMF or furfural. WH200 and WH250 contained higher concentrations of phenol, HMF and furfural; all inhibitory compounds with the potential to impede biomethane generation. Table 6.5 shows peak biomethane production rate for WH150 (43.6 mL CH_4/g COD/d) was over three times greater than WH200 or WH250 (11.6-14.2 mL CH_4/g COD/d). Additionally, the technical digestion time (T^{80}) for WH150 (5-days) occurred in half the time of WH200 or WH250 (10-days). Therefore, WH150 showed more favourable digestion kinetics compared to WH200 and WH250. The BMP_{ex} of WH-derived HTC process waters has not yet been reported in previous literature. However, using the values reported by Hudakorn and Sritrakul [85] the water squeezed from a combination of WH leaf and petioles had an approximate BMP_{ex} of 138 mL CH_4/g COD. Therefore, Figure 6.5d indicates that HTC processing at 150°C can improve the biodegradability of the WH aqueous phase. Although, this result must be interpreted with caution, as Hudakorn and

Sritrakul [85] used a WH sample harvested from a different location. Therefore, geographical variation in biochemical composition is expected.

Figure 6.5e showed the BMP_{ex} of GR150 (209.3 mL CH_4/g COD) was higher than GR200 (158.7 mL CH_4/g COD) and GR250 (152.4 mL CH_4/g COD). This continues the trend observed throughout Figure 6.5, in which the process water generated at the lowest temperature (150°C) generated higher biomethane yields than higher temperature process waters (200°C and 250°C). Again, this could be linked to the formation of inhibitory compounds; with GR200 and GR250 showing increased phenol and NH_4^+-N concentrations, compared to GR150 (Chapter 5). Table 6.5 shows that GR150 has slightly improved digestion kinetics compared to GR200 and GR250; however, this improvement is not as significant as the improvement observed between WH150 and WH200/WH250.

Pagés-Díaz *et al*. [190] investigated the generation of biomethane from lignocellulosic-derived HTC process waters. The study determined the BMP_{ex} of HTC process waters produced at 220°C (1-hr) using a range of different lignocellulosic biomass types: pine sawdust (253 mL CH_4/g COD), canola oil production residues (108 mL CH_4/g COD), olive oil production residues (91 mL CH_4/g COD) and vineyard waste (119 mL CH_4/g COD). It was concluded that lower biomethane yields were linked to the presence of recalcitrant nitrogen-containing compounds [190].

Overall, all the HTC process waters presented in Figure 6.5 demonstrated the capacity for biomethane generation during AD. Although, across all feedstocks, the lower temperature process waters (150°C) generated higher levels of biomethane compared to the process waters generated at 200°C and 250°C. However, there appears to be a varied degree of magnitude between the difference in BMP_{ex} yields of process waters produced at 150°C and higher temperatures (200°C and 250°C), depending on the feedstock. This is exemplified in Figure 6.6, which compares the percentage reduction in BMP_{ex} of the higher temperature process waters, compared to process waters produced at 150°C. Lignocellulosic-derived, high temperature process waters display a greater reduction in BMP_{ex} compared to macroalgal-derived high temperature process waters. Figure 6.6 showed that WH200 and WH250 had a respective 35% and 30% reduction in BMP_{ex} compared to WH150; the highest of any feedstock investigated. GR200 and GR250 showed respective BMP_{ex} reductions of 24% and 27%. Kelp species (SL and LD) had similar reductions in BMP_{ex}: 16-18% (200°C) and 19-22% (250°C). Whereas, the higher temperature process waters generated from FS displayed the minimal reduction in BMP_{ex}: 6% and 11%, respectively for FS200 and FS250.

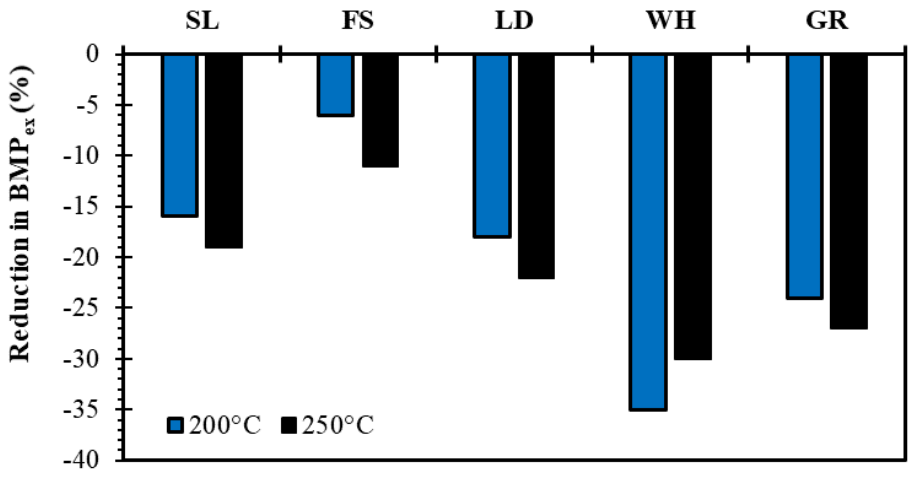

Figure 6.6. Reductions in BMP_{ex} between high temperature process waters (200°C and 250°C), comparative to low temperature process waters (150°C).

In order to understand how the composition of the process waters affects the biomethane yields, Figure 6.7 shows generalised correlations of different the concentrations of different process water components, determined in Chapter 5, to the corresponding BMP_{ex} yields, shown in Figure 6.7. The correlations in Figure 6.7 combines the data of the process waters derived from SL, FS, LD WH and GR. Therefore, potential behavioural differences between process waters produced from macroalgal and lignocellulosic biomass has not been accounted for, due to a limited number of correlation points. As a result of this, only generalised conclusions can be suggested. A Pearson's Correlation analysis was conducted to determine the significance of each correlation.

Figure 6.7a suggests the initial pH of the process water had no significant effect ($p>0.05$) on BMP_{ex} yields. Generally, the pH of process waters was acidic (Figure 5.19). However, once the process waters were mixed with inoculum during the BMP_{ex} experiment, the pH became closer to the optimal range of between 6.8-7.2 [17]. The data presented in Figure 6.7a was not normally-distributed; therefore, a Spearman's Rank analysis was conducted. Further to pH, the process water ash concentration and BMP_{ex} showed no significant ($p>0.05$) correlation (Figure 6.7b).

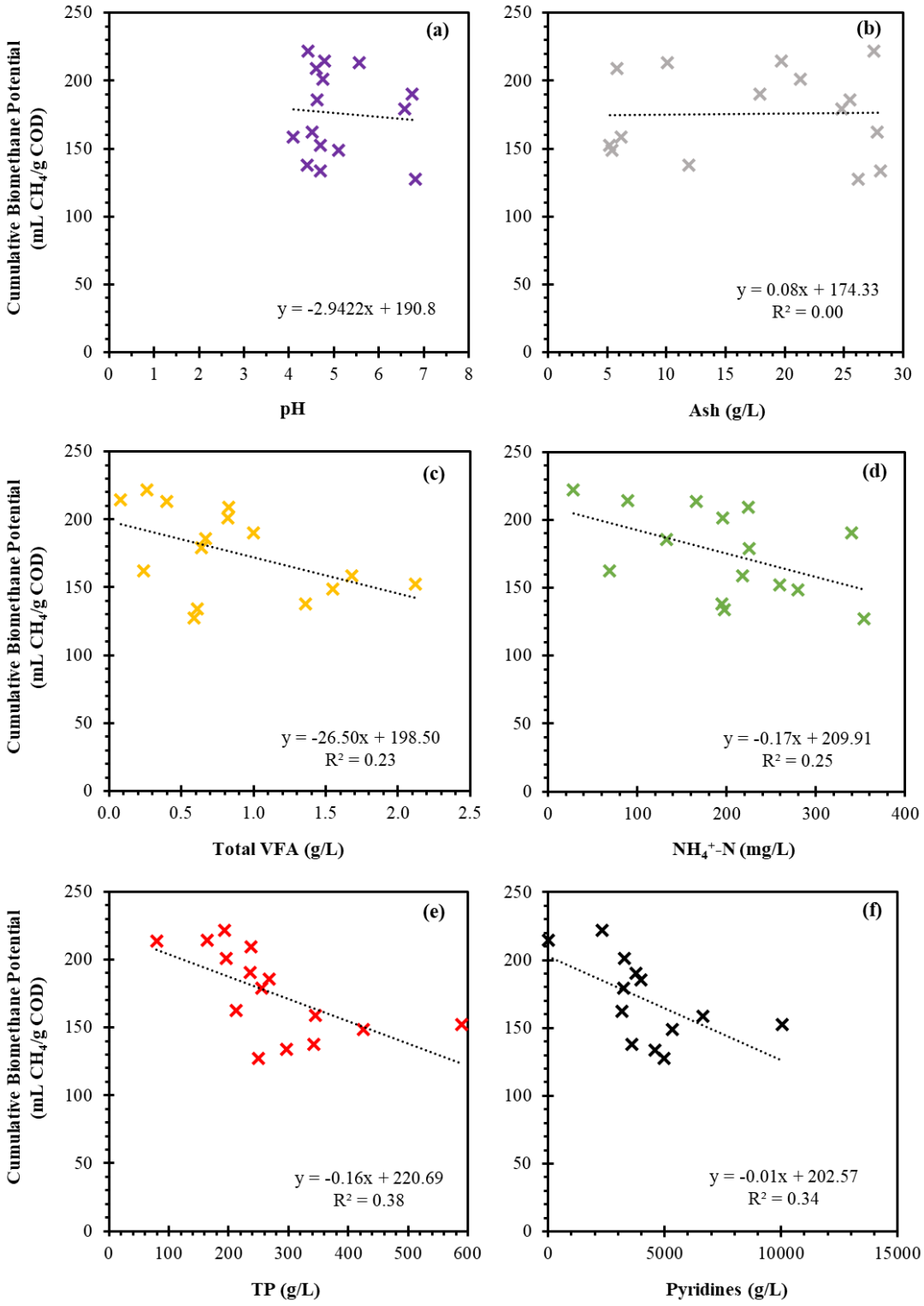

Figure 6.7. Effect of process water composition on experimental biomethane potential (BMP_{ex}) yields: (a) pH, (b) ash, (c) total volatile fatty acids, (d) NH_4^+-N, (e) total phenols (f) pyridines.

Figure 6.7c shows that BMP_{ex} reduced with increased VFA concentration, although this correlation was not significant (p>0.05). VFA concentrations were determined using GC-FID. Acetic acid is the pre-cursor to acetoclastic methanogenesis; whereas other VFAs, such as

propionic and butyric acid can be metabolised to acetic acid during the acetogenesis stage of AD. Therefore, a higher VFA concentration in the process water could be associated with greater biomethane generation. However, VFAs can be inhibitory to anaerobic systems in large enough concentrations through penetrating the cell walls of microorganisms, causing an intracellular pH imbalance [205]. Oligomers and polysaccharides within the process water can be further metabolised into acetic acid. Therefore, VFA production may continue beyond the initial concentration determined. Figure 6.7d shows a negative correlation between NH_4^+-N and BMP_{ex} of the process waters, although, this relationship was not significant (p>0.05). Free ammonia (NH_3) has been reported to have a greater inhibitory effect over ammonium (NH_4^+) [190]. Although, both are inhibitory to the AD process [254].

A significant (p<0.05) negative correlation was identified for between both BMP_{ex} and total phenol concentration (Figure 6.7e) as well as pyridine concentration (Figure 6.7f). Phenols are known inhibitors of the AD process, altering the selective permeability of microbial cell membranes, causing disruption of essential enzymatic pathways [192]. Previous studies find that an anaerobic microbial consortium can degrade phenols at lower concentrations [207]. However, increased concentrations of between 1 g/L [205] and 2 g/L [207] can cause complete inhibition of anaerobic systems. The phenol concentrations shown in Figure 6.7e ranged between 80-590 mg/L; therefore are below the limits to completely inhibit the process. Pyridine concentration in the process waters also showed a negative correlation with BMP_{ex}. Pyridines were determined by GC-MS and were mainly present in the form of 3-hydroxypridine.

WH and GR process waters produced at 200°C and 250°C contain higher concentrations of phenols and pyridines compared to macroalgal-derived process waters generated at the same temperatures (Chapter 5). This could help to explain the greater reduction in BMP_{ex} of high-temperature lignocellulosic-derived process water, compared to high-temperature macroalgal-derived process waters (Figure 6.6). Although the phenol and pyridine concentrations appear to have the greatest impact on BMP_{ex} in Figure 6.7, the R^2 values remain low (0.38 and 0.34, respectively), signifying a weak correlation. The chemical composition of HTC process waters are a complex mixture of organic and inorganic constituents. Therefore, influence of process water composition on the biomethane yields generated is likely to be associated with a combination of biochemical factors which promote or inhibit biomethane generation, rather than one single factor, as shown in Figure 6.7. These factors are not likely to have additive effects; but have combined synergistic or antagonistic effects.

6.4.1.2 Theoretical Biomethane Potential

The BMP_{th} of process waters can be assumed using the theoretical biomethane yield of 1g COD: 350mL of biomethane, under standard conditions [97]. Therefore, the BI can be calculated by dividing the BMP_{ex} values (mL CH_4/g COD) by 350 (mL CH_4/g COD). Figure 6.8 displays the BI of each process water determined using this method. SL, FS, WH and GR process waters generated at 150°C had the highest BIs of between 60-63%.

Alternatively, BMP_{th} can be calculated stoichiometrically, using the Boyle's equation, as reported in previous studies [80,170]. However, Chapter 5 highlighted the potential difficulties in calculating the CHNS-O concentration of process waters, due to losses of volatile organics during the drying process and losses of volatile inorganics during ashing. Table 6.6 displays the BMP_{th} of each process water, calculated by applying the re-calculated CHNS-O values to the Boyle's Equation. The Boyle's Equation predicts the BMP_{th} using a unit of mL CH_4/g VS. Therefore, in order to determine the BI of the process waters the theoretical biomethane yield must be converted to the same unit used to determined BMP_{ex} (mL CH_4/g COD). This was achieved by multiplying the BMP_{th} obtained from the Boyle's Equation by the VS:COD ratio of the process waters, also shown in Table 6.6.

A general trend which is observed in Table 6.6 is the process waters generated at 150°C display a higher BI compared to those produced at 200°C or 250°C. This is observed across SL, FS, WH and GR process waters, with the exception of LD. Although, this method of determining BMP_{th} is assumed to be associated with error. This is reflected in the BI values of SL150 and SL250 being >100%; which is theoretically impossible, as biomethane yields are determined stoichiometrically. In addition, the BMP_{th} of WH200 is unusually high, due to a negative O-content (-14.0%), which was calculated whilst attempting to adjust the CHNS-O values to account for evaporative organic and inorganic losses. Therefore, currently, this method of determining the BI of process waters is unsuitable, due to the associated errors of accounting for volatile losses during drying and ashing. An alternative method to determine the CHNS-O content of process waters would be through direct liquid injection into an elemental analyser. Unfortunately this technique was unavailable during this time of laboratory work.

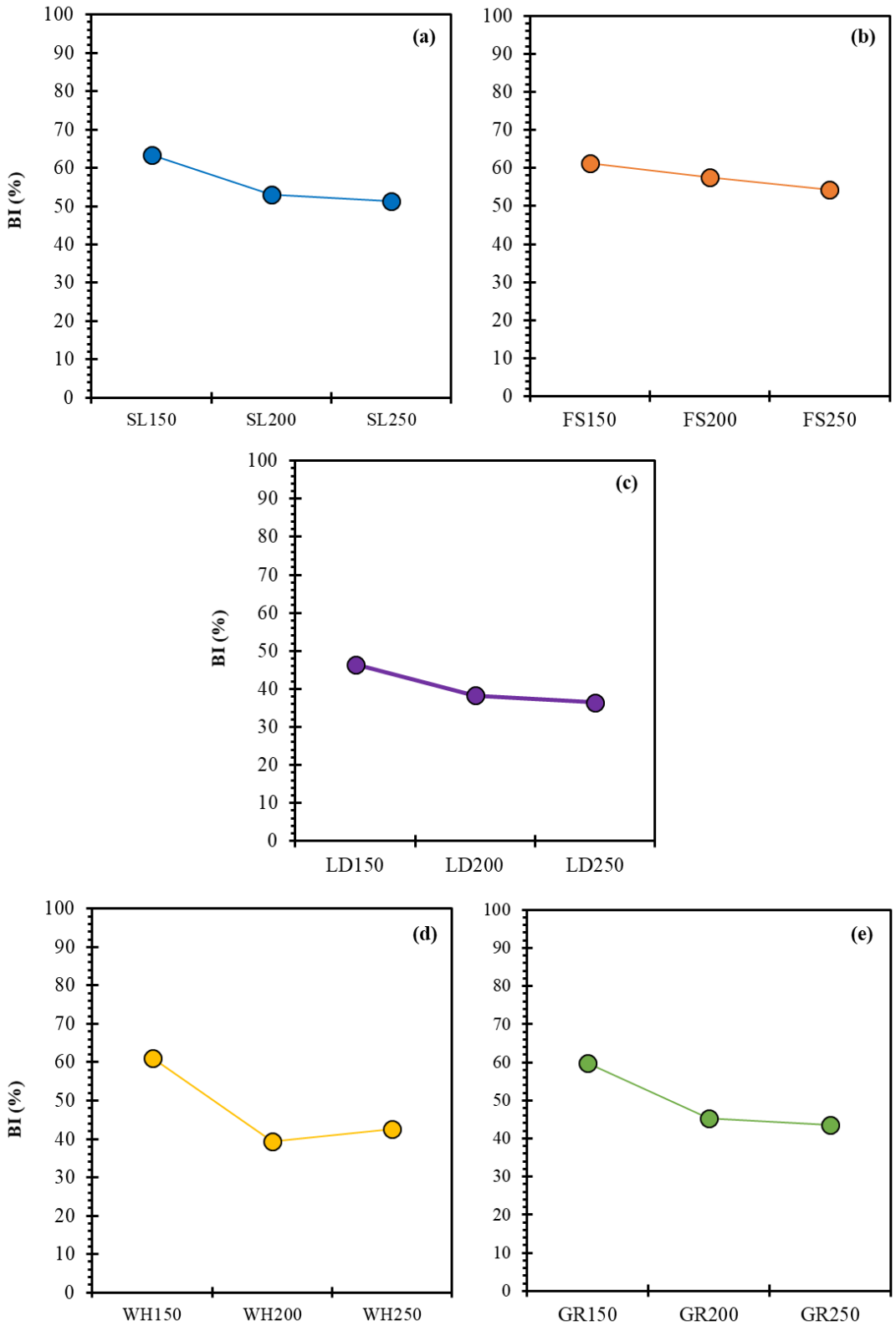

Figure 6.8. Biodegradabilities of HTC process waters from (a) SL, (b) FS, (c) LD, (d) WH and (e) GR.

Table 6.6. Theoretical biomethane potential and calculated biodegradabilities of HTC process waters.

Sample	BMP_{th} (mL CH_4/ g VS)	VS:COD	BMP_{th} (mL CH_4/ g COD)	BMP_{ex} (mL CH_4/ g COD)	BI (%)
SL150	206.9	0.95	196.7	221.9	113
SL200	292.6	0.79	232.5	185.7	80
SL250	231.6	0.73	168.3	179.2	106
FS150	302.7	1.02	307.6	214.5	70
FS200	403.1	0.94	378.7	201.2	53
FS250	270.0	1.19	321.5	190.4	59
LD150	318.4	0.87	278.5	162.4	58
LD200	246.1	0.76	186.3	133.9	72
LD250	475.0	0.67	317.8	127.4	40
WH150	576.6	0.63	363.7	213.4	59
WH200	1157.7	0.70	809.4	137.9	17
WH250	666.0	0.43	228.2	148.8	52
GR150	382.6	0.79	301.2	209.3	69
GR200	610.3	0.63	387.0	158.7	41
GR250	766.3	0.53	407.6	152.4	37

BMP_{th}=theoretical biomethane potential. BMP_{ex}=experimental biomethane potential. BI=biodegradability index. VS=volatile solids. COD=chemical oxygen demand.

6.4.2 Biohydrogen Generation

The following section investigates the comparative production of biohydrogen from the process waters, through dark fermentation (DF). The generation of biohydrogen poses significant advantages over biomethane generation by generating only water as combustion product [205] decarbonising emissions from the energy sector. The metabolic pathways of DF are similar to AD: hydrolysis, acidogenesis and acetogenesis; however, the methanogenesis stage is inhibited to facilitate biohydrogen accumulation [137]. Therefore, there is potential for the solubilised organic metabolites within process water to generate biohydrogen.

6.4.2.1 Method Development

Initially, it was important to establish a method of determining biohydrogen potential (BHP_{ex}). The inoculum used in the BHP_{ex} experiments originated from Esholt WWTP; the same source used to conduct the BMP_{ex} experiments. Therefore, an inoculum pre-treatment step was required to deactivate methanogens. The effectiveness of a number of pre-treatment methods have been investigated in previous studies, which can be broadly grouped into thermal, pH or chemical [145]. However, there is disagreement across studies as to the most effective inoculum pre-treatment to deactivate methanogens [267,268], with variation between feedstocks suggested [267]. The most widely cited method for the pre-treatment of inoculum to deactivate methanogens appears to be thermal treatment [72,124,144,216,269–272]. Heat shock treatment of the inoculum deactivates hydrogenotrophic microorganisms, in this case methanogens, whilst allowing for the proliferation of spore-forming microorganisms, such as *Clostridia* [145], which are involved in the metabolic generation of biohydrogen [138]. However, the conditions used to heat-treat inoculum varies between studies; (90°C, 30 min), [270]; un-specified, [144,271]; (104°C, 24 hours), [72,124,216,272]. Yang and Wang [267] found a thermal treatment of (100°C, 15 min) was sufficient to ensure only biohydrogen and carbon dioxide were detected during the DF of ryegrass; with no detectable biomethane. Therefore, in this study, a thermal pre-treatment of 115°C, 30 min was selected.

The operation of DF can be sensitive to pH, with an acidic pH<4 causing microbial inhibition and an alkaline pH>7 favouring propionate generation [205]; associated with hydrogen consumption [138]. Optimal pH ranges of between 5-6 have been suggested [138,205]. Therefore, in order obtain the optimal starting pH for this study, the BHP_{ex} of glucose were compared after adjusting the starting pH of the bioreactors to pH 5, pH 6 and pH 7.

The biohydrogen yields obtained from glucose, following pH adjustment to pH 5, pH 6 and pH 7 are displayed in Figure 6.9, with final BHP_{ex} yields reported in Table 6.7. Final biohydrogen yields were similar, although the glucose adjusted to pH 6 gave a slightly higher BHP_{ex} (224.5 mL H_2/g VS), compared to pH 5 (212.5 mL H_2/g VS) and pH 7 (197.9 mL H_2/g VS). This is equivalent to 1.71 mol H_2/mol glucose (pH 5), 1.80 mol H_2/mol glucose (pH 6) and 1.60 mol H_2/mol (pH 7). The biohydrogen yields shown in Figure 6.9 are below the theoretical yields obtained from the metabolism of glucose into acetate (4 mol H_2/mol) or butyrate (2 mol H_2/mol) [138]. Although, these stoichiometric yields are unlikely to be achieved in an experimental system due to the energy considerations of microbial growth [138] and propionate production or hydrogen consumption by homoacetogens [137]. Biohydrogen yields in literature typically range from 0.48-2.3 mol H_2/mol glucose [273] using a mixed culture system. Higher yields can be achieved using monocultures [205], although

operational costs would increase with scale-up due to contamination issues. Yin *et al*. [268] found a biohydrogen yield of 1.39 mol H_2/mol glucose, using heat-treated anaerobic sludge as inoculum. Although, irradiation inoculum pre-treatment yielded a higher biohydrogen yield (2.15 mol H_2/mol glucose) [268]. Therefore, overall the values obtained from Figure 6.9 appear to align with literature values.

Further to biohydrogen yield, the adjustment of pH appears to influence digestion kinetics. Table 6.7 presents the kinetics of each BHP_{ex} curves shown in Figure 6.9. Kinetics are described using the modified Gompertz Model [229], peak fermentation time (T_m) [44] and technical digestion time (T^{80}) [226].

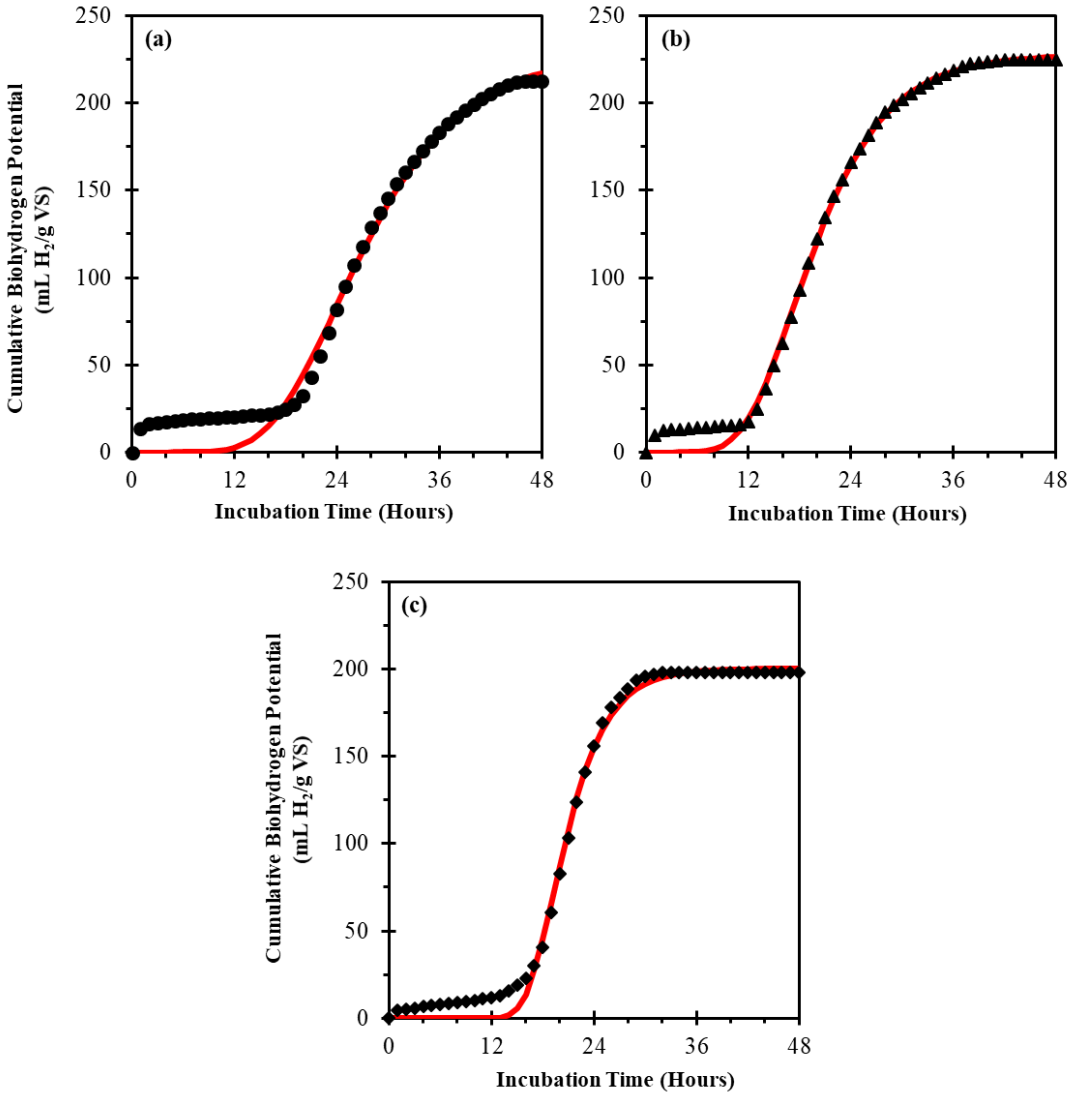

Figure 6.9. Experimental biohydrogen potential (BHP_{ex}) yields of glucose adjusted to (a) pH 5, (b) pH 6 and (c) pH 7. The red line indicates the modified Gompertz model fit.

Table 6.7. Digestion kinetics from the dark fermentation of glucose.

Glucose Sample	BHP_{ex} mL H_2/g VS	Modified Gompertz Model				T_m (h)	T^{80} (h)
		H_m mL H_2/g VS	R_m mL H_2/g VS/h	λ (h)	R^2		
pH 5	212.5	228.4	10.5	16.0	0.96	24.0	27
pH 6	224.5	227.6	14.1	14.4	0.99	17.3	24
pH 7	197.9	200.2	21.6	16.0	0.99	19.4	25

BHP_{ex}=experimental biohydrogen potential. H_m=maximum biohydrogen yield. R_m=peak biohydrogen production rate. λ=lag phase. T_m=peak time of fermentation. T^{80}=technical digestion time.

Adjustment to pH 6 provides the most favourable digestion kinetics; displaying the shortest lag period (λ), as well as the fastest peak fermentation time (T_m) and technical digestion time (T^{80}). Adjustment to pH 7 gave a more rapid peak biohydrogen production rate (R_m) compared to glucose at pH 6. However, this is compromised by the lower overall BHP_{ex} yield. Overall, Figure 6.9 and Table 6.7 suggest that adjusting the reaction medium to pH 6 provided the optimal BHP_{ex} yields and digestion kinetics, compared to pH 5 and pH 7. Therefore, any further BHP_{ex} experiments discussed throughout this thesis adjusted the reaction medium to pH 6 before beginning the experiment.

The AMPTS II measures the volume of accumulated biogas through calibrated (c. 10mL) flow cells, according to the principle of liquid displacement and buoyancy. However, the composition of biogas is not measured. Multiple studies have previously used the AMPTS II to determine biohydrogen yields of a range of substrates [72,124,144,216,269–272]. However, the inoculum pre-treatment methodology varies between studies. Therefore, further evidence was required to confirm the inoculum pre-treatment used in this study was sufficient to deactivate methanogens and therefore, result in the generation of biohydrogen as opposed to biomethane.

The generation of biohydrogen was confirmed using sodium acetate to identify any residual methanogenic activity [269]. Biohydrogen generation originates from the metabolism pyruvate into acetic and butyric acids [138]. Therefore, acetate can be considered a metabolic end-point for biohydrogen production; with no further biohydrogen generation expected. Conversely, methanogens can further metabolise acetate into biomethane via the acetoclastic methanogenesis pathway. Therefore, generation of biogas from sodium acetate would indicate the remaining presence of active methanogens.

Figure 6.10 shows negligible biohydrogen yields (c. 3 mL H_2/g VS) from sodium acetate, using heat-treated inoculum. Negligible biohydrogen yields continued throughout the 12-day experiment. Figure 6.11 shows the biomethane yield of sodium acetate, once methanogen-containing inoculum was added to the effluent from DF. The BMP_{ex} yields of sodium acetate reached 623.2 mL CH_4/g VS after 10-days of digestion; highlighting the use of sodium acetate to identify residual methanogen activity. The high BHP_{ex} yields of glucose (197.9-224.5 mL H_2/g VS) shown in Figure 6.9, coupled with the negligible BHP_{ex} yields of sodium acetate (Figure 6.10) suggests the inoculum pre-treatment is sufficient to remove methanogens, whilst maintaining an active population of hydrogen-producing bacteria.

After establishing the optimal experimental conditions for determining the BHP_{ex} of glucose (Figure 6.9), a similar experiment was conducted for more complex carbohydrates: cellulose and starch, as shown in Figure 6.10. The incubation time use to digest the complex carbohydrates was significantly longer than the incubation time required for glucose. Additionally, the biohydrogen generation from starch appears to remain in the exponential generation phase; therefore, the experiment should have been conducted for a longer duration. Despite this, after a 12-day incubation period, both glucose and starch showed much lower BHP_{ex} yields than glucose after a 2-day incubation period. The BHP_{ex} yields of cellulose and starch were 25.4 mL H_2/g VS and 32.5 mL H_2/g VS, respectively. Therefore, indicating reduced biohydrogen yields for complex substrates, potentially due to limited hydrolysis. Guo *et al.* [137] found 89% of the variability of biohydrogen production of feedstocks linked to the carbohydrate content of the feedstock. Therefore, perhaps pre-treatment methods are required to liberate the soluble carbohydrate fraction from complex carbohydrates; improving biohydrogen yields.

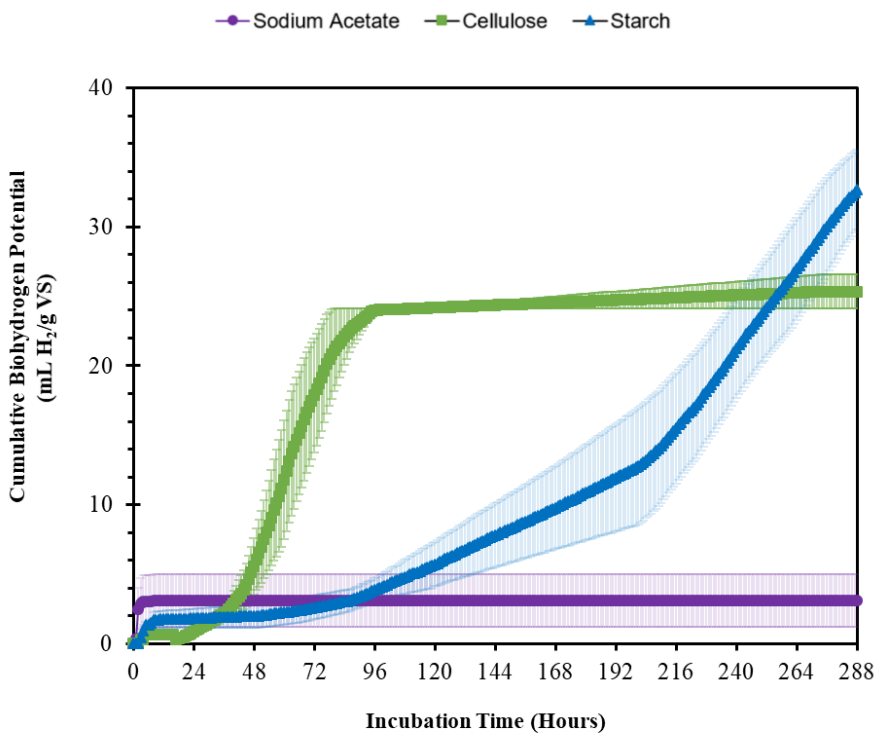

Figure 6.10. Experimental biohydrogen potential (BHP_{ex}) of sodium acetate, cellulose and starch. Data is presented as average values. Error bars represent the standard error (n=3).

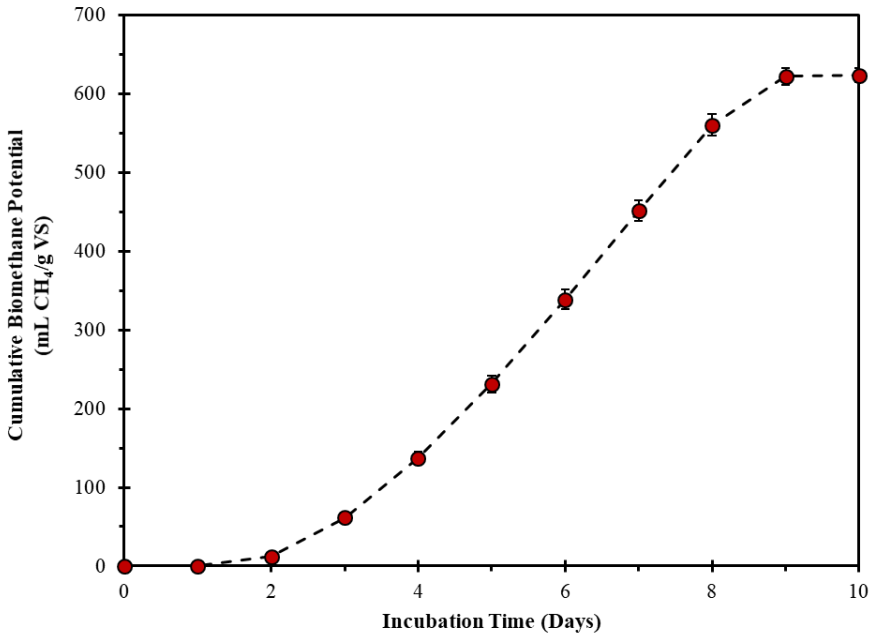

Figure 6.11. Experimental biomethane potential (BMP_{ex}) of sodium acetate. Data is presented as average values. Error bars represent the maximum and minimum values (n=2).

6.4.2.2 HTC Process Waters

Figure 6.12 displays the biohydrogen yields for the process waters generated from SL, FS, LD and WH. In addition, Table 6.8 describes the final BHP_{ex} yields and the digestion kinetics of the BHP_{ex} curves. Unfortunately, due to limited sample and time constraints, the BHP_{ex} of GR-derived process waters was unable to be determined.

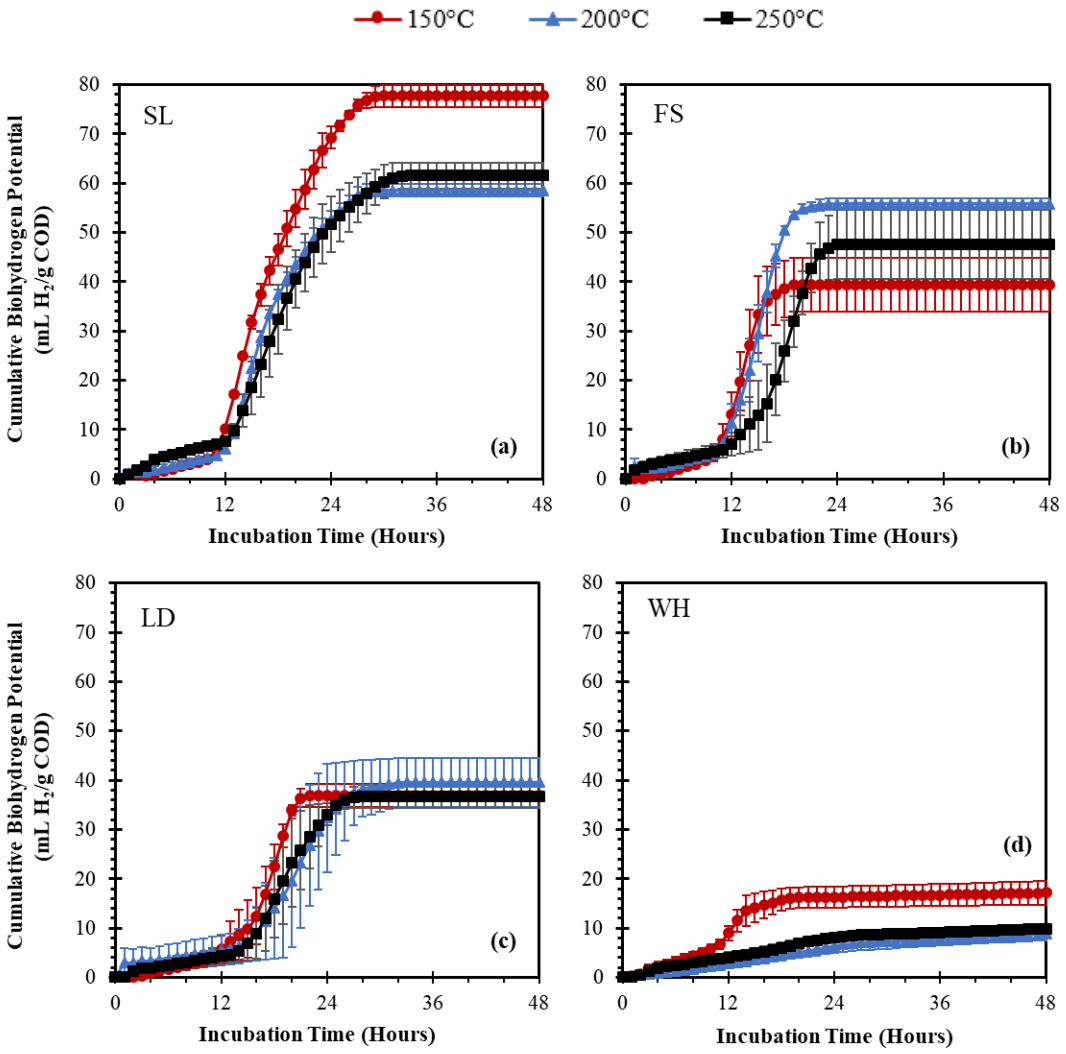

Figure 6.12. Experimental biohydrogen potential (BHP_{ex}) of HTC process waters from (a) SL, (b) FS, (c) LD and (d) WH. Data is presented as average values. Error bars represent the standard error (n=3).

Table 6.8. Digestion kinetics from the dark fermentation of HTC process waters.

Sample	BHP_{ex} mL H_2/g COD	Modified Gompertz Model				T_m (h)	T^{80} (h)
		H_m mL H_2/g COD	R_m mL H_2/g COD /h	λ (d)	R^2		
SL150	77.7	78.6	6.4	10.4	0.99	14.9	22
SL200	58.6	59.0	5.4	11.0	0.99	15.0	22
SL250	61.6	62.7	4.5	10.5	0.99	15.7	23
FS150	39.4	39.6	7.3	10.0	0.99	12.0	15
FS200	55.8	56.2	8.2	10.9	0.99	13.4	17
FS250	47.5	48.3	5.3	12.3	0.99	15.7	21
LD150	36.9	37.4	4.8	12.6	0.99	15.5	20
LD200	39.5	40.6	3.1	12.8	0.99	17.6	24
LD250	36.8	37.4	3.6	13.2	0.99	17.0	23
WH150	17.1	17.0	1.5	4.9	0.99	9.2	14
WH200	8.9	9.0	0.3	2.9	0.99	13.7	23
WH250	9.9	10.0	0.4	0.8	0.99	10.6	21

BHP_{ex}=experimental biohydrogen potential. H_m=maximum biohydrogen yield. R_m=peak biohydrogen production rate. λ=lag phase. T_m=peak time of fermentation. T^{80}=technical digestion time.

Figure 6.12a shows SL-derived process waters generated the highest BHP_{ex} yields compared to all other process waters from FS, LD and WH. The recorded biohydrogen yields were 77.7 mL H_2/g COD (SL150), 58.6 mL H_2/g COD (SL200) and 61.6 mL H_2/g COD (SL250). Therefore, the process water generated at the lowest HTC temperature (150°C) generated the highest BHP_{ex} yields; a similar trend to BMP_{ex} yields. This is likely due to a higher sugar concentration [72]. Table 6.8 shows the digestion kinetics of SL-derived process waters were broadly similar.

FS-derived process waters display different behaviours to SL process waters. Figure 6.12b shows FS150 generated the least biohydrogen (39.4 mL H_2/g COD); whereas FS200 displayed the highest yields (55.8 mL H_2/g COD). Although, the error bars associated with Figure 6.12b are large; indicating there was no significant differences between the biohydrogen yields of FS-process waters generated at different temperatures. The large error

bars indicate a potential limitation with the methodology of determining BHP_{ex}. The flow cells of the AMPTS II have a calibrated volume of approximately 10mL and only record gas accumulation once the gas occupies the volume of the flow cell, causing it to tip upwards in water. The biohydrogen yields being registered in Figure 6.12 are much lower than the biomethane yields registered in Figure 6.5; which is the primary function of the AMPTS II. Therefore, in order to improve the accuracy of the AMPTS II for determining biohydrogen production, flow cells with smaller volume sizes are required.

LD-derived process waters all generated similar levels of biohydrogen: 36.9 mL H_2/g COD (LD150), 39.5 mL H_2/g COD (LD200) and 36.8 mL H_2/g COD (LD250). These yields are all lower than the corresponding SL-derived process waters produced at the same temperature, despite SL and LD both being kelp species. Again, this could be related to LD being harvested in the winter, resulting in a lower initial carbohydrate fraction [61] compared to the summer-harvested SL.

The biohydrogen yield was higher for WH150 (17.1 mL H_2/g COD) than WH200 (8.9 mL H_2/g COD) or WH250 (9.9 mL H_2/g COD) (Figure 6.12d). Although, WH-derived process waters produced the lowest biohydrogen yields of all of the process waters in Figure 6.12. This could be linked to the higher total phenol content of the process waters, as phenols have been shown to exhibit stronger inhibitions over DF than AD [204].

Overall, it is observed that the yields of biohydrogen from HTC process waters are lower than the yields of biomethane which can be obtained. Therefore, indicating AD is a more favourable valorisation technology for process waters, compared to DF.

6.5 Energetic Balance

The overall aim of this chapter was to assess different conversion routes of the separated products from HTC. This included the comparative utilisation of hydrochar as a solid combustion fuel, or as a feedstock for AD. The generation of biomethane and biohydrogen from the process waters was also compared. In this section the energy output of each conversion route is assessed and compared, in order to determine the most energetically feasible applications for the separated hydrothermal products.

The energy output of each conversion route is calculated based on a starting material of 1-kg of oven dried biomass. To clarify, in this context, ‘oven dried biomass’ refers to the biomass once it has undergone preservation by oven drying, freeze drying or air drying. Therefore, moisture has not been completely eliminated and remains between 5.1-7.6%; as shown by the

proximate analysis in Chapter 5. The calculations subsequently account for the changing mass yield distributions across each of the three HTC processing temperatures.

6.5.1 Hydrochar Conversion Routes

The calculated energy outputs for the combustion of hydrochars, compared to the AD of hydrochars are displayed in Table 6.9. The energy outputs based on the AD of the untreated biomass are also shown, to ease comparison. Combustion of the untreated biomass feedstocks are not considered, due to inherent high moisture contents and unfavourable inorganic compositions.

Table 6.9. Comparative energy output generated from the combustion or anaerobic digestion of hydrochars. Based off a starting material of 1-kg oven dried biomass.

Sample	Energy Output from Combustion (MJ/kg dried biomass)	Energy Output from AD (MJ/kg dried biomass)
SL	-	6.53
SL150	5.58	2.35
SL200	4.53	1.55
SL250	4.22	0.20
FS	-	4.12
FS150	7.19	2.33
FS200	6.29	1.40
FS250	5.85	0.77
LD	-	5.46
LD150	5.61	-
LD200	4.85	-
LD250	4.02	-
WH	-	3.02
WH150	10.23	4.59
WH200	9.11	3.33
WH250	7.83	0.51
GR	-	8.76
GR150	11.55	5.22
GR200	10.85	3.10
GR250	9.01	0.65

A reduced energy output was observed with increased HTC temperature for both hydrochar combustion and AD conversion routes. The hydrochar yield and biodegradability both decrease with increasing HTC temperature, as shown by Chapter 5 and Figure 6.5, respectively. Therefore, explaining the reduced energy output from the AD of hydrochars

generated at higher HTC temperatures. Similar conclusions were determined from the digestion of coffee-ground-derived hydrochars [161]. The energy output obtained from the combustion of hydrochars also decreased from hydrochars generated at higher temperatures, despite an increased energy densification and HHV. However, decreased hydrochar yields at higher HTC processing temperatures reduced the energy yield of the hydrochar and the overall energy output obtained.

The energy output obtained from the combustion of the hydrochars was consistently higher than the corresponding energy output obtained from the AD of hydrochars, across all samples presented in Table 6.9. WH150 and WH200 were the only hydrochar samples to show an improvement in energy output compared to the parent biomass, when treated by AD. WH150 and WH200 displayed an improvement in energy output of 52% and 10%, respectively, compared to the parent biomass (WH). Whereas, AD of WH250 demonstrated an 83% reduction in energy output compared to WH. Although, combustion of WH150 and WH200 produced over double the corresponding energy output from AD. All additional hydrochars presented in Table 6.9 showed a reduced energy output, compared to their parent biomass when converted using AD.

Consequently, mono-digestion of hydrochars through AD does not appear a suitable valorisation strategy to maximise the energy recovery from hydrochars. Especially once the energy input required for the HTC reactions is considered. In addition, this HTC-AD integration strategy would require an alternative application for the HTC process water such as re-circulation into AD [179,264] or as a nutrient-rich fertiliser [262]. Recent research has focussed on the use of hydrochar as an additive to AD, rather than use as a mono-digestion feedstock [166–168,195,197,198,274]. Hydrochar additives can improve the digestion kinetics and yields by improving direct interspecies electron transfer (DIET) between microbial communities [195]. Although, a recent study has shown hydrochar addition to be inhibitory to AD, compared to biochar addition, due to their acidic nature and presence of inhibitory compounds [198].

The combustion of hydrochars generated a higher energy output compared to AD; suggesting combustion is a more suitable valorisation route to maximise the energy recovery from hydrochars. The energy output obtained from lignocellulosic-derived hydrochars is higher than that recovered from macroalgal-derived hydrochars; due to greater hydrochar yields (Chapter 5), leading to greater EYs. Combustion of WH-derived hydrochar improved the energy output by 239% (WH150), 201% (WH200) and 159% (WH250) compared to the energy obtained from AD of WH. Combustion of GR-derived hydrochar improved the energy output by 32% (GR150), 24% (GR200) and 3% (GR250) compared to the energy obtained from AD of GR. WH displays a greater energy improvement compared to GR as the energy

output from the AD of untreated-WH (3.02 MJ/kg) was lower than untreated-GR (8.76 MJ/kg). Combustion of FS-derived hydrochars produced the greatest energy output, compared to SL and LD-derived hydrochars. Combustion of FS150, FS200 and FS250 corresponds to a respective 74%, 53% and 42% increase in energy output, compared to AD of untreated-FS. Alternatively, combustion of SL150, SL200, SL250, LD200 and LD250 is associated with a reduction in energy output, compared to AD of untreated-SL or untreated-LD. This could be a result of the untreated kelp seaweed species displaying the highest initial ECE; therefore, meaning it could be the most difficult to improve.

6.5.2 Process Water Conversion Routes

The energy recovery efficiency of the feedstocks can be further improved though separate biological conversion of the process waters. Therefore, creating separate energy vectors from the HTC products, to maximise the obtainable energy from each biomass. Table 6.10 compares the calculated energy outputs from the HTC process waters treated by AD and DF, based on a starting material of 1-kg oven dried biomass.

Table 6.10. Comparative energy output generated from the anaerobic digestion or dark fermentation of process waters. Based off a starting material of 1-kg oven dried biomass.

Sample	Energy Output from AD (MJ/kg dried biomass)	Energy Output from DF (MJ/kg dried biomass)
SL150	3.62	0.40
SL200	3.36	0.34
SL250	3.05	0.33
FS150	3.68	0.22
FS200	3.12	0.28
FS250	2.80	0.22
LD150	2.40	0.17
LD200	2.05	0.19
LD250	1.86	0.17
WH150	1.50	0.04
WH200	1.44	0.03
WH250	1.80	0.04
GR150	2.93	-
GR200	2.14	-
GR250	2.15	-

The conversion of the process waters through AD consistently provided a higher energy output compared to conversion through DF. The volumes of biomethane generated during AD (Figure 6.5) were higher than the equivalent volumes of biohydrogen generated (Figure 6.12). This, coupled with the higher HHV of methane (39.8 MJ/m^3) compared with hydrogen (12.7 MJ/m^3) is the reason for a higher energy output from the AD of process waters. Previously, Smith and Ross [80] concluded DF yielded a greater energy output than AD for seaweed-derived HTC process waters. However, this was based on theoretical, stoichiometric predictions of biomethane and biohydrogen yields; highlighting the complexities of predicting biodegradability during experimental digestions.

Table 6.10 shows the energy output from AD of seaweed-derived and GR-derived HTC process waters decreased with increasing HTC processing temperature. Decreased energy output is likely because of the reduced BMP_{ex} yields for higher-temperature HTC process waters (Figure 6.6). However, the energy output of WH250 (1.80 MJ/kg) is greater than WH150 (1.50 MJ/kg), despite showing reduced BMP_{ex} yields. This is as a result of the increasing COD concentration of higher temperature WH-derived process waters. Whereas, the COD concentrations of seaweed and GR-derived process waters remain relatively similar.

Smith and Ross [80] predicted the theoretical energy output obtained from the AD of HTC process waters produced from *A. esculenta*, *L. digitata* and *L. hyperborea*; the latter across a range of seasons. Across all the process waters analysed, the average energy output predicted by [80] was 4.4 MJ/kg and 4.5 MJ/kg for HTC processing temperatures of 200°C and 250°C, respectively. The calculations conducted by Smith and Ross [80] were based on a starting point of 1-kg of seaweed undergoing HTC at an approximate solid loading ratio of 10%; therefore, the results should be comparable to Table 6.10. The theoretical energy output predictions obtained by [80] are higher than the values obtained by this study at 200°C: SL200 (3.12 MJ/kg), FS200 (3.12 MJ/kg), LD200 (2.05 MJ/kg), as well as 250°C: SL250 (3.05 MJ/kg), FS250 (2.80 MJ/kg) and LD250 (1.86 MJ/kg). This highlights the nature of theoretical BMP predictions to enhance BMP yields, due to un-predictable biodegradability during experimental digestions. Smith and Ross [80] assumed a biodegradability of 75%; higher than suggested by Figure 6.8. In addition, the change of biodegradability at different HTC temperatures was not accounted for. This highlights an additional limitation with predicting theoretical biomethane yields, as the effects of inhibitory compound formation cannot be predicted.

6.5.3 Integrated Approach

According to the previous sections, the combustion of hydrochar and AD of process waters appears to provide the greatest energy output when separating the products from HTC. However, as the hydrochars and process waters are utilised as separate energy vectors, the energy outputs from both products can be combined for utilisation as an integrated HTC-AD systems approach. Combining the energy outputs obtained from combustion and AD means the overall energy output can be further increased. Figure 6.13a-c displays the energy outputs from the hydrochar combustion and biomethane generation from the process waters, as well as a combined energy output of the two factors. The energy output based on the AD of the untreated biomass is also included on each Figure, for ease of comparison.

The combined energy outputs obtained from both hydrochar combustion and process water digestion were consistently higher than the AD of the parent biomass, across all feedstocks presented in Figure 6.13. The scale of improvement varies across feedstock types, however a common conclusion is the recovered energy output reduces with increasing HTC processing temperature.

The combined energy outputs of SL150, SL200 and SL250 were 9.19 MJ/kg, 7.89 MJ/kg and 7.27 MJ/kg, respectively (Figure 6.13a); corresponding to a 41%, 21% and 12% improvement in energy output, compared to the AD of SL. The ECE of SL was 64%, whereas, an improvement in ECE was observed for SL150 (90%), SL200 (77%) and SL250 (71%). Figure 6.13c suggests the integration of HTC and AD for LD shows similar improvements in ECE compared to SL. The ECEs of LD, LD150, LD200 and LD250 were 59%, 87%, 75% and 64%, respectively. HTC-treated FS (Figure 6.13b) showed a greater improvement in energy output, than SL and LD, when compared to their respective parent feedstocks. The combined energy outputs of FS150, FS200 and FS250 were 10.87 MJ/kg, 9.42 MJ/kg and 8.65 MJ/kg, respectively; corresponding to a 164%, 129% and 110% improvement in energy output, compared to the AD of FS. The ECE of FS was 35%, whereas, an improvement in ECE was observed for FS150 (91%), FS200 (79%) and FS250 (72%). This highlights the significance of inter-species differences, suggesting integration of HTC and AD may be better suited to selected feedstocks.

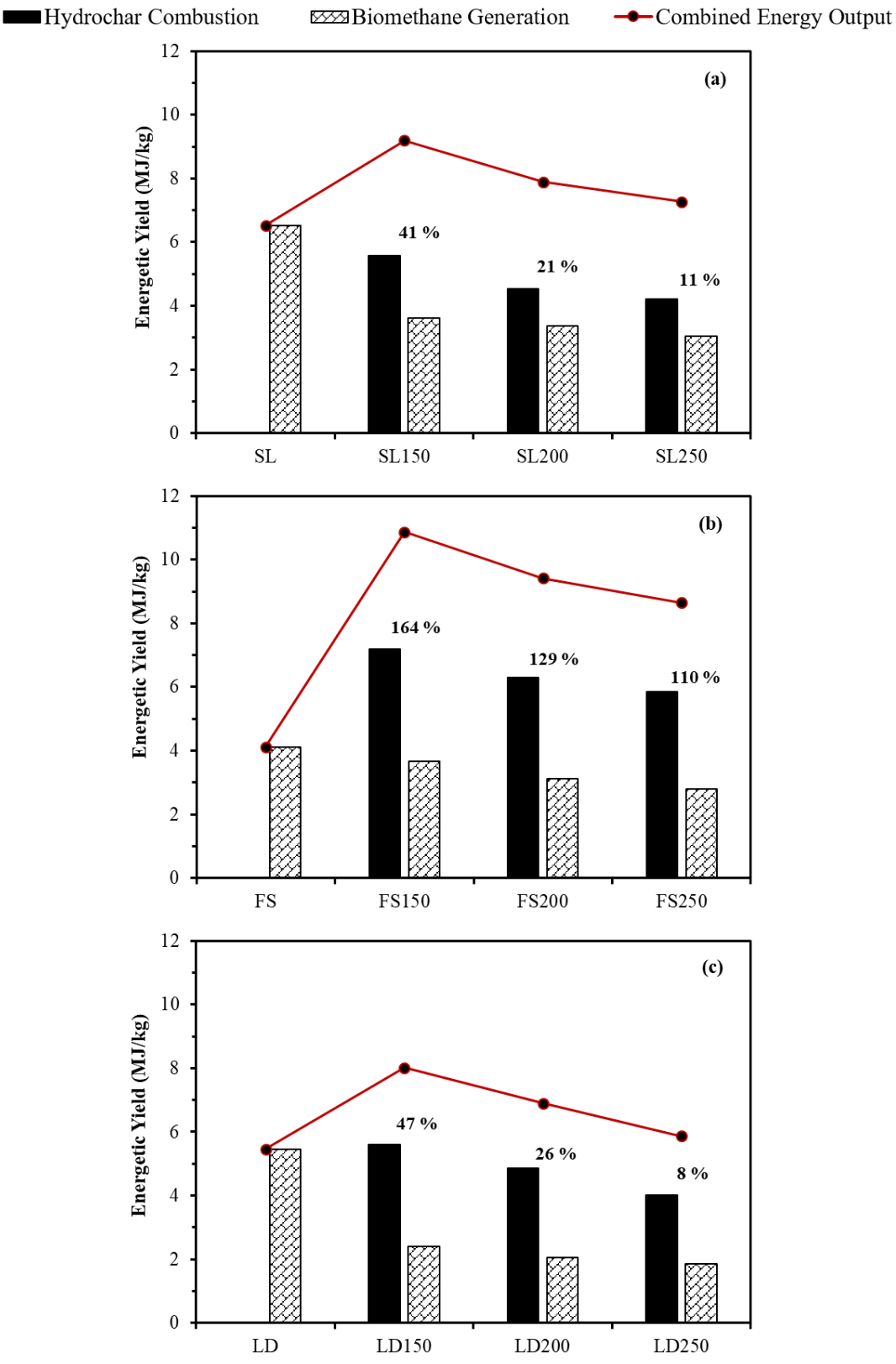
Hydrochar Combustion
Biomethane Generation
Combined Energy Output
(a)
Energetic Yield (MJ/kg)
41 %
21 %
11 %
SL
SL150
SL200
SL250
(b)
Energetic Yield (MJ/kg)
164 %
129 %
110 %
FS
FS150
FS200
FS250
(c)
Energetic Yield (MJ/kg)
47 %
26 %
8 %
LD
LD150
LD200
LD250

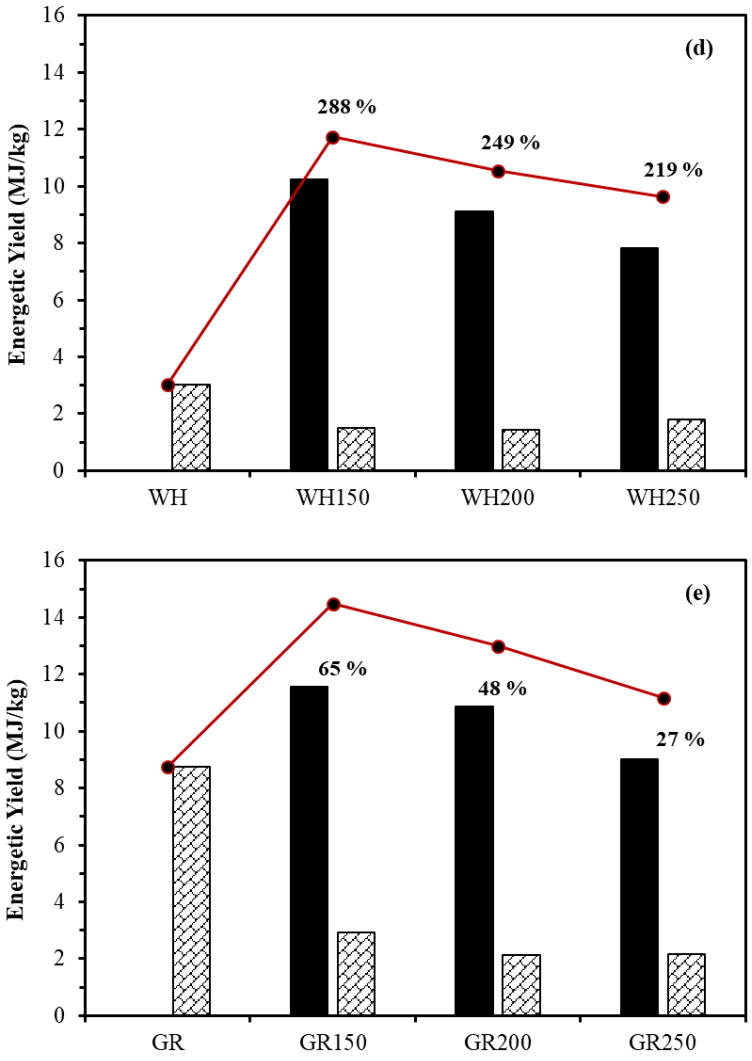

Figure 6.13. Energetic output from hydrochar combustion, anaerobic digestion of process waters and a combined energy output for (a) SL, (b) FS, (c) LD, (d) WH and (e) GR. Calculated based on a starting material of 1-kg oven dried biomass. The percentages above the bars represent the increase in total energy output compared to the anaerobic digestion of the untreated biomass.

The greatest improvement in energy output is observed in hydrothermally-treated WH; Figure 6.13d. The combined energy outputs of WH150, WH200 and WH250 were 11.73 MJ/kg, 10.54 MJ/kg and 9.63 MJ/kg, respectively; corresponding to a 288%, 249% and 219% improvement in energy output, compared to the AD of WH. This represents an improvement in ECE, from 25% (WH) to: 97% (WH150), 87% (WH200) and 79% (WH250). Integrating HTC and AD also improved the energy output of GR, shown in Figure 6.13e. The combined energy outputs of GR150, GR200 and GR250 were 14.48 MJ/kg, 12.99 MJ/kg and 11.16 MJ/kg, respectively; corresponding to an 65%, 48% and 27% improvement in energy output, compared to the AD of GR. This represents an improvement in ECE, from 50% (GR) to: 82% (GR150), 74% (GR200) and 63% (GR250). Therefore, the greatest improvements in energy output are observed in FS and WH; the feedstocks which yielded the lowest biomethane yields

from the untreated biomass. Although, the integration of HTC and AD showed improvements in the ECE of all feedstocks tested in this study.

Separation of hydrochars for combustion and process waters for AD has been investigated for sewage sludge digestate [170], microalgae [160], cow manure [84] and the organic fraction of municipal solid waste [209]. Each study found an improved energetic return using this HTC-AD integration strategy, compared to AD of the parent feedstock. Generally, a lower HTC processing temperature yielded a greater energy output, similar to this study.

One of the major differences between macroalgal and lignocellulosic biomass in Figure 6.13 is the distribution of the energy output obtained from either the hydrochars or process waters. The energy obtained from seaweed-derived process waters represented a higher proportion of the combined energy output, compared to lignocellulosic-derived process waters. The energy from process waters represented 39-42%, 32-34% and 30-32% of the combined energy output of hydrothermally treated SL, FS and LD, respectively. Whereas, WH process waters represented between 13-19% of the overall energy balance; whilst GR process waters represented between 16-20%. This is linked to a greater carbon distribution to seaweed HTC process waters, compared to lignocellulosic HTC process waters (Chapter 5). The hydrochar represents a greater energy carrier across all samples in Figure 6.13; demonstrating the energy densification properties of hydrochars.

Figure 6.13 demonstrates the potential for integrating HTC and AD to improve the energy conversion efficiency of feedstocks. However, in order to be an energetically-feasible process, the energy input required to heat the HTC reactor must be less than the obtainable energy output. Table 6.11 displays the energy balance of integrating HTC and AD. Energy input is determined as the energy required to heat the contents of the HTC reactor; based on a starting point of 1-kg oven dried biomass. Whereas, the energy output is determined as the combined energy output, derived from Figure 6.13.

Sensibly, the energy input increased as the HTC processing temperature increased. The energy input values are slightly lower for WH, compared to the other biomass types, because a larger HTC reactor was used with a slightly different solid loading ratio. However, energy returned upon energy invested (EROI) values are directly comparable.

The EROIs presented in Table 6.11 are displayed as two values; no assumed energy recovery efficiency and 55% energy recovery efficiency. Previous studies have assumed an 85% energy recovery efficiency for the HTC process [234]. However, in this study a more conservative assumption of 55% energy recovery efficiency was used.

Table 6.11. Energy balance for the integration of HTC and AD, by hydrochar combustion and process water AD.

Biomass	HTC Processing Temperature (°C)	Energy Input (MJ/kg dried[1] biomass)	Energy Output (MJ/kg dried[1] biomass)	EROI	EROI[2]
SL	150	5.44	9.19	1.69	3.75
	200	7.61	7.89	1.04	2.31
	250	9.79	7.27	0.74	1.65
FS	150	5.44	10.87	2.00	4.44
	200	7.61	9.42	1.24	2.75
	250	9.79	8.65	0.88	1.96
LD	150	5.44	8.01	1.47	3.27
	200	7.61	6.89	0.91	2.01
	250	9.79	5.87	0.60	1.33
WH	150	4.99	11.73	2.36	5.22
	200	6.99	10.54	1.51	3.35
	250	8.99	9.63	1.07	2.38
GR	150	5.44	14.48	2.66	5.92
	200	7.61	12.99	1.71	3.79
	250	9.79	11.16	1.14	2.53

[1]oven dried biomass. [2]55% assumed energy recovery efficiency. EROI=energy returned upon energy invested.

Across all biomass types, the EROI decreased as HTC processing temperature increased. This is due to a combination of increased energy input and a reduced energy output. Therefore, HTC treatment at 150°C provides the most energetically feasible HTC and AD integration option. Lignocellulosic biomass obtain a higher EROI than macroalgal biomass. When no energy recovery is assumed, the EROIs of SL250, FS250, LD200 and LD250 are all <1; suggesting energetically un-feasible integration routes. However, once 55% energy recovery efficiency is assumed, all the HTC and AD integration options presented in Table 6.11 become energy positive (EROI>1).

Further to use as a combustion fuel, hydrochar has a multitude of alternative applications, including: soil amendment, sorbent, carbon sequestration and use as a capacitor [146,154]. However, such applications negate the energetic value associated with the combustion of hydrochars. Therefore, the recovered energy would originate from the HTC process waters. Assuming a 55% energy recovery efficiency, the energy input for the HTC of SL, FS, LD and GR would be 2.45 MJ/kg, 3.42 MJ/kg and 4.41 MJ/kg at temperatures of 150°C, 200°C and

250°C, respectively. Whereas, the energy input for WH HTC would be 2.25 MJ/kg (150°C), 3.15 MJ/kg (200°C) and 4.05 MJ/kg (250°C). Therefore, the energy output obtained from the WH-process waters would not be sufficient to balance the energy input of HTC. Alternatively, lower temperature process waters: SL150, FS150, LD150 and GR150 generate a sufficient energy output to balance the energy input of the HTC reaction. Although, higher temperature process waters (200°C and 250°C) would require an external source of energy to heat the HTC reactor, should the hydrochar be utilised for an alternative application.

However, the calculations presented within this section are based on an approximate SLR of 10%. Increased solid loading ratios would can improve the energetics of the process, with Parmar and Ross [171] conducting HTC of a range of digestates up to a 30% SLR. Higher SLRs would provide a greater mass of hydrochar, improving energy output. Additionally, the specific heat capacity of water (4200 J/kg/K) [72] is higher than biomass (1455 J/kg/K) [177]. Therefore, displacing water with biomass will, in turn require less energy to heat the HTC reactor contents. Although, inherent biomass properties may instil limitations on the solid loading ratio which can be used. For example, the hydrochar and process water generated by WH treated at 150°C could not be separated through Bücher filtration, due to the 'sponge-like' properties of WH. Therefore, increasing the solid loading ratio further would create complications associated with material handling.

6.6 Conclusions

The separation of hydrothermal-products: hydrochar and process waters allows for the generation of bioenergy as separate energy vectors. This chapter involved the comparison of different conversion routes for both hydrochars: combustion or AD, and process waters: AD or DF, in order to maximise the energy recovery efficiency of the selected macroalgal and lignocellulosic feedstocks.

HTC has the potential to improve the behaviour of hydrochars during combustion by altering the ash chemistry to reduce the likelihood of slagging and fouling. Predictive slagging and fouling indices suggested no real improvements in the ash behaviour of hydrochars. However, ash fusion tests revealed hydrochars derived from SL, FS, LD and GR displayed a reduced slagging propensity compared to the parent biomass. Generally, hydrochars generated at higher temperatures (250°C) showed the greatest improvements, due to more efficient removal of problematic alkali metals. Although, WH-derived hydrochars displayed no improvement in slagging propensity. Therefore, alternative applications for WH-derived hydrochars can be considered, such as: small-scale combustion, soil amendment or low-cost sorbents.

The generation of biomethane from hydrochars is possible, although the biodegradability is typically lower than the untreated feedstock; with the exception of WH150 and WH200. Hydrochars produced at 250°C have low biodegradabilities (4-12%), due to an increased aromatic structure, which is recalcitrant to microbial degradation. From an energetic perspective the combustion of hydrochars yields a greater energy output compared to the AD of hydrochars.

HTC process waters have the capacity to generate biomethane through AD, or biohydrogen through DF. However, the obtainable yields of biomethane are much higher than the obtainable yields of biohydrogen. Therefore, the conversion of process waters through AD appears a more suitable valorisation route, compared to DF. Overall, lower temperature process waters (150°C) have an increased biodegradability, compared to higher-temperature process waters (200°C and 250°C). This is due to the increased concentrations of inhibitory compounds at higher temperatures, such as phenols. Lignocellulosic-derived process waters experience a greater reduction in biodegradability at higher processing temperatures (200°C and 250°C), compared to macroalgal-derived process waters.

Integration of HTC and AD through the combustion of hydrochars and AD of process waters provides the most energetically feasible valorisation strategy. Although, higher HTC processing temperatures results in a reduced energy recovery; generally due to lower hydrochar yields and the reduced biodegradability of process waters. Hydrochars represent the greatest energy carrier; although process waters contribute between 30-43% of the overall energy from seaweeds and between 13-20% of the energy from lignocellulosic biomass.

The EROI of this integration strategy is energy positive with an assumed 55% energy recovery efficiency. However, this reduces with increasing HTC temperature. Therefore, a compromise between hydrochar quality and favourable energetics is generated for the macroalgal feedstocks and GR. Higher HTC processing temperatures produced hydrochars with more favourable ash behaviours. However, this compromises the energetics of the process. The greatest improvement in energy recovery is observed during the integration of HTC and AD using WH; however, inherent slagging and fouling tendencies may limit the application of WH-hydrochars during large-scale combustion.

Chapter 7
Biological Processing of High Ash Feedstocks Following Hydrothermal Pre-treatment

Previously, Chapter 6 investigated the separation of HTC products for applications as separate energy vectors, to improve the ECE of high ash feedstocks. However, the aim of this chapter is to investigate the comparative use of different hydrothermal pre-treatment technologies to enhance the biodegradability of high ash feedstocks during biological conversion processes. The two hydrothermal pre-treatments investigated as part of this chapter are: hydrothermal carbonisation (HTC) and steam explosion (SE). Hydrothermal pre-treatments were investigated across a range of conditions, described in Table 7.1. The severity of each pre-treatment was calculated according to the severity factor (SF), also presented in Table 7.1. HTC pre-treatment was conducted on macroalgal species: SL and FS, as well as lignocellulosic biomass: WH and GR. Whereas, SE pre-treatment was conducted on two macroalgal species: FS[19] and LD[19], as well as WH. The effectiveness of HTC and SE pre-treatments for enhancing biomethane yields was assessed, with the enhancement of two-stage digestion assessed for selected samples.

Table 7.1. Severity factor of each hydrothermal treatment.

Hydrothermal Treatment	Temperature (°C)	Retention Time (min)	Severity Factor (SF)
HTC	150	60	3.3
HTC	200	60	4.7
HTC	250	60	6.2
SE	150	15	2.6
SE	200	15	4.1

7.1 Objectives

The objectives of this chapter are to:

- Compare the effectiveness of two HTC-AD integration strategies to improve the ECE of high ash feedstocks. These include: separation of hydrochars for combustion and AD of process waters separately and AD of the combined HTC-slurries.
- Compare the effect of HTC and SE pre-treatment conditions on the generation of biomethane from macroalgal and lignocellulosic biomass.
- Compare the influence of HTC and SE pre-treatments on the ECE of WH during one-stage and two-stage digestion.

7.2 Hydrothermal Carbonisation Pre-Treatment

The following section assesses the effectiveness of HTC pre-treatment to enhance the generation of biomethane from SL, FS, WH and GR. HTC utilises subcritical water as a reactant medium for the conversion of biomass. Under elevated pressures and temperatures, the structure of the biomass is broken down, with hydrolysed products solubilised into the process water. The overall aim of this HTC pre-treatment is to promote hydrolysis of biomass to subsequently improve the biomethane yields.

7.2.1 Experimental Biomethane Potential

Figure 7.1 shows the BMP_{ex} yields obtained from the untreated biomass feedstocks and corresponding HTC slurries. Alongside, Table 7.2 reports the final BMP_{ex} yields and describes the process kinetics of each of the BMP_{ex} curves presented in Figure 7.1.

According to Figure 7.1a, HTC pre-treatment had little effect on the BMP_{ex} yields of SL. The BMP_{ex} yields of SL, SL150, SL200 and SL250 were 249.5 mL CH_4/g VS, 217.4 mL CH_4/g VS. 202.4 mL CH_4/g VS and 196.0 mL CH_4/g VS, respectively. Therefore, BMP_{ex} yields were reduced by 13%, 19% and 21%, for SL150, SL200 and SL250, compared to untreated SL. This suggests the hydrothermal pre-treatment conditions used in this study were not suitable to enhance the biomethane yields of SL. Lin *et al*. [72] found optimal hydrothermal pre-treatment conditions of 140°C, 30-min for *S. latissima*; increasing biomethane yields by 23%, linked to optimised solubilisation of mannitol. In addition, Ding *et al*. [216] reported a 26.8% increase in the biomethane yield of *L. digitata*; another kelp species, following hydrothermal pre-treatment at 140°C, 20-min. This suggests the hydrothermal conditions used to process SL in Figure 7.1a were too severe to generate a significant improvement in BMP_{ex}. This is reflected in the findings of Lin *et al*. [72], who found increasing the severity of *S. latissima* hydrothermal treatment to 180°C, 30-min resulted in a slight (1%) reduction in biomethane yield, compared to untreated *S. latissima*. The reduction in biomethane yield was linked to the increased formation of inhibitory compounds, produced through Maillard reactions. The SFs of the optimal and more severe conditions used by Lin *et al*. [72] were 2.7 (140°C, 30-min) and 3.8 (180°C, 30-min), respectively. Therefore, the optimal conditions identified by Lin *et al*. [72] were much less severe than the severity of hydrothermal conditions used during HTC within this thesis (Table 7.1).

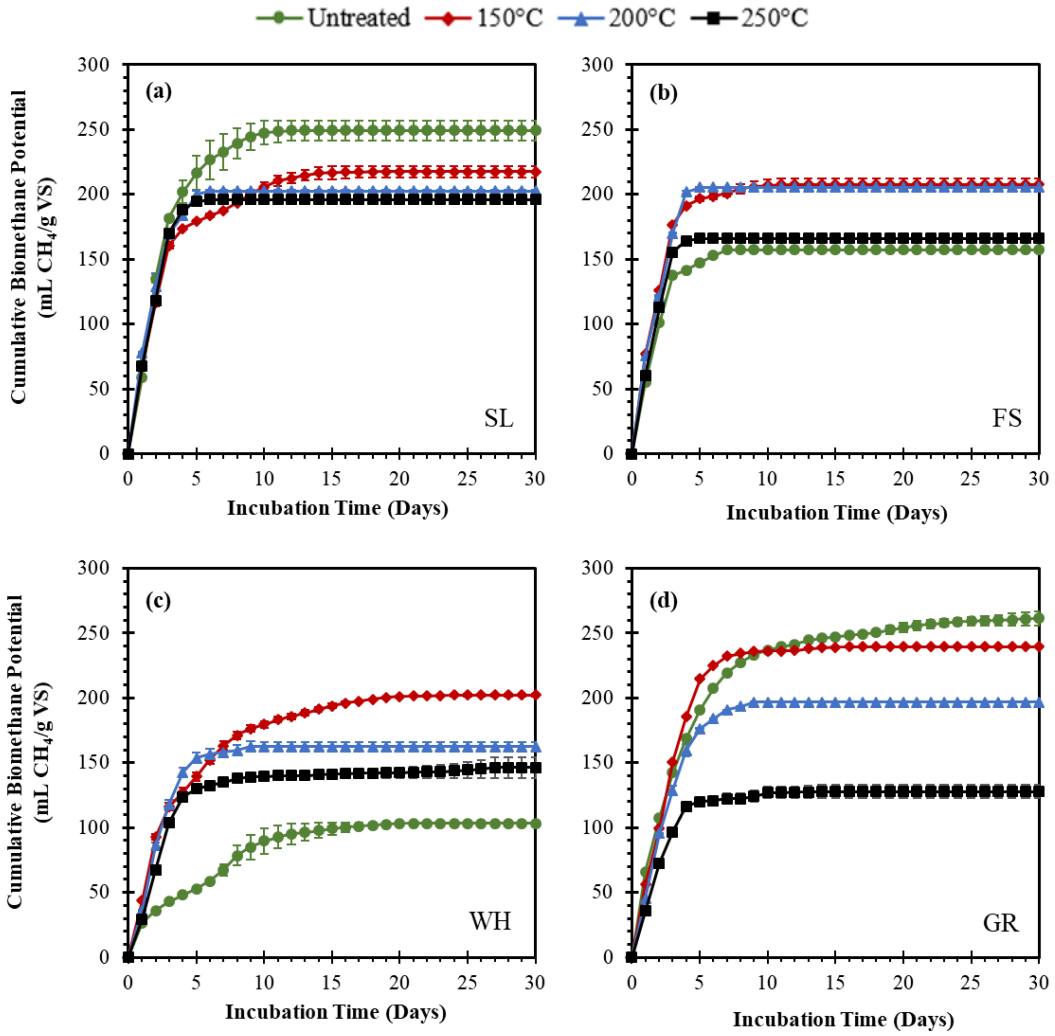

Figure 7.1. Experimental biomethane potential (BMP_{ex}) of untreated biomass and HTC slurries for (a) SL, (b) FS, (c) WH and (d) GR. Data is presented as average values. Error bars represent the maximum and minimum values (*n*=2).

Conversely, Figure 7.1b showed all FS-HTC slurries generated a higher BMP_{ex}, compared to untreated FS. The BMP_{ex} yields of FS150 (207.8 mL CH_4/g VS), FS200 (205.4 mL CH_4/g VS) and FS250 (165.9 mL CH_4/g VS) represent a 32%, 30% and 5% increase, compared to untreated FS. Table 7.2 also shows the FS-HTC slurries have a higher peak biomethane production rate (R_m) and similar technical digestion time (T^{80}) compared to untreated FS. This highlights differences in the effectiveness of HTC pre-treatment on different macroalgal species; with greater improvements observed for the seaweed species with the lowest initial biodegradability.

Table 7.2. Digestion kinetics from the anaerobic digestion of untreated biomass and HTC slurries.

Sample	BMP_{ex} mL CH_4/g VS	Modified Gompertz Model				T_m (d)	T^{80} (d)
		H_m mL CH_4/g VS	R_m mL CH_4/g VS/d	λ (d)	R^2		
SL	249.5	248.0	62.1	0.0	0.99	1.5	4
SL150	217.4	212.9	53.5	0.0	0.97	1.5	5
SL200	202.4	202.4	69.0	0.0	0.99	1.1	3
SL250	196.0	196.3	68.4	0.1	0.99	1.1	3
FS	157.4	157.0	53.4	0.0	0.99	1.1	3
FS150	207.8	206.9	68.5	0.0	0.99	1.1	3
FS200	205.4	206.0	68.4	0.0	0.99	1.1	3
FS250	165.9	166.2	70.4	0.2	0.99	1.1	3
WH	103.1	103.1	11.2	0.0	0.99	3.4	9
WH150	202.1	197.6	32.4	0.0	0.97	2.2	7
WH200	162.4	162.2	47.6	0.2	0.99	1.5	4
WH250	146.3	142.2	39.4	0.3	0.99	1.6	4
GR	261.2	252.0	44.3	0.0	0.98	2.1	7
GR150	239.3	239.2	53.8	0.1	0.99	1.7	5
GR200	196.9	197.0	46.1	0.0	0.99	1.6	4
GR250	127.7	127.1	36.7	0.0	0.99	1.3	4

BMP_{ex}=experimental biomethane potential. H_m=maximum biomethane yield. R_m=peak biomethane production rate. λ=lag phase. T_m=peak time of fermentation. T^{80}=technical digestion time.

Figure 7.1c shows that all WH-HTC slurries generated higher BMP_{ex} yields compared to untreated WH. WH150 (202.1 mL CH_4/g VS), WH200 (162.4 mL CH_4/g VS) and WH250 (146.3 mL CH_4/g VS) increased the BMP_{ex} by 96%, 57% and 42%, respectively, compared to untreated WH. Again, HTC-slurries improved the biomethane yields of a biomass with an initially low biodegradability (22%); similar to the observations made for FS (Figure 7.1b). Table 7.2 shows all WH-HTC-slurries showed enhanced digestion kinetics, compared to the untreated WH. Both WH200 and WH250 had a higher peak biomethane production rate (R_m)

and lower peak time of fermentation (T_m), compared to WH150. However. WH150 generated a higher biomethane yield compared to WH200 or WH250. The reduced BMP_{ex} of higher-temperature WH-HTC slurries could be linked to a dual synergy of factors, including; the formation of inhibitory compounds and the reduced biodegradability of the solid fraction; as discussed in Chapter 6. The improvement in biomethane yields obtained by WH150 are greater than the improvements observed in previous studies investigating subcritical water pre-treatment of WH [112,121]. Ali and Sun [112] found hydrothermal pre-treatment conditions of 121°C, 30-min (SF=2.1) improved biomethane yields from WH by 33%. Whereas, Putra *et al.* [121] found hydrothermal pre-treatment conditions of 170°C, 30-min (SF=3.5) improved biomethane yields from WH by 51%. Alternatively, Ferrer *et al.* [114] found a much lower hydrothermal treatment severity of 80°C, 180-min (SF=1.7) did not significantly improve the biomethane yields of WH. Therefore, the results of Figure 7.1c, combined with the results of [112,114,121] suggest there is an optimal SF which provides ideal pre-treatment conditions to balance the hydrolysis and solubilisation of organic matter, whilst limiting the formation of inhibitory or recalcitrant compounds. According to Figure 7.1c and [112,114,121] this range appears to a SF of 3.3-3.8. However, it is important to point out the variability in the biochemical composition of WH samples reported across literature studies. The analysis of WH presented in review papers [34,275] reports a wide range in the biochemical composition of WH, including: cellulose (17.3-31.0%), hemicellulose (20.3-43.4%) and lignin (1.1-26.4%) compositions. Therefore, not all WH sources would be expected to behave similarly. For instance, WH150 may show a greater improvement in biomethane generation compared to [112,121], due to the initially low biodegradability of the untreated WH used in this study (22%). The pre-treatment of a recalcitrant biomass with low biomethane generation is likely to show a greater improvement in BI, compared to the pre-treatment of a more readily-digestible biomass.

This hypothesis is supported by Figure 7.1d where all GR-HTC slurries generate a lower BMP_{ex}, compared to untreated GR. GR150 (239.3 mL CH_4/g VS), GR200 (196.9 mL CH_4/g VS) and GR250 (127.7 mL CH_4/g VS) decreased the BMP_{ex} by 8%, 25% and 51%, respectively, compared to untreated GR. Therefore, suggesting the HTC conditions used in this thesis were too severe to enhance the biomethane yields of GR. Digestion of GR-slurries were conducted at an ISR of 1.9:1, due to the initial VS of the inoculum batch being slightly lower. Again, higher temperature HTC slurries generated the lowest BMP_{ex} yields. This is echoed in the findings of Lin *et al.* [276], who found hydrothermal treatment at 140°C, 20-min (SF=2.5) generated the highest sugar yield from grass silage; however, increasing the temperature further to 180°C, 20-min (SF=3.7) favoured the degradation of sugars into inhibitory products, such as HMF and furfural. The SF of the optimal conditions for maximising sugar yields from grass silage found by Lin *et al.* [276] were lower than the SF

of GR150 (SF=3.3); suggesting degradation of sugars into inhibitors at this temperature. Wang *et al*. [214] found hydrothermally treated rice straw processed at 90°C, 15-min (SF=0.9), 150°C, 15-min (SF=2.6) and 180°C, 15-min (SF=3.5) had little effect on biomethane yields compared to untreated rice straw. However, increasing the severity of the processing conditions to 210°C, 15-min (SF=4.4) resulted in a 30% reduction in biogas generation, due to the presence of fermentative inhibitors.

Overall, Figure 7.1 shows that HTC pre-treatment enhanced the biomethane yields of FS and WH biomass. FS150 and WH150 demonstrated the greatest improvement in biomethane yields, compared to the parent feedstock; suggesting the more severe pre-treatment conditions resulted in the formation of recalcitrant or inhibitory compounds.

7.2.2 Biodegradability Index (BI)

The BI of each biomass and HTC slurry is shown in Figure 7.2, according to the BMP_{ex} yields, shown in Figure 7.1. The elemental composition of the HTC slurries was assumed to be the same as the untreated parent biomass, therefore, the BMP_{th} was also assumed to be the same.

According to Figure 7.2a, the BIs of SL150 (45%), SL200 (42%) and SL250 (41%) were all lower than untreated SL (52%). Figure 7.2b shows the BIs of FS150 (43%), FS200 (43%) and FS250 (35%) were all higher than untreated FS (33%). WH-derived HTC slurries display a similar behaviour to FS-derived HTC slurries; with the BIs of WH150 (42%), WH200 (34%) and WH250 (31%) all being higher than untreated WH (22%) (Figure 7.2c). Although, BI decreases with increased HTC severity. Figure 7.2d shows the BIs of GR150 (46%), GR200 (38%) and GR250 (24%) were all lower than untreated GR (50%).

Therefore, only HTC slurries produced from FS or WH significantly improve the BI compared to the parent biomass. Lower HTC processing conditions reflect greater biodegradability of the biomass, with BI typically decreasing at increased HTC temperatures. The reduction of BI under more severe conditions is linked to the formation of inhibitory compounds in the process waters, as well as increasing recalcitrance of the solid fraction; as described in Chapter 6. Therefore, overall FS150 and WH150 appear suitable HTC pre-treatment to enhance the biodegradability of FS and WH, respectively. Although the enhancement in biomethane yields may be further improved by exploring a wider range of HTC severity conditions, for example a reduction in retention time.

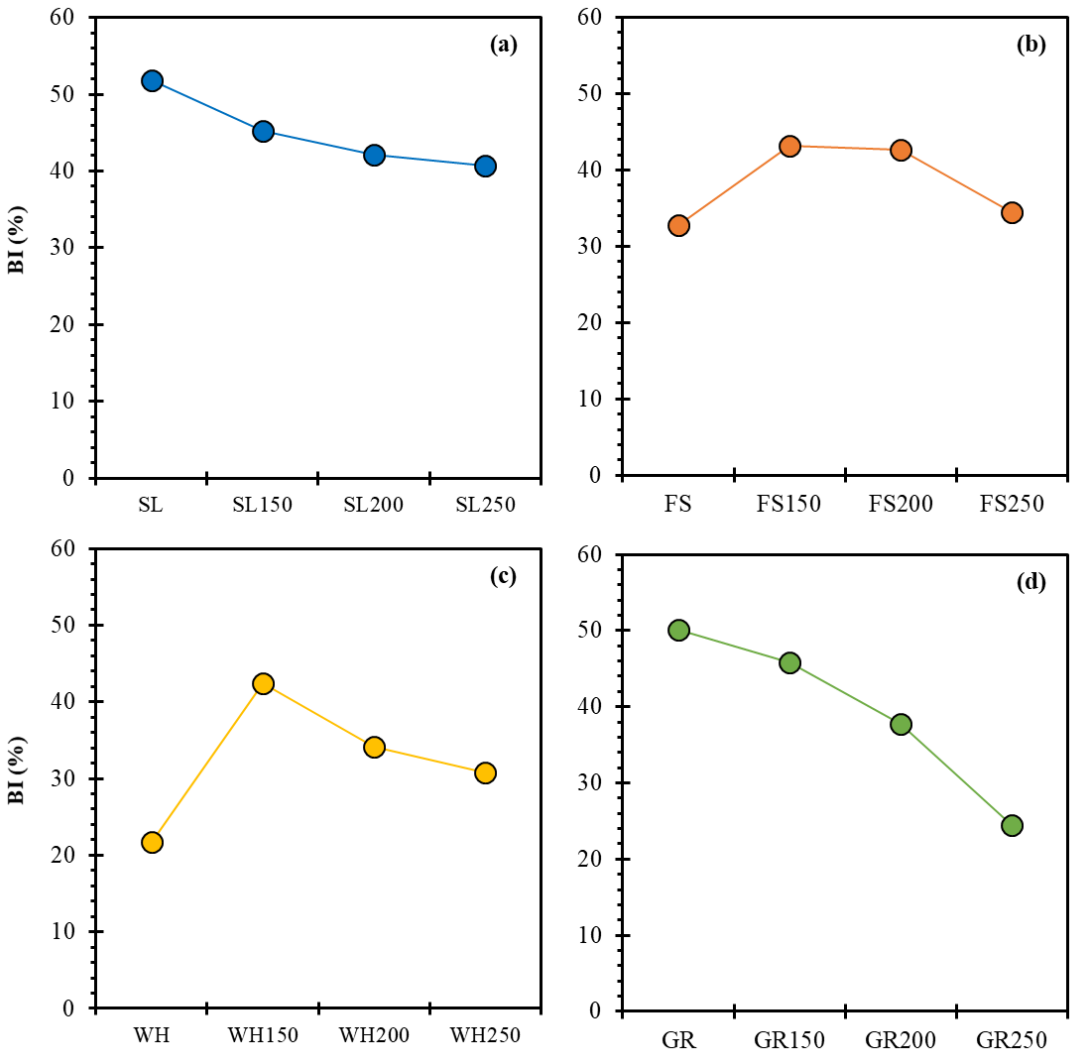

Figure 7.2. Biodegradability index of untreated biomass and HTC slurries for (a) SL, (b) FS, (c) WH and (d) GR.

7.2.3 Energetic Balance

7.2.3.1 Energy Return Upon Energy Invested

The energy balance calculated for the AD of each HTC slurry are shown in Table 7.3. Energy input is calculated according to the energy required to heat the contents of the HTC reactor, based on a starting material of 1-kg oven dried biomass. Whereas, the energy output is based on the HHV of the volume of biomethane generated from the HTC slurry; according to the BMP_{ex} yield shown in Figure 7.1.

Generally, Table 7.3 shows the EROI reduced with increasing HTC temperature across all biomass types. This is linked to an increased energy input to heat up the reactor, coupled with a reduced energy output; due to the formation of inhibitory compounds and increasing

recalcitrance of the solid fraction. The energy input of WH-HTC reactions was slightly lower than the other biomass types, due to the use of a larger reactor and slightly different solid loading ratios. Without any assumed energy recovery efficiency, only reactions conducted at 150°C were considered energy positive. However, with an assumed 55% energy recovery efficiency, reactions carried out at 200°C also become energy positive; although all have a reduced EROI compared to reactions conducted at 150°C.

Table 7.3. Energy balance for the integration of HTC and AD, through the AD of the HTC slurries.

Sample	Energy Input (MJ/kg dried[1] biomass)	Energy Output (MJ/kg dried[1] biomass)	EROI	EROI[2]
SL	-	6.53	-	-
SL150	5.44	6.17	1.13	2.52
SL200	7.61	4.86	0.64	1.42
SL250	9.79	3.80	0.39	0.86
FS	-	4.12	-	-
FS150	5.44	6.89	1.27	2.81
FS200	7.61	5.31	0.70	1.55
FS250	9.79	4.40	0.45	1.00
WH	-	3.02	-	-
WH150	4.99	5.78	1.16	2.57
WH200	6.99	4.15	0.59	1.32
WH250	8.99	2.44	0.27	0.60
GR	-	8.76	-	-
GR150	5.44	8.55	1.57	3.49
GR200	7.61	4.75	0.62	1.39
GR250	9.79	2.54	0.26	0.58

[1]oven dried biomass. [2]55% assumed energy recovery efficiency. EROI=energy returned upon energy invested.

Table 7.3 shows the energy output of untreated SL is greater than any SL-HTC slurries. A similar observation is made for GR and GR-HTC slurries. Therefore, HTC slurry AD, using the HTC conditions used in this thesis appears not to be suitable for the treatment of SL or GR; where AD of the untreated biomass would be a more viable option.

Alternatively, AD of all FS-HTC slurries were associated with a higher energy output, compared to the AD of untreated FS. FS150, FS200 and FS250 were associated with a respective 67%, 29% and 7% increases in energy output, compared to untreated FS.

Therefore, HTC treatment at 150°C would be the most suitable for FS; associated with the greatest improvement in energy output and displaying the most favourable EROI (Table 7.3).

WH150 and WH200 HTC slurries show respective increases in energy output of 91% and 37%, compared to the AD of untreated WH. However, the energy output of WH250 (2.44 MJ/kg) was associated with a 19% reduction in energy output compared to untreated WH. Therefore, similarly to FS; HTC treatment at 150°C would be the most suitable for WH; due to the most favourable EROI. Overall, higher temperature HTC is not recommended as a pre-treatment for AD, supporting the conclusions obtained by [72,214].

7.2.3.2 Comparison of HTC-AD Integration Options

Previously, Chapter 6 identified the separation of hydrochars for combustion and process waters for AD is a viable HTC-AD integration option to improve the ECE of macroalgal and lignocellulosic feedstocks. Furthermore, Table 7.3 shows the AD of the residual HTC slurry can be another viable HTC-AD integration option to improve the ECE of FS and WH. The two HTC-AD strategies can be compared, in order to understand which is the most feasible approach for each biomass type. Table 7.4 displays the comparative energy output, ECE and EROI for both integration options. The values for the untreated biomass feedstocks have also been included in Table 7.4 under the 'HTC slurry AD' column, to allow easier comparison to HTC-AD integration options.

The separation of hydrochars for combustion and process waters for AD is a more feasible HTC-AD integration strategy for SL, compared to AD of SL-HTC slurries. Table 7.4 shows the ECE of SL-HTC slurries did not improve the ECE of SL. Whereas, separation of HTC products improved the ECE of SL, as well as displaying more favourable EROI values.

Digestion of FS150 slurry returned an ECE of 58%; which was higher than the ECE of untreated FS (35%). AD of FS200 slurry also displayed an improvement in ECE compared to untreated FS. However, the energy output and EROI of FS150 was greater. Therefore, the digestion of the lower-temperature (150°C) FS-slurry was favoured. The separation of FS hydrochars for combustion and FS process waters for AD yielded a higher ECE, across all HTC temperatures, compared to the AD of FS150 slurry. However, the ash fusion tests reported in Chapter 6 suggest FS-derived hydrochars needed to be produced at temperatures of 200°C or 250°C to drastically reduce their slagging propensities; important to future applications in large-scale combustion. Table 7.4 shows the AD of FS150 slurry had a more favourable EROI (2.81), compared to the separation of FS200 (EROI=2.75) or FS250 (EROI=1.96) HTC products, for applications as separate energy vectors. However, the ECE

achieved from the separated HTC products of FS200 (79%) and FS250 (72%) were higher than the AD of FS150-slurry (58%), resulting in a compromise between EROI and ECE. However, on balance, perhaps the separation of FS200 products for combustion and AD is the most feasible option, due to a higher ECE and similar EROI, compared to FS150-slurry AD, as well as a reduction in the slagging potential of the hydrochars.

Table 7.4. Comparison of improvements in ECE and EROI using two HTC-AD integration strategies: (i) hydrochar combustion combined with process water AD (ii) HTC slurry AD.

Sample	(i) Hydrochar Combustion and Process Water AD			(ii) HTC Slurry AD		
	Energy Output (MJ./kg)	ECE (%)	EROI[1]	Energy Output (MJ./kg)	ECE (%)	EROI[1]
SL	-	-	-	6.53	64	-
SL150	9.19	90	3.75	6.17	60	2.52
SL200	7.89	77	2.31	4.86	47	1.42
SL250	7.27	71	1.65	3.80	37	0.86
FS	-	-	-	4.12	35	-
FS150	10.87	91	4.44	6.89	58	2.81
FS200	9.42	79	2.75	5.31	44	1.55
FS250	8.65	72	1.96	4.40	37	1.00
WH	-	-	-	3.02	25	-
WH150	11.73	97	5.22	5.78	48	2.57
WH200	10.54	87	3.35	4.15	34	1.32
WH250	9.63	79	2.38	2.44	20	0.60
GR	-	-	-	8.76	50	-
GR150	14.48	82	5.92	8.55	48	3.49
GR200	12.99	74	3.79	4.75	27	1.39
GR250	11.16	63	2.53	2.54	14	0.58

[1]55% assumed energy recovery efficiency. EROI=energy returned upon energy invested.

Table 7.4 shows all HTC-AD integration strategies improved the ECE of WH, with the exception of the digestion of WH250 slurry. AD of WH150 slurry provided a greater ECE (48%) and EROI (2.57), compared to WH200 slurry (ECE=34%, EROI=1.32). Therefore, AD of WH-slurry generated at 150°C is more favourable compared to 200°C. Separation of WH hydrochar for combustion and WH process waters for AD shows a consistently higher ECE compared to AD of WH150 slurry, across HTC all temperatures. However, the ash fusion tests reported in Chapter 6 suggested WH-hydrochars showed no real improvement in slagging behaviour, compared to untreated WH. This suggests the large-scale combustion of

WH-hydrochars is not suitable and perhaps applications in small-scale combustion is a more feasible option. Therefore, the integration strategy best applied to WH is dependent on whether a market exists for WH-hydrochars as a small scale combustion fuel. Alternatively, WH-hydrochars could be used as a soil amendment product.

Finally, Table 7.4 shows GR follows similar conclusions to SL; where separation of GR hydrochars for combustion and GR process waters for AD is a more suitable HTC-AD integration option, compared to GR-HTC slurry digestion. This is because the AD of GR150, GR200 and GR250 slurries all display a lower ECE than untreated GR. Whilst the strategy of separating products consistently shows higher ECEs, compared to untreated GR.

The conclusions obtained from Table 7.4 reflect the conclusions by Lucian *et al*. [209] where the separation of hydrochars for combustion and process waters for AD was deemed a more energetically feasible HTC-AD integration strategy, compared to HTC slurry AD, using the organic fraction of municipal solid waste as a feedstock.

7.3 Steam Explosion Pre-treatment

Steam explosion (SE) is an alternative hydrothermal treatment which is used to disrupt the biochemical structure of biomass, to facilitate enhanced biodegradation during biological conversion processes, such as AD. SE differs from HTC, as high pressure steam is used as a reactant medium, rather than subcritical water. The biomass is retained under high-pressure conditions for a specific retention time, before undergoing rapid pressure discharge to atmospheric conditions. Decompression causes mechanical disruption to the biochemical structure of biomass. Such treatment can enhance biomass hydrolysis and improve the digestion kinetics in downstream biological conversion processes.

This section investigates the effect of SE pre-treatment on the biomethane yields generated from two seaweeds: *F. serratus* (FS[19]) and *L. digitata* (LD[19]) and a lignocellulosic biomass: water hyacinth (WH). SE conditions of 150°C, 15-min (SF=2.6) and 200°C, 15-min (SF=4.1) were investigated to understand the effect of SE severity on the resulting biomethane yields from the biomass.

7.3.1 Characterisation of Steam Exploded Slurries

Following SE pre-treatment, the SE slurries were separated into the solid and aqueous fractions, through centrifugation. Each fraction was subsequently characterised; allowing a greater understanding of the hydrolysis behaviour of each biomass under the selected SE conditions.

7.3.1.1 Mass Balance

The mass balances of the solid and aqueous phases following SE reactions are displayed in Figure 7.3. Following each SE reaction, the aqueous phase represents the greatest mass fraction (93-99%). Increased SE reaction severity from 150°C to 200°C resulted in a reduction of the proportional mass of the solid fraction across all feedstocks. Therefore, indicating potential enhanced hydrolysis of the biomass and increased solubilisation into the aqueous phase, under the more severe reaction conditions. However, this must be interpreted with caution, as the SE reactor uses an exogenous steam to pressurise the reactor to the chosen conditions: 150°C (4.5bar) and 200°C (14.5bar). Hence, SE reactions are not conducted in a closed system, unlike HTC. More severe SE reactions require the introduction of a greater volume of steam to pressurise the reaction chamber. This is likely to lead to increased condensation of steam onto the biomass, during the decompression stage; creating a dilution effect, reducing the solid yield of the SE slurry.

To further investigate this phenomenon, the addition of excess water during SE was calculated through the gravimetric difference between the sample input and sample output. The increase in sample masses, associated with the addition of water, are presented in Table 7.5. The data is compared across duplicate SE runs, conducted on each sample. The addition of water generally represents a significant increase in the mass of the SE slurry; with all LD[19] and WH SE slurries showing the increase in sample mass was >100%. The difference in water addition between duplicate runs appears to be much greater during SE reactions conducted at 200°C, compared to 150°C. For example, the average addition of water for WH-SE150 and WH-SE200 was 118 ± 3 w/w% and 158 ± 76 w/w%, across the respective duplicate runs. FS[19]-SE150 experienced the least significant addition of water; with duplicate 1 showing no addition of water and duplicate 2 showing a 38 w/w% increase in water addition. This is reflected in the higher solid yield of FS[19]150, shown in Figure 7.3.

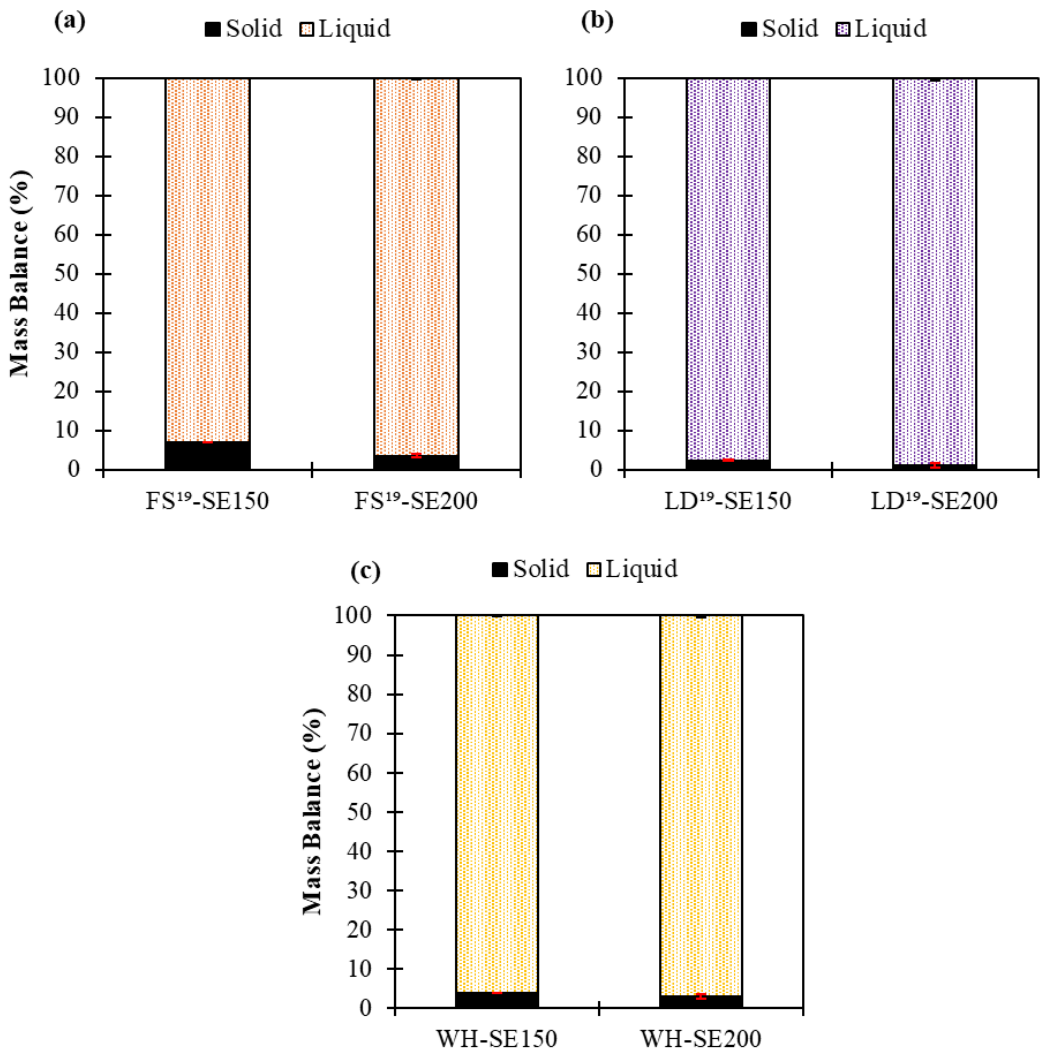

Figure 7.3. Mass balance of the solid and liquid fractions following the SE of (a) FS[19], (b) LD[19] (c) and WH. Error bars represent the standard deviation (*n*=2).

The addition of excess water from condensed steam makes it difficult to compare the properties of the aqueous phases across SE runs, or to the HTC process waters. A further complication is the distribution of water vented during decompression and water condensed onto the biomass surface is unknown. This highlights the limitations of using a batch-based 30-L CAMBI system. However, for the purposes of this study, the SE reactor was sufficient to pre-treat samples in order to understand potential improvements in biodegradability.

Table 7.5. Mass increase of biomass, associated with water addition.

Sample	Duplicate Number	Mass Increase of Biomass Related to Water Addition (w/w%)
FS[19]-SE150	1	0
FS[19]-SE150	2	38
FS[19]-SE200	1	190
FS[19]-SE200	2	66
LD[19]-SE150	1	116
LD[19]-SE150	2	114
LD[19]-SE200	1	216
LD[19]-SE200	2	104
WH-SE150	1	120
WH-SE150	2	116
WH-SE200	1	212
WH-SE200	2	104

7.3.1.2 Solid Fraction Characterisation

Following SE reactions the solid fraction was recovered through centrifugation and freeze drying. The residual solid from duplicate SE runs were combined and characterised. The proximate and ultimate composition of the solid residues from SE are presented in Table 7.6, alongside the composition of the original biomass. The C-contents of the solid SE residues from FS[19] and LD[19] were higher during greater SE severity; coupled with an increase in the FC content. FS[19] and LD[19] SE solid residues also showed a reduction in ash content compared to the parent material. This suggests solubilisation of the inorganic matter; likely due to the removal of free ionic salts, such as NaCl and KCl [64]. Conversely, SE residues from WH shows the inverse effect; with C-content reducing and ash content increasing under more severe SE conditions. Although, an increase in FC is observed.

The increasing C-content of FS[19] and LD[19] solid residues suggests similar energy densification reactions are occurring; similar to HTC. Whereas, WH does not undergo these similar energy densification reactions during SE. This could be a result of the seaweed polysaccharides undergoing degradation at lower temperatures than cellulose or hemicellulose.

Table 7.6. Proximate and ultimate composition of biomass feedstocks and solid residues from steam explosion.

Sample	Ultimate analysis (wt%) *db*					Proximate analysis (wt%) *db*		
	C	H	N	S	O*	VM	FC	Ash
FS[19]	33.7 ± 0.2	4.2 ± 0.2	2.1 ± 0.0	1.6 ± 0.4	26.8 ± 0.0	77.0	9.8	13.2
FS[19]-SE150	43.6 ± 0.1	2.5 ± 0.4	2.7 ± 0.1	ND	27.0 ± 0.3	75.1	17.7	7.1
FS[19]-SE200	49.8 ± 0.2	2.5 ± 0.1	3.0 ± 0.1	ND	23.1 ± 1.1	73.5	20.9	5.6
LD[19]	33.5 ± 0.1	4.4 ± 0.1	1.5 ± 0.1	0.8 ± 0.2	30.0 ± 0.0	81.0	9.4	9.6
LD[19]-SE150	39.7 ± 0.0	2.2 ± 0.1	2.4 ± 0.0	ND	28.7 ± 0.0	76.1	17.2	6.8
LD[19]-SE200	44.4 ± 0.0	2.8 ± 0.1	2.4 ± 0.0	ND	26.5 ± 1.6	76.7	17.4	6.0
WH	38.7 ± 0.0	3.4 ± 0.0	2.7 ± 0.1	0.1 ± 0.1	27.4 ± 0.5	85.5	ND	14.5
WH-SE150	37.4 ± 0.2	3.4 ± 0.1	2.1 ± 0.0	ND	26.5 ± 0.3	66.6	13.2	20.2
WH-SE200	32.1 ± 0.3	3.9 ± 0.0	2.0 ± 0.0	ND	22.9 ± 0.5	56.6	9.8	33.6

*Oxygen measured directly. ND=not detected. *db*= dry basis. VM=volatile matter. FC=fixed carbon.

Figure 7.4 shows the HHV and ED of the SE solid residues. The HHVs of FS[19]-SE150 (13.5 MJ/kg) and FS[19]-SE200 (16.3 MJ/kg) were higher than the untreated FS[19] (12.6 MJ/kg); corresponding to respective EDs of 1.07 and 1.29. The increased HHVs are because of an increased C-content (Table 7.6). Chapter 4 showed FS[19] and FS showed a similar HHV (12.6-12.7 MJ/kg); as the samples were collected from a similar location, during a similar season. Chapter 5 demonstrated HTC of FS at 150°C and 200°C generated hydrochars with respective EDs of 1.32 and 1.55; higher than the EDs of the SE solid residues produced at the corresponding temperatures (Figure 7.4).

Figure 7.4b shows a decrease in HHV between LD[19] (12.2 MJ/kg) and LD[19]-SE150 (11.5 MJ/kg); despite an increase in C-content (Table 7.6). In fact, the lower H-content of LD[19]-SE150 (2.2%), compared to LD[19] (4.4%) is the reason for the reduced HHV. LD[19]-SE200 displayed an increase in HHV, compared to LD[19]; corresponding to an ED of 1.17 (Figure 7.4b). Chapter 5 demonstrated that the HTC of LD at 150°C and 200°C produced hydrochars with an energy densification of 1.48 and 1.68, respectively. Therefore, despite LD being harvested in winter and LD[19] being harvested in summer, HTC shows improved ED, compared to SE for *L. digitata.*

Figure 7.4c shows that the HHVs of the SE solid residues: WH-SE150 (12.8 MJ/kg) and WH-SE200 (12.4 MJ/kg) were both lower than the HHV of WH (13.0 MJ/kg). Whereas, Chapter 5 found HTC treatment of WH at 150°C and 200°C yielded hydrochars with corresponding EDs of 1.03 and 1.25. Therefore, validating the trend highlighted by Figure 7.4a and Figure 7.4b that the ED of SE solid residues is lower than hydrochars generated by HTC at

corresponding temperatures. This emphasises key differences between SE and HTC technologies: HTC is often considered to simulate the natural coalification process [159]; generating an energy densified solid (hydrochar), whereas, SE is a technique used to facilitate hydrolysis [115]. Overall, Figure 7.4 suggests the use of the solid residue from SE is not suitable as a solid combustion fuel. A more likely application of SE is to maintain the solid and aqueous phases as a mixed slurry for downstream biological conversion.

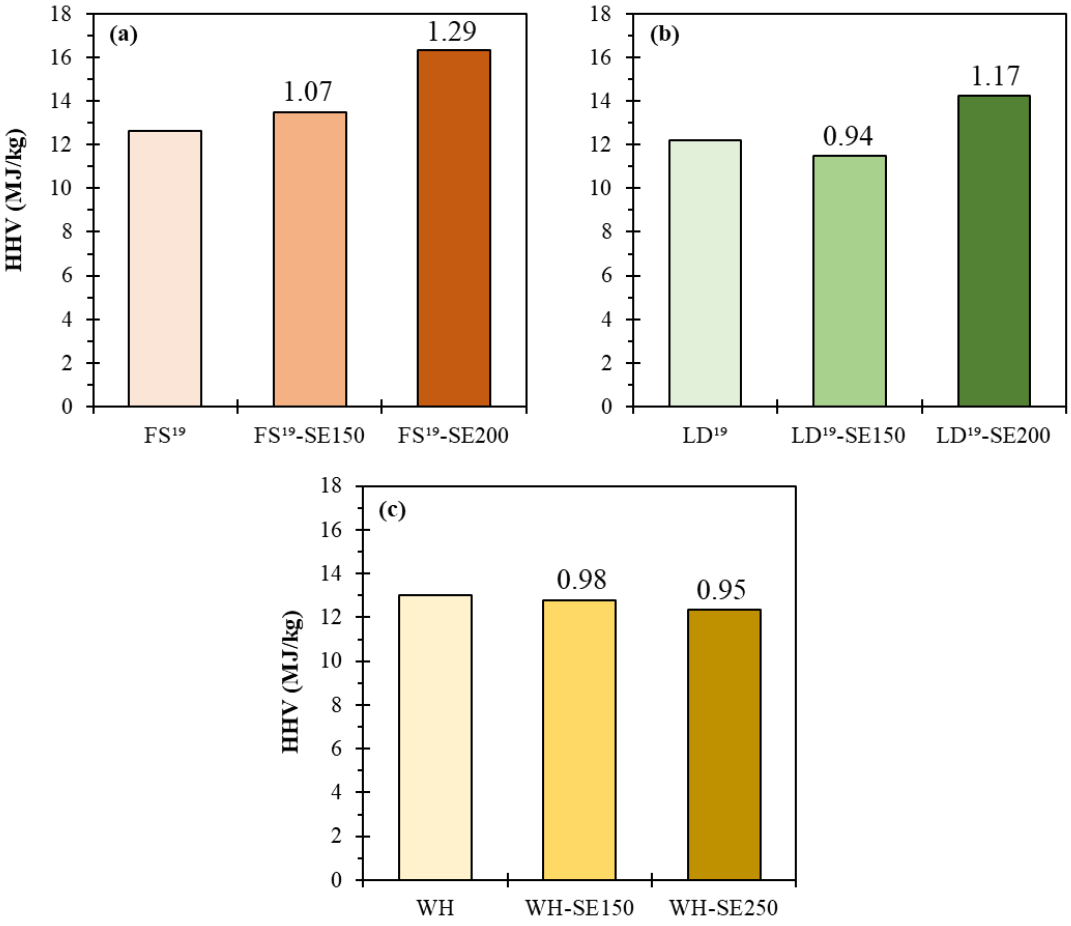

Figure 7.4. HHV of untreated biomass and solid residues from steam explosion for (a) FS[19] (b) LD[19] and (C) WH. HHV values presented on a dry basis (*db*). Numbers above the bars corresponds to the energy densification (ED) of the solid, compared to the original biomass.

7.3.1.3 Aqueous Fraction Characterisation

Characterisation of the aqueous fraction from SE allows an assessment of the degree of biomass hydrolysis during each SE reaction. Table 7.7 shows the properties of the aqueous phases from SE, using data directly measured from the process waters. However, the results

shown in Table 7.7 do not account for the varying quantities of excess water added to the biomass during the different SE reactions; as described in Table 7.5. Therefore, it is difficult to compare these results, due to the differential dilution effects resulting from the addition of different amounts of water, during SE reactions. As a result of this, Table 7.8 shows the properties of the aqueous fractions from SE, which have been corrected to account for the dilution effect described in Table 7.5; allowing the data to be more easily compared. The aqueous phases from each SE run was analysed in singlet and the results corrected for the dilution effect of that individual run. The average values across each duplicate run were then averaged and presented in Table 7.8.

Table 7.7. Characteristics of the aqueous fraction from steam explosion, uncorrected data.

Sample	COD (g/L)	TOC (g/L)	Total Phenol (mg/L)	Total VFA (mg/L)	pH
FS[19]-SE150	68.9 ± 2.4	35.1 ± 0.0	191.5 ± 24.0	204.2 ± 45.7	4.7
FS[19]-SE200	40.5 ± 9.9	17.4 ± 3.8	215.0 ± 60.1	386.8 ± 105.0	4.5
LD[19]-SE150	38.6 ± 0.4	17.5 ± 0.4	36.3 ± 2.4	84.4 ± 5.2	4.3
LD[19]-SE200	33.6 ± 4.8	14.5 ± 2.7	187.8 ± 52.7	209.1 ± 30.8	4.1
WH-SE150	4.4 ± 0.0	2.3 ± 0.0	59.3 ± 4.6	139.4 ± 11.0	6.2
WH-SE200	15.2 ± 4.0	6.2 ± 1.6	123.0 ± 36.8	315.5 ± 50.8	5.6

COD=chemical oxygen demand. TOC=total organic carbon. VFA=volatile fatty acids.

Table 7.8. Characteristics of the aqueous fraction from steam explosion. Data corrected to account for the addition of exogenous water during steam explosion.

Sample	COD (g/L)	TOC (g/L)	Total Phenol (mg/L)	Total VFA (mg/L)
FS[19]-SE150	71.3 ± 5.8	41.8 ± 9.4	231.1 ± 80.1	258.3 ± 86.5
FS[19]-SE200	97.4 ± 13.1	38.0 ± 6.6	463.9 ± 51.1	825.8 ± 43.2
LD[19]-SE150	83.0 ± 0.3	37.6 ± 1.1	78.1 ± 4.6	181.4 ± 10.9
LD[19]-SE200	85.3 ± 14.0	36.5 ± 4.4	467.3 ± 11.7	545.8 ± 159.7
WH-SE150	9.5 ± 0.1	5.1 ± 0.0	129.1 ± 8.3	302.7 ± 21.0
WH-SE200	37.8 ± 1.4	15.5 ± 0.5	303.3 ± 0.9	850.2 ± 85.6

COD=chemical oxygen demand. TOC=total organic carbon. VFA=volatile fatty acids.

According to Table 7.8, the macroalgal-derived SE aqueous phases have greater COD and TOC concentrations compared to WH-derived SE aqueous phases. Therefore suggesting the biochemical structure of FS[19] and LD[19] undergo more enhanced hydrolysis during SE, compared to WH. This echoes the conclusions found in Chapter 5; where the COD and TOC

values of macroalgal-derived HTC process waters were consistently higher than WH-derived HTC process waters generated at 150°C and 200°C. Although, the COD and TOC concentrations of macroalgal-derived HTC process waters ranged from 34.6-42.9 g COD/L and 13.0-16.8 g TOC/L. These values are much lower than the values reported in Table 7.8: 71.3-97.4 g COD/L and 36.5-41.8 g TOC/L, again suggesting more efficient hydrolysis of seaweeds using SE, rather than HTC.

The SE aqueous phase of WH-SE150 had lower COD and TOC values (9.5 g COD/L and 5.1 g TOC/L), compared to WH150 HTC process water (19.0 g COD/L and 7.1 g TOC/L). Whereas, the SE aqueous phase of WH-SE200 had higher COD and TOC concentrations (37.8 g COD/L and 15.5 g TOC/L), compared to WH200 HTC process water (27.5 g COD/L and 11.1 g TOC/L). Therefore, at 150°C HTC provides more efficient hydrolysis of WH, compared to SE. However, at 200°C this trend is reversed. Alfageme *et al*. [115] obtained a COD concentration of 9.3 g/L from the aqueous phase of SE WH (210°C, 10-min); similar to the values in Table 7.7. Although, the authors did not account for the dilution effect obtained from the addition of exogenous steam.

Both FS[19] and WH show an increased COD and TOC concentration at higher SE severity; indicating enhanced hydrolysis of these feedstocks, at higher temperatures. Whereas, COD and TOC concentrations remained similar for LD[19], across the two SE temperatures; suggesting little difference in the hydrolysis of LD[19] across the different SE severities.

Similarly to HTC process waters, Table 7.8 suggests the composition of the aqueous fraction from SE changes according to the SE severity. All feedstocks display an increase in VFA at 200°C, compared to 150°C. Weber *et al*. [277] previously reported an increased concentration of VFA during the SE of *Agave tequilana* bagasse. Acetic acid represents the highest concentration of VFA, similar to HTC process waters. WH200 shows a slightly higher VFA concentration (850.2 mg/L), compared to FS[19]200 (825.8 mg/L) and LD[19]200 (545.8 mg/L); again similar to HTC process waters (Chapter 5). Although, the standard deviation of the VFAs in Table 7.8 remains high; due to complications in correcting the data for the excess water added to the system.

The total phenol concentrations of the SE aqueous phases also increased under more severe reaction conditions. Therefore, suggesting the formation of inhibitory compounds at higher SE temperatures. Although, the concentrations shown in Table 7.8 are not likely to fully inhibit AD [115,277]. Alfageme *et al*. [115] studied the SE of WH; finding a linear increase in the formation of phenols with increasing temperature (120°C, 170°C and 210°C); up to a concentration of 700 mg/L. This concentration appears higher than the values presented in Table 7.8. However, as previously mentioned, it is difficult to compare these values between studies due to largely different reactor operations. Alfageme *et al*. [115] found a decrease in

phenols as the retention time increased for the highest temperature SE treatment (210°C). Although, less severe reaction conditions are shown in Table 7.8, so this trend is not observed.

Following SE treatment at 200°C, FS^{19}-SE200 and LD^{19}-SE200 displayed a greater total phenol concentration, compared to WH-SE200 (Table 7.8). This is opposite to the effect observed during HTC (Chapter 5); where the WH200 HTC process water had a higher total phenol concentration than SL200, FS200 or LD200. Suggesting, a reduced degradation of lignin during SE, compared to HTC.

In addition to the measurements of process water composition displayed in Table 7.7 and Table 7.8. The concentrations of total sugars, HMF and furfural were also determined for the SE aqueous fractions; using similar methodologies to those used in Chapter 5. Although, due to the large variations in excess water addition (Table 7.5), a large range of values were obtained across sample duplicates. The following values have been corrected to account for the addition of excess water. The total sugar content of FS^{19} aqueous phases generally increased from between 0-8.9 g/L (150°C) to 9.5-19.2 g/L (200°C); although as previously discussed, the method of quantifying sugars for seaweeds may be subject to overestimation. No detectable HMF or furfural was present in FS^{19}-SE150, however HMF and furfural increased to between 0-767 mg/L and 657-1639 mg/L, respectively, in FS^{19}-SE200. LD^{19} followed a similar trend to FS^{19}, with sugar content increasing at higher temperatures: 2.4-6.2 g/L (150°C) and 6.8-12.9 g/L (200°C). Furfural was not detected in any LD^{19}-derived process water. Whereas HMF was undetected for LD^{19}-150, but increased to 13237-15664 mg/L in LD^{19}-200: although this is possibly an overestimation.

The total sugar range of WH-SE150 was slightly higher (0.9-2.2 g/L) compared to WH-SE200 (1.3-2.0 g/L). However, the concentration range of both HMF and furfural increased under more severe conditions: 150°C (HMF= 0-552 mg/L, furfural= 0-645 mg/L) and 200°C (HMF= 0-1116 mg/L, furfural= 0-6303 mg/L). Again, large variations between duplicate samples are observed. Generally, higher severity SE results in a reduction in sugar yield and an increase in HMF and furfural concentrations. Steinbach *et al*. (2019) also [219] report an increase in HMF formation with increasing SF during the SE of rice straw; due to the higher prevalence of glucose dehydration. HMF and furfural are formed from the dehydration of solubilised sugar derivatives [120,150,204], typically forming around 200°C [278] where cellulose begins to degrade to monomeric sugars and subsequent furanic compounds [152,163].

7.3.1.4 Physical Characteristics

SE has the potential to not only enhance the hydrolysis of biomass, but also improve the handling properties of the material. Figure 7.5 shows the changing appearance of FS^{19} after SE treatment at 150°C and 200°C. Whereas, Figure 7.6 shows the changing appearance of WH following SE treatment at 150°C and 200°C. Both FS^{19} and WH show a gradual reduction in the presence of visible fibres, with increasing SE temperature. Therefore, improving the processing properties of the biomass, including the potential to pump and more easily transport the slurry. This effect is particularly significant with WH (Figure 7.6), because of the difficult handling of the untreated biomass, related to the 'sponge-like' physical properties.

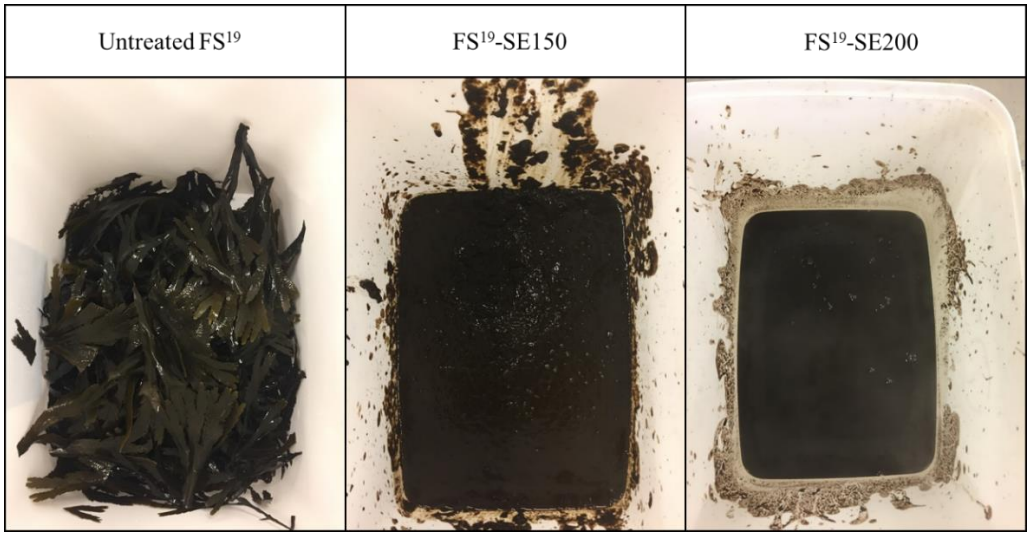

Figure 7.5. Physical appearance of FS^{19} following steam explosion at 150°C and 200°C.

Figure 7.6. Physical appearance of WH following steam explosion at 150°C and 200°C.

7.3.2 Experimental Biomethane Potential

The BMP_{ex} values obtained from the digestion of SE slurries obtained from FS^{19}, LD^{19} and WH are shown in Figure 7.7a-c and Table 7.9; with the corresponding digestion kinetics also described in Table 7.9. BMP_{ex} experiments for SE-slurries were ran for 27-days. However the data in Figure 7.7 has only been reported up until 25-days. At this time point, biomethane production had plateaued for all SE-slurries and untreated biomass. The VS of SE slurries was determined by drying at 60°C and subsequently ashing at 550°C. Therefore, in order to maintain similar experimental conditions, the VS-content of the untreated biomass was determined at respective drying and ashing temperatures of 105°C and 550°C [223]. A slightly reduced drying temperature (60°C) was used to determine the VS of SE slurries, in order to minimise the losses of volatile organics from hydrolysed slurry.

The BMP_{ex} yields of both FS^{19}-SE slurries generated a higher BMP_{ex} compared to untreated FS^{19} (Figure 7.7a). The SE slurries improved biomethane yields by 82% (FS^{19}-SE150) and 72% (FS^{19}-SE200), compared to untreated FS^{19}. FS^{19}-SE150 generated a slightly higher biomethane yield (261.3 mL CH_4/g VS), compared to FS^{19}-SE200 (247.8 mL CH_4/g VS). This could be linked to an increased presence of fermentative inhibitors: HMF, furfural and phenols, produced during the more severe reaction conditions. Although, due to the variation in BMP_{ex} yields shown in Figure 7.7a, it is unlikely this difference is significant. Table 7.9 shows the digestion kinetics of both FS^{19}-SE slurries are also similar. The improvement in biomethane yields is due to the enhanced hydrolysis of FS^{19} during SE. Whereas, Figure 7.7b shows that SE pre-treatment does not enhance the biomethane yields generated from LD^{19}. In fact, untreated LD^{19} generated the higher biomethane yields (307.6 mL CH_4/g VS) compared to LD^{19}-SE150 (289.4 mL CH_4/g VS) and LD^{19}-SE200 (259.5 mL CH_4/g VS). Therefore, highlighting interspecies differences of the effectiveness of SE to improve the digestion of different seaweed species during AD; with an enhancement observed with *F. serratus*, but not *L. digitata*. Perhaps hydrothermal pre-treatments are more effective for fucoid species, compared to kelp species. This reflects the findings of Table 7.3; where HTC pre-treatment found to be effective at improving the energy output obtained from FS, but not SL. The effect of SE on the biomethane generation from fucoids has not been reported in previous studies. However, Vivekanand *et al*. [132] investigated the use of SE to enhance the biodegradability of the kelp species *S. latissima*. SE treatment conditions of 130°C, 10-min (SF=1.9) reflected a 20% improvement in the biomethane yields of *S. latissima* from 223 mL CH_4/g VS to 268 mL CH_4/g VS [132]. Although, more severe reaction conditions of 130°C, 10-min (SF=2.8) resulted in a biomethane yield of 260 mL CH_4/g VS; slightly lower than the less severe reaction conditions, but slightly higher than the untreated *S. latissima*. SE of LD^{19} at 150°C

or 200°C were associated with respective reaction SFs of 2.6 and 4.1, respectively; both higher than the optimal SF conditions identified by Vivekanand *et al.* [132] (SF=1.9). Therefore, perhaps the SE conditions used in this thesis were too severe to enhance the biodegradability of LD^{19}. In addition, the BMP_{ex} yield obtained by LD^{19} (307.6 mL CH_4/g VS) is generally higher than typically reported biomethane yields for *L. digitata* [60,71,127]. As a result, improving the biomethane yields of an already high-yielding biomass can prove challenging.

The behaviour of WH during SE treatment is different compared to the macroalgal species. Figure 7.7c demonstrates WH-SE150 showed slightly improved biomethane yields compared to untreated WH. The BMP_{ex} yields of untreated WH and WH-SE150 were 103.1 mL CH_4/g VS and 121.9 mL CH_4/g VS, respectively. Whereas, WH-SE200 had a BMP_{ex} yield of 200.2 mL CH_4/g VS; reflecting a 94% increase in biomethane production, compared to untreated WH. Therefore, unlike the macroalgal species, the more severe SE conditions; conducted at 200°C, resulted in the greatest improvement in biomethane generation, compared to the less severe SE reaction conditions, conducted at 150°C. These results indicate limited hydrolysis of WH during SE at 150°C, which is also reflected in the lower COD and TOC concentrations present in the aqueous phase. The dissimilarities between the behaviour of macroalgal biomass and WH during SE is likely linked to the differences in biochemical compositions. As previously mentioned, macroalgal-derived carbohydrates break down between temperatures of 140-160°C [69,72,243], whereas hemicellulose and cellulose degrade at higher temperatures (180-230°C) [159,242]. Therefore, less severe conditions are required to facilitate the hydrolysis of macroalgal biomass, compared to WH.

Table 7.9 shows the digestion kinetics of WH-SE150 were slower than untreated WH. For example, the technical digestion time (T^{80}) of WH-SE150 was 13-days, whereas for untreated WH it was 9-days. The slower digestion of WH-SE150 could be related to differences in particle size used during the BMP_{ex} experiment. A particle size of <1-mm was used for untreated WH, whereas SE reactions were conducted on WH with a particle size of 20-30cm and the SE slurries maintained as received after the SE pre-treatment. Figure 7.6 indicated the visible presence of fibres within the WH-SE150 slurry. A smaller particle size creates an increased surface area for the accessibility of microbial interactions; therefore facilitating digestion [279]. WH-SE200 showed an improvement in digestion kinetics compared to untreated WH or WH-SE150 (Table 7.9) which could be linked to the elimination of visible fibres in the SE slurry (Figure 7.6).

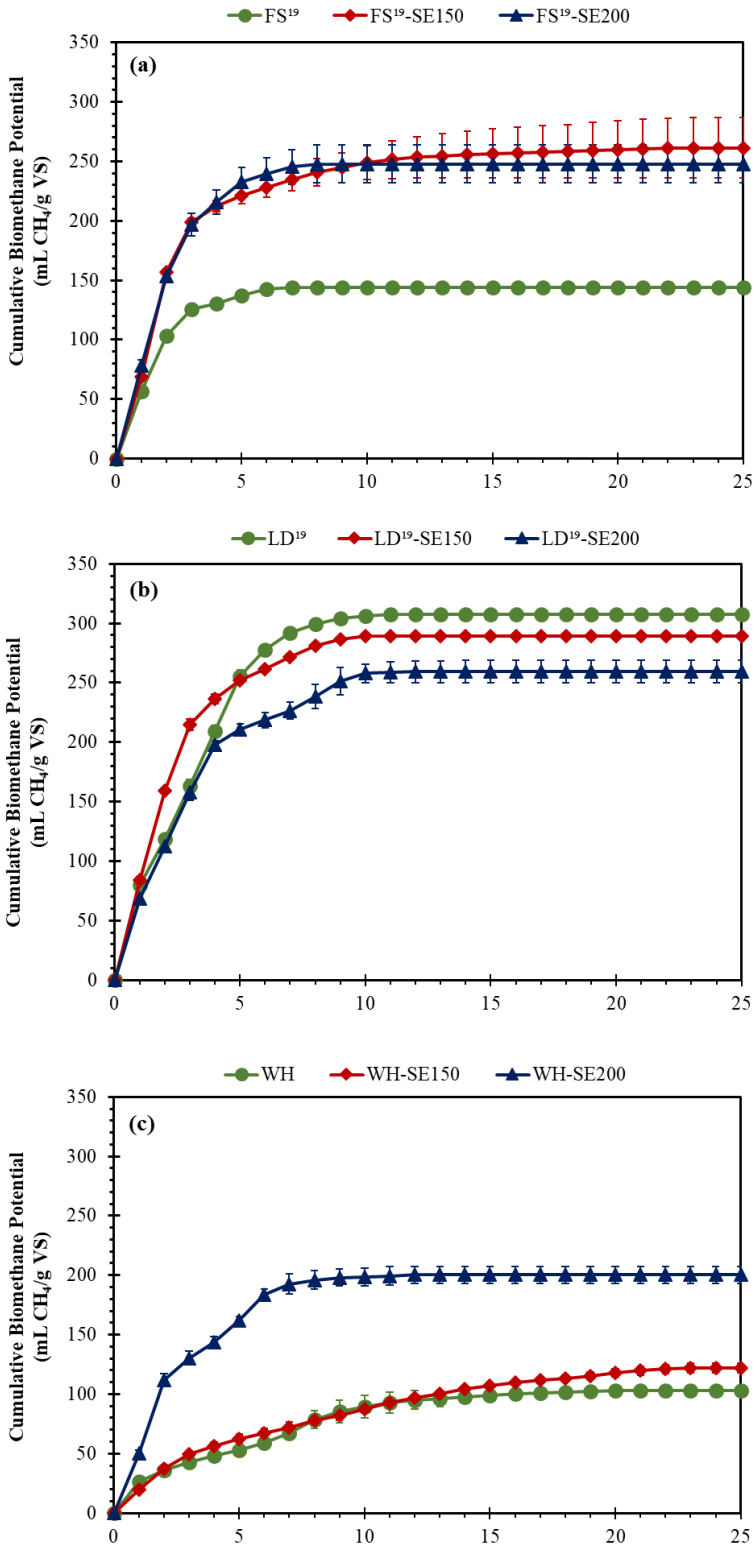

Figure 7.7. Experimental biomethane potential (BMP_{ex}) of untreated biomass and SE slurries for (a) FS^{19}, (b) LD^{19} and (c) WH. Data is presented as average values. Error bars represent the maximum and minimum values (n=2).

Table 7.9. Digestion kinetics from the anaerobic digestion of untreated biomass and SE slurries.

Sample	BMP_{ex}	Modified Gompertz Model				T_m	T^{80}
		H_m	R_m	λ	R^2		
	mL CH_4/g VS	mL CH_4/g VS	mL CH_4/g VS/d	(d)		(d)	(d)
FS^{19}	143.8	143.5	54.2	0.0	0.99	1.0	3
FS^{19}-SE150	261.3	254.3	70.5	0.0	0.98	1.3	4
FS^{19}-SE200	247.8	247.3	75.6	0.0	0.99	1.2	4
LD^{19}	307.6	308.8	58.6	0.0	0.99	1.9	5
LD^{19}-SE150	289.4	287.5	75.1	0.0	0.99	1.4	4
LD^{19}-SE200	259.5	257.9	52.2	0.0	0.99	1.8	5
WH	103.1	103.1	11.2	0.0	0.99	3.4	9
WH-SE150	121.9	118.9	10.8	0.0	0.97	4.1	13
WH-SE200	200.2	200.0	44.8	0.0	0.99	1.6	5

BMP_{ex}=experimental biomethane potential. H_m=maximum biomethane yield. R_m=peak biomethane production rate. λ=lag phase. T_m=peak time of fermentation. T^{80}=technical digestion time.

The digestion behaviours of WH-HTC slurries (Figure 7.1c) and WH-SE slurries (Figure 7.7c) are directly comparable, as the same source of WH was used across each experiment. The optimal HTC pre-treatment conditions for WH were 150°C, 60-min (SF=3.3); yielding a BMP_{ex} of 202.1 mL CH_4/g VS. The less severe reaction conditions of WH-SE150 (SF=2.6) generated a biomethane yield of 121.9 mL CH_4/g VS; suggesting these conditions are not severe enough to effectively hydrolyse the WH. WH-SE200 generated similar biomethane yields to WH-150 HTC slurry, despite the more severe reaction conditions (SF=4.1). However, WH-HTC200 slurry (SF=4.7) had a reduced biomethane yield, compared to WH-SE200 slurry. This suggests an optimal pre-treatment severity between a SF of 3.3-4.1. Alfageme *et al*. [115] investigated the effect of SE pre-treatment on the biomethane yields of WH, across a range of reaction severities. Optimal SE conditions of 170°C, 60-min (SF=3.8) were identified, improving the biomethane yields of WH by 33% [115]; which falls within the optimal range identified in this work (SF=3.3-4.1). Less severe SE conditions used by Alfageme *et al*. [115]: 120°C, 60-min (SF=2.4) gave a biomethane yield lower than untreated WH. Whilst more severe SE conditions 210°C, 10-min (SF=4.2) showed a 21% increase in

biomethane production; therefore, showing a reduced effectiveness compared to the more intermediate SE conditions of 170°C, 60-min (SF=3.8) [115]. Kist *et al*. [113] report optimal pre-treatment conditions of 170°C, 30-min (SF=3.5) showed the greatest improvement in biomethane generation from WH-slurries, using sequential thermal hydrolysis and SE. Again, this falls within the ideal SF range of 3.3–4.1. Therefore, results from this study and across literature conclude that a hydrothermal pre-treatment using moderate conditions pre-treatment allows for sufficient hydrolysis of the lignocellulosic matrix, whilst limiting formation of inhibitory compounds.

7.3.3 Biodegradability Index (BI)

The biodegradability index (BI) of the SE slurries and the untreated biomass are displayed in Figure 7.8. SE pre-treatment improves the biodegradability of FS^{19} from 29% to 53% (FS^{19}-SE150) or 51% (FS^{19}-SE200). Alternatively, SE pre-treatment reduced the BI of LD^{19} from 67% to 63% (LD^{19}-SE150) or 56% (LD^{19}-SE200). This suggests SE treatment at 150°C, 15-min provides the most effective conditions to improve the biomethane yields from FS^{19}. Whereas, untreated LD^{19} provided a higher biodegradability compared to SE-treated LD^{19}. WH-SE200 had a BI of 42%; greater than untreated WH (22%), or WH-SE150 (26%). The BIs shown in Figure 7.8c are directly comparable with the BIs derived from the AD of HTC-slurries, shown in Figure 7.2. The BI of the WH-HTC slurry generated at 150°C (42%) was the same as WH-SE200; suggesting similar pre-treatment effectiveness.

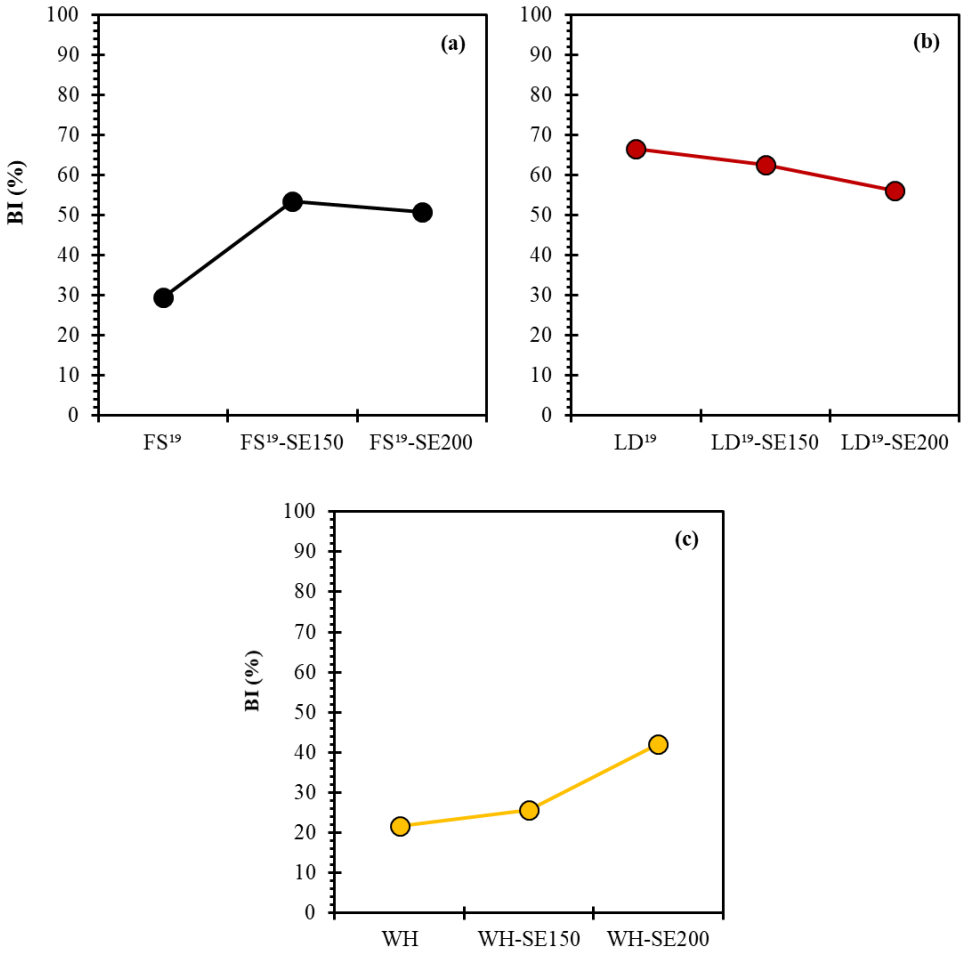

Figure 7.8. Biodegradability index of untreated biomass and SE slurries for (a) FS^{19}, (b) LD^{19}, and (c) WH.

7.3.4 Energy Balance

Similarly to HTC pre-treatment, the energy balance of SE was calculated, in order to compare the energetics of both hydrothermal pre-treatments and determine which is the most energetically feasible. The calculation of the energy input required for SE is more complex than for HTC, as wet or rehydrated biomass was added to the reactor, each with a slightly different moisture content. The moisture content of the as received FS^{19} was 76.2%, whilst the moisture content of LD^{19} was 87.2%. The WH biomass was initially dried to ease transportation. However, the WH was rehydrated to an approximate moisture content of 90%. The energy input for SE was initially calculated based on the combined energy required to heat the wet biomass from ambient temperature (25°C) to the treatment temperature (150°C or 200°C) as well as the energy required to generate the volume of steam to pressure the SE reactor, inclusive of 20% assumed vapour losses. However, this method does not account for the addition of water to the biomass. The energy output of the SE slurries is based on the

calorific value of the volume of biomethane produced during AD. Initially the energy balance was calculated according to the energy input required to heat 1-kg of wet biomass and the energy output obtained from the AD of the residual slurry. The results of this energy balance calculation are presented in Table 7.10.

Table 7.10. Energy balance for the application of SE as a pre-treatment for AD. Calculated based on a starting point of 1-kg wet biomass.

Sample	Energy Input (MJ)	Energy Output (MJ)	EROI	EROI[1]
FS[19]-SE150	0.42	1.44	3.43	7.62
FS[19]-SE150	0.95	1.32	1.39	3.09
LD[19]-SE150	0.61	1.30	2.13	4.74
LD[19]-SE150	1.22	0.96	0.79	1.75
WH-SE150	0.72	0.43	0.60	1.33
WH-SE200	1.38	0.63	0.46	1.01

[1]55% assumed energy recovery efficiency. EROI=energy returned upon energy invested.

Generally, Table 7.10 shows the SE macroalgal-slurries generated a higher energy output compared to the WH-SE slurries; due to higher BMP_{ex} yields (Figure 7.7). In addition, the EROI values were higher for SE reactions conducted at 150°C, compared to 200°C; especially for macroalgal-derived SE slurries. However, in order to compare these EROI values to the ones obtained for the AD of HTC slurries (Table 7.3), the energy input and output values needed to be corrected to a unit of MJ/kg dried biomass. The corrected energy balance values are presented in Table 7.11, alongside the energy balance for the AD of the untreated biomass. The energy input values shown in Table 7.11 are slightly different for each biomass, due to the differing moisture contents. The biomass with the highest moisture content; WH, displays the highest energy input values, as the specific heat capacity of water (4200 J/kg/K) is higher than biomass (1455 J/kg/K).

According to Table 7.11, SE pre-treatment improves the ECE of FS[19] from 31%, up to 51% (FS[19]-SE150), due to the improved biodegradability (Figure 7.8a). SE at 150°C also yields a positive energy balance, showing an EROI value of 4.76; assuming 55% energy recovery efficiency. The *F. serratus* sample: FS[19] has a comparable biochemical composition to FS (Chapter 4), due to similar harvesting locations and seasons. Table 7.3 showed HTC at 150°C was the most effective HTC pre-treatment temperature for FS. The energy output from HTC pre-treatment of FS at 150°C was 6.17 MJ/kg dry biomass; slightly higher than the energy output for SE pre-treatment of FS[19] at 150°C. However, the EROI value was more favourable

for SE (7.58), than HTC (2.81), assuming a 55% energy recovery efficiency. Therefore, suggesting SE may be a more energetically feasible pre-treatment technology for *F. serratus*, compared to HTC. Although, Table 7.11 also suggests that the ECE of LD[19]-SE150 (89%) was higher than untreated LD[19] (76%), despite Figure 7.7b and Figure 7.8b showing untreated LD[19] had higher BMP_{ex} yields and BI. Again, this highlights the difficulties in calculating the energy balance of SE.

Table 7.11. Energy balance and energy conversion efficiencies for the application of SE as a pre-treatment for AD. Calculated based on a starting point of 1-kg dry biomass.

Sample	Energy Input (MJ/kg dry biomass)	Energy Output (MJ/kg dry biomass)	ECE (%)	EROI	EROI[1]
FS[19]	-	3.63	31	-	-
FS[19]-SE150	1.77	6.04	51	3.41	7.58
FS[19]-SE200	3.99	5.56	47	1.39	3.10
LD[19]	-	8.74	76	-	-
LD[19]-SE150	4.77	10.18	89	2.13	4.74
LD[19]-SE200	9.53	7.51	66	0.79	1.75
WH	-	3.02	25	-	-
WH-SE150	7.21	4.28	35	0.59	1.32
WH-SE200	13.79	6.31	52	0.46	1.02

[1]55% assumed energy recovery efficiency. ECE=energy conversion efficiency. EROI=energy returned upon energy invested.

WH-SE200 showed a greater improvement in ECE of WH, compared to WH-SE150. Although, according to Table 7.11 the EROI of WH-SE150 was greater than WH-SE200. Interestingly, without any assumed energy recovery efficiency, the EROI values of both WH-derived SE slurries suggested an energy negative process. The energy output obtained from the AD of WH-HTC slurry generated at 150°C was 5.78 MJ/kg dry biomass (Table 7.3); lower than WH-SE200: 6.31 MJ/kg dry biomass. However, the EROI value were more favourable for HTC at 150°C (2.57), compared to SE at 200°C (1.02); assuming 55% recovered energy efficiency. Consequently, from an energetic perspective, HTC pre-treatment is more suitable for WH, compared to SE. Although, from a practical perspective, SE has the advantage of producing a slurry which is easier to pump and transport (Figure 7.6).

The calculation of the energy balance for SE presented in Table 7.11 is not able to fully incorporate heating efficiencies and energy recovery which would be experienced in a full-

scale SE unit. Despite this, using the energy balance values provided by Kobayashi *et al*. [221], SE of bamboo (234°C, 5-min) to improve biomethane yields, had an EROI value of 5.08; similar to FS^{19}-SE150. Therefore, suggesting SE is an energetically feasible process.

7.4 Two-stage Digestion of Water Hyacinth Following Hydrothermal Pre-treatment

The following section investigates the use of two-stage digestion to further enhance the ECE of WH. Two-stage digestions were conducted on untreated WH and pre-treated WH: HTC at 150°C, 60-min (WH-HTC150) and SE at 150°C, 15-min (WH-SE150). These pre-treatment conditions were selected for further investigation as they appear to be the most energetically feasible conditions, for each respective WH pre-treatment technology, according to the EROI values reported in Table 7.3 and Table 7.11. The BMP_{ex} yields, ECE and EROI values were subsequently compared to the one-stage AD values, presented earlier in this Chapter, to understand any potential benefits of two-stage digestion.

7.4.1 Biohydrogen Generation

The yields of biohydrogen generated from the DF of untreated WH, WH-HTC150 and WH-SE150 were measured over an incubation period of 5-days. However, biohydrogen generation ceased for all samples after 17-hours; therefore, only the yields of biohydrogen produced in the first 24-hour period are presented in Figure 7.9.

WH-HTC150 generated the highest biohydrogen yield of 16.1 mL H_2/g VS; higher than both untreated WH (9.9 mL H_2/g VS) or WH-SE150 (10.2 mL H_2/g VS), which generated similar BHP yields. Fermentative biohydrogen generation originates from pyruvate metabolism into acetate and butyrate [138] with up to 89% of the variability of biohydrogen production of feedstocks linked to the carbohydrate content of the feedstock [137]. The improved hydrogen production from WH-HTC150 could be linked to the increased total soluble sugar content, compared to WH-SE150. Chapter 5 showed the aqueous phase of WH-HTC150 had a total sugar concentration of 2.5 g/L, whilst the sugar content of the WH-SE150 aqueous phase ranged from 0.9-2.2 g/L, once corrected for the addition of excess water during SE. In addition, WH-HTC150 showed no detectable HMF or furfural, whereas GC-MS analysis recorded the presence of HMF or furfural in the WH-SE150 aqueous phase. These compounds have been previously reported to be inhibitory to DF [204–206].

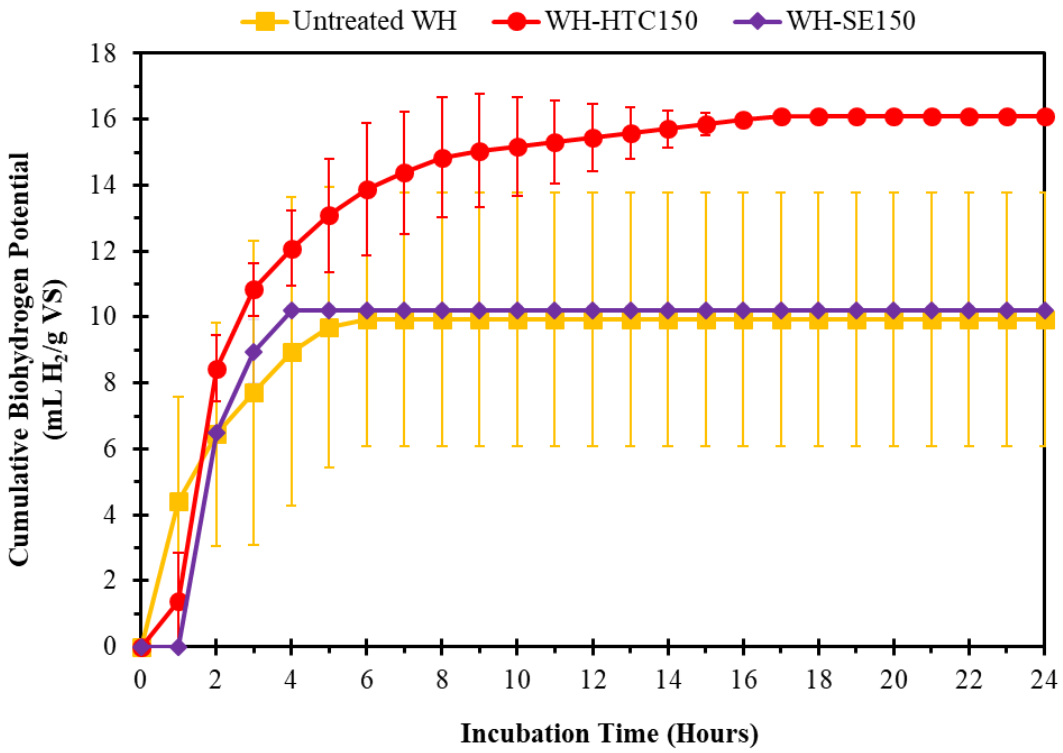

Figure 7.9. Biohydrogen potential of untreated WH, WH-HTC slurry (150°C) and WH-SE slurry (150°C). Data is presented as mean values ± one standard deviation (*n*=3).

The biohydrogen yield of the untreated WH in this study was 9.9 mL H_2/g VS. Chuang *et al*. [280] examined the generation of biohydrogen from a similar two-stage digestion of untreated WH. Using a value of 0.7825g VS/g dried WH, applied by [120] a biohydrogen yield of 4.5 H_2/g VS was found [280]. In comparison, a pre-treated WH yielded between 47.9-63.9 mL H_2/g VS using sequential microwave-heated alkali pre-treatment and enzymatic hydrolysis [120]. Additionally, Su *et al*. [281] compared a range of pre-treatments to enhance the biohydrogen yields from WH. The most effective pre-treatment was found to be using a combination of steam heating, microwave heating, alkali treatment and enzymatic hydrolysis; yielding 64.0-76.7 mL H_2/g VS. Therefore, both [120,281] showed a significantly higher biohydrogen yield from pre-treated WH compared to this study. This could be linked to varying initial biochemical composition of the initial WH sample. However, Su *et al.* [281] also investigated the impact of steam heating only (121°C , 15 min); finding a yield of 0.0-14.0 mL H_2/g VS. The greater hydrogen yield associated with sequential steam heating, microwave heating, alkali treatment and enzymatic hydrolysis is linked to the greater reducing sugar yield compared to steam heating alone. Therefore, hydrothermal treatment alone may not release sufficient concentrations of sugars to facilitate enhanced biohydrogen production, as additional pre-treatments; microwave, alkali and enzymatic hydrolysis are required to further destroy the recalcitrant lignocellulosic structure [281] and produce higher yields of reducing sugars. Therefore, pre-treated WH samples in this study generated similar

biohydrogen yields to [280], as hydrothermal treatment alone produces a lower reducing sugar yield [281].

The VFA contents of the DF effluents are displayed in Figure 7.10. Production of acetic and butyric acid during acidogenesis reactions yields 4-mol and 2-mol of hydrogen, respectively from 1-mol of glucose [138]. HTC-150 has the greatest total VFA, acetic acid and butyric acid content in the residual dark fermentation effluent, compared to untreated WH and SE-150; indicating an increased biohydrogen generation. The effluents produced from DF, across a 5-day period, contained solubilised metabolites (Figure 7.10), which can be readily digested and utilised by *Archaea* during methanogenesis. Residual VFAs can be used directly in conventional methanogenesis [72]. The synergistic benefits of biohydrogen production and generation of VFAs for methanogenesis could offer a greater energy recovery compared to methanogenesis alone [144].

7.4.2 Biomethane Generation

The comparative BMP_{ex} yields for one-stage and two-stage digestions of untreated WH, WH-HTC150 and WH-SE150 are presented in Figure 7.11. The values for one-stage digestion have been extracted from Figure 7.1c and Figure 7.7c. Unfortunately, due to time limitations, two-stage digestions were only conducted across a 14-day incubation time. However, this provides an indication of the effectiveness of two-stage digestion on the generation of biomethane.

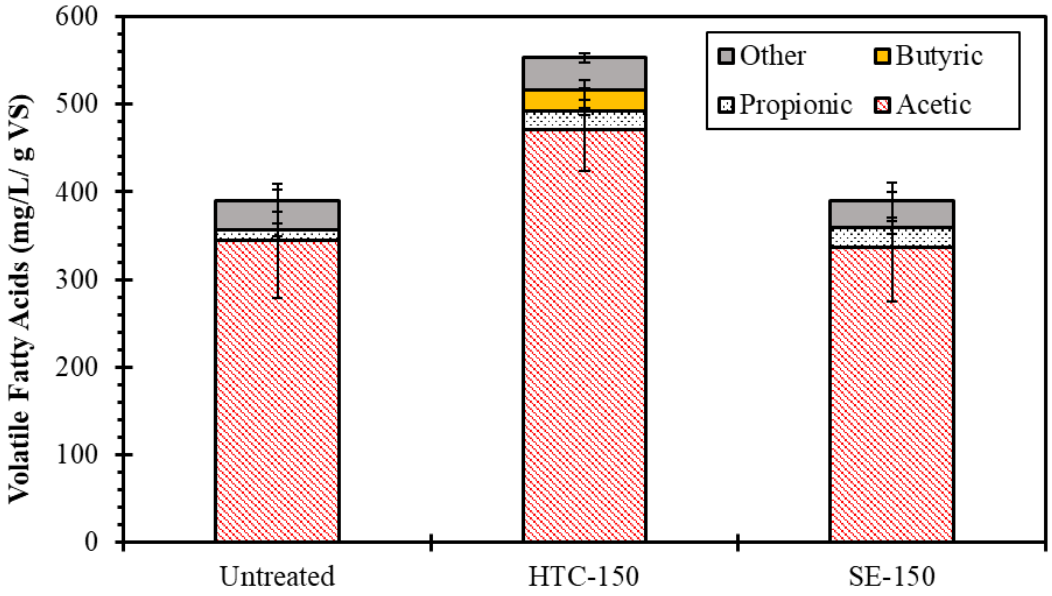

Figure 7.10. Solubilised volatile fatty acids in the dark fermentation effluent, after a 5-day digestion. Data is displayed as the average total concentration minus the average VFA concentration of the blank reactors. Data is presented as mean values ± one standard deviation (*n*=3).

The comparative biomethane yields obtained from untreated WH were similar across one-stage digestion (97.8 mL CH_4/g VS) and two-stage digestion (114.0 mL CH_4/g VS). WH-SE150 showed a higher biomethane generation during two-stage digestion (169.4 mL CH_4/g VS), compared to one-stage digestion (104.1 mL CH_4/g VS), after 14-days. Furthermore, WH-HTC150 also showed an increased biomethane yield during a two-stage (255.7 mL CH_4/g VS) digestion compared to a one-stage digestion (191.3 mL CH_4/g VS), after 14-days. Two-stage digestion of WH-HTC150 yielded the highest biomethane yield; representing a 161% increase in the biomethane yields compared to one-stage untreated WH and a 34% increase compared to one-stage WH-HTC150, after 14-days of digestion.

A previous study [120] reported a reduction in ECE for a two-stage digestion, compared to a one-stage digestion of microwave-heated alkali combined with enzymatic hydrolysis pre-treated WH. This was linked to the reduction of biomethane yields at similar pre-treatment conditions: 237.4 and 172.5 mL CH_4/g VS for one-stage and two-stage digestion respectively. This highlights the variation of gas yields than can be achieved for different pre-treatments, other studies have shown microwave-heated alkali combined with enzymatic hydrolysis pre-treatment are effective at enhancing biohydrogen yields [120,281]. However, the HTC-150 pre-treatment is more effective at enhancing biomethane yields; potentially due to the higher accumulation of VFAs shown in Figure 7.10, or through the enhancement of hydrolysis. Improving the production of biomethane from WH is recommended over biohydrogen production, due to improved yields and improved volumetric heating values [120].

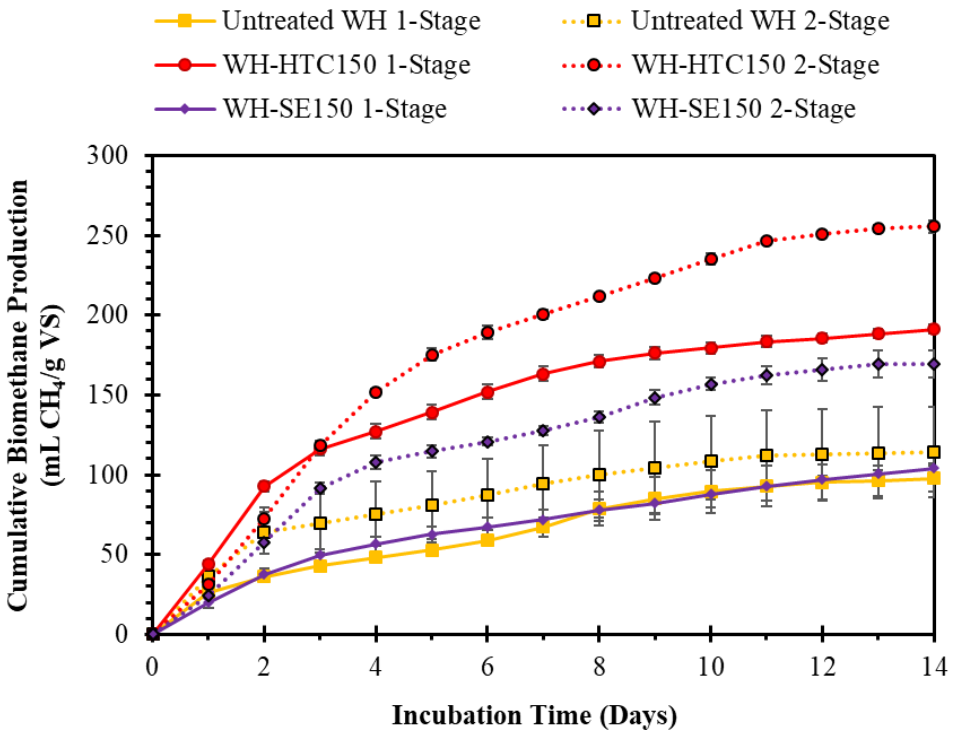

Figure 7.11. Comparative **e**xperimental biomethane potential (BMP_{ex}) of untreated WH, WH-HTC150 and WH-SE150 from one-stage and two-stage digestion. Data is presented as average values. Error bars represent the maximum and minimum values for one-stage digestions (*n*=2) and the standard deviation of two-stage digestions (*n*=3).

7.4.3 Energy Balance

The comparative energy balance of one-stage and two-stage digestion of untreated WH, WH-HTC150 and WH-SE150; alongside the BI and ECE of each sample are shown in Table 7.12. Two-stage digestion improved the BI and ECE of all samples. However, this improvement in BI and ECE was greater for hydrothermally pre-treated WH, compared to untreated WH; linked to the greater improvement in BMP_{ex} yields (Figure 7.11). Biohydrogen generation only contributed between 2-3% of the total energy outputs shown in Table 7.12. Again, suggesting hydrothermal treatments of WH should be directed towards enhancing biomethane yields.

Two-stage digestion, yields a greater EROI, compared to one-stage digestion for pre-treated WH. Table 7.12 shows the EROI from the two-stage digestion of WH-HTC150 and WH-SE150 were 37% and 65% higher than the corresponding EROI from the one-stage digestion of the same sample. Two-stage digestion of WH-HTC150 displayed the greatest conversion efficiencies (BI=54%, ECE=62%) and EROI value (3.32); suggesting this is the most energetically feasible pre-treatment method.

Table 7.12. Comparative energy balance and conversion efficiencies for one-stage and two-stage digestion of WH. Calculated based on a starting point of 1-kg oven dried biomass.

Sample	Energy Input (MJ/kg)	One-stage Digestion				Two-stage Digestion			
		Energy Output (MJ/kg)	EROI[1]	BI (%)	ECE (%)	Energy Output (MJ/kg)	EROI[1]	BI (%)	ECE (%)
Untreated WH	-	2.87	-	21	24	3.43	-	24	28
WH-HTC150	4.99	5.47	2.43	40	45	7.46	3.32	54	62
WH-SE150	7.21	3.66	1.13	22	30	6.06	1.87	36	50

[1]55% assumed energy recovery efficiency. EROI=energy returned upon energy invested. BI=biodegradability index. ECE=energy conversion efficiency.

The application of hydrothermal pre-treatment to enhance the digestion of WH is not only focussed upon the energetic feasibility of the process, but is also reliant on the infrastructure available in the countries applying this technology. In this study, WH was collected from Uganda. However, Uganda has limited capacity for energy intensive pre-treatments, such as; HTC and SE at 150°C, due to limited energy infrastructure. Table 7.12 shows hydrothermal pre-treatment processes (HTC and SE) are energetically feasible. However, the net energy balance could be further improved using an integrated solar-thermal biomass conversion technology. Green *et al*. [177] found a low temperature HTC (150-250°C) treatment is a suitable thermochemical conversion technology which can be heated by concentrated solar-thermal energy, for biomasses including WH in Uganda. Additionally, rural Ugandan areas may not have the capacity for establishing complex multi-stage digesters; such as sequential DF and AD. Therefore, these practical and socioeconomic factors must be considered during the potential scale-up of hydrothermal pre-treatment of WH.

7.5 Conclusions

The aim of this chapter was to investigate the use of hydrothermal pre-treatment to enhance the biodegradability of alternative, high ash feedstocks, during biological conversion processes. This included the comparison of the effectiveness of HTC and SE pre-treatments across both one-stage and two-stage digestion.

HTC reactions were conducted at 150°C, 60-min (SF=3.3), 200°C, 60-min (SF=4.7) and 250°C, 60-min (SF=6.2). All HTC pre-treatment conditions were shown to reduce the ECE of both SL and GR, compared to the AD of the respective untreated biomass. However, lower severity HTC pre-treatment (150°C) improved the ECE of FS from 35% to 58% and WH

from 25% to 48%. Highlighting differences in behaviour between different feedstock types (macroalgal and lignocellulosic biomass), as well as species (*S. latissima* and *F. serratus*). Generally, feedstocks with an initially lower biodegradability showed the greatest enhancement in ECE, following HTC pre-treatment. Lower severity HTC pre-treatment generally resulted in the production of higher biomethane yields, compared to more severe HTC conditions. This is likely due to the increased formation of inhibitory compounds and increasing recalcitrance of the solid fraction at the higher processing temperatures.

The separation of hydrochars for combustion and process waters for AD consistently provides a greater energy output, ECE and EROI, compared to AD of the HTC-slurry across all feedstocks and HTC processing temperatures. Although, typically higher HTC temperatures (200°C and 250°C) are required to effectively reduce the slagging and fouling potential of hydrochars, during combustion; which is associated with a higher energy input. As a result of this, the AD of FS-HTC slurry produced at 150°C can be considered a suitable HTC-AD integration options, as this displays an improved EROI compared to the separation of HTC products for application as separate energy vectors at 200°C and 250°C. Although, this does compromise the ECE of FS; which are greater during hydrochar and process water separation. AD of WH-HTC slurry generated at 150°C could also be considered a suitable HTC-AD integration option due to the improvement in ECE from 25% to 48% and the positive EROI value. In addition, WH-derived hydrochars showed no improvement in slagging and fouling propensity, therefore, the hydrochars would be less suitable for large-scale combustion.

The use of SE pre-treatment proved effective for improving the biodegradability of *F. serratus* (FS^{19}); with the less severe SE conditions: 150°C, 15-min (SF=2.6); reflecting the greatest increase in biomethane yields, compared to 200°C, 15-min (SF=4.1). The ECE of FS^{19} undergoing SE at 150°C (51%) was slightly lower than FS-HTC at 150°C (58%). Although, EROI values suggest SE is a more energetically feasible hydrothermal pre-treatment for FS^{19}. On the other hand, SE pre-treatment of *L. digitata* (LD^{19}) showed a reduced biodegradability, compared to the untreated LD^{19}; suggesting SE is not a suitable pre-treatment for this kelp species. Alternatively, the more severe SE reaction conditions (200°C, 15-min) reflected the greatest improvement in biomethane yields from WH, compared to SE at 150°C. The less severe SE conditions were not effective at hydrolysing the WH. HTC (150°C) and SE (150°C) pre-treatments both improved the ECE of WH from 25%, to 48% (HTC) and 52% (SE). Although, according to the EROI values, HTC was a more energetically feasible pre-treatment for WH, compared to SE; showing the inverse relationship found for *F. serratus.* Two-stage digestion can further improve the ECE of hydrothermally pre-treated WH, compared to one-stage digestion. This is because of the generation of higher biomethane yields; linked to enhanced hydrolysis of the WH. AD of WH-HTC150 slurry had the highest ECE after two-stage digestion (62%), compared to one-stage digestion (45%).

Chapter 8
Comparative HTC of Macroalgal Biomass Using Seawater or Freshwater as a Reactant Medium

The work conducted in previous chapters suggests the integration of HTC and AD can improve the ECE of biomass, compared to AD of the untreated feedstock. The separation of hydrochars for combustion and process waters for AD was identified as the integration strategy which provided the greatest improvement in ECE. However, throughout this thesis, the experiments have been conducted using oven dried biomass, in order to prolong sample storage and facilitate more accurate measurements during laboratory work. However, a significant advantage of the HTC is the inherent capacity to process feedstocks with a high moisture content [159,282], in which the energy-intensive pre-drying of biomass can be negated. Therefore, during the scale-up of HTC, it is likely feedstocks will be processed as received.

A further consideration to the HTC processing of seaweeds is the reactant medium used during the HTC process. Seaweeds are a marine-based biomass and are therefore, naturally surrounded by seawater. As a result, a suitable valorisation route could be to conduct HTC reactions of wet, or as received seaweeds using a seawater reactant medium. Using seawater in HTC would reduce the fresh water demand of the process, as currently less than 1% of the world's fresh water is accessible for human consumption [283]. In addition, using seawater to treat seaweeds provides logistical benefits; where the biomass and water source can both be harvested from the sea at the same time. This would negate the requirement for energy intensive biomass preservation and allow the development of localised HTC reactors, situated close to the sea. However, seawater is rich in alkali metals salts which may compromise the quality of hydrochar as a solid combustion fuel, or the suitability of the HTC process waters for AD. Only limited studies exist which uses seawater as a HTC reactant medium for the treatment of marine plastic waste [181] and *Ulva*: a green macroalgal biomass [182]. However, a comparison of product characteristics using both seawater and fresh water has not been conducted.

Therefore, this chapter investigates the effect of different HTC processing conditions on the integration of HTC and AD, using macroalgal biomass. This includes a comparison of treating freeze dried seaweed in distilled water (DIS) and treating wet, as received seaweed in seawater (SEA). HTC reactions were conducted at 150°C, 200°C and 250°C for two different types of seaweed, an inter-tidal kelp; *Laminaria digitata* (LD^{19}) and a sub-tidal wrack; *Fucus serratus* (FS^{19}). The effect of processing conditions on the properties of the hydrochars and process waters was assessed, alongside the impact on the ECE of the seaweeds.

8.1 Objectives

The objectives of this chapter are to:

- Compare the combustion properties of hydrochars produced from HTC using seawater and distilled water.
- Compare the digestion properties of process waters produced from HTC using seawater and distilled water.
- Assess the influence of reactant medium on the ECE of *F. serratus* and *L. digitata* during the integration of HTC and AD.

8.2 HTC Yields

8.2.1 Mass Yields

The mass yields of the hydrochars, process waters and gaseous phases for each seaweed HTC reaction are shown in Table 8.1. Hydrochar yield decreased with increasing HTC temperature; as reaction products become distributed between the process water and gaseous phase.

Table 8.1. Yields of products following HTC reactions.

Sample	Yield (wt%)		
	Hydrochar	**Process Water**	**Gas**
FS[19]SEA-150	40.9 ± 8.1	58.1 ± 8.0	1.0 ± 0.1
FS[19]SEA-200	33.3 ± 5.0	65.6 ± 4.7	1.1 ± 0.2
FS[19]SEA-250	21.9 ± 1.6	76.4 ± 1.6	1.7 ± 0.0
FS[19]DIS-150	40.9 ± 0.5	58.3 ± 0.8	0.7 ± 0.3
FS[19]DIS-200	34.0 ± 0.2	65.2 ± 0.5	0.9 ± 0.3
FS[19]DIS-250	28.7 ± 0.8	70.2 ± 1.1	1.1 ± 0.2
LD[19]SEA-150	68.5 ± 3.7	30.4 ± 3.7	1.1 ± 0.0
LD[19]SEA-200	53.7 ± 18.2	44.5 ± 18.4	1.8 ± 0.2
LD[19]SEA-250	35.9 ± 5.3	61.7 ± 4.6	2.4 ± 0.7
LD[19]DIS-150	27.2 ± 2.3	72.1 ± 2.4	0.7 ± 0.2
LD[19]DIS-200	25.1 ± 1.3	73.8 ± 1.4	1.1 ± 0.1
LD[19]DIS-250	18.4 ± 2.5	80.5 ± 2.7	1.2 ± 0.2

Data is presented as average ± standard deviation.

Both FS^{19}SEA and FS^{19}DIS hydrochar yields are generally comparable to the yields obtained from *F. serratus* (FS) in Chapter 5. FS and FS^{19} were both harvested from a similar location, during summer months; therefore, similar behaviour would be expected from both samples during HTC. The hydrochar yields generated by FS^{19}SEA and FS^{19}DIS were similar at HTC processing temperatures of 150°C (40.9%) and 200°C (33.3-34.0%). However, the hydrochar yield from FS^{19}DIS-250 (28.7%) was higher than FS^{19}SEA-250 (21.9%).

Alternatively, LD^{19}SEA and LD^{19}DIS hydrochar yields were different to those generated by *L. digitata* (LD) in Chapter 5. The hydrochar yields previously reported for LD were 40.4% (LD150), 30.3% (LD200) and 22.1% (LD250). HTC of LD^{19} in seawater (LD^{19}SEA) consistently produced higher hydrochar yields than LD, at comparable temperatures. While LD^{19}DIS consistently showed lower hydrochar yields than LD, at comparable HTC temperatures. LD^{19} was harvested during July 2019 and LD harvested during January 2009. The carbohydrate fraction of *L. digitata* is seasonally variable; peaking during the summer months [60]. As a result of this, LD^{19} is likely to contain a higher carbohydrate fraction, compared to LD. As previously mentioned, macroalgal-derived polysaccharides typically undergo hydrolysis between 140°C-160°C [69,72,243]. Therefore, enhanced hydrolysis of LD^{19} is expected, potentially resulting in reduced hydrochar yields. This is reflected in the results described by Smith and Ross [80] , who found *L. hyperborea* hydrochar yields were generally higher during autumn and winter months, compared to spring and summer. Additionally, Smith and Ross [80] found summer-harvested *L. digitata* produced hydrochar yields of 21.8% (200°C) and 18.4% (250°C); similar to LD^{19}DIS-200 and LD^{19}DIS-250, described in Table 8.1. Although, it is worth pointing out that the particle size differences between LD (<1mm) and LD^{19} (5-10cm) is likely to result in differences in the carbonisation process [180,250].

LD^{19}SEA consistently showed higher hydrochar yields, compared to LD^{19}DIS, at comparable HTC temperatures. Therefore, suggesting the salts within the seawater could be displaying a catalytic effect to increase hydrochar yield [179]. However, this trend is not observed by FS^{19}SEA and FS^{19}DIS; where the hydrochar yields are more comparable; highlighting potential interspecies differences.

A further observation from Table 8.1 is the yield standard deviations obtained from the HTC of as received seaweed (FS^{19}SEA and LD^{19}SEA) are higher than those obtained from the HTC of dried seaweed (FS^{19}DIS and LD^{19}DIS). This is particularly observed for LD^{19}SEA-200: showing a hydrochar yield of 53.7 ± 18.2% and a process water yield of 44.5 ± 18.5%; highlighting the inconsistencies of working with fresh, or wet biomass. Unfortunately, due to time and logistical constraints the LD^{19}SEA-200 HTC reactions could not be repeated. For

the sake of interest, subsequent data related to this sample has been included in this chapter; however, this must be interpreted with caution.

8.2.2 Carbon Distribution

The distribution of carbon between the hydrochar and process water from each seaweed HTC reaction is shown in Table 8.2. However, all LD^{19}SEA reactions and LD^{19}DIS-150 show a large overestimation of the carbon balance of the system. This is particularly prevalent with LD^{19}SEA-150, which calculates a 200% carbon yield; 124% of which is suggested to be concentrated in the process water fraction. Therefore, in order to overcome this overestimation, the normalised carbon distribution between the hydrochar and process water is displayed in Figure 8.1.

Table 8.2. Carbon distribution between hydrochars and process waters.

Sample	Carbon Yield (%)		
	Hydrochar	**Process Water**	**Total**
FS^{19}SEA-150	50	57	107
FS^{19}SEA-200	49	44	93
FS^{19}SEA-250	37	40	78
FS^{19}DIS-150	56	52	108
FS^{19}DIS-200	54	48	102
FS^{19}DIS-250	48	47	95
LD^{19}SEA-150	76	124	200
LD^{19}SEA-200	71	93	164
LD^{19}SEA-250	51	82	133
LD^{19}DIS-150	35	85	120
LD^{19}DIS-200	38	68	105
LD^{19}DIS-250	29	65	94

FS^{19} exhibits an almost even distribution of carbon between the hydrochar and process water, whether HTC was conducted using seawater (Figure 8.1a) or distilled water (Figure 8.1b). This is reflective of a similar carbon distribution found for *F. serratus* (FS) in Chapter 5. Alternatively, LD^{19} shows a higher distribution of carbon towards the process water fraction. LD^{19}SEA-150, LD^{19}SEA-200 and LD^{19}SEA-250 process waters had a normalised carbon distribution of 62%, 57% and 61%, respectively (Figure 8.1c). Whereas, LD^{19}DIS-150, LD^{19}DIS-200 and LD^{19}DIS-250 process waters had a normalised carbon distribution of 71%, 64% and 69%, respectively (Figure 8.1c). Therefore, a LD^{19}DIS had a greater carbon

distribution to the process water, compared to LD^{19}SEA; likely due to a higher process water yield (Table 8.1).

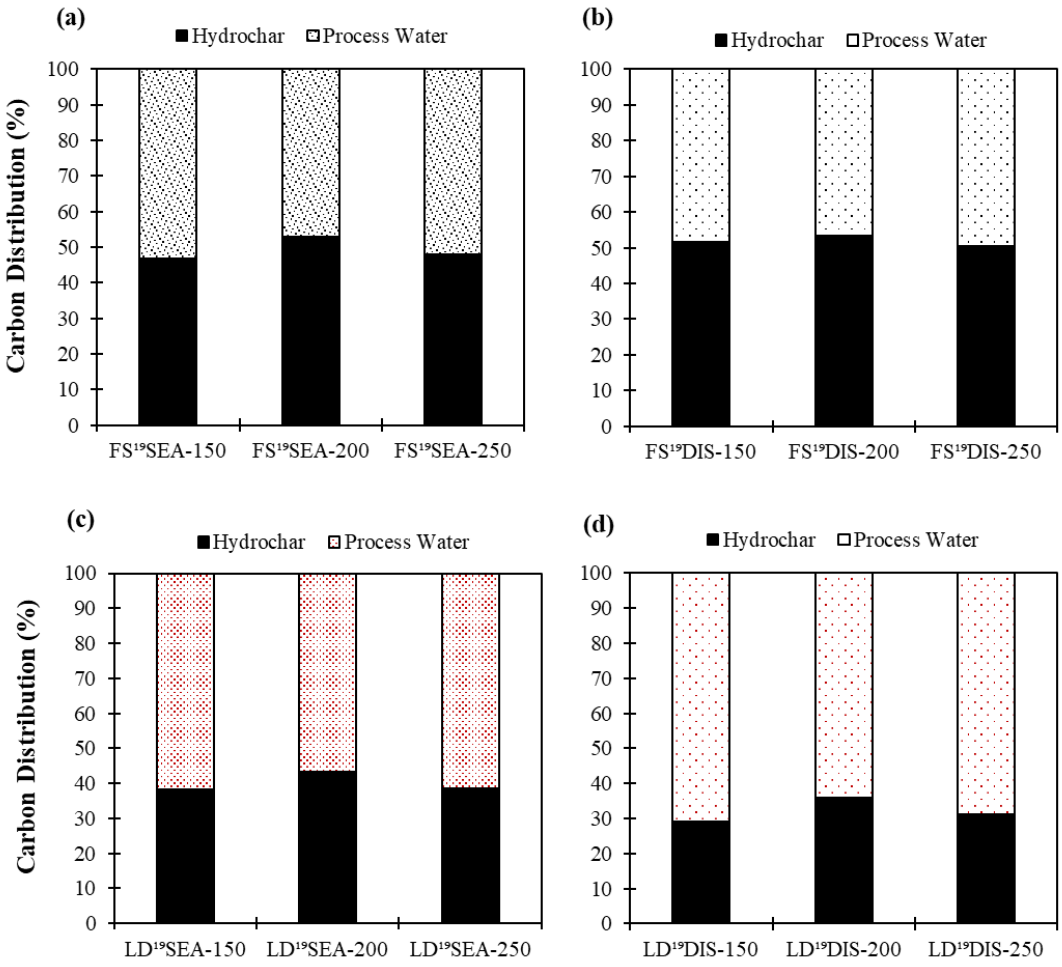

Figure 8.1. Normalised carbon distribution between hydrochars and process waters following the HTC of (a) FS^{19}SEA (b) FS^{19}DIS (c) LD^{19}SEA and (d) LD^{19}DIS. Gaseous phase is excluded from the carbon distribution.

8.3 Hydrochar Characteristics

Following HTC reactions, the hydrochar and process waters were separated for subsequent characterisation. Hydrochars were characterised in terms of proximate, ultimate and inorganic composition, as well as energy densification and ash behaviour, in order to assess their suitability as a solid combustion fuel.

8.3.1 Proximate and Ultimate Analysis

The proximate and ultimate analysis of the seaweed-derived hydrochars are presented in Table 8.3, alongside the composition of the untreated seaweeds. Following a similar trend to observations in Chapter 5, the C-content of hydrochars were consistently higher than the parent biomass, whilst the O-content of hydrochars are consistently lower than the parent biomass. Additionally, the C-content of hydrochars increased, whilst the O-content decreased, at higher HTC temperatures. This results in a general reduction in the H:C and O:C ratios, due to dehydration and decarboxylation reactions [64]. This is exemplified by the Van Krevelen diagram in Figure 8.2; which shows higher-temperature hydrochars becoming more 'coal-like' in their composition. Although, a slight increase in H:C was observed for FS^{19}-DIS and LD^{19}-SEA hydrochars between 200°C and 250°C.

Table 8.3. Proximate and ultimate composition of seaweeds and hydrochars.

Sample	Ultimate Analysis (wt% *db*)					Proximate Analysis (wt% *db*)		
	C	H	N	S	O*	VM	FC	Ash
FS^{19}	33.7 ± 0.2	4.2 ± 0.2	2.1 ± 0.0	1.6 ± 0.4	26.8 ± 0.0	77.0	9.8	13.2
FS^{19}SEA-150	41.0 ± 0.1	5.8 ± 0.2	2.5 ± 0.0	1.2 ± 0.1	21.7 ± 0.3	72.6	21.9	5.5
FS^{19}SEA-200	48.3 ± 0.1	6.0 ± 0.2	2.2 ± 0.0	1.2 ± 0.0	18.9 ± 0.1	66.4	28.2	5.5
FS^{19}SEA-250	55.1 ± 0.7	4.4 ± 2.3	2.4 ± 0.2	0.9 ± 1.3	15.5 ± 0.6	62.0	27.8	10.3
FS^{19}DIS-150	45.6 ± 0.3	3.4 ± 0.1	3.1 ± 0.0	1.1 ± 0.0	24.2 ± 0.3	80.2	13.8	6.0
FS^{19}DIS-200	52.4 ± 0.2	2.6 ± 1.1	2.9 ± 0.1	1.1 ± 0.0	21.3 ± 0.2	65.0	28.0	7.0
FS^{19}DIS-250	54.4 ± 0.0	4.1 ± 0.1	2.7 ± 0.1	1.3 ± 0.0	18.4 ± 0.4	61.9	28.5	9.6
LD^{19}	33.5 ± 0.1	4.4 ± 0.1	1.5 ± 0.1	0.8 ± 0.2	30.0 ± 0.0	81.0	9.4	9.6
LD^{19}SEA-150	36.9 ± 0.1	2.8 ± 1.5	2.1 ± 0.0	0.9 ± 0.1	27.4 ± 0.3	76.3	17.7	6.0
LD^{19}SEA-200	43.0 ± 0.0	2.5 ± 1.0	2.3 ± 0.0	1.4 ± 0.1	22.9 ± 0.1	69.3	22.6	8.1
LD^{19}SEA-250	46.2 ± 0.1	3.5 ± 0.5	2.4 ± 0.0	2.0 ± 0.1	20.0 ± 0.7	65.1	23.1	11.9
LD^{19}DIS-150	42.1 ± 0.1	3.8 ± 2.2	2.4 ± 0.1	ND	26.9 ± 0.3	77.0	18.9	5.1
LD^{19}DIS-200	48.8 ± 0.1	2.8 ± 0.1	2.5 ± 0.0	ND	23.6 ± 0.5	67.7	26.2	6.1
LD^{19}DIS-250	51.2 ± 0.2	2.9 ± 0.4	2.5 ± 0.0	ND	19.3 ± 0.7	64.6	25.8	9.7

VM=volatile matter. FC=fixed carbon. *db*=dry basis. ND=not detected.

Table 8.3 shows FS^{19}DIS-150 and FS^{19}DIS-200 had a higher C-content compared to FS^{19}SEA-150 and FS^{19}SEA-200, respectively. Although, an increase in HTC temperature to 250°C resulted in FS^{19}SEA-250 having a higher C-content (55.1%) than FS^{19}DIS-250 (54.4%). The O-content was consistently higher for FS^{19}DIS hydrochars, compared to FS^{19}SEA hydrochars, at comparable temperatures. The C-content of LD^{19}DIS hydrochars were consistently higher than LD^{19}SEA hydrochars. In addition, FS^{19}-derived hydrochars had lower O-contents compared to LD^{19}-derived hydrochars at comparable temperatures.

The N-content of all FS[19]-derived and LD[19]-derived hydrochars were higher, compared to their untreated parent seaweed. Generally, a higher N-content is observed in hydrochars produced from HTC in distilled water, compared to hydrochars produced in seawater. Again, this could result in higher NO_x emissions, during the combustion of hydrochars; however this requires further investigation. The higher S-content of LD[19]SEA-200 and LD[19]SEA-250 may also contribute to increased SO_x emissions, although using LD[19]DIS hydrochars appear to successfully remove the problematic S-fraction.

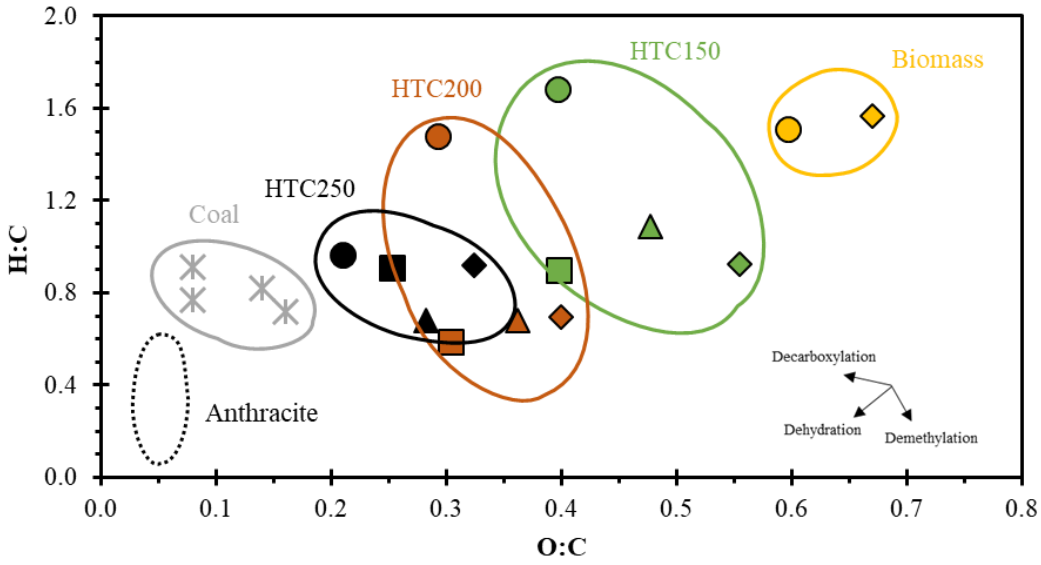

Figure 8.2. Van Krevelen diagram for seaweeds and resultant hydrochars. Coal values adapted from [165], anthracite zone adapted from [160]. H:C and O:C atomic ratios are presented on a dry ash free basis. ●= FS[19]SEA. ■= FS[19]DIS. ♦= LD[19]SEA. ▲= LD[19]DIS.

In a similar finding to Chapter 5; an increasing HTC temperature results in a general reduction of the VM-content, with a simultaneous increase in the FC-content (Table 8.3). The ash contents of FS[19]-derived hydrochars are lower than that observed in untreated FS[19]; although, an increase in ash is still observed between 200°C and 250°C. A similar trend was observed for LD[19]-derived hydrochars; however, LD[19]SEA-250 and LD[19]DIS-250 have a higher ash content than untreated LD[19]. Due to the presence of inorganics in the seawater, it would be expected that hydrochars generated using seawater would contain a higher ash content than hydrochars generated using distilled water. Table 8.3 shows this is true for LD[19]-derived hydrochars. However, FS[19]SEA-150 and FS[19]SEA-200 hydrochars have a lower ash content than FS[19]DIS-150 and FS[19]DIS-200 hydrochars; which could be linked to losses of volatile inorganics, such as alkali salts.

8.3.2 HHV and Energy Densification

The higher heating value (HHV), energy densification (ED) and energy yield (EY) of each of the hydrochars produced from FS^{19} and LD^{19} are shown in Table 8.4. HHV was calculated using Dulong's equation, using the O-content measured directly. The HHVs of all FS^{19}-derived hydrochars were greater than FS^{19}; with higher HHVs observed at higher HTC processing temperatures; due to increased C-contents and decreased O-contents (Table 8.3). The HHVs of FS^{19}SEA-150 (18.2 MJ/kg), FS^{19}SEA-200 (21.5 MJ/kg) and FS^{19}SEA-250 (22.2 MJ/kg) were higher than FS^{19} hydrochars produced using distilled water, at comparable temperatures: FS^{19}DIS-150 (16.0 MJ/kg), FS^{19}DIS-200 (17.6 MJ/kg) and FS^{19}DIS-250 (21.0 MJ/kg); due to a reduced O-content. However, despite FS^{19}SEA-250 having the highest HHV in Table 8.4, the EY (38.4%) is less than FS^{19}DIS-250 (47.6%), due to the greater hydrochar yield of FS^{19}DIS-250 (Table 8.1). Chapter 5 found the HHV of *F. serratus* hydrochars were 16.8 MJ/kg (FS150), 19.7 MJ/kg (FS200) and 21.5 MJ/kg (FS250), and therefore display similar HHVs to FS^{19}DIS-hydrochars than FS^{19}SEA-hydrochars.

Table 8.4. Higher heating value (HHV), energy densification (ED) and energy yield (EY) of seaweed hydrochars.

Sample	HHV (MJ/kg) *db*	ED	EY (%)
FS^{19}	12.6	-	-
FS^{19}SEA-150	18.2	1.44	58.9
FS^{19}SEA-200	21.5	1.70	56.6
FS^{19}SEA-250	22.2	1.75	38.4
FS^{19}DIS-150	16.0	1.26	51.7
FS^{19}DIS-200	17.6	1.39	47.3
FS^{19}DIS-250	21.0	1.66	47.6
LD^{19}	12.2	-	-
LD^{19}SEA-150	11.7	0.95	65.3
LD^{19}SEA-200	14.0	1.14	61.4
LD^{19}SEA-250	17.1	1.40	50.3
LD^{19}DIS-150	14.9	1.22	33.2
LD^{19}DIS-200	16.2	1.33	33.4
LD^{19}DIS-250	18.0	1.47	27.1

db=dry basis.

LD[19]-derived hydrochars show consistently lower HHVs than FS[19]-derived hydrochars. Reflecting similar conclusions discussed in Chapter 5, where hydrochars produced from wracks (*F. serratus*) have higher HHVs compared to kelps (*L. digitata*). Contradictory to FS[19], Table 8.4 shows the HHVs of LD[19]-SEA derived hydrochars are lower than LD[19]-DIS derived hydrochars. In fact, LD[19]SEA-150 had a lower HHV (11.7 MJ/kg) compared to LD[19] (12.2 MJ/kg); resulting in an ED of 0.95. Despite this, the EY of LD[19]SEA hydrochars (50.3-65.3%) were higher than LD[19]DIS hydrochars (27.1-33.2%) or FS[19]-derived hydrochars. The reason for this was the higher hydrochar yields from LD[19]SEA; shown in Table 8.1. Chapter 5 reported the HHVs of a winter-harvested *L. digitata* sample: 14.4 MJ/kg (LD150), 16.3 MJ/kg (LD200) and 18.5 MJ/kg (LD250); consistent with the HHVs of LD[19]DIS-derived hydrochars shown in Table 8.4.

Therefore, Table 8.4 suggests the presence of seawater as a reactant medium can improve the HHV of *F. serratus* hydrochars, but decrease the HHV of *L. digitata* hydrochars. The salinity of seawater is typically 3.5 wt% [183]. Table 8.5 displays the average concentrations of the most abundant elements present in seawater. Cl and Na represent the highest concentration of inorganics in seawater; likely in the form of NaCl. Xu *et al*. [284] found the addition of NaCl during the HTC of sewage sludge facilitated hydrolysis; enhancing solubilisation into the process water. Although, there was little influence on the HHV of sewage sludge. NaCl has been reported to facilitate the depolymerisation and solubilisation of cellulose [285] due to interactions between the Cl- and the glucose intermolecular hydrogen bonds. Although $CaCl_2$ has been shown to increase the energy density of lignocellulosic-derived hydrochars [249], this effect has not been reported for macroalgal-derived hydrochars.

Table 8.5. Typical composition of the major elements in seawater, according to [183]**.**

Element	Concentration (ppm)
Chlorine	19,500
Sodium	10,770
Magnesium	1,290
Sulphur	905
Calcium	412
Potassium	380

8.3.3 Inorganic Composition

The inorganic composition of the seaweed-derived hydrochars are shown in Table 8.6, with the resultant inorganic removal efficiencies shown in Table 8.7; accounting for the reductions in hydrochar yields. As mentioned in previous chapters, high concentrations of alkali metals (Na and K) and Cl leads to problematic slagging, fouling and corrosion issues during the thermal conversion of biomass. However, HTC also possesses the capability to selectively remove these problematic inorganics [64,74,80], especially at higher HTC processing temperatures. The major inorganic components of both FS^{19} and LD^{19} are Na, Cl and K; suggesting problematic ash behaviour during seaweed combustion.

FS^{19}DIS-derived hydrochars all show a reduced concentration of Na, Cl and K compared to untreated FS^{19} (Table 8.6). Additionally, the concentrations of Na, Cl and K reduced as the temperature of HTC increases. This is reflected in Table 8.7, which shows the removal efficiencies of Na, K and Cl all increase at higher HTC temperatures: FS^{19}DIS-150 (Na=77%, K=70%, Cl=76%), FS^{19}DIS-200 (Na=85%, K=80%, Cl=84%) and FS^{19}DIS-250 (Na=87%, K=86%, Cl=85%). However, the Na and Cl concentrations are higher for FS^{19}SEA-150 (Na=4.8%, Cl=7.8%) and FS^{19}SEA-200 (Na=4.9%, Cl=9.0%), compared to FS^{19} (Na=4.1%, Cl=6.6%). This is likely because of the higher concentrations of Na and Cl associated with the seawater (Table 8.5). As a result of this, Table 8.7 shows the removal efficiencies of Na and Cl in FS^{19}SEA-150 (Na=52%, Cl=51%) and FS^{19}SEA-200 (Na=60%, Cl=54%) were lower than those observed for FS^{19}DIS-150 and FS^{19}DIS-200, respectively. Although, once the HTC temperature reaches 250°C, Table 8.6 shows FS^{19}SEA-250 has a lower Na (2.6%) and Cl (4.9%) concentration, compared to FS^{19} (Na=4.1%, Cl=6.6%). Therefore, FS^{19}SEA-250 and FS^{19}DIS-250 display similar Na and Cl removal efficiencies (Table 8.7). Interestingly, seawater contains relatively low concentrations of K, compared to Na and Cl (Table 8.5). FS^{19}SEA-derived hydrochars contain lower concentrations of K compared to FS^{19}DIS-derived hydrochars, across comparable HTC temperatures (Table 8.6); resulting in higher K-removal efficiencies across FS^{19}SEA-derived hydrochars.

Table 8.7 shows the Na and Cl removal efficiencies are also lower for LD^{19}SEA-hydrochars, compared to LD^{19}DIS-hydrochars; again due to the high concentrations of Na and Cl in the seawater being incorporated into the hydrochars. Unlike FS^{19}SEA-250, the Na and Cl removal efficiency of LD^{19}SEA-250 (66-68%) remains lower than any LD^{19}DIS-derived hydrochar (82-91%). The K removal efficiency is also lower for LD^{19}SEA-hydrochars, compared to LD^{19}DIS-hydrochars, despite similar K concentrations in the hydrochars (Table 8.6).

Table 8.6. Inorganic composition of seaweed hydrochars.

Sample	Inorganic content (% feedstock *db*)						
	Na	Mg	P	Cl	K	Ca	Fe
FS[19]	4.1	0.8	0.2	6.6	3.9	1.8	0.1
FS[19]SEA-150	4.8	0.8	0.1	7.8	2.0	1.1	0.0
FS[19]SEA-200	4.9	1.0	0.1	9.0	2.2	1.0	0.0
FS[19]SEA-250	2.6	1.5	0.3	4.9	1.1	2.3	0.1
FS[19]DIS-150	2.3	0.6	0.2	3.8	2.9	1.4	0.1
FS[19]DIS-200	1.8	0.5	0.4	3.2	2.3	1.7	0.1
FS[19]DIS-250	1.8	1.1	0.5	3.2	2.1	1.9	0.1
LD[19]	3.6	0.7	0.1	6.1	3.1	1.0	0.0
LD[19]SEA-150	5.3	0.9	0.1	6.7	1.9	1.2	0.0
LD[19]SEA-200	4.2	0.9	0.2	6.0	2.2	1.5	0.0
LD[19]SEA-250	3.5	1.1	0.4	5.3	1.8	2.4	0.1
LD[19]DIS-150	2.4	0.6	0.2	4.0	2.1	1.2	0.0
LD[19]DIS-200	2.0	0.5	0.4	3.5	1.7	1.3	0.0
LD[19]DIS-250	1.8	1.1	0.8	3.1	1.7	2.3	0.0

Table 8.7. Removal efficiencies of individual inorganic species from seaweed hydrochars, compared to the original biomass.

Sample	Inorganic Removal Efficiency (%)						
	Na	Mg	P	Cl	K	Ca	Fe
FS[19]	-	-	-	-	-	-	-
FS[19]SEA-150	52	53	76	51	79	74	74
FS[19]SEA-200	60	61	86	54	81	82	68
FS[19]SEA-250	86	62	64	84	94	72	69
FS[19]DIS-150	77	72	62	76	70	69	40
FS[19]DIS-200	85	78	23	84	80	69	45
FS[19]DIS-250	87	62	20	86	85	70	52
LD[19]	-	-	-	-	-	-	-
LD[19]SEA-150	-1	14	24	24	60	15	25
LD[19]SEA-200	38	34	20	47	62	16	12
LD[19]SEA-250	66	42	-6	68	80	12	-40
LD[19]DIS-150	82	79	49	82	82	67	50
LD[19]DIS-200	86	81	28	86	87	66	57
LD[19]DIS-250	91	71	-16	91	90	56	63

8.3.3.1 Slagging and Fouling Propensities

The tendencies of the seaweeds and seaweed hydrochars to cause slagging and fouling issues can be predicted using the indices shown in Table 8.8. These predictive indices are calculated using the inorganic oxide content of the biomass; determined by modifying the values in Table 8.6. Table 8.8 shows the AI, Rb/a, SI and SVI indices predict high or certain slagging and fouling inclinations for all seaweeds and hydrochars; regardless of whether HTC was conducted using seawater or distilled water. This is a consequence of high concentrations of alkali metals across all samples. The only suggested improvement in ash behaviour is predicted by the FI for FS^{19}SEA-250 and LD^{19}DIS-250.

Table 8.8. Slagging and fouling indices for seaweed and resultant hydrochars.

Sample	Slagging and Fouling Index					
	AI	BAI	$R\frac{b}{a}$	SI	FI	SVI
FS^{19}	8.11	0.01	27.1	41.8	277.8	8.7
FS^{19}SEA-150	4.88	0.00	40.7	49.2	361.2	5.9
FS^{19}SEA-200	4.31	0.01	34.1	47.7	315.4	7.0
FS^{19}SEA-250	2.17	0.02	7.2	12.0	34.5	18.5
FS^{19}DIS-150	4.10	0.01	18.8	19.7	122.8	10.6
FS^{19}DIS-200	2.94	0.02	14.9	16.8	76.8	10.0
FS^{19}DIS-250	2.35	0.02	9.0	10.1	44.2	16.3
LD^{19}	7.09	0.00	68.7	57.2	595.2	4.6
LD^{19}SEA-150	8.07	0.00	97.5	85.0	917.1	3.1
LD^{19}SEA-200	5.96	0.00	47.5	57.9	395.3	4.8
LD^{19}SEA-250	3.99	0.01	12.9	20.9	87.8	12.3
LD^{19}DIS-150	3.89	0.01	40.8	27.5	236.1	5.3
LD^{19}DIS-200	2.88	0.01	35.6	23.4	166.9	5.7
LD^{19}DIS-250	2.44	0.01	9.1	8.8	40.0	16.3

However, as highlighted in Chapter 5, these predictive slagging and fouling indices must be interpreted with caution, because they are empirically designed for characterising coal samples, rather than biomass [74]. Therefore, ash fusion tests were conducted on the seaweed and seaweed hydrochar ashes in order to further understand their propensity to cause slagging issues. The temperatures at which each transitional stage of ash behaviour occurs is displayed in Figure 8.3; with higher temperatures representing a reduced slagging potential. The furnace

used to conduct the ash fusion tests had a temperature limit of 1550°C; therefore, any transitional change beyond this temperature cannot be determined.

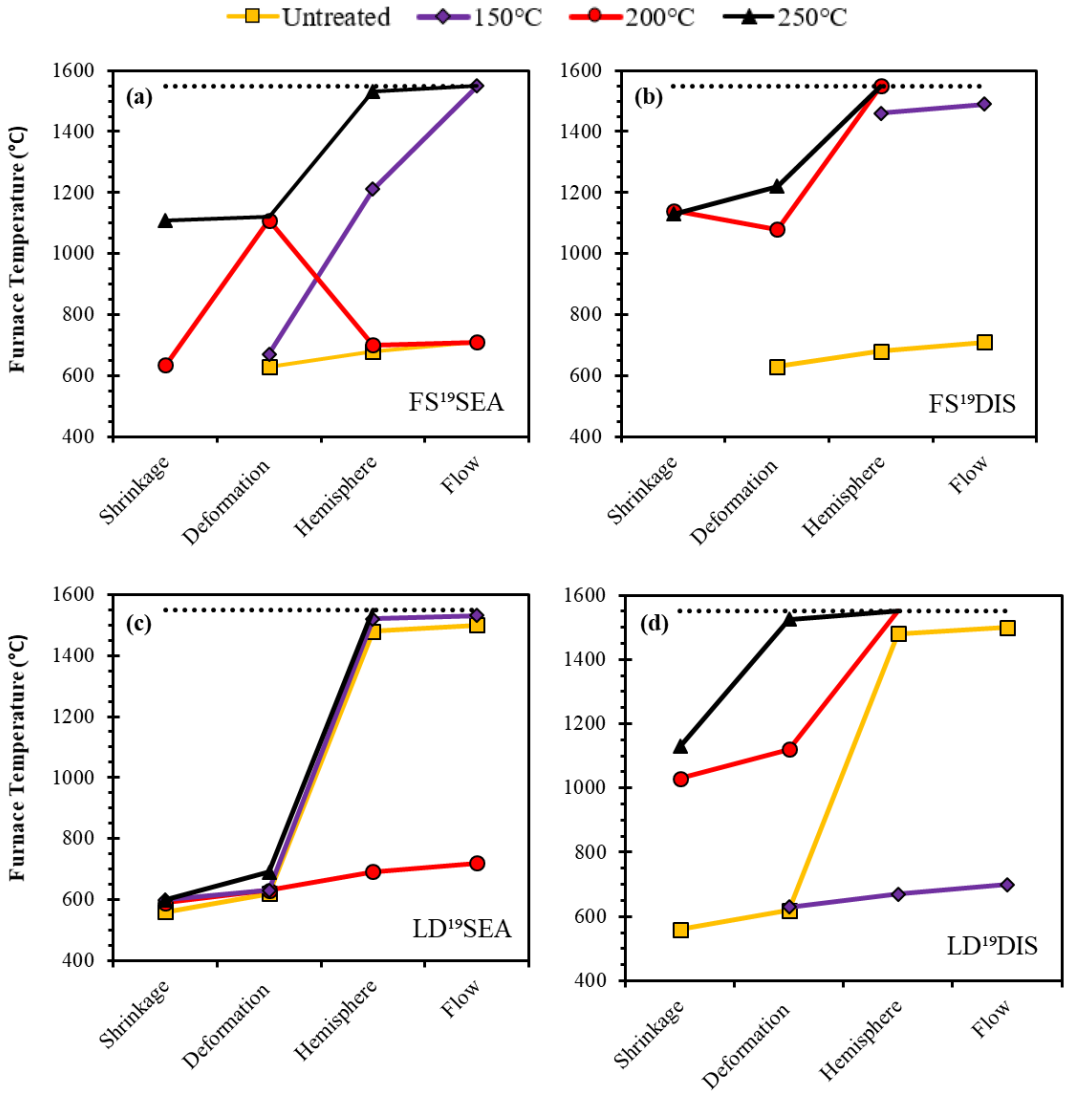

Figure 8.3. Ash fusion transition temperatures of untreated seaweeds and hydrochars for (a) FS[19]SEA (b) FS[19]DIS (c) LD[19]SEA and (d) LD[19]DIS. The dotted line depicts the furnace temperature limit (1550°C).

Untreated FS[19] ash undergoes deformation, hemisphere and flow at relatively low temperatures; 630°C, 680°C and 710°C, respectively (Figure 8.3). These values are similar to the values obtained for *F. serratus* (FS) in Chapter 5, and indicate a high slagging potential. Figure 8.3a displays the temperatures of the different transitional stages for FS[19]SEA-derived hydrochar ashes. FS[19]SEA-150 displayed higher hemisphere (1210°C) and flow (1550°C) temperatures compared to FS[19]; although the deformation temperature (670°C) was comparable to FS[19]. Deformation is the point where the ash becomes sticky and likely to begin

coating the surfaces within a furnace [64]. On the other hand, FS^{19}SEA200 exhibits a higher deformation temperature (1110°C) than FS^{19}; but the flow temperature (710°C) occurred at a comparable temperature to FS^{19}, suggesting limited improvement in ash behaviour. It is worth mentioning some of the seaweed derived ashes did not undergo the ash deformation stages in the normal sequential order. For example, the deformation temperature was higher than the flow temperature for FS^{19}SEA200; highlighting the complexities of working with biomass ash. Table 8.6 shows FS^{19}SEA200 had Na, K and Cl concentrations which were higher than FS^{19}SEA150 or FS^{19}SEA250; perhaps explaining the reduction in flow temperature. Ultimately, FS^{19}SEA250 showed the greatest improvement in ash behaviour in Figure 8.3; with an higher deformation (1120°C), hemisphere (1530°C) and flow (>1550°C) compared to FS^{19}. Table 8.7 shows FS^{19}SEA250 had the greatest removal of Na, K and Cl of any FS^{19}SEA-derived hydrochars.

Figure 8.3b shows FS^{19}DIS-250 demonstrates the greatest improvement in ash behaviour, compared to FS^{19} or lower-temperature FS^{19}-DIS-derived hydrochars. The deformation temperature of FS^{19}DIS-250 was: 1220°C and both the hemisphere and flow temperatures were >1550°C. Again, this is due to the significant removal of alkali metals and chlorine (90-91%), compared to the FS^{19} (Table 8.7). Both FS^{19}DIS-200 and FS^{19}DIS-250 showed higher deformation, hemisphere and flow temperatures compared to FS^{19}SEA-200 and FS^{19}DIS-250, respectively. Therefore, suggesting the introduction of seawater increased the slagging potential of FS^{19}-derived hydrochars, through the introduction of NaCl. This is reflected in Table 8.6, where FS^{19}-SEA hydrochars show a consistently higher Na or Cl concentration, compared to FS^{19}-DIS hydrochars, generated at comparable temperatures.

LD^{19} has a comparable deformation temperature (620°C) to FS^{19} (Figure 8.3). However, the hemisphere (1480°C) and flow (1500°C) are much higher than FS^{19}. Chapter 5 found the flow temperature of *L. digitata* (LD) to be low: 720°C. The high alkali metal content of LD^{19} (Table 8.6) means it is unlikely this seaweed would display a low slagging propensity [65,80]. Therefore, suggesting seaweed ashes may not always behave as expected during an ash fusion test; similar to the observations of *S. latissima*, observed in Chapter 5.

LD^{19}SEA-250 was the only hydrochar in Figure 8.3c to show an improvement in ash behaviour compared to LD^{19}; with both the hemisphere and flow temperature being above the furnace limit. LD^{19}SEA-150 displayed deformation, hemisphere and flow temperatures of: 360°C, 1520°C and 1530°C, respectively; all similar to LD^{19}, indicating no significant reduction in slagging propensity. LD^{19}SEA-200 displayed an increased slagging tendency compared to LD^{19}, with decreased hemisphere (690°C) and flow temperatures (720°C). This reflects a similar conclusion to Figure 8.3, where the hydrochar generated in seawater at

200°C had an increased slagging propensity, compared to hydrochars produced in seawater at both 150°C and 250°C.

Both LD[19]DIS-200 and LD[19]DIS-250 showed improved ash behaviour compared to LD[19]SEA-200 and LD[19]SEA-250, respectively. The temperatures of LD[19]DIS-200 deformation (1120°C) and flow (>1150°C) were higher than LD[19]SEA-200: 690°C (deformation) and 720°C (flow). Again, suggesting the introduction of seawater increases the risk of slagging, through the introduction of NaCl (Table 8.6). Although, Figure 8.3d shows the deformation, hemisphere and flow temperatures of LD[19]DIS-150 are: 630°C, 690°C and 720°C, respectively. All lower than LD[19] or LD[19]SEA-150.

Overall, Figure 8.3 suggests conducting HTC using seawater is likely to increase the slagging propensity of hydrochars, compared to using a distilled water medium; due to the introduction of NaCl. Although, higher HTC temperatures (250°C) provide the most effective reduction in hydrochar slagging tendencies, compared to the parent seaweeds.

8.4 Process Water Characterisation

Following separation from the hydrochars, the process waters were characterised in order to understand how the feedstock, HTC temperature and presence of seawater or distilled water affected the process water composition. Subsequently, the biochemical methane potential of the process waters was determined, in order to assess their suitability of an AD feedstock.

8.4.1 Process Water Composition

The COD concentration of each HTC process water is shown in Figure 8.4. The COD concentrations of FS[19]DIS150, FS[19]DIS200 and FS[19]DIS250 process waters were: 39.2 g/L, 34.7 g/L and 35.1 g/L. Therefore, showing a slight decline in COD concentration between 150°C and 200°C, although remaining constant between 200°C and 250°C. These results are generally comparable with the COD concentrations of *F. serratus*, determined in Chapter 5: 41.4 g/L (FS150), 37.1 g/L (FS200) and 35.2 g/L (FS250). FS[19]SEA-process waters display a slightly reduced COD concentration compared to FS[19]DIS-process waters, at higher HTC processing temperatures (200°C and 250°C). The COD concentrations of FS[19]SEA150, FS[19]SEA200 and FS[19]SEA250 process waters were: 39.9 g/L, 30.6 g/L and 28.7 g/L.

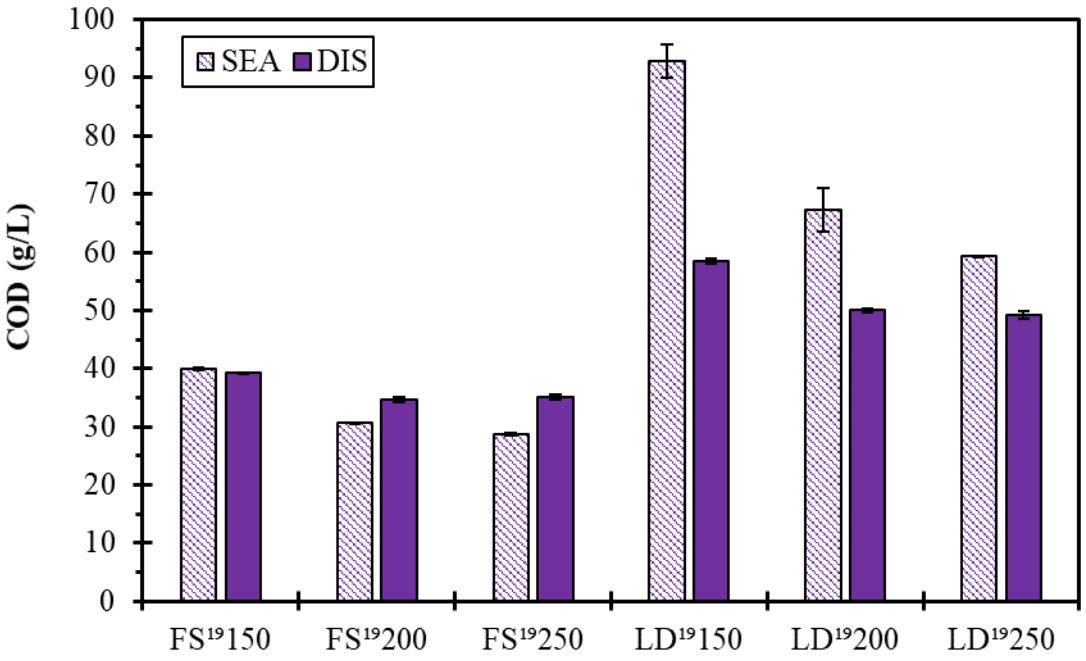

Figure 8.4. Chemical oxygen demand (COD) concentrations of seaweed HTC process waters.

Figure 8.4 shows LD[19]DIS-derived process waters have a higher COD concentration than FS[19]DIS-derived process waters. The COD concentrations of LD[19]DIS150, LD[19]DIS200 and LD[19]DIS250 process waters was: 58.4 g/L, 50.0 g/L and 49.3 g/L. Therefore, again a decline in COD is observed between 150°C and 200°C. The COD concentrations of LD[19]DIS-derived process waters are higher than those determined from *L. digitata* in Chapter 5: 35.7 g/L (LD150), 36.6 g/L (LD200) and 34.6 g/L (LD250). This is potentially linked to LD[19] being harvested in the summer, which is likely to contain a higher carbohydrate fraction than the winter-harvested LD [60]. Therefore, LD[19] has a greater availability of polysaccharides to undergo hydrolysis and subsequent solubilisation into the process water.

LD[19]SEA-derived process waters display the highest COD values of 92.9 g/L (LD[19]SEA-150), 67.3 g/L (LD[19]SEA-200) and 59.3 g/L (LD[19]SEA-150). Therefore, contrasting effects are observed between FS[19] and LD[19], when converted using HTC using a seawater medium. Seawater has no effect on the COD of FS[19]-derived process waters, whilst an increase in COD concentration is observed LD[19]-derived process waters, when conducting HTC with seawater.

The COD concentration of LD[19]SEA-150 is much higher than is observed in HTC process waters from other feedstocks, including: orange pomace [163], cow manure [84], digestates [171], lignocellulosic biomass [190] and microalgae [160]. Although, Wang *et al*. [179] reported *Laminaria* HTC process concentrations between 23 g/L to 185 g/L; of which the increase was related to the recirculation of process water back into HTC reactor 12 times. Initially, the high COD value of LD[19]SEA-150 indicates some form of overestimation. As

previously mentioned, the COD can be overestimated due to the presence of chlorides (BS 6068-2.34:1988) [253]. In the case of the LCK014 HACH cuvettes, Cl concentrations of >5g/L can cause high-bias results. Table 8.5 shows seawater alone contains approximately 19.5 g/L Cl and Table 8.7 shows that during HTC, Cl is removed from the seaweeds and solubilised into the process water; further increasing the Cl concentration; a trend also observed by [181]. However, each HTC process water was pre-diluted, prior to COD analysis, using 1-in-10 dilution with distilled water. The dilution was conducted for two reasons; to dilute the COD concentrations to within the detectable limits of the HACH cuvette and to reduce the Cl concentration, to prevent interference. In order to confirm that a 1-in-10 dilution prevents the overestimation of COD concentration, undiluted seawater was analysed using the LCK014 HACH cuvette kits, yielding a result of 11.3 ± 1.0 g COD/L; above the limit of the cuvette kit (10 g COD/L). However, the same seawater, diluted 1-in-10 with distilled water resulted in a concentration of 0.0 ± 0.0 g/L; confirming the dilution eliminates Cl-related overestimation. Interestingly, Table 8.6 shows the Cl concentration of FS^{19} (6.6%) is higher than LD^{19} (6.1%) and Table 8.7 suggests a higher Cl-removal efficiency for FS^{19}SEA-derived hydrochars, compared to LD^{19}SEA-derived hydrochars. Therefore, it can be assume the FS^{19}SEA-process waters contain a higher Cl concentration than LD^{19}SEA-process waters. However, the COD concentrations remain lower (Figure 8.4); suggesting Cl concentration does not cause COD overestimation, in this situation.

The TOC concentrations of each seaweed HTC process water is displayed in Figure 8.5. The trends associated with process water TOC concentrations mirror the trends observed for COD concentrations; shown in Figure 8.4. Interestingly, the TOC concentration represents between 39-43% of the COD concentrations; representing a similar proportion that was observed in Chapter 5.

LD^{19}SEA-derived process waters showed the highest TOC concentrations: 38.0 g/L (LD^{19}SEA-150), 28.3 g/L (LD^{19}SEA-150) and 24.6 g/L (LD^{19}SEA-150). However, these high COD and TOC values creates discrepancies between the yield data reported in Table 8.1. The high LD^{19}-SEA hydrochar yields suggest a significant proportion of the biomass is distributed towards the solid phase. Conversely, high TOC concentrations indicate a significant proportion of the biomass is solubilised within the process water. This disparity is the reason why the total carbon balance distribution, described in Table 8.2 is greater than 100% for LD^{19}SEA-150 (200%), LD^{19}SEA-200 (164%) and LD^{19}SEA-250 (133%).

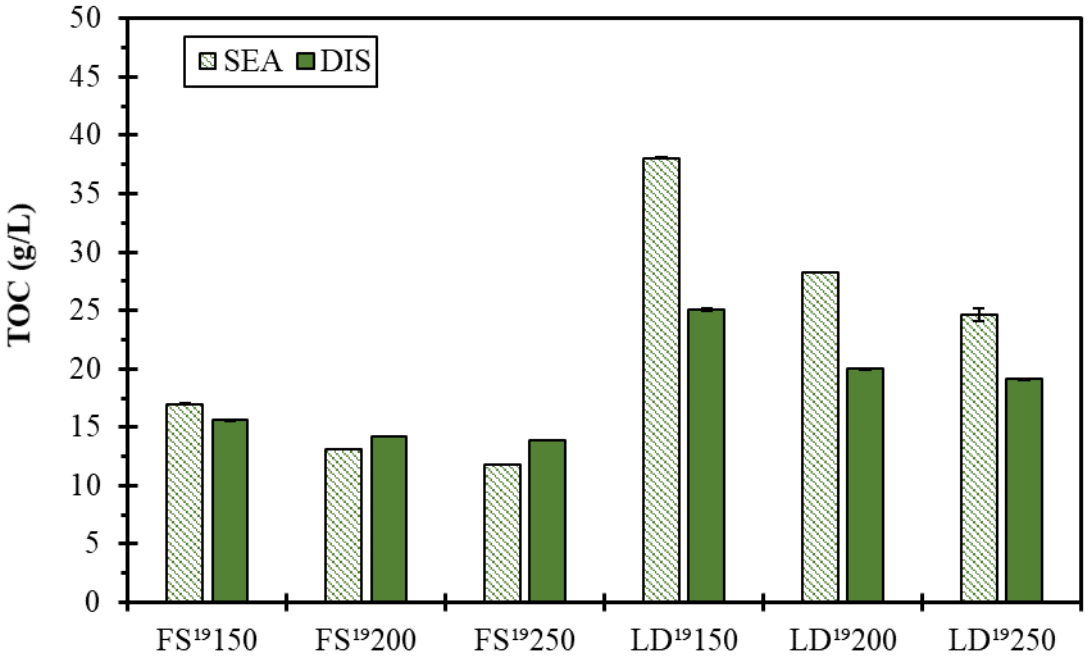

Figure 8.5. Total organic carbon (TOC) concentrations of seaweed HTC process waters.

The disagreement between the mass distributions of LD[19]SEA-HTC reactions continues into Table 8.9; which displays the TS, VS and ash concentrations of the process waters; where drying was conducted at 60°C and ashing at 550°C. Table 8.9 shows the VS concentrations of LD[19]SEA process waters were consistently higher than LD[19]DIS process waters; suggesting the reactions conducted in seawater show an enhanced hydrolysis of organic matter to the process water phase. The typical C-content of seawater is typically 28 ppm; present in the form of carbonates and CO_2 [183]; therefore the solubilised organics present in the seawater are not expected to significantly contribute to the VS fraction of LD[19]SEA process waters. Overall, it is clear the mass distribution of LD[19]SEA-HTC reactions is overestimated; however it remains unclear as to the cause of the overestimation.

Table 8.9 shows FS[19]SEA process waters have a slightly increased VS concentration, compared to FS[19]DIS process waters. Again, suggesting the seawater enhances the solubilisation of biomass into the process water, echoing conclusions presented by [284]. Sensibly, the ash concentrations of FS[19]SEA process waters were higher than corresponding FS[19]DIS process waters, due to the presence of inorganics within the seawater. However, interestingly the ash content, as a proportion of TS was much higher in FS[19]-derived process waters, compared to LD[19]-derived process waters. The highest ash concentration was observed for FS[19]SEA-250; where the ash fraction represented 61.6% of the overall total solids.

Table 8.9. Proximate composition of seaweed HTC process waters.

Sample	TS	VS	Ash	Ash
		(g/L)		(%TS)
FS[19]SEA-150	76.5 ± 0.3	39.2 ± 0.2	37.3 ± 0.4	48.8
FS[19]SEA-200	59.9 ± 0.1	24.3 ± 0.4	35.6 ± 0.4	59.4
FS[19]SEA-250	53.1 ± 0.6	20.4 ± 0.4	32.7 ± 0.7	61.6
FS[19]DIS-150	52.9 ± 0.1	33.6 ± 0.2	19.3 ± 0.2	36.5
FS[19]DIS-200	44.8 ± 0.6	26.5 ± 0.1	18.3 ± 0.6	40.8
FS[19]DIS-250	41.9 ± 0.9	24.9 ± 0.5	17.0 ± 1.0	40.6
LD[19]SEA-150	110.1 ± 0.6	80.2 ± 0.1	29.9 ± 0.6	27.2
LD[19]SEA-200	84.2 ± 0.2	54.8 ± 0.2	29.4 ± 0.3	34.9
LD[19]SEA-250	74.0 ± 0.0	47.1 ± 0.1	26.9 ± 0.1	36.4
LD[19]DIS-150	60.7 ± 0.5	45.8 ± 0.6	14.9 ± 0.8	24.5
LD[19]DIS-200	53.9 ± 0.4	40.5 ± 0.4	13.4 ± 0.6	24.9
LD[19]DIS-250	51.2 ± 0.3	36.7 ± 0.3	14.5 ± 0.4	28.3

TS=total solids. VS=volatile solids.

The work conducted in Chapter 5 revealed that the composition of process water changes across different HTC temperatures. Table 8.10 shows the composition of each seaweed HTC process water, across the three processing temperatures. As before, lower temperature process waters (150°C) had a lower VFA concentration, compared to higher temperature process waters (200°C and 250°C). A similar trend is generally observed for the TN concentrations. Higher temperature process waters are also associated with the increased formation of inhibitory NH_4^+-N and phenols. Unusually, LD[19]-derived process waters have higher phenol concentrations than FS[19]-derived process waters, despite *F. serratus* containing a higher polyphenol content than *L. digitata* [128]. Although, this was also observed in Chapter 5. Overall, Table 8.10 reveals that although higher temperature process waters show enhanced VFA solubilisation, this is compromised through the increased presence of inhibitory compounds.

The use of seawater as a reactant medium appears to facilitate the hydrolysis of the seaweeds; with Table 8.10 showing increased VFA concentrations for SEA-derived process waters, compared to DIS-derived process waters. Although, there appears to be no real trend towards the solubilisation of TN, NH_4^+-N and phenols.

Table 8.10. Seaweed HTC process water composition.

Sample	Total VFAs (mg/L)	TN (mg/L)	NH_4^+-N (mg/L)	NH_4^+-N (%TN)	Total Phenol (mg/L)	pH
FS^{19}SEA-150	333 ± 15	561 ± 16	80 ± 2	14	142 ± 10	4.3
FS^{19}SEA-200	1458 ± 277	672 ± 25	175 ± 2	26	171 ± 2	4.2
FS^{19}SEA-250	2136 ± 30	662 ± 62	251 ± 1	38	236 ± 8	6.3
FS^{19}DIS-150	681 ± 4	593 ± 9	106 ± 1	18	144 ± 4	4.8
FS^{19}DIS-200	1512 ± 348	753 ± 14	200 ± 2	26	224 ± 5	4.8
FS^{19}DIS-250	1394 ± 166	763 ± 4	273 ± 6	36	289 ± 6	6.6
LD^{19}SEA-150	772 ± 121	839 ± 9	93 ± 1	11	299 ± 1	4.2
LD^{19}SEA-200	1074 ± 541	949 ± 16	138 ± 1	15	374 ± 24	4.4
LD^{19}SEA-250	2256 ± 53	836 ± 0	222 ± 0	27	390 ± 8	6.4
LD^{19}DIS-150	934 ± 43	731 ± 4	109 ± 2	15	286 ± 1	4.6
LD^{19}DIS-200	1465 ± 106	562 ± 93	78 ± 2	14	298 ± 3	4.3
LD^{19}DIS-250	1659 ± 11	674 ± 34	182 ± 1	27	331 ± 1	6.5

VFA=volatile fatty acid. TN=total nitrogen.

8.4.2 Biomethane Potential

As identified across previous chapters, the separation of hydrochars for combustion and process waters for AD appears the most suitable HTC-AD integration strategy to maximise the ECE of macroalgal biomass. Consequently, the BMP_{ex} of the seaweed HTC process waters was determined in order to identify differences between seawater-derived process waters and distilled-water derived process waters. The BMP_{ex} yields of FS^{19}SEA and FS^{19}DIS process waters are shown in Figure 8.6a and Figure 8.6b. Whereas, the BMP_{ex} yields of LD^{19}SEA and LD^{19}DIS process waters are shown in Figure 8.7a and Figure 8.7b. The final BMP_{ex} yields and digestion kinetics of each HTC process water are described in Table 8.11.

Figure 8.6a shows the BMP_{ex} of FS^{19}SEA-150 (200.0 mL CH_4/g COD) was higher than FS^{19}SEA-200 (174.8 mL CH_4/g COD) or FS^{19}SEA-250 (168.4 mL CH_4/g COD). Therefore, reflecting the conclusions of Chapter 6, in which the lower-temperature process waters generated a higher BMP_{ex} than higher-temperature process waters. However, Figure 8.6b shows the BMP_{ex} of FS^{19}DIS process waters were similar: 227.0 mL CH_4/g COD (FS^{19}DIS-150), 216.2 mL CH_4/g COD (FS^{19}DIS-200) and 232.8 mL CH_4/g COD (FS^{19}DIS-250). This builds on an observation seen in Chapter 6; where macroalgal-derived process waters showed a lesser reduction in BMP_{ex} between low temperature (150°C) and high temperature (200°C and 250°C) process waters, compared to lignocellulosic biomass. However, Figure 8.6b

suggests that, in some instances, the BMP_{ex} yields of seaweed-derived process waters is unaffected by HTC temperature, despite the increased concentrations of inhibitory NH_4^+-N and phenols (Table 8.10). This observation is not normally observed in literature; with BMP_{ex} yields of process waters typically reducing at higher HTC temperatures [84,160,163,209]. Therefore, suggesting the degradation products from the biochemical products of seaweeds are not as inhibitory as other biomass sources.

Overall, the BMP_{ex} yields obtained from $FS^{19}SEA$ process waters are lower than $FS^{19}DIS$ process waters, at corresponding temperatures. In addition, Table 8.11 shows more favourable digestion kinetics for $FS^{19}DIS$ process waters, compared to $FS^{19}SEA$ process waters; displaying consistently higher R_m and consistently lower T_m and T^{80} values. Table 8.10 shows the concentrations of inhibitory NH_4^+-N and phenols are relatively similar between $FS^{19}SEA$ and $FS^{19}DIS$ process waters. Therefore, indicating an inhibitory effect from the increased presence of inorganics in the seawater. High concentrations of salinity within *L. digitata* have been shown to reduce biomethane yields [67]. Although, the high levels of salts within the seawater were not present at a level to completely inhibit the process; as Figure 8.6b shows $FS^{19}SEA$-process waters still generate sufficient yields of biomethane. This result is backed up by Wang *et al*. [179], who investigated the generation of biomethane from *Laminaria* HTC process waters, following various repetitions of process water circulation. After zero recirculations, the process water had a salinity of 15.8%, which increased to 153.3% after 12 recirculations; due to an increased solubilisation of inorganic matter into the process water, similarly described in Table 8.7. Despite the higher salinity of the recirculated process waters, similar or higher biomethane yields were obtained, compared to the process water with no recirculations. Therefore, suggesting high salinity process waters can generate sufficient yields of biomethane during AD.

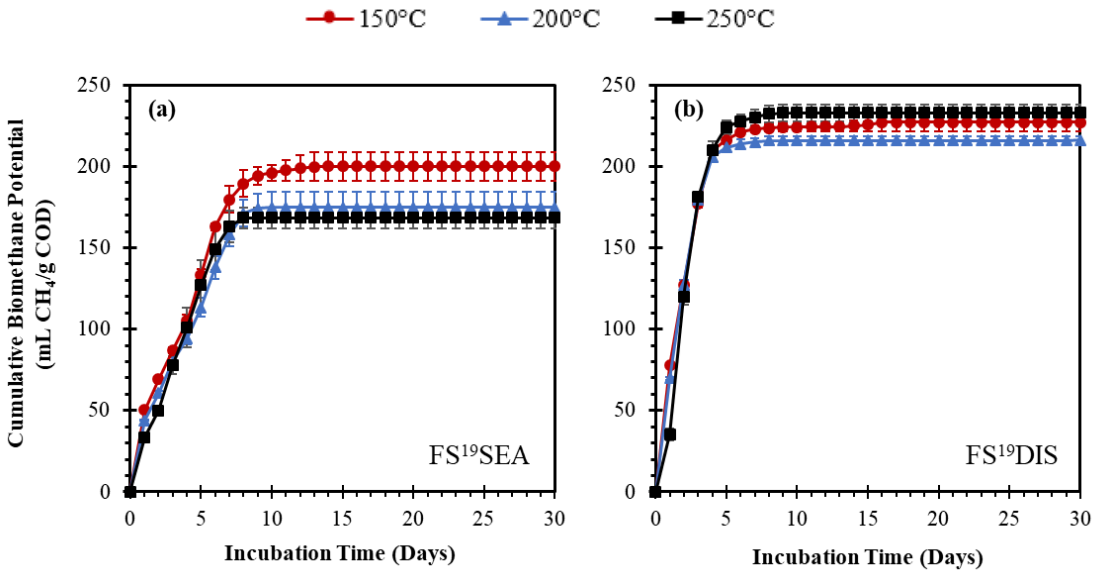

Figure 8.6. Experimental biomethane potential (BMP_{ex}) of HTC process waters from (a) $FS^{19}SEA$ (b) $FS^{19}DIS$. Data is presented as average values. Error bars represent the maximum and minimum values (*n*=2).

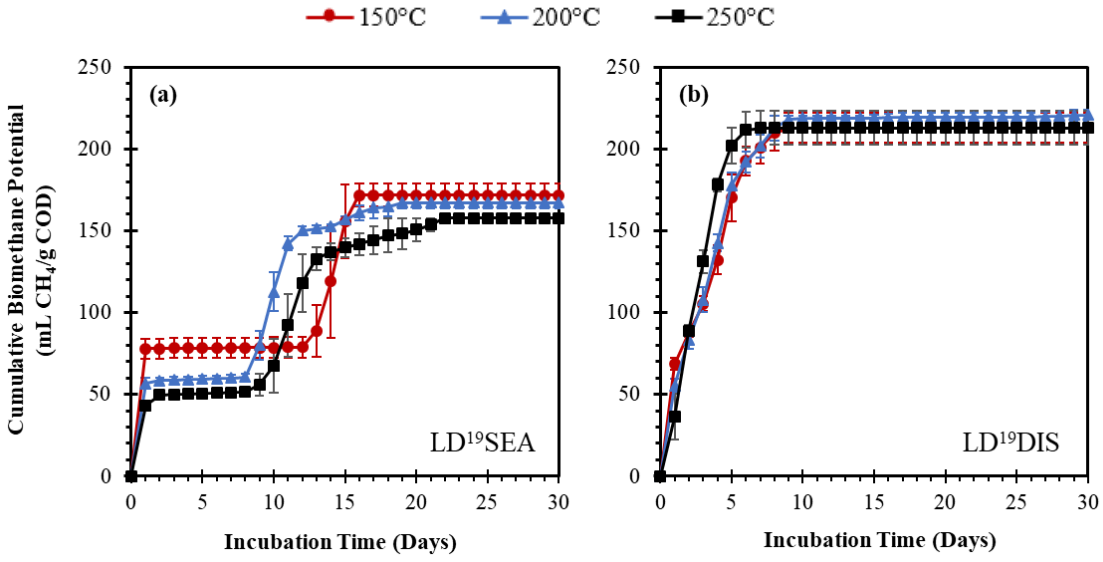

Figure 8.7. Experimental biomethane potential (BMP_{ex}) of HTC process waters from (a) $LD^{19}SEA$ (b) $LD^{19}DIS$. Data is presented as average values. Error bars represent the maximum and minimum values (*n*=2).

Table 8.11. Digestion kinetics from the anaerobic digestion of seaweed HTC process waters.

Sample	BMP_{ex}	Modified Gompertz Model				T_m	T^{80}
		H_m	R_m	λ			
	mL CH_4/g COD	mL CH_4/g COD	mL CH_4/g COD /d	(d)	R^2	(d)	(d)
$FS^{19}SEA$-150	200.0	201.3	30.4	0.0	0.99	2.4	6
$FS^{19}SEA$-200	174.8	176.4	26.9	0.0	0.99	2.4	7
$FS^{19}SEA$-250	168.4	170.0	31.4	0.4	0.99	2.4	6
$FS^{19}DIS$-150	227.0	226.2	68.2	0.0	0.99	1.2	4
$FS^{19}DIS$-200	216.2	216.1	72.0	0.1	0.99	1.2	3
$FS^{19}DIS$-250	232.8	232.6	85.3	0.6	0.99	1.6	4
$LD^{19}SEA$-150	171.8	189.0	10.1	0.0	0.83	6.9	15
$LD^{19}SEA$-200	167.0	175.6	12.0	0.0	0.92	5.4	11
$LD^{19}SEA$-250	157.8	171.4	9.3	0.0	0.94	6.8	13
$LD^{19}DIS$-150	212.6	213.7	39.1	0.0	0.99	2.0	5
$LD^{19}DIS$-200	220.5	220.3	39.5	0.0	0.99	2.1	5
$LD^{19}DIS$-250	212.8	213.5	59.7	0.5	0.99	1.9	4

BMP_{ex}=experimental biomethane potential. H_m=maximum biomethane yield. R_m=peak biomethane production rate. λ=lag phase. T_m=peak time of fermentation. T^{80}=technical digestion time.

Figure 8.7a shows the BMP_{ex} yields of $LD^{19}SEA$-150, $LD^{19}SEA$-200 and $LD^{19}SEA$-250 are 171.8 mL CH_4/g COD, 167.0 mL CH_4/g COD and 157.8 mL CH_4/g COD, respectively. Again, showing the lower temperature process water (150°C) generated the highest BMP_{ex} yield. Although, each of the process waters shown in Figure 8.7a displays an initial lag period between Day 1 and Day 8-12. This lag periods is similar to that observed in Chapter 6 for the *L. digitata* process water LD200. Interestingly LD200 process water had an ash content of 28.2 g/L (Chapter 5); the highest of the seaweed-derived process waters investigated in Chapter 5. This ash content is similar to $LD^{19}SEA$ process waters, but lower than $LD^{19}DIS$ process waters. Although Table 8.9 shows $FS^{19}SEA$ process waters contain an even higher concentration of ash. Therefore, perhaps there is some interaction between degradation products from *L. digitata* which become more inhibitory under high-ash conditions. However,

at this point this is a speculatory assumption, with a greater understanding of HTC reaction pathways from macroalgal biomass required to confirm this suggestion.

The BMP_{ex} values for LD^{19}DIS-derived process waters are shown in Figure 8.7b: LD^{19}DIS-150 (212.6 mL CH_4/g COD) was higher than LD^{19}DIS-200 (220.5 mL CH_4/g COD) or LD^{19}DIS-250 (212.8 mL CH_4/g COD). Therefore, final BMP_{ex} values are similar, agreeing with the conclusions of Figure 8.6b. Again, Table 8.11 showed improved digestion kinetics for LD^{19}DIS process waters, compared to LD^{19}SEA process waters; although, the latter had reduced R^2 values due to the lag period observed in Figure 8.7a. Therefore, suggesting the increased presence of inorganics from the seawater had an inhibitory effect on AD; although the effect was not completely inhibitory.

8.5 Energy Balance and Future Considerations

8.5.1 Energy Output

The data obtained in this chapter can be used to calculate the obtainable energy outputs from the combined combustion of hydrochars and AD of process waters from 1-kg of dried FS^{19} or LD^{19}, across each of the HTC processing temperatures. The total energy output can subsequently be compared to the obtainable energy output from the AD of 1-kg of dried FS^{19} or LD^{19}; determined in Chapter 4. Therefore, allowing any improvements in the ECEs to be identified.

The obtainable energetic outputs of FS^{19}SEA and FS^{19}DIS HTC reactions are shown in Figure 8.8a and Figure 8.8b, respectively. The combined energy outputs of FS^{19}SEA-150, FS^{19}SEA-200 and FS^{19}SEA-250 were 10.31 MJ/kg, 9.06 MJ/kg and 6.72 MJ/kg, respectively; reflecting a 184%, 150% and 85% increase in the energy output, compared to the AD of FS^{19} (3.63 MJ/kg). Hydrochar combustion represented between 68-75% of the combined energy balance; therefore representing the greater energy carrier. The energy output obtained from hydrochar combustion decreased as HTC temperature increased: FS^{19}SEA-150 (6.97 MJ/kg), FS^{19}SEA-200 (6.83 MJ/kg) and FS^{19}SEA-250 (4.68 MJ/kg); due to a reduced hydrochar yield (Table 8.1). The process water energy output was higher for FS^{19}SEA-150 (3.34 MJ/kg), compared to FS^{19}SEA-200 (2.23 MJ/kg) or FS^{19}SEA-250 (2.04 MJ/kg), due to the higher BMP_{ex} value (Figure 8.6) and increased COD concentration of FS^{19}SEA-150 process water (Figure 8.4).

Figure 8.8b shows the combined energy output of FS^{19}DIS-150 (9.85 MJ/kg) and FS^{19}DIS-200 (8.83 MJ/kg) are similar to FS^{19}SEA-150 and FS^{19}SEA-200, respectively. Although, FS^{19}DIS-250 yields a greater energy output (9.19 MJ/kg) than FS^{19}SEA-250; due to a higher

hydrochar yield (Table 8.1), process water COD concentration (Figure 8.4) and BMP_{ex} (Figure 8.6). The FS^{19}DIS-derived process waters generated a higher energy output than FS^{19}SEA-process waters: FS^{19}DIS-150 (3.72 MJ/kg), FS^{19}DIS-200 (3.13 MJ/kg) and FS^{19}DIS-250 (3.41 MJ/kg); due to higher BMP_{ex} yields (Figure 8.6).

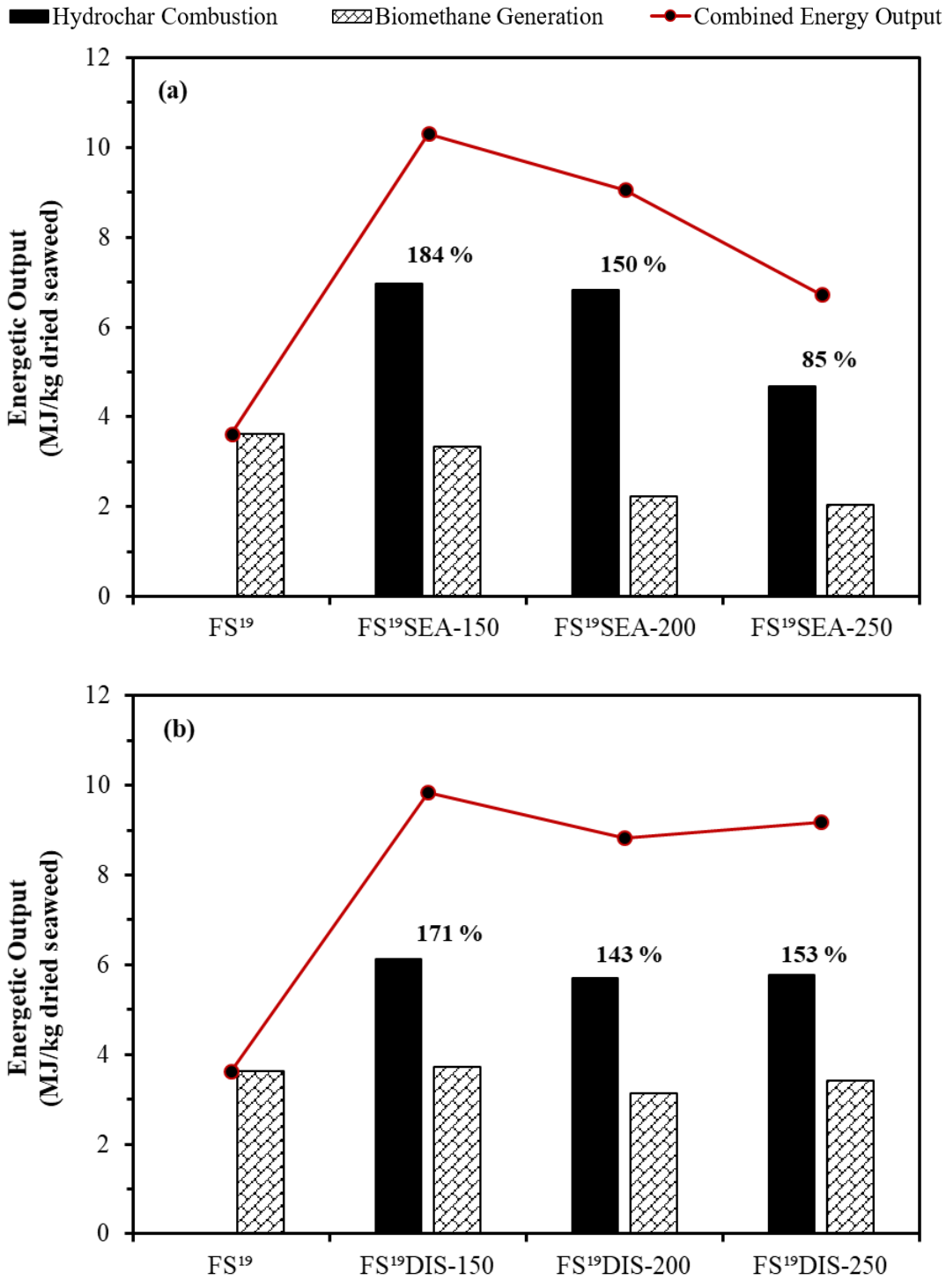

Figure 8.8. Energetic output from hydrochar combustion, anaerobic digestion of process waters and a combined energy output for (a) FS^{19}SEA (b) FS^{19}DIS. Calculated based on a starting material of 1-kg dried FS^{19}. The percentages above the bars represent the increase in total energy output compared to the anaerobic digestion of the untreated biomass.

The obtainable energy outputs from LD[19]SEA and LD[19]DIS HTC reactions are shown in Figure 8.9a and Figure 8.9b, respectively. Figure 8.9a shows all HTC-AD integration strategies improved the energetic output compared to the AD of LD[19]. LD[19]SEA-150, LD[19]SEA-200 and LD[19]SEA-250 improved the energy output by 61%, 36% and 12%. However, due to the issue of the overestimation of the yield distribution of LD[19] between the hydrochar and process water (Table 8.2) the results displayed in Figure 8.9a must be approached with caution. The reason for this cautious approach is reflected by the findings of Figure 8.9b; in which the integration of HTC-AD of LD[19] in distilled water shows either a negligible increase, or a decrease in the obtainable energy output, compared to the AD of LD[19]. LD[19]DIS-150 displays a slight improvement (4%) in energy output, compared to LD[19]. However, LD[19]DIS-200 and LD[19]DIS-250 show declines in energy outputs of -2% and -13%, respectively. Hydrochar energy yields: 3.87 MJ/kg (LD[19]DIS-150), 3.93 MJ/kg (LD[19]DIS-200) and 3.21 MJ/kg (LD[19]DIS-250) are all lower than LD[19]SEA hydrochars, due to the lower hydrochar yields (Table 8.1). LD[19]DIS hydrochars also have lower hydrochar yields and HHVs, compared to FS[19]SEA and FS[19]DIS hydrochars. In this, instance, the process waters generate a higher energy output that the hydrochars; meaning process waters are the greater energy carrier for LD[19].

The overall improvement in energy output, using this HTC-AD integration strategy is lower for LD[19], than FS[19]; reflecting the conclusions of Chapter 6. Typically *F. serratus* has limited a biodegradability compared to other seaweeds [71,127,134]; in particular kelp species, such as *L. digitata*. Therefore, the integration of HTC-AD could act a potential valorisation route for utilising under-performing species, such as *F. serratus* as a suitable feedstock for bioenergy production.

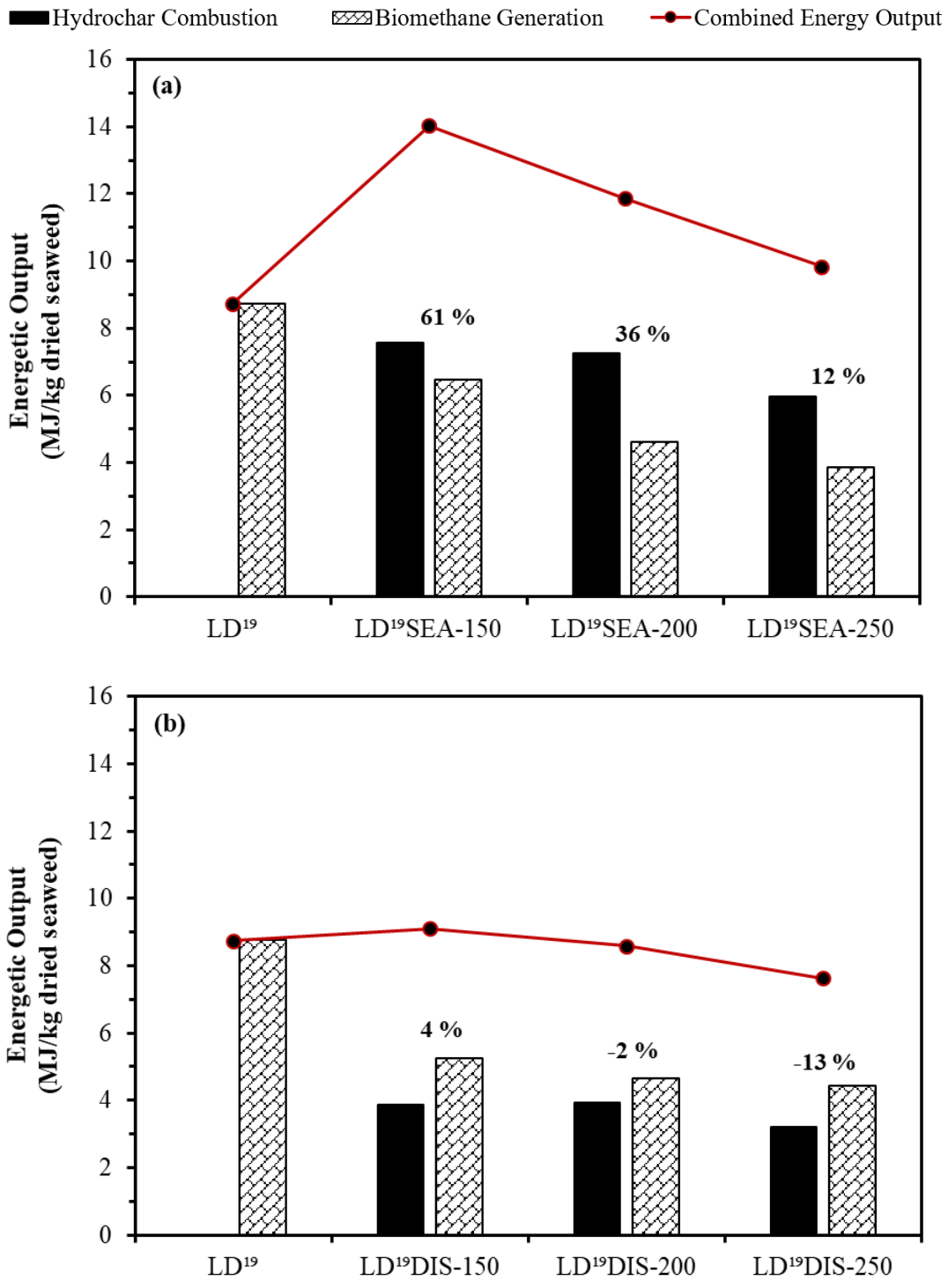

Figure 8.9. Energetic output from hydrochar combustion, anaerobic digestion of process waters and a combined energy output for (a) LD[19]SEA (b) LD[19]DIS. Calculated based on a starting material of 1-kg dried LD[19]. The percentages above the bars represent the increase in total energy output compared to the anaerobic digestion of the untreated biomass.

8.5.2 Energy Return upon Energy Invested

In order to determine whether the HTC-AD integration option of hydrochar combustion and process water digestion is energetically feasible, the EROI was calculates for each seaweed HTC condition, displayed in Table 8.12. EROI is shown as two values; one with no assumed energy recovery efficiency and another with 55% energy recovery efficiency. Energy input is calculated based on the energy to heat the contents of the HTC reactor; assuming 1-kg dried seaweed input. Whereas, energy output is determined as the combined energy output values shown in Figure 8.8 and Figure 8.9. Table 8.12 also shows the ECE values for the AD of untreated seaweeds and the HTC-AD integration options.

Table 8.12. Energy balance for the integration of HTC and AD.

Sample	Energy Input (MJ/kg)	Energy Output (MJ/kg)	EROI	EROI[1]	ECE (%)
FS^{19}	-	3.63	-	-	31
FS^{19}SEA-150	5.44	10.31	1.90	4.21	88
FS^{19}SEA-200	7.61	9.06	1.19	2.65	77
FS^{19}SEA-250	9.79	6.72	0.69	1.53	57
FS^{19}	-	3.63	-	-	31
FS^{19}DIS-250	5.44	9.85	1.81	4.02	84
FS^{19}DIS-250	7.61	8.83	1.16	2.58	75
FS^{19}DIS-250	9.79	9.19	0.94	2.09	78
LD^{19}	-	8.74	-	-	76
LD^{19}SEA-150	5.44	14.04	2.58	5.74	123
LD^{19}SEA-200	7.61	11.86	1.56	3.46	104
LD^{19}SEA-250	9.79	9.83	1.00	2.23	86
LD^{19}	-	8.74	-	-	76
LD^{19}DIS-150	5.44	9.11	1.67	3.72	80
LD^{19}DIS-200	7.61	8.58	1.13	2.51	75
LD^{19}DIS-250	9.79	7.63	0.78	1.73	67

[1]55% assumed energy recovery efficiency. ECE=energy conversion efficiency. EROI=energy returned upon energy invested.

The EROI values of FS^{19}SEA150 (1.90) and FS^{19}SEA200 (1.19) are similar to FS^{19}DIS150 (1.81) and FS^{19}DIS200 (1.16); each reflecting an energy positive process, without an assumed energy recovery efficiency. Both FS^{19}SEA250 and FS^{19}DIS250 require a heat recovery efficiency in order to be energetically feasible. Similar conclusions are observed for LD^{19}SEA and LD^{19}DIS HTC-AD integration options; although LS^{19}SEA150 appears energy neutral (EROI=1.00).

Table 8.12 shows the ECE of FS[19]SEA-150 (88%) and FS[19]DIS-150 (84%) are similar. The same is observed for FS[19]SEA-200 (77%) and FS[19]DIS-200 (75%). Therefore, at HTC temperatures of 150°C or 200°C a similar ECE of *F. serratus* is obtained regardless of whether seawater or distilled water is used as a HTC reaction medium. However, an increase in temperature to 250°C shows a greater ECE with FS[19]DIS-250 (78%), compared to FS[19]SEA-250 (57%). Despite the decrease in ECE with increasing temperature, all FS[19] HTC-AD integration options show an improvement in ECE compared to AD of untreated FS[19].

Table 8.12 shows the ECEs of LD[19]SEA-150 (123%) and LD[19]SEA-200 (104%) are both >100%. Again, this reflects the overestimation in the mass yield distribution of LD[19]SEA-HTC reactions between the hydrochar and process water; therefore these results cannot be interpreted with confidence. The ECE of LD[19]DIS-150 (80%) is slightly increased compared to the AD of untreated LD[19] (76%). However, this slight increase would not justify the separate infrastructure required to conduct HTC, rather than just AD. Therefore, in this scenario AD of untreated LD[19] is recommended, as opposed to the HTC-AD integration strategy. This is further exemplified by the ECE of LD[19]DIS-200 (75%) and LD[19]DIS-250 (67%); both lower than the ECE of untreated LD[19]. Overall, this suggests the integration of HTC-AD may be better suited towards valorising biomass feedstocks with a lower biodegradability and therefore ECE during AD.

8.5.3 Future Considerations

The integration of HTC-AD has been highlighted as a suitable technology for improving the ECE of *F. serratus*. This chapter investigated the use of seawater as a HTC reaction medium in order to simulate real world processing conditions and to reduce fresh water consumption. Only limited studies exist which use seawater as a HTC reactant medium [181,182]. Therefore, there is a number of future considerations to examine before scale-up of this technology, using seawater as a reactant medium, can be considered.

The HTC reactions conducted as part of this work were carried out using a 600 mL stainless steel Parr bench top reactor, within a custom quartz liner. A liner was used to facilitate easier transition of material out of the reactor, following HTC. In reality, a quartz liner is unlikely to be used, due to added complications to the reactor design and increased cost. Therefore, an unexplored limitation of using seawater as a reactant medium is likely to be corrosion issues of the stainless-steel HTC reactor caused by the increased presence of salts and Cl. In order to overcome this, the reactors can be constructed using different materials. For example, Castello *et al*. [286] investigated the use of an alumina ceramic-lined reactor to reduce corrosion in a supercritical water gasification reactor. Although the authors recommend the

use of this material, this would increase the capital cost of the HTC reaction. Therefore, a full techno-economic assessment would be required to assess the feasibility of using these types of reactors.

The associated issues of salts and Cl also follows through to AD. Figure 8.6a showed that sufficient volumes of biomethane can be generated from FS[19]SEA-process waters. During AD, the carbon-containing fraction of the feedstock is reduced, during the metabolic production of biomethane; effectively concentrating down the nutrient and inorganic fraction of the feedstock, generally recovered as digestate, which can be typically applied as a natural fertiliser [56]. However, the HTC process waters generated in seawater contain a high ash fraction; the majority of which is likely salts and Cl. For example, Table 8.9 shows the ash content of FS[19]SEA-150, FS[19]SEA-200 and FS[19]SEA-250 process waters was 37.3 g/L, 35.6 g/L and 32.7 g/L, respectively. Wang *et al*. [179] demonstrated the inhibitory nature of *Laminaria* HTC process waters on seed germination, suggested to be linked to the high salinity and high concentration toxic organic compounds; such as HMF or furfural. Therefore, the use of seaweed HTC process waters produced in seaweed is likely to generate a digestate that is inhibitory to crop growth. Perhaps a potential use of this digestate is an application as a fertiliser in the artificial cultivation of future macroalgal or marine microalgal crops, due to their inherent salinity tolerance. However, this requires further investigation.

This chapter has highlighted differences between the suitability for applying the HTC-AD integration strategy across different species of seaweeds. Significant improvements in the ECE of *F. serratus* were observed, whereas limited improvements were observed for *L. digitata*. Therefore, one possible integration route could be to co-digest *F. serratus*-derived process waters with untreated *L. digitata*, in order to maximise biomethane yields whilst considering both wracks and kelps as bioenergy feedstocks. The co-digestion of HTC process waters with an untreated biomass feedstock has already been previously investigated [287,288]. Although, Choe *et al*. found co-digesting bamboo-residue HTC process waters with fish waste did not show any significant enhancements on biomethane production, compared to the mono-digestion of fish waste. Whereas, Wang *et al*. [288] found the co-digestion of corn-stover HTC process water with untreated corn stover slightly enhanced biomethane yields compared to untreated corn-stover. Therefore, the co-digestion of *F. serratus* HTC process waters and untreated kelps may be an option worth exploring.

8.6 Conclusions

The focus of this chapter was to compare the effectiveness of integrating HTC-AD to improve the ECE of seaweeds, under different HTC processing conditions. This included a comparison of typical laboratory-based conditions; freeze dried seaweeds processed in a distilled water medium and a ‘real-world’ processing scenario; processing wet, as received seaweed in a

seawater medium. The influence of HTC processing conditions was assessed in terms of hydrochar and process water properties. The overall aim is to generate a hydrochar with suitable properties for combustion and a process water with suitable properties for AD; in order to improve the ECE of the seaweeds, compared to the AD of untreated seaweeds.

The integration of HTC-AD can significantly improve the ECE of *F. serratus*, compared to the AD of untreated *F. serratus*. Conducting HTC at lower temperatures provides the greatest improvement in ECE, as well as the most favourable energetics. Processing *F. serratus* at 150°C or 250°C shows a similar improvement in ECE, regardless of whether the seaweed is processed in distilled water, or seawater. At 150°C the ECE of *F. serratus* is 84-88% and at 200°C the ECE of *F. serratus* is 75-77%. However, the hydrochars generated in seawater at 150°C and 200°C appear to be subject to slagging and fouling tendencies, due to the incorporation of NaCl from the seawater into the hydrochar structure. At 250°C sufficient quantities of alkali metals and Cl is removed from the hydrochar; drastically reducing the slagging and fouling potential of the hydrochars. Therefore, if seawater is to be used as reactant medium for the HTC of *F. serratus*, a higher processing temperature of 250°C is recommended. Although, using a distilled water reactant medium at 250°C yields a higher ECE (78%) compared to seawater at 250°C (57%); due to higher hydrochar yields and biomethane yields from process waters. The use of seawater in HTC also appears to improve the ECE of *L. digitata* compared to the AD of untreated *L. digitata*. However, these results appear to be subject to overestimation of the product yields between the hydrochar and process water and therefore, cannot be reliably interpreted. Despite this, the integration of HTC-AD using distilled water for *L. digitata* yields a negligible improvement or a reduction in ECE, compared to the AD of untreated *L. digitata*. Therefore, suggesting the integration of HTC-AD is not a suitable valorisation route for *L. digitata*. The ECE of untreated *L. digitata* was 76%. Therefore perhaps the HTC-AD integration strategy is more suitable to improving the ECE of biomass with more limited biodegradabilities during AD.

Overall, the integration of HTC-AD appears to be a more suitable valorisation route of *F. serratus* compared to *L. digitata*. The use of seawater as a HTC reactant medium appears to more suitable at higher HTC processing temperatures (250°C); allowing for sufficient removal of alkali metals and Cl, reducing the slagging and fouling propensity of the resultant hydrochars. A higher ECE is obtained when processing *F. serratus* at 250°C using distilled water, rather than seawater. However, treatment with seawater showed an improvement in ECE, compared to the AD of untreated *F. serratus* and is associated with a reduced fresh water demand and facilitates easier processing of marine-based biomass.

Chapter 9
Conclusions and Future Recommendations

The overall aim of this study was to investigate the potential of integrating hydrothermal and biological conversion processes, to improve the energy conversion efficiency of alternative, high ash feedstocks. This included an assessment of different hydrothermal and biological integration strategies, across a range of hydrothermal reaction severities. The comparative valorisation of lignocellulosic and macroalgal biomass was assessed, in order to provide recommendations for optimised integration conditions, across a range of different feedstocks.

The following section will outline the key conclusions of this thesis and how these achieve the overall aims and objectives of this study. In addition, future directions of work are highlighted in order to further develop the concept of integrated hydrothermal and biological processing of high ash biomass feedstocks.

9.1 Conclusions

This section presents the main conclusions obtained throughout this thesis, placed in context to research objectives:

(i) Assessment of the suitability of high ash feedstocks for conventional conversion routes.

Chapter 4 compared the differences in biochemical compositions between the different feedstocks used in this thesis. Each biomass contained a high ash content (9.6-15.2 wt% *db*, determined by TGA) which, in turn, contained high concentrations of problematic alkali metals (Na and K) and Cl, posing an increased risk of slagging, fouling and corrosion issues during thermochemical conversion processes. **Chapters 5 and 8** demonstrated the high slagging and fouling tendencies of these feedstocks through a combination of predictive indices and ash fusion testing. Macroalgal biomass displayed an increased slagging propensity compared to lignocellulosic biomass, due to a higher concentration of problematic inorganics. However, WH and GR still appear to display slagging and fouling tendencies.

The high-ash feedstocks used in this thesis contained high concentrations of alkali metals and chlorine. This proved particularly problematic during the determination of ash and oxygen content of biomass; due to losses of Na, K and Cl through volatilisation at higher ashing temperatures (900°C). However, lower ashing temperatures (550°C), can result in an underestimation of ash content, due to the presence of unburnt carbon. The method of ash determination created discrepancies in the measured VS-content and both theoretical and

experimental biomethane potential. Overall, lower ashing temperatures (550°C) were deemed the most suitable for high-ash biomass, although longer retention times (c. 12-hrs) are recommended to eliminate the presence of unburnt carbon in the ash.

The HHV of the macroalgal samples (9.7-12.7 MJ/kg), WH (13.0 MJ/kg) and GR (18.8 MJ/kg) are typically lower than coal. High ash biomass feedstocks have a low energy density, due to the high ash and oxygen concentrations. Overall, the thermochemical conversion of the high ash feedstocks was deemed unsuitable, due to a low energy density and problematic ash behaviour.

Chapter 4 determined the behaviour of the high ash feedstocks during AD. The ECE of feedstocks during AD was largely varied (25-76%), due to variations in biochemical composition. Kelp species SL, LD and LD[19] demonstrated the highest ECE (59-76%). Whereas, the ECE was particularly low for *F. serratus* (FS= 35% and FS[19]=31%), WH (25%) and GR (50%). Therefore, suggesting the ECE of these feedstocks can be further improved through the integration of hydrothermal and biological conversion technologies.

(ii) Understand the effect of reaction severity on the yields and properties of HTC products.

Chapter 5 determined the product yields and characteristics obtained from the HTC of high ash feedstocks, at different reaction severities: 150°C, 200°C and 250°C. The hydrochar yield decreased with increasing HTC temperature, due to a higher mass distribution towards the aqueous phase. Macroalgal biomass displayed lower hydrochar yields (22.0-44.7%) compared to lignocellulosic biomass (37.4-79.9%).

The HHV of hydrochars increased with increasing HTC temperature, linked to an increased C-content and reduction of O-content, due to dehydration and decarboxylation reactions. Hydrochars produced at higher temperatures displayed more ‘coal-like’ properties, in terms of lower H:C and O:C and higher FC:VM. Although, the EY obtained from hydrochars decreased with increasing HTC temperature, due to a reduced hydrochar yield. The ED of macroalgal-derived hydrochars was higher than lignocellulosic-derived hydrochars, due to the initially lower HHV of macroalgal feedstocks. Limited ED of lignocellulosic biomass is observed at 150°C. The EY of lignocellulosic-derived hydrochars was greater than macroalgal-derived hydrochars, due to higher hydrochar yields.

HTC selectively removes problematic inorganics, such as Na, K and Cl from biomass, which can improve the ash behaviour of the fuel. The removal efficiency of problematic inorganics increases with increasing HTC temperature, to greater than 90% at 250°C. Therefore,

improving the properties of hydrochar as a combustion fuel. However, the ash content and N-content still remains high.

Chapter 5 also assessed the changing composition of HTC process waters across different reaction temperatures. A significant proportion of carbon was distributed towards the process water phase during HTC. However, this was greater for macroalgal biomass (43-61%), compared to lignocellulosic biomass (18-33%). Largely, the concentrations of COD and TOC remained unchanged across the different reaction severities, with the exception of WH. However, higher HTC temperatures displayed an increase in inhibitory compound formation, such as: phenols and ammonia. This was confirmed by **Chapter 6** where lower-temperature (150°C) process waters displayed a higher biodegradability, compared to higher-temperature process waters (200°C and 250°C). This effect was particularly significant for lignocellulosic-derived HTC process waters.

(iii) Assess the potential applications of hydrochars and process waters as separate energy vectors.

Chapter 6 compared the generation of different energy vectors from the separated hydrochars and process waters, from the HTC reactions conducted as part of **Chapter 5**. The effectiveness of hydrochars as a solid combustion fuel or AD feedstock were compared. Whereas, the potential for generating either biomethane or biohydrogen from the HTC process waters was compared.

Chapter 6 determined the slagging and fouling tendencies of the hydrochars. Hydrochars produced from SL, FS, LD and GR displayed a reduced slagging propensity compared to the respective parent biomass. Generally, hydrochars generated at higher temperatures (250°C) displayed the greatest reduction in slagging tendency, due to a greater removal efficiency of problematic inorganics (**Chapter 5**). WH-derived hydrochars showed no improvement in ash behaviour, potentially limiting their application as a combustion fuel.

The energy output obtained from the combustion of hydrochars was greater than that obtained from the AD of hydrochars. All hydrochars showed a reduced biodegradability compared to the parent feedstock, except FS150, WH150 and WH200. In particular, higher temperature hydrochars (250°C) showed reduced biodegradabilities (4-12%), linked to a recalcitrant aromatic structure.

The energy output obtained from the combustion of hydrochars decreased as HTC temperature increased, despite higher HHVs. This is due to reduced hydrochar yields at higher temperatures. The energy output from the combustion of lignocellulosic-derived hydrochars

(7.83-11.55 MJ/kg) was greater than macroalgal-derived hydrochars (4.02-7.19 MJ/kg), again due to higher hydrochar yields.

The generation of biomethane from process waters appeared to be a more suitable valorisation route compared to biohydrogen production. A higher yield of biomethane was produced, compared to biohydrogen, resulting in a greater energetic recovery. Lower temperature (150°C) process waters generally yield a higher energy output, due to the increase presence of inhibitory compounds found within higher-temperature HTC process waters.

Overall, the use of hydrochars as a solid combustion fuel and biomethane generation from HTC process waters is the most energetically feasible valorisation route for separated HTC products. Although, the obtainable energy recovery is dependent on HTC temperature.

Chapter 6 found that hydrochars represents the greater energy carrier, compared to the process waters, across all feedstocks and processing conditions. Although the process waters contribute between 30-43% of the overall energy output for macroalgal species, compared to between 13-20% for lignocellulosic biomass.

(iv) Understand the effect of hydrothermal pre-treatment severity on the behaviour of high ash feedstocks during biological conversion.

Chapter 7 investigated the use of HTC and SE pre-treatments to improve the biodegradability of high ash feedstocks during biological conversion. HTC pre-treatments were conducted at 150°C, 200°C and 250°C, with corresponding SFs of: 3.3, 4.7 and 6.2 respectively. All HTC-pre-treatments reduced the ECE of SL and GR, compared to the untreated biomass. However, an optimal pre-treatment temperature of 150°C (SF=3.3) was identified for both FS and WH. The ECE of FS improved from 35% to 58% and WH from 25% to 48%. More severe HTC pre-treatment conditions resulted in a reduced ECE, due to the formation of inhibitory compounds (**Chapter 5**) and increasing recalcitrance of the solid fraction (**Chapter 6**).

SE pre-treatments were conducted at 150°C (SF=2.6) and 200°C (SF=4.1). SE-150°C showed the greatest improvement in biomethane yields for FS[19]; improving the ECE from 31% to 51%. Whereas, SE pre-treatment did not improve the ECE of LD[19]. SE at 200°C provided the greatest improvement in biomethane yields from WH; improving the ECE from 25% to 52%. The less severe SE conditions (150°C) did not prove effective in hydrolysing the WH. HTC-150°C pre-treatment of *F. serratus* results in a slightly higher ECE (58%), compared to SE-150°C (51%). Although, an EROI calculation suggests SE may be more energetically feasible than HTC for *F. serratus*. Alternatively, HTC appears a more energetically-feasible pre-treatment for WH, compared to SE, due the optimal WH pre-treatment temperature being lower during HTC (150°C), than SE (200°C). Although, SE appears to improve the material

handling properties of WH, by reducing the presence of fibres, allowing for easier pumping and transportation of WH.

Two-stage digestion of pre-treated WH can further enhance the ECE compared to one-stage digestion. The two-stage digestion enhanced the hydrolysis of WH, which resulted in a higher biomethane generation. HTC-150°C pre-treatment showed the greatest improvement in ECE of WH, from 45% during one-stage digestion, to 62% during two-stage digestion.

Overall, **Chapter 7** found that hydrothermal pre-treatment is only suitable for feedstocks which display an initially low ECE. **Chapter 4** found the ECEs of SL, LD[19] and GR were 64%, 76% and 50%, respectively. Hydrothermal pre-treatment did not enhance the ECE of SL, LD[19] or GR. Whereas, hydrothermal pre-treatment improved the ECE of feedstocks with an initially low ECE: FS, FS[19] and WH.

(v) Compare the effectiveness of different hydrothermal and biological integration strategies to improve the energy conversion efficiency of high ash feedstocks.

Overall, **Chapter 7** showed that the separation of hydrochars for combustion and HTC process waters for AD consistently provided the greatest improvement in energy output and ECE, compared to AD of the HTC slurry, across all feedstocks and HTC processing temperatures. Although, **Chapter 5** shows that higher HTC processing temperatures are associated with a reduced energy output and ECE. According to **Chapter 5** and **Chapter 6**, conducting HTC at lower processing temperatures can compromise hydrochar quality by limiting energy densification or removal of problematic ash species. As a result, the optimised hydrothermal and biological integration strategy varies according to the behaviour of different feedstocks. Therefore, the following conclusions section discusses each feedstock-type individually, in order to provide recommendations to maximise the ECE obtained from each feedstock.

According to **Chapter 4** the ECE of kelp macroalgal species are the highest of any feedstocks investigated as part of this thesis. HTC or SE pre-treatment did not improve the ECE of kelps, therefore, hydrothermal pre-treatment is not recommended as suitable valorisation strategy. Separation of hydrochars for combustion and process waters for AD improved the ECE of both SL and LD, although lower HTC temperatures yielded the greatest energetic return. The ECE of SL was improved from 64% to 90% (150°C), 77% (200°C) and 71% (250°C), whereas LD was improved from 59% to 87% (150°C), 75% (200°C) and 64% (250°C). Higher HTC processing temperatures reduces the overall EROI, however, each option was energy positive, if 55% energy recovery is assumed. **Chapter 5** showed higher HTC temperatures generally produces hydrochars with improved ash chemistry during combustion. Therefore, creating a compromise between hydrochar quality and process energetics.

Chapter 4 showed that wrack species *F. serratus* displayed an initially lower ECE during AD, compared to kelps: FS=35% and FS^{19}=31%. Separation of FS-derived hydrochars for combustion and process water AD improved the ECE from 35% to 91% (150°C), 79% (200°C) and 72% (250°C). According to **Chapter 6** HTC temperatures of 200-250°C reflect the greatest improvement in ash chemistry, during the combustion of FS-derived hydrochars. As a result, hydrothermal pre-treatment can also be considered a suitable valorisation strategy for *F. serratus*. **Chapter 7** found HTC-150°C to be the optimal pre-treatment conditions for FS, improving the ECE to 58%. Although this is lower than the ECE obtained by the separation of hydrochars and process waters at 200°C or 250°C, the EROI is lower. SE pre-treatment at 150°C could also act as a valorisation route for *F. serratus*. On balance, the separation of FS-HTC products generated at 200°C for combustion and AD appears the most feasible hydrothermal and biological integration option.

Untreated WH displayed an ECE during AD of 25% (**Chapter 4**); the lowest of any feedstock investigated as part of this thesis. Again, separation of hydrochars for combustion and process waters for digestion provided the greatest improvement in ECE of WH, up to: 97% (150°C), 87% (200°C) and 79% (250°C). However, **Chapter 5** showed WH hydrochars produced at lower temperatures (150°C) showed limited energy densification. Furthermore, **Chapter 6** reported WH-hydrochars showed no improvement in ash chemistry during combustion. Therefore, WH-derived hydrochars may not be suitable as a combustion fuel, but may be useful in alternative applications, such as soil amendment. **Chapter 7** determined hydrothermal pre-treatment could be a suitable valorisation route for WH. HTC-150°C pre-treatment appears more energetically feasible than SE: improving the ECE of WH to 48%. Two-stage digestion of HTC-150°C WH slurry can further improve the ECE to 62%. However, this is compromised by the increasing complexity of infrastructure required for this process.

Similar to kelps, **Chapter 7** determined that hydrothermal pre-treatment did not improve the ECE of GR. **Chapter 4** found the ECE obtained from the AD of GR was 50%. **Chapter 6** determined the separation of hydrochars for combustion and process waters for AD improved the ECE of GR up to: 82% (150°C), 74% (200°C) and 63% (250°C). However, hydrochars produced at 250°C showed a much greater reduction in slagging and fouling tendencies, compared to those produced at lower temperatures. GR-hydrochars produced at 150°C exhibited limited energy densification. Therefore, higher HTC processing conditions are recommended. EROI reduced with increased HTC temperature, but remained energy positive, if 55% energy recovery is assumed.

One of the key findings of this thesis is that the recommended hydrothermal and biological integration strategy is different between different biomass sources, even within similar

categories. For example, kelp and wrack macroalgal species behave differently during hydrothermal pre-treatment, as do WH and GR: both classed as lignocellulosic biomass.

(vi) Assess the potential for using seawater as a HTC reactant medium for macroalgal biomass.

The conclusions of **Chapters 6 and 7** identified that separation of HTC products for separate combustion and AD provided the greatest improvement in the ECE of macroalgal species. Following on from this, **Chapter 8** investigated the comparative use of seawater or distilled water as a HTC reactant medium for macroalgal biomass.

A higher HTC temperature (250°C) was required to effectively remove the excess alkali metals and Cl, associated with seawater, from the FS^{19}-derived hydrochar. Processing FS^{19} in seawater at lower temperatures (150°C and 200°C) resulted in unfavourable ash behaviour from the hydrochars during combustion. Integration of HTC-AD improved the ECE of FS^{19}, compared to biological processing alone. A higher ECE was obtained whilst processing FS^{19} in distilled water (78%), compared to seawater (57%) at 250°C. Although the use of seawater is associated with easier processing of marine biomass and a reduced fresh water demand.

Chapter 4 determined LD^{19} displayed the greatest ECE during AD (76%). **Chapter 8** found the use of seawater as a HTC reactant medium also appears to improve the ECE of LD^{19} at 250°C to 86%. However, these results appear to be subject to overestimation of the product yields and therefore, cannot be reliably interpreted. Despite this, LD^{19} HTC-AD using distilled water yields a negligible improvement or a reduction in ECE, compared to the AD of untreated LD^{19}. Again, suggesting the integration of HTC-AD is not a suitable valorisation route for *L. digitata*.

9.2 Future Work

This work has highlighted the potential of integrating hydrothermal and biological conversion technologies to enhance the ECE of alternative, high-ash feedstocks, for utilisation as part of the future sustainable bioeconomy. However, a number of further future work directions exist to advance the knowledge in this area and lead to a scaling-up in the process.

9.2.1 Limitations of the Biomethane Potential Test

Throughout this thesis, the calculation of obtainable biomethane yields from untreated biomass and hydrothermally-derived biomass residues were determined using biochemical methane potential experiments (BMP_{ex}). Numerous publications exist which provide set criteria and recommendations for conducting valid BMP_{ex} experiments [240,266,289]. However, methodologies remain insufficiently standardised across different research laboratories [290]. The purpose of this section is to discuss the limitations of the BMP_{ex} methodology used within this thesis, in context to the guidelines and recommendations required to conduct a valid BMP_{ex} experiment; provided by: [240,266,289]. Reflecting on the validity of the BMP_{ex} methodology used within this thesis highlights key areas of development for further applications during future work.

9.2.1.1 Inoculum Collection and Storage

The inoculum used in a BMP_{ex} experiment contains the population of active microorganisms involved in the biodegradation of organic matter into biogas. The complex nature and microbial biodiversity of inocula means it is one of the most difficult aspects to standardise for a BMP_{ex} experiment [97]. Recent efforts have investigated the development of a standardised inoculum; utilising freeze drying as a microbial preservation method [291]. Although, issues were encountered with an increasing lag phase of the freeze-dried inoculum. Therefore, the existence of a universal, standardised inoculum is unlikely to be available in the near future.

In order to maintain a degree of consistency between BMP_{ex} experiments, it is recommended that inoculum is sourced from an active anaerobic digester, digesting complex organic matter; such as waste water, and the reactor is in a steady-state at the time of collection [240,266]. The inoculum source used throughout this thesis was collected from an active wastewater treatment plant digester (Esholt), during steady-state operation. This inoculum source has proved sufficient for the digestion of food waste [226], sewage sludge [170] and digestate-derived HTC process waters [170,171], in published studies from our research group; highlighting its suitability for applications in BMP_{ex} experiments.

It is recommended that the inoculum is used as fresh as possible [240,266,292]. However, from a logistical perspective, this was not always possible for the work conducted in this thesis. As a result, the collected inoculum was stored at 4°C for a maximum duration of 1-month, before replacing with another batch of fresh inoculum. However, prolonged storage of inoculum can have an impact on both biomethane yields and digestion kinetics [289,292].

Although, this effect is dependent upon storage conditions and duration. Hagen *et al*. [292] found storage of inoculum up to 1-month obtained similar biomethane yields to using freshly collected inoculum, whilst digesting cellulose. Biomethane yields were most similar for inoculum stored at 4°C or room temperature, whilst storage at -20°C showed a decrease in biomethane yields after 1-month storage. Prolonged storage of inoculum beyond 1-month resulted in decreased biomethane yields from cellulose, regardless of storage temperature. Koch *et al*. [289] also investigated the effect of a 2-week long storage period of inoculum during the digestion of pelletised dog food; comparing two different storage temperatures: 4°C and 38°C. Again, storage at 4°C showed a similar digestion performance to the fresh inoculum; albeit with a slight impact on the digestion kinetics. Whereas, inoculum storage at 38°C resulted in reduced biomethane yields and slower digestion kinetics. Further evidence by Astals *et al*. [293] showed that inoculum methanogenic activity decreases with prolonged storage, regardless of temperature (4°C, 22°C and 37°C). However, inoculum stored at 4°C is recommended, as this was found to maintain similar methanogenic activity to the fresh inoculum up to a storage duration of 14-days. Therefore, although using fresh inoculum is a more favourable option, the storage of inoculum at 4°C, for a maximum of 1-month appears a sufficient strategy to overcome the logistical complications of inoculum collection experienced in this work.

9.2.1.2 Inoculum Dilution

A further limitation identified during the experimental work of this thesis was validating the cross-comparison of BMP_{ex} data across multiple experimental runs. BMP_{ex} was determined for a large range of samples in this thesis, which in turn, were all compared to identify optimal hydrothermal and biological integration strategies, as well as differences between biomass types. Due to the limited capacity of AMPTS equipment available, not all samples could be analysed using the same inoculum, before surpassing the pre-determined 1-month expiry date. Therefore, the assumption was made that each batch of inoculum collected from Esholt would provide similar digestion kinetics. Filer *et al*. [294] previously reported that an AD reactor for a waste water treatment plant could provide biologically consistent inoculum for BMP_{ex} experiments; although this was only determined over a 1-month period. Furthermore, Chiumenti *et al*. [51] determined the variation in biogas yields of grass collected in spring and summer, using inocula from the same AD reactor, but collected at the corresponding seasonal time points. The authors found the two inoculum samples performed similarly during BMP_{ex} experiments; likely because the digester which the inoculum is collected from only digests a single feedstock (cow manure), therefore, inoculum samples are expected to be seasonally analogous [51].

In order to further ensure that the different BMP_{ex} tests used throughout the thesis were comparable, the same amount of inoculum-VS was added to each reactor, when determining the BMP_{ex} of solid samples. As detailed in Chapter 3, the inoculum was diluted to 20 g VS/L for BMP_{ex} reactions. This enabled greater control over the inoculum solid loading ratio, to ensure this was uniform across experiments. Therefore, facilitating similar digestion kinetics between different BMP_{ex} reactions. Likewise, for aqueous samples, such as HTC process waters, the inoculum was diluted to 20 g COD/L. The exceptions to this were during the two-stage digestions of WH (Chapter 7); where the DF inoculum was diluted to 15 g VS/L and the AD inoculum to 30 g VS/L; this was to allow both stages of the digestion to be conducted in the same reactor. In addition, the inoculum used to digest GR hydrochars and slurries had an initial VS-content of 18.6 g VS/L; slightly below the target VS concentration.

However, accounting for these dilutions may have resulted in a further issue; as Holliger *et al*. [240] indicate the dilution of inoculum should be avoided. Koch *et al*. [289] further investigate the impact of inoculum dilution on the digestion of pelletised dog food; testing inoculum dilutions of 1:0.5, 1:1 and 1:2. The inoculum was diluted with distilled water. Increasing inoculum dilution resulted in reduced BMP_{ex} yields, compared to un-diluted inoculum [289]; with the highest dilution (1:2) showing a negative decline in the BMP_{ex} curve, once the plateau-phase was reached. This was believed to be a result of the distilled water reducing the buffering capacity of the reactor contents, leading to an accumulation of VFAs, subsequently inhibiting methanogens.

The declining nature of the BMP_{ex} curves was a behaviour observed for some of the samples used in this thesis. This is exemplified by Figure 9.1, which shows that the BMP_{ex} curve obtained from the AD of WH-SE200 slurry slightly declines once the biomethane yields begin to plateau. The maximum BMP_{ex} yield was obtained after 12-days (200.2 mL CH_4/ g VS). Whereas, at day-27 this value had declined to 192 mL CH_4/ g VS. All BMP_{ex} data from previous chapters was reported from the highest point of biomethane generation.

The declining BMP_{ex} observed in Figure 9.1 does not appear to be as severe as that observed by Koch *et al*. [289]. However, this trends could still be linked to the dilution of inoculum. The average VS concentration for the Esholt inoculum was approximately 27 g VS/L, which was subsequently diluted to 20 g VS/L; therefore, representing a dilution of <1:0.5, approximately 1:0.3. This dilution is lower than the least severe dilution used by Koch *et al*. [289]; which showed the least impact on BMP_{ex} yields. Overall, results from Figure 9.1 and Koch *et al*. [289] suggests that inoculum dilution could impact the determination of maximum BMP_{ex} yields, however, the extent of this impact is unknown. Future work would aim to determine the BMP_{ex} yields of selected feedstocks using undiluted inoculum.

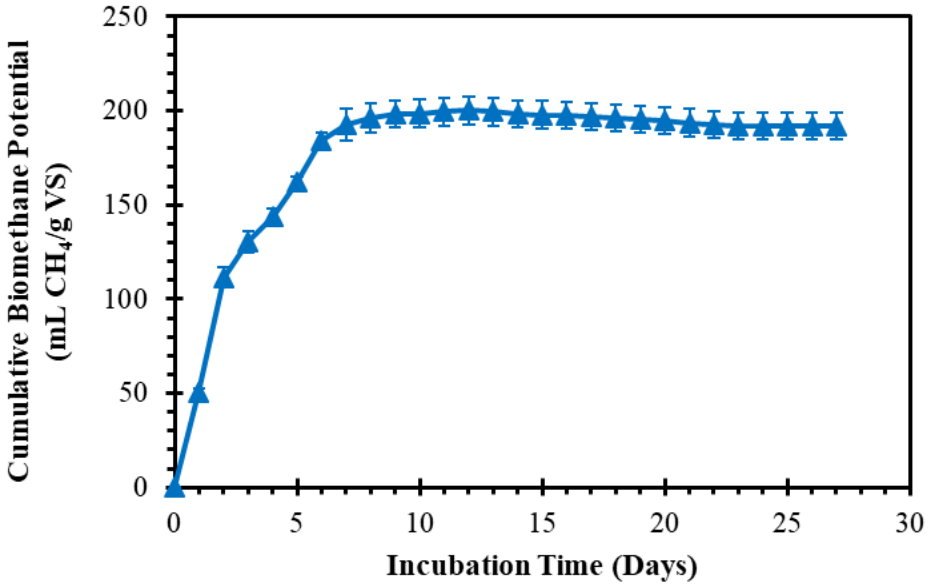

Figure 9.1. Experimental biomethane potential (BMP_{ex}) of water hyacinth steam exploded slurry, generated at 200°C (WH-SE200) showing a declining BMP_{ex} curve. Data is presented as average values. Error bars represent the maximum and minimum values (*n*=2).

9.2.1.3 Use of Positive Controls

A widely-used method of confirming sufficient microbial activity is the inclusion of a positive control [240,266,295]. The most widely used positive control is microcrystalline cellulose which should yield a BMP_{ex} value between 352-414 mL CH_4/g VS; between 85-100% of the maximum theoretical biomethane yield [240]. Although, a positive control was not regularly included throughout the BMP_{ex} experiments in this thesis, a singlet run of cellulose generated 299.2 mL CH_4/g VS, below the indicated range [240]. Therefore, suggesting that the inoculum dilution may exhibit slightly reduced BMP_{ex} values. Development of future methods would aim to limit the dilution of inoculum, whilst simultaneously including positive controls with each run; to validate sufficient microbial activity. Interestingly, Koch *et al*. [295] have also investigated the applications of conventionally-bought supermarket products as positive controls, including: Tic tacs, gummi bears, Cornflakes and coffee filters. The aim of this study was to generate a data set for more widely-available sources of positive controls. However, in future work, microcrystalline cellulose will be applied as a positive control, due to extensive applications across literature [97,240,266]. Finally, one additional future modification to the BMP_{ex} methodology used in this thesis would be to repeat each reaction in triplicate (*n*=3) in order to ensure true validity of the BMP_{ex} test and to allow a more robust statistical analysis of the data. The majority of BMP_{ex} experiments conducted as part of this work were conducted in duplicate (*n*=2).

9.2.2 HTC Reaction Conditions

The HTC reaction conditions explored as part of this work were conducted across a range of temperatures (150°C, 200°C and 250°C), with a fixed retention time (60-min) and a fixed solid loading ratio (approximately 10%).

Chapter 7 suggests that the hydrothermal pre-treatment conditions used in this study were potentially too severe during the AD of HTC slurries. Therefore, optimised pre-treatment conditions were not achieved. Hydrothermal pre-treatment of high-ash feedstocks should be conducted over a much broader range of reaction severities, in particular, pre-treatments with a lower reaction severity than the mildest conditions used in this study.

The solid loading ratio of HTC reactions was maintained at approximately 10%. However, increasing the solid loading ratio has the potential to improve the energy balance of the process. The specific heat capacity of water (4200 J/kg/K) [72] is higher than biomass (1455 J/kg/K) [177], therefore displacing water with biomass with reduce the energy requirement of the HTC reaction. However, the physical properties of different biomass types may limit the maximum solid loading ratio which can be achieved. For example, WH has a porous sponge-like structure, which made separation of the hydrochar and process water difficult, even at lower temperatures. Therefore, the feasibility of increasing the HTC solid loading ratio needs to be determined on a case-by-case basis.

A useful area of future work would be to obtain the optimised HTC conditions which results in the greatest improvement in ECE of high ash feedstocks. It is recommended this be carried out using a multivariate design of experiments approach to obtain the optimised HTC conditions (temperature, retention time and solid loading ratio) to maximise the energy obtained from high ash feedstocks. Although, the results are expected to vary between different biomass types.

9.2.3 Further Assessment of the Applications of HTC Products

This study identified that the separation of hydrochars for combustion and process waters for AD provided the greatest improvement of ECE for high ash feedstocks. Hydrochars generally displayed increased energy densification and improved ash chemistry compared to the parent feedstocks. However, further work is required to assess the quality of hydrochars as a solid combustion fuel. **Chapter 5** identified that the N-content of hydrochars remains relatively high (2-3 wt% *db*), whilst **Chapter 8** found the S-content of macroalgal-derived hydrochars also remains high (1-2 wt% *db*). Therefore, the potential generation of NO_x and SO_x emissions

needs to be considered, as production of high levels of emissions would be disadvantageous for the application of hydrochars as a solid combustion fuel. The emissions from hydrochars could be assessed by TGA-FTIR or by measured experimentally using small-scale domestic combustion apparatus, such as that described by Mitchell *et al*. [236]. Furthermore, the hydrochars generated in this study can be further assessed to determine their suitability as solid combustion fuels. Such analyses include: derivative thermogravimetric (DTG) burning profiles and assessing the friability and hydrophobic properties of hydrochars. In addition to applications as a solid combustion fuel, hydrochars have been identified for a wide range of alternative applications, such as soil amendment, extraction of humic acids, use as a low-cost sorbent, capacitors or inclusion as an additive for AD. The possibilities and opportunities for alternative hydrochar applications provides an interesting area for future development. The comparative assessment of hydrochar application is likely to require both a techno-economic and life cycle assessment to provide recommendations to the most cost-effective utilisation of hydrochars.

Chapters 5 and 8 identified the potential of generating biomethane from HTC process waters to recover the value associated with the solubilised organic fraction. However, limited knowledge exists on the performance of process waters during mono-digestion in a full-scale system. It is likely that future research will investigate the co-digestion of process waters with other feedstocks. This could include the co-digestion of process waters with readily-digestible biomass, where the integration of HTC-AD is not as effective, such as kelps. In addition, the potential applications of HTC process-water derived digestate have not yet been considered. Typically a process waters display between 60-80% COD removal during batch-AD systems [86], suggesting a large amount of organic matter remains in the digestate; potentially associated with GHG emissions. Furthermore, **Chapter 5 and 8** determined that large quantities of alkali metals and Cl are solubilised into the process water during the HTC process. Therefore, the process water-derived digestate could be unsuitable for applications as a fertiliser, meaning alternative valorisation streams need to be identified.

9.2.4 Feedstock Selection

The majority of work in this thesis has focussed on the HTC of macroalgal biomass. However, the fundamental chemical reaction pathways of macroalgal biomass during HTC are not yet fully understood. Future work would aim to model the behaviour of seaweed-derived carbohydrates: laminarin, alginate, fucoidan and mannitol across a range of HTC reaction severities. The yields and properties of both the hydrochars and process waters should be analysed to obtain an understanding of the HTC reaction pathways.

The biochemical composition of macroalgal biomass is known to seasonally vary [60], which can have an impact on the yields and characteristics HTC products [80]. However, the effect of seasonality on the subsequent digestion properties of the process waters during AD is unknown and therefore, poses an interesting direction for future research.

The HTC reactions carried out as part of this thesis were conducted on single feedstocks, in order to obtain a fundamental understanding of the behaviour of these feedstocks during integrated HTC-AD. However, the co-blending of biomass in HTC acts as a strategy to optimise the properties of HTC products. For example, **Chapter 5** found hydrochar generated from lignocellulosic biomass at higher HTC temperatures (250°C) had a greater HHV and hydrochar yield, compared to macroalgal-derived hydrochars. Whereas, **Chapter 6** found the process waters generated from macroalgal biomass at higher HTC temperatures (250°C) generally displayed a higher biodegradability index (BI) and energy output, compared to lignocellulosic-derived process waters. Therefore, the co-blending of lignocellulosic and macroalgal biomass could draw upon the simultaneous benefits of each feedstock during HTC-AD. However, this would require an assessment of resource availability across an area of land and sea, to determine the potential yields of biomass available for co-blending.

Chapter 1 and 2 determined that WH displays large variability in biochemical composition and biomethane potential across literature studies. **Chapter 7** determined both HTC and SE hydrothermal pre-treatments were effective at enhancing the biodegradability of WH during AD. However, the work carried out in this thesis was conducted on one sample of WH. Therefore, it is difficult to determine whether the improvements in biodegradability would be a universal observation across all samples of WH. In order to address this, the same hydrothermal pre-treatment should be conducted on a range of WH samples and the improvements in biodegradability assessed.

The work in this thesis was conducted on WH, GR and macroalgal biomass: representing a narrow range of high-ash feedstocks. Despite this, differences in behaviour were observed during the integration of HTC-AD. Future work would aim to assess the behaviour of additional of a range of high-ash feedstocks as part of a systematic study to identify key trends for the effect of biochemical composition on the effectiveness of integrated HTC-AD to improve the ECE of the biomass.

9.2.5 Scale-Up and Technoeconomic Assessment

Most of the work conducted on the integration of HTC-AD has been based on laboratory data, often using batch-based HTC or AD systems. Therefore, making assumptions or ‘real-world’

performance difficult. Future work would aim to conduct integrated HTC-AD as part of a continuous pilot-scale system. The scale-up of HTC technology would allow for more accurate predictions of the energy recovery efficiency potential, allowing a more accurate process energy balance to be calculated. Understanding the behaviour of integrated HTC-AD at scale would allow an assessment of the economic feasibility of integrated HTC-AD: which has not yet been demonstrated.

References

1. Fawzy, S.; Osman, A.I.; Doran, J.; Rooney, D.W. Strategies for mitigation of climate change: a review. *Environ. Chem. Lett.* **2020**, *18*, 2069–2094, doi:10.1007/s10311-020-01059-w.
2. IPCC. Climate Change 2021: The Physical Science Basis. Contribution of Working Group I to the Sixth Assessment Report of the Intergovernmental Panel on Climate Change, Cambridge University Press. In Press. **2021**.
3. Wrigley, E.A. Energy and the English industrial revolution. *Philos. Trans. R. Soc. A* **2013**, *371*, 20110568, doi:10.5860/choice.48-4603.
4. Lindsey, R. Climate Change: Atmospheric Carbon Dioxide Available online: https://www.climate.gov/news-features/understanding-climate/climate-change-atmospheric-carbon-dioxide (accessed on Aug 25, 2021).
5. UNFCCC. Adoption of the Paris Agreement. **2015**.
6. IPCC. Global Warming of 1.5°C. An IPCC Special Report on the impacts of global warming of 1.5°C above pre-industrial levels and related global greenhouse gas emission pathways, in the context of strengthening the global response to the threat of climate change, sustainable development, and efforts to eradicate poverty. Cambridge University Press, **2018.**
7. IPCC. Climate Change 2014: Mitigation of Climate Change. Contribution of Working Group III to the Fifth Assessment Report of the Intergovernmental Panel on Climate Change; Cambridge, United Kingdom and New York, NY, USA, **2014**.
8. McKendry, P. Energy production from biomass (part 1): Overview of biomass. *Bioresour. Technol.* **2002**, *83*, 37–46, doi:10.1016/S0960-8524(01)00118-3.
9. Kraan, S. Mass-cultivation of carbohydrate rich macroalgae , a possible solution for sustainable biofuel production. *Mitigating Adapt. Strateg. Glob. Chang.* **2013**, *18*, 27–46, doi:10.1007/s11027-010-9275-5.
10. REN21. Renewables 2021 Global Status Report, Paris, **2021.**
11. UK Government. Climate Change Act 2008, London, **2008**.
12. DECC-DfT-DEFRA. UK Bioenergy Strategy, London, **2012**.;
13. Brown, T.R.; Brown, R.C. Biorenewable resources: engineering new products from agriculture.; John Wiley & Sons, **2013**.
14. Basu, P. Biomass Gasification, Pyrolysis and Torrefaction: Practical Design and Theory; Academic press, **2013**.
15. Kumar, M.; Oyedun, A.O.; Kumar, A. A review on the current status of various hydrothermal technologies on biomass feedstock. *Renew. Sustain. Energy Rev.* **2018**, *81*, 1742–1770, doi:10.1016/j.rser.2017.05.270.
16. Ekpo, U.; Ross, A.B.; Camargo-Valero, M.A.; Williams, P.T. A comparison of product yields and inorganic content in process streams following thermal hydrolysis and hydrothermal processing of microalgae, manure and digestate. *Bioresour. Technol.* **2016**, *200*, 951–960, doi:10.1016/j.biortech.2015.11.018.
17. Ward, A.J.; Hobbs, P.J.; Holliman, P.J.; Jones, D.L. Optimisation of the anaerobic digestion of agricultural resources. *Bioresour. Technol.* **2008**, *99*, 7928–7940, doi:10.1016/j.biortech.2008.02.044.
18. Kumar, S.; Singh, S.P.; Mishra, I.M.; Adhikari, D.K. Recent advances in production

of bioethanol from lignocellulosic biomass. *Chem. Eng. Technol.* **2009**, *32*, 517–526, doi:10.1002/ceat.200800442.

19. Kumar, M.; Oyedun, A.O.; Kumar, A. A review on the current status of various hydrothermal technologies on biomass feedstock. *Renew. Sustain. Energy Rev.* **2018**, *81*, 1742–1770, doi:10.1016/j.rser.2017.05.270.
20. Montingelli, M.E.; Tedesco, S.; Olabi, A.G. Biogas production from algal biomass: A review. *Renew. Sustain. Energy Rev.* **2015**, *43*, 961–972, doi:10.1016/j.rser.2014.11.052.
21. Ho, D.P.; Ngo, H.H.; Guo, W. A mini review on renewable sources for biofuel. *Bioresour. Technol.* **2014**, *169*, 742–749, doi:10.1016/j.biortech.2014.07.022.
22. Chandra, R.; Takeuchi, H.; Hasegawa, T. Methane production from lignocellulosic agricultural crop wastes: A review in context to second generation of biofuel production. *Renew. Sustain. Energy Rev.* **2012**, *16*, 1462–1476, doi:10.1016/j.rser.2011.11.035.
23. Kumar, G.; Bakonyi, P.; Periyasamy, S.; Kim, S.H.; Nemestóthy, N.; Bélafi-Bakó, K. Lignocellulose biohydrogen: Practical challenges and recent progress. *Renew. Sustain. Energy Rev.* **2015**, *44*, 728–737, doi:10.1016/j.rser.2015.01.042.
24. Sawatdeenarunat, C.; Surendra, K.C.; Takara, D.; Oechsner, H.; Khanal, S.K. Anaerobic digestion of lignocellulosic biomass: Challenges and opportunities. *Bioresour. Technol.* **2015**, *178*, 178–186, doi:10.1016/j.biortech.2014.09.103.
25. Monlau, F.; Barakat, A.; Trably, E.; Dumas, C.; Steyer, J.P.; Carrère, H. Lignocellulosic materials into biohydrogen and biomethane: Impact of structural features and pretreatment. *Crit. Rev. Environ. Sci. Technol.* **2013**, *43*, 260–322, doi:10.1080/10643389.2011.604258.
26. Lee, H.V.; Hamid, B.A.; Zain, S.K. Conversion of Lignocellulosic Biomass to Nanocellulose: Structure and Chemical Process. *Sci. World J.* **2014**, doi:http://dx.doi.org/10.1155/2014/631013 Review.
27. Patel, S. Threats, management and envisaged utilizations of aquatic weed Eichhornia crassipes: An overview. *Rev. Environ. Sci. Biotechnol.* **2012**, *11*, 249–259, doi:10.1007/s11157-012-9289-4.
28. Gaurav, G.K.; Mehmood, T.; Cheng, L.; Klemeš, J.J.; Shrivastava, D.K. Water hyacinth as a biomass: A review. *J. Clean. Prod.* **2020**, *277*, doi:10.1016/j.jclepro.2020.122214.
29. Güereña, D.; Neufeldt, H.; Berazneva, J.; Duby, S. Water hyacinth control in Lake Victoria: Transforming an ecological catastrophe into economic, social, and environmental benefits. *Sustain. Prod. Consum.* **2015**, *3*, 59–69, doi:10.1016/j.spc.2015.06.003.
30. Albright, T.P.; Moorhouse, T.G.; McNabb, T.J. The rise and fall of water hyacinth in Lake Victoria and the Kagera River basin, 1989-2001. *J. Aquat. Plant Manag.* **2004**, *42*, 73–84.
31. Villamagna, A.M.; Murphy, B.R. Ecological and socio-economic impacts of invasive water hyacinth (Eichhornia crassipes): A review. *Freshw. Biol.* **2010**, *55*, 282–298, doi:10.1111/j.1365-2427.2009.02294.x.
32. Rezania, S.; Ponraj, M.; Din, M.F.M.; Songip, A.R.; Sairan, F.M.; Chelliapan, S. The diverse applications of water hyacinth with main focus on sustainable energy and production for new era: An overview. *Renew. Sustain. Energy Rev.* **2015**, *41*, 943–954, doi:10.1016/j.rser.2014.09.006.
33. Sindhu, R.; Binod, P.; Pandey, A.; Madhavan, A.; Alphonsa, J.A.; Vivek, N.; Gnansounou, E.; Castro, E.; Faraco, V. Water hyacinth a potential source for value

addition: An overview. *Bioresour. Technol.* **2017**, *230*, 152–162, doi:10.1016/j.biortech.2017.01.035.

34. Gunnarsson, C.C.; Petersen, C.M. Water hyacinths as a resource in agriculture and energy production: A literature review. *Waste Manag.* **2007**, *27*, 117–129, doi:10.1016/j.wasman.2005.12.011.

35. Munjeri, K.; Ziuku, S.; Maganga, H.; Siachingoma, B.; Ndlovu, S. On the potential of water hyacinth as a biomass briquette for heating applications. *Int. J. Energy Environ. Eng.* **2016**, *7*, 37–43, doi:10.1007/s40095-015-0195-8.

36. Mishra, S.; Maiti, A. The efficiency of Eichhornia crassipes in the removal of organic and inorganic pollutants from wastewater: a review. *Environ. Sci. Pollut. Res.* **2017**, *24*, 7921–7937, doi:10.1007/s11356-016-8357-7.

37. Luu, K.T.; Getsinger, K.D. Seasonal Biomass and Carbohydrate Allocation in Waterhyacinth. *J. Aquat. Plant Manag.* **1990**, *28*, 3–10.

38. Shafy, H.I.; Farid, M.R.; El-Din, A.M. Water-Hyacinth from Nile River: Chemical contents, nutrient elements and heavy metals. *Egypt. J. Chem.* **2016**, *59*, 131–143, doi:10.21608/ejchem.2016.934.

39. Prochnow, a; Heiermann, M.; Plöchl, M.; Linke, B.; Idler, C.; Amon, T.; Hobbs, P.J. Bioenergy from permanent grassland--a review: 1. Biogas. *Bioresour. Technol.* **2009**, *100*, 4931–4944, doi:10.1016/j.biortech.2009.05.070.

40. Wall, D.M.; O'Kiely, P.; Murphy, J.D. The potential for biomethane from grass and slurry to satisfy renewable energy targets. *Bioresour. Technol.* **2013**, *149*, 425–431, doi:10.1016/j.biortech.2013.09.094.

41. Rodriguez, C.; Alaswad, A.; Benyounis, K.Y.; Olabi, A.G. Pretreatment techniques used in biogas production from grass. *Renew. Sustain. Energy Rev.* **2017**, *68*, 1193–1204, doi:10.1016/j.rser.2016.02.022.

42. Ceotto, E. Grasslands for bioenergy production. A review. *Agron. Sustain. Dev.* **2008**, *28*, 47–55, doi:10.1051/agro.

43. Mehmood, M.A.; Ibrahim, M.; Rashid, U.; Nawaz, M.; Ali, S.; Hussain, A.; Gull, M. Biomass production for bioenergy using marginal lands. *Sustain. Prod. Consum.* **2017**, *9*, 3–21, doi:10.1016/j.spc.2016.08.003.

44. Andriamanohiarisoamanana, F.J.; Matsunami, N.; Yamashiro, T.; Iwasaki, M.; Ihara, I.; Umetsu, K. High-solids anaerobic mono-digestion of riverbank grass under thermophilic conditions. *J. Environ. Sci.* **2017**, *52*, 29–38, doi:10.1016/j.jes.2016.05.005.

45. Nitsche, M.; Hensgen, F.; Wachendorf, M. Using grass cuttings from sports fields for anaerobic digestion and combustion. *Energies* **2017**, *10*, doi:10.3390/en10030388.

46. Brown, A.E.; Ford, J.S.; Bale, C.S.E.; Camargo-Valero, M.A.; Cheffins, N.J.; Mason, P.E.; Price-Allison, A.M.; Ross, A.B.; Taylor, P.G. An assessment of road-verge grass as a feedstock for farm-fed anaerobic digestion plants. *Biomass and Bioenergy* **2020**, *138*, 105570, doi:10.1016/j.biombioe.2020.105570.

47. Cadavid Rodríguez, L.S.; Bolaños Valencia, I.V. Grass from public green spaces an alternative source of renewable energy in tropical countries. *Rev. Investig. Optim. y Nuevos procesos en Ing.* **2016**, *29*, 109–116, doi:10.18273/revion.v29n1-2016009.

48. Hidaka, T.; Arai, S.; Okamoto, S.; Uchida, T. Anaerobic co-digestion of sewage sludge with shredded grass from public green spaces. *Bioresour. Technol.* **2013**, *130*, 667–672, doi:10.1016/j.biortech.2012.12.068.

49. Smith, A.M.; Whittaker, C.; Shield, I.; Ross, A.B. The potential for production of

high quality bio-coal from early harvested Miscanthus by hydrothermal carbonisation. *Fuel* **2018**, *220*, 546–557, doi:10.1016/j.fuel.2018.01.143.

50. Watson, L. The grass family, *Poaceae*. In G.P. Chapman (Ed), Reproductive Versatility in the Grasses.; Cambridge University Press, **1990**.

51. Chiumenti, A.; Boscaro, D.; Da Borso, F.; Sartori, L.; Pezzuolo, A. Biogas from fresh spring and summer grass: Effect of the harvesting period. *Energies* **2018**, *11*, doi:10.3390/en11061466.

52. Nizami, A.S.; Orozco, A.; Groom, E.; Dieterich, B.; Murphy, J.D. How much gas can we get from grass? *Appl. Energy* **2012**, *92*, 783–790, doi:10.1016/j.apenergy.2011.08.033.

53. Nizami, A.S.; Korres, N.; Murphy, J. Review of the integrated process for the production of grass biomethane. *Environ. Sci. Technol.* **2009**, *43*, 8496–508, doi:10.1021/es901533j.

54. Prochnow, A.; Heiermann, M.; Drenckhan, A.; Schelle, H. Seasonal Pattern of Biomethanisation of Grass from Landscape Management. *Agric. Eng. Int. CIGR Ejournal* **2005**, *VII*, 1–17.

55. Jung, K.A.; Lim, S.R.; Kim, Y.; Park, J.M. Potentials of macroalgae as feedstocks for biorefinery. *Bioresour. Technol.* **2013**, *135*, 182–190, doi:10.1016/j.biortech.2012.10.025.

56. Torres, M.D.; Kraan, S.; Domínguez, H. Seaweed biorefinery. *Rev. Environ. Sci. Bio/Technology* **2019**, *18*, 335–388, doi:10.1007/s11157-019-09496-y.

57. Chen, H.; Zhou, D.; Luo, G.; Zhang, S.; Chen, J. Macroalgae for biofuels production: Progress and perspectives. *Renew. Sustain. Energy Rev.* **2015**, *47*, 427–437, doi:10.1016/j.rser.2015.03.086.

58. Gao, G.; Burgess, J.G.; Wu, M.; Wang, S.; Gao, K. Using macroalgae as biofuel: current opportunities and challenges. *Bot. Mar.* **2020**, *1*, doi:10.1515/bot-2019-0065.

59. Bruhn, A.; Dahl, J.; Nielsen, H.B.; Nikolaisen, L.; Rasmussen, M.B.; Markager, S.; Olesen, B.; Arias, C.; Jensen, P.D. Bioenergy potential of Ulva lactuca : Biomass yield , methane production and combustion. *Bioresour. Technol.* **2011**, *102*, 2595–2604, doi:10.1016/j.biortech.2010.10.010.

60. Adams, J.M.M.; Toop, T.A.; Donnison, I.S.; Gallagher, J.A. Seasonal variation in Laminaria digitata and its impact on biochemical conversion routes to biofuels. *Bioresour. Technol.* **2011**, *102*, 9976–9984, doi:10.1016/j.biortech.2011.08.032.

61. Adams, J.M.M.; Ross, A.B.; Anastasakis, K.; Hodgson, E.M.; Gallagher, J.A.; Jones, J.M.; Donnison, I.S. Seasonal variation in the chemical composition of the bioenergy feedstock Laminaria digitata for thermochemical conversion. *Bioresour. Technol.* **2011**, *102*, 226–234, doi:10.1016/j.biortech.2010.06.152.

62. Schiener, P.; Black, K.D.; Stanley, M.S.; Green, D.H. The seasonal variation in the chemical composition of the kelp species Laminaria digitata, Laminaria hyperborea, Saccharina latissima and Alaria esculenta. *J. Appl. Phycol.* **2014**, *27*, 363–373, doi:10.1007/s10811-014-0327-1.

63. Fletcher, H.R.; Biller, P.; Ross, A.B.; Adams, J.M.M. The seasonal variation of fucoidan within three species of brown macroalgae. *Algal Res.* **2017**, *22*, 79–86, doi:10.1016/j.algal.2016.10.015.

64. Smith, A.M.; Singh, S.; Ross, A.B. Fate of inorganic material during hydrothermal carbonisation of biomass : Influence of feedstock on combustion behaviour of hydrochar. *FUEL* **2016**, *169*, 135–145, doi:10.1016/j.fuel.2015.12.006.

65. Ross, A.B.; Jones, J.M.; Kubacki, M.L.; Bridgeman, T. Classification of macroalgae

as fuel and its thermochemical behaviour. **2008**, *99*, 6494–6504, doi:10.1016/j.biortech.2007.11.036.

66. Kantarli, İ.C.; Pala, M.; Yildirim, Y.; Yanik, J.; Abrreu, M.H. Fuel characteristics and combustion behavior of seaweed-derived hydrochars. *Turkish J. Chem.* **2019**, *43*, 475–491, doi:10.3906/kim-1807-7.

67. Tabassum, M.R.; Xia, A.; Murphy, J.D. The effect of seasonal variation on biomethane production from seaweed and on application as a gaseous transport biofuel. *Bioresour. Technol.* **2016**, *209*, 213–219, doi:10.1016/j.biortech.2016.02.120.

68. Black, W.A.P. Seasonal variation in chemical composition of some of the littoral seaweeds common to scotland. Part II. Fucus serratus. Fucus Vesiculosus. Fucus spiralis and pelvetia canaliculata. *J. Soc. Chem. Ind.* **1949**, *68*, 183–189.

69. Fletcher, H. Microwave Assisted Hydrothermal Extraction of Carbohydrates from Macroalgae and the Impact of Seasonal Variation, PhD Thesis, University of Leeds, **2016**.

70. Nielsen, M.M.; Manns, D.; D'Este, M.; Krause-Jensen, D.; Rasmussen, M.B.; Larsen, M.M.; Alvarado-Morales, M.; Angelidaki, I.; Bruhn, A. Variation in biochemical composition of Saccharina latissima and Laminaria digitata along an estuarine salinity gradient in inner Danish waters. *Algal Res.* **2016**, *13*, 235–245, doi:10.1016/j.algal.2015.12.003.

71. Allen, E.; Wall, D.M.; Herrmann, C.; Xia, A.; Murphy, J.D. What is the gross energy yield of third generation gaseous biofuel sourced from seaweed ? *Energy* **2015**, *81*, 352–360, doi:10.1016/j.energy.2014.12.048.

72. Lin, R.; Deng, C.; Ding, L.; Bose, A.; Murphy, J.D. Improving gaseous biofuel production from seaweed Saccharina latissima : The effect of hydrothermal pretreatment on energy efficiency. *Energy Convers. Manag.* **2019**, *196*, 1385–1394, doi:10.1016/j.enconman.2019.06.044.

73. Black, W.A.P. The seasonal variation in the cellulose content of the common Scottish Laminariaceae and Fucaceae. *J. Mar. Biol. Assoc. United Kingdom* **1950**, *29*, 379–387, doi:10.1017/S0025315400055429.

74. Reza, M.T.; Lynam, J.G.; Uddin, M.H.; Coronella, C.J. Hydrothermal carbonization: Fate of inorganics. *Biomass and Bioenergy* **2013**, *49*, 86–94, doi:10.1016/j.biombioe.2012.12.004.

75. Kambo, H.S.; Dutta, A. A comparative review of biochar and hydrochar in terms of production, physico-chemical properties and applications. *Renew. Sustain. Energy Rev.* **2015**, *45*, 359–378, doi:10.1016/j.rser.2015.01.050.

76. Zhang, C.; Ma, X.; Chen, X.; Tian, Y.; Zhou, Y.; Lu, X.; Huang, T. Conversion of water hyacinth to value-added fuel via hydrothermal carbonization. *Energy* **2020**, *197*, 117193, doi:10.1016/j.energy.2020.117193.

77. Román, S.; Ledesma, B.; Álvarez, A.; Coronella, C.; Qaramaleki, S.V. Suitability of hydrothermal carbonization to convert water hyacinth to added-value products. *Renew. Energy* **2020**, *146*, 1649–1658, doi:10.1016/j.renene.2019.07.157.

78. Gao, Y.; Wang, X.; Wang, J.; Li, X.; Cheng, J.; Yang, H.; Chen, H. Effect of residence time on chemical and structural properties of hydrochar obtained by hydrothermal carbonization of water hyacinth. *Energy* **2013**, *58*, 376–383, doi:10.1016/j.energy.2013.06.023.

79. Guo, S.; Dong, X.; Liu, K.; Yu, H.; Zhu, C. Chemical, energetic, and structural characteristics of hydrothermal carbonization solid products for lawn grass. *BioResources* **2015**, *10*, 4613–4625, doi:10.15376/biores.10.3.4613-4625.

80. Smith, A.M.; Ross, A.B. Production of bio-coal, bio-methane and fertilizer from seaweed via hydrothermal carbonisation. *Algal Res.* **2016**, *16*, 1–11, doi:10.1016/j.algal.2016.02.026.

81. Smith, K.L.; Smoot, L.D.; Fletcher, T.H.; Purgmire, R.J. *The structure and reaction processes of coal*; Springer Science & Business Media, **1994**;

82. Caillat, S.; Vakkilainen, E. Large-scale biomass combustion plants: An overview; Woodhead Publishing Limited, **2013**; pp.189-224.

83. Vassilev, S. V; Baxter, D.; Andersen, L.K.; Vassileva, C.G. An overview of the composition and application of biomass ash . Part 1 . Phase – mineral and chemical composition and classification. *Fuel* **2013**, *105*, 40–76, doi:10.1016/j.fuel.2012.09.041.

84. Marin-Batista, J.D.; Villamil, J.A.; Qaramaleki, S. V.; Coronella, C.J.; Mohedano, A.F.; Rubia, M.A. d. la Energy valorization of cow manure by hydrothermal carbonization and anaerobic digestion. *Renew. Energy* **2020**, *160*, 623–632, doi:10.1016/j.renene.2020.07.003.

85. Hudakorn, T.; Sritrakul, N. Biogas and biomass pellet production from water hyacinth. *Energy Reports* **2020**, *6*, 532–538, doi:10.1016/j.egyr.2019.11.115.

86. Ipiales, R.P.; de la Rubia, M.A.; Diaz, E.; Mohedano, A.F.; Rodriguez, J.J. Integration of Hydrothermal Carbonization and Anaerobic Digestion for Energy Recovery of Biomass Waste: An Overview. *Energy & Fuels* **2021**, doi:10.1021/acs.energyfuels.1c01681.

87. Xie, S.; Wickham, R.; Nghiem, L.D. Synergistic effect from anaerobic co-digestion of sewage sludge and organic wastes. *Int. Biodeterior. Biodegrad.* **2017**, *116*, 191–197, doi:10.1016/j.ibiod.2016.10.037.

88. Angelidaki, I.; Treu, L.; Tsapekos, P.; Luo, G.; Campanaro, S.; Wenzel, H.; Kougias, P.G. Biogas upgrading and utilization: Current status and perspectives. *Biotechnol. Adv.* **2018**, *36*, 452–466, doi:10.1016/j.biotechadv.2018.01.011.

89. Weiland, P. Biogas production: Current state and perspectives. *Appl. Microbiol. Biotechnol.* **2010**, *85*, 849–860, doi:10.1007/s00253-009-2246-7.

90. Bharathiraja, B.; Sudharsanaa, T.; Bharghavi, A.; Jayamuthunagai, J.; Praveenkumar, R. Biohydrogen and Biogas – An overview on feedstocks and enhancement process. *Fuel* **2016**, *185*, 810–828, doi:10.1016/j.fuel.2016.08.030.

91. Demirel, B.; Scherer, P. The roles of acetotrophic and hydrogenotrophic methanogens during anaerobic conversion of biomass to methane: A review. *Rev. Environ. Sci. Biotechnol.* **2008**, *7*, 173–190, doi:10.1007/s11157-008-9131-1.

92. Kondusamy, D.; Kalamdhad, A.S. Pre-treatment and anaerobic digestion of food waste for high rate methane production - A review. *J. Environ. Chem. Eng.* **2014**, *2*, 1821–1830, doi:10.1016/j.jece.2014.07.024.

93. Bharathiraja, B.; Sudharsanaa, T.; Bharghavi, A.; Jayamuthunagai, J.; Praveenkumar, R. Biohydrogen and Biogas – An overview on feedstocks and enhancement process. *Fuel* **2016**, *185*, 810–828, doi:10.1016/j.fuel.2016.08.030.

94. Mosey, F.E. Mathematical modelling of the anaerobic digestion process: regulatory mechanisms for the formation of short-chain volatile acids from glucose. *Water Sci. Technol.* **1983**, *15*, 209–232, doi:https://doi.org/10.2166/wst.1983.0168.

95. Lesteur, M.; Bellon-Maurel, V.; Gonzalez, C.; Latrille, E.; Roger, J.M.; Junqua, G.; Steyer, J.P. Alternative methods for determining anaerobic biodegradability: A review. *Process Biochem.* **2010**, *45*, 431–440, doi:10.1016/j.procbio.2009.11.018.

96. Angelidaki, I.; Sanders, W. Assessment of the anaerobic biodegradability of

macropollutants. *Rev. Environ. Sci. Biotechnol.* **2004**, *3*, 117–129, doi:10.1007/s11157-004-2502-3.

97. Raposo, F.; Fernández-Cegrí, V.; de la Rubia, M.A.; Borja, R.; Béline, F.; Cavinato, C.; Demirer, G.; Fernández, B.; Fernández-Polanco, M.; Frigon, J.C.; Ganesh, H.; Kaparaju, P.; Koubova, J.; Méndez, R.; Menin, G.; Peene, A.; Scherer, P.; Torijos, M.; Uellendahl, H.; Wierinck., de Wilde, V. Biochemical methane potential (BMP) of solid organic substrates: Evaluation of anaerobic biodegradability using data from an international interlaboratory study. J. Chem. Technol. Biotechnol. 2011, 86, 1088–1098, doi:10.1002/jctb.2622.

98. Symons, G.E.; Buswell, A.M. The Methane Fermentation of Carbohydrates. *J. Am. Chem. Soc.* **1933**, *55*, 2028–2036, doi:10.1021/ja01332a039.

99. Buswell, M.; Mueller, H.F. Mechanisms of Methane Fermentation. *Ind. Eng. Chem.* **1952**, *44*, 550–552, doi:10.1021/ie50507a033.

100. Nielfa, A.; Cano, R.; Fdz-Polanco, M. Theoretical methane production generated by the co-digestion of organic fraction municipal solid waste and biological sludge. *Biotechnol. Reports* **2015**, *5*, 14–21, doi:10.1016/j.btre.2014.10.005.

101. Koch, K.; Hafner, S.D.; Weinrich, S.; Astals, S.; Holliger, C. Power and Limitations of Biochemical Methane Potential (BMP) Tests. *Front. Energy Res.* **2020**, *8*, 63, doi:10.3389/fenrg.2020.00063.

102. Labatut, R.A.; Angenent, L.T.; Scott, N.R. Biochemical methane potential and biodegradability of complex organic substrates. *Bioresour. Technol.* **2011**, *102*, 2255–2264, doi:10.1016/j.biortech.2010.10.035.

103. Allen, E.; Wall, D.M.; Herrmann, C.; Murphy, J.D. A detailed assessment of resource of biomethane from first, second and third generation substrates. *Renew. Energy* **2016**, *87*, 656–665, doi:10.1016/j.renene.2015.10.060.

104. Chen, Y.; Cheng, J.J.; Creamer, K.S. Inhibition of anaerobic digestion process: A review. *Bioresour. Technol.* **2008**, *99*, 4044–4064, doi:10.1016/j.biortech.2007.01.057.

105. Paul, S.; Dutta, A. Challenges and opportunities of lignocellulosic biomass for anaerobic digestion. *Resour. Conserv. Recycl.* **2018**, *130*, 164–174, doi:10.1016/j.resconrec.2017.12.005.

106. Patil, J.H.; AntonyRaj, M.; Gavimath, C.C. Study on Effect of Pretreatment Methods on Biomethanation of Water Hyacinth. *Int. J. Adv. Biotechnol. Res.* **2011**, *2*, 143–147.

107. Priya, P.; Nikhitha, S.O.; Anand, C.; Nath, R.D.; Krishnakumar, B. Biomethanation of water hyacinth biomass. *Bioresour. Technol.* **2018**, *255*, 288–292, doi:10.1016/j.biortech.2018.01.119.

108. Patil, J.H.; AntonyRaj, M.; Shankar, B.B.; Shetty, M.K.; Kumar, B.P. Anaerobic co-digestion of Water Hyacinth and Sheep Waste. *Energy Procedia* **2014**, *52*, 572–578, doi:10.1016/j.egypro.2014.07.112.

109. O'Sullivan, C.; Rounsefell, B.; Grinham, A.; Clarke, W.; Udy, J. Anaerobic digestion of harvested aquatic weeds: Water hyacinth (Eichhornia crassipes), cabomba (Cabomba Caroliniana) and salvinia (Salvinia molesta). *Ecol. Eng.* **2010**, *36*, 1459–1468, doi:10.1016/j.ecoleng.2010.06.027.

110. Varanasi, J.L.; Kumari, S.; Das, D. Improvement of energy recovery from water hyacinth by using integrated system. *Int. J. Hydrogen Energy* **2018**, *43*, 1303–1318, doi:10.1016/j.ijhydene.2017.11.110.

111. Gao, J.; Chen, L.; Yan, Z.; Wang, L. Effect of ionic liquid pretreatment on the composition, structure and biogas production of water hyacinth (Eichhornia

crassipes). *Bioresour. Technol.* **2013**, *132*, 361–364, doi:10.1016/j.biortech.2012.10.136.

112. Ali, S.S.; Sun, J. Effective thermal pretreatment of water hyacinth (Eichhornia crassipes) for the enhancement of biomethanation: VIT ® gene probe technology for microbial community analysis with special reference to methanogenic Archaea. *J. Environ. Chem. Eng.* **2019**, *7*, 102853, doi:10.1016/j.jece.2018.102853.

113. Kist, D.L.; Pérez-Elvira, S.I.; Monteggia, L.O. Evaluation of the steam explosion pretreatment upon the anaerobic digestion of water hyacinth biomass : influence on liquid and solid fractions. *Am. Sci. Res. J. Eng. Technol. Sci.* **2018**, *40*, 298–317.

114. Ferrer, I.; Palatsi, J.; Campos, E.; Flotats, X. Mesophilic and thermophilic anaerobic biodegradability of water hyacinth pre-treated at 80°C. *Waste Manag.* **2010**, *30*, 1763–1767, doi:10.1016/j.wasman.2009.09.020.

115. Alfageme, E.R.; Fujiwara, M.; Toda, T. Steam explosion and thermal hydrolysis for pretreating Eichhornia crassipes to enhance anaerobic digestion. In Proceedings of the Proceedings of the Annual Conference of Japan Society of Material Cycles and Waste Management; Sendai, Japan, 19–21 September 2019; Japan Society of Material Cycles and Waste Management; Tokyo, Japan, **2019**; p. 551-552.

116. Rasam, S.; Talebkeikhah, F.; Talebkeikhah, M.; Salimi, A.; Moraveji, M.K. Physico-chemical properties prediction of hydrochar in macroalgae Sargassum horneri hydrothermal carbonisation. *Int. J. Environ. Anal. Chem.* **2019**, 1–22, doi:10.1080/03067319.2019.1700973.

117. Shiralipour, A.; Smith, P.H. Conversion of biomass into methane gas. *Biomass* **1984**, *6*, 85–92, doi:10.1016/0144-4565(84)90011-8.

118. Xia, Y.; Sheng, K.; Kloss, R.; Chen, Z.; Zhou, R. Effects of silage pretreatment on the anaerobic digestion of different parts of water hyacinth. In Proceedings of the American Society of Agricultural and Biological Engineers Annual International Meeting 2013, ASABE 2013; Kansas City, Missouri, 2013; p. 131620187.

119. Baura, V.B.; Kalamdhad, A.S. Effect of various types of thermal pretreatment techniques on the hydrolysis , compositional analysis and characterization of water hyacinth. *Bioresour. Technol.* **2017**, *227*, 147–154, doi:10.1016/j.biortech.2016.12.036.

120. Lin, R.; Cheng, J.; Song, W.; Ding, L.; Xie, B.; Zhou, J.; Cen, K. Characterisation of water hyacinth with microwave-heated alkali pretreatment for enhanced enzymatic digestibility and hydrogen / methane fermentation. *Bioresour. Technol.* **2015**, *182*, 1–7, doi:10.1016/j.biortech.2015.01.105.

121. Putra, Y.; Murni, D.; Kurniawan, T. Study of Biogas Production Rate from Water Hyacinth by Hydrothermal Pretreatment with Buffalo Dung as a Starter. *Waste Technol.* **2014**, *2*, 26–30, doi:10.12777/wastech.2.2.26-30.

122. Mähnert, P.; Heiermann, M.; Linke, B. Batch- and Semi-continuous Biogas Production from Different Grass Species. *Agric. Eng.* **2005**, *VII*, 1–11.

123. Raju, C.S.; Ward, A.J.; Nielsen, L.; Møller, H.B. Comparison of near infra-red spectroscopy, neutral detergent fibre assay and in-vitro organic matter digestibility assay for rapid determination of the biochemical methane potential of meadow grasses. *Bioresour. Technol.* **2011**, *102*, 7835–7839, doi:10.1016/j.biortech.2011.05.049.

124. Deng, C.; Lin, R.; Cheng, J.; Murphy, J.D. Can acid pre-treatment enhance biohydrogen and biomethane production from grass silage in single-stage and two-stage fermentation processes ? *Energy Convers. Manag.* **2019**, *195*, 738–747, doi:10.1016/j.enconman.2019.05.044.

125. Yu, L.; Bule, M.; Ma, J.; Zhao, Q.; Frear, C.; Chen, S. Enhancing volatile fatty acid (VFA) and bio-methane production from lawn grass with pretreatment. *Bioresour. Technol.* **2014**, *162*, 243–249, doi:10.1016/j.biortech.2014.03.089.

126. Thompson, T.M.; Young, B.R.; Baroutian, S. Advances in the pretreatment of brown macroalgae for biogas production. *Fuel Process. Technol.* **2019**, *195*, 106151, doi:10.1016/j.fuproc.2019.106151.

127. Vanegas, C.H.; Bartlett, J. Green energy from marine algae : biogas production and composition from the anaerobic digestion of Irish seaweed species. *Environ. Technol.* **2013**, *34*, 2277–2283, doi:10.1080/09593330.2013.765922.

128. Heffernan, N.; Smyth, T.J.; Soler-Villa, A.; Fitzgerald, R.J.; Brunton, N.P. Phenolic content and antioxidant activity of fractions obtained from selected Irish macroalgae species (Laminaria digitata, Fucus serratus, Gracilaria gracilis and Codium fragile). *J. Appl. Phycol.* **2015**, *27*, 519–530, doi:10.1007/s10811-014-0291-9.

129. Tabassum, M.R.; Xia, A.; Murphy, J.D. Seasonal variation of chemical composition and biomethane production from the brown seaweed Ascophyllum nodosum. *Bioresour. Technol.* **2016**, *216*, 219–226, doi:10.1016/j.biortech.2016.05.071.

130. Tabassum, M.R.; Xia, A.; Murphy, J.D. Biomethane production from various segments of brown seaweed. *Energy Convers. Manag.* **2018**, *174*, 855–862, doi:10.1016/j.enconman.2018.08.084.

131. Tabassum, M.R.; Xia, A.; Murphy, J.D. Comparison of pre-treatments to reduce salinity and enhance biomethane yields of Laminaria digitata harvested in different seasons. *Energy* **2017**, *140*, 546–551, doi:10.1016/j.energy.2017.08.070.

132. Vivekanand, V.; Eijsink, V.G.H.; Horn, S.J. Biogas production from the brown seaweed Saccharina latissima : thermal pretreatment and codigestion with wheat straw. *J. Appl. Phycol.* **2012**, *24*, 1295–1301, doi:10.1007/s10811-011-9779-8.

133. Tedesco, S.; Daniels, S. Optimisation of biogas generation from brown seaweed residues: Compositional and geographical parameters affecting the viability of a biorefinery concept. *Appl. Energy* **2018**, *228*, 712–723, doi:10.1016/j.apenergy.2018.06.120.

134. Tedesco, S.; Stokes, J. Valorisation to biogas of macroalgal waste streams: A circular approach to bioproducts and bioenergy in Ireland. *Chem. Pap.* **2017**, *71*, 721–728, doi:10.1007/s11696-016-0005-7.

135. Guneratnam, A.J.; Xia, A.; Murphy, J.D. Comparative study of single- and two-stage fermentation of the brown seaweed Laminaria digitata. *Energy Convers. Manag.* **2017**, *148*, 405–412, doi:10.1016/j.enconman.2017.06.013.

136. Wong, Y.M.; Wu, T.Y.; Juan, J.C. A review of sustainable hydrogen production using seed sludge via dark fermentation. *Renew. Sustain. Energy Rev.* **2014**, *34*, 471–482, doi:10.1016/j.rser.2014.03.008.

137. Guo, X.M.; Trably, E.; Latrille, E.; Carrere, H.; Steyer, J.P. Predictive and explicative models of fermentative hydrogen production from solid organic waste: Role of butyrate and lactate pathways. *Int. J. Hydrogen Energy* **2014**, *39*, 7476–7485, doi:10.1016/j.ijhydene.2013.08.079.

138. Li, C.; Fang, H.H.P. Fermentative Hydrogen Production From Wastewater and Solid Wastes by Mixed Cultures. *Crit. Rev. Environ. Sci. Technol.* **2007**, *37*, 1–39, doi:10.1080/10643380600729071.

139. Gioannis, G. De; Muntoni, A.; Polettini, A.; Pomi, R.; Spiga, D. Energy recovery from one- and two-stage anaerobic digestion of food waste. *Waste Manag.* **2017**, *68*, 595–602, doi:10.1016/j.wasman.2017.06.013.

140. Roy, S.; Das, D. Biohythane production from organic wastes : present state of art.

Enivronmental Sci. Pollut. Res. **2016**, *23*, 9391–9410, doi:10.1007/s11356-015-5469-4.

141. De Gioannis, G.; Muntoni, A.; Polettini, A.; Pomi, R. A review of dark fermentative hydrogen production from biodegradable municipal waste fractions. *Waste Manag.* **2013**, *33*, 1345–1361, doi:10.1016/j.wasman.2013.02.019.

142. Schievano, A.; Tenca, A.; Lonati, S.; Manzini, E.; Adani, F. Can two-stage instead of one-stage anaerobic digestion really increase energy recovery from biomass? *Appl. Energy* **2014**, *124*, 335–342, doi:10.1016/j.apenergy.2014.03.024.

143. Massanet-Nicolau, J.; Dinsdale, R.; Guwy, A.; Shipley, G. Utilising biohydrogen to increase methane production, energy yields and process efficiency via two stage anaerobic digestion of grass. *Bioresour. Technol.* **2015**, *189*, 379–383, doi:10.1016/j.biortech.2015.03.116.

144. Arreola-vargas, J.; Flores-Larios, A.; González-Álvarez, V.; Corona-González, R.I.; Méndez-Acosta, H.O. Single and two-stage anaerobic digestion for hydrogen and methane production from acid and enzymatic hydrolysates of Agave tequilana bagasse. *Int. J. Hydrogen Energy* **2016**, *41*, 897–904, doi:10.1016/j.ijhydene.2015.11.016.

145. Liu, D.; Liu, D.; Zeng, R.J.; Angelidaki, I. Hydrogen and methane production from household solid waste in the two-stage fermentation process. *Water Res.* **2006**, *40*, 2230–2236, doi:10.1016/j.watres.2006.03.029.

146. Reza, M.T.; Andert, J.; Wirth, B.; Busch, D.; Pielert, J.; Lynam, J.G.; Mumme, J. Hydrothermal Carbonization of Biomass for Energy and Crop Production. *Appl. Bioenergy* **2014**, *1*, 11–29, doi:10.2478/apbi-2014-0001.

147. Wirth, B.; Mumme, J. Anaerobic Digestion of Waste Water from Hydrothermal Carbonization of Corn Silage. *Appl. Bioenergy* **2013**, *1*, 1–10, doi:10.2478/apbi-2013-0001.

148. Funke, A.; Ziegler, F. Hydrothermal carbonization of biomass: a summary and discussion of chemical mechanisms for process engineering. *Biofuels, Bioprod. Biorefining* **2010**, *4*, 160–177, doi:10.1002/bbb.

149. Nicolae, S.A.; Au, H.; Modugno, P.; Luo, H.; Szego, A.E.; Qiao, M.; Li, L.; Yin, W.; Heeres, H.J.; Berge, N.; Titirici, M.M. Recent advances in hydrothermal carbonisation: from tailored carbon materials and biochemicals to applications and bioenergy. Green Chem. 2020, 22, 4747–4800, doi:10.1039/d0gc00998a.

150. Kruse, A.; Funke, A.; Titirici, M.M. Hydrothermal conversion of biomass to fuels and energetic materials. *Curr. Opin. Chem. Biol.* **2013**, *17*, 515–521, doi:10.1016/j.cbpa.2013.05.004.

151. Ruiz, H.A.; Rodríguez-Jasso, R.M.; Fernandes, B.D.; Vicente, A.A.; Teixeira, J.A. Hydrothermal processing, as an alternative for upgrading agriculture residues and marine biomass according to the biorefinery concept: A review. *Renew. Sustain. Energy Rev.* **2013**, *21*, 35–51, doi:10.1016/j.rser.2012.11.069.

152. Machado, N.T.; de Castro, D.A.R.; Santos, M.C.; Araújo, M.E.; Lüder, U.; Herklotz, L.; Werner, M.; Mumme, J.; Hoffmann, T. Process analysis of hydrothermal carbonization of corn Stover with subcritical H 2 O. *J. Supercrit. Fluids* **2018**, *136*, 110–122, doi:10.1016/j.supflu.2018.01.012.

153. Pauline, A.L.; Joseph, K. Hydrothermal carbonization of organic wastes to carbonaceous solid fuel – A review of mechanisms and process parameters. *Fuel* **2020**, *279*, 118472, doi:10.1016/j.fuel.2020.118472.

154. Fang, J.; Zhan, L.; Ok, Y.S.; Gao, B. Minireview of potential applications of hydrochar derived from hydrothermal carbonization of biomass. *J. Ind. Eng. Chem.*

2018, *57*, 15–21, doi:10.1016/j.jiec.2017.08.026.

155. Fernández-Sanromán, Á.; Lama, G.; Pazos, M.; Rosales, E.; Sanromán, M.Á. Bridging the gap to hydrochar production and its application into frameworks of bioenergy, environmental and biocatalysis areas. *Bioresour. Technol.* **2021**, *320*, 124399, doi:10.1016/j.biortech.2020.124399.

156. Higgins, L.J.R.; Brown, A.P.; Harrington, J.P.; Ross, A.B.; Kaulich, B.; Mishra, B. Evidence for a core-shell structure of hydrothermal carbon. *Carbon N. Y.* **2020**, *161*, 423–431, doi:10.1016/j.carbon.2020.01.060.

157. Becker, R.; Dorgerloh, U.; Paulke, E.; Mumme, J.; Nehls, I. Hydrothermal carbonization of biomass: Major organic components of the aqueous phase. *Chem. Eng. Technol.* 2014, *37*, 511–518.

158. Nakason, K.; Panyapinyopol, B.; Kanokkantapong, V.; Viriya-empikul, N.; Kraithong, W.; Pavasant, P. Hydrothermal carbonization of unwanted biomass materials: Effect of process temperature and retention time on hydrochar and liquid fraction. *J. Energy Inst.* **2017**, 1–11, doi:10.1016/j.joei.2017.05.002.

159. Reza, M.T.; Andert, J.; Wirth, B.; Busch, D.; Pielert, J.; Lynam, J.G.; Mumme, J. Hydrothermal Carbonization of Biomass for Energy and Crop Production. *Appl. Bioenergy* **2014**, *1*, 11–29, doi:10.2478/apbi-2014-0001.

160. Marin-Batista, J.D.; Villamil, J.A.; Rodriguez, J.J.; Mohedano, A.F.; Rubia, M.A. De Valorization of microalgal biomass by hydrothermal carbonization and anaerobic digestion. *Bioresour. Technol.* **2019**, *274*, 395–402, doi:10.1016/j.biortech.2018.11.103.

161. Luz, F.C.; Volpe, M.; Fiori, L.; Manni, A.; Cordiner, S.; Mulone, V.; Rocco, V. Spent coffee enhanced biomethane potential via an integrated hydrothermal carbonization-anaerobic digestion process. *Bioresour. Technol.* **2018**, *256*, 102–109, doi:10.1016/j.biortech.2018.02.021.

162. Nizamuddin, S.; Baloch, H.A.; Griffin, G.J.; Mubarak, N.M.; Bhutto, A.W.; Abro, R.; Mazari, S.A.; Ali, B.S. An overview of effect of process parameters on hydrothermal carbonization of biomass. *Renew. Sustain. Energy Rev.* 2017, *73*, 1289–1299.

163. Erdogan, E.; Atila, B.; Mumme, J.; Reza, M.T.; Toptas, A.; Elibol, M.; Yanik, J. Characterization of products from hydrothermal carbonization of orange pomace including anaerobic digestibility of process liquor. *Bioresour. Technol.* **2015**, *196*, 35–42, doi:10.1016/j.biortech.2015.06.115.

164. Smith, A.M.; Ross, A.B. The influence of residence time during hydrothermal carbonisation of miscanthus on bio-coal combustion chemistry. *Energies* **2019**, *12*, 523, doi:10.3390/en12030523.

165. Hatcher, P.G.; Breger, I.A.; Earl, W.L. Nuclear magnetic resonance studies of ancient buried wood-I. Observations on the origin of coal to the brown coal stage. *Org. Geochem.* **1981**, *3*, 49–55, doi:10.1016/0146-6380(81)90013-9.

166. Choe, U.; Mustafa, A.M.; Lin, H.; Xu, J.; Sheng, K. Effect of bamboo hydrochar on anaerobic digestion of fish processing waste for biogas production. *Bioresour. Technol.* **2019**, doi:10.1016/j.biortech.2019.03.084.

167. Xu, J.; Mustafa, A.M.; Lin, H.; Choe, U.Y.; Sheng, K. Effect of hydrochar on anaerobic digestion of dead pig carcass after hydrothermal pretreatment. *Waste Manag.* **2018**, *78*, 849–856, doi:10.1016/j.wasman.2018.07.003.

168. Guo, W.; Li, Y.; Zhao, K.; Xu, Q.; Jiang, H.; Zhou, H. Performance and Microbial Community Analysis of Anaerobic Digestion of Vinegar Residue with Adding of Acetylene Black or Hydrochar. *Waste and Biomass Valorization* **2019**, 1–11,

doi:10.1007/s12649-019-00664-3.

169. Wang, F.; Wang, J.; Li, Z.; Zan, S.; Du, M. Promoting anaerobic digestion by algae-based hydrochars in a continuous reactor. *Bioresour. Technol.* **2020**, *318*, 124201, doi:10.1016/j.biortech.2020.124201.

170. Aragón-Briceño, C.; Ross, A.B.; Camargo-Valero, M.A. Evaluation and comparison of product yields and bio-methane potential in sewage digestate following hydrothermal treatment. *Appl. Energy* **2017**, *208*, 1357–1369, doi:10.1016/j.apenergy.2017.09.019.

171. Parmar, K.R.; Ross, A.B. Integration of Hydrothermal Carbonisation with Anaerobic Digestion; Opportunities for Valorisation of Digestate. *Energies* **2019**, *12*, 1586, doi:10.3390/en12091586.

172. Gao, Y.; Chen, H.; Wang, J.; Shi, T.; Yang, H.-P.; Wang, X.-H. Characterization of products from hydrothermal liquefaction and carbonation of biomass model compounds and real biomass. *J. Fuel Chem. Technol.* **2011**, *39*, 893–900, doi:10.1016/S1872-5813(12)60001-2.

173. Gao, Y.; Yu, B.; Wu, K.; Yuan, Q.; Wang, X.; Chen, H. Physicochemical, pyrolytic, and combustion characteristics of hydrochar obtained by hydrothermal carbonization of biomass. *BioResources* **2016**, *11*, 4113–4133, doi:10.15376/biores.11.2.4113-4133.

174. Zhang, C.; Ma, X.; Huang, T.; Zhou, Y.; Tian, Y. Co-hydrothermal carbonization of water hyacinth and polyvinyl chloride: Optimization of process parameters and characterization of hydrochar. *Bioresour. Technol.* **2020**, *314*, 123676, doi:10.1016/j.biortech.2020.123676.

175. Munawer, M.E. Human health and environmental impacts of coal combustion and post-combustion wastes. *J. Sustain. Min.* **2018**, *17*, 87–96, doi:10.1016/j.jsm.2017.12.007.

176. Rezania, S.; Md Din, M.F.; Kamaruddin, S.F.; Taib, S.M.; Singh, L.; Yong, E.L.; Dahalan, F.A. Evaluation of water hyacinth (Eichhornia crassipes) as a potential raw material source for briquette production. *Energy* **2016**, *111*, 768–773, doi:10.1016/j.energy.2016.06.026.

177. Green, T.; Miria, O.I.; Crook, R.; Ross, A. Energy Calculator for Solar Processing of Biomass with Application to Uganda. *Energies* **2020**, *13*, 1485, doi:https://doi.org/10.3390/en13061485.

178. Qadi, N.; Takeno, K.; Mosqueda, A.; Kobayashi, M.; Motoyama, Y.; Yoshikawa, K. Effect of Hydrothermal Carbonization Conditions on the Physicochemical Properties and Gasification Reactivity of Energy Grass. *Energy and Fuels* **2019**, *33*, 6436–6443, doi:10.1021/acs.energyfuels.9b00994.

179. Wang, F.; Wang, J.; Gu, C.; Han, Y.; Zan, S.; Wu, S. Effects of process water recirculation on solid and liquid products from hydrothermal carbonization of Laminaria. *Bioresour. Technol.* **2019**, *292*, 121996, doi:10.1016/j.biortech.2019.121996.

180. Xu, Q.; Qian, Q.; Quek, A.; Ai, N.; Zeng, G.; Wang, J. Hydrothermal carbonization of macroalgae and the effects of experimental parameters on the properties of hydrochars. *ACS Sustain. Chem. Eng.* **2013**, *1*, 1092–1101, doi:10.1021/sc400118f.

181. Iñiguez, M.E.; Conesa, J.A.; Fullana, A. Hydrothermal carbonization (HTC) of marine plastic debris. *Fuel* **2019**, *257*, 116033, doi:10.1016/j.fuel.2019.116033.

182. Polikovsky, M.; Gillis, A.; Steinbruch, E.; Robin, A.; Epstein, M.; Kribus, A.; Golberg, A. Biorefinery for the co-production of protein, hydrochar and additional co-products from a green seaweed Ulva sp. with subcritical water hydrolysis. *Energy*

Convers. Manag. **2020**, *225*, 113380, doi:10.1016/j.enconman.2020.113380.

183. Brown, E.; Colling, A.; Park, D.; Phillips, J.; Rothery, D.; Wright, J. Seawater: its composition, properties, and behaviour; 2nd ed.; Pergamon, **1995**; pp. 85-124.

184. Shrestha, A.; Acharya, B.; Farooque, A.A. Study of hydrochar and process water from hydrothermal carbonization of sea lettuce. *Renew. Energy* **2021**, *163*, 589–598, doi:10.1016/j.renene.2020.08.133.

185. Patel, N.; Acharya, B.; Basu, P. Hydrothermal Carbonization (HTC) of Marine Seaweed (Macroalgae) for Producing Hydro-Char. *Energies* **2021**, *14*, 1805.

186. Steinbruch, E.; Drabik, D.; Epstein, M.; Ghosh, S.; Prabhu, M.S.; Gozin, M.; Kribus, A.; Golberg, A. Hydrothermal processing of a green seaweed Ulva sp. for the production of monosaccharides, polyhydroxyalkanoates, and hydrochar. *Bioresour. Technol.* **2020**, *318*, 124263, doi:10.1016/j.biortech.2020.124263.

187. Méndez, A.; Gascó, G.; Ruiz, B.; Fuente, E. Hydrochars from industrial macroalgae "Gelidium Sesquipedale" biomass wastes. *Bioresour. Technol.* **2019**, *275*, 386–393, doi:10.1016/j.biortech.2018.12.074.

188. Nakason, K.; Panyapinyopol, B.; Kanokkantapong, V.; Viriya-empikul, N.; Kraithong, W.; Pavasant, P. Characteristics of hydrochar and liquid fraction from hydrothermal carbonization of cassava rhizome. *J. Energy Inst.* **2018**, *91*, 184–193, doi:10.1016/j.joei.2017.01.002.

189. Volpe, M.; Wüst, D.; Merzari, F.; Lucian, M.; Andreottola, G.; Kruse, A.; Fiori, L. One stage olive mill waste streams valorisation via hydrothermal carbonisation. *Waste Manag.* **2018**, *80*, 224–234, doi:10.1016/j.wasman.2018.09.021.

190. Pagés-Díaz, J.; Alvarado, A.O.C.; Montalvo, S.; Diaz-Robles, L.; Curio, C.H. Anaerobic bio-methane potential of the liquors from hydrothermal carbonization of different lignocellulose biomasses. *Renew. Energy* **2020**, *157*, 182–189, doi:10.1016/j.renene.2020.05.025.

191. Hoekman, S.K.; Broch, Amber; Robbins, C. Hydrothermal carbonization (HTC) of lignocellulosic biomass. *Energy & Fuels* **2012**, *25*, 1802–1810, doi:10.1016/j.biortech.2012.05.060.

192. Monlau, F.; Sambusiti, C.; Barakat, A.; Quéméneur, M.; Trably, E.; Steyer, J.P.; Carrère, H. Do furanic and phenolic compounds of lignocellulosic and algae biomass hydrolyzate inhibit anaerobic mixed cultures? A comprehensive review. *Biotechnol. Adv.* **2014**, *32*, 934–951, doi:10.1016/j.biotechadv.2014.04.007.

193. Ahmed, B.; Aboudi, K.; Tyagi, V.K.; Álvarez-Gallego, C.J.; Fernández-Güelfo, L.A.; Romero-García, L.I.; Kazmi, A.A. Improvement of Anaerobic Digestion of Lignocellulosic Biomass by Hydrothermal Pretreatment. *Appl. Sci.* **2019**, *9*, 3853.

194. Milledge, J.J.; Nielsen, B. V.; Harvey, P.J. The inhibition of anaerobic digestion by model phenolic compounds representative of those from Sargassum muticum. *J. Appl. Phycol.* **2019**, *31*, 779–786, doi:10.1007/s10811-018-1512-4.

195. Zhao, K.; Li, Y.; Zhou, Y.; Guo, W.; Jiang, H.; Xu, Q. Characterization of hydrothermal carbonization products (hydrochars and spent liquor) and their biomethane production performance. *Bioresour. Technol.* **2018**, *267*, 9–16, doi:10.1016/j.biortech.2018.07.006.

196. Mumme, J.; Srocke, F.; Heeg, K.; Werner, M. Use of biochars in anaerobic digestion. *Bioresour. Technol.* **2014**, *164*, 189–197, doi:10.1016/j.biortech.2014.05.008.

197. Ren, S.; Usman, M.; Tsang, D.C.W.; O-Thong, S.; Angelidaki, I.; Zhu, X.; Zhang, S.; Luo, G. Hydrochar-Facilitated Anaerobic Digestion: Evidence for Direct Interspecies Electron Transfer Mediated through Surface Oxygen-Containing

Functional Groups. *Environ. Sci. Technol.* **2020**, *54*, 5755–5766, doi:10.1021/acs.est.0c00112.

198. Quintana-Najera, J.; Blacker, A.J.; Fletcher, L.A.; Ross, A.B. The effect of augmentation of biochar and hydrochar in anaerobic digestion of a model substrate. *Bioresour. Technol.* **2020**, *321*, 124494, doi:10.1016/j.biortech.2020.124494.

199. De la Rubia, M.A.; Villamil, J.A.; Rodriguez, J.J.; Mohedano, A.F. Effect of inoculum source and initial concentration on the anaerobic digestion of the liquid fraction from hydrothermal carbonisation of sewage sludge. *Renew. Energy* **2018**, *127*, 697–704, doi:10.1016/j.renene.2018.05.002.

200. Oliveira, I.; Blöhse, D.; Ramke, H.G. Hydrothermal carbonization of agricultural residues. *Bioresour. Technol.* **2013**, *142*, 138–146, doi:10.1016/j.biortech.2013.04.125.

201. Villamil, J.A.; Mohedano, A.F.; Rodriguez, J.J.; de la Rubia, M.A. Valorisation of the liquid fraction from hydrothermal carbonisation of sewage sludge by anaerobic digestion. *J. Chem. Technol. Biotechnol.* **2018**, *93*, 450–456, doi:10.1002/jctb.5375.

202. Weide, T.; Brügging, E.; Wetter, C. Anaerobic and aerobic degradation of wastewater from hydrothermal carbonization (HTC) in a continuous , three-stage and semi-industrial system. *J. Environ. Chem. Eng.* **2019**, *7*, 102912, doi:10.1016/j.jece.2019.102912.

203. Wirth, B.; Reza, T.; Mumme, J. Influence of digestion temperature and organic loading rate on the continuous anaerobic treatment of process liquor from hydrothermal carbonization of sewage sludge. *Bioresour. Technol.* **2015**, *198*, 215–222, doi:10.1016/j.biortech.2015.09.022.

204. Monlau, F.; Sambusiti, C.; Barakat, A.; Quéméneur, M.; Trably, E.Steyer, J.-P.; Carrère, H. Do furanic and phenolic compounds of lignocellulosic and algae biomass hydrolyzate inhibit anaerobic mixed cultures? A comprehensive review. *Biotechnol. Adv.* **2014**, *32*, 934–951, doi:10.1016/j.biotechadv.2014.04.007.

205. Elbeshbishy, E.; Dhar, B.R.; Nakhla, G.; Lee, H.S. A critical review on inhibition of dark biohydrogen fermentation. *Renew. Sustain. Energy Rev.* **2017**, *79*, 656–668, doi:10.1016/j.rser.2017.05.075.

206. Lin, R.; Cheng, J.; Ding, L.; Song, W.; Zhou, J.; Cen, K. Inhibitory effects of furan derivatives and phenolic compounds on dark hydrogen fermentation. *Bioresour. Technol.* **2015**, *196*, 250–255, doi:10.1016/j.biortech.2015.07.097.

207. Wirth, B.; Krebs, M.; Andert, J. Anaerobic degradation of increased phenol concentrations in batch assays. *Environ. Sci. Pollut. Res.* **2015**, *22*, 19048–19059, doi:10.1007/s11356-015-5100-8.

208. Jiang, Y.; McAdam, E.; Zhang, Y.; Heaven, S.; Banks, C.; Longhurst, P. Ammonia inhibition and toxicity in anaerobic digestion: A critical review. *J. Water Process Eng.* **2019**, *32*, 100899, doi:10.1016/j.jwpe.2019.100899.

209. Lucian, M.; Volpe, M.; Merzari, F.; Wüst, D.; Kruse, A.; Andreottola, G.; Fiori, L. Hydrothermal carbonization coupled with anaerobic digestion for the valorization of the organic fraction of municipal solid waste. *Bioresour. Technol.* **2020**, *314*, 123734, doi:10.1016/j.biortech.2020.123734.

210. Aragón-Briceño, C.I.; Ross, A.B.; Camargo-Valero, M.A. Mass and energy integration study of hydrothermal carbonization with anaerobic digestion of sewage sludge. *Renew. Energy* **2021**, *167*, 473–483, doi:10.1016/j.renene.2020.11.103.

211. Heidari, M.; Norouzi, O.; Salaudeen, S.; Acharya, B.; Dutta, A. Prediction of Hydrothermal Carbonization with Respect to the Biomass Components and Severity Factor. *Energy & Fuels* **2019**, *33*, 9916–9924, doi:10.1021/acs.energyfuels.9b02291.

212. Hoekman, S.K.; Broch, A.; Felix, L.; Farthing, W. Hydrothermal carbonization (HTC) of loblolly pine using a continuous, reactive twin-screw extruder. *Energy Convers. Manag.* **2017**, *134*, 247–259, doi:10.1016/j.enconman.2016.12.035.

213. Chandra, R.; Takeuchi, H.; Hasegawa, T. Hydrothermal pretreatment of rice straw biomass: A potential and promising method for enhanced methane production. *Appl. Energy* **2012**, *94*, 129–140, doi:10.1016/j.apenergy.2012.01.027.

214. Wang, D.; Shen, F.; Yang, G.; Zhang, Y.; Deng, S.; Zhang, J.; Zeng, Y.; Luo, T.; Mei, Z. Can hydrothermal pretreatment improve anaerobic digestion for biogas from lignocellulosic biomass? *Bioresour. Technol.* **2018**, *249*, 117–124, doi:10.1016/j.biortech.2017.09.197.

215. He, L.; Huang, H.; Zhang, Z.; Lei, Z.; Lin, B. Le Energy Recovery from Rice Straw through Hydrothermal Pretreatment and Subsequent Biomethane Production. *Energy and Fuels* **2017**, *31*, 10850–10857, doi:10.1021/acs.energyfuels.7b01392.

216. Ding, L.; Cheng, J.; Lin, R.; Deng, C.; Zhou, J.; Murphy, J.D. Improving biohydrogen and biomethane co-production via two-stage dark fermentation and anaerobic digestion of the pretreated seaweed Laminaria digitata. *J. Clean. Prod.* **2020**, *251*, 119666, doi:10.1016/j.jclepro.2019.119666.

217. Ahmad, F.; Silva, E.L.; Bernadete, M.; Varesche, A. Hydrothermal processing of biomass for anaerobic digestion – A review. *Renew. Sustain. Energy Rev.* **2018**, *98*, 108–124, doi:10.1016/j.rser.2018.09.008.

218. Thompson, T.M.; Young, B.R.; Baroutian, S. Efficiency of hydrothermal pretreatment on the anaerobic digestion of pelagic Sargassum for biogas and fertiliser recovery. *Fuel* **2020**, *279*, 118527, doi:10.1016/j.fuel.2020.118527.

219. Steinbach, D.; Wüst, D.; Zielonka, S.; Krümpel, J.; Munder, S.; Pagel, M.; Kruse, A. Steam Explosion Conditions Highly Influence the Biogas Yield of Rice Straw. *Molecules* **2019**, *24*, 3492, doi:10.3390/molecules24193492.

220. Baêta, B.E.L.; Cordeiro, P.H. de M.; Passos, F.; Gurgel, L.V.A.; de Aquino, S.F.; Fdz-Polanco, F. Steam explosion pretreatment improved the biomethanization of coffee husks. *Bioresour. Technol.* **2017**, *245*, 66–72, doi:10.1016/j.biortech.2017.08.110.

221. Kobayashi, F.; Take, H.; Asada, C.; Nakamura, Y. Methane production from steam-exploded bamboo. *J. Biosci. Bioeng.* **2004**, *97*, 426–428, doi:10.1016/S1389-1723(04)70231-5.

222. Grasham, O.; Dupont, V.; Camargo-Valero, M.A.; García-Gutiérrez, P.; Cockerill, T. Combined ammonia recovery and solid oxide fuel cell use at wastewater treatment plants for energy and greenhouse gas emission improvements. *Appl. Energy* **2019**, *240*, 698–708, doi:10.1016/j.apenergy.2019.02.029.

223. APHA Standard methods for the examination of water and wastewater. *Am. Public Heal. Assoc.* **2005**.

224. The British Standards Institution. BS ISO 1928:2009 Solid mineral fuels. Determination of gross calorific value by the bomb calorimetric method andcalculation of net calorific value, **2009**.

225. European Committee for Standardization (CEN). DD CEN/TS 15370-1: 2006. Solid Biofuels—Method for the Determination of Ash Melting Behaviour Part 1: Characteristic Temperatures Method, **2006**.

226. Okoro-Shekwaga, C.K.; Suruagy, M.V.T.; Ross, A.; Camargo-Valero, M.A. Particle size, inoculum-to-substrate ratio and nutrient media effects on biomethane yield from food waste. *Renew. Energy* **2020**, *151*, 311–321, doi:10.1016/j.renene.2019.11.028.

227. Madsen, R.B.; Jensen, M.M.; Mørup, A.J.; Houlberg, K.; Christensen, P.S.; Klemmer, M.; Becker, J.; Iversen, B.B.; Glasius, M. Using design of experiments to optimize derivatization with methyl chloroformate for quantitative analysis of the aqueous phase from hydrothermal liquefaction of biomass. *Anal. Bioanal. Chem.* **2016**, *408*, 2171–2183, doi:10.1007/s00216-016-9321-6.

228. Boyle, W.C. Energy Recovery From Sanitary Landfills - a Review. In *Microbial Energy Conversion*; Pergamon, **1977**; pp. 119–138.

229. Deng, C.; Lin, R.; Kang, X.; Wu, B.; O'Shea, R.; Murphy, J.D. Improving gaseous biofuel yield from seaweed through a cascading circular bioenergy system integrating anaerobic digestion and pyrolysis. *Renew. Sustain. Energy Rev.* **2020**, *128*, 109895, doi:10.1016/j.rser.2020.109895.

230. Moset, V.; Al-zohairi, N.; Møller, H.B. The impact of inoculum source, inoculum to substrate ratio and sample preservation on methane potential from different substrates. *Biomass and Bioenergy* **2015**, *83*, 474–482, doi:10.1016/j.biombioe.2015.10.018.

231. Cano, R.; Nielfa, A.; Fdz-Polanco, M. Thermal hydrolysis integration in the anaerobic digestion process of different solid wastes: Energy and economic feasibility study. *Bioresour. Technol.* **2014**, *168*, 14–22, doi:10.1016/j.biortech.2014.02.007.

232. The Engineering Toolbox. Properties of Saturated Steam - Pressure in Bar. Available online: https://www.engineeringtoolbox.com/saturated-steam-properties-d_457.html (accessed on May 12, 2020).

233. The Engineering Toolbox. Higher and Lower Calorific Values. Available online: https://www.engineeringtoolbox.com/fuels-higher-calorific-values-d_169.html (accessed on Jul 29, 2020).

234. Yuan, T.; Cheng, Y.; Zhang, Z.; Lei, Z.; Shimizu, K. Comparative study on hydrothermal treatment as pre- and post-treatment of anaerobic digestion of primary sludge: Focus on energy balance, resources transformation and sludge dewaterability. *Appl. Energy* **2019**, *239*, 171–180, doi:10.1016/j.apenergy.2019.01.206.

235. Kohn, R.A.; Allen, M.S. Storage of fresh and ensiled forages by freezing affects fibre and crude protein fractions. *J. Sci. Food Agric.* **1991**, *58*, 215–220, doi:10.1002/jsfa.2740580209.

236. Mitchell, E.J.S.; Lea-Langton, A.R.; Jones, J.M.; Williams, A.; Layden, P.; Johnson, R. The impact of fuel properties on the emissions from the combustion of biomass and other solid fuels in a fixed bed domestic stove. *Fuel Process. Technol.* **2016**, *142*, 115–123, doi:10.1016/j.fuproc.2015.09.031.

237. Xiao, R.; Chen, X.; Wang, F.; Yu, G. The physicochemical properties of different biomass ashes at different ashing temperature. *Renew. Energy* **2011**, *36*, 244–249, doi:10.1016/j.renene.2010.06.027.

238. Anastasakis, K. The Potential of the Production of Fuels and Chemicals from Marine Biomass, PhD Thesis, University of Leeds, 2011.

239. Parikh, J.; Channiwala, S.A.; Ghosal, G.K. A correlation for calculating HHV from proximate analysis of solid fuels. *Fuel* **2005**, *84*, 487–494, doi:10.1016/j.fuel.2004.10.010.

240. Holliger, C.; Alves, M.; Andrade, D.; Angelidaki, Irini; Astals, S.; Baier, U.; Bougrier, C.; Buffiere, P.; Carballa, M.; de Wilde, V.; Ebertseder, F.; Fernandez, B.; Ficara, E.; Fotidis, Ioannis; Frigon, J.-C.; de Laclos, H. F.; Ghasimi, D. S. M.; Hack, G.; Hartel, M.; Heerenklage, J.; Horvath, I. S.; Jenicek, P.; Koch, K.; Krautwald, J.; Lizasoain, J.; Liu, J.; Mosberger, L.; Nistor, M.; Oechsner, H.; Oliveira, J. V.;

Paterson, M.; Pauss, A.; Pommier, S.; Porqueddu, I.; Raposo, F.; Ribeiro, T.; Rusch Pfund, F.; Stromberg, S.; Torrijos, M.; van Eekert, M.; van Lier, J.; Wedwitschka, H.; Wierinck, I. Towards a standardization of biomethane potential tests. Water Sci. Technol. **2016**, 74, 2515–2522, doi:10.2166/wst.2016.336.

241. Paul, R. Anaerobic Digestion of Saccharina latissima, PhD Thesis, Birmingham City University, **2018**.

242. Sevilla, M.; Fuertes, A.B. The production of carbon materials by hydrothermal carbonization of cellulose. *Carbon N. Y.* **2009**, *47*, 2281–2289, doi:10.1016/j.carbon.2009.04.026.

243. Jeon, W.; Ban, C.; Park, G.; Yu, T.K.; Suh, J.Y.; Woo, H.C.; Kim, D.H. Catalytic hydrothermal conversion of macroalgae-derived alginate: Effect of pH on production of furfural and valuable organic acids under subcritical water conditions. *J. Mol. Catal. A Chem.* **2015**, *399*, 106–113, doi:10.1016/j.molcata.2015.01.011.

244. Reza, M.T.; Freitas, A.; Yang, X.; Hiibel, S.; Lin, H.; Coronella, C.J. Hydrothermal Carbonization (HTC) of Cow Manure: Carbon and Nitrogen Distributions in HTC Products. *Environ. Sci. Technol.* **2016**, *35*, 1002–1011, doi:10.1002/ep.

245. Becker, R.; Dorgerloh, U.; Helmis, M.; Mumme, J.; Diakité, M.; Nehls, I. Hydrothermally carbonized plant materials: Patterns of volatile organic compounds detected by gas chromatography. *Bioresour. Technol.* **2013**, *130*, 621–628, doi:10.1016/j.biortech.2012.12.102.

246. Kruse, A.; Koch, F.; Stelzl, K.; Wüst, D.; Zeller, M. Fate of Nitrogen during Hydrothermal Carbonization. *Energy and Fuels* **2016**, *30*, 8037–8042, doi:10.1021/acs.energyfuels.6b01312.

247. Sommersacher, P.; Brunner, T.; Obernberger, I. Fuel indexes: A novel method for the evaluation of relevant combustion properties of new biomass fuels. *Energy and Fuels* **2012**, *26*, 380–390, doi:10.1021/ef201282y.

248. Zhao, B.; Su, Y.; Liu, D.; Zhang, H.; Liu, W.; Cui, G. SO2/NOx emissions and ash formation from algae biomass combustion: Process characteristics and mechanisms. *Energy* **2016**, *113*, 821–830, doi:10.1016/j.energy.2016.07.107.

249. Lynam, J.G.; Toufiq Reza, M.; Vasquez, V.R.; Coronella, C.J. Effect of salt addition on hydrothermal carbonization of lignocellulosic biomass. *Fuel* **2012**, *99*, 271–273, doi:10.1016/j.fuel.2012.04.035.

250. Heidari, M.; Dutta, A.; Acharya, B.; Mahmud, S. A review of the current knowledge and challenges of hydrothermal carbonization for biomass conversion. *J. Energy Inst.* **2019**, *92*, 1779–1799, doi:10.1016/j.joei.2018.12.003.

251. He, C.; Giannis, A.; Wang, J.Y. Conversion of sewage sludge to clean solid fuel using hydrothermal carbonization: Hydrochar fuel characteristics and combustion behavior. *Appl. Energy* **2013**, *111*, 257–266, doi:10.1016/j.apenergy.2013.04.084.

252. Pagés-Díaz, J.; Huiliñir, C. Valorization of the liquid fraction of co-hydrothermal carbonization of mixed biomass by anaerobic digestion: Effect of the substrate to inoculum ratio and hydrochar addition. *Bioresour. Technol.* **2020**, *317*, 123989, doi:10.1016/j.biortech.2020.123989.

253. The British Standards Institution. BS 6068-2.34:1988. Water quality. Physical, chemical and biochemical methods. Method for the determination of the chemical oxygen demand, **1988.**

254. Yenigün, O.; Demirel, B. Ammonia inhibition in anaerobic digestion: A review. *Process Biochem.* **2013**, *48*, 901–911, doi:10.1016/j.procbio.2013.04.012.

255. O'Flaherty, V.; Collins, G.; Mahony, T. The microbiology and biochemistry of anaerobic bioreactors with relevance to domestic sewage treatment. *Rev. Environ.*

Sci. Biotechnol. **2006**, *5*, 39–55, doi:10.1007/s11157-005-5478-8.

256. Shao, Y.; Long, Y.; Zhou, Y.; Jin, Z.; Zhou, D.; Shen, D. 5-Hydroxymethylfurfural production from watermelon peel by microwave hydrothermal liquefaction. *Energy* **2019**, *174*, 198–205, doi:10.1016/j.energy.2019.02.181.

257. Jung, K.W.; Kim, D.H.; Shin Hang-Sik, H.S. Fermentative hydrogen production from Laminaria japonica and optimization of thermal pretreatment conditions. *Bioresour. Technol.* **2011**, *102*, 2745–2750, doi:10.1016/j.biortech.2010.11.042.

258. Nakason, K.; Panyapinyopol, B.; Kanokkantapong, V.; Viriya-empikul, N.; Kraithong, W.; Pavasant, P. Characteristics of hydrochar and hydrothermal liquid products from hydrothermal carbonization of corncob. *Biomass Convers. Biorefinery* **2018**, *8*, 199–210, doi:10.1007/s13399-017-0279-1.

259. Ding, L.; Cheng, J.; Qiao, D.; Yue, L.; Li, Y.; Zhou, J.; Cen, K. Investigating hydrothermal pretreatment of food waste for two-stage fermentative hydrogen and methane co-production. *Bioresour. Technol.* **2017**, *241*, 491–499, doi:10.1016/j.biortech.2017.05.114.

260. The British Standards Institution. ISO 1171:2010. Solid mineral fuels — Determination of ash. **2010**.

261. The British Standards Institution. BS EN 14775:2009. Solid biofuels — Determination of ash content. **2009**.

262. Chen, X.; Lin, Q.; He, R.; Zhao, X.; Li, G. Hydrochar production from watermelon peel by hydrothermal carbonization. *Bioresour. Technol.* **2017**, *241*, 236–243, doi:10.1016/j.biortech.2017.04.012.

263. Lu, X.; Pellechia, P.J.; Flora, J.R.V.; Berge, N.D. Influence of reaction time and temperature on product formation and characteristics associated with the hydrothermal carbonization of cellulose. *Bioresour. Technol.* **2013**, *138*, 180–190, doi:10.1016/j.biortech.2013.03.163.

264. Kabadayi Catalkopru, A.; Kantarli, I.C.; Yanik, J. Effects of spent liquor recirculation in hydrothermal carbonization. *Bioresour. Technol.* **2017**, *226*, 89–93, doi:10.1016/j.biortech.2016.12.015.

265. Ariunbaatar, J.; Panico, A.; Esposito, G.; Pirozzi, F.; Lens, P.N.L. Pretreatment methods to enhance anaerobic digestion of organic solid waste. *Appl. Energy* **2014**, *123*, 143–156, doi:10.1016/j.apenergy.2014.02.035.

266. Angelidaki, I.; Alves, M.; Bolzonella, D.; Borzacconi, L.; Campos, J.L.; Guwy, A.J.; Kalyuzhnyi, S.; Jenicek, P.; Van Lier, J.B. Defining the biomethane potential (BMP) of solid organic wastes and energy crops: A proposed protocol for batch assays. *Water Sci. Technol.* **2009**, *59*, 927–934, doi:10.2166/wst.2009.040.

267. Yang, G.; Wang, J. Kinetics and microbial community analysis for hydrogen production using raw grass inoculated with different pretreated mixed culture. *Bioresour. Technol.* **2018**, *247*, 954–962, doi:10.1016/j.biortech.2017.09.041.

268. Yin, Y.; Hu, J.; Wang, J. Enriching hydrogen-producing bacteria from digested sludge by different pretreatment methods. *Int. J. Hydrogen Energy* **2014**, *39*, 13550–13556, doi:10.1016/j.ijhydene.2014.01.145.

269. Teli, A.; Ficara, E.; Malpei, F. Bio-Hydrogen Production from Cheese Whey by Dark Fermentation. *Chem. Eng. Trans.* **2014**, *37*, 613–618, doi:10.3303/CET1437103.

270. Patterson, T.; Esteves, S.; Dinsdale, R.; Guwy, A.; Maddy, J. Life cycle assessment of biohydrogen and biomethane production and utilisation as a vehicle fuel. *Bioresour. Technol.* **2013**, *131*, 235–245, doi:10.1016/j.biortech.2012.12.109.

271. Valdez-Guzmán, B.E.; Rios-Del Toro, E.E.; Cardenas-López, R.L.; Méndez-Acosta, H.O.; González-Álvarez, V.; Arreola-Vargas, J. Enhancing biohydrogen production from Agave tequilana bagasse: Detoxified vs. Undetoxified acid hydrolysates. *Bioresour. Technol.* **2019**, *276*, 74–80, doi:10.1016/j.biortech.2018.12.101.

272. Ding, L.; Cheng, J.; Xia, A.; Jacob, A.; Voelklein, M.; Murphy, J.D. Co-generation of biohydrogen and biomethane through two-stage batch co-fermentation of macro- and micro-algal biomass. *Bioresour. Technol.* **2016**, *218*, 224–231, doi:10.1016/j.biortech.2016.06.092.

273. Elbeshbishy, E.; Hafez, H.; Nakhla, G. Enhancement of biohydrogen producing using ultrasonication. *Renew. Energy* **2010**, *35*, 6184–6193, doi:10.1016/j.ijhydene.2010.03.119.

274. Wang, X.; Zhao, J.; Yang, Q.; Sun, J.; Peng, C.; Chen, F.; Xu, Q.; Wang, S.; Wang, D.; Li, X.; Zeng, G. Evaluating the potential impact of hydrochar on the production of short-chain fatty acid from sludge anaerobic digestion. Bioresour. Technol. 2017, 246, 234–241, doi:10.1016/j.biortech.2017.07.051.

275. Rezania, S.; Din, M.F.M.; Taib, S.M.; Sohaili, J.; Chelliapan, S.; Kamyab, H.; Saha, B.B. Review on fermentative biohydrogen production from water hyacinth , wheat straw and rice straw with focus on recent perspectives. *Int. J. Hydrogen Energy* **2017**, *42*, 20955–20969, doi:10.1016/j.ijhydene.2017.07.007.

276. Lin, R.; Deng, C.; Rajendran, K.; Bose, A.; Kang, X.; Murphy, J.D. Competing Reactions Limit Production of Sugars in Hydrothermal Hydrolysis of Grass Silage: An Assessment of the Effect of Temperature on Sugar Production and Parasitic Energy Demand. *Front. Energy Res.* **2020**, *8*, 1–11, doi:10.3389/fenrg.2020.575523.

277. Weber, B.; Estrada-Maya, A.; Sandoval-Moctezuma, A.C.; Martínez-Cienfuegos, I.G. Anaerobic digestion of extracts from steam exploded Agave tequilana bagasse. *J. Environ. Manage.* **2019**, *245*, 489–495, doi:10.1016/j.jenvman.2019.05.093.

278. Wijngaard, H.; Brunton, N. The Optimization of Extraction of Antioxidants from Apple Pomace by Pressurized Liquids. *J. Agric. Food Chem.* **2009**, *57*, 10625–10631, doi:10.1021/jf902498y.

279. Yang, L.; Xu, F.; Ge, X.; Li, Y. Challenges and strategies for solid-state anaerobic digestion of lignocellulosic biomass. *Renew. Sustain. Energy Rev.* **2015**, *44*, 824–834, doi:10.1016/j.rser.2015.01.002.

280. Chuang, Y.S.; Lay, C.H.; Sen, B.; Chen, C.C.; Gopalakrishnan, K.; Wu, J.H.; Lin, C.S.; Lin, C.Y. Biohydrogen and biomethane from water hyacinth (Eichhornia crassipes) fermentation: Effects of substrate concentration and incubation temperature. *Int. J. Hydrogen Energy* **2011**, *36*, 14195–14203, doi:10.1016/j.ijhydene.2011.04.188.

281. Su, H.; Cheng, J.; Zhou, J.; Song, W.; Cen, K. Hydrogen production from water hyacinth through dark- and photo- fermentation. *Int. J. Hydrogen Energy* **2010**, *35*, 8929–8937, doi:10.1016/j.ijhydene.2010.06.035.

282. Heidari, M.; Salaudeen, S.; Norouzi, O.; Acharya, B.; Dutta, A. Numerical Comparison of a Combined Hydrothermal Carbonization and Anaerobic Digestion System with Direct Combustion of Biomass for Power Production. *Processes* **2020**, *8*, 43.

283. Saidi, R.; Liebgott, P.P.; Gannoun, H.; Ben Gaida, L.; Miladi, B.; Hamdi, M.; Bouallagui, H.; Auria, R. Biohydrogen production from hyperthermophilic anaerobic digestion of fruit and vegetable wastes in seawater: Simplification of the culture medium of Thermotoga maritima. *Waste Manag.* **2018**, *71*, 474–484, doi:10.1016/j.wasman.2017.09.042.

284. Xu, Z.X.; Shan, Y.Q.; Zhang, Z.; Deng, X.Q.; Yang, Y.; Luque, R.; Duan, P.G.

Hydrothermal carbonization of sewage sludge: Effect of inorganic salts on hydrochar's physicochemical properties. *Green Chem.* **2020**, *22*, 7010–7022, doi:10.1039/d0gc02615h.

285. Jiang, Z.; Yi, J.; Li, J.; He, T.; Hu, C. Promoting effect of sodium chloride on the solubilization and depolymerization of cellulose from raw biomass materials in water. *ChemSusChem* **2015**, *8*, 1901–1907, doi:10.1002/cssc.201500158.

286. Castello, D.; Rolli, B.; Kruse, A.; Fiori, L. Supercritical water gasification of biomass in a ceramic reactor: Long-time batch experiments. *Energies* **2017**, *10*, 1–17, doi:10.3390/en10111734.

287. Choe, U.; Mustafa, A.M.; Lin, H.; Choe, U.; Sheng, K. Anaerobic co-digestion of fish processing waste with a liquid fraction of hydrothermal carbonization of bamboo residue. *Bioresour. Technol.* **2020**, *297*, 122542, doi:10.1016/j.biortech.2019.122542.

288. Wang, F.; Yi, W.; Zhang, D.; Liu, Y.; Shen, X.; Li, Y. Anaerobic co-digestion of corn stover and wastewater from hydrothermal carbonation. *Bioresour. Technol.* **2020**, *315*, 123788, doi:10.1016/j.biortech.2020.123788.

289. Koch, K.; Hafner, S.D.; Weinrich, S.; Astals, S. Identification of Critical Problems in Biochemical Methane Potential (BMP) Tests From Methane Production Curves. *Front. Environ. Sci.* **2019**, *7*, 178, doi:10.3389/fenvs.2019.00178.

290. Hafner, S.D.; de Laclos, H.F.; Koch, K.; Holliger, C. Improving Inter-Laboratory Reproducibility in Measurement of Biochemical Methane Potential (BMP). *Water* **2020**, *12*, 1752, doi:https://doi.org/10.3390/w12061752.

291. Heerenklage, J.; Rechtenbach, D.; Atamaniuk, I.; Alassali, A.; Raga, R.; Koch, K.; Kuchta, K. Development of a method to produce standardised and storable inocula for biomethane potential tests – Preliminary steps. *Renew. Energy* **2019**, *143*, 753–761, doi:10.1016/j.renene.2019.05.037.

292. Hagen, L.H.; Vivekanand, V.; Pope, P.B.; Eijsink, V.G.H.; Horn, S.J. The effect of storage conditions on microbial community composition and biomethane potential in a biogas starter culture. *Appl. Microbiol. Biotechnol.* **2015**, *99*, 5749–5761, doi:10.1007/s00253-015-6623-0.

293. Astals, S.; Koch, K.; Weinrich, S.; Hafner, S.D.; Tait, S.; Peces, M. Impact of storage conditions on the methanogenic activity of anaerobic digestion inocula. *Water* **2020**, *12*, 1321, doi:10.3390/W12051321.

294. Filer, J.; Ding, H.H.; Chang, S. Biochemical Methane Potential (BMP) Assay Method for Anaerobic Digestion Research. *Water* **2019**, *11*, 921, doi:https://doi.org/10.3390/w11050921.

295. Koch, K.; Hafner, S.D.; Astals, S.; Weinrich, S. Evaluation of Common Supermarket Products as Positive Controls in Biochemical Methane Potential (BMP) Tests. *Water* **2020**, *12*, 1223, doi:https://doi.org/10.3390/w12051223.

Appendices

Appendix A.

Example calculation for the conversion of proximate or ultimate data across different bases

Proximate and/or ultimate data can be presented as a number of bases: as received basis (*ar*), dry basis (*db*) or dry ash-free basis (*daf*). The definitions of each are as follows for this thesis:

- *ar* = analysis of biomass which been preserved through either through oven or freeze drying, as described by Section 3.1.1.1. Biomasses contain between 5-8% moisture. Preserved biomass is also referred to as 'oven dried biomass'.
- *db* = analysis of biomass following the complete theoretical removal of moisture content.
- *daf* = analysis of biomass following the complete theoretical removal of both moisture and ash content.

Appendix Equation A.1. demonstrates the calculation used for the conversion of an as received (*ar*) analysis to a dry basis (*db*), using the carbon (C) content as an example. Where, $C\%_{db}$ is the carbon-content on a dry basis (%), $C\%_{ar}$ is the carbon-content on an as received basis (%) and M is the moisture content, on an as received basis. M-content was determined by TGA analysis, described in Section 3.3.1.1.

Appendix Equation A.1: Conversion of C-content from *ar* to *db*.

$$C\%_{db} = \left(\frac{C\%_{ar}}{100 - M}\right) \times 100$$

Appendix Equation A.2, demonstrates the calculation used for the conversion of a dry basis (*db*) analysis to a dry ash-free basis (*daf*), using the carbon (C) content as an example. Where, $C\%_{daf}$ is the carbon-content on a dry ash-free basis (%), $C\%_{db}$ is the carbon-content on a dry basis (%) and Ash_{db} is the ash content, on a dry basis. Ash-content was determined by TGA analysis, described in Section 3.3.1.1.

Appendix Equation A.2: Conversion of C-content from *db* to *daf*.

$$C\%_{daf} = \left(\frac{C\%_{db}}{100 - Ash_{db}}\right) \times 100$$

Appendix B.

Example calculation of HHV using Dulong's equation, with oxygen-content measured by difference

Appendix Table B.1. shows the proximate and ultimate composition of *L. digitata* (LD) on an as received (*ar*) basis. Initially, the H-content was corrected for moisture by applying Appendix Equation B.1 and O-content was calculated by difference, according to Appendix Equation B.2, each discussed in Section 3.3.1.2. Proximate data determined by TGA (Section 3.3.1.1). Corrected results are presented in Appendix Table B.2.

Appendix Table B.1. Proximate and ultimate data of *L. digitata* (LD), on an as received (*ar*) basis.

Ultimate Analysis (% *ar*)					Proximate analysis (% *ar*)			
C	**H**	**N**	**S**	**O***	**M**	**VM**	**FC**	**Ash**
25.14	3.82	2.02	ND	-	5.13	65.66	14.78	14.43

*O-content measured by difference. M=moisture. VM=volatile matter. FC=fixed carbon. ND=not detected.

Appendix Equation B.1: Correction of H-content for moisture.

$$\text{Corrected H}(\%) = 3.82 - (5.13 \times \left(\frac{2}{18}\right))$$

Appendix Equation B.2: Calculation of O-content by difference.

$$\text{O}(\%) = \ 100 - (5.13 + 14.43 + 25.14 + 3.25 + 2.02)$$

Appendix Table B.2. Proximate and ultimate data of *L. digitata* (LD), on an as received (*ar*) basis, following the correction of both hydrogen and oxygen for moisture.

Ultimate Analysis (% *ar*)					Proximate analysis (% *ar*)			
C	**H**	**N**	**S**	**O***	**M**	**VM**	**FC**	**Ash**
25.14	3.25	2.02	ND	50.03	5.13	65.66	14.78	14.43

*O-content measured by difference. M=moisture. VM=volatile matter. FC=fixed carbon. ND=not detected.

CHNS-O values were subsequently converted from an as received (*ar*) basis to a dry basis (*db*), according to Appendix Equation A.1. An example calculation for the conversion of C-content is shown in Appendix Equation B.3. Proximate and ultimate data is reported on a dry basis in Appendix Table B.3.

Appendix Equation B.3: Conversion of *L. digitata* (LD) C-content from *ar* to *db*.

$$\text{C}\%_{db} = \left(\frac{25.14}{100 - 5.13}\right) \times 100$$

Appendix Table B.3. Proximate and ultimate data of *L. digitata* (LD), on a dry basis (*db*).

Ultimate Analysis (% *ar*)					**Proximate analysis (% *ar*)**		
C	H	N	S	O*	VM	FC	Ash
26.50	3.43	2.13	ND	52.74	69.21	15.58	15.21

*O-content measured by difference. M=moisture. VM=volatile matter. FC=fixed carbon. ND=not detected.

C, H and O values presented in Appendix Table B.3. were subsequently applied to Dulong's equation, described in Section 3.3.3.1 and shown in Appendix Equation B.4. The HHV for LD was 4.46 MJ/kg (*db*).

Appendix Equation B.4: Correction of O-content for moisture.

$$\text{HHV (MJ/kg)}(db) = (0.3383 \times 26.50) + (1.422 \times (3.43 - \left(\frac{52.74}{8}\right))$$

HHV = 4.46 MJ/kg (*db*)

Appendix C.

Example calculation of HHV using Dulong's equation with oxygen-content measured directly

Appendix Table C.1. shows the proximate and ultimate composition of *L. digitata* (LD) on an as received (*ar*) basis. Initially, the H-content and O-content were corrected for moisture by applying Appendix Equation C.1 and Appendix Equation C.2, respectfully; as discussed in Section 3.3.1.2. Proximate data determined by TGA (Section 3.3.1.1). Corrected results are presented in Appendix Table C.2.

Appendix Table C.1. Proximate and ultimate data of *L. digitata* (LD), on an as received (*ar*) basis.

Ultimate Analysis (% *ar*)					Proximate analysis (% *ar*)			
C	**H**	**N**	**S**	**O***	**M**	**VM**	**FC**	**Ash**
25.14	3.82	2.02	ND	26.55	5.13	65.66	14.78	14.43

*O-content measured directly. M=moisture. VM=volatile matter. FC=fixed carbon. ND=not detected.

Appendix Equation C.1: Correction of H-content for moisture.

$$\text{Corrected H}(\%) = 3.82 - (5.13 \times \left(\frac{2}{18}\right))$$

Appendix Equation C.2: Correction of O-content for moisture.

$$\text{Corrected O}(\%) = 26.55 - (5.13 \times \left(\frac{16}{18}\right))$$

Appendix Table C.2. Proximate and ultimate data of *L. digitata* (LD), on an as received (*ar*) basis, following the correction of both hydrogen and oxygen for moisture.

Ultimate Analysis (% *ar*)					Proximate analysis (% *ar*)			
C	**H**	**N**	**S**	**O***	**M**	**VM**	**FC**	**Ash**
25.14	3.25	2.02	ND	21.99	5.13	65.66	14.78	14.43

*O-content measured directly. M=moisture. VM=volatile matter. FC=fixed carbon. ND=not detected.

CHNS-O values were subsequently converted from an as received (*ar*) basis to a dry basis (*db*), according to Appendix Equation A.1. An example calculation for the conversion of C-content is shown in Appendix Equation C.3. Proximate and ultimate data is reported on a dry basis in Appendix Table C.3.

Appendix Equation C.3: Conversion of *L. digitata* (LD) C-content from *ar* to *db*.

$$\mathrm{C}\%_{db} = \left(\frac{25.14}{100 - 5.13}\right) \times 100$$

Appendix Table C.3. Proximate and ultimate data of *L. digitata* (LD), on a dry basis (*db*).

Ultimate Analysis (% *ar*)					**Proximate analysis (% *ar*)**		
C	H	N	S	O*	VM	FC	Ash
26.50	3.43	2.13	ND	23.18	69.21	15.58	15.21

*O-content measured directly. M=moisture. VM=volatile matter. FC=fixed carbon. ND=not detected.

C, H and O values presented in Appendix Table C.3. were subsequently applied to Dulong's equation, described in Section 3.3.3.1 and shown in Appendix Equation C.4. The HHV for LD was 9.72 MJ/kg (*db*).

Appendix Equation C.4: Calculation of HHV of LD by Dulong's equation.

$$\mathrm{HHV\ (MJ/kg)}(db) = (0.3383\ \times 26.50) + (1.422\ \times (3.43 - \left(\frac{23.18}{8}\right))$$

HHV = 9.72 MJ/kg (*db*)

Appendix D.

Grouping structures for compounds identified by derivatization GC-MS methodology

Appendix Table D.1. Grouping structures of compounds from process waters, identified by derivatization GC-MS methodology.

Compound Group	Compounds Included
Carboxylic Acids	Acetic Acid
	Isobutyric Acid
	Butyric Acid
	Isovaleric Acid
	Crotonic Acid
	5-Hexenoic Acid
	Malonic Acid
	Levulinic Acid
	Succinic Acid
	Glutaric Acid
	Glycolic Acid
	3-Methylpentanoic Acid
	Valeric Acid
Aromatic Carboxylic Acids	Benzoic Acid
	Glycolic Acid
Aromatic Ketones	Cyclopentanone
	2-Methyl-2-Cyclopenten-1-one
	3-Methyl-2-Cyclopentenone
	2,3-Dimethyl-2-Cyclopenten-1-one
Phenolics	Phenol
	P-cresol
Pyrazines	2-Methyl-Pyrazine
	2,5-Dimethylpyrazine
	Ethylpyrazine
	2,3-Dimethylpyrazine
	2,3,5-Trimethylpyrazine
Pyridines	3-Hydroxypyridine